Advanced Modelling of Sports Footwear

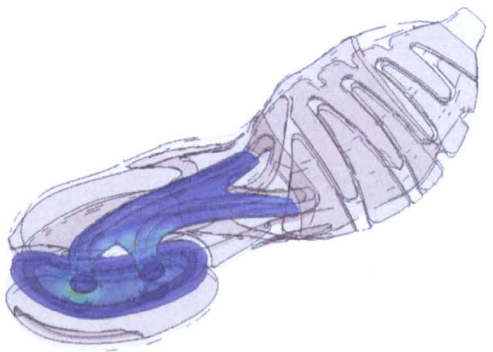

by

Paul J. Gibbs

A Doctoral Thesis
Submitted in Partial Fulfilment of the Requirements
for award of

Doctor of Philosophy
of
Loughborough University

Abstract

A need to reduce the number of design iterations, coupled with a requirement to reduce the weight of the new generation of TPU running shoes has lead to the use of finite element analysis (FE) within the athletic shoe industry. The collaborators in this research, adidas, were already using the technology, but only on individual parts, and on a reverse engineered basis.

This thesis presents a thorough review into the materials used in athletic footwear, their application within running shoes and the methods of testing non-linear, highly deformable polymers and polymer foams. The fundamentals of the FE process are examined, along with a discussion of the current testing methods for shoes.

The novelty in this work comes mainly from the comprehensive, logical progression through the modelling process as applied to this new area. Sample materials were tested, revealing new test methods. These were then analysed and converted for use in ABAQUS v6.5 which was the FE software used. The modelling of the sample materials, their tests, then shoe parts and midsole assemblies are discussed at length.

At each stage the required complexities were added to the model, and these are detailed. This includes the import, conversion and repair of highly complex geometry, meshing techniques for this geometry, methods of building models of shoe assemblies and all relevant issues that arose from these processes.

In addition, a shoe with an internal mechanism was modelled to assist in the design process. The effect of damage to shoe materials was also studied.

Physical tests were carried out to verify all the FE models, and the results are presented. In addition, shoes taken from the end of the production line with the uppers attached were tested in order to compare the change in performance between the component parts and a finished product.

The results of the modelling showed that was possible to construct and run full shoe assemblies within a reasonable time. Fair prediction of the physical response of the assemblies was seen using material data taken directly from the sample data, but a method of correcting the initial error in the material test is presented which gives very good force/deflection results in TPU parts. A method of adjusting the entire assembly's material models is then presented, which improves the initial verification.

In addition to force/deflection readings, digital image processing was used to monitor the structural response of the shoe during loading, and a set of structural metrics is put forward. The results of these indicated that while the shoe models were representing the cushioning response well, the shape of the shoe was not replicated, suggesting that the model in its present state would be unsuitable for use in some forms of test. Suggestions for improvement are made.

Comparison of the structural metrics between shoe assemblies and production shoes suggests the possibility of a quantifiable metric for what would be considered a 'good' shoe. The repercussions of this are discussed in the conclusions.

Acknowledgements

I would like to thank all the people who have helped me with this research. My supervisors, Andy Harland and Sean Mitchell for providing guidance and support, thanks to Tim Lucas, Tim Robinson and all the team at adidas for their assistance providing test samples, support and the opportunity to work on this challenging project (along with some memorable trips around the globe).

I'd also like the thank all of the Wolfson School technicians for helping me build my (quote) 'shoe pounding rig', and special thanks to Andy Sandaver for his help with all the materials testing, who remained ever cheerful despite his lab becoming festooned with small chunks of foam and black paint from the video metric testing.

Thanks also go out to my undergraduate assistants Siân Slawson and Chris Baker for all their help with the practical testing.

'A computer lets you make more mistakes faster than any invention in human history, with the possible exceptions of hand guns and tequila.'

Mitch Ratliffe

Contents

Chapter 1

Introduction

1.1 Context of Research

Today's market for training shoes is highly competitive, and one where fashion can play as much of a role as performance. To maintain a competitive advantage, a shorter time between initial design and full production is desirable, as this allows manufacturers to follow trends closely. The use of new materials in shoe design is allowing manufacturers to produce shoes that have much longer life spans; a traditional foam midsole shoe is expected to last 500-600 miles, while one made from solid polymers can last up to 2000 miles. Solid polymers are however much denser than foams and as runners consider heavy shoes to be a disadvantage, less material must be used. This has resulted in a wave of new intricate components that require more stringent engineering than has ever been used in the running footwear industry.

The bulk of shoe sales come from the recreational sector - the shoes are bought as fashion accessories and are not subjected to the same stresses as they would be if used for competitive running (at any level of competition). These shoes provide the main source of income for large shoe companies and are therefore critical to business performance. Customers often choose one brand of recreational shoes over another for non-performance reasons such as appearance, branding or price. The appearance and price of a shoe can be controlled, but enhancing the branding of a shoe relies more on public opinion, which is fuelled by advertising, media reports and in most cases, the 'perceived performance' advantage in a shoe. The general public's logic could be thought of in this way - people may not want to run, but if they had to, their chosen shoes would make them run better.

To enhance perceived performance many manufacturers create expensive, low-volume, high-performance shoes and advertise these shoes heavily. The message given out is that the brand understands the technical aspects of shoe design, and can apply this to their entire range of shoes. They may not necessarily do this, but the emphasis is there. This process is not just seen in the footwear industry, for example, Vauxhall produced the VX220 - a high performance sports car that used the engine from its range of more sedate Vectra cars. The message was that consumers could 'buy into' the performance of the VX220 by owning a car with the same engine.

In the same way, by filtering technology down from the low-profit performance shoes to the mass market models, shoe manufacturers can boost sales. The ability to develop and filter down new technology faster than competitors is a distinct advantage in increasing the perceived performance of a brand.

While the appearance of a shoe might be assessed on the drawing board, at present the only way of fully testing the performance of a shoe is to make prototypes and subject these to physical tests. The prototyping process takes a significant amount of time and

money, as moulds and templates for the individual parts must be made. This means that any design changes will require new moulds to be made, new prototypes created and tested. The reduction in number of these design iterations would be financially beneficial, not only in direct manufacturing costs, but also in the costs associated with delaying production.

The highly competitive nature of this industry means that up-to-date information concerning the design and manufacture of shoes is commercially sensitive and will be severely restricted in the public domain. To allow progress in this field, this research is conducted in collaboration with adidas, the second largest sports shoe manufacturer in the world. Their involvement will allow access to sensitive information within adidas, but will exclude any assistance from any other shoe manufacturers. For the purpose of this research, this is considered an acceptable compromise.

1.2 Design and Manufacture

For the majority of shoe manufacturers the design of the shoe is carried out in a separate location to the manufacture, which is predominantly contracted out to factories in Asia. This is due to the considerably reduced costs of low technology, high labour mass production in countries such as China.

1.2.1 Design

The design considerations of a shoe can be split into three factors: style, function and cost. The balance between these three depends on the purpose of the shoe - a fashion shoe will focus on style, a performance shoe on function and the large volume, mid to low range shoes on cost.

From information gathered during visits to the adidas headquarters, it is apparent that different groups of people are broadly (but not exclusively) responsible for each of the factors: Graphic Designers and Marketing (style), Biomechanists and Engineers (function), Finance and Production (cost). The company runs a production group consisting of all the groups mentioned that work to a seasonal timescale, working with existing technology, but controlling the entire shoe manufacture process from styling to sales. New technology is generated by a satellite group which works on a separate timescale, exchanging information with the production groups. This group has to prove any new technology before it can be incorporated into production (Figure 1.1).

Communication is vital between the various departments to ensure that one factor is not overly compromised. However, the function of the shoe manufacturers is to turn a profit, so emphasis is often put on being able to sell the shoe at a profit, while still producing a product that will not adversely affect future sales.

Shoe designs themselves are generated with surface modelling software (for 3D shapes) and 2D CAD for uppers and any parts that are to be stamped/cut from fabric. The designs are generally created to scale, and they will require some adjustment if the part is to be moulded as the cooling process during manufacture warps the produced part, and this distortion must be accounted for. These adjustments are carried out by the factories producing the moulds.

1.2.2 Design Analysis

It is common business knowledge that if a manufacturer can consistently produce and sell a product that satisfies the customer's requirements then the customer is likely to return to the same manufacturer's product when they need to replace said product. If the customer is

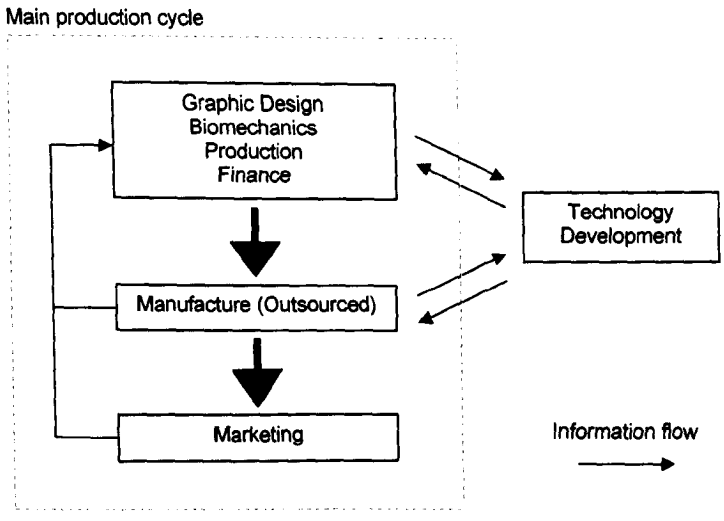

Figure 1.1: Flow chart illustrating the information flow within a large shoe manufacturer.

not satisfied then they are likely not to buy the same product again, and are more likely to complain to others about the poor product, reducing overall sales.

This wisdom is relevant to the running shoe market, so while cost is very important, a 'poor' shoe can seriously damage a company's reputation and therefore its sales. Due to the need to produce new shoes on a seasonal basis, there is little time to design, prototype, test, analyse and re-design a shoe. As most of the critical performance components in the midsole are moulded, the ability to predict the performance of a shoe component, without the time-consuming and expensive process of making moulds, would be a distinct competitive advantage.

The aim of this research is to develop such a predictive capacity, using Finite Element Analysis (FEA or FE, see Chapter 4 for details). FE analyses are already used within the industry's technology groups, but on a small scale for the analysis of parts of shoes, and are performed as a reverse engineering exercise, without any predictive capacity.

1.2.3 Manufacture

The manufacture of a shoe midsole (from a finally approved design) follows this process:

1. Repair/conversion of 2D/3D geometry (to account for changes that will happen to the part depending on the exact production process used) and production of CNC code.
2. CNC machining of moulds for moulded parts (with hand finishing/cleaning of moulds).
3. Injection/compression moulding of parts.
4. Hand assembly.

For each of the aforementioned stages, the following issues may cause differences between a produced shoe and the finally approved design (and between two assumed identical shoes):

Stage 1 Approximation or correction of geometry to allow for tooling or control system capabilities.

Stage 2 Deviation from the finally approved design to create qualitatively/quantitatively acceptable moulds.

Stage 3 Variation in the production of the constituent materials (within a batch, i.e. inhomogeneity in foam parts, or between different batches). Variation in the production process for a given part (e.g. moulding temperature variation, random fluid flow within the moulds etc.).

Stage 4 Variation in any of the assembly processes (including variation that is allowed within a process that is inspected for quality).

It is hypothesised that the issues in stages 1 and 2 will cause differences between the performance of a shoe based on the finally approved design, and the performance of an actual shoe, but not from one shoe to another produced with the same tooling. Issues in stages 3 and 4 are likely to cause differences in performance between any two shoes from the same tooling.

The accuracy of the computer models to be produced needs to be understood within the context of likely production variability. There are two implications: Firstly, model validation needs to allow for potential sample deviation from 'designed' performance (model predictions could be accompanied by an appropriate confidence level or accuracy tolerance). Secondly models could be used to explore performance sensitivity to production parameters and so improve quality/efficiency.

1.3 Research Question

An 'ideal' solution to the problem of predicting shoe performance would provide results in a shorter time than it takes to physically make and test prototypes, and would be able to provide quantitative results from all testing done on the computer model (henceforth referred to as the *virtual shoe* or *virtual model/tests*). This would be an improvement over the current methods of runner questionnaires and simple mechanical testing (see Section 2.9), and would reduce the number of design iterations, saving large sums of money and shortening the production life-cycle of a shoe.

The use of FEA is the proposed method as it is suited to the application of complex part geometry seen in present day shoes. The aim of this research is therefore to address the following question:

Can shoes/shoe components be modelled using FEA techniques purely on the basis of anticipated geometry and sample material properties, with sufficient accuracy to permit reliable prediction of satisfactory/unsatisfactory shoe performance under laboratory testing conditions and enable subsequent design improvement without physical prototypes?

The objectives that are required to answer the research question include:

Literature and shoe technology reviews (Chapters 2-4) To assess the current level of knowledge in the fields of material science, FEA and biomechanics, relative to this research. The technology used to develop shoes within a company is also studied, including; the design and manufacture process, manufacturer shoe assessment and time/cost implications. There will be difficulty obtaining current information concerning manufacturer testing from companies other than adidas, due to the commercially sensitive nature of the information.

Laboratory testing of materials (Chapter 7) It is known that the materials used in shoes are compounds specific to a company and its products. Information on material properties therefore may not be available publicly (or exist at all) and that laboratory testing is required to determine said properties.

FEA model construction (Chapter 4) Initial research suggests that FEA has not been used extensively within the footwear industry. Where it has been used, models have been very simple. It is expected that the FE software to be used (ABAQUS v6.4/5), combined with meshing software (Hypermesh 6.0) will be capable of creating a model of a shoe, but this is to be confirmed in Chapter 4.

FEA model performance analysis If it can be proven that the FE technique can create shoe models, then the ability of these models to predict the performance of shoes must be assessed. This will be done by comparing results from models of full shoes and parts of shoes against experimental data. New methods of comparison may have to be devised.

Laboratory testing of real components To facilitate the assessment of FE model performance, data concerning physical properties and responses of parts and shoes is required. Initial research suggests that the current tests are aimed at deducing biomechanical performance, but it may be the case that there are more suitable tests that could be devised.

Model development and enhancement If it can be proved that the FE method can create models of shoes, and that the performance of these models can be verified against experimental data, then the level of agreement between the models and experiments needs to be at a level where the models can be used to predict performance independently of experiment. It is not expected that this will be the case with the initial models, so a process of model development and enhancement will be needed to advance the technology to a level where it can progress from a thorough proof of concept into a commercially viable method. This may include the development of procedures for the creation of models to be followed by commercial developers.

Based on these objectives, this thesis will first present a summary of the history of running, putting the project into context. This will be followed by a review of the current technology used in the shoe industry. Literature reviews of the material theory and computational methods will conclude the theoretical research part of this thesis.

Chapter 5 details test equipment and methods used in the subsequent chapters, which in turn present an increase in modelling complexity from material samples through to production shoes and those with mechanisms. A suggested workflow appropriate for use in industry is then presented in Section 12.5.1.

Chapter 2

Literature Review: Shoe Technology

2.1 Introduction

This chapter presents a concise history of the technologies used in running shoes, and their relation to society, as this needs to be considered to understand why there is a need for 'better' shoes at all. The latter part of the chapter covers the running shoe construction methods used at present.

2.2 The History of the Running Shoe

It has been argued that running has been part of human life since we descended out of the trees many thousands of years ago (O'Neil 2004, Anon 2004). The need to catch food, run from predators and generally interact with the world required speed and agility - so much so that over the years the human body has adapted itself to cope with the motions involved with running; curved spine, wider hips and aligned toes when compared with our simian ancestors (Diagram 2004). While historians have evidence of the ability of people to construct basic clothes from 50,000 years ago, the oldest recognisable shoe was found in a cave in Oregon and is estimated to be only 10,000 years old. Made from woven bark it probably would have been used to do pretty much everything in, and this non-specific shoe tendency would continue until the 1800's (Savannah 1980).

The first recorded instances of running as more than just a necessity come from the ancient Greeks, where sport and competitive 'games' were an important part of the culture. A vase dating from around 1300 BC is thought to show the first depictions of running as a sport, pre-dating the first Olympic event by 700 years. While running, the contestants didn't wear shoes, in fact nearly all of them ran naked.

To find the first running shoes we have to go forward in time, past the Romans (who preferred more brutal pursuits and abandoned the ancient Greeks' athletic events) and into the Middle Ages where the 'pump' first appeared. Made from canvas with a leather or early rubber sole, these were used for indoor sports but were too flimsy for any outdoor activities (Underbill 1998).

It took nearly 2000 years for athletics to come back into popularity, but the shoes used to compete in were simply lightly built 'dress shoes', that people would wear everyday. Usually made from leather, with heavy leather soles, these shoes were not designed for running in, and invariably caused pain, blisters and provided poor traction as the soles were made for

stability and durability instead of grip. It was 1839 when rubber vulcanisation was invented and recognisable, modern rubber soles were introduced. The first true running shoe was in fact designed for playing cricket; a light leather shoe with spikes in the forefoot. This was quickly adapted for use on running tracks and spawned many similar spike shoe designs.

Running came back to the masses at the turn of the 20th century, with the re-introduction of the Olympics and the holding of distance running events of various lengths (up to the awe inspiring 'Long Distance' events which lasted six days and saw runs of over 600 miles). These longer events went outside the stadiums and so needed non-spiked shoes, which were again made mostly from leather, with similar constructions to today's football boots - all leather uppers and thin, stiff soles with attachments for different surfaces. Running shoe technology evolved slowly along these lines for the next 50 years.

In the early 1970s, the first midsoles (separate cushioning layers) began to appear, as a progression from gradually thickening rubber soles. When the shoe manufacturer Brookes started working with the Monarch Rubber Company they came up with the foundation of the modern shoe: ethylene vinyl acetate (EVA) foam. EVA is a polymer with small gas bubbles that give it excellent cushioning properties while having a very low density when compared to rubber compounds (Cavanagh 1980).

With renewed public interest in running coming from the popularity of marathons during the 1970s & 80s, and the range of new materials available, there was an explosion in sales and the variety of shoes increased dramatically. In the past 20 years the materials used have undergone gradual development, but the design of running shoes has changed out of all recognition from the shoes at the start of the last century.

2.3 Present Day Running

Competitive running has increased steadily in popularity since the 1970s, but the keep-fit craze of the late 1980s boosted sales dramatically (Vanderbilt 1998). Three categories of shoe buyers emerged: serious recreational runners, requiring technically superior footwear that would give at least a mental advantage on the Sunday morning run, multi-sport keep-fit types who needed shoes that would cope with the odd run, game of tennis, gym session etc. while still retaining an element of fashion, and finally, those who wanted shoes purely to follow a trend.

With ruthlessly efficient marketing and advertising machines, today's running shoe is more than a shoe - it is a statement of aspiration, allegiance or style. The manufacturers that helped create this culture must also bow to its demands, and so new models are turned out on a seasonal basis in an attempt to hold on to market share. But there are still a large number of runners who will look past the hype and buy the shoes that make them run faster, longer and more comfortably, so the performance of the technology, as well as the right look, is crucial.

2.4 Technology Introduction

As this thesis is concerned more with the creation of realistic FEA assemblies to be used within more realistic tests, and not the creation of the tests themselves, only a short introduction to the extensive field of biomechanics is presented. For the reader without a biomechanics background, the main terms relating to the technologies studied in this thesis are shown in Figure 2.1. In addition, an extensive glossary of manufacturer's terms can be found on the Runner's World website (Runner's World 2004).

Figure 2.1: Key features and terms used in the design of running shoes.

Although running styles vary, a typical running step (or footstrike) has three main phases:

Heel Strike First contact of the heel onto the ground (the forefoot is still in the air).

Mid-Phase Rolling forward of the ankle joint, progressively transferring the load from the heel forward to the mid-foot.

Forefoot Strike/Push-Off Impact of the 'ball' of the foot with the ground. The foot then bends about the metatarsal heads and power is applied to push the body off the ground.

The mechanism used to drive the foot off the forefoot is shown in Figure 2.2. The load during heel strike is taken by the calcaneus bone, then transferred to the whole foot during the mid-phase, and finally to the heads of the metatarsals during push-off/forefoot strike. Loads are at their highest at the heel and forefoot regions due to the need to decelerate/accelerate the body using a small area of the foot.

During the entire footstrike, the ankle joint can rotate about the horizontal, anterior-posterior axis. This is known as pronation/supination. If the ankle rolls outwards relative to a pivot at the outsole/ground contact point, this is known as supination. If the ankle rolls inward it is known as pronation. The amount and direction of the rolling is affected by factors including running style, body geometry and the running shoe used.

2.5 Shoe Types

While there are almost as many types of footwear as there are different sports (and a vast array of fashion specific shoes), this research is concerned with the 'standard' running shoe. This type of shoe is designed to enhance the runner's performance and reduce injury, on a variety of surfaces and can be divided into a number of sub-categories (Runner's World 2004):

Cushioned Shoes The simplest shoes, these have the softest midsoles and least support in the medial region (the inside of the foot) and are suitable for people who don't roll their feet during a running strike (pronation/suplination).

Motion Control Shoes The most rigid shoes - designed to limit overpronation. Often heavy, but very durable due to the use of denser foams.

Stability Shoes A blend of cushioning, medial support and durability. Typically will have dual density midsoles and some kind of hard plastic medial post (see Section 2.6.3).

Performance Training Shoes Lighter versions of any of the above, built for fast-paced training or racing. Not as durable as other shoes, due to lighter but weaker parts.

Racing Shoes Super-lightweight shoes, usually without extra cushioning and stability features found on other shoes. Designed for elite professional runners only as their durability is very poor.

Off-Road (Trail) Shoes Normally built around stability midsoles, these shoes feature toughened weatherproof uppers, aggressive tread patterns and extra toe protection.

This is not necessarily an exhaustive list, but the shoe types listed comprise of a similar midsole construction, so modelling processes developed for one should be applicable to the others. Other sports-specific shoes such as ski-boots, cycling shoes and even sprint-running spikes will not be considered as part of this research as their major components differ considerably from running shoes.

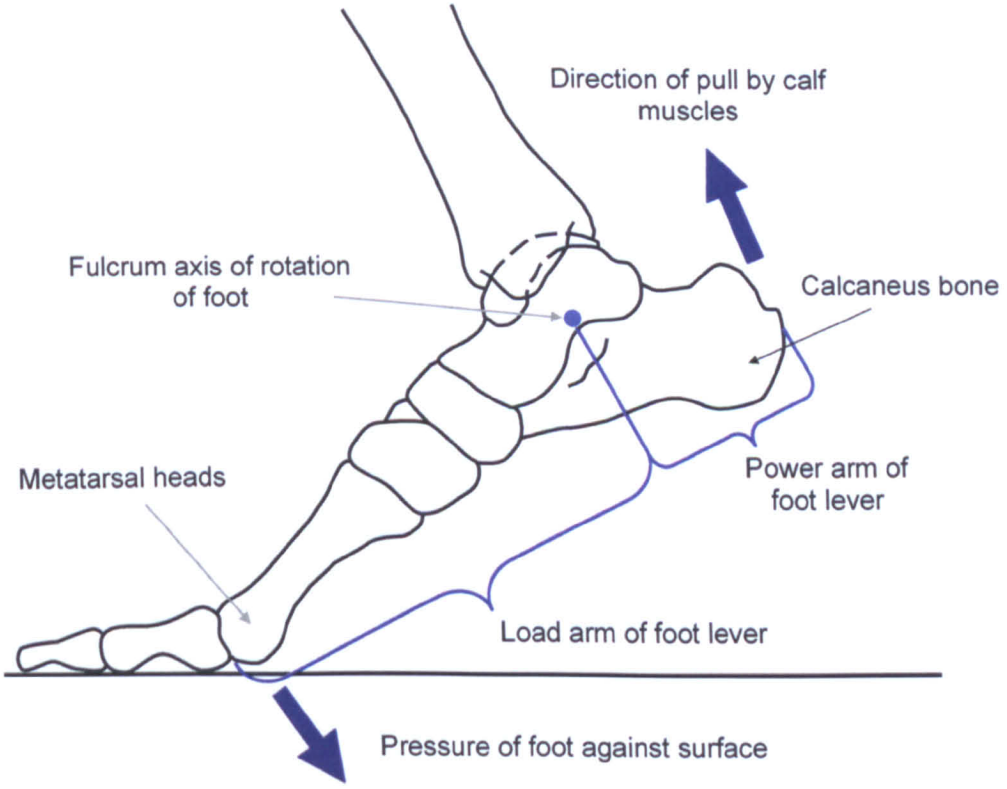

Figure 2.2: Schematic of the right foot, viewed from the medial side (Reproduced from Krantz 1972).

2.6 Materials

2.6.1 Uppers

Shoe uppers are primarily made from man-made woven fabrics, with non-fabric detailing for aesthetic and strengthening purposes. Leather has been all but abandoned for the serious running shoe for weight and cost reasons (fashion variations of running shoes are available in a whole host of materials however). Some lighter shoes feature Lycra-based fabrics to give better fit, and virtually all modern shoes have laces, as these are light, cheap and give a customisable fit. Most shoes incorporate a stiff 'cup' in the heel (known as a heel counter, depicted in Figure 2.1), to locate the heel on the midsole and stop the foot slipping off during foot strike. Foam that moulds and retains the shape of the ankle for a better fit ('memory foam') has been used to pad the inside of the heel counter by Asics.

2.6.2 Outsoles

With the exception of trail shoes, the outsole of a shoe generally consists of a rubber (or substitute) strip, usually 3-6mm thick. Its function is to protect the softer midsole from wear and to provide the runner with grip. The tread pattern varies greatly between shoes, dependant on the surface it was designed for, the mechanical properties of the material used and the level of protection and grip required.

2.6.3 Midsoles

While the materials used in the midsole are less varied than those in the uppers, it is the midsole that forms the core of the shoe and affects the entire motion of the foot strike.

Section 2.8 gives a more detailed account of the biomechanics of a running step in terms of shock absorption and energy return, but in summary the aim is to absorb the shock loading at the heel, optimise the motion of the foot through the midfoot phase by controlling pronation, then provide a firm (but not rigid) base for the forefoot to launch off.

The most common midsole material is EVA (ethylene vinyl acetate) foam. Each manufacturer has their own specific mix of EVA (e.g. adiPRENE from adidas, Phylon from Nike), usually with differing formulations for different parts of the shoe. For example, in the heel region high-hysteresis materials are used to absorb and dissipate (as heat) the heel shock loading, whereas in the forefoot more elastic materials are used to absorb the initial impact, then return the energy as an elastic rebound, pushing the runner along.

In addition to the above, most shoes contain some kind of stiff plastic inserts to provide support in specific areas (e.g. heel counter, torsion bar, see Figure 2.1).

EVA is not the only midsole material in use; sealed PU (polyurethane) pockets filled with gas have been used (a Nike patent, held by Rudy 1980) to provide cushioning. TPU (thermoplastic PU) technology is advancing rapidly, and recent developments have enabled the conventional foam to be replaced by a series of 'independent' structures to provide the cushioning in some shoe designs (e.g. Nike Shox, adidas Ultraride). TPU has excellent wear resistance when compared with EVA, but is much denser. The use of structures also allows the stiffness of sections of the midsole to be controlled more easily than using EVA. While the aim is to provide at least as 'good' cushioning as EVA shoes with much longer shoe lifetimes (the reasons for which are discussed in Section 3), some commercially successful shoes have employed a combination of EVA and TPU structure technology (e.g. Mizuno Wave, Onoda 1985).

2.7 Midsole Construction

2.7.1 Introduction

Early modern (1970 onwards) running midsoles were of very simple construction: cut sheets of foam/rubber with a carbon rubber outsole. These shoes were designed only to reduce the shock experienced by the runner. In contrast, today's shoes can assist with almost every aspect of foot/shoe/ground interaction; cushioning, pronation control, torsion control (relative axial motion between the forefoot and heel of a shoe), push-off, temperature control and so on.

With improvements in moulding and material technologies, more complex shapes are possible, and some manufactures are deliberately designating parts of the shoe to specific functions (e.g. adidas a^3, Asics IGS). For the purposes of explaining of the technologies, the principle functions have been split in a similar manner in the following sections.

2.7.2 Cushioning

The general aim is to absorb more impact at the heel than the forefoot, so as to assist, but not slow down, the running strike. To do this, most of the heel cushioning uses viscoelastic (high-hysteresis, rate-dependant materials) whereas the forefoot is more elastic. The vast majority of running shoes use some form of EVA foam as cushioning. There are many different variations on the theme, such as Nike's Phylon (lower density), Asics SpEVA (faster rebound/recovery). Adjustment of the cushioning can be achieved through changes in the EVA recipe (New Balance Abzorb, adidas adiPRENE/adiPRENE+ as shown in Figure 2.3), or by adding inserts of other materials such as gel (Asics Gel) or air (Nike Air, sealed TPU inserts). The response of the air/gel filled shoes can be tuned dependent on the shape of the insert and flow of fluid inside it. While these innovations theoretically allow improvements in performance, the results on performance of their application to running shoes is mostly reported by the relevant companies' marketing departments, so the information may be heavily biased. Experimental data from tests performed on shoes is limited, and often only available from the manufacturer if they consider it a commercial advantage to broadcast this information (if it exists at all).

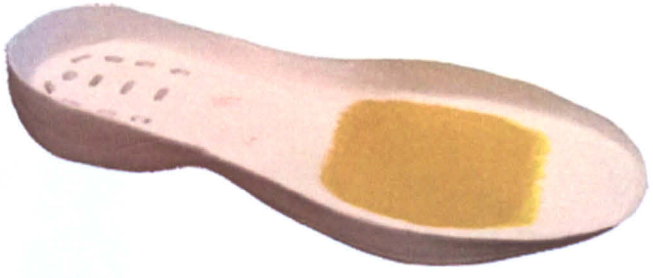

Figure 2.3: adidas basketball shoe midsole with highly elastic adiPRENE+ insert (yellow).

With new materials coming into the market, small structural elements have begun to appear in shoes, the most publicised being Nike Shox: a set of (roughly) cylindrical hollow columns replacing the EVA midsole for the entire length of the shoe, or just in the heel (Figure 2.4). The mechanical properties of these separate columns can be tuned relative to their position in the footstrike (though it must be noted that at present the midsole requires a stiff load distribution plate above and below the structures).

Figure 2.4: Nike Shox Turbo (Nike Inc. 2004)

The adidas a^3 series follows a similar scheme of thought, by using different EVA types in a TPU 'hinge' in the Ride series, and TPU/PU and TPU structures in the Ultraride (Figure 2.5). Again these individual structures can be tuned to best fit their position in the footstrike.

Figure 2.5: adidas a^3 Ultraride. (left) Whole shoe, (right top) heel TPU structures, (right bottom) PU foam filled TPU heel crash structure (adidas 2004).

Saucony has introduced the 'Grid', a mesh of thermoplastic polyester elastomer ('Hytrel') covering the EVA midsole with the aim of spreading the load across more of the EVA and thus improving cushioning and lifetime of the shoe. (Figure 2.6).

(a) (b)

Figure 2.6: Saucony 3D Grid. (a) Detail of Grid insert, (b) Triumph model. (Saucony Inc. 2003).

Mizuno has a similar plan with its use of Wave inserts: a stiff plate to spread the impact load (Onoda 1985). The Wave is one of the most successful shoes currently, with the Creation model being awarded 'Best Update' in the 2004 Runner's World Shoe Buying Guide (Figure 2.7).

(a) (b)

Figure 2.7: (a) Mizuno Skeleton Composite Wave insert, (b) Wave Creation shoe (Runners World 2004a).

Reebok introduced the Shear Strip, a layer in the heel that can move backward relative to the rest of the midsole (Figure 2.8), with the aim of reducing the peak impact forces by spreading the total force over a longer time (this also has the effect of slightly extending the runners stride). A new system from adidas, the GCS (Ground Control System) uses a more pronounced movement with a spherical bearing in the heel that deforms on the heel strike.

Figure 2.8: Reebox Premier Road Lite with DMX Shear Strip in heel (Reebok 2004).

In summary, the manufacturers are attempting to create products that reduce the amount of stress on the body without adversely affecting the runner's speed or levels of exertion. This is primarily done by using EVA foams to provide cushioning and TPU inserts to distribute the load onto the foam. Only adidas and Nike have produced shoes with significantly reduced amounts of foam, although at present virtually all running shoes still contain some kind of foam for cushioning. Another factor that should be considered is that the appearance of foam may not be desired, as shown by the 'hiding' of foams within the upper in shoes such as the adidas Ultraride and Nike Shox (Figures 2.5 and 2.4).

2.7.3 Stability

Control over the motion of the foot during footstrike is as important as the cushioning, according to some researchers (James 1978). Most manufacturers use harder plastic inserts in the heel to control the seating of the heel onto the cushioning part of the midsole (heel counter), and in the arch area, which controls the amount of twist or torsion the foot experiences. Figure 2.9 shows the range of torsion control inserts used for shoes for different sports - by changing the shape of these inserts, the pronation of the foot can be controlled to some extent.

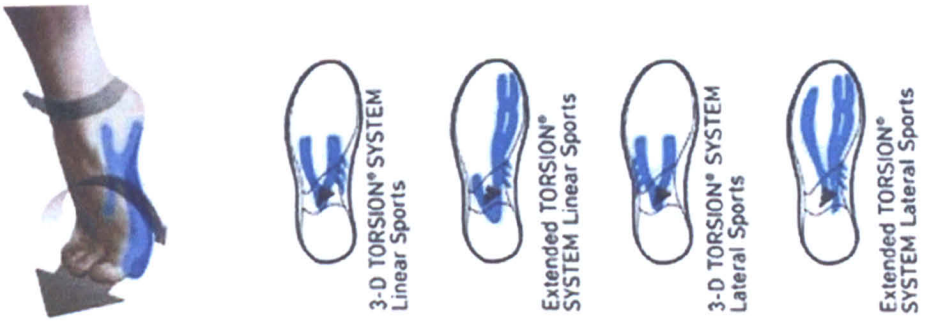

Figure 2.9: Selection of adidas midsole Torsion inserts, used to control twisting of the midsole during footstrike (Reproduced from Anon 2003).

Another way to control the motion of the foot is to vary the density/stiffness of areas of the midsole. These shoes are often known as 'control' shoes. Figure 2.10 shows a stiffer section of foam on the medial side of the midsole (in this shoe the stiffer foam has a blue vein pattern, while the 'normal' foam is white).

Figure 2.10: Motion control insert foam on the medial side of the adidas Chino running shoe.

2.7.4 Drive

The components of the shoe under load during push-off for most running shoes are more simplistic than the heel cushioning and stability elements. Most 'performance' shoes use more elastic foam inserts in the forefoot region (Figure 2.3), but this is usually adequate as the loadings at push off are more progressive than the shock loading in the heel. Load is distributed over a much larger area in the forefoot so there can be a reduction in energy dissipation, resulting in a larger proportion of energy returned to the runner (pushing the runner upward and forward).

2.8 Running Biomechanics

2.8.1 Introduction

The body of research on modelling the behaviour of running shoes is dwarfed by that on the biomechanics of running itself. A vast number of publications can be found that cover the movements of the joints, muscles and tissues during the motion of running, but for the purpose of the first part of this research, these complex motions are simplified into force/time loading that can be applied by simple mechanical devices.

2.8.2 Impacts During Running

The motion of running is not a smooth process. Before the forward foot touches the ground, the rear foot has left it, and so the body will be accelerating toward the ground when the forward foot 'strikes' (makes contact). The body must then absorb the energy of impact, stabilise itself, and propel the body back up ready for the next impact[1]. The function of the shoe is to assist in absorbtion of the impact forces without having a detrimental effect on the stabilisation of the foot or removing too much energy from the push-off phase.

Fundamentally, the shoe must transfer the ground reaction impulse to the foot. For a normal running gait (at constant velocity, on a flat surface), the magnitude of this impulse, determined predominantly by the leg muscles, is sufficient to maintain the horizontal momentum and reverse the vertical momentum of the runner. The heel contact phase is generally associated with retardation of the runner, certainly vertically, but the midfoot and forefoot phases can be involved in both retardation and acceleration, resulting in unequal impulses transferred during these phases. It must be noted that while this is considered the general case for the purpose of most testing (and for the scope of this research), variations in the runner's gait can significantly alter the impacts.

The magnitudes of the forces are greatest in the vertical direction and although there are forces in both the anterior/posterior and medial/lateral directions, these are often considered negligible during testing (see Figure 2.11).

The duration and magnitude of these impacts is dependant on many factors, Frederick (1986) mentions at least 10 variables that affect the heel impact, and 7 that affect the forefoot impact. The tests were carried out with barefoot runners, and on the same surface (a force plate), so all of these variables are biomechanical and therefore not necessarily controllable by shoe designers.

One of the primary factors affecting impact is the pronation of the foot on heel strike. Pronation is the rolling in of the foot around the ankle joint through the foot strike, i.e. landing on the lateral edge of the heel and pushing off from the big toe. Runners are categorised into over-pronators (too much roll), under-pronators (to little roll, or rolling outward of the ankle joint) and neutral. The latter type are generally considered not to need any correction, but the under/over-pronators can improve their running motion with the correct type of shoe. This may not necessarily make them run faster, but will minimise the risk of injury from excessive ankle movement (Arendse 2003).

2.8.3 Effects of Impacts on the Body

Although values vary significantly from subject to subject (Bates 1983), it is generally considered that the peak forces during a heel strike are 2-3 times the runner's body weight, and

[1]There are many styles of running, but non-sprint shoes are generally designed to be used by heel strikers, i.e. people who exhibit a distinct heel-mid-forefoot running style, as opposed to those who strike the ground first with their mid or forefoot.

that the number of impacts is around 1500 per mile (Frederick 1984). Given these facts and the high loading rates of running (Figure 2.11), it is no surprise that injuries occur to the bones and tissues of (mainly) the legs (Radin 1973).

One of the primary functions of the leg/foot system is to provide locomotion over a variety of terrains, whilst minimising the shock to more vulnerable areas of the body. The body has two main shock absorbing mechanisms, the first of which is running style: bending the legs and feet to absorb the impacts. The second is a pad of fatty tissue on the heel, which can deform by around 12 mm, absorbing energy and distributing the load (Aerts 1993). These two systems work exceedingly well (some world-class athletes still race competitively without shoes), but they have evolved to be used on softer ground, while the vast majority of runners will be running on tarmac or concrete at some point.

Figure 2.12 shows the difference in impact between shod and barefoot running, the most noticeable feature of the barefoot strike being the short, hard impact spike as the heel first makes contact with the ground. Heavy use, combined with this shock loading, is thought to cause acute injuries such as fractures and sprains, along with degenerative changes in the joint tissues, stress fractures and a host of other aliments (Radin 1973).

A study by James (1978) into the prevention of injuries in runners, emphasises that control of the foot motion through the running step is as important as controlling the impact magnitude. The design of the shoe can influence the motion of the foot in various ways (see Section 2.7), which is useful if the runner's natural style is physically damaging.

There is however some debate on the actual effects of wearing running shoes, and while there is research supporting and disagreeing with the need for running shoes, at the present time there have not been enough studies of a wide enough range of subjects to draw any concrete conclusions (Burge 2001).

2.8.4 Effects of Shoes on Impacts

The primary function of the running shoe is to reduce the shock loading to the body. There are two main ways of achieving this: reduce the peak accelerations by increasing the time the loads occur for, or dissipate the energy by some means. Most materials used in shoes perform a combination of these functions - the compressibility of the material extends the impact time, while any hysteresis (energy loss between loading and unloading the material) absorbs and dissipates the impact energy, usually as heat.

High quality running shoes are designed to enhance performance, so the level of energy absorption needs to be controlled; the runner must not expend a significant amount of energy heating up their shoes. To this end the heel of the shoe is usually fitted with a high-hysteresis material to absorb shock, while the forefoot is fitted with an elastic material. However, Thomson (1999) states that "contrary to expectations, no significant difference was found in oxygen uptake, heart rate or perceived exertion" for runners testing a selection of air and non-air soled shoes with different midsole stiffnesses, although it must be noted that no hysteresis measurements are detailed in the report.

Henning (1995a) performed a series of tests using a subject in a harness being impacted against a force plate on a wall. The report concludes "soft midsole materials may reduce the severity of impacts and also energy expenditure". A similar, but more thorough test was performed by Aerts (1993), who looked at the direct influence on loading of various shoes, and compared them with the barefoot condition. To eliminate the effect of running style the subject's legs were fixed in position and the load applied by a pendulum. The authors conclude that the effect on transmitted forces is a complex combination of shoe material, heel pad response and the magnitude and rate of the loadings.

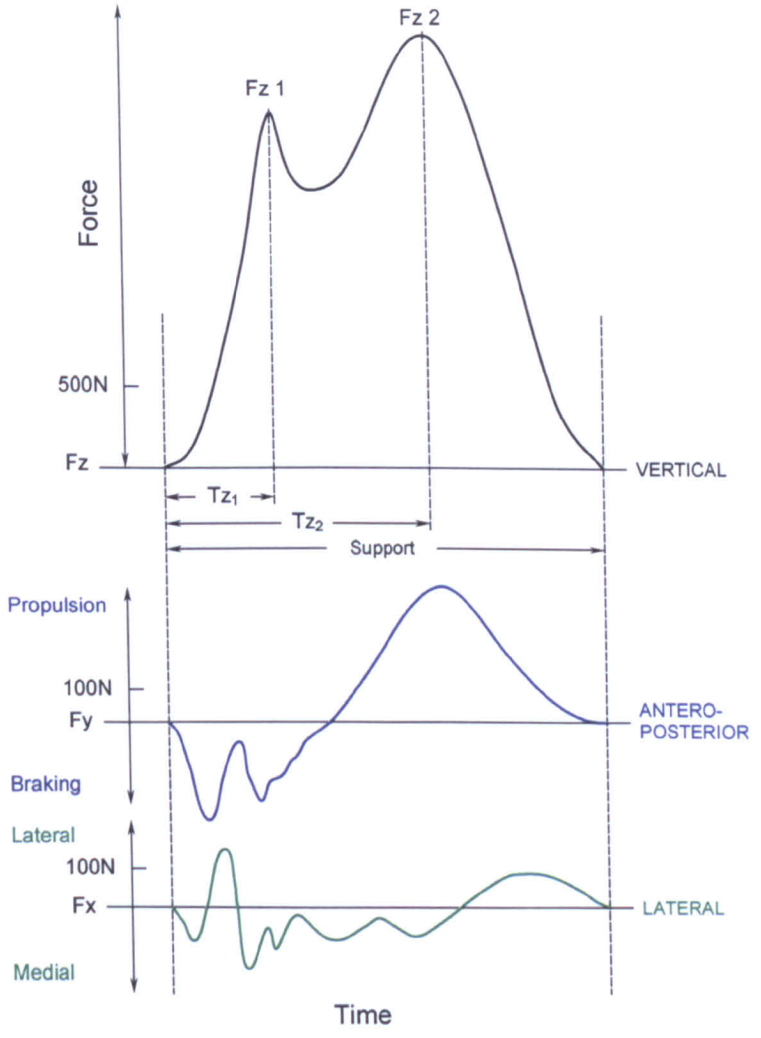

Figure 2.11: Force/time curves in three dimensions for shod running (Adapted from Bates 1981). Typically, Fz_1 ≈30 ms (heel maximum), Fz_2 ≈100 ms (forefoot maximum).

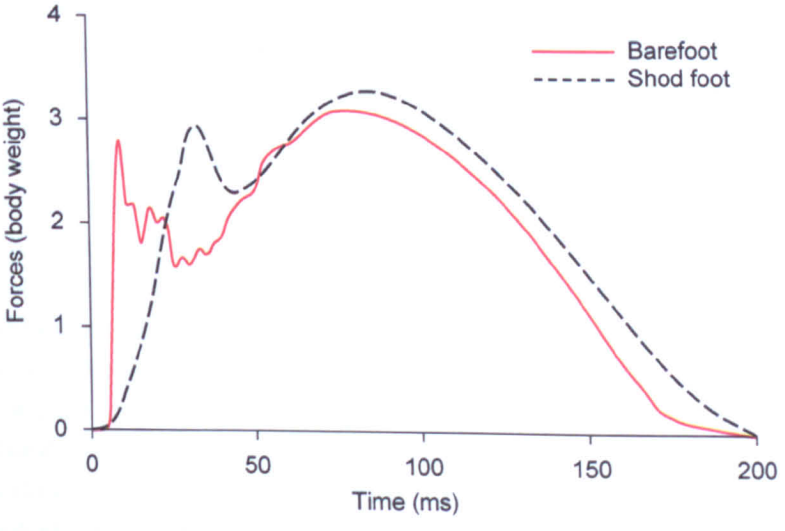

Figure 2.12: Difference in ground reaction force for bare and shod running (Reproduced from De Wit 2000). Note the reduction in initial shock loading at around 10 ms.

The authors also note that the fit of the shoe affects the results:

> "...findings strongly suggest that overall shock reduction in the hard-shoe foot system is worse than could be expected from the basic mechanical principles and the elastic behaviour of the shoe alone, because an increase in midsole hardness is accompanied by an additional stiffening of the heel pad due to its confinement in the shoe."

Other published research by De Clercq (1994) also shows a change in the properties of the heel pad due to the compression of the pad after insertion of the foot into the shoe. This study actually measured the deformation of the heel pad using X-ray cinematography. The difference in deformation of the heel pad during heel strike between bare foot and shod running was found to be significant (60% and 35% respectively). The author argues that embedding the foot in a well fitting shoe increases the stiffness of the heel pad.

2.8.5 Effects of Shoes on Running Style

The studies noted in the previous sections are only one stage of complexity ahead of a basic material test; they do not consider the effect that the shoe can have on the running style. Nigg (1987) looked at the influence of running velocity and midsole hardness on impact forces using subjects running on a force platform (four velocities and three hardnesses). The report concludes that "running velocity does influence external impact force peaks" but "midsole hardness does not influence magnitude and loading rate of the external vertical impact forces". This is contrary to the results obtained from material and pendulum studies.

Henning (1995b) investigated the in-shoe pressures for 19 different running shoes and concluded that substantial differences in pressures and loads are possible through shoe design, but does not detail what shoes were used in the study. This does appear to disagree with Nigg (1987), but this may be due to selection of the shoes used in the study.

De Wit (1995) performed a similar test to that of Henning (1995b), but also looked at the motion of the joints when running with different midsole hardnesses. The study shows that harder midsoles give smaller peak impact forces (measured from a force plate) and offers an explanation on the basis that different joint rotation speeds absorb energy in different ways. This is supported by the findings of Luethi (1987), demonstrating a relationship between angular motion of the joints and the magnitude of the impact forces.

There is another theory to account for the conflicting material/subject test results: that the human nervous system adapts the body's running style to keep the impact forces constant. This is most noticeable when comparing barefoot running with shod running; Bates (1981) hypothesised that "the mind sensed a potential danger and modified performance technique". Further studies have supported this statement; Snel (1983) states, "It seems that the runner anticipates the expected impact force, in such a way that the stiffness of the sole can influence the neuromuscular control system".

Two reports by De Wit (1996 & 2000) also conclude that there is some kind of "actively induced adaptation strategy" to the particular shoe the runner is wearing. It would appear that runners instinctively land harder when they know that adequate cushioning is available, and softer when the ground is hard. This presents a significant problem when assessing the effect of different midsole hardness (as will be discussed in Section 2.9).

The structural stiffness of the heel region of the midsole, essential to rearfoot control, is also important as medio-lateral instability (unnecessary motion of the heel during impact) is assumed to be connected with overuse injuries (Nigg 1987).

2.9 Shoe Testing

2.9.1 Introduction

It was only in the latter half of the 20th Century that footwear testing began to appear, before then any technological advances were a result of trial and error. Only when photographic technology advanced sufficiently to allow the use of high-speed video recording of running strides, was real scientific testing carried out. The early tests were focused on the biomechanics of running and how different shoes affect the runner, but no focused research was directed at the shoes themselves. A summary of the techniques currently used to assess the performance of running shoes is presented in the following sections.

2.9.2 Force Plates

A force plate is one of the simplest (and most common) ways of recording the forces beneath the shoe during actual running. This consists of a suspended plate fitted with piezo washers or strain gauges (or similar) that record the motion and resistance of the plate when a force is applied to it. This is usually placed so the top of the plate sits at ground level, allowing it to form part of the running surface (so as not to disrupt the natural running motion). Both uni-axial plates (as used in Clarke (1983) and Shiba (1995) for the variation of vertical forces with different midsole and insole materials respectively) and tri-axial plates (such as those used to obtain the results in Figure 2.11) are available. Warren-Forward (1992) details an in-shoe 3D force/displacement sensor that performs a similar function to force plates, but without the need for specialist running surfaces with force plate 'pits'.

2.9.3 Pressure Measurement

While the external force measurements from force plates can be useful in shoe design, they do not show the interaction between the foot and the shoe directly. This internal measurement is necessary to deduce any pressure points on the foot which could cause soreness and blistering (especially in people with diabetes), and to allow complete measurement of the pressures on or compression of the midsole only, when used in conjunction with a force plate.

Measurement systems generally employ a grid of pressure sensors printed onto a flexible plastic sheet, which is then placed between the foot and the inner shoe. A novel device for the measurement of in-shoe shear is suggested by Akhlaghi (1996), using shear sensors embedded in insoles.

Pressure measurement sensors can also be placed on the running surface, giving an above and below reading of pressure in the midsole when combined with in-shoe sensors.

2.9.4 Body Measurement

As discussed in Section 2.8.5, the human body adapts to the material of the shoe, making it difficult to isolate the effects of a change in material properties. Nishiwaki (2002) attempted to overcome this problem by assessing the reaction of participants dropped onto various materials (including a hard floor) without them knowing what they were bring dropped onto. To assess the force impulses from a human perspective, accelerometers were attached to the skin covering the participant's tibia. The study reports good correlation between the material cushioning property and human feeling.

A more common approach is to measure the biomechanical response using markers, such as the CODA system, which can be used to determine body kinetics from small infrared LED markers placed at points of interest on the body (Dixon et al. 2000).

The accuracy of on-body measurement has been called into question by Valiant (1987), reporting an overestimate of 20-30% in acceleration due to the sensing device being attached to the non-rigid skin of subjects. Greater accuracy can be gained by connecting the accelerometers directly to the skeleton (e.g. Bergmann (1995) uses sensors embedded in an artificial hip joint), but this method is drastic, very expensive, and likely to use only a small amount of willing subjects.

2.9.5 Mechanical Testing

The first well-recognised set of mechanical tests was carried out by Dr. Peter Cavanagh, the results featuring in the Runner's World Shoe Survey 1977. They no longer feature in more recent Shoe Surveys, but many of the tests have been adopted by the shoe industry to evaluate and compare products as they attempt to simulate the various conditions and responses deemed important by a combination of runner questioning, clinical experience and biomechanical research (Bates 1985). Some of the features/loads on a shoe considered most important are detailed below (Knoerr 2002):

Heel Impact High and rapid vertical deformation of the heel part (over 50% of the thickness, given a power/time profile of $\approx$2000 N in $\approx$30 ms, affected area $\approx$20cm^2).

Forefoot Impact High and slightly slower vertical deformation under the forefoot (over 50 % of the thickness, given a power/time profile of $\approx$2000 N in $\approx$100 ms, affected area $\approx$43 cm^2).

Stability Test The horizontal thrust forces that must be borne by the rear foot part as well as by the forefoot part without being considerably deformed horizontally (less than 3 mm) are up to a maximum of 3000 N. This means the sole should be very stable in both horizontal directions (anterior/posterior, medial/lateral).

Longitudinal Flexibility The flexibility of the sole in the longitudinal direction must be minimal in the heel and midfoot area, but very high in the forefoot area. The forefoot bending angle is up to 60°.

Lateral Flexibility The lateral flexibility should be minimal.

Torsional Stiffness The torsional stiffness of the sole should not exceed 0.3 Nm/degree in the midfoot, between the metatarsal heads and the ankle. The anatomical torsion between forefoot and rearfoot is at a maximum of 35° (in both directions).

Longevity The shoe should be able to endure at least 1,000,000 load cycles prior to a drastic modification of its mechanical properties.

These test values are still not a true representation of the response of a shoe during running, but they allow fast and repeatable quantitative testing.

2.9.5.1 Standardised Testing

Standardised shoe tests do exist, though their main aims are to prevent confusion between manufacturers and suppliers with relation to basic performance characteristics, and to ensure the safety of users of the shoes. These tests are summarised in Section 3.4.3, and consist mainly of tests to determine stiffness and energy absorption from simple drop devices.

2.9.5.2 Mechanical vs. Real Performance

There have been several attempts to directly compare material measurements with shoe performance, for example: Ujihashi (1998) used material impact tests and subject questioning and found that "the mechanical evaluation functions defined by the measurements have definite correlations with the sensory evaluations of the distance runners", while Baumann (1995) compared the wear properties of shoes undergoing actual running with those subjected to mechanical impact tests, concluding that a simulation of the entire life of the running shoe is possible in a single day (although this test only considered a single material stiffness value).

Currently there is no fully predictive method of shoe evaluation; all shoe manufacturers use a combination of material, machine and human testing, the latter two requiring some form of prototype shoe to be manufactured.

2.9.5.3 Mechanical Testing at adidas

All the standardised tests discussed by Knoerr are performed in-house as part of adidas' development of a shoe. As this thesis is concerned more with developing the underlying material responses of an FEA model, only three tests are to be modelled: forefoot flexibility (longitudinal), forefoot cushioning and rearfoot cushioning. Figures 2.13-2.16 illustrate the set up of each test. The forefoot flexibility (or 'bend') test is performed by depressing the stamp sinusoidally to a maximum of 15 mm in a total time of 0.2 seconds. The cushioning tests are performed by specifying a force-time relationship, with a force-feedback loop in the test device fitting the load to the required curve. Maximum load for both forefoot and rearfoot cushioning is 2 kN. The result from heel impacts (rearfoot cushioning) on a Supernova midsole is shown in Figure 2.17; some difference is seen in the force/displacement results of the shoe, even though the impacts are under identical conditions and within milliseconds of each other. This is illustrative of the need to standardise the breaking-in of shoes, as this midsole appears to be exhibiting some kind of stress relaxation (this could be due to a number of variables in the test, which are detailed in Section 3.3).

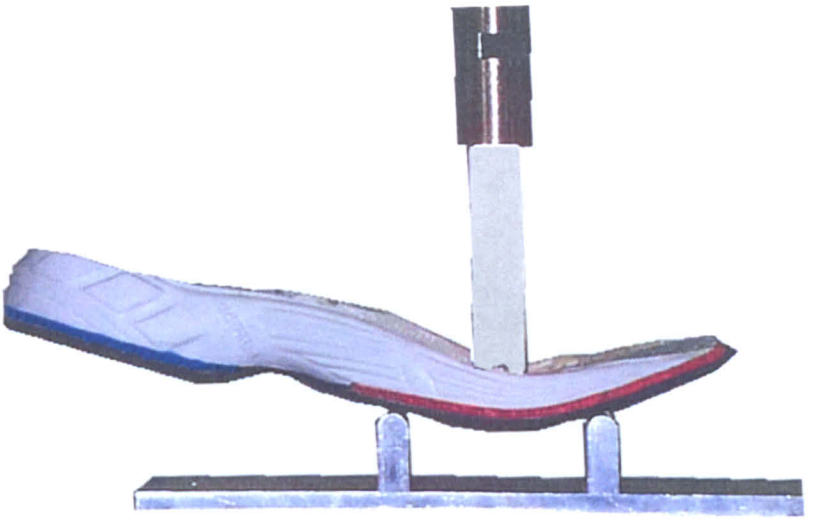

Figure 2.13: Forefoot flexibility (also known as forefoot bend) test set-up.

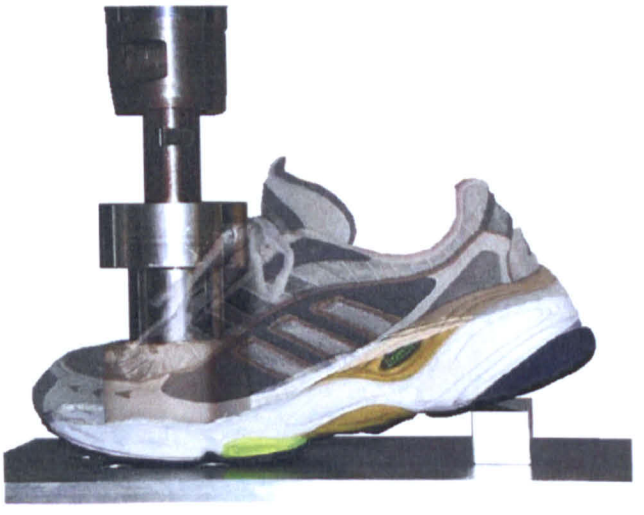

Figure 2.14: Forefoot cushioning test set-up (with optional heel lifting block).

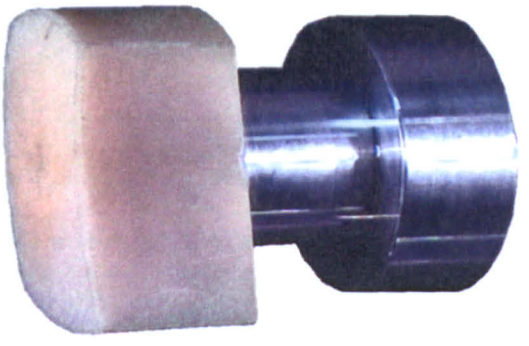

Figure 2.15: Detail of the stamp used in forefoot cushioning test.

Figure 2.16: Rearfoot cushioning test set-up. The stamp used is 50 mm in diameter, which approximates the dimensions of the calcaneus (see Figure 2.2).

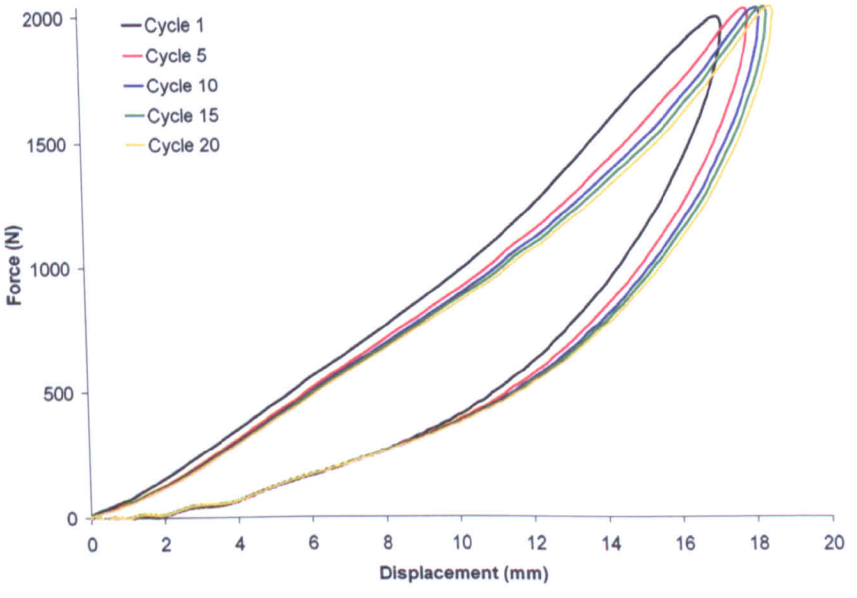

Figure 2.17: Force/displacement results from multiple consecutive impacts of a Supernova midsole heel). Note the change in response over the cycles.

2.10 Chapter Summary

The main points put forward by this chapter can be summarised as follows:

- Sportswear is a global multi-billion dollar industry where competition is fierce so any performance gain (proven or otherwise) is considered an advantage.
- The majority of shoe sales are of fashion shoes - those that are not required to improve athletic performance. Brand association is high so improvements in performance products (those that are required to improve athletic performance) will boost the overall profile of a brand.
- Performance shoes are mostly designed to improve comfort through cushioning, though some are also designed to correct faults in the runner's gait.
- Currently the majority of shoes provide cushioning with foam parts, though TPU is emerging as a longer-lasting but heavier alternative.
- The body adapts to the shoe it is wearing, so the only way to repeatedly assess shoe performance is with testing that is not affected by human response, such as mechanical testing.
- Current mechanical testing attempts to mimic some parts of the running strike, be it range of motion, strain rate or overall force. They do not replicate a full running strike due to the shoe-foot-body interaction being far too complex to create a practical testing machine.
- The use of computer simulation has the potential to overcome the human-adaptation issue and allow complex (and more realistic) loading conditions to be created.
- This research could use available equipment to perform adidas' standard mechanical testing, but it is likely that some of the tests will have to be adapted or new equipment constructed for testing to be carried out at Loughborough. This will add to the time constraint on the research.

Chapter 3

Literature Review: Materials

3.1 Introduction

In order to create a shoe model, the underlying physical principles of the materials must be understood to allow the relevant material responses to be added into the model. In this chapter the different types of material currently used in athletic footwear are presented, followed by a review of previous research into properties of these materials. Stress/strain, strain rate, hysteresis, Poisson's ratio, foam gas, temperature, density and wear/failure effects are all discussed in depth. Equations are not presented however, as many require a significant amount of space to present and this research concentrates on the application of these material models rather than their development.

3.2 Material Types

A typical running shoe is made from a variety of materials, both structural and cosmetic, but this research concentrates on the materials used in the midsole. While natural materials are used in other sports footwear (particularly soccer boots), running shoe midsoles are usually made from ethylene vinyl acetate (EVA), polyurethane (PU), thermoplastic polyurethane (TPU) or a combination of these materials. PVC has also been used, but stricter environmental controls on its usage are making it less favourable.

EVA is used in foam form, and has provided good cushioning characteristics from its first use in the 1970s, where it was moulded into a simple wedge shape, to the complex injection moulded structures of the present. EVA foam is often used 'remoulded' (under various trade names, e.g. Nike's Phylon); a sheet of the foam is produced by heating the polymer to activate the blowing agents which release gas to create the foam structure. This sheet is then roughly cut and compression moulded into the desired final shape. The remoulding process increases the density slightly (Table 3.1), but the material retains similar cushioning properties as the sheet foam.

EVA can also be injection moulded (Nike's version is called Injection Phylon or IP), which eliminates a lot of the waste foam generated by remoulding, but does not overcome the biggest problem with EVA: compression set. Over a period of time the cell structure of the foam starts to collapse, reducing its ability to cushion. Due to this, most running magazines recommend changing shoes every 500-600 miles. Even so, EVA is still used in the majority of running shoes due to its good 'ride' quality, a factor that Nike engineers put down to the level of impact energy absorption (Alley 1999), and its low density.

TPU/PU has been used predominantly in fashion and basketball shoes, due to its high durability compared with EVA, but not in running shoes because of its high density. PU

materials in general fell into decline in the late 1990s because of quality issues; PU foam can be moulded into visually acceptable parts without strict controls, so sub-standard parts were often manufactured. These were prone to failure, leading to consumer perception that PU was a poor quality material (Alley 1999).

The current trend in shoe design is for combination shoes that use TPU/PU and some other stiff plastics, in conjunction with EVA. As discussed in Section 2.4, some shoes separate out the resistance and dampening functions between different structures (e.g. adidas a^3 Ride) while others use the shape of the structures to provide both (e.g. Nike Shox, adidas a^3 Ultraride). These complex shapes are easier to mould in TPU/PU and will last longer than the EVA equivalents. Both Nike and adidas have study programs looking into this combined approach (Alley 1999, Knoerr 2002).

Property	EVA Wedge	PU Foam	Phylon	IP
Density (g/cm^3)	0.15-0.25	0.30-0.40	0.20-0.25	0.17-0.22
Hardness (Asker C)	50-65	56-60	50-56	50-56
Compression Set	50-60%	<30%	50-60%	50-70%
Peak Impact Force (G)	-	10-11	11-12	11-12
Impact Energy Loss	-	48-50%	34-36%	34-36%

Table 3.1: Property table for various Nike midsole materials (Alley 1999).

3.3 Stress/Strain Response of Shoe Materials

In terms of properties, the shoe materials can be divided into three categories: flexible elastomers (TPU structures), foams (EVA, PU) and the 'stiff' inserts used for heel counters, torsion stabilisers etc. In general, all three types behave in a similar manner, but the foams have a plateau region in their compression curve and experience unusual creep and compression set behaviour.

The foams used are of the closed-cell type (Figure 3.1); gas pockets are formed in the polymer and can only escape by diffusing through the cell walls (open-cell foams are usually found in packaging or furniture). The effect of the gas in the foam is discussed in Section 3.3.6.

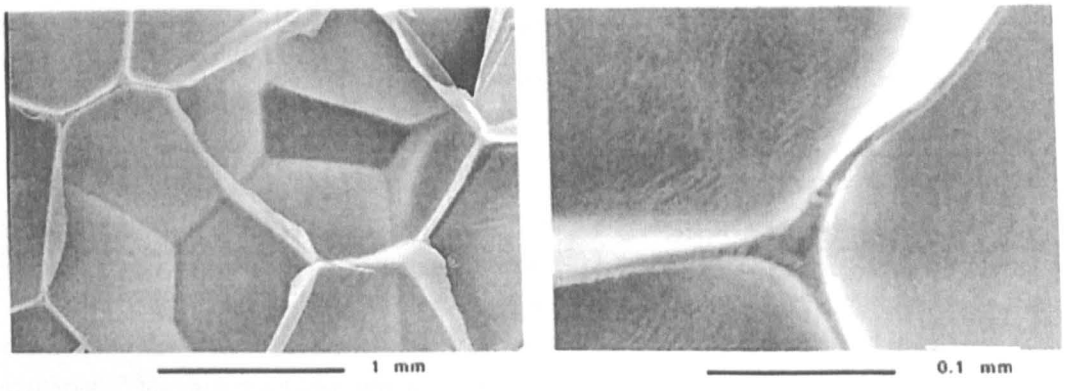

Figure 3.1: Scanning Electron Microscope (SEM) images of closed-cell foam. Each cell is enclosed, preventing large-scale transfer of gas between cells. The closer view on the right highlights that walls between cells are thin, allowing them to buckle under loading (Mills 1999).

3.3.1 The Shape of the Stress/Strain Curve

Bauman (1998) presents a thorough description of the theory behind the elastomer stress strain curve, the relevant sections are summarised as follows:

A block of moulded, vulcanised elastomer consists of a mass of polymer chains cross-linked every 100-1000 carbon atoms. In addition to these cross-links, the chains are also connected by entanglements (a common analogy would be spaghetti). The stress-strain response of the material can be related directly to the behaviour of these molecules.

Each molecule consists primarily of a series of carbon atoms linked in single C-C bonds at an angle of 153° to each other. These molecule chains are often referred to as coils, and behave in a similar way to coil springs (at low strains); as force is applied to the overall structure, the molecules deform due to torsion at the bonds. This gives a linear response, which is a good approximation of the linear-elastic section of the curve (Figure 3.2(a)).

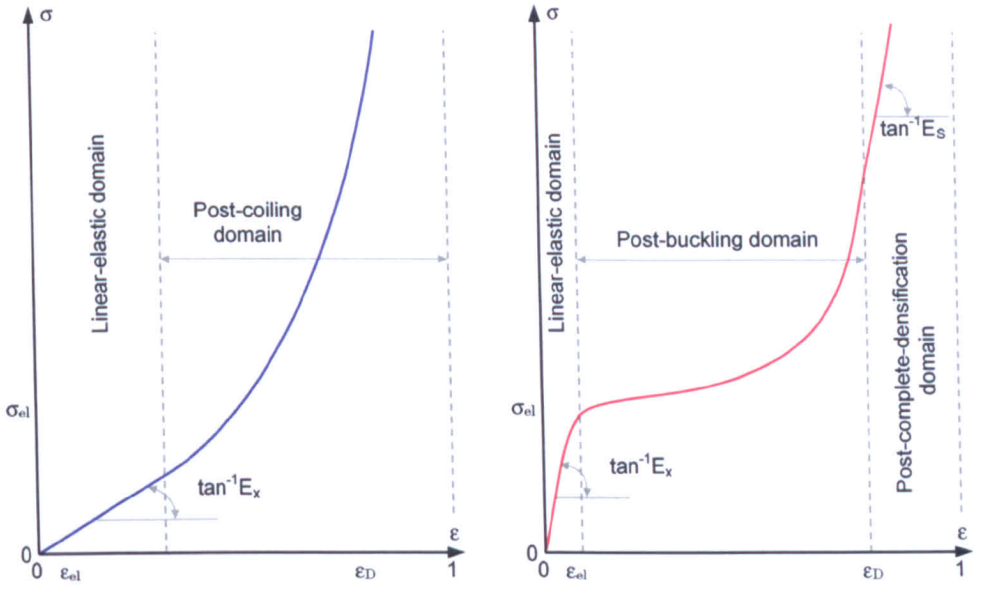

(a) Solid Polymer

(b) Polymer Foam (compression)

Figure 3.2: Polymer stress/strain responses. Note the change in stiffness in the post-buckling domain as the proportion of cells that are fully collapsed (densification) increases. Solid polymers will not generally show this plateau region. Reproduced from Ben-Dor (1996b).

When the chain has been fully uncoiled, other deformation modes occur. Bending, axial deformation and finally, breaking of the 153° C-C bonds requires a significantly larger amount of energy, and so the stress/strain curve steepens at high strains.

This example assumes that all the molecular coils are oriented in the direction of applied load, but this is not the case as the molecules are randomly distributed throughout the material. This causes a smoothing of the stress/strain curve, as differently oriented molecules will uncoil at different rates.

However, the sprung coil analogy will over-predict the deformation for a given force (as it gives a purely elastic response). The proximity of the entangled molecules leads to weaker Van der Waals bonds forming along the chains. Any relative motion of molecules will use energy to break these bonds resulting in an increased stiffness above the elastic curve in extension and a reduction below it (i.e. the sample resists a change in its dimensions).

These are the basic principles involved in solid elastomers, but foamed materials have additional deformation mechanisms resulting in considerably different deformation curves. In tension, foams exhibit a rising stress/strain curve as the cell walls are rotated about their joining edge (Figure 3.3), then stretched until failure. In compression, the material will have a near-elastic region to begin with (the same as in tension), but the curve then flattens out as the cell walls buckle and finally collapse into each other, causing the material to densify and the stiffness to increase dramatically (Figure 3.2(b)).

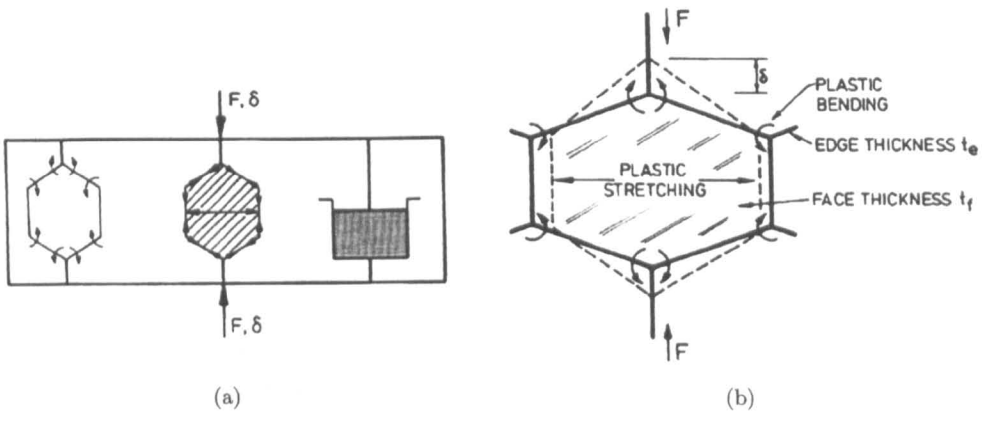

Figure 3.3: Deformation mechanisms in closed cell foams. (a) Main deformation mechanisms (left to right): Cell wall join bending, cell wall extension/compression, gas isotropic gas compression. (b) Detail of plastic deformation of a cell under loading. Reproduced from Gibson (1998).

There have been many models proposed for the prediction of foam behaviour (the equations are not shown here due to the space needed to present each model). Gent (1959) proposes a model of foam based on a network of thin threads joined at the cell edges (Figure 3.4), which gives "satisfactory agreement" between theory and measurement (uni-axial extension/compression), for small strains and finite compressions for a foamed rubber. The author does note however, that the inhomogeneity of the material would affect the properties significantly, especially in compression.

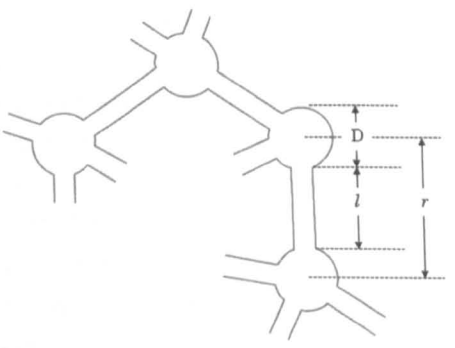

Figure 3.4: Connected thin thread foam model, where D is the diameter of the 'node' where cell walls join, l is the length of the connecting wall and r is the centre to centre distance between two nodes. Reproduced from Gent (1959).

Blatz (1962) uses a simple finite elastic model to predict the response of foamed rubber over a more extensive range of tests; uni-axial, homogeneous-biaxial and two types of strip-biaxial tension. The need for these different tests is explained in Section 3.4. The report comments on previously reported compression data, but no new compression tests were performed. The resulting strain energy function "correlates all the data to a high degree of accuracy".

Throne (1984) presents three models predicting the behaviour of low-density foams, and notes that during compression, the cells do not buckle in a consistent manner; some foams will collapse from the outside in, while others distort uniformly, even though there is no apparent difference in cell dimensions or geometry from centre to edge. The author offers no explanation for this behaviour.

Gibson (1998) provides a thorough review of a very wide range of cellular materials and their properties, including closed cell polymer foams. The book is cited by a number of the publications reviewed here. The deformation model for closed cell foam in compression presented includes the bending of cell wall edges, extension of cell walls and the compression of the gas inside the cell (Figure 3.3).

Across two papers, Ben-Dor (1996a & 1996b) reports on the stress/strain relation for elastomeric foams, and presents models based on Gibson (1998, 1st Ed. 1988) that are still valid at the extremes of strain allowing the densification part of the curve to be modelled. Further equations are developed to fit uni-, bi- and tri-axial compression modes for both open and closed cell foams. No new experiments are reported in these two papers; the results are verified against data presented in other papers.

Mills (1999) and Zhu (1997), both based at Birmingham University, analysed the compression of closed and open-celled foams respectively. Their model is based on a base-centre-cubic (BCC) lattice of tetrakaidecahedral cells. Open cell foams are modelled in a similar way to Gent (1959), but with a more complex overall structure, while the closed-cell foam walls are modelled as buckling walls. Their closest experimental/theory match is shown in Figures 3.5-3.6. The results for closed-cell foams are considerably better than for open-cells, although the predictions in Mills (1999) are only sufficient for low-density foams. If a relative density of more than 0.1 is required (e.g. 10% polymer, 90% gas), then shear forces in the thicker cell walls would need to be considered. Mills later extended this work (Mills 2000a) to look at the high-strain extension of open-cell foams, using a similar BCC lattice technique.

Shulmeister (1997) uses a micromechanical random model of the closed-cell foam based on the geometry of real foam to predict the material behaviour. Cell structure is generated by 3D Voronoi space tessellation (a mesh generating algorithm where the final structure depends entirely on random nuclei or nodes). Finite element analysis (FEA) is then used to compute the overall stiffness of this mesh. The study looks at the effect of adjusting the percentage of material contained in the faces and struts (edges of a cell, e.g. node to node connections which are usually thicker than the cell walls, shown in Figure 3.1). It concludes that the effect of cell randomness (material inhomogeneity) is greater for open-cell foams.

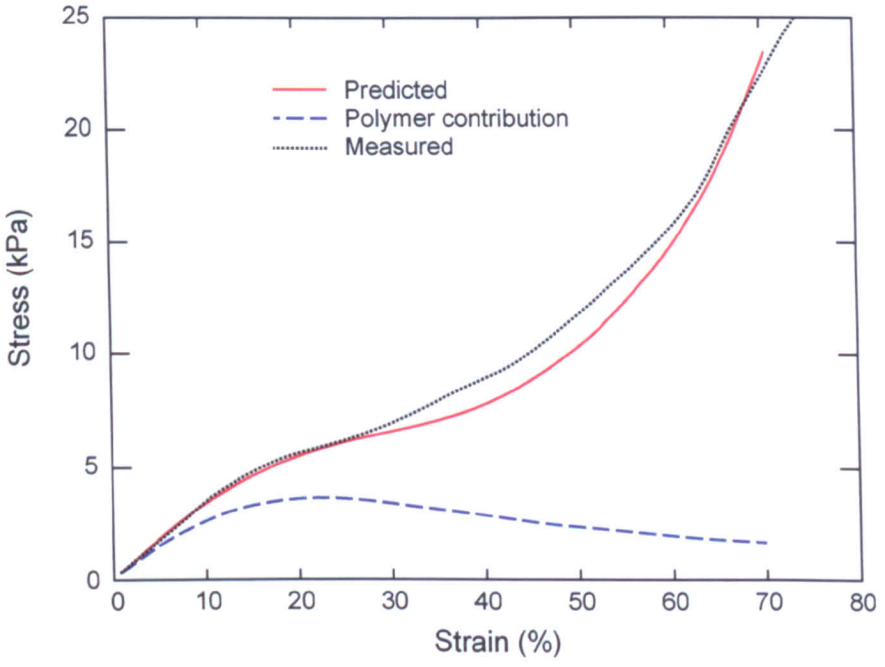

Figure 3.5: Predicted and measured compressive stress-strain curve for LDPE foam of relative density 0.025. Reproduced from Mills (1999)

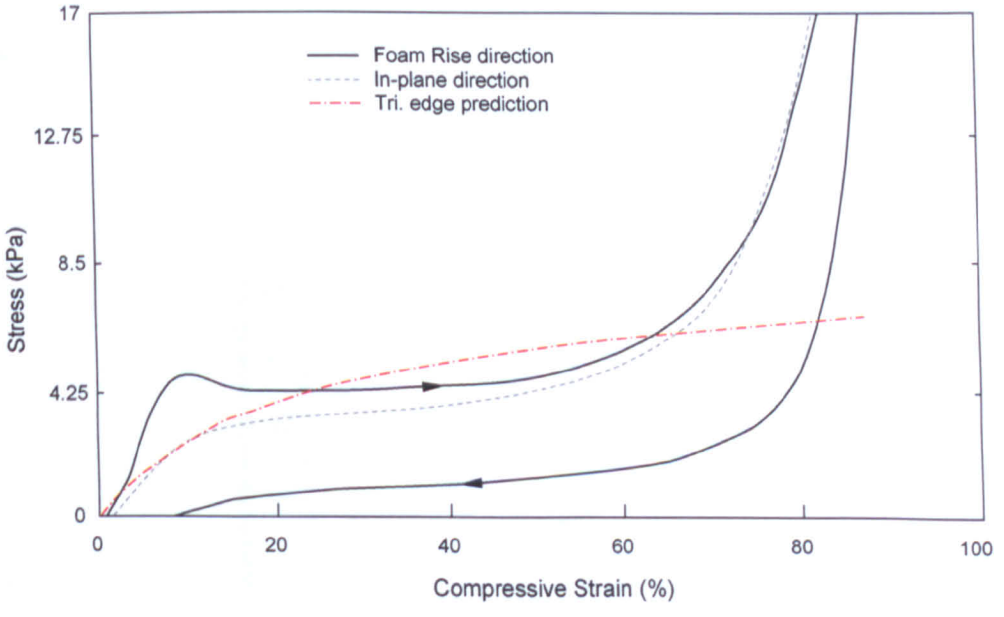

Figure 3.6: Stress-strain data for an open cell PU foam of density 31 kg.m^{-3}, compressed in the foam-rise and in-plane direction, compared with the triangular edge prediction [111] direction compression. Reproduced from Mills (1999)

3.3.2 Hysteresis

As discussed in the previous section, the proximity of the molecular chains causes Van der Waals forces to be generated between them. Moving the molecules relative to each other requires energy to break these bonds; energy is then released as new bonds are formed, but this is mostly dissipated as heat. As a consequence, the material resists a change in its dimensions and even if the sample is deformed and returned to its original shape, energy has been lost as heat in the material (Bauman 1998). This effect is known as hysteresis and is illustrated in Figure 3.7, where load/displacement curves for an elastic forefoot and a viscoelastic heel material are shown. The heel material has a wider loop corresponding to a greater absorption of energy.

Hysteresis increases dramatically at high strains (Figure 3.8) due to the effect of partial crystallisation. A crystal is an ordered arrangement of molecules and is almost always the lowest energy state of the material. As the sample is deformed to high strains the molecules are forced into close proximity. This is easier to visualise in tension; when the string-like molecules are pulled tight, they form into an ordered, dense structure. A larger amount of energy is required to separate these ordered molecules than randomly arranged ones.

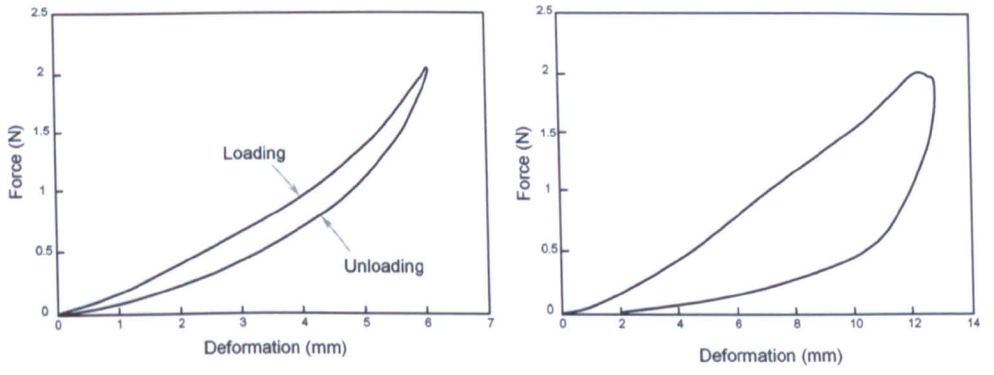

Figure 3.7: Load/displacement curves showing hysteresis for forefoot (left) and heel (right) materials. Upper curve on each chart is loading, lower is unloading. The forefoot material is more elastic and thus shows less hysteresis and consequently has a smaller area within the curve. Reproduced from Knoerr (2002).

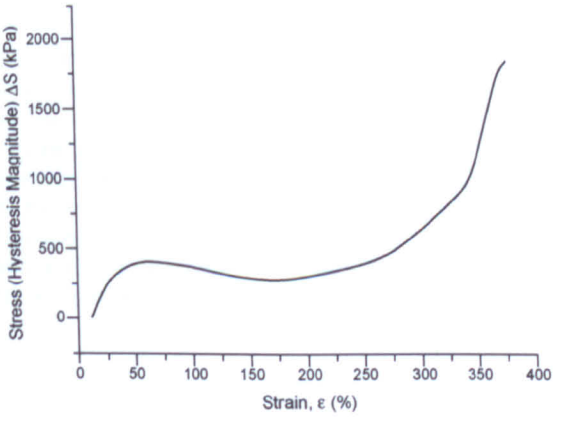

Figure 3.8: Variation of measured hysteresis magnitude with strain. Note that the amount of energy lost is dependent on how far the material is strained. Reproduced from Bauman (1998).

3.3.3 The Mullins Effect

The Mullins effect can be seen when an elastomer is extended to greater strains on successive cycles (Figure 3.9). It is caused by deformation of the molecule chain segments, where a segment is a continuous section of the chain (e.g. no branches or entanglements with other molecules - a 'free' string-like molecule).

If l is the length of the segment and r is the straight line distance between the ends, then a segment is fully extended when $l/r = 1$, and its ends are touching when $l/r = \infty$. When the material is formed there will be a distribution of ratios, l/r_0 (as shown in Figure 3.10). As the sample is distorted, those segments with a ratio close to one are stretched past their limits and break, causing plastic deformation. So for the next cycle, a given strain has a lower corresponding stress, as the material has not returned to its original state, and less molecular chains support the load. When the strain has reached the limit of the previous cycle, it joins back onto the 'original' curve (Bauman 1998).

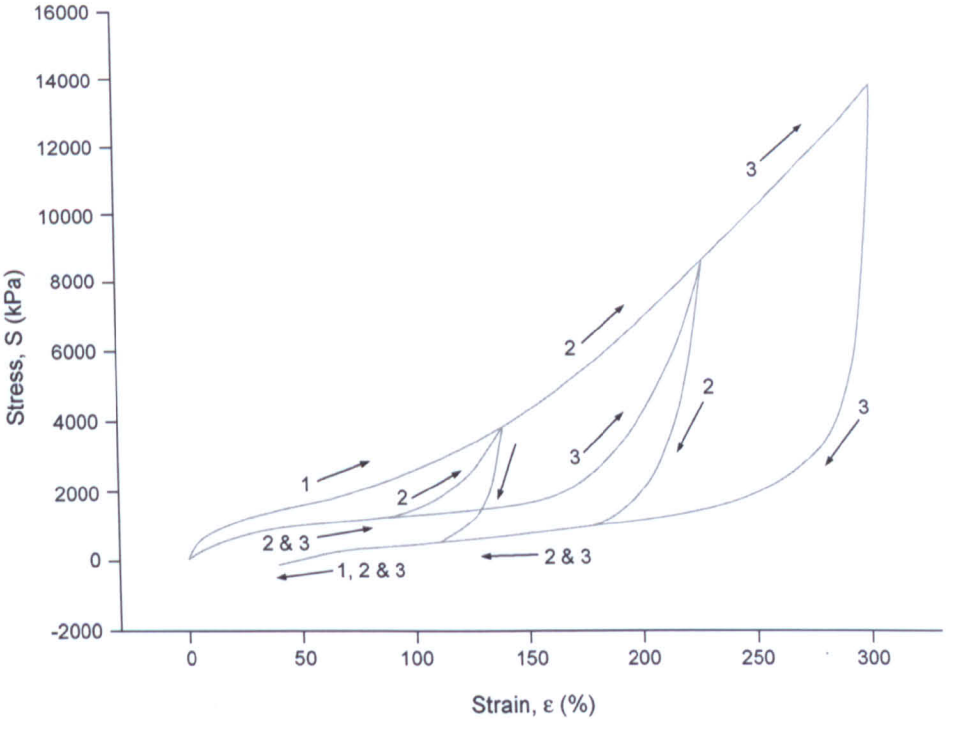

Figure 3.9: Mullins Effect. Points to note are:
1. The second and subsequent extension cycles pass through previously visited strains at a greatly reduced stress.
2. After the first cycle to a given extension, the next cycle curve always returns to the same peak stress recorded at the maximum strain of the previous cycle. It returns to the original curve.
3. The retractions decrease slightly from cycle to cycle but are nearly coincident.
4. The effect is the same whether the elastomer is reinforced or not and does not vary significantly with strain rate or temperature. Reproduced from Bauman (1998).

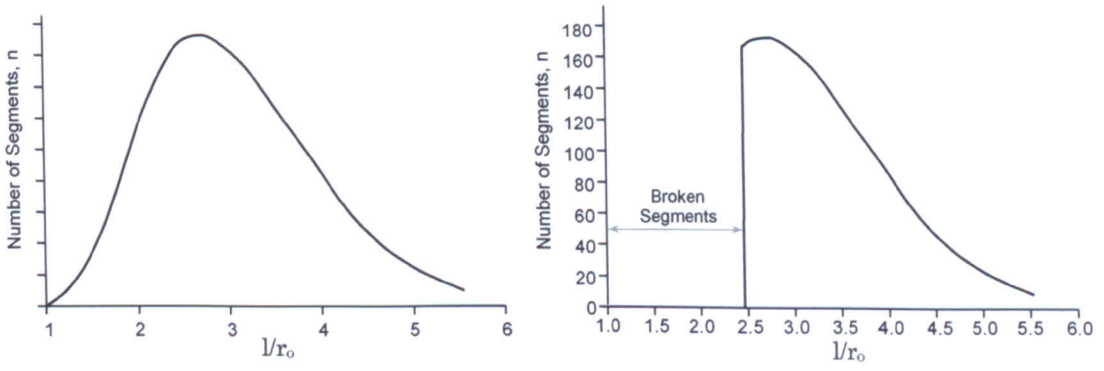

Figure 3.10: Statistical variation of segment length (l) / segment end distance (r). Reproduced from Bauman (1998).

3.3.4 Poisson's Ratio

Poisson's ratio, v, is defined as the ratio of lateral contraction to longitudinal extension for a rectangular sectioned test sample (Figure 3.11). For "incompressible" materials (most metals and rubbers) their Poisson's ratio is constant, as the volume of the material does not change significantly (there is almost always some compression, though it is considered negligible). Foams however, can have a range of Poisson's ratios as their gas pockets can be compressed allowing large volume changes.

The majority of materials will exhibit positive Poisson's ratios - that is, when a cube of the material is compressed uniaxially, its sides will bow outward in an attempt to retain its volume. A cube of material with zero Poisson's ratio will not bow out, but retain a square cross-section as it is compressed (Figure 3.12). Some foam materials can also exhibit negative Poisson's ratios; as they are compressed, they contract, and if extended, they expand. The manufacture and uses of such materials are discussed in Brandel (2001).

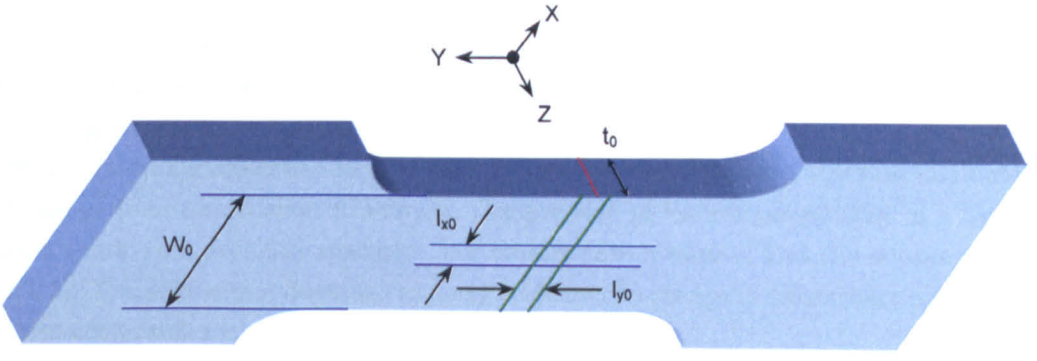

Figure 3.11: Lateral (I_{y0}), longitudinal (I_{x0}) and thickness (t_0) measurement definitions. W_0 is taken as the width of the sample. Reproduced from El-Ratal (1996).

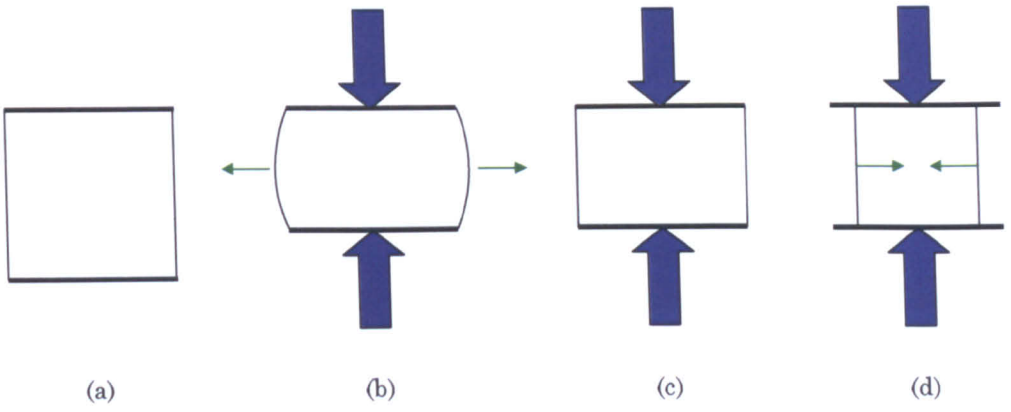

Figure 3.12: Effect of variation of Poisson's ratio: (a) uncompressed shape, (b) positive Poisson's ratio, (c) zero Poisson's ratio, (d) negative Poisson's ratio.

El-Ratal (1996) details experiments concerning the elastic response of flexible polyurethane foams in uniaxial tension. Looking at data from Blatz (1962) and new tests, the report concludes that for rubbers the Poisson's ratio is constant, but due to the highly non-linear behaviour of polyurethane foams, new relationships must be formed:

1. The minor stretch ratio $\lambda_2 (= y/y_0)$ is a non-linear function of the major stretch ratio $\lambda_1 (= x/x_0)$.

2. The volume increases initially with increasing values of λ_1, attains a maximum and then decreases at higher values of λ_1.

3. Both elastic modulus and Poisson's ratio are non-linear functions of the major stretch ratio λ_1. The relationship proposed by Blatz (1962), between the volume ratio and an apparent Poisson's ratio (calculated thus: $\nu = -\frac{ln\lambda_2}{ln\lambda_1}$), has excellent correlation with the experimental data.

The Poisson's ratio for a foam is also dependent on the loading and structure of the foam. Mills (2000a) uses a Kelvin foam model to predict the stress/strain response of open-cell foams, but notes that the response of the foam is anisotropic (direction dependent) due to the manufacture of the foam giving elliptical cells. This results in a higher Poisson's ratio in one loading direction.

Mills (2003a) also describes another instance of anisotropic response, this time attributed to a change from compression to tension. Compression of the sample resulted in a 'small' Poisson's ratio (not explicitly specified), but tension gave a value of 0.44 (for strains greater than 0.1). The difference is described as being evidence of a change in deformation mechanism between compression and tension.

3.3.5 Strain Rate Effects

It is well documented that the rate at which a sample is deformed affects its stress/strain response. If inertia effects are ignored, then for a solid polymer this can be explained by the need to break and re-make the Van der Waals bonds between molecules (see Section 3.3.1) at a higher rate, so for the shorter deformation time a higher force is required to keep the absorbed energy constant (Bauman 1998). For foamed polymers, the presence of gas in the foam can cause an additional strain rate dependent effect (discussed further in Section 3.3.6). The need to test material samples at strain rates similar to those experienced by the material in practical use is a matter for debate, as indicated by the findings of the following researchers.

Throne (1985b) performed dynamic loading of closed cell polystyrene foams, up to rates of 50,800 mm/min, and concluded that "essentially no strain-rate dependent effects" were found. Typical rates seen in heel cushioning tests are 45,000 mm/min. However, the polystyrene foam used in Thrones' paper may differ substantially from the EVA used in shoes.

Most of the other available research describes a definite strain-rate effect; Garcia (1992) used an Instron dynamic tester to apply loads of 250 kg in 12 ms to a sample of a "viscoelastic material used in running insoles". The results show a variation of the rigidity of the sample with the loading frequency. As the sample was displaced by the same amount for each frequency, this corresponds to a change in rigidity with rate of strain.

Zysk (1992) performed both static (100 mm/min) tension and load-controlled tension-tension and compression-compression tests at a frequency of 0.35 Hz, with stress ratios (stress/original stress) of 0.01 and 10 for tension and compression respectively. The failure limits of the material were recorded in each case. The report concludes "the investigation of four types of TPU shows that the static stress/strain behaviour is not able to describe the dynamic fatigue".

Raue (1997) investigates the testing of creep and stress relaxation response of TPU by using dynamic testing. This differs from most other published work, where quasi-static tests are used to replicate dynamic situations. The report finds a "good correlation" between tests at 200 mm/min and long-term static tests up to 1000 hours for a particular TPU.

Mills (2003a) states that polyurethanes are rate dependent, and that foam characterisation testing should be carried out in impact tests lasting 0.05 sec, but does not back this up with any experimental data or equations.

Chakravarty (2003) uses a modified Split Hopkinson Pressure Bar to compression-load PVC based closed-cell foams over a range of strain-rates, concluding that peak stress varies moderately, and energy absorption varies strongly with strain rate (Figure 3.13).

The effect of material creep is reviewed in Section 3.3.9, where it is considered as part of the wear of a shoe material - in normal use the shoe is not loaded constantly for long periods.

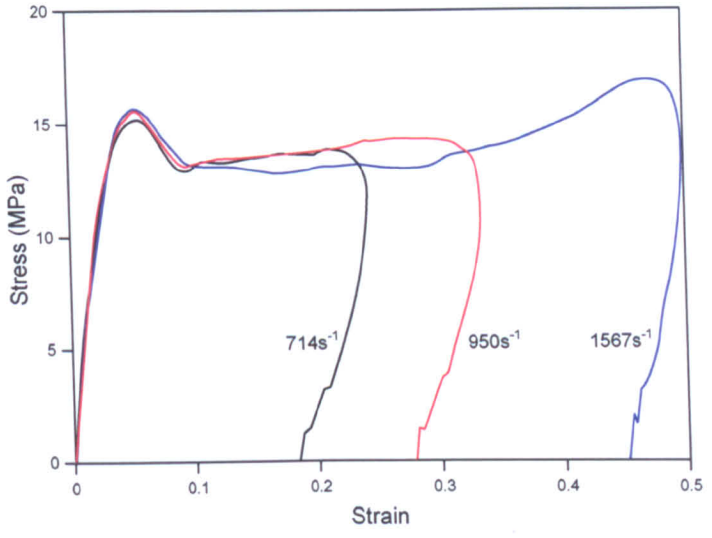

Figure 3.13: Stress/strain curves under different strain rate for R300 foam. Reproduced from Chakravarty (2003).

3.3.6 Gas Considerations

A large proportion of the volume of elastomeric foams is made up of the gases created from the blowing agents used to form the foams. When the foam is compressed, so is the gas. In open-cell foams the gas is forced between the cells (eventually leaving the foam completely) providing a damping effect. In closed-cell foams the gas is contained within the cell, and can be considered as a piston (Mills 2003a, 2003b). The effect of gas compression is shown in Figure 3.14.

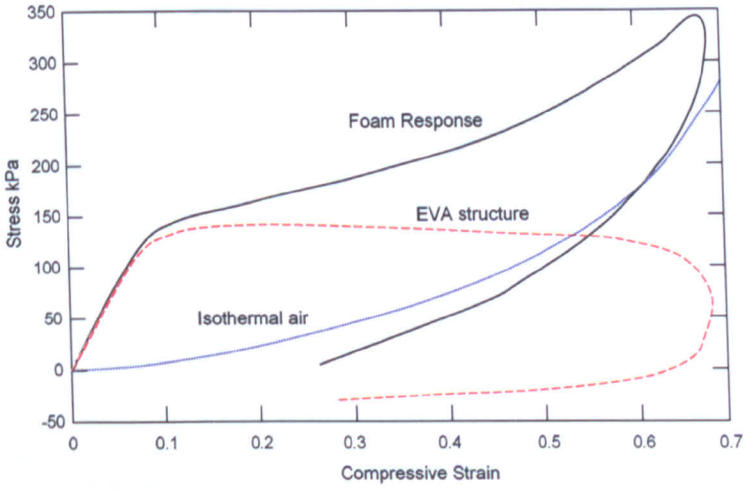

Figure 3.14: Impact compressive stress-strain curve for EVA foam of density 65kg.m^{-3}, with the contributions from the isothermally compressed air and the EVA. Reproduced from Mills (2003b).

Sims (1997) compared the cushioning performance of a variety of open and closed cell foams, with a focus on the effect of the gas flows in the materials. This was done by performing impact tests on samples with varying size cut-outs directly under the impactor. The results show that the peak G-force in the impact was independent of the size of the void, and so "the major contribution to the dynamic performance of a closed-cell polyethylene foam was from gas compression". The cushioning of open-cell foams was attributed to a "complex balance between gas flow and pressurisation".

Throne (1985a) compared a number of foam models that account for gas compressibility, and gave an equation that contained separate gas and polymer contribution terms. Throne noted that only the polymer contribution is strain-rate dependant for closed-cell foams (as the gas is not flowing, just compressing and this is assumed to be adiabatic). This assumption is contested in Section 3.3.7, by Mills (1997).

Throne's conclusion is supported by results presented in Gibson (1998), where polyethylene closed-cell foam was compressed at varying strain rates. The gas contribution to the stress-strain curve was calculated and subtracted out, resulting in a curve that was comparable to that of the solid polymer (i.e. no gas) compressed at the same strain rates as shown in Figure 3.15.

Mills (2001 & 2002) detailed the modelling of gas compression and diffusion through the foam by use of discritised layers, with an assumed transfer flow through the cell walls allowing movement of gases between layers. The 2001 paper presents a consideration of the contribution of the gas flow (open-cell) to the material stiffness while the 2002 paper reports on the compression set and creep of closed-cell foam.

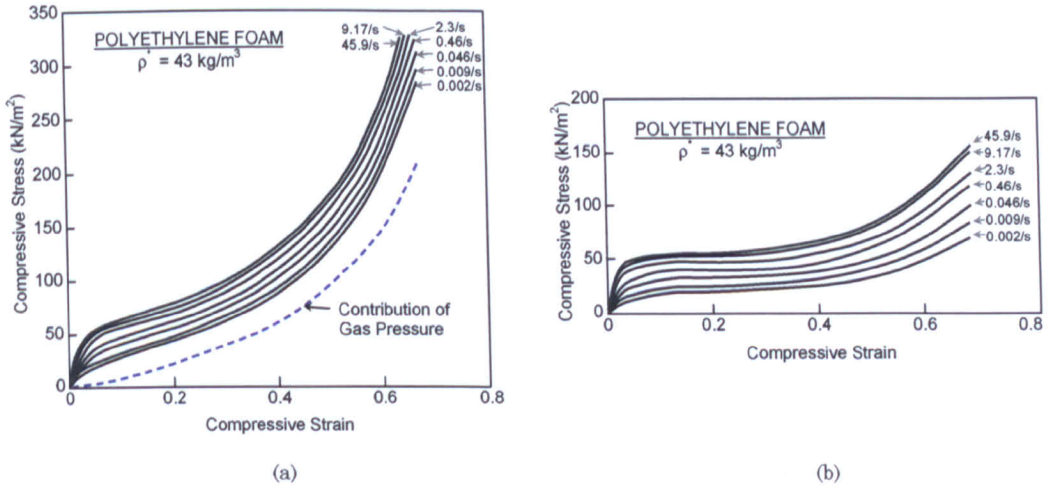

Figure 3.15: Stress-strain curves for a closed-cell polyethylene foam at strain-rates from $2x10^{-3}$ to 50 s^{-1}. (a) The broken line shows the contribution of the gas pressure in the cells, which, because the gas remains isothermal, is independent of strain-rate. (b) The stress-strain curves of (a) after subtraction of the contribution of the gas. Reproduced from Gibson 1998.

3.3.7 Temperature Effects

The temperature of the polymer has a direct effect on its properties. Within the range of temperature at which the polymer is a solid, an increase in temperature increases the rate at which the Van der Waals bonds can be broken and re-made. This reduces both the stiffness and hysteresis (and hence shock absorption) shown by the material (Bauman 1998).

Kinoshita (1996) showed that the temperature of the midsole material increases during running. Measurements of environmental, road surface and midsole minimum/maximum temperatures were taken after 40 minutes of running (Table 3.2). As the temperature of the midsole was always above that of the road or environmental temperatures, the shoe must have been experiencing a heating effect. This is thought to be due primarily to some of the impact energy being dissipated as heat by the midsole, but body heat may also be a factor, although it must be noted that temperatures in excess of body heat were recorded in the tests. Mechanical tests were also performed at different temperatures, showing a change in stress/strain response, hysteresis and the ability of the shoe to control rearfoot stability (Figure 3.16).

Condition	Season	Time	Environmental Temp.	Road Surface Temp.	—Midsole Temp.— Min.	Max.	Diff.
C1	Summer	13:30	35.0	44.5	43.6	54.3	11.2
C2	Summer	12:30	35.4	43.7	43.3	52.8	9.5
C3	Summer	08:30	29.2	29.2	31.9	40.6	8.7
C4	Spring	13:15	20.8	21.8	25.5	33.0	7.5
C5	Spring	14:05	21.1	21.0	25.5	31.9	6.4
C6	Winter	10:00	4.3	2.3	3.8	13.2	9.4
C7	Winter	07:30	0.3	-1.8	2.1	6.3	4.2

Table 3.2: Environmental and midsole temperatures (in °C) during running (Kinoshita 1996). Road surface and environmental measurements were taken prior to running.

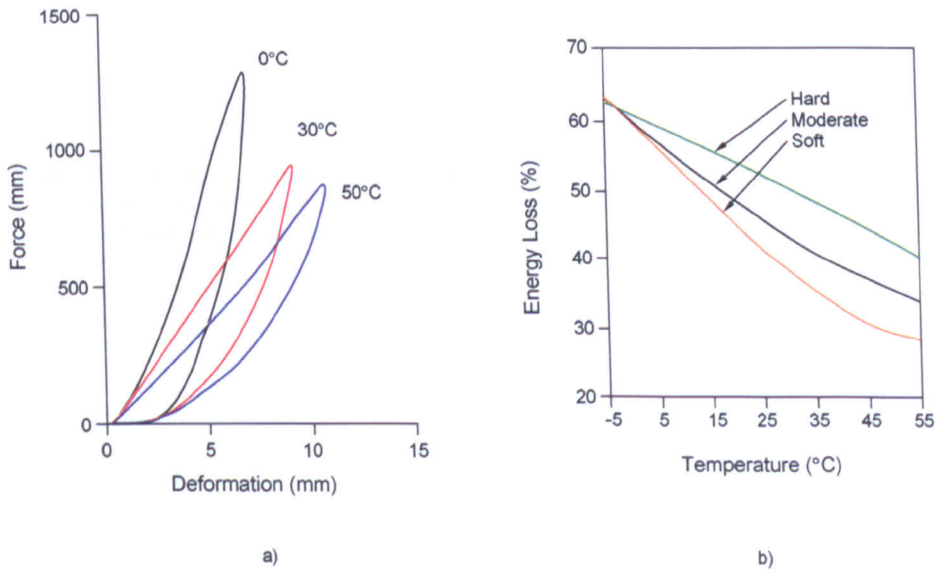

Figure 3.16: Left: Representative force-deformation relationship curves for the moderate shoe at 0, 30 and 50°C. Right: Relationship between energy absorbed and temperature. (Reproduced from Kinoshita 1996).

The direct effect on temperature of the gas compression in foam was studied by Mills (1997). Assuming adiabatic heating, the paper suggests that if a cell full of a gas is compressed to 10 % of its original size, the gas will experience a temperature rise from 23°C to 400°C, for a foam with a zero Poisson's ratio. This is above the melting point of the polymer, although no evidence has been found of melting under running forces. The heating effect in Mills (1997) shows only a ≈10°C rise for the cell sizes found in EVA foam, and that this rise is nearly isothermal even under impact conditions. The report also states that this rise is due to a combination of gas compression and polymer hysteresis from elastic and plastic deformations (Figure 3.17). The gas compression contribution to strain hardening was found to vary inversely with Poisson's ratio. Mills also considered the heat transfer between cells during impact (which was previously modelled as adiabatic), implying that another mechanism for dissipation of energy as heat within the cell structures comes from forced convection of heat from the compressed gas to the cell walls.

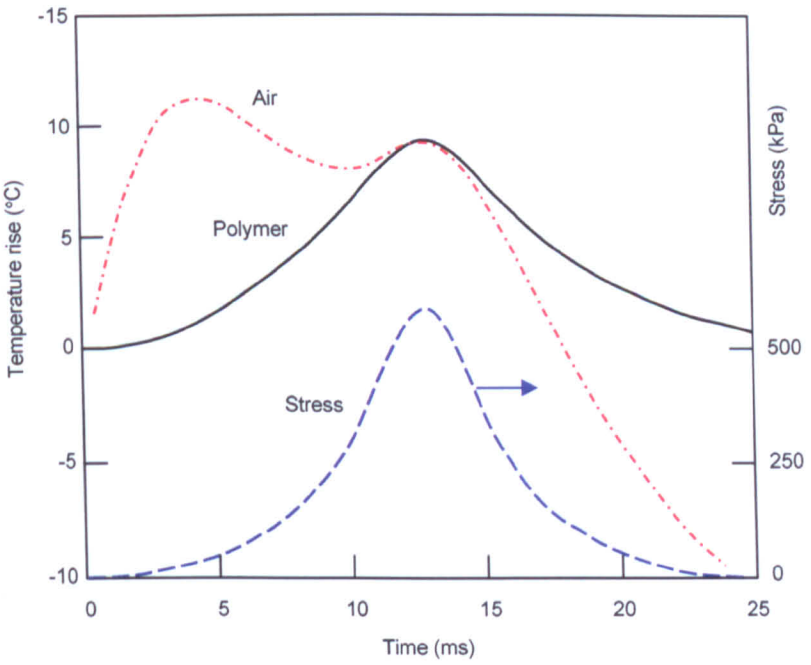

Figure 3.17: The predicated variation of the air and polymer temperatures and compressive stress with time, assuming air conduction only, for the impact of foam of Poissons ratio 0.15 and relative density 0.025, having a cell diameter of 0.1mm. (Reproduced from Mills 1997).

3.3.8 Density Effects

The moulding and setting process is complex as many factors affect the exact nature of the final product. These include the overall temperature of the mould (which can also vary across the mould), the locations and pressure of any injectors used (or if compression moulded, the shape and structure of the blown foam sheet), the orientation of the mould (as the different density components in the mix will try to stratify according to the direction of gravity) and the setting time.

Foams have been observed to exhibit densification and cell flattening near the surface of the part (Beals (1997), Mills (2001, 2003b)), as can be seen in Figure 3.22. Unpublished experiments on PU foam have found a definite variation of the density across a moulded cube, and variation of the mechanical properties with the density. A decrease in cell size toward the surface and a PU 'skin' at the surface are also reported (Lucas 2004).

Beals (1997) studied the compression behaviour of aluminium foam blocks and reported a 'significant' non-linear variation in compression properties and energy absorption values with density (Figure 3.18). Although the stress/strain response of aluminium is largely plastic, the interest in aluminium foam from major automotive and aeronautical companies could prove a useful source of analysis techniques for later research, for example Reyes (2003) used statistical variation of aluminium foam density to improve the accuracy of FEA impact models.

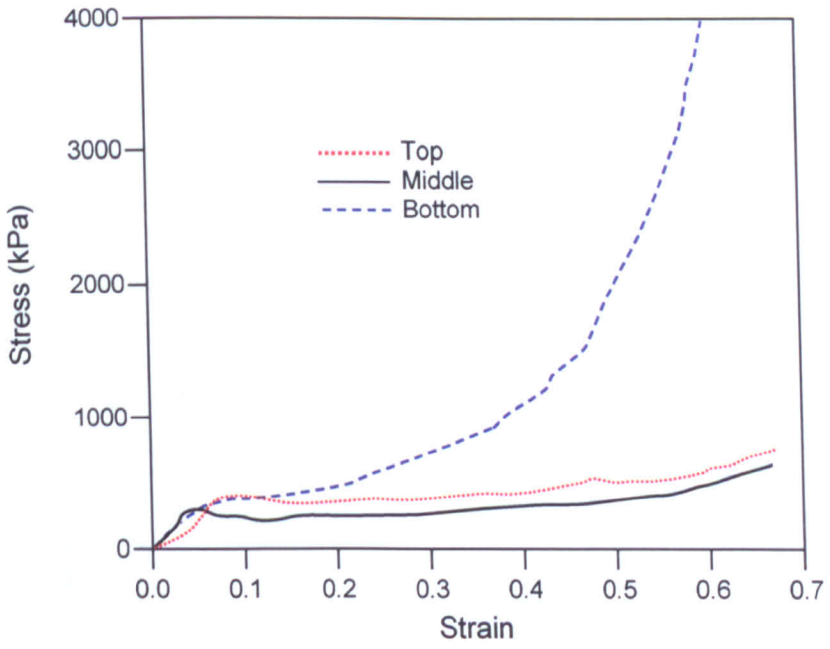

Figure 3.18: Variation of compressive stress/strain response with changing density, dotted: top surface, solid: middle, dash: bottom surface. (Reproduced from Beals 1997).

The effect of density on vinyl foam was studied by Patterson (1998) using specially made sheets of foam. ASTM standardised tests were performed to assess density, tensile strength/modulus, flexural strength/modulus, Izod impact. All tests showed a variation in their respective property with density. Tensile strength results are shown in Figure 3.19.

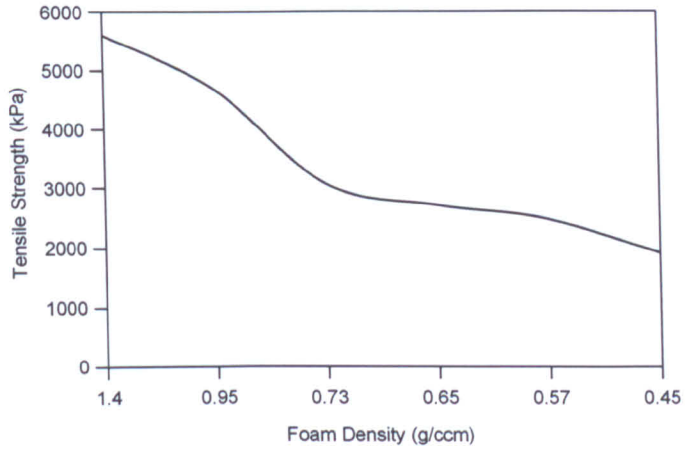

Figure 3.19: Variation of tensile strength with density. Reproduced from Patterson (1998).

Chakravarty (2003) found that the effect of foam density on the material properties of 12.5 mm cube samples, with variation across one thickness only, was greater than the variation of strain rate at which the properties were measured (Figure 3.20).

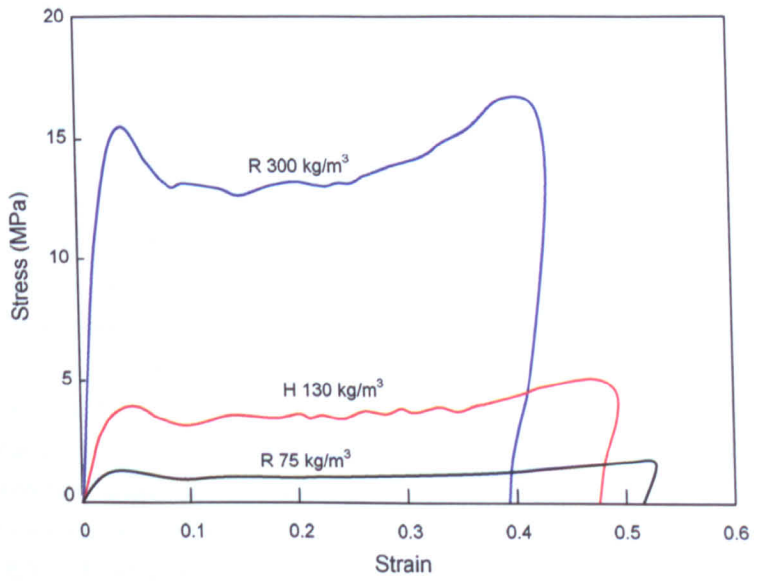

Figure 3.20: Variation for stress/strain response with foams of different densities. Reproduced from Chakravarty (2003).

3.3.9 Wear

The mechanical properties of running shoe midsole materials change with usage of the shoe. This can be attributed to two mechanisms - plastic deformation of the polymer, and loss of gas (for foamed materials only). On a molecular level, the plastic deformation occurs as the material is loaded and the molecules move relative to each other. To allow this movement, Van der Waals bonds are broken and remade in different locations. On relaxation, the material will attempt to return to its original shape, but only a proportion of the molecules can return to exactly their original position, resulting in some permanent deformation. Due to the statistical variation of the orientation of the molecules, even within the elastic limits of the material, some plastic deformation occurs in the first cycles (the Mullins effect). The amount of plastic deformation observed is dependent on the type of polymer used (Baumann 1998).

Foamed materials can also experience a loss of gas (which provides significant cushioning), due to diffusion of the gas through the cell walls. Mills (2001) attempted to model the gas-loss mechanisms in EVA foam by considering the transfer of gases through a series of cell 'layers' (Figure 3.21), and concluded the following:

- Gas diffusion parallel to the stress is the major effect for foam products with thickness much less than either lateral dimension (e.g. shoe midsoles).
- A complete gas loss model should consider the three-dimensional diffusion of gas.
- The gas diffusion rate from EVA appears to be inversely proportional to the foam density.
- Recovery of the foam after long-term loading was very slow; the process was incomplete after several weeks at 35°C and a year at roughly 20°C (Figure 3.22). When the foam is stored at 20°C it recrystallises - this may interfere with the recovery process.

The change in cushioning performance with use can be clearly seen in both mechanical testing and real running. Foto (1995) subjected PU, PE and EVA foam samples to cyclic loading (100,000 cycles, 350 kPa at 1 Hz) and recorded the rebound thickness (thickness of the material after loading) at various 'distances' (Figure 3.23). The higher resistance of PU to wear is apparent, which is the main reason manufacturers are looking to make midsoles mainly out of PU and its variants. The reduction in cushioning from actual running was reported by Ujihashi (1998), where heel impact testing was repeated on the same shoe after distances up to 840 km (Figure 3.24). As the shoe wears, the stiffness of the sole increases, while the hysteresis decreases.

Mills (2003b) noted that the thickness of the midsoles and the nature of the outsole boundary affects the total gas loss, and that gas can escape more easily in high pressure areas that are near to a free surface. Creep testing in Mills (2003c) combined with FEA shows that gas pressure in surface cells is as low as 15% of that of the rest of the material. One hypothesis that might be drawn from this is that enclosed foam structures, such as the heel crash structure in the adidas a^3 Ultraride (Figure 3.25), will lose gas at a slower rate than 'open' EVA structures, like those used in the rest of the a^3 range, due to the sealing effect of the TPU (if indeed it does provide any air sealing). It may also be of use for manufacturers to investigate the likelihood of increased wear rates for EVA structures over traditional, full-length midsole parts, due to increased surface area in the high pressure heel region.

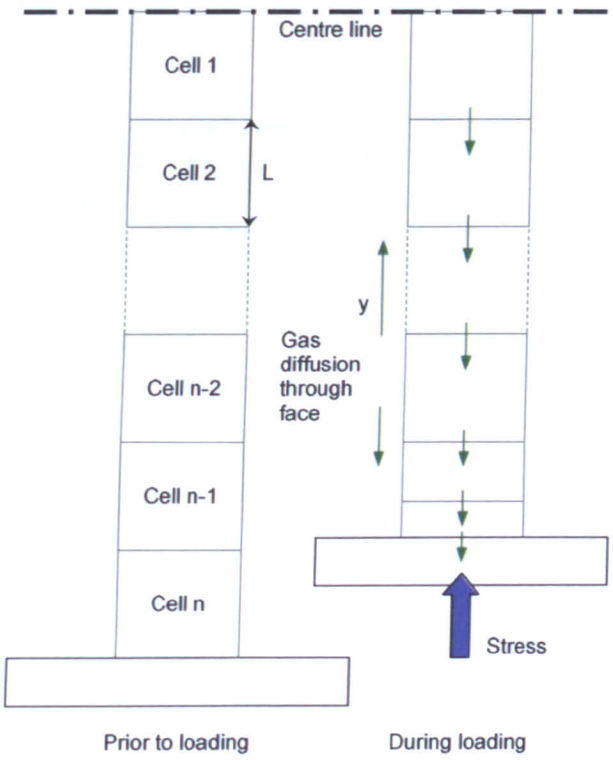

(a) Schematic of gas diffusion, parallel to the stress axis, through the faces of cubic cells.

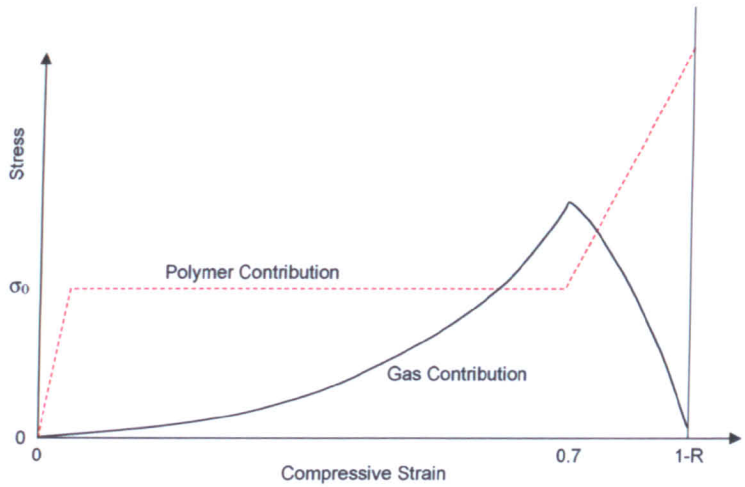

(b) The assumed contributions to the creep stress, from the cell gas and the polymeric structure as a function of compressive strain.

Figure 3.21: Modelling the gas processes within foams (Reproduced from Mills 2001).

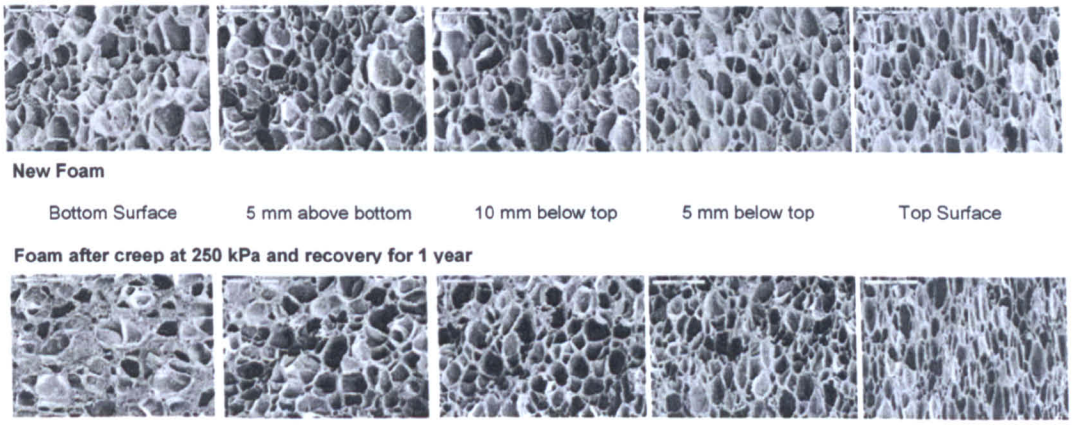

Figure 3.22: Scanning Electron Microscope (SEM) images of EVA foam in section. Note the flattening of the cell walls close to the surface and the non-recovery of original shape even after one year of rest. Adapted from Mills (2001).

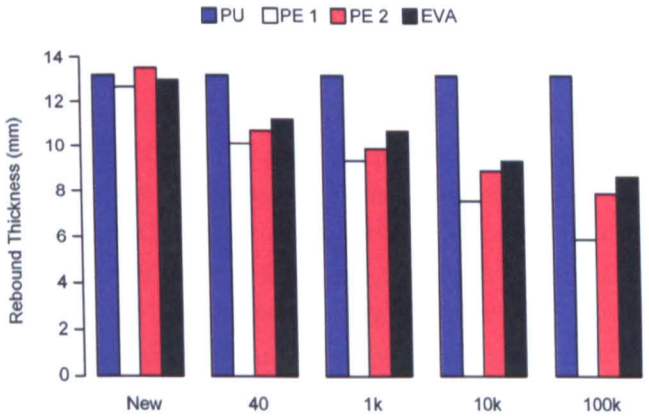

Figure 3.23: Rebound thickness of polyurethane foam (PU), medium firm polyethylene (PE1), firm polyethylene (PE2) and ethylene vinyl acetate (EVA) at various stages of wear. Reproduced from Foto (1995).

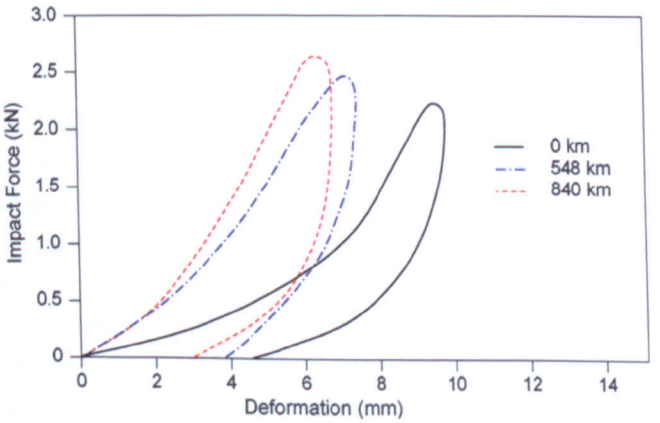

Figure 3.24: Variation of the mechanical properties of the shoe due to the service distance. Reproduced from Ujihashi (1998).

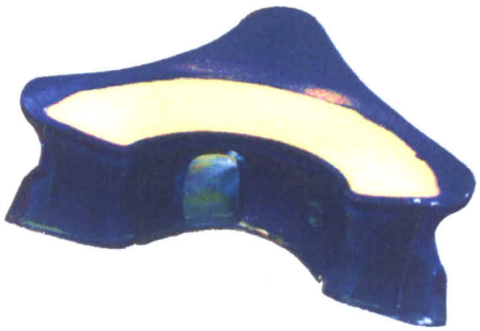

Figure 3.25: adidas a^3 Ultraride heel crash structure (EVA filled TPU).

Recovery from damage has been seen in foams; Verdejo (2004) conducted repeated impact tests on EVA foam on consecutive days, with results showing a clear improvement in cushioning at the start of the days testing (after being rested at night). However, the reason for the overall loss of cushioning is attributed to "a decrease in the initial compressive collapse stress, not a change in the air content". This conclusion is based on results from Verdejo (2003) that looks at the time required for gas to diffuse through the foam cell walls.

3.3.10 Failure

For the purpose of this section, failure is considered as the separation of one shoe material from another (or itself). For the most part, a running shoe will wear out before it fails. That is to say that its cushioning abilities will have reduced significantly due to plastic deformation (and possibly gas loss in closed cell foams). EVA foam is a very abuse tolerant material, small tears and scratches do not lead to crack propagation at the same rate as seen in metals, due to the ductility of the polymer halting the crack growth (it is because of this that complex sharp shapes can be moulded into the foam, as shown in Figure 3.26).

External sources such as extreme heat (EVA crystal melting point is $\approx$70°C, Mills (2003b)) and sharp objects can damage the foam, but these are not experienced during normal running. Some research has been carried out on the crack risks of polymers; Russell (1991) investigated predicting the strain limits of PVC compounds for a range of crack widths and depths using FEA. Samples were cycled mechanically up to 50,000 times with up to 70% strain. Good correlation between the peak values indicated by the FEA model and the results of the testing was reported.

The most likely cause of premature failures is poor manufacture; bonding failure due to improper application or drying will cause parts to separate and the shoe will not function as intended. This problem is becoming more critical as the number of parts (and therefore bonding/interface surfaces) increases, while their contact area decreases if smaller parts are used. Incorrect moulding technique is known to produce TPU parts that have seams where the releasing agent has migrated away from the mould walls and caused the molten plastic to set in the wrong geometry. Again this is becoming more important as the surface area of parts (relative to their volume) increases, resulting in greater use of releasing agents to extract these parts.

Although there is a significant volume of information on the bonding failure of polymer-based composites, at present there is little information available that specifically concerns the failure of the materials used in running shoes.

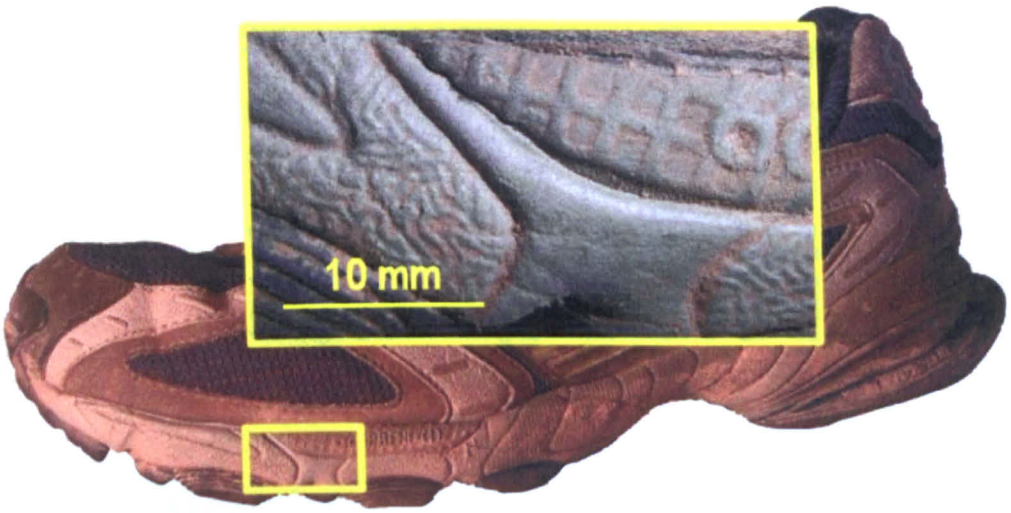

(a)

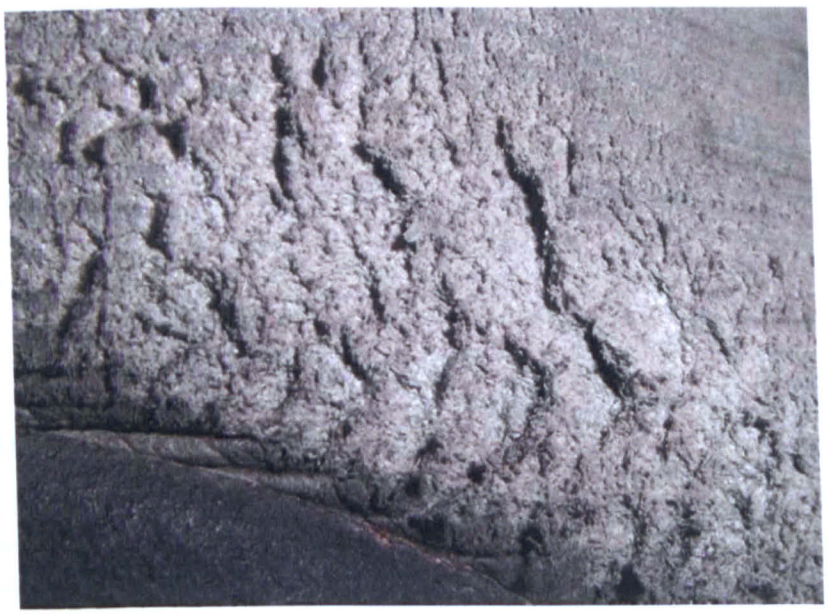

(b)

Figure 3.26: (a) Fine detail moulded into midsole, even in regions of high deformation. (b) Close-up of external damage to EVA midsole; note the lack of crack formation even after considerable wear (shoes in excess of three years old).

3.4 Shoe Material Testing

To compare and predict the behaviour of the materials used in the midsole, a number of tests are carried out on samples of each material (in addition to the tests on the whole shoe mentioned in Section 2.9). These test primarily provide the stress/strain response of the material, which can then be used within a FE model.

3.4.1 Basic Tests

The uni-axial tension test uses a dog-bone shaped sample cut from a sheet of the material under test (Figure 3.27). This sheet is often specifically manufactured for test purposes so may not be a true representation of the material in the shoe, as the moulding of complex shapes can cause inhomogeneity in the material.

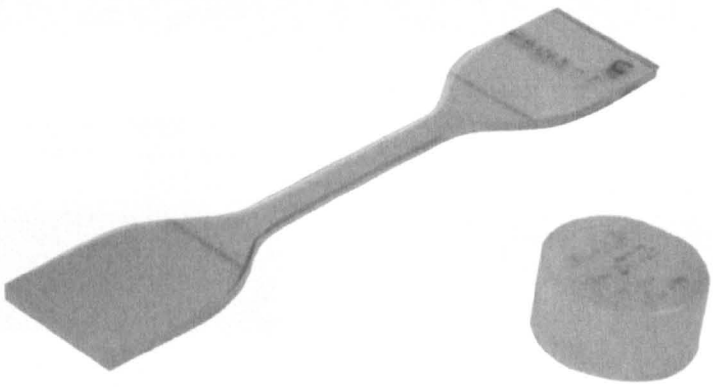

Figure 3.27: Dog bone (tension), and Button (compression), TPU material test samples.

The sample is clamped into a linear force/displacement measuring device, loaded and the stress/strain behaviour determined. Uni-axial compression is usually performed with the same device as the tension test (but in compression), on a cylindrical sample of material (Figure 3.27). Data from these two tests will describe most of the behaviour of the material, and the curves produced are often used to compare the behaviour of materials under different conditions (this can be seen in Section 3.3.1).

3.4.2 Inaccuracies in Testing

The main limitation of the tension tests is the clamping of the sample. Due to the high deformations that some of the midsole materials can undergo, the clamps must adjust to account for a thinning sample. Figure 3.28 shows the deformation of the end of a TPU dog bone; the red line was drawn on the straight edge of the clamp before the sample was loaded. The resulting stress/strain curve is assumed to be that of the thin section of the dog-bone, but it is clear that the entire sample is deforming to some extent.

The uni-axial compression test is subject to friction effects between the sample and the compressing plates. This causes the cylindrical sample to bow out at the edges, putting the surface in tension and creating inaccuracies in the results. The effect is best illustrated using FEA, where the two extremes of friction can be simulated (Figure 3.29).

Due to the inhomogeneity of foam, and the skin effects experienced by moulded parts, the size of the sample under test can affect the results. Chino (2003) investigated the effect of specimen size parameters (volume and ratio of cross sectional dimension to cell size) for a closed cell aluminium foam 'Alporas' (Shinko Wire Co., LTD., Amagasaki, Japan) in both compression and tension. The report concludes that, as size decreases, the stress and UTS

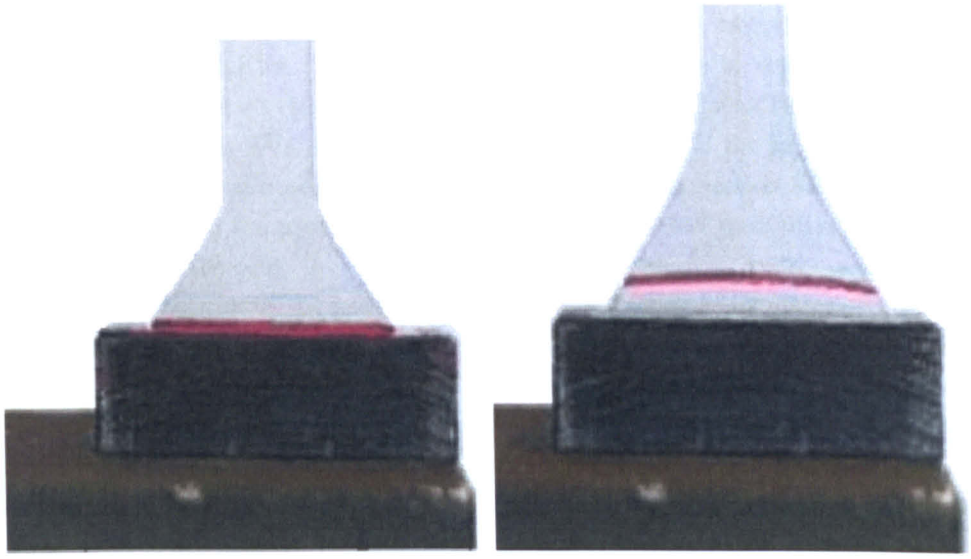

(a) (b)

Figure 3.28: Dog Bone tensile test specimen, (a) no load, (b) under load of 600N. Note the movement of the specimen in the clamp under load.

(a) (b)

Figure 3.29: Effect of friction. (a) FEA result with no friction, (b) FEA result with friction coefficient of 0.8.

(per unit area) decrease, and the scatter of results increases when the cell size is greater than one quarter of the length of the sample (Figure 3.30). Although EVA does not exhibit cell sizes proportionally as large as the samples used in this set of testing, there may be some effect if large air bubbles have been formed during the remoulding process (as have been observed during visits to EVA production lines).

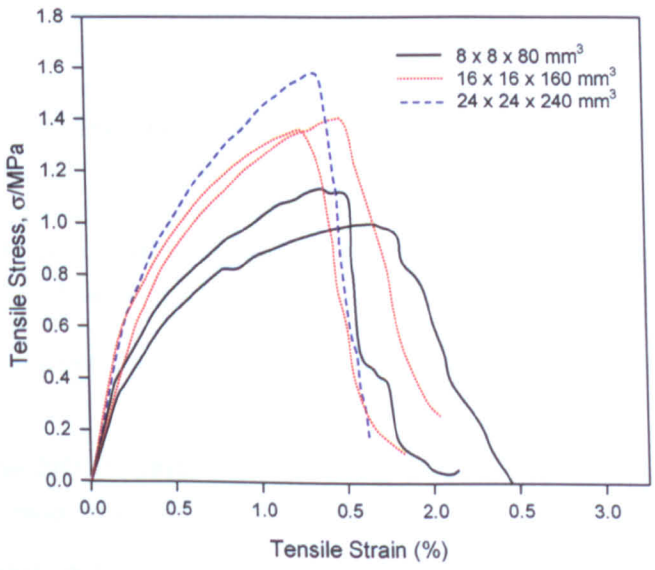

Figure 3.30: Effect of sample size on stress/strain response. (Reproduced from Chino (2003)).

The sample dimension effect can be seen in Westerman (2002), where the paper concludes that adding air to solid EVA (by the addition of blowing agents to the raw polymer, as is commonly the case) has no significant effect on the reduction of peak forces generated from impacts on thin (4 mm) EVA sheets, despite the contribution of the gas to the cushioning properties of the material observed in the papers mentioned in Section 3.3.6. This suggests that with thin samples the pressure on the cells is so great that their primary deformation mode is crushing of the cells.

Another consideration is the pre-conditioning of the sample; some materials will undergo considerable changes in properties for the first few cycles of a test, this is due to the Mullins effect (Mills 2000b, also see Section 3.3.3). Depending on where the material was constructed and stored, the sample may be 'fresh' or 'broken in' or anywhere in between at the time of testing. This is a particular problem with whole shoes as the natural tendency is for people to pick up the shoe and flex it. Transport and storage must be considered if a standardised 'break-in' cycle is not used.

For the stiffer components of the shoe (heel counters, torsion plates etc.), impact tests need to take account of the contact conditions between the impactor and the sample as predictive errors of up to 100% have been reported due to high frequency vibrations between the impact surfaces (Mills 1989).

3.4.3 Standardised Testing

This section reviews current industry standards for elastomeric materials, with a particular focus on tensile and compressive applications, and including standards for measurements and sample preparation. Attention is also given to standards supporting entire or part shoe components, as well as the terminology related to athletic footwear and biomechanics.

3.4.3.1 Standard Test Methods for Elastomeric Materials

ASTM D638, Standard test method for tensile properties of plastics, focuses on the analysis of tensile properties in plastics, namely, the tensile strength, percent elongation and modulus of elasticity. Detail is provided with regard to the test apparatus, the number of test specimens required, their geometry and sample conditioning. Detail is also given on gripping mechanisms and the specific specimen dimensions for different material types.

Analysis of compressive properties is specified in simple uni-axial form by *ASTM D575, Standard test method for rubber properties in compression.* The test method also cross references *D3183, Practice for rubber - Preparation of test pieces for test purposes from products*, and *D3767, Practice for Rubber - Measurements of dimensions.* Both of these provide information for the accurate production of test specimens.

In addition to the aforementioned ASTM methods, the BSI provides a series of tests in relation to the 'Physical testing of Rubber' and 'Rubber vulcanized or thermoplastic' the most relevant of which are listed below:

BS ISO 37:2005: Rubber, vulcanized or thermoplastic - Determination of tensile stress-strain properties.

BS 903-A35: 1995 ISO 471:1995: Physical testing of rubber - Temperatures, humidities and times for conditioning and testing of test pieces.

BS ISO 23529:2004: Rubber - General procedures for preparing and conditioning test pieces for physical test methods.

3.4.3.2 Standard Test Methods for Foam Materials

There are several ASTM test methods which deal explicitly with the testing of cellular materials. In particular *ASTM D3574, Standard test method for flexible cellular materials: slab, bonded and moulded urethane foams*, outlines in brief detail 15 test methods, the most relevant of which are: compression, force, tension and density.

In addition *ASTM D35751, Standard test method for flexible cellular materials made from olefin polymers*, outlines 12 test methods, the most significant being; compression set, compression deflection, constant compression creep, density and dynamic cushioning.

Although the above methods are designed to analyse cellular materials, the detail is simplistic in comparison to those outlined for elastomeric testing. Elastomeric foams used in athletic footwear experience high levels of deformation and it is thought that the tests outlined in these methods may need significant modifications to provide accurate repeatable results. Despite this, the methods do provide a good starting point for cellular material characterisation.

3.4.3.3 Standard Test Methods for Shoes

There are a range of test methods available for testing shoe components, separating the shoe into insoles, outsoles, uppers and liners. *BS EN13400:2002, Footwear - Sampling location, preparation and duration of conditioning of samples and test pieces*, lists 33 methods dealing with such areas as friction, stability, tear resistance, abrasion resistance, water resistance and colour migration. However it appears that methods for analysing the compressive properties of footwear are somewhat scarce in comparison.

BS EN 12743:1999, Test methods for outsoles - Compression energy, describes a test in which a heel shaped last is compressed into a shoe heel section at a rate of 10 mm/min to determine the compression energy. In this test the term outsole refers to all materials in the base of the shoe once the insole (which is not attached to the rest of the shoe) has been removed.

ASTM F1976, Standard test method for cushioning properties of athletic shoes using an impact test, takes a similar approach to *BS EN 12743:1999*. However, rather than loading the material at a slow and controlled rate it uses the impact of a falling mass to measure the material's energy absorbtion properties.

Lastly, *ASTM F1614, Standard test method for shock attenuating properties of materials systems for athletic footwear*, outlines three methods for testing a block of midsole foam. The test is to be used for general characterisation of midsole material systems and can be carried out using either a drop rig, hydraulic, pneumatic or screw driven machinery. The tests are referred to as uni-axial, however the fact that the compression impactor is smaller in diameter than the defined sample geometry would suggest an indention compression test. Furthermore there is no justification for the chosen size and geometry of the impactor.

In addition to previously stated test methods, ASTM provide standard terminology to be used alongside the methodologies. *ASTM F869, Standard Terminology relating to athletic shoes and biomechanics*, covers all the terms and notation used in relation to the previously stated methods.

3.4.3.4 Standard Test Methods for Testing Equipment

Material test methods outline the required apparatus for specific testing requirements. To ensure testing is carried accurately and to prevent any errors resulting from the test equipment, BSI provide verification standards for test machinery. The most relevant verification methods for tension and compression testing machines are outlined as follows:

BS EN ISO 7500 - 1:2004, Part1: Tension/compression testing machines - Verification and calibration of the force measuring system.

BS EN ISO 7500 - 2:1999, Part2: Tension Creep testing machines - Verification and calibration of the force measuring system.

The majority of the standardised testing attempts to achieve a 'pure' test, this is one where only the stress-strain response of the material in the required direction is recorded. Effects such as temperature and friction are significantly reduced by standardisation and special equipment respectively. Most of the standards are based on testing rubber, but have serious limitations when samples are tested to high strains. Preparation of samples, particularly foams, is also a major problem.

Details of specific issues raised and any recommended additions to the standards are included in the relevant sections of Chapter 5.

3.4.4 Advanced Tests

While the two basic uniaxial tests are very useful in describing the material behaviour, other deformation modes occur in the shoe. For example; although the main deformation in a foam heel is uni-axial compression, the upper surface is in planar tension, as demonstrated in Figure 3.31. If the material experiences a 'skin' effect (see Section 3.3.8), then this tension could provide a significant part of the material stiffness.

A more complete picture of the material behaviour can be built up by performing other tests:

Bi/Tri-Axial Tension The stress/strain behaviour in uni-axial tension is different to that in bi- or tri-axial tension. Figure 3.32 details the compression modes in multi-axial tension, while Figure 3.33 shows a test device for bi-axial tensioning of a sheet of material. Finally, Figure 3.34 shows theoretical results from the different compression modes.

Equibiaxial Tension To overcome the inaccuracies of uni-axial compression due to friction the test can be simulated by tensioning the sample in all directions about the axis. Figure 3.35 shows a device used by Day (2000) for this purpose.

Planar Compression/Tension To overcome surface effects, samples that are long in the direction perpendicular to deformation are tested. Figure 3.36 shows two forms of planar tension test equipment, the first showing significant surface effects at the edges of the sample.

Volumetric Compression The simplest way to ensure a sample is compressed in all axes (effectively tri-axially) without any friction effects is to compress it in an incompressible fluid contained in a hydraulic actuator. Pressurising the fluid causes the sample to compress evenly.

Other tests to assess the effects of temperature, cyclic loading (for wear, Mullins effect, etc.), compression set, gas loss and a range of others, may be required to fully describe the behaviour of the material.

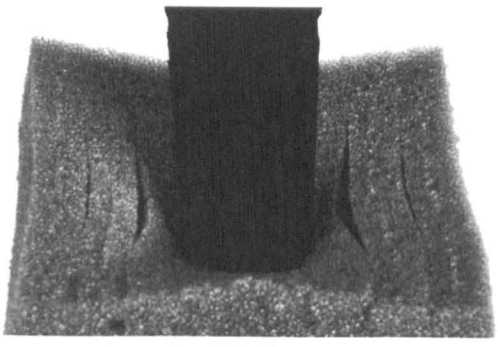

Figure 3.31: Surface tension effects in foam. The foam in the image is open cell and perforated (vertically) into 12 mm square cross-section beams. The tension in the upper surface causes the perforations to break close to the indenter.

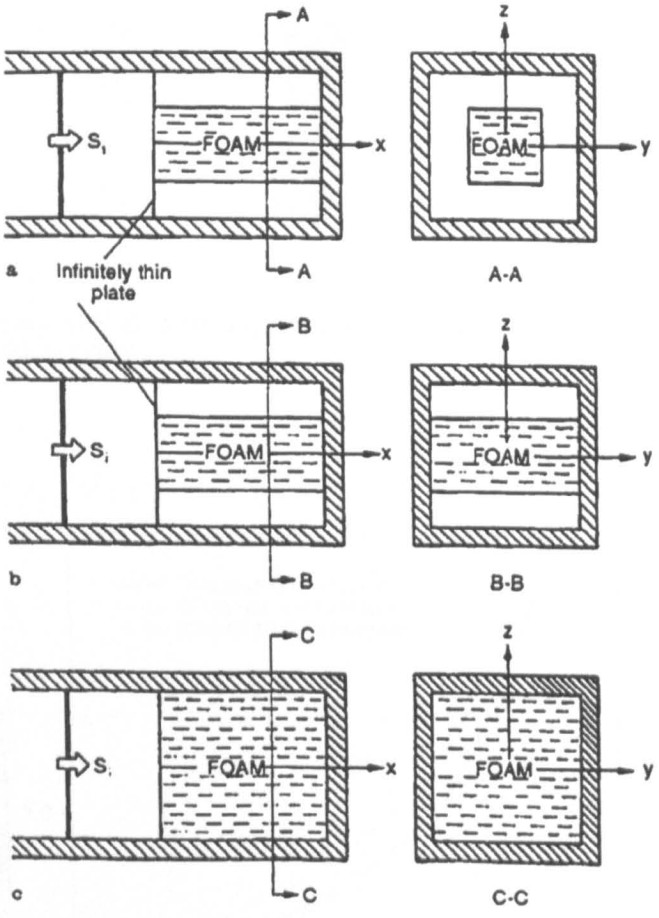

Figure 3.32: Schematics of the equipment required to achieve uni, bi and tri-axial compressive strain. Each diagram shows a sample being compressed in a piston. For uni-axial compression, the sample is compressed along one axis by a force acting on one face. The opposite face is fixed and the other four are unrestrained. For bi-axial compression the sample is loaded in the same way as for uni-axial tension, but two of the free faces are now restrained by the walls of the piston. Finally, for the tri-axial compression load case, all four free edges are restrained by the walls of the piston, such that the sample is forced to assume a cuboid shape at any point during the compression. This is different from volumetric (hydrostatic) compression in fluid, where equal pressure is maintained on all sides, allowing a single-material sample to maintain its relative dimensions. Reproduced from Ben-Dor (1996b).

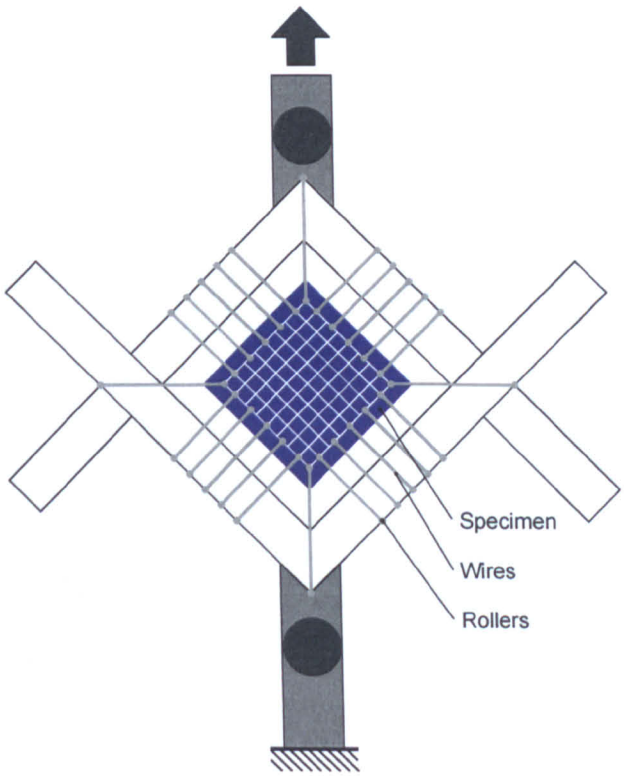

Figure 3.33: Schematic of bi-axial test apparatus for the tensioning of rubber sheet. Reproduced from Blatz (1962).

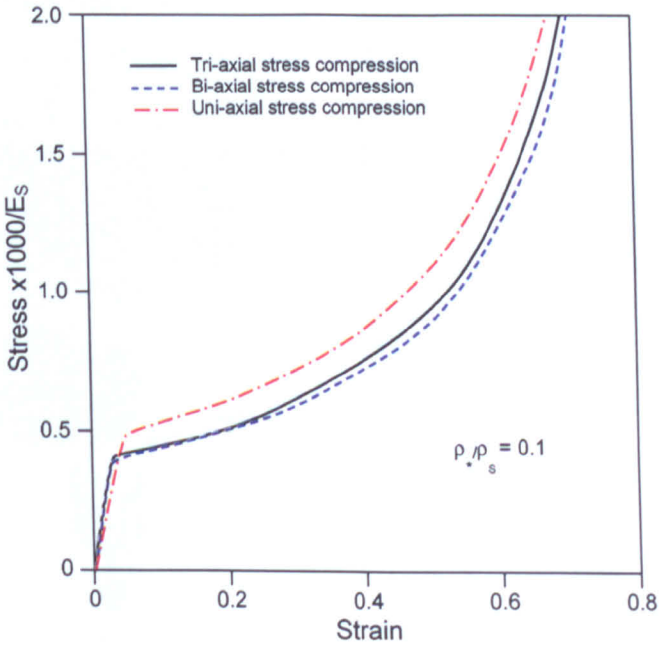

Figure 3.34: Mathematical results showing the difference in stress/strain curve for uni/bi and tri-axial strain. Reproduced from Ben-Dor (1996b).

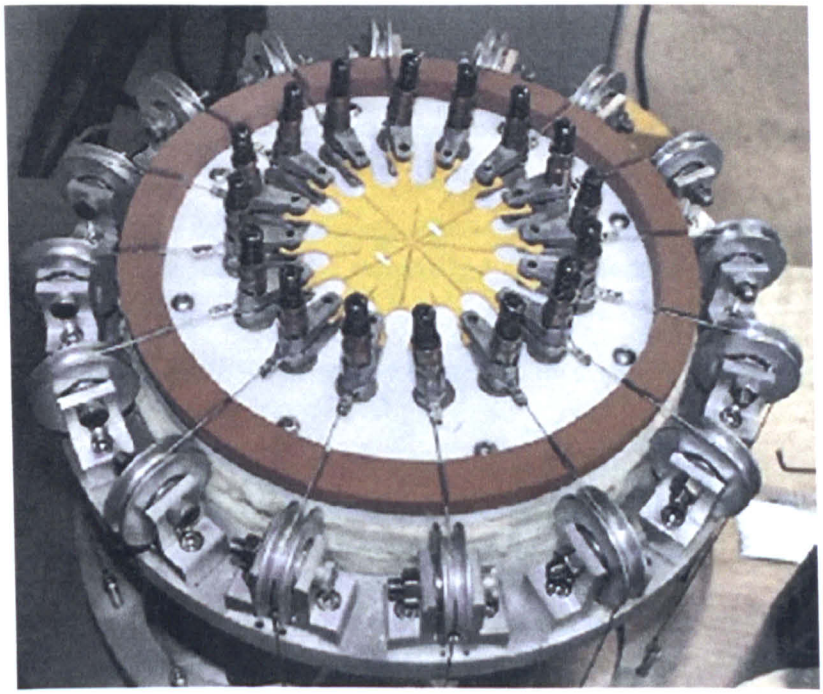

Figure 3.35: Equibiaxial test equipment, used to maintain a constant compression condition in the centre of the test piece. Day (2000).

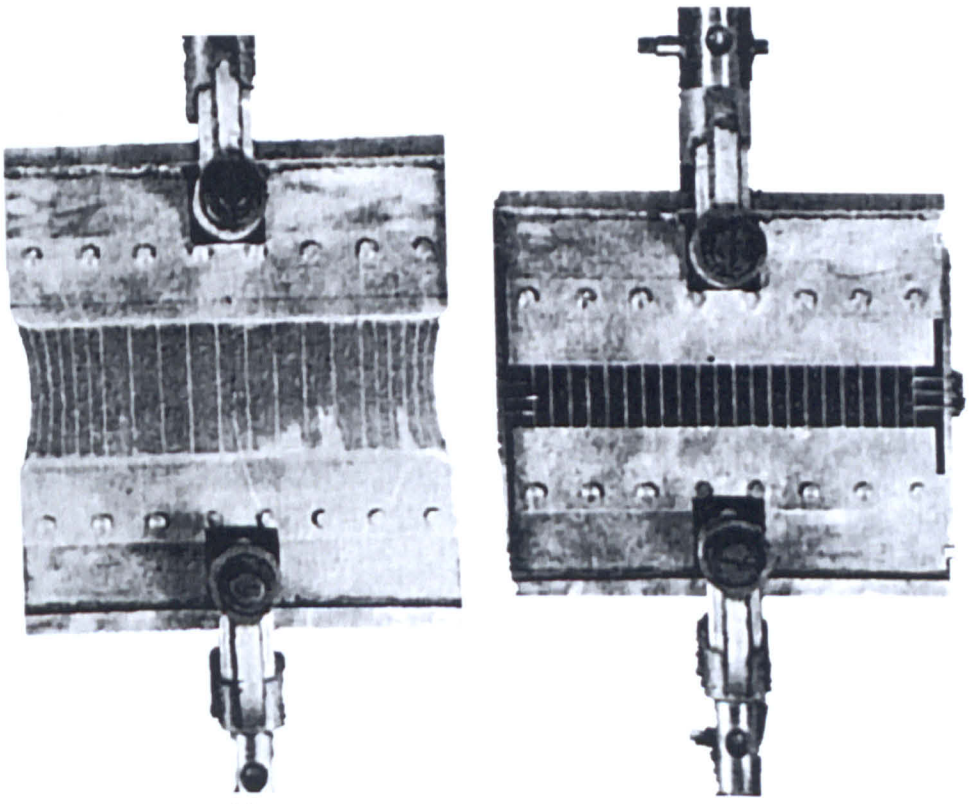

(a) (b)

Figure 3.36: (a) Planar uni-axial and (b) planar bi-axial, tension test equipment. Reproduced from Blatz (1962).

3.5 Chapter Summary

This Chapter has looked at the physical properties of materials used in running footwear. The main points that have been raised are as follows:

- The main materials that provide cushioning and make up the bulk of a midsole have a highly non-linear response.
- This response can be dependant on any combination of temperature, strain rate, strain history, deformation mode, shape and method of manufacture. This may not be an exhaustive list.
- Data concerning the physical response of specific shoe materials, especially foams, is limited and in some cases non-existent.

Any FEA model that aims to predict accurately the stress/strain response during loading must take into account these points, either by including them in the model, or by applying some correction or adjustment to the material models or the final result.

Due to the highly deformable nature of the shoe materials, the test methods are susceptible to distortion effects such as barreling and the inability to firmly hold the sample while it is under test. Initial testing has showed that new test equipment is needed to overcome these problems. Testing the material in non-uniaxial modes also requires new equipment.

Chapter 4

Literature Review: Finite Element Analysis

4.1 Introduction

This chapter presents a very brief overview of the finite element method of structural analysis - a subject which can fill many libraries. A short introduction is followed by reviews of the most advanced (and applicable) models in the public domain at the time of writing. It is expected that models of shoes are being created and used by major manufacturers, but the competitive nature of the footwear industry means these models are unlikely to be released into the public domain in the near future (if at all). Modelling of the human foot has been included as most of the work on shoes to date has come out of a need for analysis of medical footwear, almost all of which developed as an extension of a foot model. The final section goes into more detail regarding the use of ABAQUS, the finite element software used in this research.

This chapter does not aim to assess the required accuracy of the various models that will come out of this research, this is to be achieved through physical testing of footwear samples and parts, and is discussed in Chapters 7-9.

4.2 The Finite Element Method

Finite element analysis is a theoretical mathematical method of predicting the solution to a physical problem by dividing (discritising) the geometry of the problem into small sections (elements). It is normally used when the precise, analytical solution is too complex to be solved (in the time available), and practical testing is either inefficient or not possible. Each element is analysed using relatively simple mathematics and will normally have a linear or quadratic variation of the desired property with length. The large number of simple calculations required for a FEA solution are suited to processing by computer, and the vast majority of FE analyses are now done in this way (except for teaching purposes, where the problems used are very simple). A major advantage of FE over practical testing is that once a model has been verified (proven to be satisfactorily accurate), there is a high likelihood that the internal stresses in the model are similar to that in the real test situation, allowing the user to probe the inner workings of whatever is being modelled. This can be extremely difficult to do, and sometimes impossible, with real testing.

A FE model is normally constructed from geometry, which is discritised into a mesh; a representation of all the elements in the model, connected by nodes. Each node has a given

number of degrees of freedom (variables in the model). Generally these are the 6 spatial degrees of freedom, but others are available, for example: temperature, conductivity and inertia. External forces, fixings and contact between 'objects' are also assigned (known as boundary conditions) to either/both nodes or elements. The elements are assigned mechanical properties (e.g. stiffness) and the problem is then solved in matrix form with appropriate manipulations to give the solution. The size of the matrices directly affects the time taken to process the solution and this in turn is affected by the number of degrees of freedom and complexity of the boundary conditions, as well as of course the processing capabilities of the computer used.

Incorrect specification of any of the material parameters, geometry or boundary conditions, coupled with some unavoidable assumptions that must be made when using the FE technique mean that inaccuracies will be present in the model. It is the job of the FE analyst to be aware of, quantify, minimise and where possible, correct for these inaccuracies.

4.3 Material FEA

The first step in creating an accurate model of a midsole is to model the basic materials that it is made of (in this case mostly EVA foam and TPU). If mechanical tests with simple geometry cannot be modelled correctly then a complex full shoe model will be inaccurate, and therefore of limited use, unless the inconsistencies can be assessed and quantified.

A material model is usually created by fitting an equation to test data, the main equation types being linear (e.g. metals in the elastic region), hyperelastic (high strain incompressible materials, e.g. rubber, TPU) and hyperfoam (high strain, highly compressible, e.g. EVA foam). Details on which material models have been used in the shoe models in this thesis are given in Chapter 7.

Material modelling with FEA can be divided into constitutive and macro-scale models, where the former considers the atomic/molecular response of idealised materials, while the latter works on a larger scale overall response. The equations used in constitutive modelling are normally based on the mechanics of the molecular structure, while macro-scale models use curve fitting techniques. Knowledge of how the models work in principle is essential to using them correctly in a model, however this research will only use current material models' mathematics, and not attempt to develop new equations or fits.

D'Agati (1993) performed linear and non-linear elastic FEA on a simple representation of a midsole, using force input data collected from in-shoe measurements (vertical force only). A single 20-node cube (quadratic) element was used to assess the stress/strain curve, and then this data was used in the midsole model (using the same element type). No numerical results were given, but the paper quotes:

> Differences between the linear model's peak stresses and strains varied from -98% to 680% with respect to the non-linear model's results.

This is attributed to the non-linear response of the EVA material used.

Swigart (1995) used a vertical impact drop test with an 8.5 kg missile impacting onto 'midsole specimens' (the exact nature of these specimens is not specified). Tests results were then applied to an isotropic linear viscoelastic material model and FEA performed. Good correlation was reported for impact heights of 13 & 25 mm, but from 50 mm upwards, the model deviates from the practical results. As an example of this deviation the 50 mm result is shown in Figure 4.1).

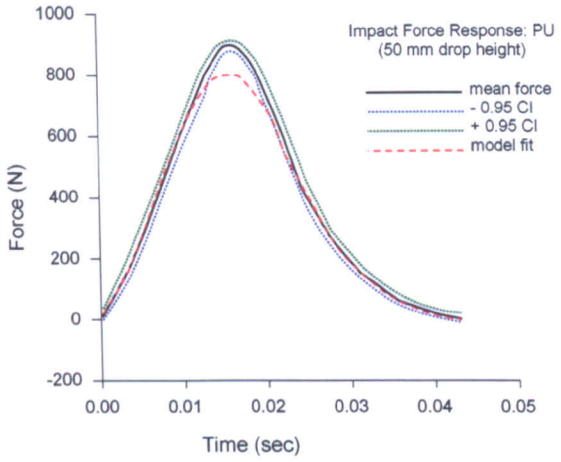

Figure 4.1: Drop tests results from 8.5 kg mass falling from 50 mm onto midsole foam; average test values and model predications are shown. Reproduced from Swigart (1995).

Shiang (1997) used FE to study the cushioning response of an unspecified midsole material. Material properties were obtained from compression of a cylindrical specimen under loading by a vertical actuator (Instron machine). Loading values were taken from in-shoe measurements and an assumed shear force of 1/10th of the peak vertical loading was applied to the model (shown in Figure 4.2). Both linear and hyperfoam material models were used, along with different boundary conditions, and models that included combinations of midsole/insole/insole board. It is not clear if the results of the study were verified by comparing real compression of the midsole with the model results.

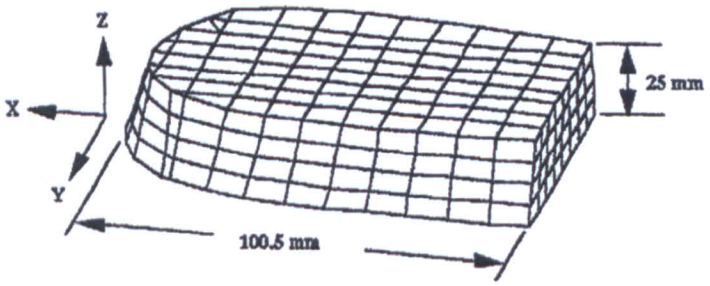

Figure 4.2: FE mesh of a simple EVA shoe heel. Shiang (1997).

The response of the foam in car seats was studied by Pajon (1996). Mechanical tests were performed and the test data used to verify the material models. The report notes the importance of verifying the simple material models with complex real parts, as the car seat foam is in a combination of compression and tension and may not be modelled accurately with uniaxial mechanical tests (as can be seen in Figure 3.31).

Thomson (1999) used uni-axial test data to create a hyperfoam material model, and used this to model the heel impact. To reduce processing time, only a cylindrical section of the heel was modelled (this allowed a 2D axisymmetric model, as shown in Figure 4.3). The model was pinned at the base and the nodes on the vertical walls were constrained to move in the vertical direction only. The accuracy of these boundary conditions is questionable and may require practical investigation, although results for this simple model are consistent with the mechanical tests (Figure 4.4).

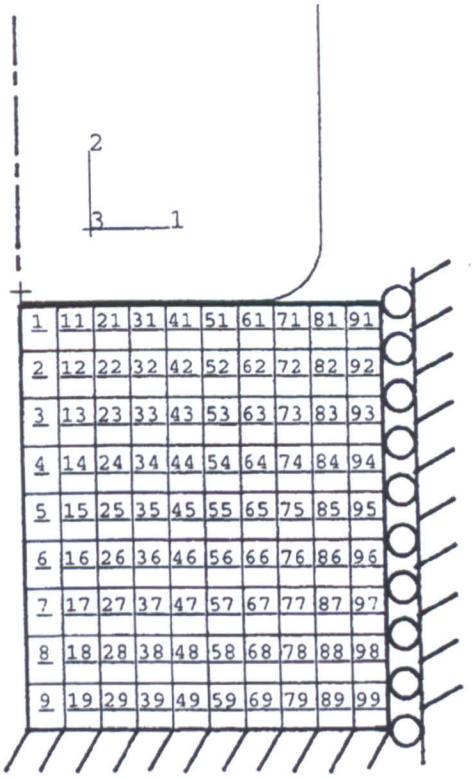

Figure 4.3: 2D axisymmetric model of a heel impact (numbers shown correspond to node numbering). Thomson (1999).

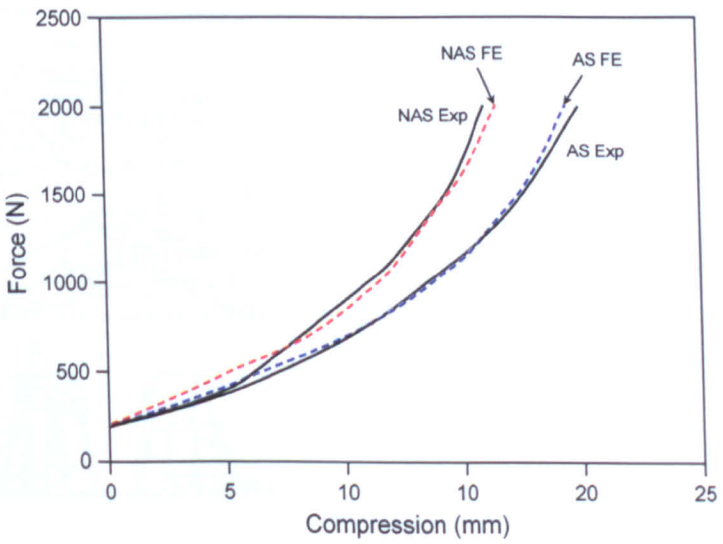

Figure 4.4: Experimental and FE results from testing of midsoles that contain (AS) or do not contain (NAS) air pouches. The no-air-pouch model is shown in Figure 4.3. Reproduced from Thomson (1999).

4.4 FEA Models of the Foot

Although the forces on the upper surface of the midsole can be measured (Section 2.9), the forces recorded are dependent on the shoe used for the test (as the foot is flexible). Where prototype shoes are available, the forces at the ground/shoe and shoe/foot interfaces can be measured, but the application of these boundary forces to models of entirely new shoes must be carefully considered. To model the forces on the shoe more accurately, some research has gone into modelling the foot. Most of the work aimed at foot-shoe interaction has been concerned with the effect of the heel pad, as this directly affects the peak forces in the heel strike (as discussed in Section 4.5).

Aerts (1993) looked at the effect of various midsoles on the forces transmitted to the leg using human test subjects, but had problems restraining the leg and so the results suffered from inaccuracies. The approach of Noe (1993), although slightly less practical, was more successful. By using fresh human cadaveric lower leg specimens, the bone could be bolted directly to a plate, eliminating any excess vibration. Tests were carried out barefoot and with different midsoles and the report concludes that any evaluation of the shock absorbency of a midsole must take into account their mechanical interaction with the body.

Nakabe (2002) used a moderately complex FEA model of a foot to assess the rotation of the joints during running with a selection of midsoles with stability correction inserts (Figure 4.5). The results were validated with barefoot running and good correlation can be seen for the modelled part of the footstrike (Figure 4.6).

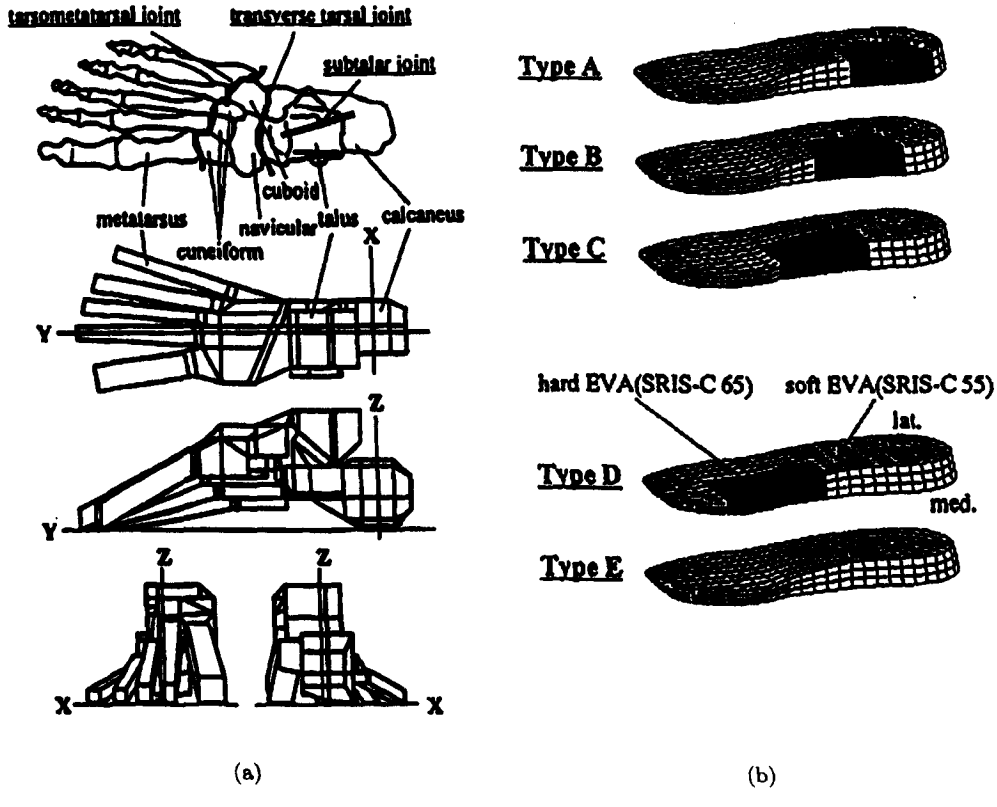

Figure 4.5: (a)FEA model of human foot, (b) FEA model of midsoles with stability correction inserts. Nakabe (2002).

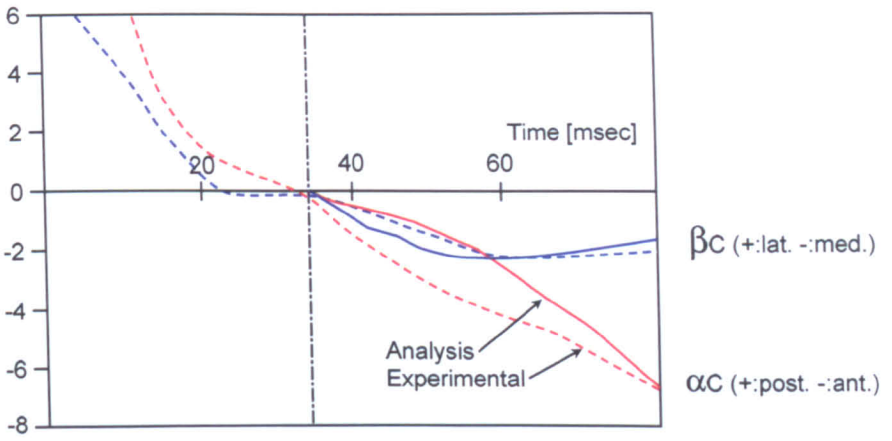

Figure 4.6: Results of FEA combined foot/midsole model. αc = rotation of the foot plantar-dorsiflextion, βc = inversion-eversion. Reproduced from Nakabe (2002).

The foot model was progressed by Chen (2003), who modelled the larger bones in the foot and used cable elements to simulate the ligaments. The bones were covered with 'skin' to allow the determination of plantar stress distributions on simple midsole surfaces (Figure 4.7). All biological materials were assumed to be linear elastic, the properties are listed in the paper, but the method of determination is not specified.

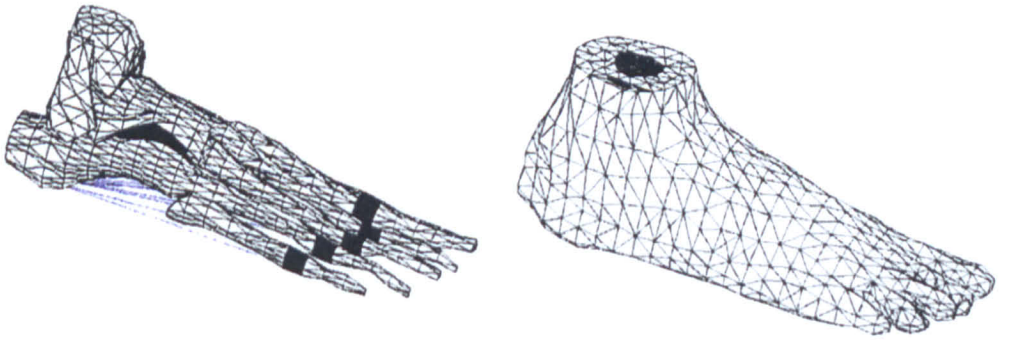

(a) (b)

Figure 4.7: (a) FEA model of the foot bones with cartilage and major plantar ligaments, (b) complete model of the foot with soft tissues. Chen (2003).

At the time of writing, Cheung (2006) has produced the most realistic foot model. Using images from magnetic resonance scans of a foot, all bones, ligaments and covering flesh are modelled (Figure 4.8). All materials are linear elastic, except the soft tissue and midsole which are modelled as a hyperelastic and hyperfoam material respectively (actual values and sources are given). The paper does not specifically state the verification process used, but in a presentation to the 2006 ABAQUS User's Conference, the author described experimental loadings of cadaveric foot samples with tendons loaded to simulate various stances. The shoe used in the report is a simple extrusion of hexahedral elements from the flat floor to a surface of a medical insert for a shoe (Figure 4.9).

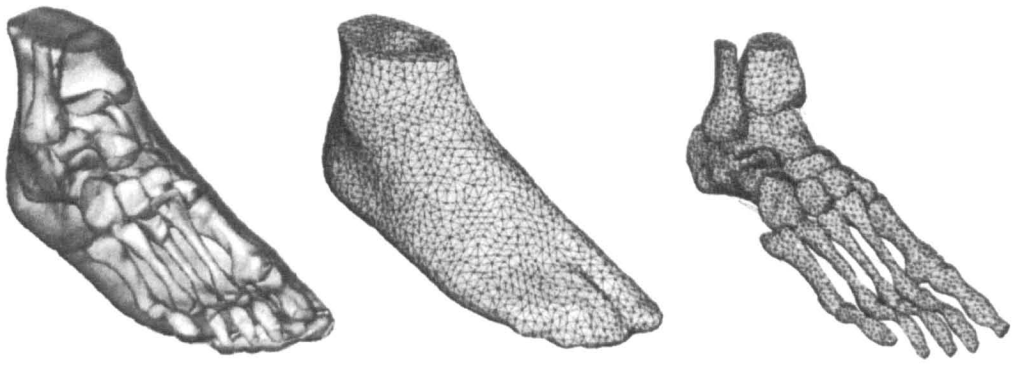

Figure 4.8: Left to right: Surface modelled of a MRI scanned foot, FE mesh of encapsulated soft tissue, FE mesh of bony structures. Cheung (2006)

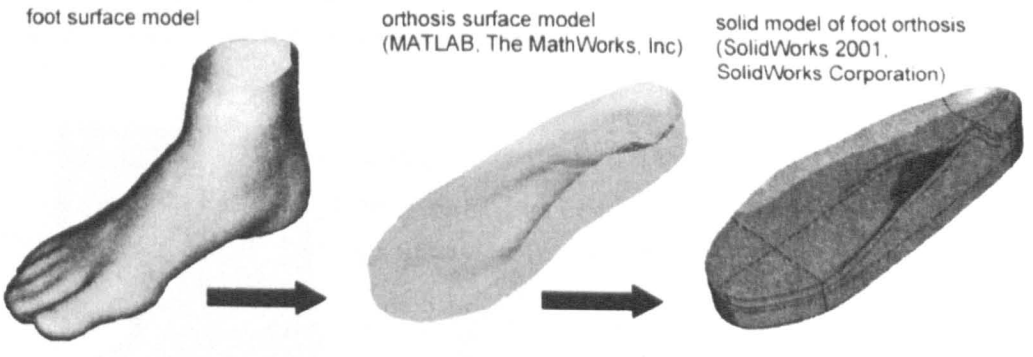

Figure 4.9: Procedures for creating the midsole (foot orthosis model). Cheung (2006).

4.5 FEA Shoe Models

There is little published research on the use of FEA to model complex 3D shoe models, due to the fact that this approaches the limits of complexity of the available technology and so is likely to be commercially sensitive information (and therefore not being released in full at this time). This section discusses models that have been found in the public domain at present.

A reasonably complex 2D model of a therapeutic shoe was performed by Lewis (2003). The model included some mesh refinement, but assumed all the materials behaved elastically. A static load case was assumed (Figure 4.10). Lewis' results show a difference in the behaviour of the shoe when certain materials are substituted. However, none of the calculations are verified with practical testing.

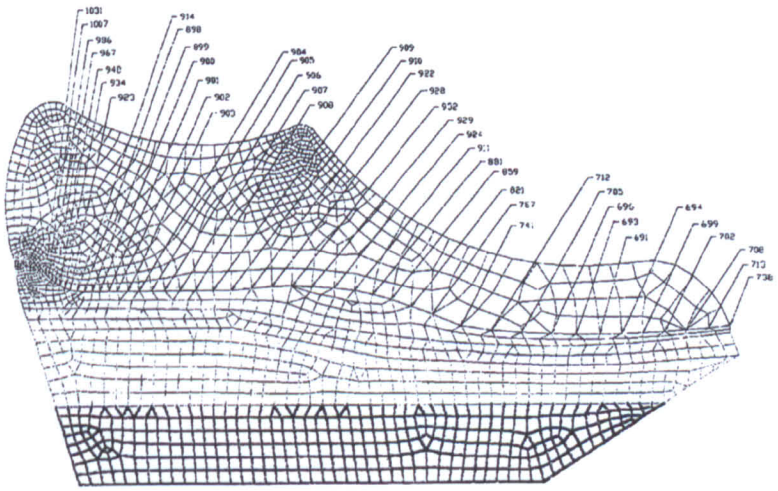

Figure 4.10: 2D model of a therapeutic shoe. Numbers indicate nodes of interest in this model. Lewis (2003).

Verdejo (2002) created a similar model to that of Thomson (1999), but with the inclusion of the heel pad. The Ogden hyperfoam material model was used, with data taken from mechanical testing. Model results were verified against ASTM mechanical testing (Figures 4.11-4.12). Verdejo reports that the ASTM testing produces a different pressure distribution on the upper surface of the EVA midsole, compared to that measured in the shoe or predicted by FEA.

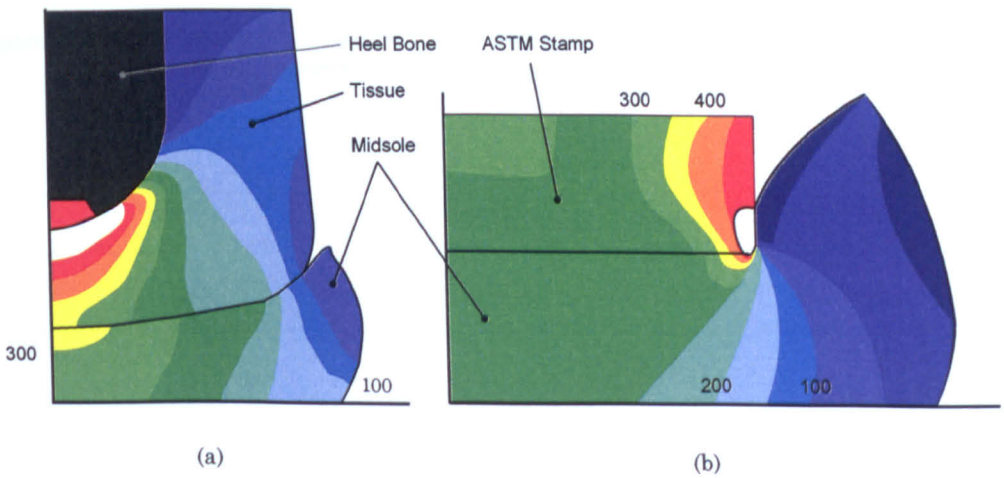

Figure 4.11: Contours (kPa) of stress distribution for (a) Heel bone and pad on EVA midsole, (b) ASTM heel on EVA midsole. Reproduced from Verdejo (2002).

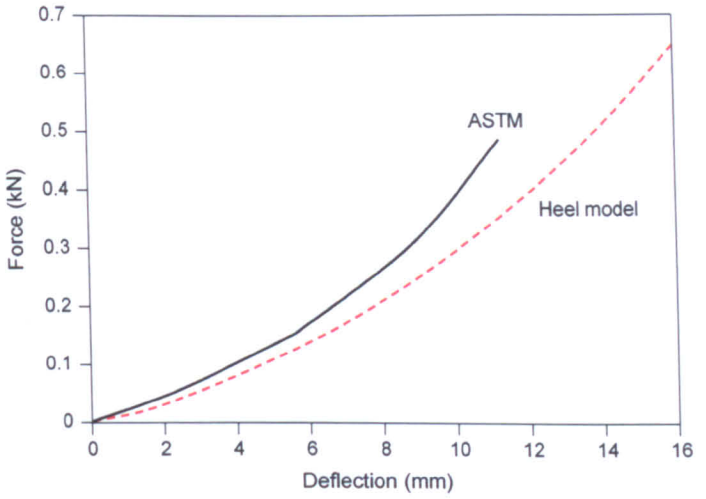

Figure 4.12: Comparison of model results and ASTM mechanical testing for model in Figure 4.11(b)). Reproduced from Verdejo (2002).

The only FEA model found to use realistic 3D midsole geometry was found in Nishiwaki (2002). It is shown as a practical implementation of a system for predicting human response to midsoles using human drop tests (see Section 2.9). Very little information is given about the FEA model but the report concludes, "the simulation method is a very powerful tool in the design of shoe soles". The result of the FEA model is shown in Figure 4.13. Results from an investigation into the effect on cushioning of varying sandwiched EVA layers are also presented in Nishiwaki's paper.

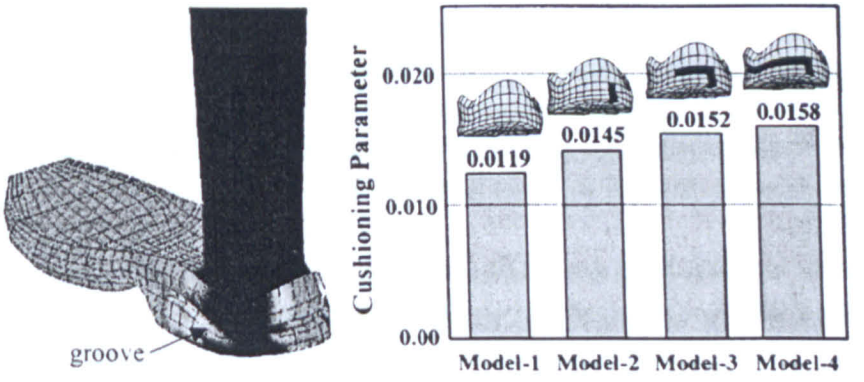

Figure 4.13: FEA model of a midsole using realistic component geometry. Black areas indicated on the chart represent areas of reduced stiffness in the model. Nishiwaki (2002).

4.6 Modelling in ABAQUS

There are a number of FEA packages available on the market at present. ABAQUS was selected as the solver primarily as it is used by adidas, but it also has a reputation as one of the most accurate mathematical solvers available.

This section will present a concise description of the physical and mathematical principles required to understand the workings of the ABAQUS code. Exhaustive mathematical proofs of all the required matrices and equations are provided in the ABAQUS instruction manuals, so only a few important equations are given here. Where necessary, some wording and quotes have been taken from the various ABAQUS manuals.

The bulk of the materials in the shoes to be modelled are classed as hyperelastic. That is to say that their stress/strain response is non-linear and modelling requires information about this response, ideally, for all strains that are to be modelled. This allows ABAQUS to create the deformation gradient matrix, $\mathbf{F}$, as follows:

$$\mathbf{F} = \frac{\partial \mathbf{x}}{\partial \mathbf{X}}$$

where $\mathbf{X}$ is the initial position of a material particle (for this purpose an integration point on an element) and $\mathbf{x}$ is its new position. For hyperelastic materials, because the stress/strain response is known over a wide range of strains, the gradient matrix can be calculated. For elastic materials, the assumption that the movement of the point is negligible is made to allow the Cauchy (or 'true') stress measure to be used.

To calculate the solution to these matrices ABAQUS comes with two primary solvers; Standard and Explicit. The main difference between these solvers is the way they solve the matrices over time; Standard is implicit - it calculates the value of the result matrix based on the values of the input matrices and the result matrix itself, that is the process is iterative. Explicit, as its name suggests, solves the matrix explicitly; assuming a negligibly small increment between one state and the next, using the result matrix with no further checks. Each of the solvers allows a computational job to be split into steps; separate calculations where the final result of one step forms the initial result of the next. In each step various conditions of the model can be altered.

Standard lends itself to efficient calculation of static and quasi-static problems, but for problems that require the inclusion of inertia, Explicit is better suited. The Explicit solver also has a more robust set of methods for the solution of complex geometry and contact problems and is used almost exclusively in this research for the modelling of shoes. Standard could be used for the modelling of small, simple parts, but the need to predict the behaviour of a part or material sample in the Explicit whole shoe model outweighs the performance advantage of using Standard for such jobs. As an example, the initial modelling of a simple shoe was performed in both Standard and Explicit; a forefoot cushioning test on the Supernova model taking 11.1 minutes in Standard, and 274.5 minutes in Explicit. These jobs modelled the boundary conditions as prescribed constraints, but when 'physical' experimental parts such as the stamp and floor were added, the Standard job failed to converge on a solution and had to be abandoned, most likely due to the required increase in contact calculations.

4.6.1 Material Models

The equations derived to form the range of material models that are available in ABAQUS are numerous and extensive, so this section will concentrate on the material models selected for use in shoe modelling. These comprise the elastic, hyperelastic and hyperfoam models. The specific forms of these models are known as strain energy potentials.

Elastic The elastic material model assumes the stress experienced by an element is directly proportional to its strain. This model has been used where there is little information on material properties, or the material shows an elastic response up to 5% strain and then deforms plastically.

Hyperelastic The hyperelastic material model was designed for use with 'rubber-like materials at finite strains' and 'provides a general strain energy potential to describe the material behaviour for nearly incompressible elastomers'. It is a non-linear elasticity model suitable for large (>5%) strains, and is therefore suitable for modelling of shoe components, in particular outsoles and the structures and mechanisms of the new generation of shoes (preliminary modelling showed strains of up to 40% for materials in both EVA and structure components in simple shoes). The hyperelastic model assumes isotropy for the following reasons:

> The initial orientation of the long-chain molecules in elastomeric materials is assumed to be random - therefore the material is initially isotropic. As the material is stretched, the molecules orient themselves, giving rise to anisotropy. However, the development of this anisotropy follows the direction of straining - hence, the material can be considered to be isotropic throughout the deformation history. As a consequence, the strain energy potential can be formulated as a function of the strain invariants.

The strain energy potential defines the strain energy stored in the material per unit of reference volume (volume in the original configuration) as a function of the strain at that point in the material. ABAQUS provides a number of different forms of strain energy potential to model the approximately incompressible elastomers, including: Arrunda-Boyce, Mooney-Rivlin, neo-Hookean, Ogden and Yeoh forms. Some of these are derived from purely polynomial curve fitting, while others are phenomenological - they are based on extrapolations of the underlying cellular/molecular structure of the material. The exception is the Marlow form, which is designed to fit any test data to a fairly smooth non-polynomial curve. The choice of a particular form should be based primarily on verified model results.

All the energy potential forms require some kind of sample data to formulate their coefficients, the most basic requirement being uni-axial tests (see Section 3.4). The uni-axial data only specifies the material property in one compression/tension mode, so assumptions are made about the other modes unless extra test data from bi-axial and tri-axial experiments are included. The use of tri-axial data is recommended when the material being modelled is compressible. Once data has been inputted, ABAQUS calculates the required energy potential form coefficients and allows the user to compare results for a given range of strain - useful for checking if any of the forms becomes unstable in the expected range of strain.

Hyperfoam The ABAQUS hyperfoam model is similar to that of the hyperelastic model, but it accounts for the difference in deformation modes in compression and tension exhibited by most elastomeric foams (see Section 3.3.1). The model is designed for materials that can deform elastically to large strains, including up to 90% in compression. Isotropy is assumed.

4.6.2 Material Model Modifications

In addition to a non-linear elastic stress-strain response, shoe materials (especially foams) can contain a number of energy-loss mechanisms (as discussed in Section 3.3). The resulting overall response of the material is vital for providing the correct performance during a running strike and so any computer model that attempts to simulate the entire footstrike accurately must contain representations of these mechanisms.

4.6.2.1 Hysteresis and Viscoelasticity

A repeatable change in the stress-strain response between the loading and unloading cycle, and the resulting energy loss, can be modelled either with the *HYSTERESIS or *VISCOELASTIC functions within ABAQUS. Both models take a defined stress-strain response and modify it with relation to the strain rate the material experiences. The main difference between the two models is that *HYSTERESIS can only be used with large-strain hyperelastic models, not hyperfoams, due to the model assuming no strain-rate dependance with a change in volume, but only in shear. The viscoelasticity model allows a range of inputs, including specification of the strain-rate response using a Prony series, normally obtained from multiple creep tests, or DMA (Dynamic Measurement Analysis) which provides a much faster physical test and is described in detail in Section 5.2.4.2.

4.6.2.2 Mullins Effect

As discussed in depth in Section 3.3.3, the Mullins effect provides a way of dissipating energy from the model via permanent deformation of the material. It is strain and strain-history dependant. To incorporate this damage into the material model, ABAQUS uses a damage calculation that removes a given amount of strain energy upon loading of the material. This can be expressed:

$$U_{Total} = (U_{stored} + U_{lost})_{Deviatoric} + (U_{stored} + U_{lost})_{Volumetric}$$

When used with *HYPERELASTIC, the *MULLINS EFFECT calculation assumes that only the deviatoric strain is subject to loss. When using *HYPERFOAM, damage occurs on both deviatoric and volumetric strain.

The variables for the damage model can be inputted directly, or derived from multiple strain-level cyclic test data by way of a least squares fit, as is done for specifying the primary behaviour via *HYPERELASTIC or *HYPERFOAM. However, the ABAQUS documentation does strongly recommend that the resulting fitted coefficients are verified by single-element models against the test data.

4.6.2.3 Combining Material Model Modifications

The materials used in shoes are subject to hysteresis, viscoelasticity and the Mullins effect. Unfortunately, these energy loss mechanisms are currently incompatible within ABAQUS; *MULLINS EFFECT cannot be used in conjunction with *VISCOELASTIC or *HYSTERESIS. Even if the material data are collected from samples pre-strained to the average maximum strain seen in use, this data will be too stiff or too soft for the majority of the material. This is not so much of a problem in simple geometry shoes where the strain is fairly constant, but it is a major issue in structure shoes. As the Mullins effect can greatly reduce the stiffness of a section of material, there is a real risk of under-prediction of stress in a component that could result in material failure. While the material model could be created from pre-stressed material data, this will only predict correct stresses in simple, homogenously strained parts.

Components with highly varying strain fields (such as the Ultraride structure plate under a heel stamp test, Figure 4.14), will not have their stress predicted correctly using a single material curve.

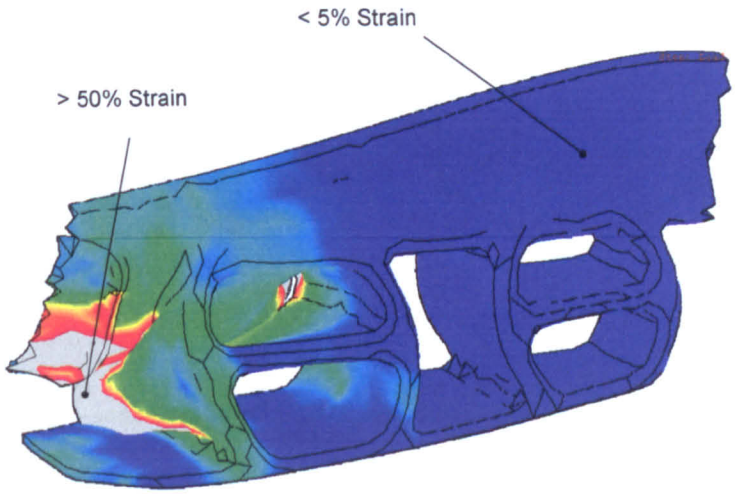

Figure 4.14: Strain result from a heel stamp test performed on the structure plate of the Ultraride, showing a large range of strains occurring in the same part.

Recent work by Bergström (2006a) has produced a phenomenological material model that extends the functionality of the ABAQUS *HYSTERESIS command to incorporate the Mullins effect and include rate-dependency. This model was not available during the research for this thesis, but it has the potential to be very useful for future work.

A less practical method of including rate-dependency and the Mullins effect is described in Section 8.5, where a model is run using *VISCOELASTIC and the results analysed for strain levels and the material model adjusted accordingly for the next iteration. This method has two main drawbacks; the material models are discrete and each iteration requires a complete re-run of the analysis, extending development time.

4.6.2.4 Bulk Viscosity

If neither viscoelasticity, hysteresis nor Mullins effect is specified, a material in a dynamic, temperature independent, elastic model has no method of dissipating energy which can result in unstable models. To this end ABAQUS applies an energy loss mechanism known as *bulk viscosity* to reduce the likelihood of elements under high strain-rates collapsing in Explicit. The application of bulk viscosity is discussed in Section 4.6.4.2.

4.6.3 Element Performance and Selection

Various element types are available in ABAQUS, but this section will pay attention only to those to be used in the modelling of shoes: three dimensional tetrahedral and hexahedral. The basic elements, C3D4 and C3D8 are shown in Figure 4.15. Across each face, and between the faces, lines of integration exist where the properties and response of the element are calculated during the analysis. The more integration points and lines an element contains, the more detailed the changes in property across the element can be modelled.

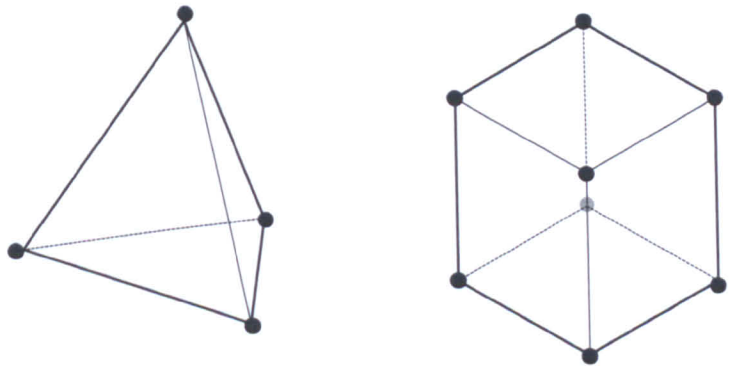

Figure 4.15: 4-node tetrahedral (C3D4) and 8-node hexahedral (C3D8) elements

These are the most mathematically simplistic of the 3D solid elements, and as such are the most computationally efficient. These elements cannot be used in all circumstances however. For example, the linear C3D8 element will become 'shear locked' when used in a direct bending model (Figure 4.16). The linear hexahedral element begins the step as shape (a). In the physical solution the element should become (b), but as the element formulation has a constant strain, the integration lines (dashed) must remain of equal length and the sides of the linear element cannot bend, generating large shear stresses (c), resulting in a stiffness modulus that approaches infinity.

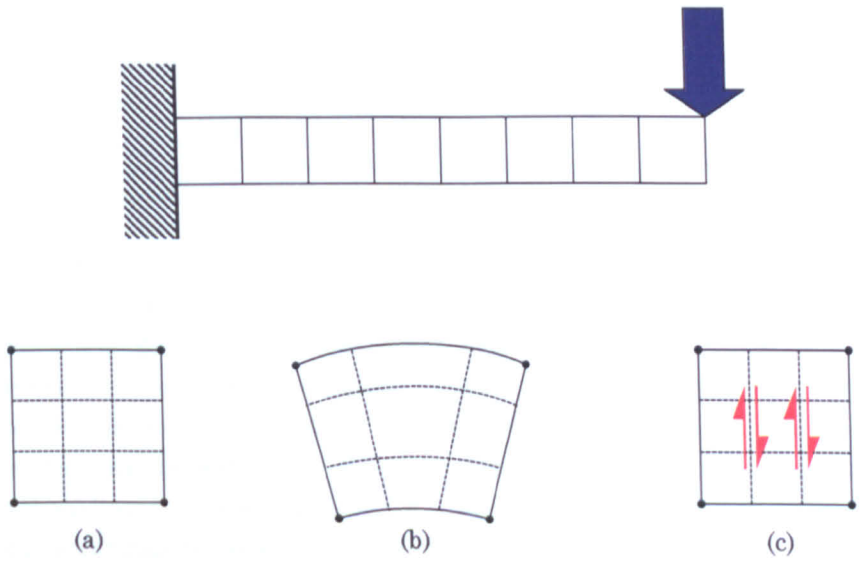

Figure 4.16: Linear hydrostatic elements in a simple bending model (top). (Note: For simplification of the diagram, only 2D elements are shown, but the principles also apply to the 3D).

To overcome this problem the element must be substituted for the quadratic version (C3D10 and C3D20, Figure 4.17), which allows a variation in strain, or have its integration modes reduced (C3D8R) giving a single deformation gradient across each face. A fine mesh of reduced elements arranged in layers more than one element thick is recommended for meshes that are likely to see high distortion.

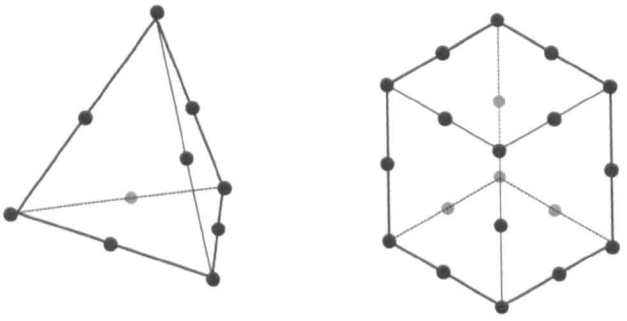

Figure 4.17: 10-node tetrahedral (C3D10) and 20-node hexahedral (C3D20) elements

Reduced integration elements can however exhibit hourglassing modes (Figure 4.18) where the stiffness of the element is effectively zero as a change in the shape of the element does not always result in a change in the length, or relative angle, of the integration lines.

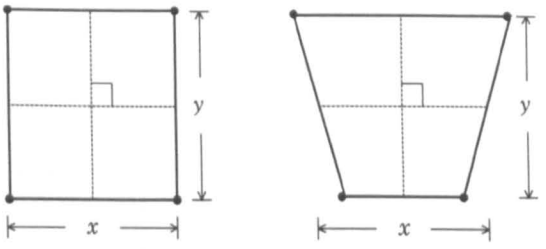

Figure 4.18: An element exhibiting an hourglassing mode. Note the change in shape of the element with no change in the deformation gradients.

To combat this behaviour, a number of controls are available to modify the behaviour of the element. The default control in Explicit is 'Viscoelastic', where the rate of volume change of the element is artificially damped at the start of a step, after which control is based on the stiffness response of the material. This initially stops the hourglassing, but assumes that the maximum load change will occur at the beginning of the step, which is not always the case.

This problem can be overcome by using the 'Enhanced' hourglassing control, which combines a stiffness based and viscoelastic based control of the deformation throughout the step. This results in a small decrease in element efficiency, but is vital for some jobs to run with realistic results (the use of a purely viscoelastic control, while more efficient, can result in severe hourglassing in quasi-static conditions during a step).

Another method of avoiding the shear locking problem is the use of incompatible mode elements (C3D8I, Figure 4.19). Additional integration modes are added on the diagonals of the element to control the trapezoidal distortion associated with locking.

In general all elements produce more accurate results the closer to their ideal shape they are (e.g. square faces at 90° for hexahedral elements). Generally tetrahedral elements have lower sensitivity to distortion so are recommended for meshes undergoing high strains, though

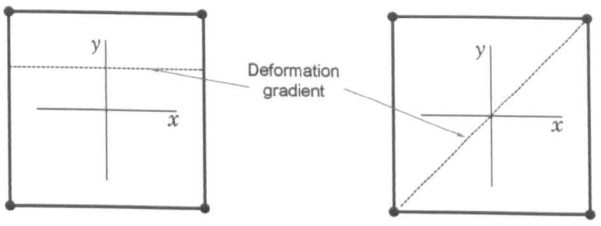

Figure 4.19: Face of a C3D8 element with normal (left) and incompatible (right) density gradient modes.

the increased numbers required to fill the same volume will create a slower running job.

The modelling of incompressible substances (where the Poisson's ratio, ν, of the material is close to 0.5), can give rise to problems due to round off errors, as the stress increase for a given deformation approaches infinity as ν approaches 0.5. To avoid this, hybrid elements are offered that calculate the pressure stress and displacement stiffness as separate, but coupled, variables.

4.6.4 Job Controls

It is often the case that a more accurate finite element model requires the addition of more physical processes into the calculations with a resulting increase in the time taken to process. Although performance of easily available desktop computers is increasing at a steady rate, there still may be a need to reduce the time taken to achieve a useful result from FEA. These controls are discussed here in theory and in Section 8.4.2 with relation to practical application.

4.6.4.1 DOF Reduction

The most obvious way of reducing the processing time of a job is to reduce the amount of calculations required. This can be achieved by reducing the number of degrees of freedom (DOF) in the model. Replacing quadratic elements with linear ones is a quick method of achieving this (provided any interactions or boundary conditions are specified on an element basis), though there is a notable performance difference between some types of elements, as discussed in Section 4.6.3.

If a reduction in accuracy is acceptable, then physical processes can also be removed (such as viscoelasticity). However, if removing these process destabilises the model, causing vibration and extra movement, the number of iterations a job needs can increase, having the reverse effect and slowing the overall job time down.

If parts of the model have a negligible effect on the current test, then they can be removed or substituted. For example, if the interest is in the performance of a heel part under heel cushioning, then the forefoot of the model could be meshed coarsely, or removed entirely. This can give significant reductions in job times, but the effects on the results should be checked.

4.6.4.2 Mass Scaling

As discussed at the start of this section, for simple problems ABAQUS/Standard is a very fast solver, but it drastically loses efficiency as the models increase in complexity, and in some contact models cannot provide a solution. To provide faster solutions using ABAQUS/Explict,

a number of solution controls are used, the most powerful (and complex) of these being mass scaling.

The total time a job will take to process is roughly dependant on the number of degrees of freedom to be solved in each increment and the number of increments to be solved. The solver automatically limits the size of the time increment based on the global stable time (Δt) of the model. Fundamentally this is a measure of the shortest time it takes a stress wave to propagate across any of the elements, this is based on factors including stiffness, size and damping, following the equation:

$$\Delta t = min\left(L_e\sqrt{\frac{\rho}{\hat{\lambda}+2\hat{\mu}}}\right) \tag{4.1}$$

where L_e is the characteristic length of an element (in an undamped material this is the length of the shortest side), ρ is the density and $\hat{\lambda}$ and $\hat{\mu}$ are the effective Lamé's constants, which are derived:

$$\hat{\lambda} = \lambda_0 = \frac{\nu E}{(1+\nu)(1-2\nu)}$$

$$\hat{\mu} = \mu_0 = \frac{E}{2(1+\nu)}$$

where ν is Poisson's ratio and E the Young's modulus of the material (ABAQUS Analysis User Manual 6.3.3).

As a result of this, any model with unrealistic, super light or stiff materials will produce a very small time increment. Elements with super light or soft properties are likely to be deformed and crushed, also producing a short wave speed and thus a small time increment.

However, using mass scaling, the time increment can be controlled by varying the density of the material with values selected to either fit to a user-specified time increment or level of scaling. The level of scaling is specified as a multiple and reported as a percentage increase in overall mass. Mass scaling is excluded from gravitational calculations, so the extra mass cannot be "weighed" in the model, it only causes an effect through a change in inertia (ABAQUS Analysis User Manual 7.6.1).

The automatic controls can be overridden in a number of ways, ranging from specifying a set increment (for example in jobs involving only rigid bodies), to giving merely a start value and allowing the solver to adjust values throughout the job. This can decrease job time by orders of magnitude, but can affect the output significantly, and may cause job failure or non-physical results. While the ABAQUS manual recommends limiting the mass increase to around 2%, useful qualitative results have been achieved with scalings of up to 1,000,000%, corresponding to a reduction in job time of around 1000 times (see Section 10.4). While this contradicts the advice against using super-stiff materials, with shoe modelling the scaling is applied mostly to the steel impactors, which undergo very small deformations and if their movement is specified by position, then the extra mass has a negligible effect on the result.

Mass scaling is automatically applied to all Explicit jobs in the form of bulk viscosity. By adjusting the density of the material slightly, a similar effect to that of the element floating in a viscous fluid is achieved - this is very similar to directly applied mass scaling, but on a much smaller scale. Bulk viscosity (ρ_{bv}) is calculated thus:

$$\rho_{bv} = (bL_e\dot{e}_{vol})^2 \tag{4.2}$$

where b is the inputted co-efficient and $\dot{e}_{vol}$ the volumetric strain rate. The automatically-

calculated bulk viscosity has been found to be ineffective in most of the shoe models, as the time increments are quite large to begin with.

Fixed Time Increment Generally it is best to allow ABAQUS to calculate the time increment in an Explicit job automatically; this allows the time increment to reduce in response to very small elements, but also to increase when the computation becomes less demanding. However, during some models where there are stiff parts that undergo little strain (such as drop tests), the part can be made rigid (either as a new rigid part, or using *RIGID) and mass scaling can be applied to all of the model *excluding* that part. Using the fixed time increment 'drives' the job along at a constant rate, ignoring the limitations of the stiff elements in the rigid part. This method can give very fast processing jobs, but will fail if there is moderate to severe mesh distortion anywhere within the model.

4.6.5 Contact

Contact in FE models should occur when two or more objects collide. However, objects will occupy the same physical space without having an effect on each other unless a specific contact interaction has been defined between two or more surfaces (external parts of objects), which must also be pre-defined. ABAQUS allows surfaces to be specified as node-based, element-based or analytical rigid. Node based surfaces are non-continuous as nodes are intersections of element edges and are mathematically considered discrete. Element surfaces are continuous, and contain more information about a given surface as the curvature and area of each element is known - this allows more accurate calculation of the transfer of forces between two element based surfaces and leads to much better results for contact problems. Analytical rigid surfaces are a special case as they are described using straight and curved line sections, either rotated or swept to form simple shapes. They allow much better definition of curved surfaces (as they are not discritised), but their use has restrictions.

Contact between one node-based surface and another, or contact with itself, is not permitted in ABAQUS, the same is true for analytical rigid surfaces. Element-based surfaces are allowed to interact relatively freely. Each interaction requires a definition of the interaction and an algorithm for calculating the result.

4.6.5.1 Interaction Definition

Contact is a large set of complex mathematical descriptions and is treated differently within Explicit and Standard. As Explicit is used in the vast majority of the models created in this research, only this is discussed (in brief) here. Full details of all the theory and formulations is found in the ABAQUS Analysis User Manual 21.1.1.

There are two methods available for defining contact between surfaces in Explicit: general contact and contact pairs. General contact sets up every element in the model as a single surface and allows this master surface to contact itself. The contact pair method requires the User to specify a pair of surfaces. The advantages of each method are summarised:

General Contact

- A single surface can span multiple objects.
- A surface can have both rigid and deformable regions.
- A surface can have solid and shell elements.
- Nodes can have contact with more than one surface at a time (very useful for modelling objects with corners).

- T-junctions of shell elements can be modelled with one surface.
- Changes can be made to surface descriptions between modelling steps.
- General contact has a built-in surface smoothing algorithm for element based surfaces.

Each of the functions above are not available when using contact pairs. Conversely, the following functions are only available with contact pairs:

Contact Pair

- 2D surfaces can be defined.
- Analytical rigid surfaces can be defined.
- Thermal contact can be defined.

The limitations on each method are reduced with each new version of ABAQUS, for example, both methods have to be used in shoe models as the structures have too many surfaces to define as pairs, but the floor is usually modelled as an analytical rigid body, requiring a contact pair (the latter limitation is to be removed in ABAQUS version 6.6).

The default setting for the contact algorithms are also different; general contact uses the penalty enforcement algorithm while contact pair uses kinematic.

4.6.5.2 Contact Algorithms

ABAQUS includes two main methods for processing surface contact; small-sliding and finite-sliding. Small-sliding assumes a negligibly small displacement of one surface along another and does not allow separations after contact, but is much more computationally efficient. Finite-sliding allows any finite movement of the two surfaces, including separations, with a reduction in efficiency. To correctly model any interactions between surfaces in shoes the finite-sliding method must be used as separation can occur after contact.

The Explicit solver provides many options for the algorithms that deal with the finite-sliding motion, but the main choice in job set-up is the use of kinematic or penalty contact enforcement:

Kinematic For each time increment the kinematic algorithm will first displace nodes, then calculate the pressure increase generated by the penetration of one surface into the other (a non-physical condition). Corrections are then made to satisfy the pressure balance (but not necessarily the penetration). The sub-options of 'hard' and 'soft' contact can also be specified (ABAQUS Analysis User's Manual: 22.1.2), where hard contact transmits forces between surfaces with zero distance between them. Soft contact gives a linear relationship between the percentage of the force transmitted and the distance between the surfaces (this can be a positive or negative distance). Hard contact is designed to reduce the penetration of the surfaces, but the level of final penetration depends heavily on the quality of refinement of the mesh. Hard contact can leave small gaps between contacting surfaces as the kinematic algorithm disregards the inertia of the nodes on the contacting surfaces (hence they can 'bounce back' off the surface).

Penalty Penalty contact will first look for penetrations in the current configuration, then apply deformations to remove that penetration. These deformations are generated by introducing artificial stiffness increases into the slave nodes. To this end, penalty contact treats the penetration of surfaces more accurately, but the pressure distribution becomes less accurate. This increase in stiffness also has a detrimental effect on the stable time increment

(slowing down the job), although the stiffness values are chosen automatically to balance the accuracy of contact with the increment time. The use of hard contact also reduces penetration, but while there is likely to be less penetration than using kinematic, the penalty algorithm does not guarantee there will be no penetration. The penalty algorithm accounts for all the energy during contact, so the inertia of the contacting nodes is retained (useful for jobs where rebound is likely).

Both algorithms can have problems resolving contact between surfaces of significantly different masses, due to high velocities being generated in the lighter material in an attempt to conserve overall energy across the contact. In Figure 4.20(a) a less dense master surface has a high velocity of contact and penetrates the slave surface in the next increment (b). The algorithm then resolves the contact based on the slave surface deforming and providing a pressure that moves the master surface back slightly (c).

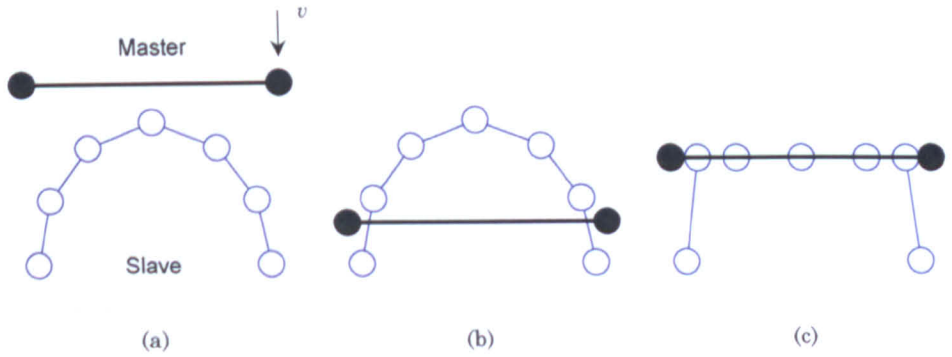

Figure 4.20: Surface contact errors due to mismatched material densities.

To overcome this problem, the master surface should be specified as the coarser, denser mesh. If this is not possible then the priority balance between master and slave surfaces can be manually over-ridden. If the default value of 1.0 gives surface 'A' as the master, then changing the priority to 0.0 gives surface 'B' as the master. Any value between 1.0 and 0.0 requires a weighted average of the results, with 0.5 giving a result generated from one calculation with A as master, and one with B as master. This method gives the most accurate results, but is the most computationally intensive.

4.6.6 Connectors

For the efficient modelling of mechanisms, ABAQUS provides a set of specialist connector elements. These act as packaged boundary constraints, specifying a particular linked relationship between two nodes in the model.

While the aim of the connector elements is to provide a quick method of simulating joints etc., they have proven to be unreliable in models with complex geometry. They are very sensitive to overconstraints; where a single degree of freedom is constrained more than once. As overconstraints can be formed from a change in contact conditions throughout the job, the use of connectors requires very careful job set-up, and if a job fails, lengthy debugging and adjustments to the model are needed to allow successful execution (see Chapter 9).

4.7 Chapter Summary

This chapter has reviewed the state of knowledge of finite element analysis, applied to a footwear modelling application. It is apparent that there is a good depth of knowledge in the mathematical modelling of hyperelastic materials, however the application of these models into FEA has been limited to more traditional industrial applications. Specific modelling of footwear has been concentrated on the biomechanical or medical (orthopedic) use of models, with complex foot assemblies but only very simple midsoles.

Looking at the techniques offered in one of the most popular FE programs, ABAQUS, shows that the technology is available to model the materials, geometry and interactions involved in footwear. Simple models have given reasonable results in the past and the application of FE mechanism modelling used in other engineering areas should allow the modelling of the increasingly complex modern shoes.

It must be noted that while there is a range of data available for the biomechanical inputs into the system and some general data on material properties, there is no apparent quantifiable information detailing the variation between one shoe and another of the same size, make and model. This information is lacking both in the public domain and within adidas.

The literature review in Chapters 2-4 proves that the methods proposed in this research will provide new insights and fill in vital gaps in knowledge in this field:

- FEA modelling of simple and complex running shoes.
- Laboratory determination of the properties of the materials in said shoes.
- Material model validation with FEA.
- Shoe model validation using practical mechanical testing.
- Determination of the overall variability of the shoes modelled.

With enough time, this kind of analysis should be possible, but for it to be applicable to industry it must be able to be carried out within a production time scale (e.g. a few weeks) with little manpower resources. The following issues are believed to be critical in achieving the correct speed/accuracy balance for the FEA models:

- The level of model complexity, specifically mesh densities, use of component bonds, contact and complex material behaviour such as Mullins effect and viscoelasticity.
- The level of accuracy of geometry required to produce adequate meshes (as the geometry may need repair, as discussed in Chapter 8).
- The sensitivity of the model to slight changes in any of the aforementioned model parameters and geometry.
- The level of repeatability of performance of manufactured shoes.

Investigations into all of the above are carried out in Chapters 7-11 to address these questions. The use of FE models within a production time scale, along with suggested workflows is discussed in Section 12.5.1.

Chapter 5

Test Equipment and Methods

5.1 Introduction

This thesis will be presented to the industrial sponsors of the research, who have expressed an interest in using it as an aid to teaching with respect to the FE modelling of sports footwear. To provide a better layout of the work, Chapters 7-11 detail the FE modelling processes and present results from testing, while this chapter contains the technical details of the test equipment and methods used to determine those processes and results. This chapter is split into the following sections:

Material Samples Specifically manufactured regularly shaped samples of the materials used in the shoes under test (a list of which can be found in Section 7.2).

Shoe Parts Individual, moulded shoe components.

Assembled Midsoles Components of a shoe, bonded together and taken from the production line before any of the upper of the shoe is attached.

Production Shoes Taken from the end of the production line, these shoes have most of the uppers cut from them in preparation for mechanical testing. Insoles are also removed.

Figure 5.1 shows examples of the parts and shoes (these are all modelled in Chapters 7-11, in order of increasing complexity). Each of the above sections covers the following;

- The measurements required from the test(s).
- How the sample/part/shoe is prepared for the test(s).
- Descriptions of the test method(s).
- Recommendations for improvements to any standard test methods.

The testing of assembled midsoles and production shoes uses a structural tracking process, which is detailed in its own section (5.5). Overall recommendations for the relevance and importance of physical testing with relation to the industrial application of this research are made at the end of the chapter.

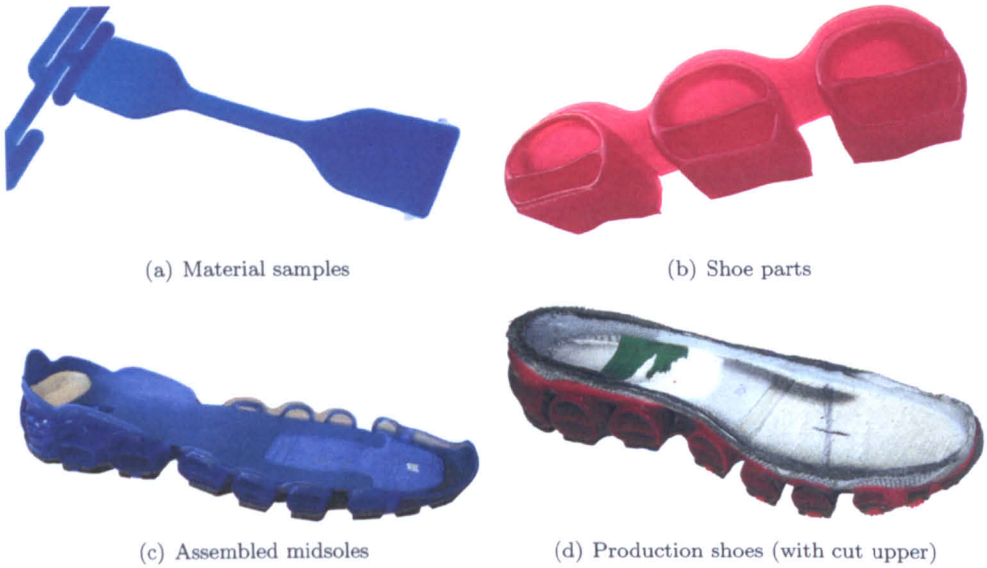

(a) Material samples

(b) Shoe parts

(c) Assembled midsoles

(d) Production shoes (with cut upper)

Figure 5.1: The four stages of modelling complexity (Gigaride used as an example).

5.1.1 Use Of Data Within A Modelling Strategy

The finite element method is one that requires the engineer to make many assumptions and estimations. To achieve an accurate model, these assumptions must at the very least be understood, and ideally, numerically accounted for. In its commercial application, this technology might take material data from specifically manufactured test samples or from previous measurements of a similar material, and use them to predict the response of a part that has yet to be made. The primary assumption to be made in this case is that the material in the sample is the same as that in the shoe part. For the purpose of development of this technology within the athletic footwear industry, the shoes, parts and materials being modelled are taken from shoe lines that are in, or have been in full production. This allows all the stages of shoe to be tested: material samples, moulded parts, assembled midsoles and production shoes.

Comparison of results from testing on these shoe stages will give quantitative information concerning any changes seen in the material properties during the entire production process. By covering the range of material types (elastic, hyperelastic, hyperfoam, elastic-plastic) and the two main types of midsole (foam block and TPU structures) the aim is to produce a record of these changes for the different shoe types that will, in future, allow analysts to adjust their material properties derived from material samples, into those found in the final product. The accuracy of this estimation will depend on the amount of information generated from shoe part and shoe assembly testing, this information gathering process is expected to continue after this research is concluded. For more details on the recommended overall predictive process that has come from this research, see Section 12.5.1.

5.2 Material Sample Testing

5.2.1 Required Measurements

Nominal stress/strain results from sample tests are inputted directly into ABAQUS to form a material model. The minimum amount of data required is the Young's modulus and Poisson's ratio, which is enough to define a purely elastic material. For hyperelastic and hyperfoam materials, the non-linear nominal stress-strain response is required. All data are obtained

from uniaxial compression and tension testing. The range of stress and strains that are required for a good material model are investigated in Chapter 7.

By cycling the samples over a range of increasing strains, the Mullins effect can be recorded, and the basic stress-strain response extracted from the data. This allows the breaking-in effect of the material to be modelled within ABAQUS using the *MULLINS EFFECT command (see Section 4.6.2.2).

Hyperelastic materials are assumed to be incompressible by ABAQUS, so Poisson's ratio is not required. For compressible foams, a constant Poisson's ratio can be specified, or data from volumetric compression testing can be included in the form of pressure vs. volume ratio.

Planar tension and compression testing data are not required, but ABAQUS recommends the inclusion of as much data as possible to create an accurate material model (this is also inputted as nominal stress-strain). Again, the range of data required to create such a model is discussed in Chapter 7.

Due to the likely rate dependency of some materials (see Section 3.3.5), it is preferable to test samples at the same speed as that material would see in normal use within the shoe (its operating condition). Due to limitations of available equipment, this may not possible, so the rate-dependant behaviour of the material must be measured by other means than simple uniaxial, planar and volumetric testing, Section 5.2.4 covers these tests.

Data from other sample testing, such as ball indentation and quasi-static tests at various strain-rates (below operating condition) are used to verify results from modelling of these tests within ABAQUS; if the model is producing false results at this relatively simple stage, then the material model may need to be adjusted and that adjustment recorded for future reference.

5.2.2 Sample Preparation

Samples of TPU materials were cut from 2 mm sheets using a BS 903-A2:1995 dog-bone stamp cutter. TPU compression samples were delivered pre-shaped in 25 mm diameter, 12 mm high cylinders. On closer inspection it was found that these were not cylindrical, but had a chamfer on the upper edge, and an indented upper surface (Figure 5.2).

Figure 5.2: View of a compression button cut down the centre. Dashed lines indicate the height of the surface at the cut face.

While the TPU samples could be cut using the stamp cutter, the thicker foam samples could not. Due to the highly compressible nature of the material, it deformed under the cutting load and so the cut was made in deformed material, which then reforms into a distorted sample (Figure 5.3). This is likely to induce the Mullins effect within the sample due to high deformation. Attempts have been made to find other methods of cutting, such as laser cutting (Figure 5.4) but this destroys the samples, even on the lowest possible power settings. Freezing of the samples before cutting was attempted, but only in a domestic freezer at -18°C, liquid nitrogen freezing was not attempted, and may provide better results.

Figure 5.3: Foam compression sample cut with a stamp. Note the non-cylindrical result and rough edges.

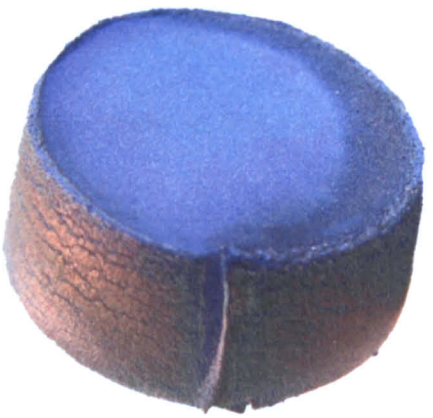

Figure 5.4: Foam compression sample cut with a low power laser cutter. Note the non-cylindrical test shape, edge burning and melt area at the start of the cut.

Stiffer PU foams (such as the ETH046 used in the Ultraride heel crash piece) have been successfully cut with a fine bandsaw (Figure 5.5), though repeating this with EVA resulted in similar 'wave' patterns as those visible in Figure 5.3. The bandsaw could also cause significant compression of the sample at the cutting edge resulting in an uncontrolled amount of pre-loading of the material.

Figure 5.5: Close-up view of a PU foam sample cut using a bandsaw.

Best results were obtained using a new scalpel blade and hand cutting the samples. Reasonably straight edges could be produced with a little practice and the blade cut the sample with very little compression when a ruler was used to spread the load of the sheet-retaining hand (Figure 5.6).

Based on the amount of material available, foam samples were created with dimensions of 10 x 20 x 150 mm - in an attempt to maximise the number of samples from limited material sheets, while still maintaining a width-height ratio similar to that in BS 903-A2:1995.

Figure 5.6: Close-up view an EVA foam cut with a scalpel.

The samples were cut as rectangles to give a more constant cross-section as it was exceedingly difficult to cut consistent curves by hand. A typical sheet cutting pattern for foam is shown in Figure 5.7, and for rubber in Figure 5.8. The TPU cut lines show up poorly on photographs so the schematic in Figure 5.9 shows the pattern used for materials with only two sample sheets available. Due to on-going production, Gigaride materials were relatively plentiful so samples were taken from multiple sheets in similar places to those illustrated here, and compared (see Section 7.3.2).

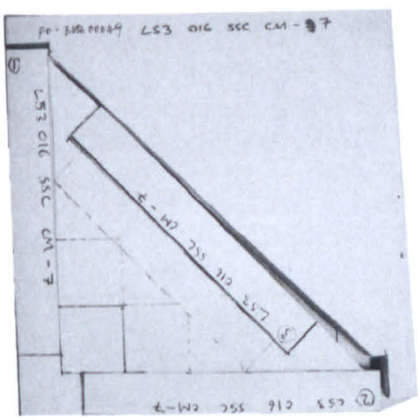

Figure 5.7: View of cutting pattern on a 180 x 180 mm foam sheet. 5 mm strips have been cut from around the edges to avoid distorted areas. Half the sheet is used to allow further testing on a limited number of sample sheets if required. Tensile samples are taken at 0, 45 and 90° to test for any stiffness variation with grain direction.

Before testing the dimensions of each sample were measured with a vernier caliper. Measurement was carried out by hand in one sitting, by the same person as the high compressibility of foam creates difficulty with gauging at what point the faces of the caliper are just in contact with the sample. By using the same person, in the same sitting, a consistent 'feel' is achieved as to where the touch point is. It is estimated that this point can be measured to within 0.1 mm with good consistency. Samples are measured for thickness, width and height at positions shown in Figure 5.10. Compression buttons were found in most cases to have warped after moulding (most probably during the cooling process). Because of this, these parts are measured for their extreme height (including distortion) and also their edge height, which was fairly consistent throughout the samples. Injection-sheet parts (Figure 5.11), especially polyamide ones were found to be the most distorted (Figure 5.12). Sample dimensions used in calculations were then obtained from the average of the readings.

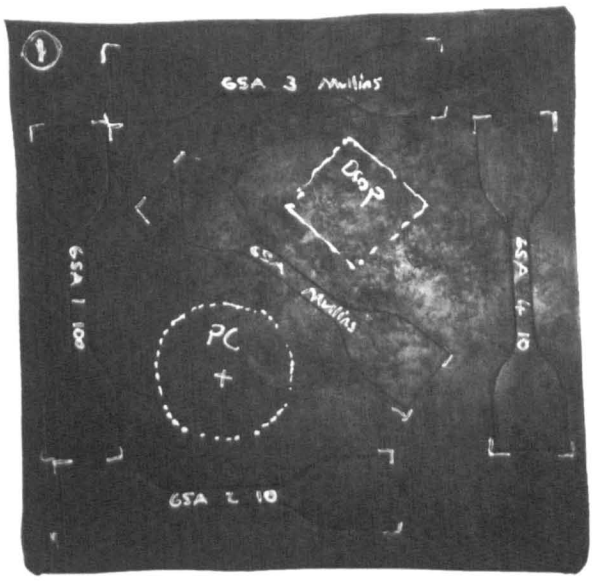

Figure 5.8: View of cutting pattern on a rough 200 x 200 mm carbon black rubber sheet. Unlike the foam sheets (Figure 5.7), many rubber samples were available so the whole sheet is used.

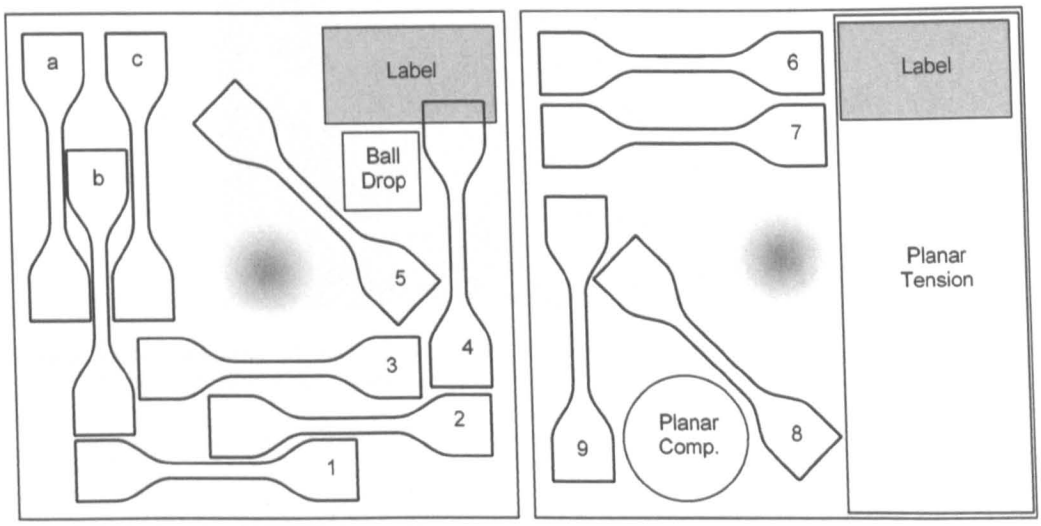

Figure 5.9: Typical cutting pattern for the two available sheets of Ultraride and Supernova TPU materials. Samples a-c were used in preliminary equipment testing, while 1-9, ball drop, planar comp. and planar tension were used for extraction of material properties. Note the grey area in the centre indicating the point of injection, which is far stiffer to the touch than the surrounding area.

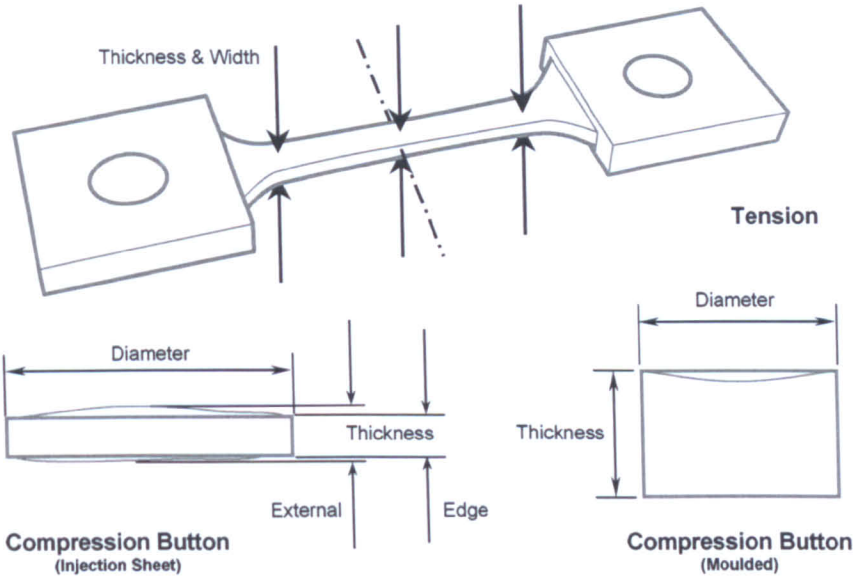

Figure 5.10: Schematic detailing the measurement points used to determine the specimen dimensions. Tension: Points are at limits of constant cross-sectional area and centre of specimen. Similar points are used for foam specimens, but measurement begins approx. 10 mm from the bonded areas. Compression: Injection sheets and moulded button parts are measured for their extreme thickness (including distortion) and edge thickness as well as diameter.

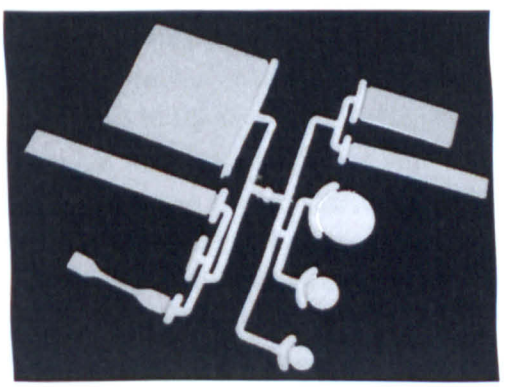

Figure 5.11: 'Injection sheet' - injection moulded set of standard parts (large dog bone sample has been removed for testing in this image).

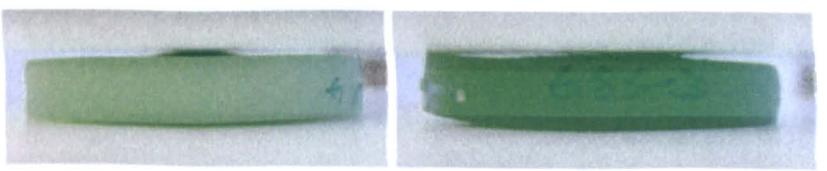

(a) (b)

Figure 5.12: Distorted samples between parallel plates. (a) 685, (b) LX materials.

5.2.3 Quasi-Static Tests

Due to the unavailability of a high-speed compression/tension measurement device for sample testing, an Instron 3366 series (screw-thread) uni-axial machine was used. This machine has a reliable maximum head speed of 500 mm/min. All quasi-static testing was carried out on this machine. The machine outputted load and displacement of the crosshead, which was then converted into nominal (engineering) stress and strain.

5.2.3.1 Uniaxial Tension

To attempt to minimise the inaccuracies discussed in Section 3.4.2, new test equipment was manufactured that allowed the sample to be suspended between two 10 mm diameter bolts. The sample had four 30 x 30 mm steel plates bonded on with cyanoacrylate (Figure 5.13). These plates had holes cut in for the bolts to pass through. After bonding was complete two 10 mm diameter holes were drilled into the sample. This allowed the sample to be held in place over a greater range of strains than when using clamps (Figure 5.14). The position of the holes did not change relative to the measuring equipment (as it did with moveable clamping, Figure 5.15) giving higher accuracy. Eventually the plates did become de-bonded, but this was indicated by a sharp fall in stress and could be observed and accounted for easily (Figure 3.30 shows a stress/strain curve where the material clamping fails while Figure 5.16 shows detail of the debonding of a sample used in the research). The same process was carried out for foam samples, though these were cuboid shaped, as it was not possible to cut dog-bones from the foam. As testing was not to failure, use of this shape was acceptable (Miller 2000a).

It should be noted that for small strains it is quicker and more accurate to use an extensiometer for measuring strain, but these are normally limited to around 10 mm extension so are unsuitable for the very large strains seen in some of the materials under test.

Testing Speeds The aim of the testing was primarily to determine the static stress/strain response of the sample materials, as the shoes operate at effective speeds above 20,000 mm/min and the machine is limited to 500 mm/min. As the test machine was only available for a limited period of time and a large number of tests were required, the shortest time of test that would give a static response was needed. An initial check was done to determine if the sample was significantly rate-dependant over the speeds at which the test machine could operate. The majority of material exhibited a small difference over the range 0.1-10 mm/min in compression (showing a strain rate of 0.0016-0.016 s^{-1}). Higher rates were not performed in compression as use of the small samples risked damage to the machine. Materials showing negligible rate-dependency were tested at 10 mm/min. Materials showing significant rate-dependency were tested at 0.1, 1 and 10 mm/min. TPU tension samples were tested at 10, 100 and 500 mm/min as more samples were available. Details of test speed for various tests and materials are given with the individual material property results.

Repeats In accordance with ASTM D3574 1995, at least three samples from each material were tested. For key components, where samples were available, as many tests as possible were carried out.

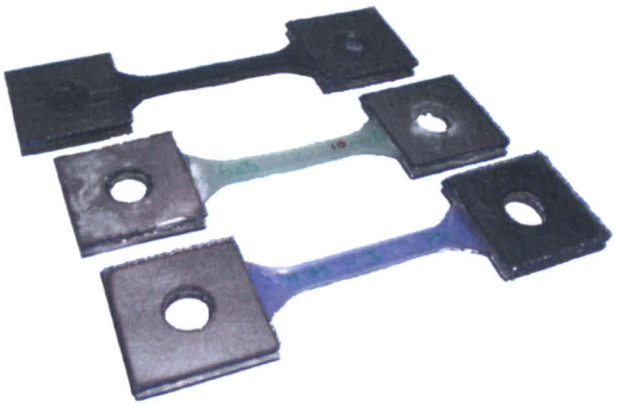

Figure 5.13: Test samples with metal plates bonded on to aid clamping. The holes allow 12 mm bolts to be passed through the samples, anchoring them to the test machine.

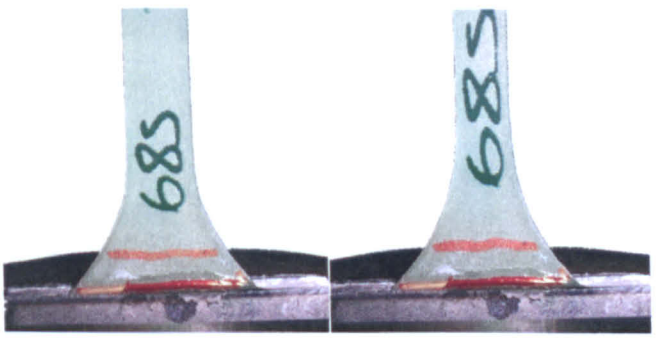

Figure 5.14: Image showing the performance of bonded plate samples under no load (left) and at 100% strain (right). Note the difference in slip (shown by the red lines) when compared to clamped samples (shown in Figure 3.28).

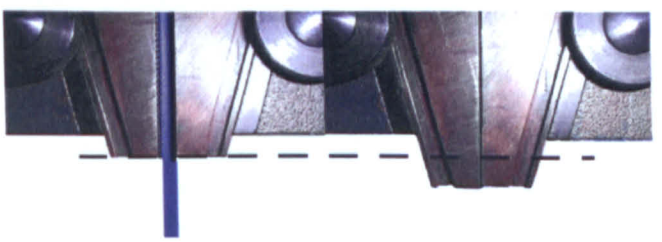

Figure 5.15: Effect of a change in sample thickness caused by contraction. Note the change in effective original length due to clamp movement.

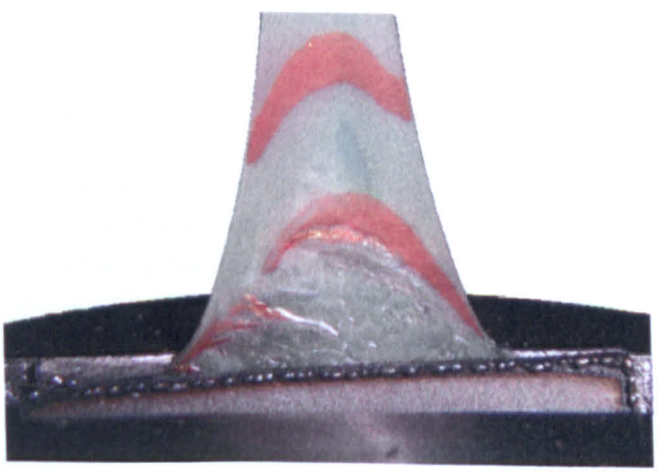

Figure 5.16: De-bonding of plates at high strains (in this case >400% strain).

5.2.3.2 Uniaxial Compression

To reduce the friction between the metal plates and the test sample during uniaxial compression (Figure 3.29), each sample was sandwiched between two PTFE plates (Figure 5.17). As the modulus of PTFE is low, and may interfere with the results, each PTFE sheet was preloaded to 10kN (the load limit of the test machine used for uniaxial testing) and cycled until a repeatable response was achieved. This response was recorded and could then be subtracted from the test result for any given strain:

$$\varepsilon_{[sample]} = \varepsilon_{[output]} - \varepsilon_{[PTFE]} \tag{5.1}$$

Figure 5.17: Uniaxial compression testing with the test sample between two 6 mm thick PTFE sheets.

While compression testing on foams using PTFE was successful, testing the stiffer TPUs from the Ultraride and the stiffer still polyamides from the Gigaride caused permanent plastic deformation in the PTFE sheets. The resulting indentations in the PTFE (Figure 5.18) restricted the movement of the next sample to be tested, voiding any increases in accuracy provided by the low friction surfaces. Because of this, all non-foam tests were repeated on new samples without the PTFE sheets in place.

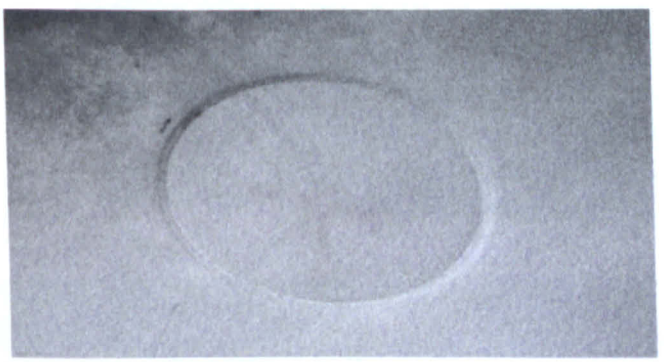

Figure 5.18: Images of a dent in the PTFE sheet caused by compression of a sample of material with a similar modulus to that of PTFE (Image enhanced).

5.2.3.3 Planar Tension

The planar tension testing set-up was very similar to that of uniaxial tension, with the samples having holed metal plates bonded onto them. However, it was much more difficult to achieve a uniform bond along the plates which resulted in early failure of the bond (Figure 5.19). It had also proved difficult to align the plates in parallel with each other before the adhesive set. In the uniaxial tension tests misalignment of the plates causes small rotations at the bolts, but this effect is greatly magnified with planar tension. With a test area of 20 x 200 mm, a misalignment of 1 mm at one end will cause an initial difference of 5% strain at opposite ends of the sample, which can produce significantly erroneous results as a constant stress is not achieved.

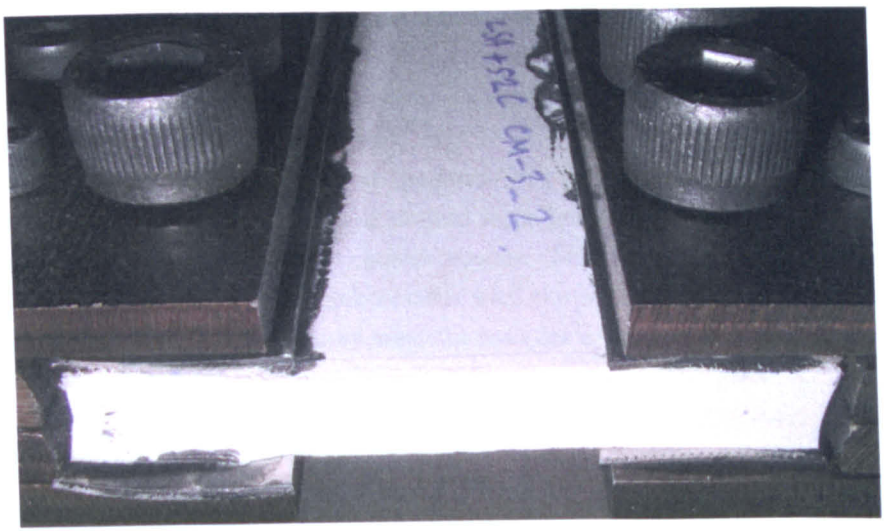

(a)

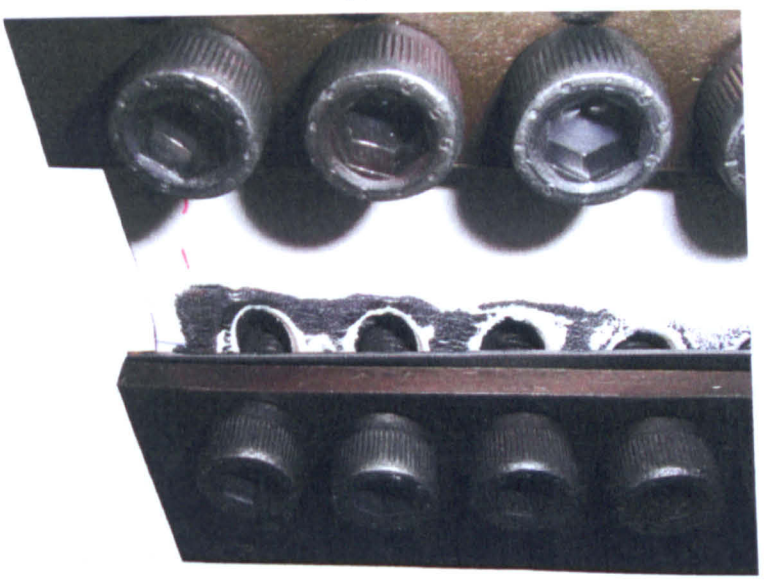

(b)

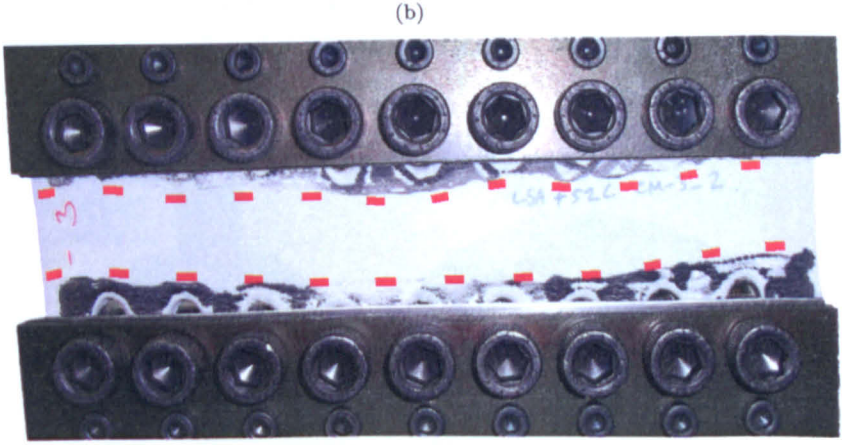

(c)

Figure 5.19: Images of planar tension testing: (a) Pre-testing, (b) Close up of bonding failure during test (left edge), (c) Failure viewed from front, dotted lines indicate original bond lines.

5.2.3.4 Planar Compression

Planar compression testing is not normally carried out, as the results from planar tension, uniaxial compression and tension, and volumetric tests are enough to characterise the material, according to advice from the ABAQUS documentation. However, due to the difficulties experienced with planar tension it was deemed a useful to investigate if planar results from compression could be obtained more easily.

Initial tests using PTFE showed that the foam/PTFE interface was not frictionless - the foam would not expand in diameter and showed some barrelling. Use of the TPUs with the PTFE sheet was not possible, as they caused damage. This meant that reliable 'pure' planar data that ABAQUS required was unobtainable with the available equipment. To give some comparison of compression over a large area, the samples were indented with a flat-bottomed 45 mm diameter stamp (as used in ASTM F-1614-99) up to an 8kN load.

5.2.3.5 Volumetric Compression

Volumetric compression was achieved using a hydrostatic compression chamber, manufactured to allow the piston to fit the Instron (Figure 5.20). Figure 5.21 shows a schematic of the device. As the seals in the chamber are rubber, and of a similar modulus to that of the test samples, the base response of the chamber was recorded by running a pressure test to full load (10kN) with no sample in the device. Re-running this test at the different test speeds allowed the rate of pressure loss due to leakage, seal distortion and expansion of the steel to be accounted for in a similar way to that used to account for the compression of PTFE sheets in Section 5.2.3.2.

ABAQUS advises that foam samples should be sealed from ingress of the oil used in a hydrostatic chamber. However, it does not advise how to do this effectively, and with the relatively delicate foam samples the application of a sealing layer of a polymer or resin is likely to change the stiffness of the material. Putting the sample in some kind of hermetically sealed bag is another solution, but this raises serious difficulties when it comes to accounting for the amount of air contained within the bag. To this end the samples were not sealed based on the assumption that a foam operates primarily as a polymer-air composite which can be modelled as a set of pistons in series (Figure 5.21), a similar assumption was made by Mills (2001) as described in Section 3.3.9.

This assumption was believed to be valid in this case as the uniform pressure within the chamber prevented an individual cell from distorting, that is to say it should have theoret-

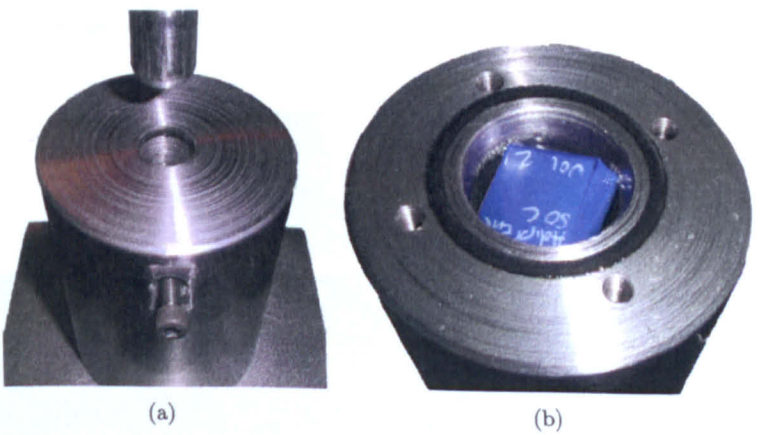

(a) (b)

Figure 5.20: Volumetric test chamber. (a) Chamber with sample and oil in place, (b) sample being inserted in the (unbolted) underside of the chamber.

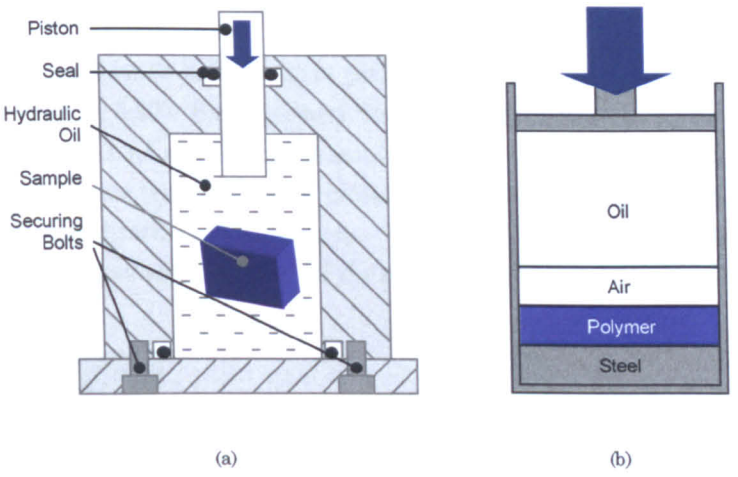

Figure 5.21: Schematics of the volumetric compression test. Left: Test equipment. Right: Illustrating the assumption made about the material behaviour during the volumetric compression test.

ically shrunk whilst maintaining its shape. In this instance the resistance to compression comes directly from the molecular structure of the polymer, not the shape of the cell. This assumption would be invalid if the cells ruptured and allowed oil to ingress into some cells as the oil-filled cells would not have to change shape during a pressure increase in the chamber, while those air-filled cells would have shrunken, causing an overall distortion in the shape of the sample. If this was the case, then significant pressure had been used to force oil in and air out (so that it collected at the top of the chamber), so some oil would remain in the sample after it was removed from the chamber. To check this the samples were accurately weighed before and after each test. If no mass change was observed, then it was assumed that there had been no oil ingress and thus the results could be considered reliable.

Results showed a maximum weight gain of 0.07g corresponding to 1.65% of the air volume of a 20 x 20 x 10 mm sample for the DOT 5.1 brake fluid (ρ=1.05) used in the chamber. This is a small difference and could have easily come from not completely cleaning the excess oil from the surface of the sample after testing, and so was considered negligible.

5.2.3.6 Indentation

Quasi-static indentation tests were performed on all materials, to obtain the broken-in steady state stiffness response of the material from indentation with a spherical object (Figure 5.22). This stress-strain response will differ from the purely elastic as areas of the sample will be under different stresses at a given instant, and skin effects (as mentioned in Section 3.4.4) may occur.

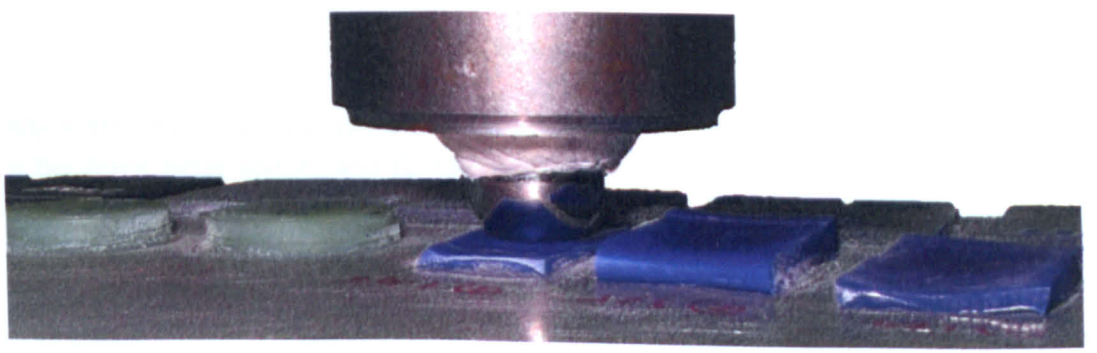

Figure 5.22: Set-up of the ball indentation test.

5.2.3.7 Bend

Bend testing was performed using a three point bend mount with 10 mm diameter circular contact points (Figure 5.23). Samples were tested at a crosshead speed of 10 mm/min, and cycled to a depth of 1,2,3,4 and 5% of the sample length. For this test the nominal strain was taken to be the distance traveled by the crosshead of the machine, divided by the thickness of the sample in the direction of movement. The nominal stress was taken as the detected load divided by the cross sectional area of the sample in a vertical plane under the crosshead.

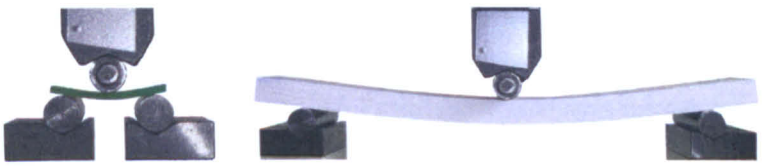

(a) (b)

Figure 5.23: Bend testing on (a) TPU sheet, (b) foam sheet.

5.2.4 Dynamic Tests

The aim of dynamic testing was to provide ABAQUS with information on how a materials' response varies with strain rate. The dynamic response of the type of materials under test was known to vary with mode and amplitude of strain so ideally the samples should be tested under operating conditions (Miller 2000).

5.2.4.1 Creep

Creep testing is a well established method of obtaining the equilibrium (static) stress-strain response of a material as well as its dynamic response. The data can be directly inputted into ABAQUS where the code will automatically generate a dynamic response for the material. However, creep or relaxation tests require prohibitively long periods of time and were replaced with Dynamic Measurement Analysis due to time constraints on the testing.

5.2.4.2 Dynamic Measurement Analysis (DMA)

DMA uses small-strain sinusoidal vibrations over a range of frequencies to determine the storage modulus (elastically stored energy) and loss modulus (energy dissipated as heat) of the material under test. It allows a much greater range of strain-rates to be achieved than with creep testing, but the trade off is that the strain amplitude is very small.

The moduli are calculated thus:

$$|M^*| = S \cdot g = \frac{F_a}{L_a}$$

where M^* is the complex modulus (Young's or shear depending on the test), S is the stiffness, g the shape factor and F_a and L_a the measured force and displacement amplitudes. By measuring the phase shift (δ) between the forced displacement of the sample and the reaction force, the loss factor ($tan\ \delta$) can be determined. A purely elastic material has a zero loss factor, and purely viscous material one of ∞. The storage (M') and loss (M'') moduli are then derived:

$$M' = |M^*| cos\ \delta \qquad M'' = |M^*| sin\ \delta \qquad tan\ \delta = \frac{M''}{M'}$$

This data is then averaged between the number of samples taken (each sample consists of two samples of material for the shear testing that was carried out) and then inputted into ABAQUS as the real and imaginary parts of frequency-dependant moduli, specified as functions of frequency in cycles per time:

$$\omega(g^*)_{Real} = \frac{M''}{G_\infty} \qquad \omega(g^*)_{Imag} = 1 - \frac{M'}{G_\infty}$$

where ω is the cyclic frequency and G_∞ is the long term modulus, taken as the value of M' at the lowest frequency recorded (0.1 Hz for this set of testing). This data is entered in the time domain, frequency data input box, *not* as "shear test data".

ABAQUS then creates a Prony series from this data in the pre-processor by performing a least squares fit. As each term added to the Prony series increases the computational cost of the material model, the smallest possible number of terms should be used, while preserving the desired fit to test data (Chen 2000). ABAQUS will automatically limit the number of terms if too few data points are available, and will also stop a job if the error tolerance of the least squares fit (set when the frequency data is inputted) is too low. If this occurs with the default values, then it is likely the test data has some errors in it and should be retaken. However, if this is not possible, then the error tolerance should be set high to ensure the job at least starts, though there may be significant errors in the resulting viscoelastic response.

5.2.5 Recommendations for Material Sample Testing

Overall, the process of characterising the physical response of shoe sample materials is beset with difficulties. The following have been identified as areas which could have a significant effect on the results:

- The material under test may not be the same as that in the shoe.
- Preparation of good, consistent samples is difficult.
- The highly deformable nature of the materials means that test equipment designed to hold stiff materials such as metals may not be sufficient.
- As discussed in Chapter 3, the response of a material is known to be dependant on any combination of temperature, strain rate, strain history, deformation mode, shape and method of manufacture. This may not be an exhaustive list.
- The dynamic properties of the material may also be dependant on the above, so if time permits the best method of obtaining the dynamic response is from operating-strain creep testing on similar size samples to those seen in the final model.

Testing samples accurately over a range of deformation modes requires very careful preparation of samples and test equipment. However, even with a "perfect" set of measurements, the sample materials may still be different from those used in the shoes. This is seen as the biggest hurdle with creating a predictive sports shoe modelling technology.

5.3 Shoe Part Testing

Shoe 'parts' are moulded/injected forms that are used in the assembly of a shoe. The parts undergo no further major chemical/physical changes (such as from moulding) during production, they are just bonded and/or sewn to other parts. These parts were tested as it was highly likely that the injection/compression moulding processes used to form the parts had affected the materials' physical response.

As each part required the fabrication of bespoke holding attachments (see Section 5.3.2), only the major parts were tested. For the Supernova this was the main midsole section, for the Ultraride, the structure plate. Both the posterior structures and the heel structure were modelled for the Gigaride. All testing was quasi-static and was performed on the Instron machine (Section 5.2.3).

5.3.1 Required Measurements

The primary measurement for shoe part testing was force-deflection, obtained directly from the Instron. As the area of material under test was not a constant cross section, the directly outputted results were used without nominalisation. To allow better verification of the FEA models, the overall structural response was recorded on video during the tests. This structural tracking method is detailed in full in Section 5.5.

5.3.2 Sample Preparation

Shoe part samples are moulded parts, and require little preparation for force-deflection measurement. Due to their irregular shapes, special fittings were created using rapid manufacture techniques to allow repeatable testing. The fitting material was assumed to be rigid as its Young's modulus was much higher than the materials under test (1800 MPa). To create the fittings, surface geometry from the part was extruded and trimmed to form a shape that, within manufacturing tolerances, conforms to the part shape on one side, and has a flat surface on the other (Figure 5.24). Preparation of the samples for structural tracking is detailed in Section 5.5.

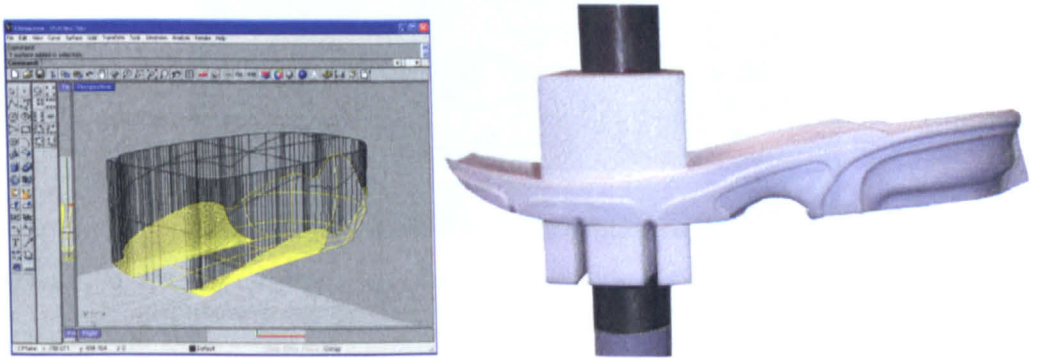

(a) (b)

Figure 5.24: (a) Creation of fitting geometry in Rhinoceros version 2.0 SR1 (McNeel 2006), (b) Resulting fittings in place between flat compression plates on Instron test machine (material: "SLS Duraform PA" from 3D Systems, Valencia, CA.

5.3.3 Controlled Boundary Condition Compression

By using special fittings bonded onto the parts, the boundary conditions of the test could be tightly controlled (the friction would be effectively infinite). This created a simpler test to model as fitting-part surface contact (and its associated increased risk of error) could be omitted.

The original aim was to produce fittings for each part sample and permanently bond them on. However, rapid manufacture production costs meant only one of each fitting could be produced, so the fittings had to be bonded and de-bonded between tests. The use of cyanoacrylate adhesive was found to be impractical with foam parts as it caused damage to both the sample part (Figure 5.25) and left a foam residue on the fitting after the first test.

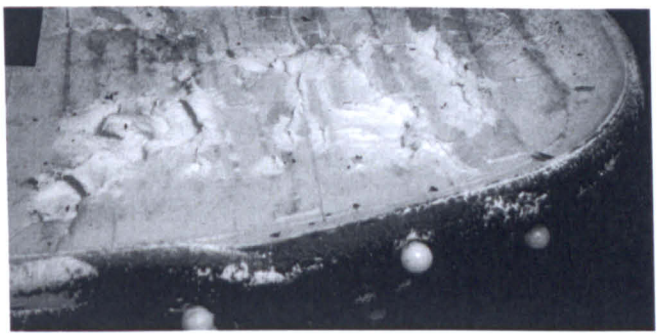

Figure 5.25: Damage to a Supernova shoe part after removal of the fitting when using cyanoacrylate and de-bonding agent.

This was replaced by a non-repositionable spray mount (3M Photo Mount) for the rest of the testing. While it did not bond as firmly as the cyanoacrylate, the spray mount allowed removal of the parts from the fittings, and showed no visible signs of slip during the test. The flat lower surface of the Ultraride structure plate allowed flat sheets of SLS to be bonded permanently onto the structure (Figure 5.26) as these were readily available.

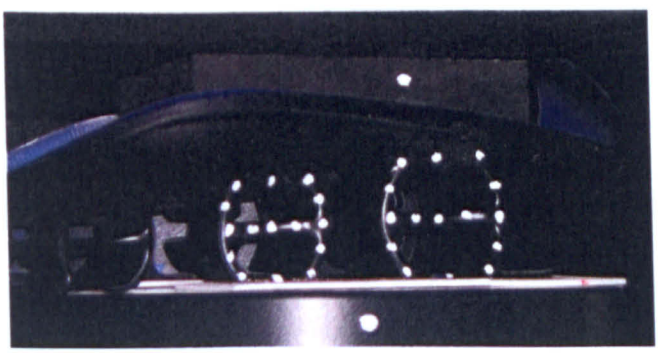

Figure 5.26: Ultraride structure plate during controlled boundary condition test. Note the use of permanently bonded SLS on the base, and temporarily bonded upper fitting.

Method As shoe parts lack the full structural strength of an assembled midsole, loading was taken only to 75% of a full heel strike (considered as 2 kN in this thesis). As the force-deflection and Mullins response and history of the shoe were unknown, the samples were broken in by cycling five times to 1500 N. Each sample was then taken to 1500 N, three times with roughly 20 seconds of rest between each cycle. Ideally the unload cycle would be recorded too, but at this stage in the testing the required adjustments to the Instron software had not taken place. Force/deflection was recorded from the load cell and the structural response was recorded on video.

5.4 Assembled Midsole Testing

Assembled midsoles are constructed of bonded shoe parts and have been removed from the production line before the addition of any part of the upper. For the Supernova this meant the assembled midsoles were lacking all of the fabric parts, while the Ultraride and Gigaride both lacked the fabric and the internal EVA midsole which was bonded into the fabric section. Testing on assembled midsoles was both static (on the Instron) and dynamic, using a specially constructed drop rig, detailed in Section 5.4.3. These dynamic tests attempted to replicate those done at adidas (see Section 2.9.5.3), although it must be noted that a drop rig cannot provide a prescribed force-deflection curve, only the speed, energy impulse or peak force can be matched. The supporting blocks seen in Figures 2.14 and 2.16 were not included in physical or FEA tests as they gave another variable that must have been accounted for.

Production Shoes These underwent the same testing as assembled midsoles, but were shoes removed from the end of the production line that have had their uppers cut off at a point approximately 15 mm above the upper surface of the midsole. For the Ultraride and Gigaride this meant the EVA 'midsole' section may have provided significant extra cushioning to the assembled midsole.

5.4.1 Required Measurements

The measurements required for assembled shoes were identical to those for shoe parts (Section 5.3). However, the use of dynamic testing allowed further structural tracking metrics to be derived. These considered the spatial distortion of the shoe as it underwent loading through the use of markers and digital video. Section 5.5 details this process.

5.4.2 Sample Preparation

The only preparation required was the marking of the samples for structural tracking, as detailed in Section 5.5.

5.4.3 Test Equipment

As ascertaining the dynamic response of the shoes under test was vital for production of a viable FEA model, a test rig to allow impacts above 500 mm/min (the limit of the Instron) was constructed. This allowed quick access to a dynamic testing machine, and permitted development of the structural tracking method (see Section 5.5). This data was supplemented by force/deflection data carried out on a high speed servo-hydraulic machine at adidas's testing facility (see Section 5.4.5).

The majority of a weight-stack exercise machine was available, and this was converted into the drop rig shown in Figures 5.27-5.28.

The rig consists of a weight stack running on two chromed stanchions, which provide a smooth uniaxial path. The stack is lifted using a hand winch and released with a bespoke catch. An interchangeable head is mounted to the bottom of the stack which allows a shoe to be impacted. The shoe is positioned on a 2 mm sheet of smoothly brushed aluminium mounted on a 20 mm thick steel plate which is in turn prevented from bending by a structural plastic block and more steel between it and the floor.

The rig was designed to be bolted to the floor, but lack of space in the engineering building meant it was located over a concrete beam on the first floor and was not bolted down. As such the structural tracking measurements also measured a point on the base plate of the rig

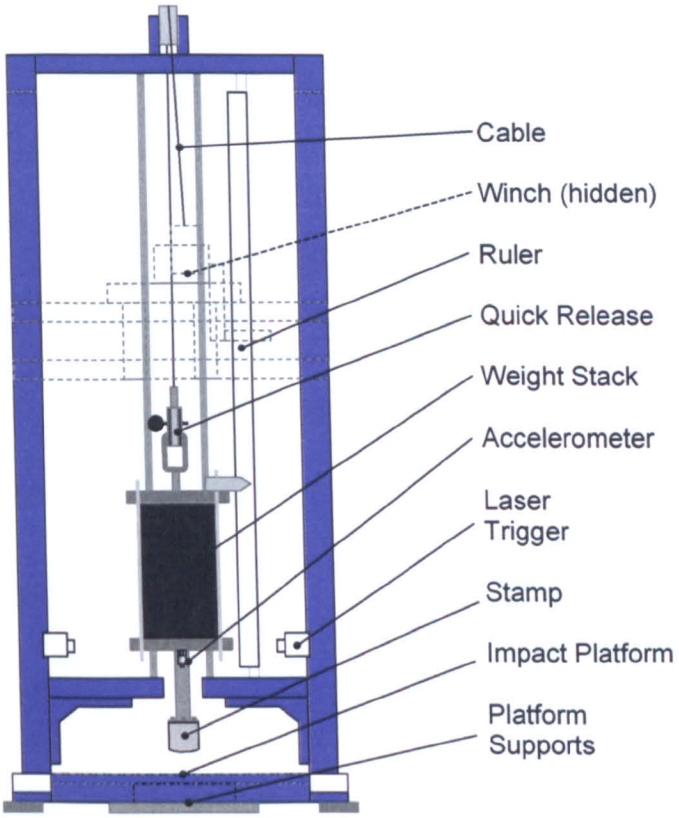

Figure 5.27: Schematic of drop rig, viewed from the front, without safety shields in place.

to determine if there was any relative movement between the rig and the camera and allowed this to be subtracted from the results.

The rig was designed to achieve similar loading rates and peak forces as that seen in running. Ideally this would be 2000 N in 30 ms for a heel strike and 2000 N over 100 ms for a forefoot strike. Assuming the runner acts as a solid mass (as our impactor will) this means the shoe must decelerate the 70 kg mass at 2.9125 g. Using the equations of motion this requires an impact speed of 0.857 m/s for a 30 ms strike time. This equates to a drop height of 37.45 mm. The rig design allowed the drop mass to be changed (with some disassembly) so the mass was initially set to 70kg. This gave an impact time of 40 ms with a 2000 N force for a heel strike, but a 30 ms impact time for the same force on a forefoot strike. As the motion of the footstrike is very different from a drop test, this result was considered to be as good as possible from the available equipment. Adjustment of the weight to change the footstrike response would change the heelstrike detrimentally.

ASTM F1614-99 Standard Test Method for Shock Attenuating Properties of Materials Systems for Athletic Footwear, also contains a drop test. There are two critical differences between the ASTM set up and the footwear drop rig; the mass of the ASTM is much smaller at 8.5 kg, and the impactor is a flat, 45 mm diameter cylinder. This ASTM was designed to test flat samples, where as the footwear rig was designed to mimic the adidas tests as closely as possible. Use of the ASTM stamp in a production shoe test would cause unrealistic pressures in the heel region (the ASTM does not have a forefoot stamp).

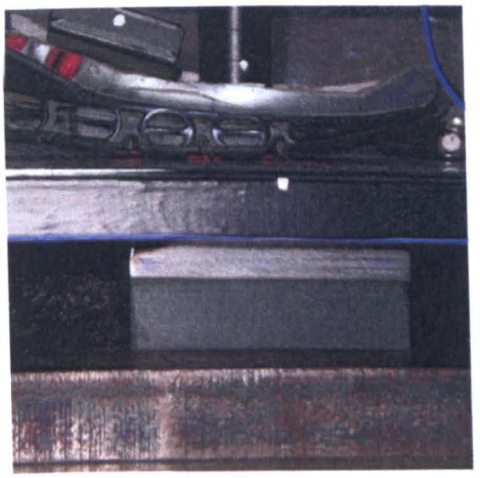

(a) Impact plate supports

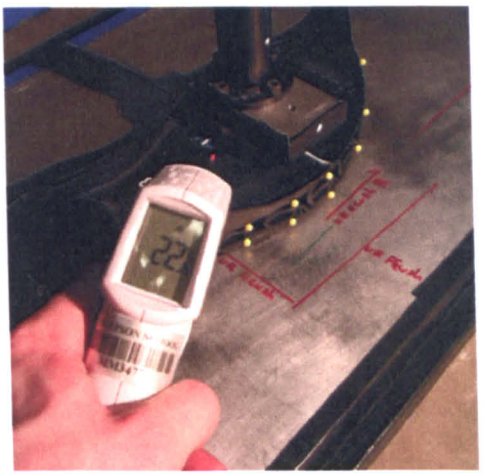

(b) Measurement of temperature

(c) Alignment of shoe using set-square and markings

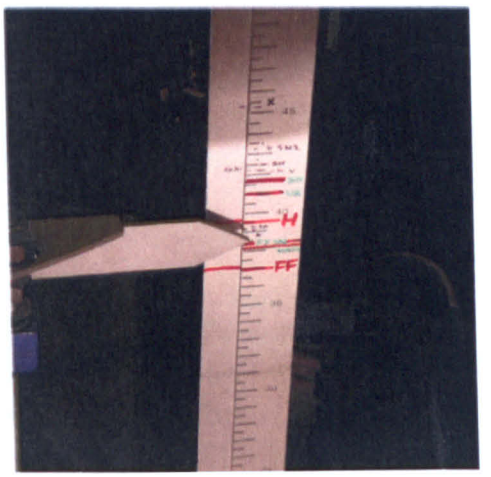

(d) Checking of height to which stack is lifted

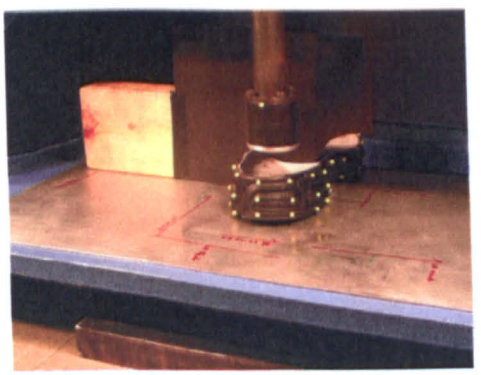

(e) Masking of forefoot pins during heel stamp from the rear

(f) Additional padding to reduce ringing in the frame caused by movement of the clamp on release

Figure 5.28: Details of drop rig testing for assembled midsoles and production shoes.

During testing, measurements were made using an ICP 353B34 Piezoelectric accelerometer which outputs a signal through a LeCroy 9304C oscilloscope via an ICP 480C02 Sensor Signal Conditioner. The signal was sampled digitally at 2 kHz. The oscilloscope was linked to a laser trigger mechanism, which permits synchronisation of the acceleration and structural tracking measurements. As the high speed camera required powerful spotlights, a 12-inch diameter desk fan was used to cool the shoe and test area. The temperature during test was recorded using a Raytek MinitempFS laser temperature gauge (Figure 5.28), accurate to $\pm 1°C$.

Figure 5.29: Drop rig set-up for testing.

Method Each test consisted of three impacts to the shoe using one of two impactors (stamps): heel and forefoot (shown in Figure 5.30). The shoe was positioned using a set-square aligned with markings on the aluminium sheet (Figure 5.28(c)). The stack was then winched to a height determined from trials using shoes of the same type (but not used in the results) to give a peak impact force of 1500 N - the same used in the quasi-static tests. The temperature of the shoe area to be impacted was recorded. The camera and oscilloscope were readied for recording and the catch was released by a sharp tug of the pin cord. The cable was then wound out, the catch attached and the stack lifted off the shoe quickly so as not to cause excessive damage to the shoe. This normally took around 15 seconds from the end of the impact. Three repeats were carried out on each of four shoes of each type before the stamp was changed and the shoes tested in repeat order.

It was found that the high-speed camera must be placed a sufficient distance away from the drop area to minimise vibration from the impact transferred through the floor. A longer zoom lens or better isolation of the camera would improve resolution for the dynamic test.

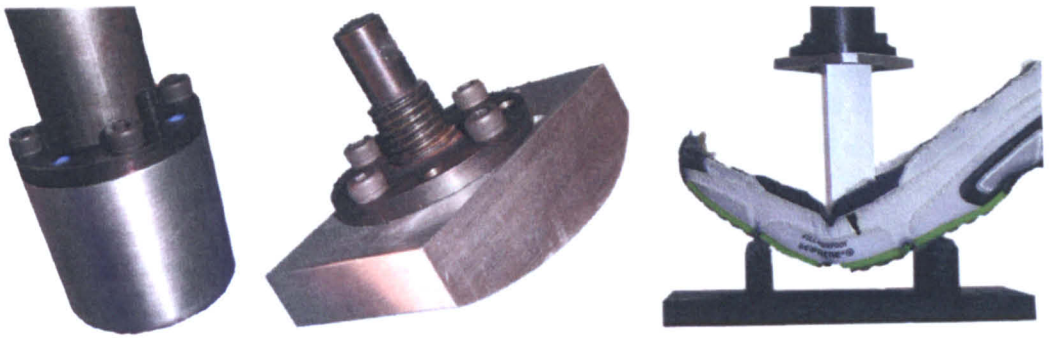

(a) (b) (c)

Figure 5.30: Stamps used for testing. (a) Heel, (b) forefoot and (c) bend test stamps.

5.4.4 Extraction of Results

Structural tracking extraction from the high speed video is detailed in Section 5.5. The results from the accelerometer came as an ASCII file, so were imported into Excel for processing. Due to the nature of release, there was some residual oscillation in the various parts of the rig which causes a noisy signal. This oscillation began before impact of the shoe and can be seen in Figure 5.31.

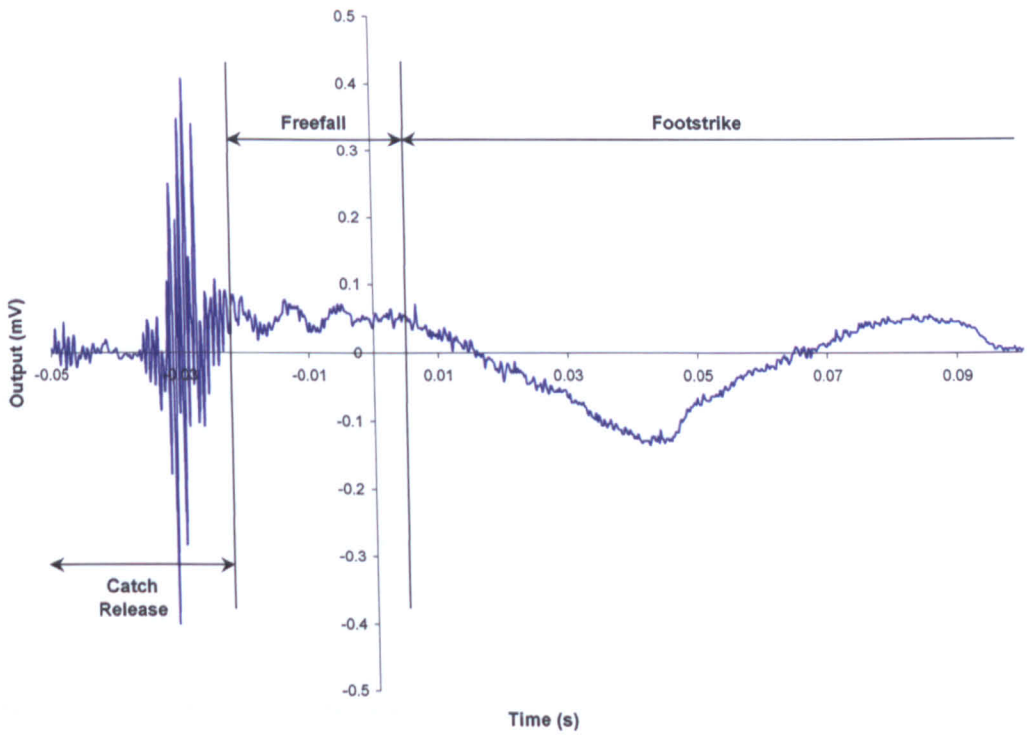

Figure 5.31: Output from accelerometer before filtering. Note the contrast between the high frequency, mixed amplitude noise on release, with the lower amplitude, low frequency output caused by the shoe impact.

The use of Fourier transform allowed removal of higher frequency signals that occurred due to residual oscillations. Figure 5.32 shows the result of running an adapted fast Fourier transform (FFT) Visual Basic macro (McCauley 1999) on a section of the results. The frequencies higher than a chosen value were removed during the process and the noise was reduced much more effectively than when using a moving average filter. Excessive filtering would remove useful data, as the figure shows, the <25 Hz filter is just beginning to 'lose' the real data curve near the points of inflexion. However, the smoother the output results, the less estimation and correction will be needed during numerical processing and extraction of results. A balance must be found.

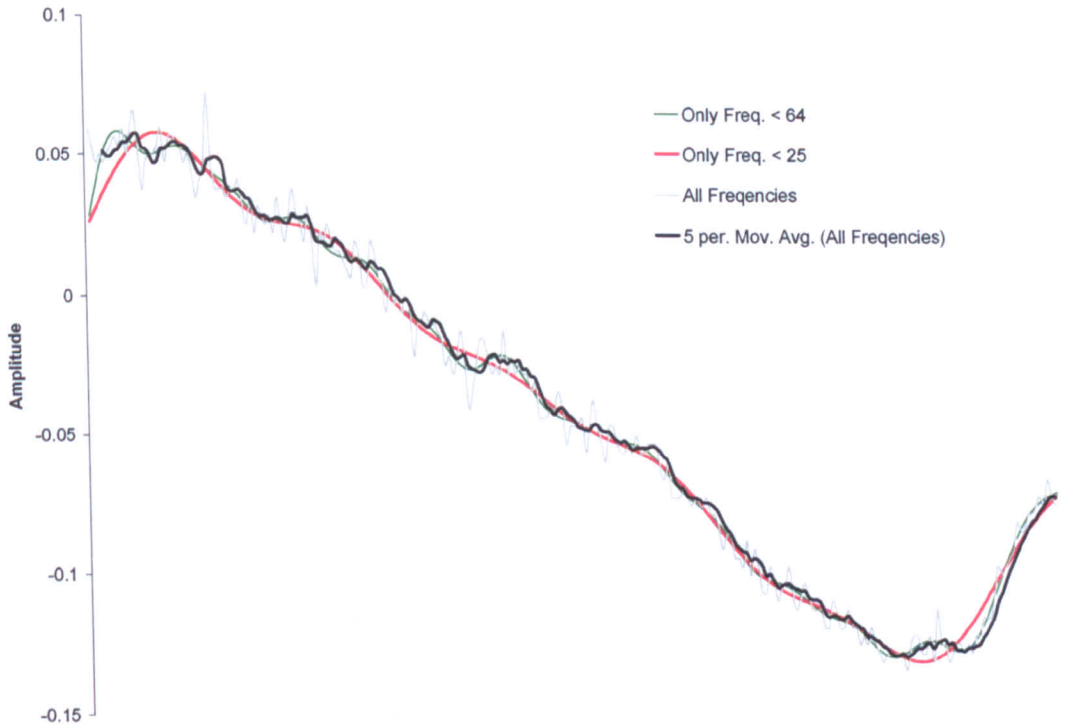

Figure 5.32: FFT filtering of the accelerometer data. Note the contrast between using a moving average filter (5 pixel range) and removing all frequencies above 25 and above 64 Hz.

As the physical testing in Chapter 9 will show, there was a high dependance of peak reaction force on displacement of the stamps, especially in the forefoot cushion test. Despite carefully filtering the results, the force/deflection response calculated from the accelerometer reading showed too much noise to allow accurate positional measurement. Any more filtering affected the peak force readings, and while the tests were repeatable (and allowed filming for the structural tracking process) another method was required to achieve accurate high speed force/deflection results.

5.4.5 High Speed Instron Testing

Force/deflection curves were obtained using a servo-hydraulic Instron, operating at realistic shoe speeds. Table 5.1 details the loading times.

	Load	Unload	Rest
Heel Cushion	35	65	710
Forefoot Cushion	100	100	710
Forefoot Bend	100	100	710

Table 5.1: Loading times for cyclic mechanical tests (all in ms).

Method While the machine was capable of moving at the high speeds required, it overshot a given load unless it was given the stiffness of the sample. This is normally done by cycling the sample multiple times. As the shoes under test had undergone less than 10 impacts at the time of testing, it was thought that this cycling may cause the shoe to settle in more. Ideally, new shoes would be available so the no-preload response could be recorded, but this was not the case so the machine was driven to a given displacement. This required one or two cycles to get the displacement within the desired range (1500 N $\pm$ 50 N), then the test was performed over 10 consecutive cycles. Care was taken not to overload the shoe and induce extra damage, softening its response. The zero point of displacement was taken as the position when the shoe showed a pre-load of 20 N. Bend tests were pre-loaded to 5 N, and driven to 15 mm displacement for all tests.

Figure 5.33: Servo-hydraulic Instron machine at adidas' test facility, with Gigaride assembled midsole undergoing a heel cushioning test.

5.5 Structural Tracking

The following method of measuring the structural response of a shoe by tracking the movement of points on its surface has been developed to allow more advanced verification of FE models than by using force-deflection curves alone.

The shoe is constructed of many parts and materials, each with different static and dynamic properties, and all interacting with their connecting parts. By using only force-deflection measurements it would be theoretically possible to create a cube of material in FE that would reproduce the impact response of a shoe. This cube (or any other simple shape) would not be able to reproduce the shape of the shoe during loading, and the use of structural measurements would show this. For example, if both a physical shoe and virtual shoe have the same force response under a heel compression test, but the very front of the physical shoe rises three times as high from the floor as the FE model, then there are some inaccuracies in the model. These may not be immediately critical in this test, but when the model is used for predictive purposes, as much information about the way in which the shoe behaves should be added to the model in order to achieve an accurate prediction in other loading scenarios.

For dynamic testing using a drop-rig, structural tracking also gives a useful method of verifying the displacement and velocity of the impact, and also any relative movement of the test rig and camera that may otherwise cause errors in the results.

5.5.1 Required Measurements

Structural tracking allows many additional measurements to be made, but for the purposes of this research the following metrics will be used, illustrated in Figures 5.34-5.39.

Drop Height Physically Measured. The distance above the floor from the bottom of the stamp before release (Figure 5.34).

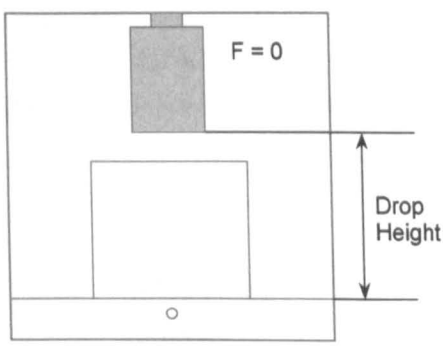

Figure 5.34: Definition of Drop Height.

Free Height Physically Measured. The distance above the floor from the top surface of the midsole directly under the stamp. This can be a difficult measurement to make as the shoe does not sit flat on the floor. To overcome this and to exclude any tilting of the shoe from affecting the results, the free height was measured on the Instron machine with a preload of 20 N on the shoe before any testing had been carried out (Figure 5.35).

Datum Height Derived from Video. The distance from the top of the video frame to the floor. This was taken as the position of the floor pin (a mark on the floor) less the physically measured difference between the floor pin and the surface of the floor (Figure 5.35).

$$(Datum\ Height)_{pix} = (Floor\ Pin)_{pix} - (Measured\ Floor - Pin\ Distance)_{mm}$$

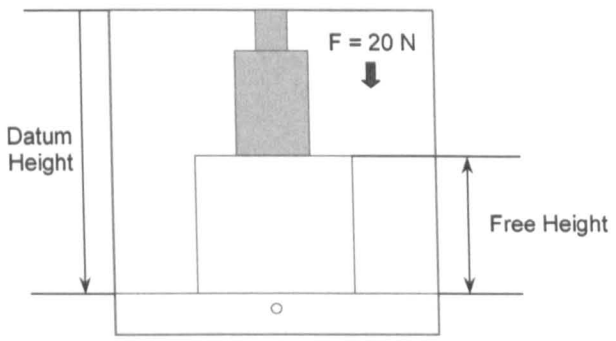

Figure 5.35: Definition of Free Height and Datum Height.

Rest Height Physically Measured. The distance above the floor from the bottom of the stamp when the weight stack has been released and slowly lowered onto the midsole (compressing the midsole). This measurement attempts to overcome not only any tilting induced in the shoe during measurement, but also the any compression in the very soft cloth surface found on production shoes (Figure 5.36). Rest height is a static measurement of compression while the other compression measures are taken under dynamic loading.

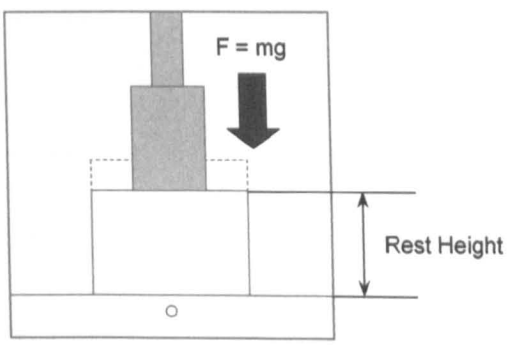

Figure 5.36: Definition of Rest Height.

Maximum Compression Derived from Video. Difference between the free height of the midsole and the lowest height above the floor achieved by the stamp (Figure 5.37).

$$(Max.Compression)_{pix} = (FreeHeight)_{mm} - [(DatumHeight)_{pix} - (Min.StampHeight)_{pix}]$$

Minimum Midsole Depth Derived from Video. The minimum height above the floor reached by the end of the stamp. Useful for picking up errors in measurement (e.g. the minimum must be positive), Figure 5.37.

$$(Min.\ Midsole\ Depth)_{pix} = (Datum\ Height)_{pix} - (Min.\ Stamp\ Height)_{pix}$$

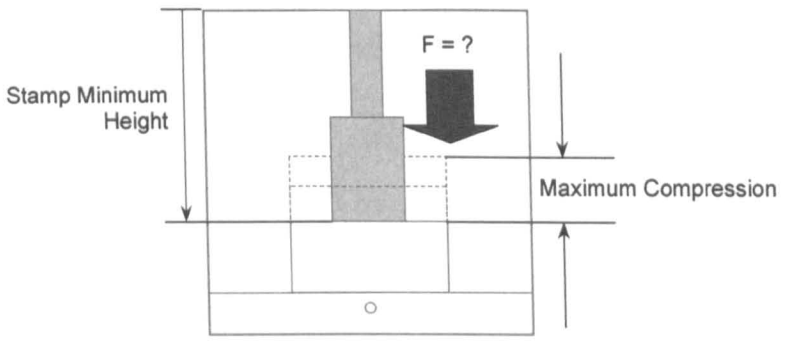

Figure 5.37: Definition of Maximum Compression and Minimum Midsole Depth.

Rebound Height Derived from Video. The difference in position of the stamp pin between maximum compression and the next maximum height of the stamp. This is measured in pixels and directly outputted from the code (Figure 5.38).

Rebound Derived from Video. The distance above the rest height to which the stamp rebounds (Figure 5.38).

$$(Rebound) = [(Min.\ Stamp\ Height)_{pix} + (Rebound\ Height)_{pix}] - (Rest\ Height)_{mm}$$

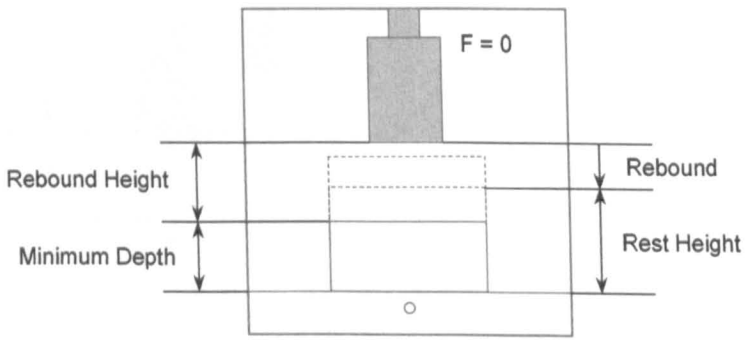

Figure 5.38: Definition of Rebound and Rebound Height.

Coefficient of Restitution (COR) Derived from Video. Ratio of input energy to output energy. Normally this is expressed as the input/output velocity ratio, but as velocity is directly related to the final height, the ratio of heights can be used:

$$v^2 = u^2 + 2as$$

where a =g,s = height, giving:

$$v^2 = 2gh$$

giving the ratio:

$$\frac{v_{out}^2}{v_{in}^2} = \frac{2gh_{out}}{2gh_{in}} = \frac{h_{out}}{h_{in}}$$

The zero height is considered as the maximum compression height, as at this point all the potential energy of the mass has been delivered into the shoe, so the input and output heights are defined as:

$$h_{in} = (Drop\ Height) - (Minimum\ Midsole\ Height)$$

$$h_{out} = Rebound\ Height$$

therefore:

$$COR = \frac{h_{in}}{h_{out}} = \frac{Rebound\ Height}{(Drop\ Height) - (Minimum\ Midsole\ Height)}$$

Tip Max. Derived from Video. The maximum displacement of the tip pin (the furthest pin from the stamp that can be tracked consistently, normally Pin 1 for heel stamp tests, and pins 16 or 24 for forefoot tests). It was measured within the code with the start point taken as t_0 (frame 1).

Tip Delay Derived from Video. Defined as the time between when the stamp achieved its minimum height, and the tip achieved its maximum height, measured in milliseconds (Figure 5.39).

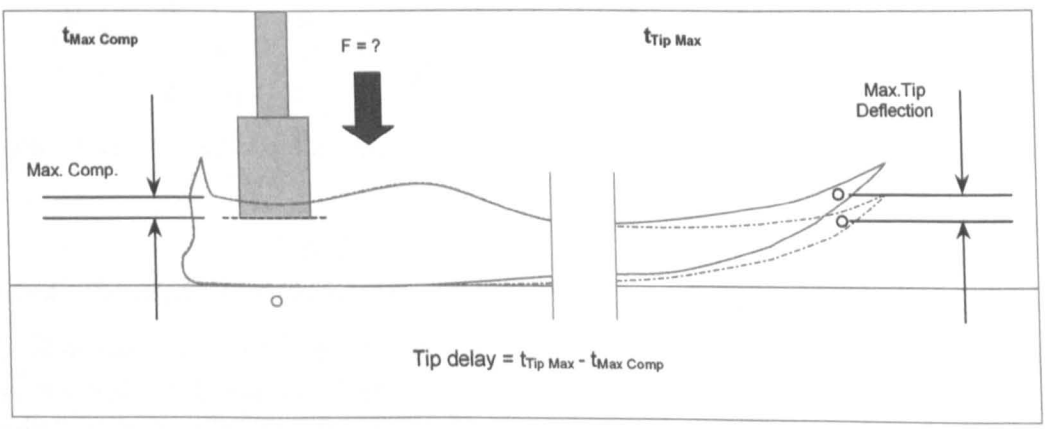

Figure 5.39: Definition of Tip Delay.

Component Strain For more detailed comparisons the strain of a section of a structure between two pins can be estimated by tracking the relative displacement of those pins. This will only be a viable method of strain measurement if the pins are placed on a part of roughly continual cross sectional area.

Visual Comparison To quickly assess the large amount of information that comes out of structural tracking, images of the physical test can be overlayed with results from FEA. This can be done as a animation overlay (Figure 5.40) or as a pin-track overlay (Figure 5.41).

It must be noted that all of the structural measurements are based on positions of pins derived from video data. Other than errors in extraction of positions and associated calculations, the main source of error that must be acknowledged when comparing physical and virtual results is that the positions of the real pins and the virtual ones (nodes) may not be in the same place. This is partly due to difficulties placing pins in a repeatable position, but more likely due to not having a node in the same place due to the density of the mesh.

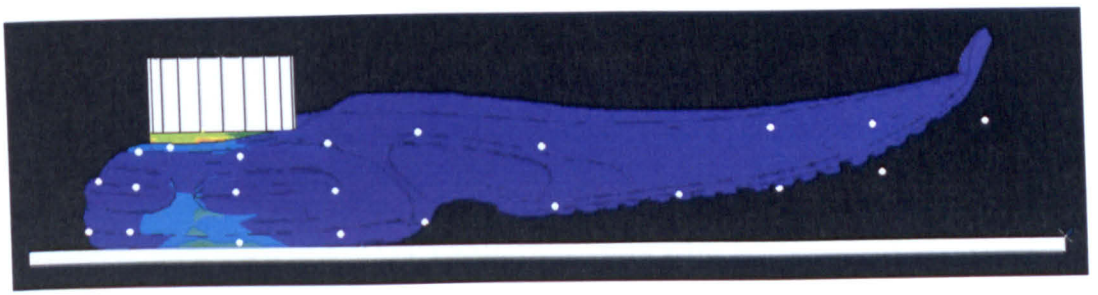

Figure 5.40: Still of a FE result animation, overlayed with pin positions (white) taken from high-speed video. Note that the FE model has rise further than the real, indicating that the front of the FE shoe is moving faster.

Figure 5.41: Screenshot of pin tracks over an entire test, displayed using the PinTracker Visual Basic program.

5.5.2 Sample Preparation

To allow tracking of points on the surface of the midsole during loading, the midsoles were sprayed with a light coating of either black or white paint, to match the colour of the main midsole material. This was done to avoid any erroneous results occurring from cracks in the paint during the tests (Figure 5.42). Pins with 4 mm spherical heads were then inserted into the samples at points of interest. Pins were used as paper was found to fall off during dynamic impacts and marking the TPU surfaces in a regular manner was difficult (though for close-up quasi-static testing Tipp-Ex was found to be acceptable, Figure 5.26). The Gigaride structure material was found to be too tough to insert pins into, so 5 mm foam squares were cut and bonded onto the midsole (Figure 5.43).

The pin points were cut down to around 5 mm to minimise any effect on the properties of the materials while still restraining the pin heads from vibration. The pins used for each shoe were of a contrasting colour; originally white pins on black shoes and red pins on white shoes (red was chosen as preliminary tests indicated it gave better contrast under the lighting conditions, Figure 5.44). Shoes were given a light coat of anti-shine spray immediately before testing to reduce unwanted glare. Tests were then performed against a background the same colour as the shoe, thus highlighting the pinheads.

(a)

(b)

Figure 5.42: (a) Cracking in paint due to testing. (b) Sectioned Ultraride structure illustrating depth of penetration of cut-down pins into material.

The positions of the pins were selected to give relevant information from the shoe. Pin 1 was always the pin at the 'tip', the very anterior of the midsole. The rest of the pins followed from that in a regular pattern. For structure shoes if there was enough room then pins were placed at either end of the structure centre, to record the strain of the centre part.

For coarsely meshed parts there was difficulty aligning the real pins with the virtual. To aid this process, physical structures are used as anchor points, as the edges of these structures also appear in the FE model. Figure 5.45 shows this process for the Supernova. The process was simpler in the structure shoes as there were more small geometries to assign pin positions too.

Figure 5.43: Foam blocks used in place of pins for Gigaride testing.

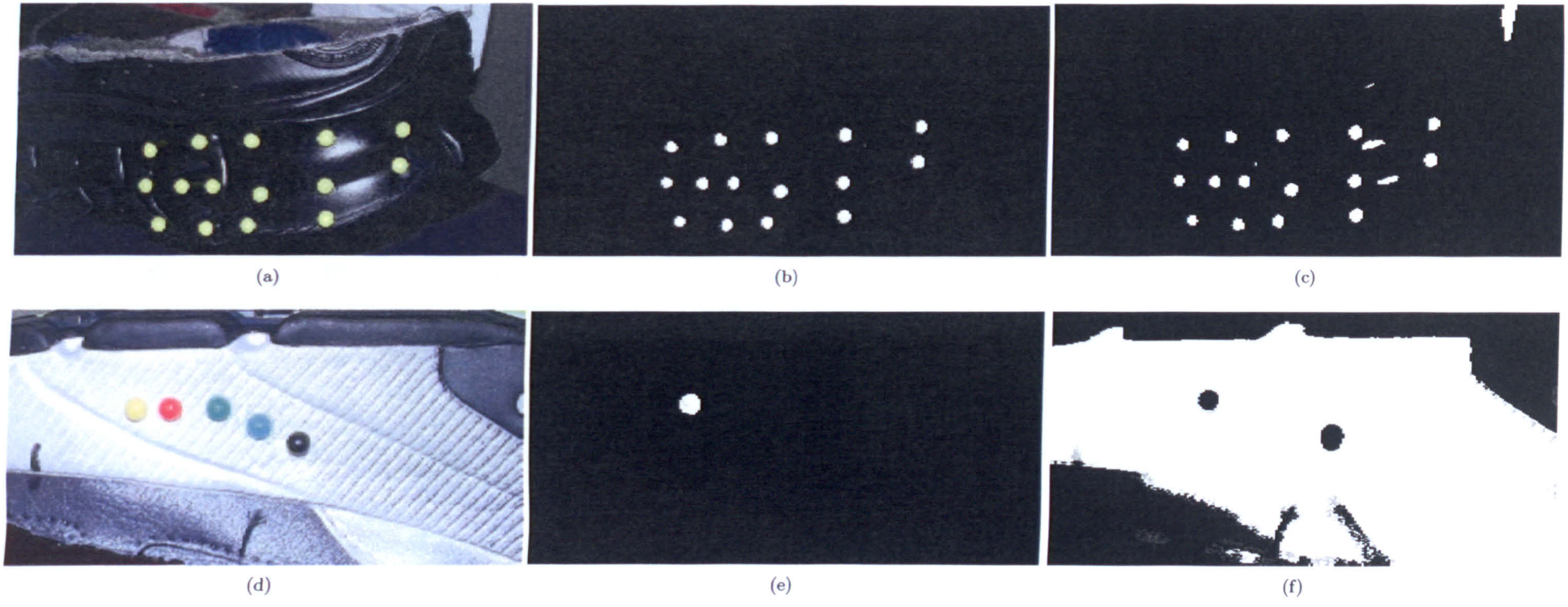

Figure 5.44: Initial testing of pin/shoe contrast and thresholding.
Ultraride:
(a) Colour video still.
(b) Colour image, saturation channel, thresholded > 169 with salt and pepper filter.
(c) Greyscale image, thresholded at > 214 with salt and pepper filter.
Supernova:
(d) Colour video still.
(e) Colour image, hue channel, thresholded > 238 with salt and pepper filter.
(f) Greyscale image, thresholded at > 159 with salt and pepper filter.

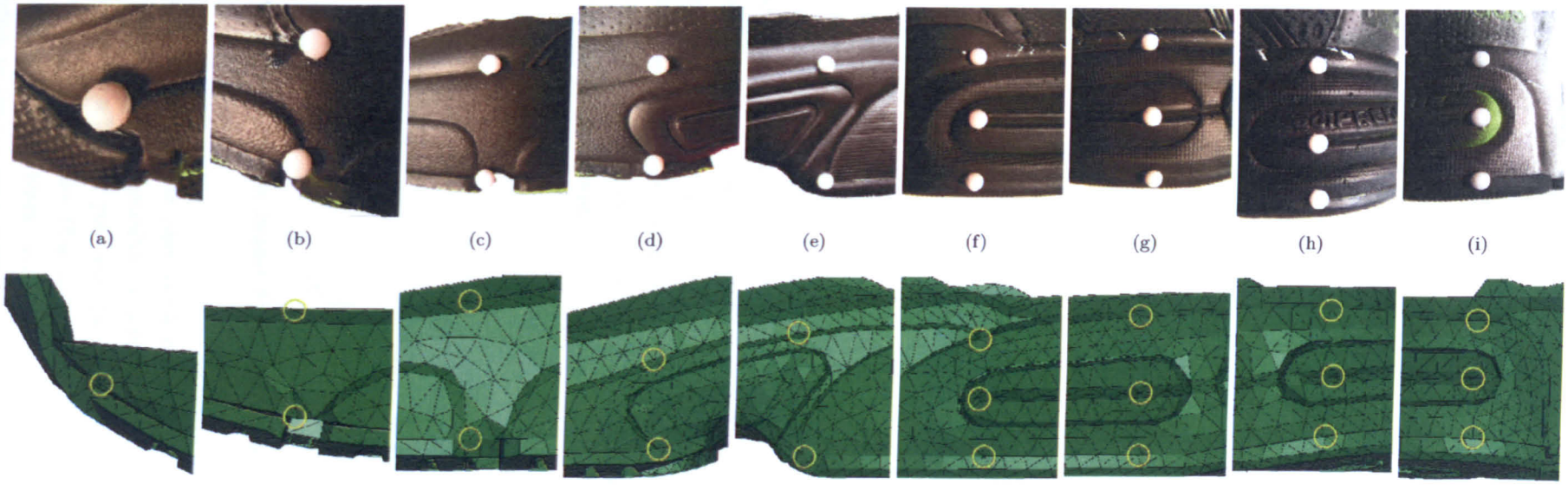

Figure 5.45: (a)Tip Pin(1): Intersection of outsole, midsole and upper.
(b)Pin 3: Intersection of outsole and lower first anterior 'arch' detail. Pin 2: Vertically above Pin 3, so the centre of the pin head is on the upper/midsole interface.
(c)Pin 5: Intersection of outsole and lower second anterior 'arch' detail Pin 4: Vertically above Pin 5, so the centre of the pin head is on the upper/midsole interface. Pins 6-7 follow the same pattern as Pins 4 & 5.
(d)Pin 9: Intersection of outsole, midsole and anterior edge of torsion bar. Pin 10: Vertically above Pin 9, on the line of the moulded detail shown.
(e)Pin 11: Intersection of outsole, midsole and midsole heel cover. Pin 10: Vertically above Pin 11, on the line of the moulded detail shown.
(f)Pin 13: Centered on the anterior end of the channel in the anterior protrusion of the adiPRENE insert. Pin 12: Vertically above Pin 13, at the intersection of the midsole heel cover, midsole and moulding. Pin 14: Vertically below Pin 13, on the outsole/midsole heel cover intersection.
(g)Pin 16: Equidistant between pins 13 and 19. Pins 18 and 20 vertically above and below.
(h)Pin 19: Center of the posterior protrusion under the 'd' of adiPRENE. Pins 18 and 20 vertically above and below.
(i)Pin 22: Posterior end of posterior adiPRENE protrusion. Pins 21 and 23 directly above and below. Note, these last three pins are only seen side-on by the camera.

5.5.3 Extraction of Results

Spatial measurement results in a large amount of data being generated. Each impact produces around 1000 images (recorded by high speed video at 4 kHz), each with approximately 30 points, so an automatic tracking system was developed. A flow chart of the process for drop tests can be seen in Figure 5.46, the process for Instron testing was similar on the video side, but took measurements directly from the Instron output.

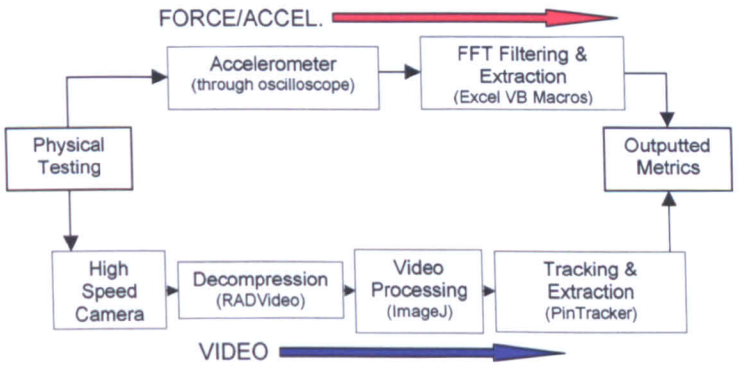

Figure 5.46: Overall process flow for obtaining results from drop testing.

5.5.3.1 Video Processing

Video from the high speed camera was first decompressed into AVI format using RADVideo (RAD Game Tools). ImageJ (Rasband 1997) was then used to create macros to automatically recognise and record positions of the midsole pins. For all the tests, the video images were first cropped, then thresholded to remove unwanted objects in the frame. The levels of crop and threshold for each test were inputted by hand as they were dependant on the camera and shoe positions and any lighting changes between each test. ImageJ's 'Analyze Particles' function was then used to find and analyse the remaining objects (Figure 5.47). This outputted the following measurements of particles in an image: height, width, perimeter,area, circularity, centre, first intercept point.

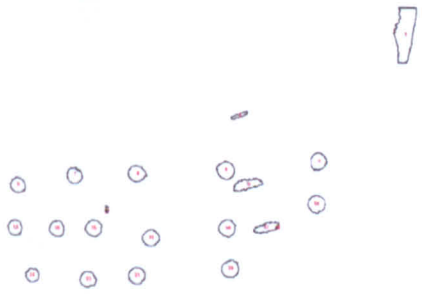

Figure 5.47: Output from ImageJ Analyze Particles function performed on the image in Figure 5.44(c).

During analysis of the quasi-static results it became apparent that when using red-on-white pins it was only possible to achieve reasonable results using a colour camera; the contrast between the red pins and the shadows in the image was not enough to distinguish them using greyscale video (Figure 5.48). As the high-speed camera was greyscale the white shoes were re-sprayed black, and white pins added. Due to the addition of a strict filtering system to the tracking program, errors caused by cracks in the paint were significantly reduced.

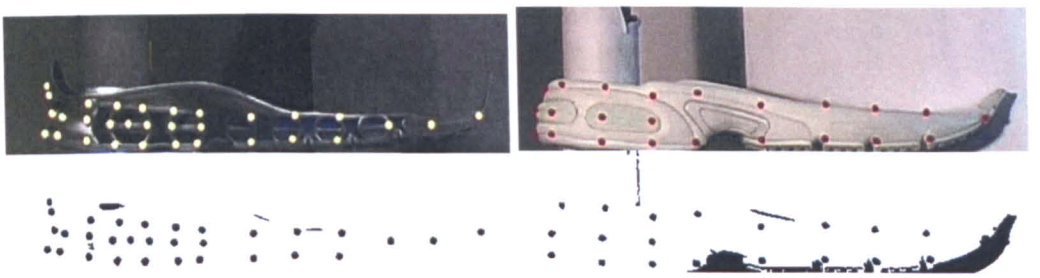

Figure 5.48: Colour video still and greyscale processed result for Ultraride and Supernova respectively. Note the much better result from yellow-on-black than red-on-white in terms of picking out only the pins from the image when the color has been removed from the image.

5.5.3.2 Tracking

A MS Visual Basic program was created to organise the files and track the pin positions through each video. Objects not fitting user-inputted criteria of height, width, area, perimeter and circularity were removed by the first stage of the program. This left only the objects corresponding to pins, or objects that were visually similar (usually reflections). As a final stage of filtration, the user could input the positions of the pins in the first frame (by clicking on the image). The tracking algorithm would then attempt to follow each selected object through to the next frame. A check was performed on each object, and the closest object within a given radius was considered to be the position of the given pin in the next frame (Figure 5.49).

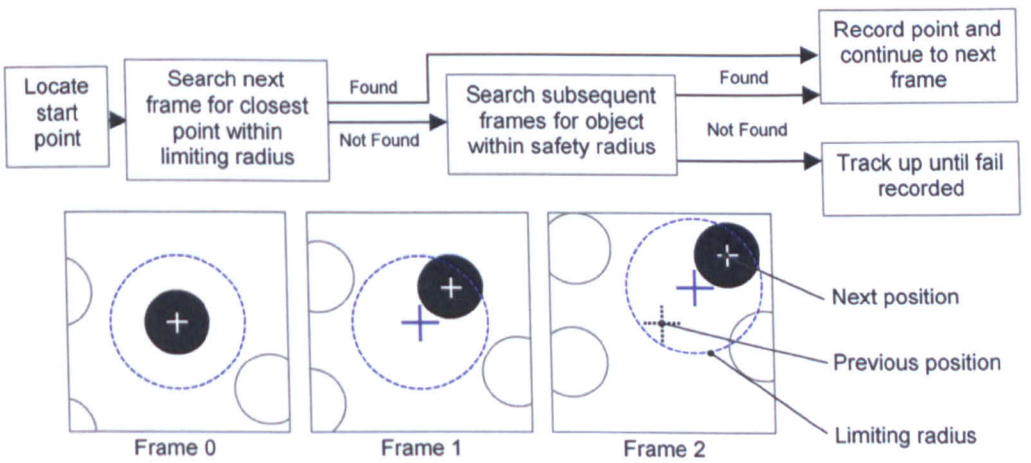

Figure 5.49: The core tracking process within PinTracker.

As the maximum speed of a pin seen on any of the results was around 1.5 pixels per frame, this method gave good results without requiring more complex tracking algorithms. Should any object be obscured during a frame (often due to it merging with a reflection and being removed) the algorithm holds the last known position of the object and picks it up when it becomes visible again - provided it has not moved out of the given tracking radius (15 pixels).

5.5.3.3 Extraction

The program performs the following steps:

1. Filtering While the data from the tracking was relatively smooth (compared with that from the accelerometer), the program looked for peaks and troughs in the data, so pixel-size noise caused problems. To avoid this the results were smoothed using a Gaussian filter (Figure 5.50).

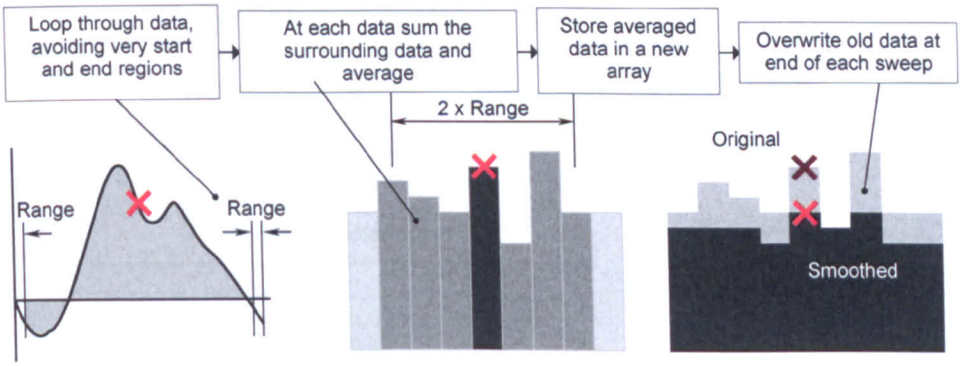

Figure 5.50: Details of the data smoothing process.

2. Synchronisation If the laser trigger mechanism fitted to the rig became dislodged between tests, the time between trigger and impact changed. To allow easier comparison, the program synchronises the peak g-force readings (corresponding to peak force) of each test.

3. Result Extraction Using the same peak-detecting function used for synchronisation, the program is able to detect the peak positional variation of an object. For testing this was chosen as the vertical limits of the stamp (giving peak compression and rebound height), and of the tip pin (giving maximum tip deflection, Figure 5.51). Recording the frame in which these events occur allows derivation of the dynamic metric, tip-delay, and the impact velocity (Figures 5.34-5.39). The resolution of the system was calculated to be 1 pixel = 0.46 mm for the high-speed camera in horizontal and vertical directions, and 1 pixel = 0.68 mm for the quasi-static camera. This process is summarised in Figure 5.52.

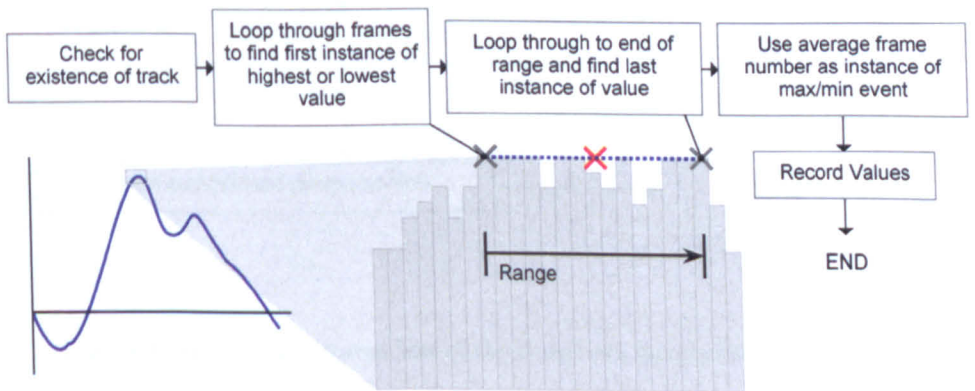

Figure 5.51: Calculation of minima and maxima points within PinTracker.

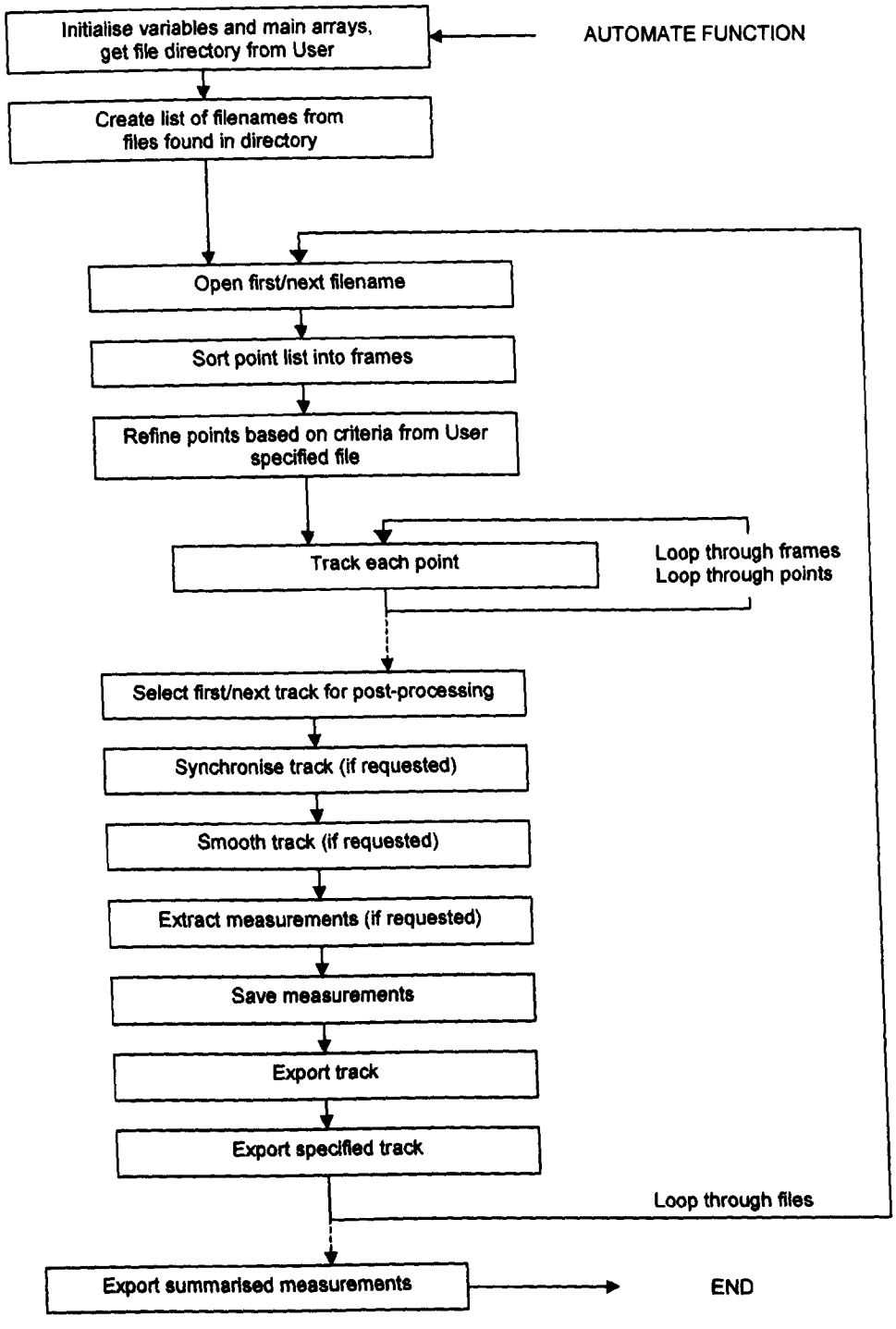

Figure 5.52: Overall process flow of the Automate function within PinTracker.

3D Structural Tracking

Accuracy of the tests were slightly compromised due to positioning of the cameras; the stereoscopic set-up meant both cameras must have the shoe fully in view, so part of the image was 'wasted' at either side on both cameras (Figure 5.53). The resolution of depth for the 3D setup was 6.81 mm, which was too poor for use in this instance (see Figure 5.54), so the 3D results are not presented here. Using one camera tightly cropped to the midsole produced better 2D results.

If 3D tracking is required in future, placement of a second camera at an angle, with the use of more complex calibration techniques, such as that detailed by Zhang (1999) should allow much better depth perception.

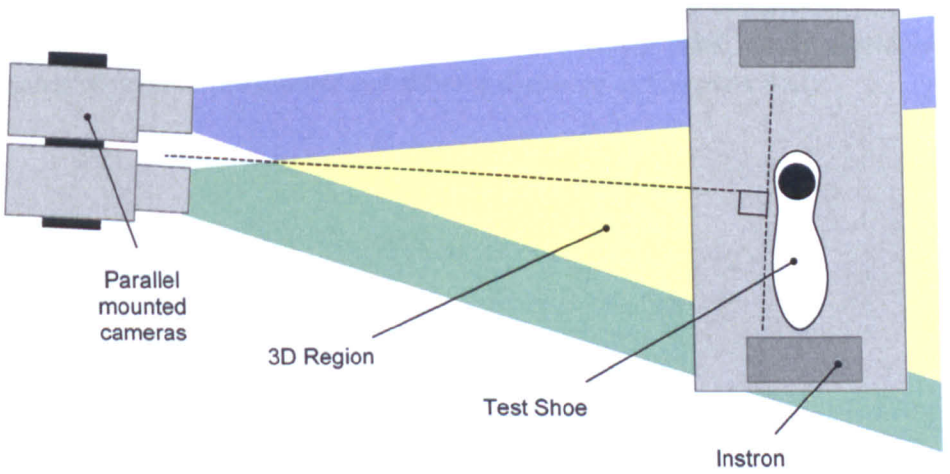

Figure 5.53: Test set-up for 3D structural tracking.

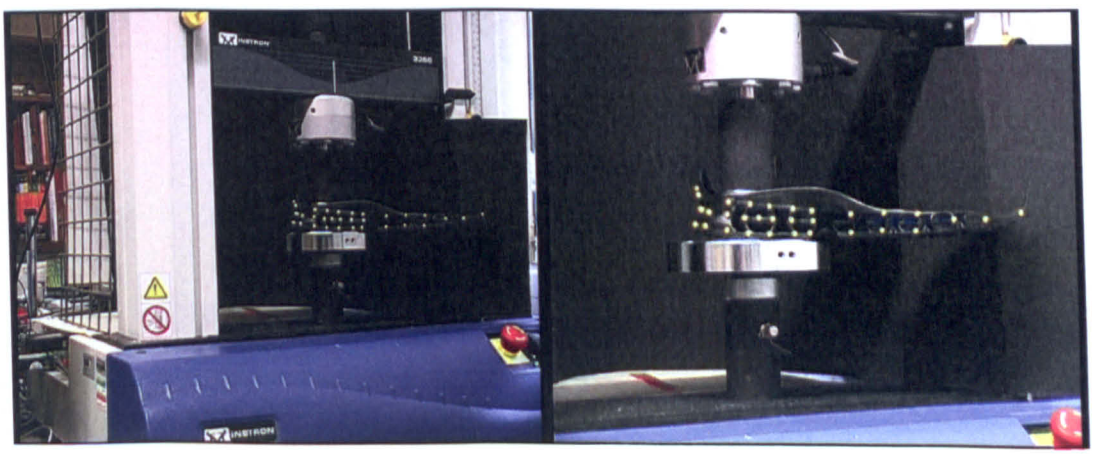

Figure 5.54: View from left and right cameras (respectively) when using 3D setup. Note the compromised resolution necessary to arrange both shoes in view of both cameras.

5.6 Chapter Summary

This chapter has presented a range of tests for shoe parts, assemblies and material samples.

Where necessary, improvements have been made to any standardised testing, and a technique for tracking the structural response of the shoe was presented. While the material sample tests are primarily for the collection of data for input into ABAQUS, the rest of the tests are crucial for verification of the FE models produced, and to gain understanding of the variations seen in physical parts.

However, to develop this understanding, prototype and production shoe parts and assemblies will need to be tested systematically and at length. If the distribution and properties of material in a moulded part can be predicted (perhaps using computational fluid dynamics techniques) then there will be less need for testing. Until that is possible, physical testing on many different parts will be required to build up a library of material performance adjustments based on material type, shape and manufacture process.

The level of accuracy required of the prediction will determine the amount and depth of the physical testing needed. The bounding limits of accuracy based on the repeatability of performance of manufactured parts and shoes is discussed in Chapters 8-11.

Chapter 6

The Modelling Process

This chapter explains the rationale for the approaches taken in Chapters 7-11 for the modelling of athletic footwear. The overall progression is illustrated in Figure 6.1.

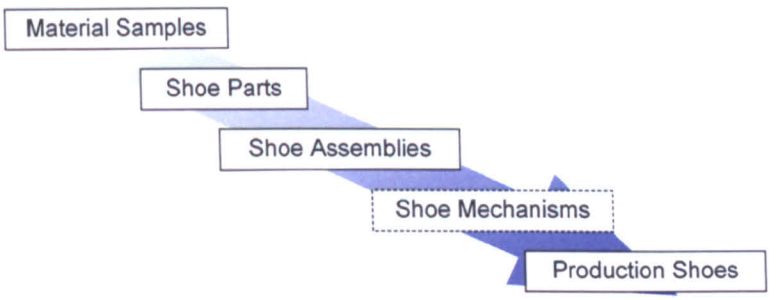

Figure 6.1: Illustration of the modelling process.

In order to produce an accurate FE model of a shoe, each component must be considered. Treating the whole shoe assembly as one part allows for rapid construction of reverse engineered models, but the aim of this research is to assess if it is possible to produce a predictive model that does not require verification by physical prototypes. To achieve this, the contribution to the shoe assemblies' performance that each part makes needs to be measured and understood.

Over the last few years the athletic footwear industry has seen new, more complex designs than the traditional solid foam shoe. If this trend continues, the ability to fully understand the roles of each component in what is effectively a suspension system, will be critical for designing and improving the performance of running shoes.

6.1 Geometrically Simple Objects

The material samples were created for the specific purpose of obtaining information about the physical response of the material. The generic uniaxial and multiaxial tests were designed to load the sample in a way that generates a homogenous stress/strain field (Figure 6.2).

This is common to material testing on many types of materials, but for polymers it is particularly relevant due to the Mullins effect. Recalling the discussion in Section 3.3.3, the stiffness of a polymer is dependant on its loading history. A sample that has been previously loaded to 50% strain will be softer than one previously loaded to 5% strain (Figure 6.3) due to breaking of more molecular chains at higher strains.

The 5% and 50% strained samples can now be considered different materials as they have different stress/strain curves (up to 50% strain) due to differing levels of plastic damage. Modelling these material samples is relatively simple, input the 5% strain data to model the 5% strain sample and so on. The results are likely to be accurate as the sample was loaded consistently (in a perfect test), so only one material state exists in each sample.

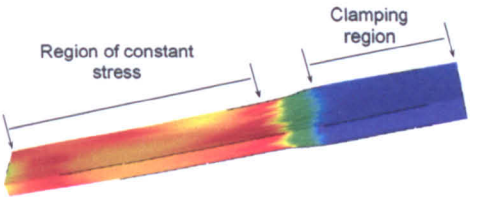

Figure 6.2: Illustration of a tension sample under uniaxial loading. Measurements are taken from the region of constant stress.

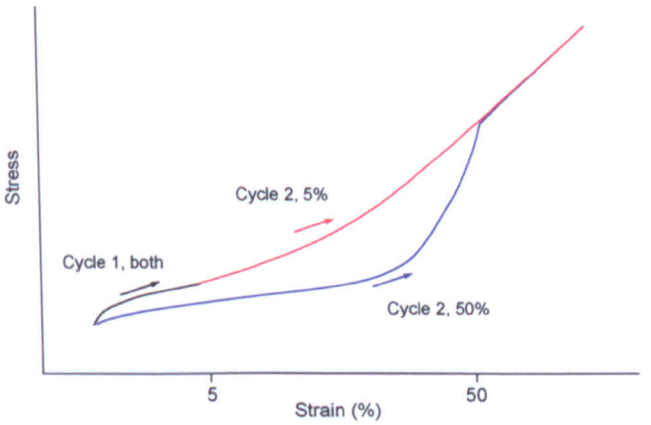

Figure 6.3: Illustration of the difference in stress/strain response for the second loading cycle of two identical objects previously strained to 5 and 50% strain. Note: not to scale.

6.2 Geometrically Complex Objects

The addition of irregular shapes complicates the problem of modelling and validating components. The structure in Figure 6.4 has been loaded such that there is a continuous range of strain occurring. For the sake of discussion, this range can be discritised into a set number of smaller strain ranges, in this case in 25% intervals.

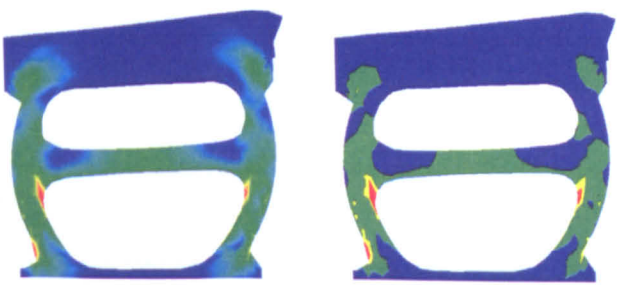

(a) (b)

Figure 6.4: Plot of the maximum strain archived during the first loading cycle of an Ultraride structure. (a) Continuous strain field, (b) Discritised strain field.

When this structure has been loaded and unloaded once, there effectively exists four different materials in the part. This is illustrated in Figure 6.5, where curves **a**, **b**, **c**, and **d** correspond to the material that has been strained to 0, 25, 50 and 75% respectively. If the Young's modulus of each material at 50% strain is measured (as indicated by the dotted trace lines), material **c** is roughly twice as stiff as **a** and **b**. Interestingly, material **d** has roughly the same stiffness as **a** and **b**, as measurements are taken just at the point where its curve begins to steepen. This highly non-linear behaviour makes modelling difficult.

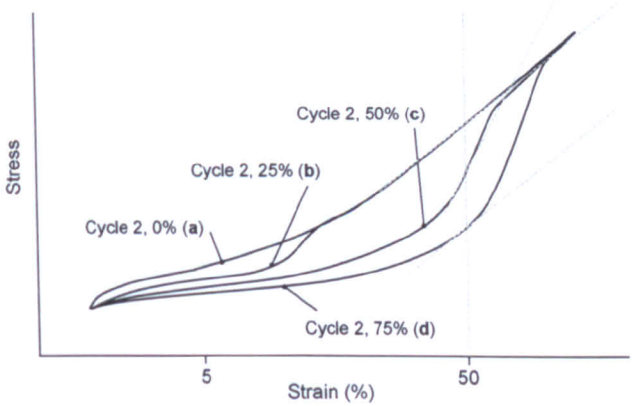

Figure 6.5: Illustration of the difference in stress/strain response for the second loading cycle of four identical objects previously strained to 0%, 25%, 50% and 75% strain. Note: not to scale.

Whilst accurate modelling of the first loading of the structure would be possible using material **a**, the second loading must include the respective stress/strain responses of all four materials, and their appropriate locations within the structure. An illustrative second loading curve from the whole object is shown in Figure 6.6. This result is not the response of any single material, it is a composite response of all four, that can only be calculated if the geometry and loading history is known, and the damage included in the model.

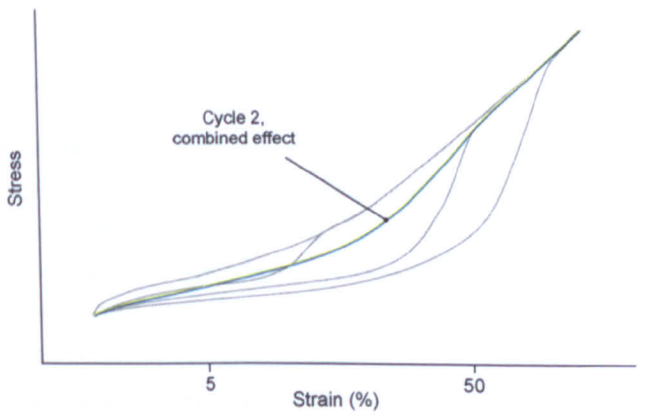

Figure 6.6: Illustration of a the overall response of a non-simple object on its second loading. Note: not to scale.

The advice in many of the material testing standards (see Section 3.4.3) is to assess what level of deformation the physical part will see under its typical loading, known as the operating strain, and pre-cycle the test piece to this strain before testing. This will theoretically give the closest match to the composite response, although it does assume the sample is loaded in the same way as the physical part.

However, a range of strains is often seen in shoe parts, so assessment of the operating strain is not straightforward. This results in the need for verification of FE results at as many modelling stages as possible.

6.3 Verification

So far, the change in behaviour of the initial material of a part into a range of different behaviours, based on the loading history of the part has been considered. The issue of what strain state of the material should be modelled, and what the results must be validated against, needs to be addressed.

In terms of modelling, the simplest and quickest approach is to model the initial **a** material, and compare this to the first loading of a sample, part or shoe. This is an acceptable approach to take for modelling of material samples, and even shoe parts. However, this method requires many physical samples as each one can only be loaded once, and the samples must reached the test apparatus in an unloaded condition.

While this may be achievable and the information gained from the process would be valuable to understanding how the FE model is performing, the results from the first loading of a shoe will be of little benefit to shoe designers if the shoe changes its response drastically in the second cycle.

Here lies the major problem with predictive shoe modelling. Unless a shoe component is loaded homogenously, or the material shows no Mullins effect at the strains it is loaded to, then the component would exhibit behaviour determined by its previous loadings and could not be accurately modelled with a single material model. The only way of doing this in FE is to model a cyclic test, which calculates the magnitude and location of the plastic damage caused throughout the component, for each cycle.

This is a lengthy process, as running 5 cycles will give a 5-fold increase in processing time, so there is scope for compromising accuracy and using a single material model for modelling the component. As samples have a different physical shape to shoe components, and are not loaded in the same way, it is difficult to assess how this material model can be created unless it is derived from reverse engineered physical prototypes. This is in conflict with the aim of creating a predictive technology, so the following approach is taken over the next chapters in an attempt to satisfy both aims to some extent.

Chapter 7: Material Samples Sets out the process used to create material models from specifically manufactured geometrically simple samples. All material tests are modelled to account for non-homogenous loadings, but only the first loading cycle is verified against for the majority of materials as the data comes from the **a** material curve. One example of the application of the Mullins effect on a geometrically simple shape in ABAQUS is considered.

A second issue discussed is the possibility that the material in the samples is different to that in the shoe components, so at this stage the material models are compared, but not adjusted. If a consistent difference is seen between the sample models and the part models, then there may also be some error in the results due to the way the mathematics is applied within the FE method.

Chapter 8: Moulded Shoe Parts The response of moulded shoe components is considered here. As the material models are derived from the **a** material data, the first loading of the part is used for verification.

Differences between the initial physical and model responses are investigated with respect to modelling errors and differences in physical properties between material samples and shoe parts. The single material models of the major components are adjusted here to fit the first loading of the physical data, so as to include the effects caused by moulding, or eliminate those caused by ABAQUS.

The Ultraride structure plate is modelled cyclicly with the Mullins effect included and the results compared to the first and subsequent physical loading cycles.

Chapter 9: Midsole Assemblies The combination of many shoe parts to form a shoe assembly is considered here. The ideal situation for the use of this technology in industry would occur if the **a** material model from the sample would give an acceptable match to the multi-cycled response of a shoe component. While this is theoretically unlikely, the difference between the unverified FE prediction and the shoe assembly has not been tested and could be small enough to be acceptable. This would result in a predictive technology without the need for cyclic modelling.

The ability to adjust whole shoe models based on the components' relative contributions to stiffness is also considered to allow the creation of material models that account for the moulding process and the effects of bonding within a shoe. This is done by verification of the model (which contains the **a** materials) against the multi-cycled shoe assemblies. The adjustments of the main components from Chapter 8 are included in the assembly model, and an estimation of the level of over/underprediction of the stiffness of the other components is made.

The Gigaride assembly is modelled cyclicly with the Mullins effect included and the results compared to the first and subsequent physical loading cycles.

Chapter 10: Mechanisms This chapter is an important consideration in the creation of accurate shoe models. It considers the addition of multi-part mechanisms into shoes (in contrast to shoes which are considered as a single object made from many bonded parts).

Chapter 11: Production Shoe Assemblies Considers the physical differences seen between the shoe assemblies and the cut-down production shoes that adidas perform their standard tests on. As no geometry or material information is currently available for shoe uppers, no FE models currently exist which contain uppers. Therefore this chapter contains only physical results. Comparisons are made between the assemblies and production shoes to give a insight into the effect of the lower part of the upper on shoe performance.

The application of the various material models to the FE modelling of athletic footwear is discussed in the conclusion (Chapter 12), along with notable conclusions and discussion points from all parts of this thesis.

Chapter 7

Modelling Stage 1: Material Samples

7.1 Introduction

This chapter charts the processes involved in creating a material model from practical tests performed on material samples. The methods of testing, along with the advantages, disadvantages and assumptions required for each have been detailed in Chapter 5.

A material model is required to give a FE mesh a physical response, without which the mesh is merely a set of connections in space. All the FE stress analysis used in this research must be run with material models (ABAQUS will not process those without).

It is possible to create material models with properties that are physically unrealistic. As long as the correct directionality is observed (compression is a negative stress, and must accompany a negative strain), then any value for stiffness can be given. However, to create a model that will output accurate values for stress and strain, accurate material models are required (assuming the rest of the model simulates the required situation correctly). These can be included in an ABAQUS analysis either as results from physical tests (as is done in this chapter) or directly as coefficients of strain energy potentials (as discussed in Section 4.6.1).

In an ideal modelling process, the creation of material models should be the first stage of the creation of a FE model, as the choice of material model can affect the elements that are required (see Section 7.5). The use of realistic physical properties within the model also allows any errors in the current job to be corrected much faster, as common sense can be applied to the results (i.e. do objects bounce or stop when they hit other objects?, is the steel impactor behaving much stiffer than the foam shoe?, etc.).

It has been shown in Section 3.3.5, that the speed at which a material is tested can have an effect on its stress/strain response. Because of this, a material should be tested to see if it exhibits a strain rate dependent effect, and if does, it should be tested at the same strain rates that it will see in the final model (in this case, during a footstrike). As the test equipment available during this research was not capable of reaching the required speeds, the overall stiffness was obtained from quasi-static testing and the change in stiffness with strain rate was determined from Dynamic Measurement Analysis (DMA).

The Mullins effect (Section 3.3.3) has also been shown to contribute heavily to a change in material stiffness over a number of loading cycles for the materials used in the shoes under test. The handling of the data collected that exhibits this effect, its input into ABAQUS and its effect on the results of models is discussed throughout this chapter.

While 14 materials have been tested and the data used to create material models, this chapter presents results from only one hyperelastic, one hyperfoam and one elastic material, to illustrate the process involved (which is summarised in Figure 7.1).

A critical element to this process is practical verification. Both the physical tests and the mathematical models created to simulate them have limitations and inherent inaccuracies, so to create a material model that is of practical use, the model must be tuned to be most accurate within the physical conditions that the end product/simulation will experience. This model must then be verified experimentally under conditions as close to the final operating conditions as possible.

For sample materials this is done in three stages: comparison of material curve fits, comparison of models of sample tests and where possible, comparison of tests on isolated shoe parts. The latter of these requires physical shoe parts to test, so cannot be part of a truly predictive technology, but is required to build up knowledge about the differences between material properties in samples and in moulded parts.

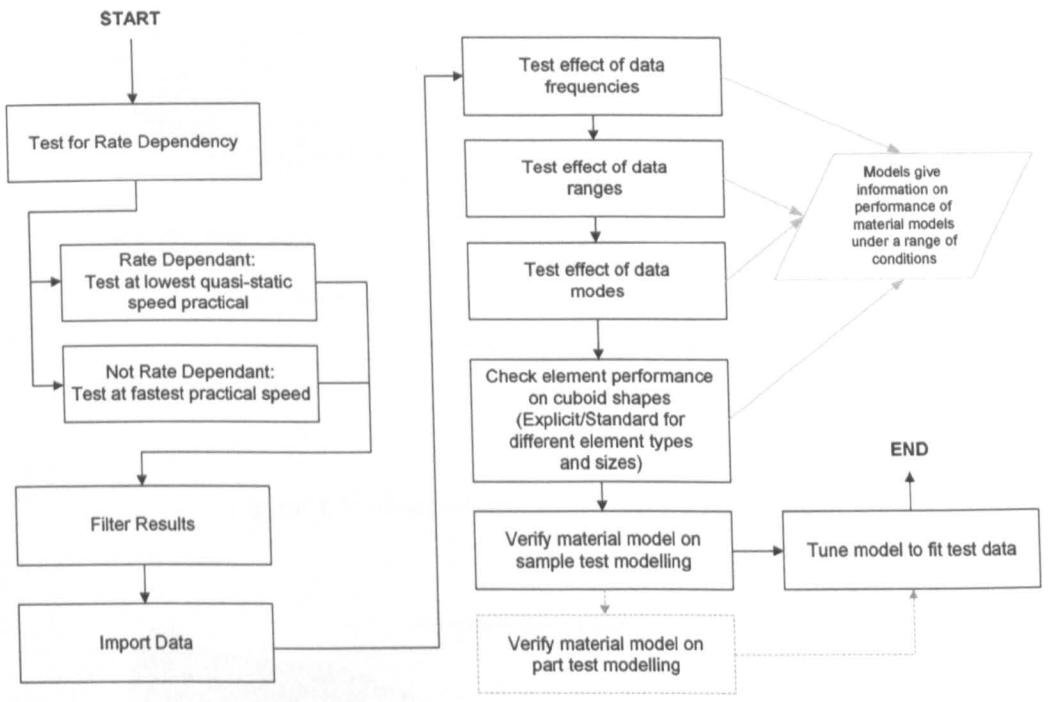

Figure 7.1: Testing/modelling process for determining the static response of shoe materials.

7.2 Materials Used

Figures 7.2-7.6 detail the materials used in the shoes and their locations. Table 7.1 gives information on the type of material and the manufacturers material codes, along with abbreviated names used throughout the rest of this chapter. It must be noted that not all the materials used in the shoes were included in the models, this is due to lack of sample materials. However, some parts (such as the outsole) changed only slightly between shoes and used very similar materials so it was assumed that the materials could be modelled with the same properties. The materials were modelled as homogeneous, although it has been shown in literature to be other otherwise (Section 3.3.8). This meant that the material was of constant stiffness, density and all other physical properties, and that one material model could be used to represent it. This decision was made on the basis that no inhomogeneity could be measured in the shoe parts, as discussed later in Section 7.3.3.

Figure 7.2: Materials used in the Supernova midsole.

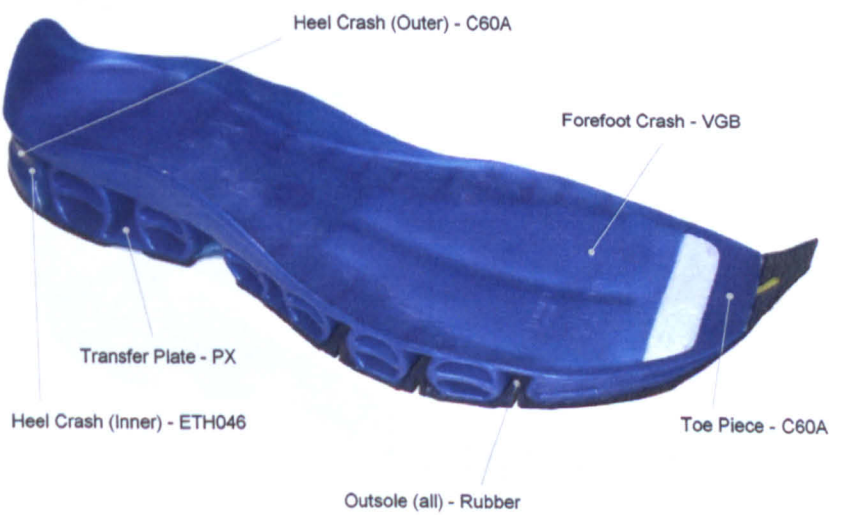

Figure 7.3: Materials used in the Ultraride midsole (part 1).

Figure 7.4: Materials used in the Ultraride midsole (part 2).

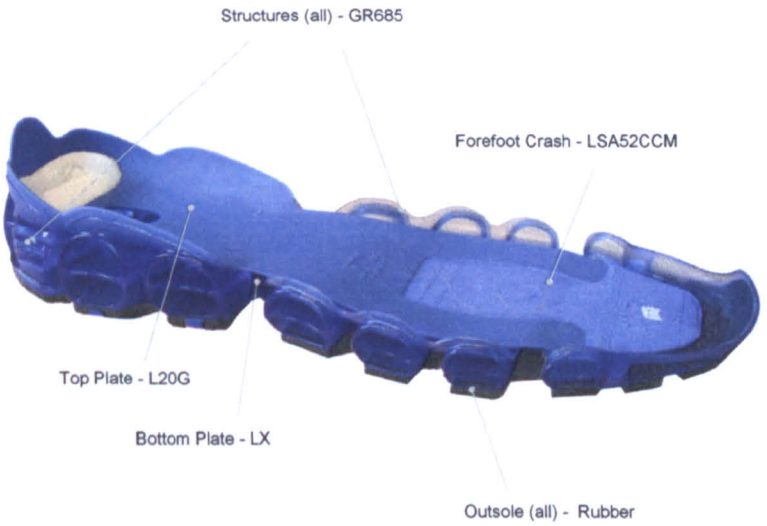

Figure 7.5: Materials used in the Gigaride midsole (part 1).

Figure 7.6: Materials used in the Gigaride midsole (part 2).

Shoe	Part	Manufacturers Name	Type	Abbreviation
Supernova	Midsole (Heel)	EVA-LS301655CCM	Hyperfoam	LS3016
Supernova	Midsole (Forefoot)	Rubber-EVA Light Strike adiPRENE +52CCM	Hyperfoam	LSA55CCM
Supernova	Midsole Heel Cover	EVA-LS301760CCM	Hyperfoam	LS3017
Supernova	adiPRENE Insert	Rubber-Foam adiPRENE CM	Hyperfoam	adi50CCM
Supernova	Torsion Bar	TPU Elastollan B 64 D Elastogran	Elastic	B64D
Supernova	Outsole	Rubber(s) 65C200BLNM/55A80SONM/65C160SMBL/65A40SOAWNM	Hyperelastic	Rubber
Ultraride	Structure Plate	Elastollan 1175AWH	Hyperelastic	UR1175
Ultraride	Heel Crash (Inner)	ETH04655CFF11802	Hyperfoam	ETH046
Ultraride	Heel Crash (Outer)	Elastollan C60A	Hyperelastic	C60A
Ultraride	Transfer Plate	Pebax 4033	Elastic	PX
Ultraride	Forefoot Crash	Rubber-EVA VGB7ACM	Hyperfoam	VGB
Ultraride	Toe Piece	Elastollan C60A	Hyperelastic	C60A
Ultraride	Outsole	adiWEAR 60A40AWNM Basic Peebax 3533 (Lug)	Hyperelastic	Rubber
Ultraride	'Midsole'	LS301655CCM	Hyperfoam	LS3016
Ultraride	'Midsole' Heel	IM adiPRENE	Hyperfoam	adi50CCM
Ultraride	'Midsole' Forefoot	Rubber-EVA VGB7A	Hyperfoam	VGB
Gigaride	Structures	Elastollan 685 AU	Hyperelastic	GR685
Gigaride	Top Plate	L 20 G EMS	Elastic	L20G
Gigaride	Bottom Plate	Vestamid LX 9012	Elastic	LX
Gigaride	Forefoot Crash	adiPRENE +52CCM	Hyperfoam	LSA52CCM
Gigaride	Outsole	65A40SOAWNM	Hyperelastic	Rubber
Gigaride	'Midsole'	EVA-LS301655CCM	Hyperfoam	LS3016

Table 7.1: Materials used in the adidas Supernova, Ultraride and Gigaride midsoles.

7.2.1 Operating Strains

In order to determine the operating strains of various shoe parts under loading, estimated material models were used in displacement-driven FE models. These material models were based on previous models of similar materials, created by adidas. The use of displacement driven tests reduced the effect of inaccurate stress prediction - and as only the strains were required this was considered to be acceptable. The three basic mechanical tests were modelled (heel cushion, forefoot cushion and forefoot bend), along with a virtual footstrike created by Mara (2006) that used the Supernova model. This was included as the material models created for this research were likely to be used in other virtual tests, so they needed to be robust for both simple mechanical tests and simulated footstrike conditions.

For parts that showed a range of strains, it was difficult to assess what the working strain of a material model should be. The following guidelines were drawn up and followed:

- Peak strain was ignored as this may be due to a single deformed element.
- Approximately 50% of the load-bearing area of the part should be in the operating strain.
- If the material of the part has shown little Mullins effect during uniaxial testing then this 50% value can be relaxed.
- If the material has shown significant Mullins effect then either this needs to be modelled, or the results verified with a physical part.

The last of these guidelines is particularly relevant for structures. As Figure 7.7 shows, under a heel cushion test there is a significant range of strains within one part. Modelling this with a single, unverified material model is likely to produce large inaccuracies in some parts of the structure. Table 7.2 details the estimated operating strain ranges for materials under various tests.

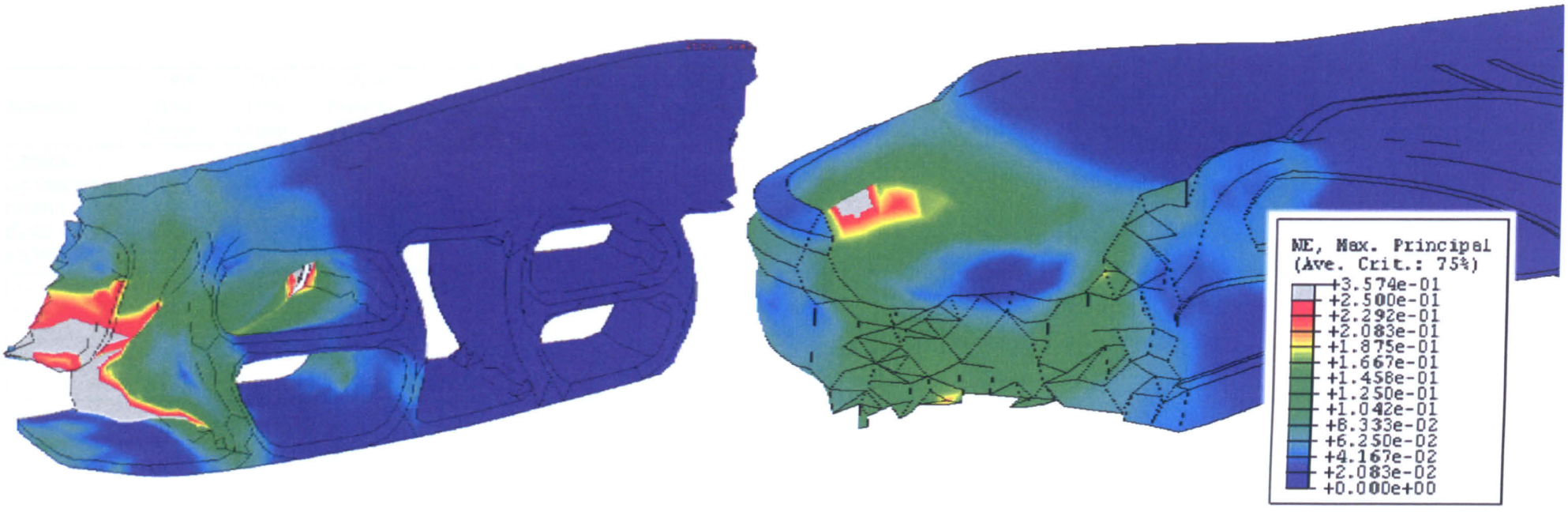

Figure 7.7: Variation in strain between structures and foam midsole under 2000N heel cushion loading. Both images are to the same scale and some elements have been hidden to show the internal strains. Note the higher variation in strain over a smaller area in the structure. The high strain spot on the foam shoe is generated by only a few elements in contact with the surface of the stamp.

Material	URS Heel Comp.	SNM Heel Comp.	SNM Forefoot Comp.	UR Heel Comp.	UR Forefoot Comp.	UR Forefoot Bend	SN Heel Comp.	SN Forefoot Comp.	SN Forefoot Bend	GR Heel Comp.	GR Forefoot Comp.	GR Forefoot Bend	—Footstrike— Heel	Forefoot
LS3016	-	5	<1	-	-	-	15	15	5	-	-	-	10	5
LSA52CCM	-	<1	5	-	-	-	15	15	5	-	-	-	5	15
LS3017	-	-	-	-	-	-	5	<1	<1	-	-	-	10	< 1
B64D	-	-	-	-	-	-	<1	<1	<1	-	-	-	<1	<1
adi50CCM	-	-	-	-	-	-	10	<1	<1	-	-	-	10	< 1
UR1175	10	-	-	30 (5-100)	15	10	-	-	-	-	-	-	-	-
C60A	20	-	-	<1	<1	<1	15	15	5	-	-	-	-	-
ETH046	-	-	-	20	<1	<1	-	-	-	-	-	-	-	-
PX	-	-	-	5	<1	<1	-	-	-	-	-	-	-	-
VGB	-	-	-	<1	15	10	-	-	-	≈1	10	5	-	-
GR685	-	-	-	-	-	-	-	-	-	25 (5-100)	20 (5-100)	5	-	-
L20G	-	-	-	-	-	-	-	-	-	5	5	≈1	-	-
LX	-	-	-	-	-	-	-	-	-	≈1	≈1	≈1	-	-
Rubber	-	-	-	5	15	10	10	5	5	10	5	5	15	20

Table 7.2: Estimated operating strain levels of the materials used in the adidas Supernova, Ultraride and Gigaride. '-' indicates material not used in this model. Values in brackets are the limits of strain seen in a sample with a large range of strain, the value outside the brackets is the estimated median value.

7.3 Selection of Test Data

ABAQUS does not accept multiple stress-strain curves from the same deformation mode as an input, so the data from the sample testing was reduced. The aim of the testing was to provide the long-term stress-strain response of the material at whatever pre-strain level was required. This was achieved by providing 0% pre-strain data coupled with a range of pre-strains into the *MULLINS EFFECT command, allowing material degradation to be modelled.

7.3.1 Rate Dependance

The material was first tested in uniaxial compression or tension at a range of strain rates to determine if it was rate dependant. If not, then the rest of the tests were performed at the highest practical speed: one which gives reliable results from the Instron machine, while minimising the impact on the limited time available for testing. If the material did show rate-dependency, then the slowest practical speed was used in the knowledge that there would be some small inaccuracies generated in the material model as the quasi-static stress-strain response was not being inputted. In future these errors could be calculated through creep and relaxation testing. Figure 7.8 shows two foam materials used in the Supernova, one rate dependant, one not.

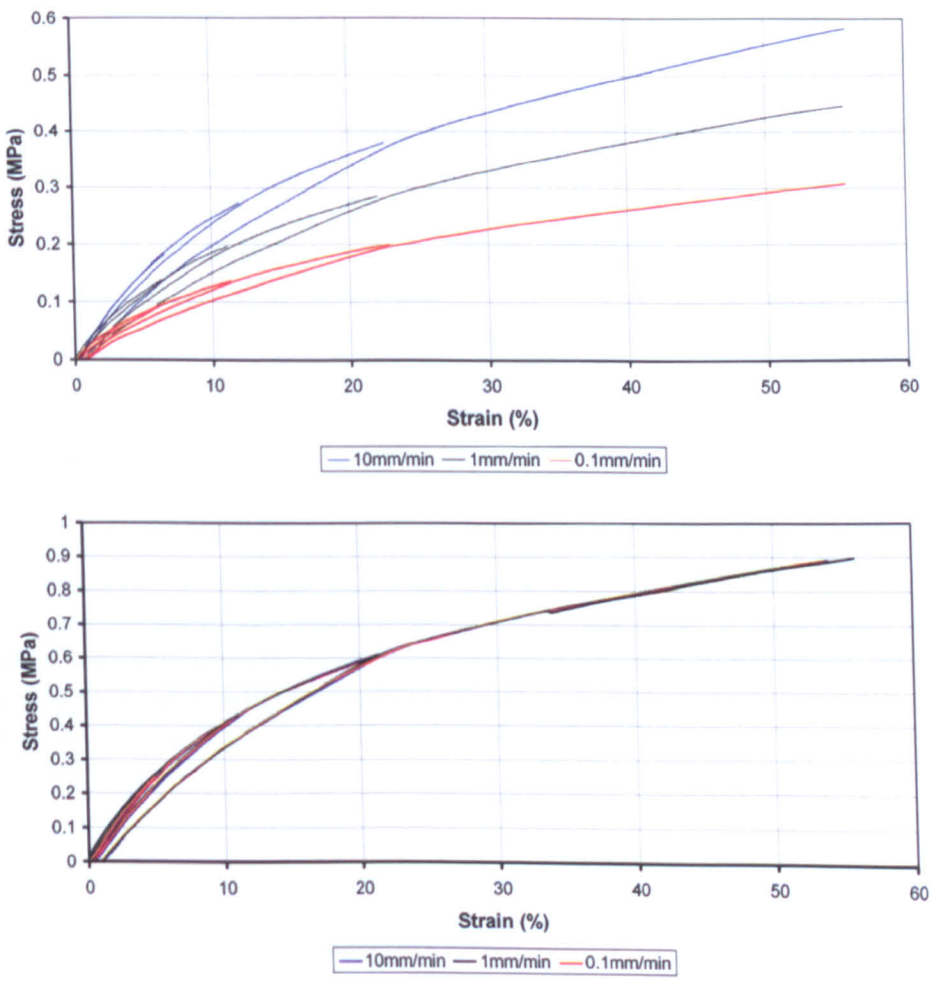

Figure 7.8: Stress-strain response of adi50CCM (top) and LSA52CCM materials tested at different crosshead speeds.

7.3.2 Grain Variation

During manufacture of the material samples, the moulding process generates inhomogeneities within the samples. This was most apparent in the sample sheets, where injection could create a visible radiating grain pattern around the injection site. Tests were carried to determine if the material sample orientation would significantly affect the results.

Samples were taken from a range of orientations for all materials (see Figure 5.9 for the TPU layout), but no significant differences were measured between orientations. Figure 7.9, shows the results for UR1175 and GR685. Neither material exhibited any orientation dependency, but the GR685 showed a difference in stiffness between samples taken from a pre-moulded bag of parts, and those cut from sheets. At strains less than 25% both samples could be considered similar, but above this range the pre-moulded samples were shown to be up to 100% stiffer.

The data used for input into ABAQUS was collected from tests on dog-bone shapes cut from sample sheets, as all the other TPU materials only came in sheet form, and the results also showed greater consistency. The sheet material was also likely to be more similar to the material seen in the structures as it was assumed that there was a variation of density with depth (thicker at the surface), as the thickness-width ratio of the structures was approximately 10, but only three for the moulded dog-bones.

7.3.3 Density Variation

While a variation due to moulding was seen in material samples taken from different moulded shapes, studying this effect in the final shoe parts was more difficult. A structure element from the Ultraride was dissected to obtain samples of material suspected to be of different densities (close to the surface, inside thick sections etc.). These samples were then weighed in air and water using an electronic balance. The sample locations and results are shown in Figure 7.10, but the results were inconclusive. The problems in preparing such small samples without altering their properties made determination of a variation of property through a section very difficult. In this test the material density was not directly affected, but the rough surface trapped air bubbles which distorted the results.

Ideally much larger samples would be available, as this would minimise any error from cutting and ensure that the effect of air bubbles was kept to a minimum. However, larger samples may not contain the same isolated density variation (assuming there is one) as found in the structures, so the results of the tests may be of little use.

Other methods were sought (such as hardness/indentation testing) but these were considered to be even less reliable than the method used. The inability to accurately measure any change in material property within a sample meant that all models had to be assumed to be homogenous, as any variations programmed into the model would be based on estimates with little physical basis, and may reduce the accuracy of the model.

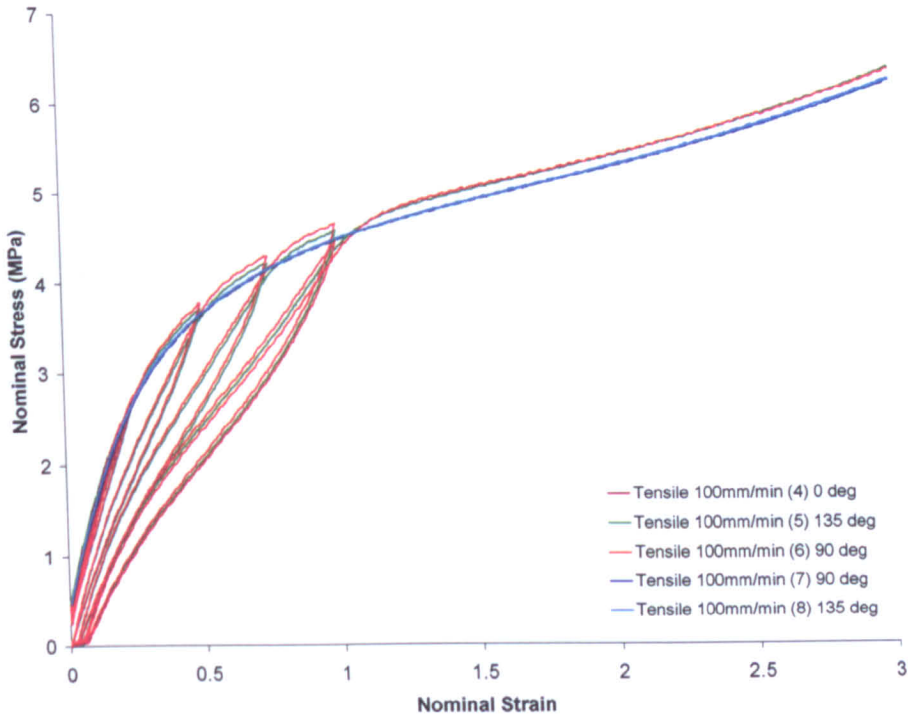

(a) UR1175

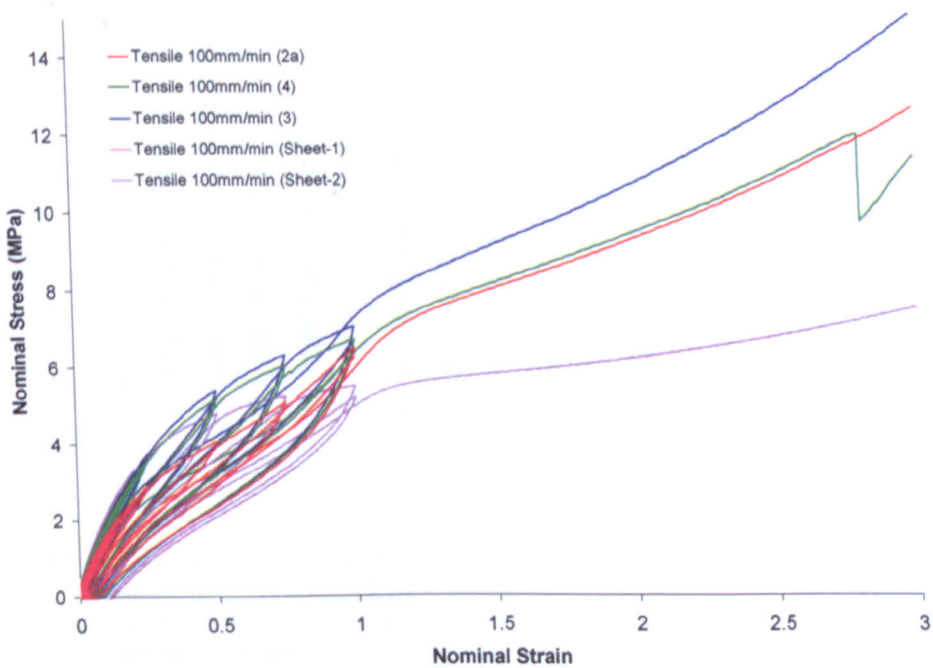

(b) GR685

Figure 7.9: Grain variation testing on (a) UR1175 and (b) GR685 (on sheets), also including tests on pre-moulded samples.

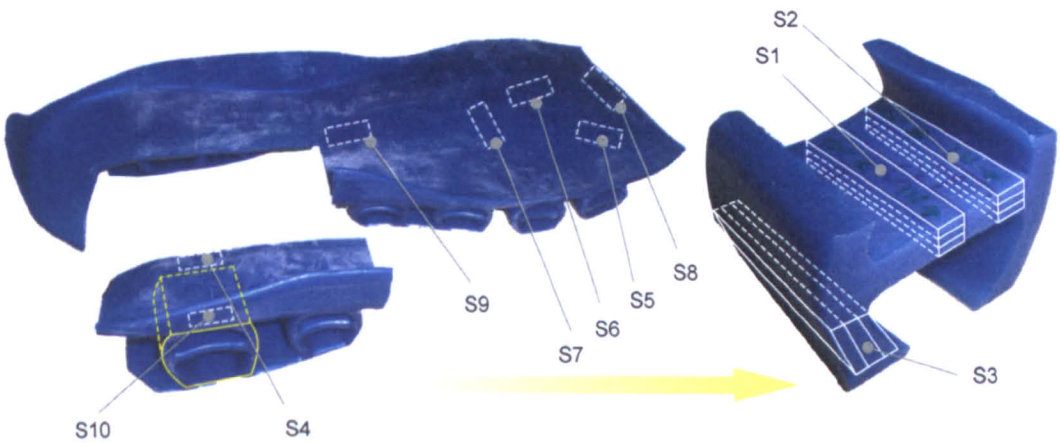

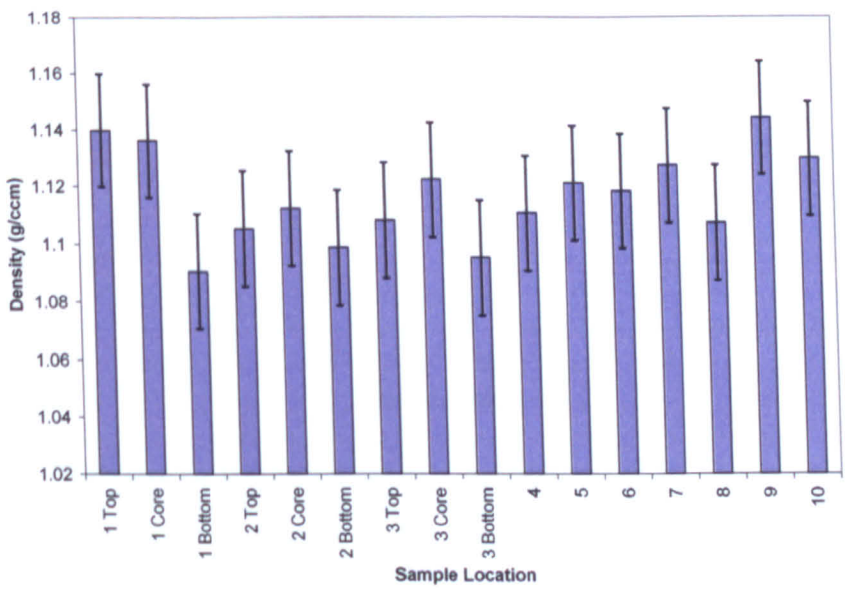

Figure 7.10: Location of samples cut from an Ultraride structure plate for density testing and the results of the tests (black bars indicate the error from weighting in the measurement - the error caused by air bubbles on the samples changing their measured volume could not be quantified).

7.3.4 Mullins Input

As the effect of pre-loading to different strains needed to be studied on a limited range of samples, the samples were cycled to successive strains to give the input data for *MULLINS EFFECT. A typical loading would be 0% strain to 5%, then returning to 0% strain, and repeating this cycle with increasing levels of strain to capture the 5, 10, 15, 20, 25, 50, 75 and 100% strain cycles.

The no pre-strain curve was then extracted from the results as described in Miller (2000b). This involves removing the plastic deformation that occurs at each strain cycle from the results, then reconstructing the overall curve from the sections of the cycles where a new high strain is reached (Figure 7.11).

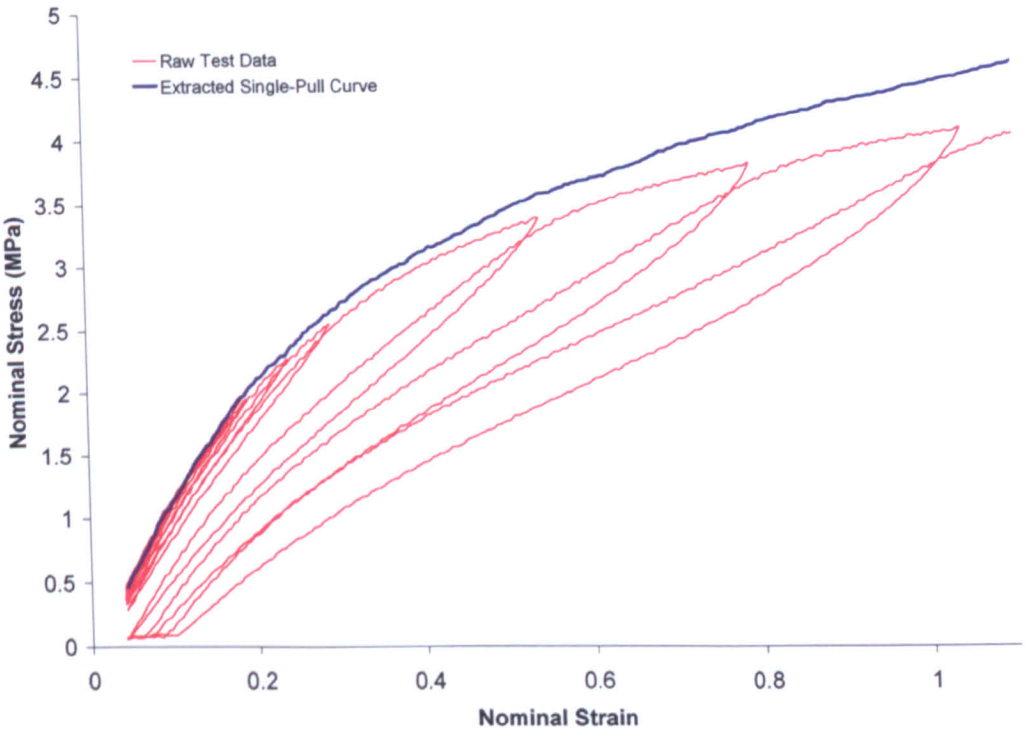

Figure 7.11: Graph showing the original test data, cycled to progressively higher strains, and the single-pull curve derived from the original by extracting sections of cyclic loops where the strain is increasing for the first time and stitching them back together. (Both curves have been pre-load corrected).

7.3.5 Preload Estimation

To remove any slack in the instrumentation and sample mounts, a small preload was applied to the sample before each test. This gave a definitive zero point for the assessment of strain, but removed a small portion of data at very low stress/strain. The stress was known at this point (as the preload was chosen) but the strain was not. The data could not be allowed to start from zero as errors were likely to be caused in the curve fitting algorithms as a kink in the data would be created. A smooth transition from compression to tension data was achieved by estimating the strain based on the apparent intersection of the curves with the zero stress/strain point. Figure 7.12 shows this process, which was carried out manually.

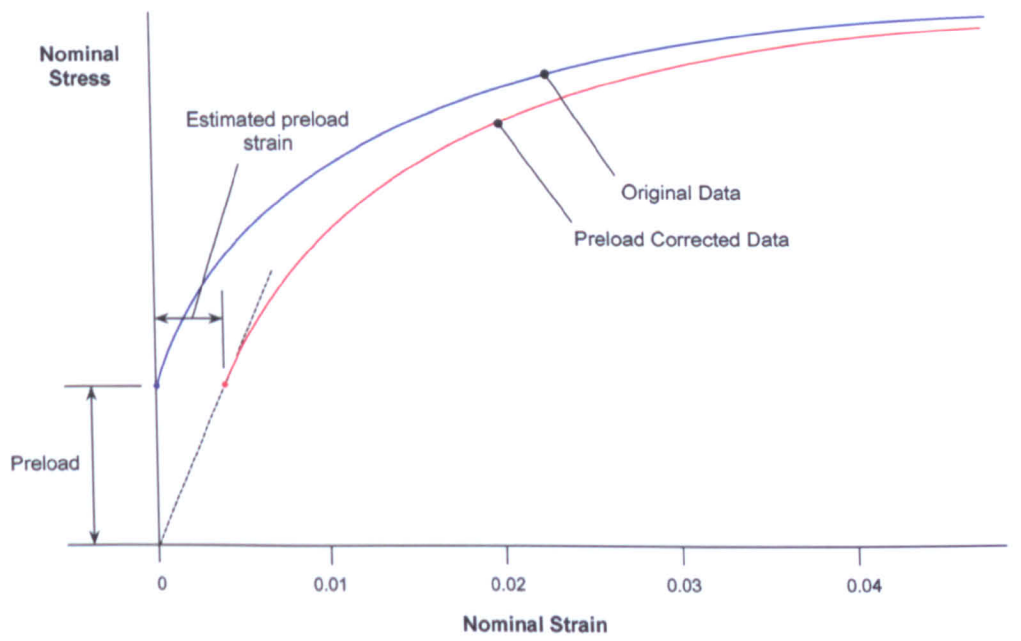

Figure 7.12: Graph illustrating how the preload required to give a consistent start point to a tension test is removed by estimating an initial strain for this preload.

7.4 Test Data Evaluation

Experimental material data were inputted into ABAQUS in a nominal stress-nominal strain tabular format. This data then underwent a series of least squares fits (minimising the stress) to attempt to fit the data to a material strain energy potential. For hyperfoams there is only one model available so the curve fitting was carried out in the pre-process phase. For hyperelastics there are a number of potentials available (such as Ogden, Marlow) so ABAQUS provides an evaluation function to allow comparison. Potentials, orders, and deformation modes are selected then evaluated against the test data using a single cuboid element. The results are plotted automatically and the user can decide which is the most appropriate for the desired application.

The results from an evaluation of UR1175 (structure material in the Ultraride) is shown in Figure 7.13. The figure shows the result from planar loading of the cube. Note that while most of the potentials give a reasonable fit, the polynomial N=2 exhibits non-physical effects in compression (that is to say its stress is positive - it would effectively pull the compression plattens together under loading). This potential is therefore unsuitable for use within the desired range (nominal strain of -0.5 to +3 in this case).

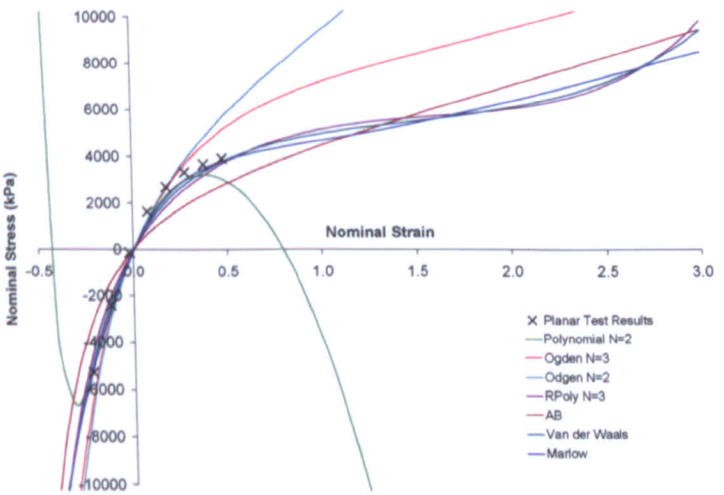

Figure 7.13: Planar results from an ABAQUS evaluation run on UR1175 for various strain energy potentials.

What is not apparent from the chart is that the Van der Waals potential is unstable. This means that a very small increase in strain does produce a change in stress, indicating that the material has a positive stiffness. This is known as the Drucker stability of the potential and is checked and reported by ABAQUS for each evaluation (see ABAQUS Analysis User's Manual: 10.5.1). It was possible to run models with unstable material models, although the quality of the results was questionable, as some elements may have been operating with a zero or negative stiffness.

7.4.1 Evaluation of Hyperfoams

As there is only one model for hyperfoam available, ABAQUS does not provide an evaluation function - the results from curve fitting are presented only in the pre-processor output files. This was acceptable if the data were known to be suitable for input, but to perform the checks in Section 7.4.3, a model containing 5 cubes loaded in uniaxial and planar tension and compression, and volumetric compression were created. With the use of a Python macro, the results were plotted in a similar way to that of the hyperelastic evaluation function.

7.4.2 Evaluation of Elastics

The evaluation was not performed on elastic materials as it was assumed that they have a good linear fit (as their Young's moduli were assessed by the user from test data and inputted directly). All the materials that showed a linear elastic response in their operating strain region were solid polyamide and TPU-ester blends and were assumed to be incompressible, with a Poisson's ratio close to 0.5. This is the automatic assumption of all hyperelastics in ABAQUS, and the code adjusts the ratio as close to 0.5 as is practical (0.475 as a default) to give the most accurate solution (without slowing the Explicit analysis down), in accordance with the information in the ABAQUS Analysis User Manual: 10.5.1.

7.4.3 Manipulation of Input Data

The input data collected from sample testing consisted of many points, as it was collected at 40 Hz for tests lasting up to 30 minutes. The ABAQUS Analysis User's Manual: 15.5.1 gives the following guidelines on how the data should be prepared for input:

Data Frequency The manual states - "as many data points can be entered as is needed" and that there should be more data points than potential coefficients. Data points should be evenly spaced.

Data Range Data should be given for the entire range of strain that the model is expected to see during the analysis. To improve the fit of the data for large strain models, some points at low strain may be omitted (and vice versa).

Deformation Mode Data from tests on samples under the modes of deformation that the model is expected to see, should be included within the test data. In addition, it is advised to include data from more than one deformation state to achieve a good fit with the phenomological models.

Despite following the guidelines laid out in the manuals, the initial curve fitting gave very poor results, so a study into the effect of variation in data range, frequency and specification of different modes was carried out.

7.4.3.1 Data Frequency

It was suspected that inputting up to 5000 points for material evaluation may cause unnecessary demands on the curve fitting algorithms, so a range of strain frequencies were inputted, as shown in Figure 7.14.

The chart shows that the best overall fit was obtained from data points sampled at 0.1 strain. This gave a better result than more dense data as it masked errors in the very low strain region due to unavoidable inaccuracies in the practical testing method. Less dense data did not provide enough information to formulate a good curve fit.

7.4.3.2 Data Range

Data ranges were selected from compression, tension and a mix of the two. While the Marlow and Ogden potentials both gave a good fit for the data sampled at 0.1 strain, the Ogden potential was used to illustrate the effects of a change in data range (as the Marlow model always attempted to fit to all of the data it was given). Figure 7.15 shows the results of this for UR1175. As the primary modes of the UR1175 material in operation were tension and bending, the best fit to the tension data was sought. For the uniaxial data this occurred when mostly tension data was specified.

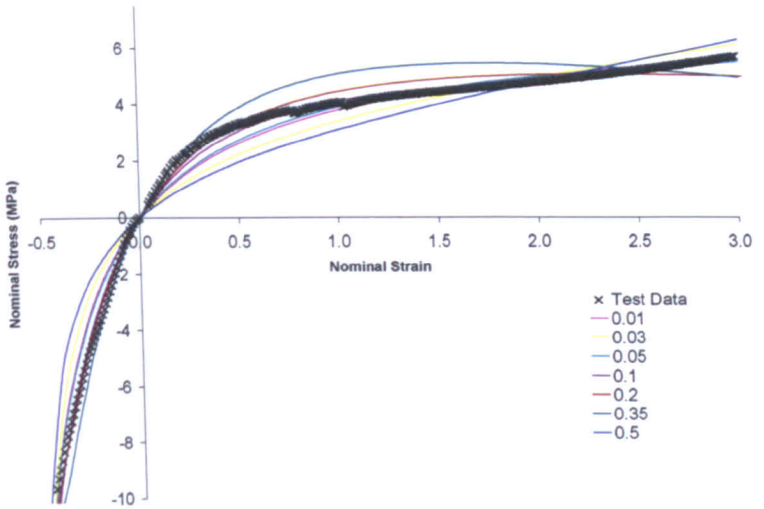

Figure 7.14: ABAQUS evaluation results (uniaxial) run on UR1175 for a range of sampling frequencies in strain.

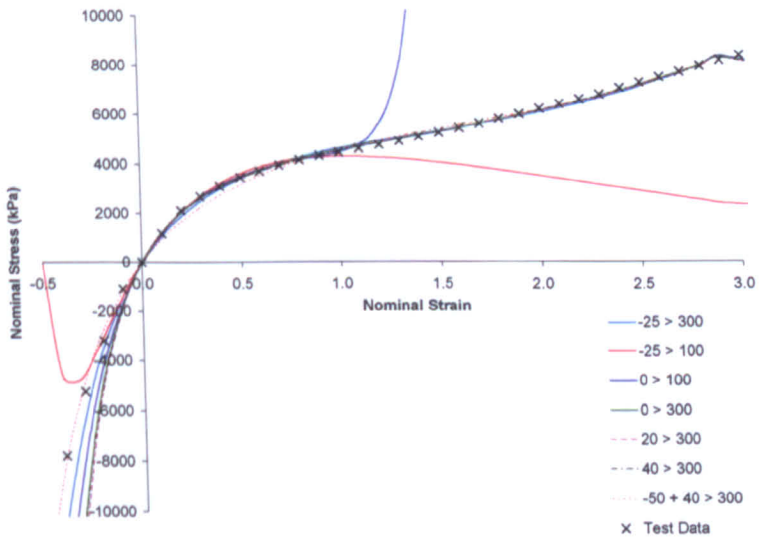

Figure 7.15: ABAQUS evaluation results (uniaxial) run on UR1175 with a variation in the range of data given.

7.4.3.3 Deformation Modes

For the UR1175 material, the planar tension test data were reasonable as the physical testing exhibited no obvious problems such as the significant de-bonding seen with the foams, and the resulting stress/strain curve was smooth. Despite this, when planar data were inputted along with uniaxial, the overall results became worse. Both the uniaxial and planar results show better agreement in the desired strain range with uniaxial input only. The addition of volumetric compression data caused all of the strain energy potentials to become unstable. This may be due to either physical testing errors, or the inability of the potentials used to accommodate the extra data. Because of this, all the material models were derived from uniaxial data only.

7.5 Element Performance in Simple Models

The type and size of element used in a model can affect the stress-strain response of the material. As one objective of this research was to obtain information about the optimum modelling process, the performance of the elements most likely to be used in the shoe models was checked. This was carried out using a simple 20-element block (6 x 2 x 35 mm) loaded in tension, to simulate the tension test detailed in Section 5.2.3.1, and the same block loaded in 3-point bending to assess the influence of elements during bending modes. Figure 7.16 shows the results of these tests in Standard and Explicit. Note the good agreement with all elements for both Standard and Explicit in tension, excluding the C3D8R with Stiffness hourglass control which has failed to restrain the hourglassing above a nominal strain of 1. For the bend test, the linear tetrahedral elements show characteristic locking, while the other elements have a very consistent response. In Explicit the linear tetrahedrals are inherently stiffer than the quadratics, and the stiffening effect of adding enhanced (stiffness and viscoelastic) hourglass controls to the hexahedral elements is shown.

7.6 Quasi-Static Modelling & Verification

Most shoe parts were manufactured either by injection moulding or by compressing a rough block of foam into a shaped mould. This has been shown to have effects on the homogeneity of the material, and can change its overall response (as discussed in Section 3.3.8).

At this stage it is expected that there will be differences in physical properties between sample materials and the materials in shoe parts.

7.6.1 Test Setups

All of the physical tests were modelled, excluding the volumetric test (as this test is independent of element size and has no distortion effects) and the simplified models are shown with their lines of symmetry in Figure 7.17. Single element thickness shapes with mirror symmetry on both sides were used for the majority of the tests in preference to 2D, axisymmetric models to include the volumetric and hourglassing effects associated with the 3D elements.

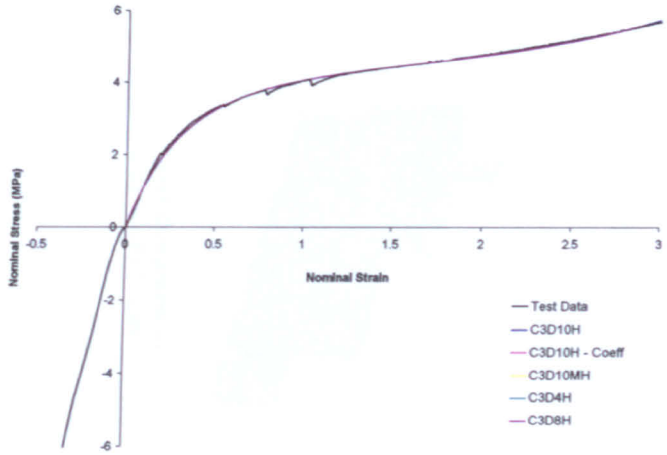

(a) Compression, Standard

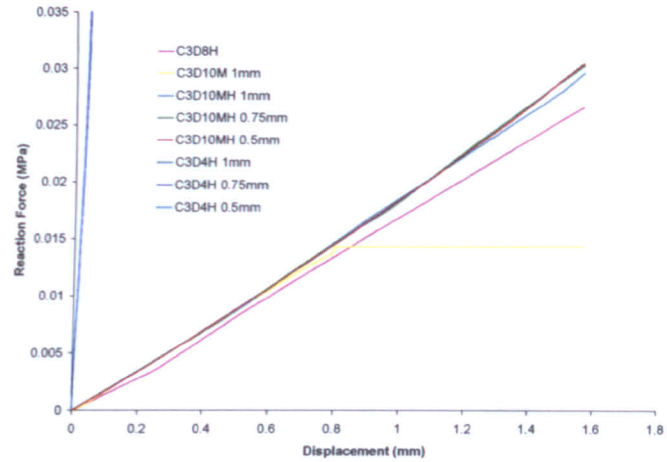

(b) Bend, Standard

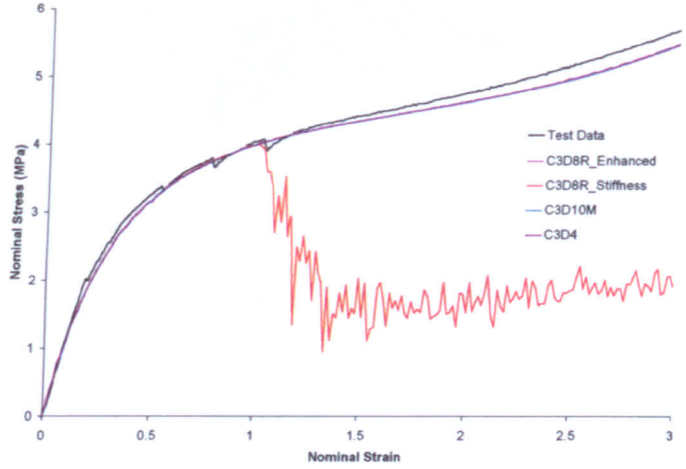

(c) Compression, Explicit

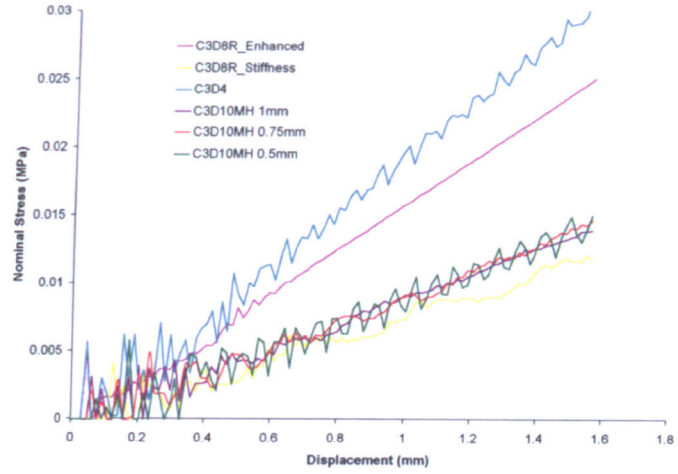

(d) Bend, Explicit

Figure 7.16: Element performance checks for UR1175.

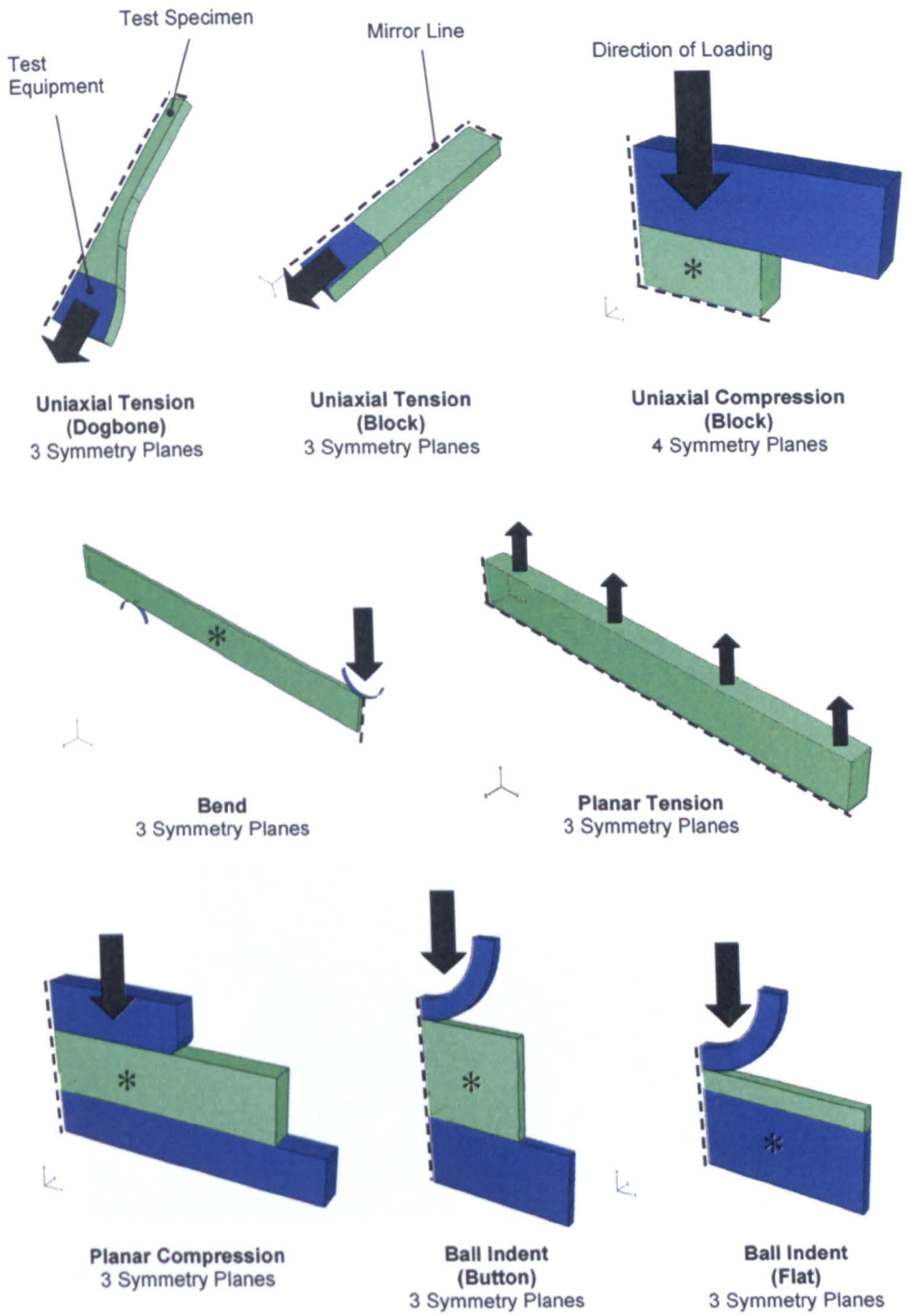

Figure 7.17: Schematics of the material sample tests. Specimens shown in green, with mountings and attachments in blue. Dashed lines indicate a mirror boundary condition along, and tests with a * are modelled as a slice: a thin representation of the test with mirror surfaces on opposing faces.

7.6.1.1 Mesh Selection

Due to the dependance of material stiffness on element size and type (see Section 8.2.1.1), any verification of a shoe part should be done on a like-for-like basis. For example if a material is to be used in a part that has 1 mm C3D4 elements (see Section 4.6.3 for element details), then any verification model should use the same element. For the majority of the shoe parts the C3D4 element is used, with a size range of 2-5 mm.

As the quadratic tetrahedral (C3D10M) element was known to give a greater accuracy with a lower computational cost when compared to a fine mesh of C3D4s, this was the element chosen for use in the performance shoe models (see Chapter 12), whose aim was maximum accuracy. The development models used in Chapters 8-11 used the C3D4 for maximum speed as relative effects were generally being studied.

As the final use of these models was in the performance models, the verification of the sample tests was done using both the C3D4 and C3D10M elements (the results presented later in this chapter use the C3D10M elements).

7.6.1.2 Friction

Despite efforts to reduce the levels of friction between the sample and test apparatus, there was always some barreling seen (a widening of the centre of the sample, relative to the upper and lower surfaces), especially in the TPU samples (Figure 7.18). The value of friction was chosen by running FE models and varying the friction levels until agreement was seen in the amount of barrel. For example; a friction value of 0.15 gave a final diameter of a compression button of 36.14 mm in the physical test and 36.5 mm in the FE model at 60% compression of an UR1175 compression button.

Figure 7.18: Barreling observed during uniaxial compression testing of UR1175.

7.6.2 Results

Figures 7.19-7.21 show the results of modelling the physical tests shown in Figure 7.17 for the materials UR1175, LS3016 and B64D (hyperelastic, hyperfoam and elastic respectively, see Section 4.6.1 for more details), using C3D10M elements.

UR1175 For this hyperelastic, both the Ogden N=3 and Marlow potentials are shown. Both give adequate results in the required uniaxial tension mode, as the stiffness is matched within the range of strains the part is expected to see (taken from the operating strains shown in Table 7.2. The Marlow potential is generally a better match for the test data, and as there were data available up to 300% strain, this potential was used for further modelling. If a smaller range of data were available, then there would be a risk of the potential becoming unstable, and it could not used.

LS3016 The only available options on the hyperfoam model were in specification of order, or adding in more deformation data. For this data set, using a 1st order fit and only uniaxial tension and compression was the only way to achieve a stable hyperfoam model. There was a trade off for this data between achieving a good compression or tension fit, so as the main deformation mode seen was compression, this mode was chosen. This gave a reasonable fit for uniaxial compression and planar compression, and a very good fit for the indentation test, which was most similar to the loading conditions seen by the shoe. However, the uniaxial tension prediction was very soft, which may explain the poor bend test results, as in bending, the sample experiences uniaxial tension on its lower surface. In general it was difficult to model the initial curve in the hyperfoam compression response without creating either unstable models, or giving a very, very stiff tension result (this was achieved by giving the material a fixed Poisson's ratio of 0.05).

B64D The elastic model shows the worst fitting for the range of modes, it performs reasonably in uniaxial modes, but is consistently soft in planar. This may be due to the need to specify a compressible Poisson's ratio to an incompressible material due to the limitations of Explicit (see Section 4.6.3). However, this component operates mainly at below 5% tension during a simulated heel strike, where the model adequately replicates the stiffness.

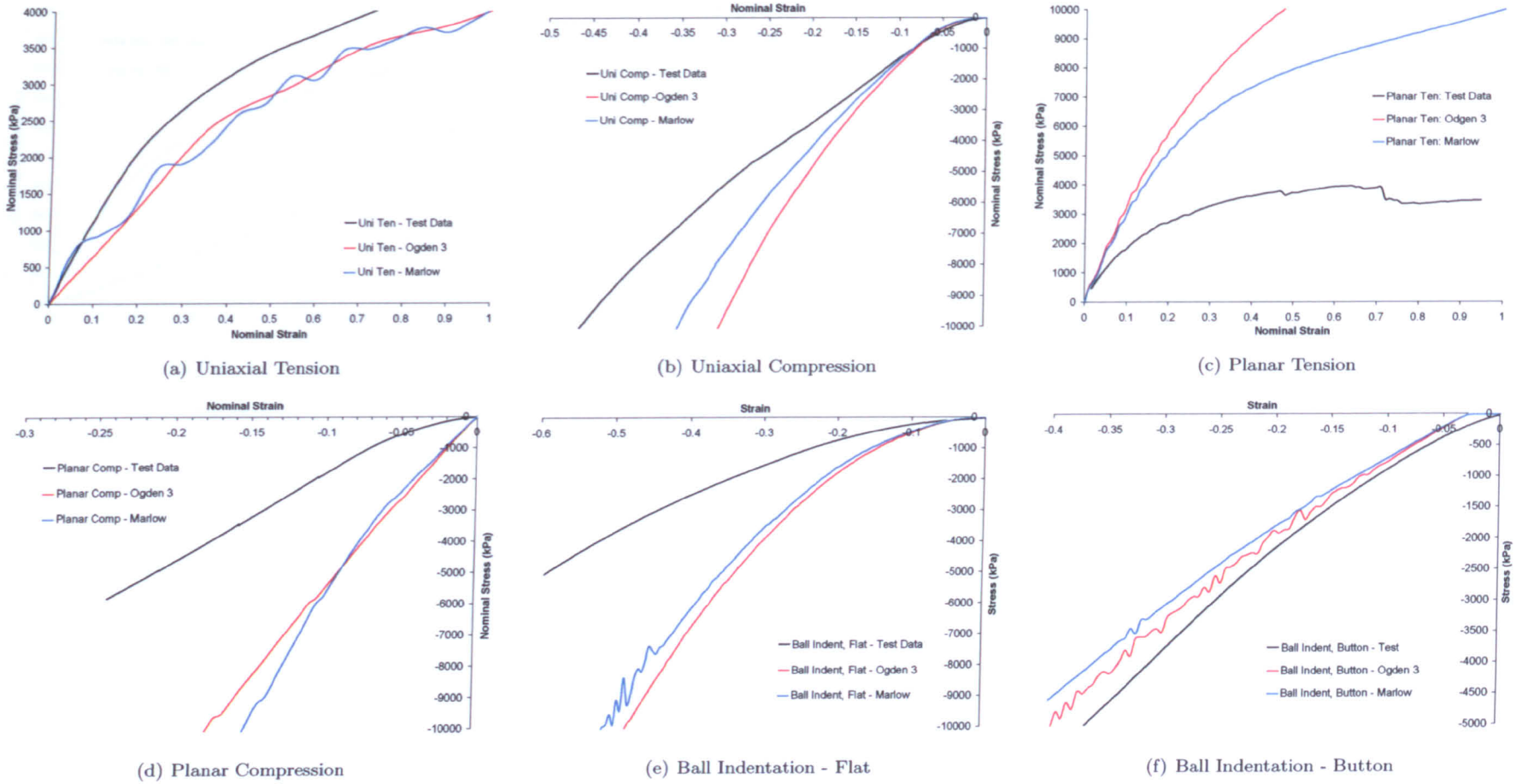

(a) Uniaxial Tension

(b) Uniaxial Compression

(c) Planar Tension

(d) Planar Compression

(e) Ball Indentation - Flat

(f) Ball Indentation - Button

Figure 7.19: Multi-deformation mode results from FE tests on UR1175.

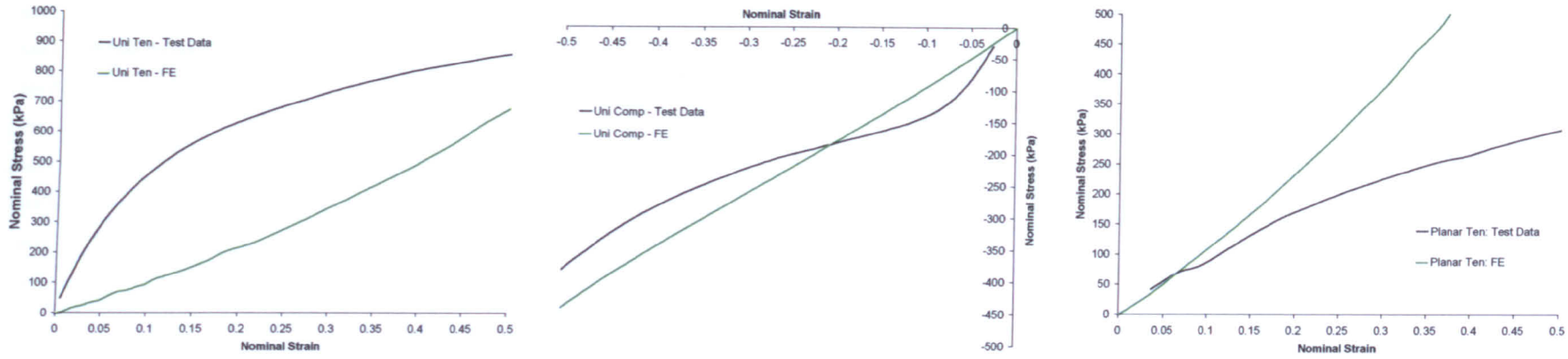

(a) Uniaxial Tension

(b) Uniaxial Compression

(c) Planar Tension

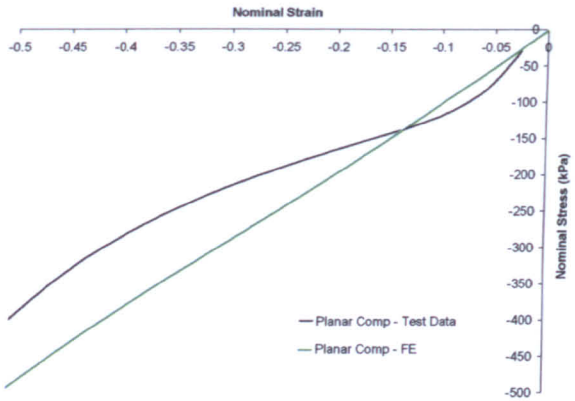

(d) Planar Compression

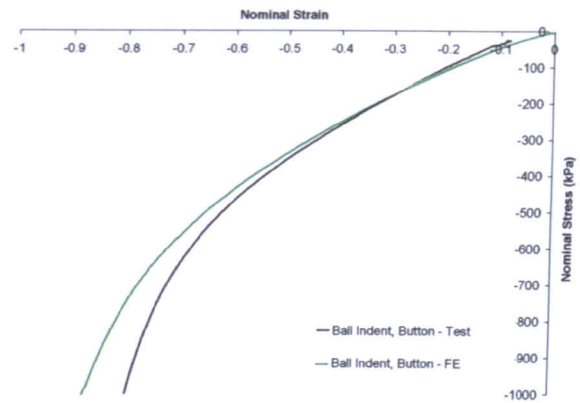

(e) Ball Indentation - Button

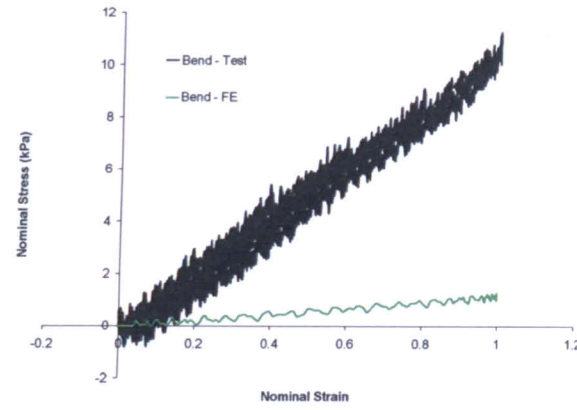

(f) Bend

Figure 7.20: Multi-deformation mode results from FE tests on LS3016.

(a) Uniaxial Tension

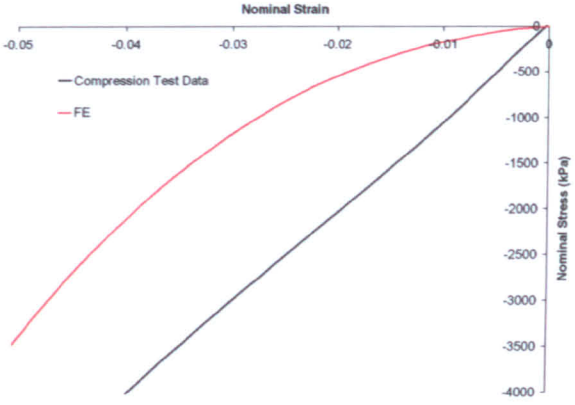

(b) Uniaxial Compression

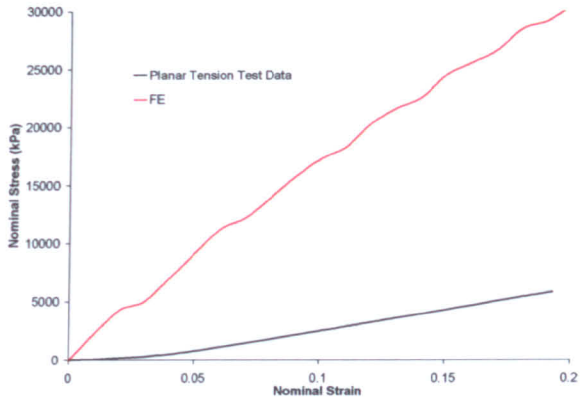

(c) Planar Tension

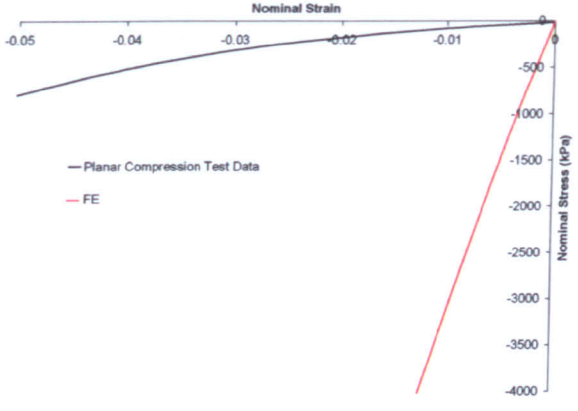

(d) Planar Compression

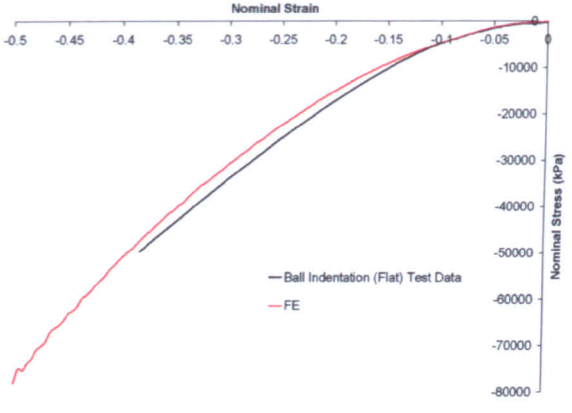

(e) Ball Indentation - Flat

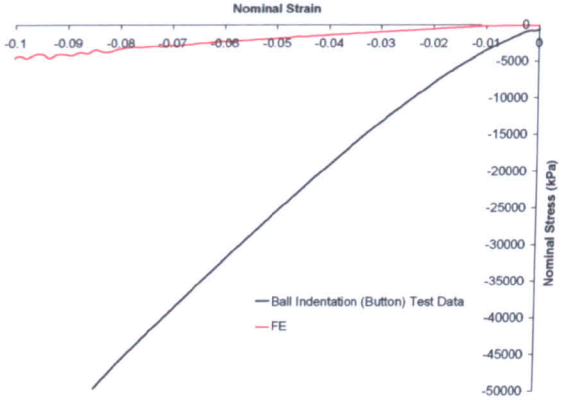

(f) Ball Indentation - Button

Figure 7.21: Multi-deformation mode results from FE tests on B64D.

7.7 Dynamic Modelling

Test data from DMA testing on all the materials are shown in Figure 7.22. Figure 7.23 highlights the response of the main midsole component materials. These data have been converted into a form which can be inputted into ABAQUS (see Section 5.2.4.2 for details). Most materials show a slight increase in stiffness between the long-term modulus (taken as 0.1 Hz) and real-life shoe impact speeds, this includes the main components of each shoe, which is taken as justification of the need to include the viscoelastic data within the models.

Due to time constraints the results were not verified against the physical tests by full-scale FE models in the same was as the stress/strain data. A check was performed on the data to verify that the effect on the long-term response (e.g. the static response) was zero; there should be a zero increase in stiffness with a zero increase in strain-rate. Figure 7.24 shows the results from uniaxial tests at a variety of different speeds performed on a 1 mm cube. A set of test data obtained from adidas that had previously been used to specify the viscoelasticity of LS3016 (data Set A) was compared to the more recent results from DMA (data Set B). If the long-term relaxation had been set correctly, then the results of deformation over a long period should be the same as those where the viscoelasticity was not included. This was the case for Set B, but not for Set A, which clearly showed a large stiffness increase even for long deformation times.

It should also be noted that the Set B data produced the same results whether the DMA results were inputted directly, or the calculated Prony series coefficients were used. Previous use of Set A data was not an issue as the models were verified directly with production samples and the extra stiffness accounted for.

The mostly likely reason for this discrepancy is that Set A (which is described directly as a Prony series) had not been converted for use in the kg, mm, s and mN unit scheme currently used. By inputting the DMA results directly with Set B, this conversion problem did not occur. It is recommended that in future this check be performed on any new viscoelastic data to ensure that, at the least, the starting point of the data is correct.

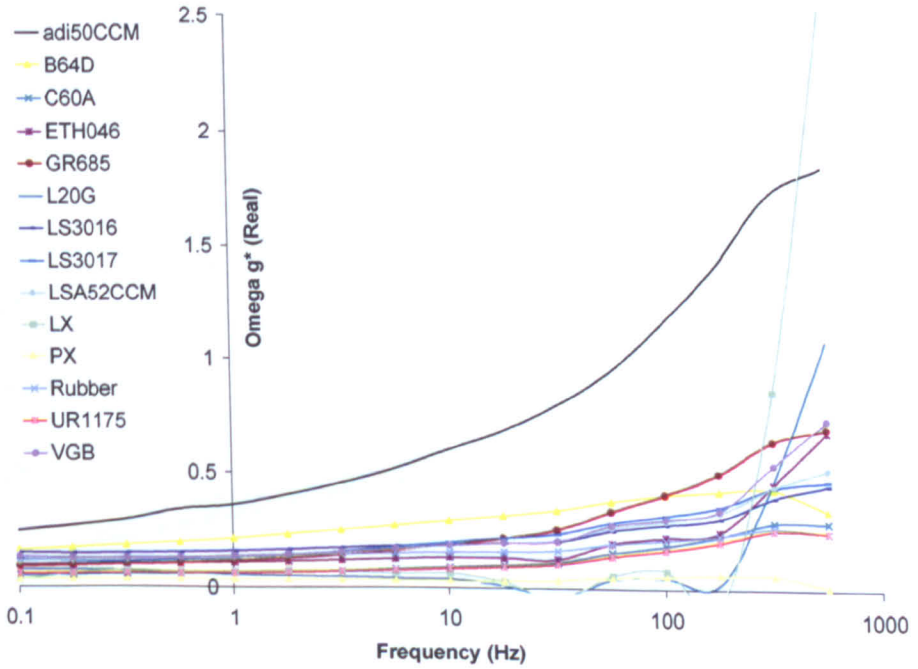

Figure 7.22: Plot of results for all materials tested using DMA. Results have been converted into ABAQUS input format, where Omega g* is a measure of the shear modulus of the material.

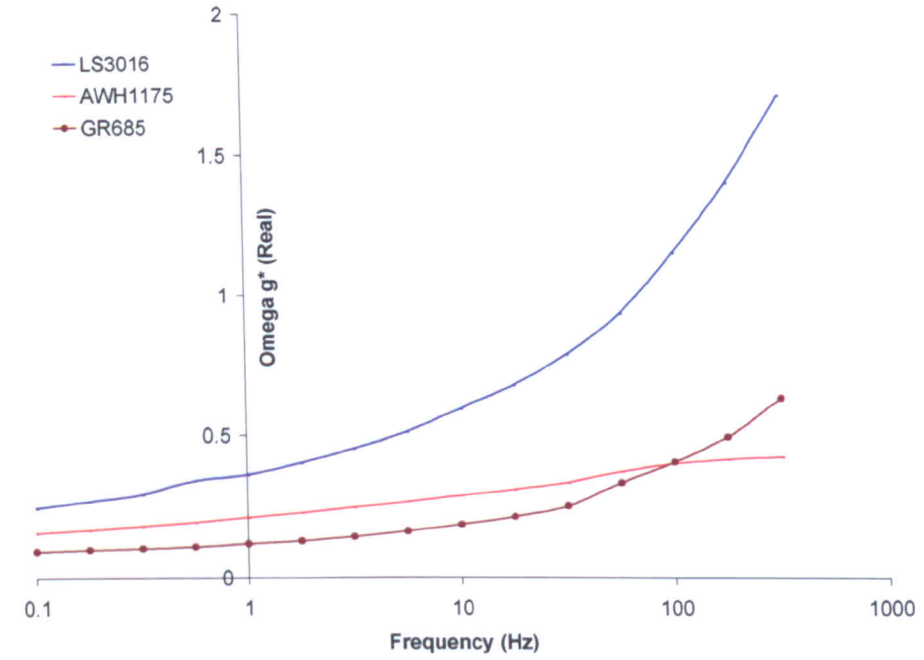

Figure 7.23: DMA results for main component materials of each shoe. Results have been converted into ABAQUS input format, where Omega g* is a measure of the shear modulus of the material.

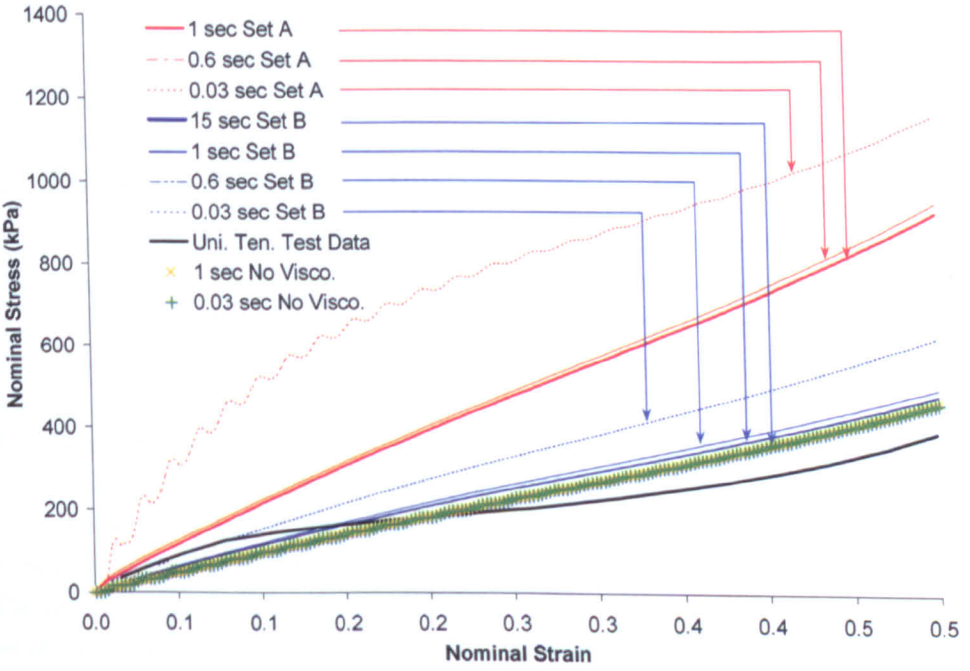

Figure 7.24: Variation between FE results for data obtained from adidas (Set A) and new data directly from DMA testing (Set B).

7.8 Material Model Adjustments

On occasions, the material models required adjustment to account for discrepancies between the physical test data and the model output. Whilst using the Marlow potential allowed adjustment by simply entering stiffened test data (by a simple multiplication of stress values), the other potentials attempted to re-fit any data, so it was quicker and simpler to adjust one or more of their coefficients and specify the potential that way. The adjustment of the polynomial and Ogden models are discussed here.

Ignoring the volumetric part of the equation (as the material is assumed to be incompressible), the polynomial strain energy potential takes the form;

$$U = \sum_{i+j=1}^{N} C_{ij}(\overline{I}_1 - 3)^i(\overline{I}_2 - 3)^j$$

where U is the strain energy per unit of reference volume; C_{ij} is a temperature-dependent material parameter and $\overline{I}_1$ and $\overline{I}_2$ are the first and second deviatoric strain invariants (ABAQUS Analysis Users Manual: 10.5.1).

Again, if the volumetric response is ignored, the Ogden potential is expressed as;

$$U = \sum_{i=1}^{N} \frac{2\mu_i}{a_i^2}(\overline{\lambda}_1^{\alpha_i} + \overline{\lambda}_2^{\alpha_i} + \overline{\lambda}_3^{\alpha_i} - 3)$$

where $\overline{\lambda}_1$ are the deviatoric principal stretches, μ_i, α_i and D_i are temperature-dependent material parameters. With incompressibility assumed, both of the equations can be adjusted for stiffness by adding a multiplier, η:

Polynomial: C_{ij} becomes ηC_{ij}

Ogden: μ_i becomes $\eta\mu_i$

Thus, changing the value of the multiplier η allows consistent adjustment of the stiffness of the material in both tension and compression.

However, due to the compressibility of the hyperfoam model, consistent adjustment in this way is not possible; some trial and error is required.

7.8.1 Dynamic Property Adjustment

Dynamic test data were obtained for this research using DMA testing, due to its much faster test times than creep or relaxation testing. The damping of the material was adjusted by changing the ratio of loss moduli to storage moduli, through a change in $tan\ \delta$ (see Section 5.2.4.2). Doubling $tan\ \delta$ and recalculating the inputs gave a doubling of the loss of the material.

If, in future, the testing is carried out by a third party, then the viscoelastic information may be available only as a Prony series (a set of coefficients). Direct adjustment of the damping characteristics of the material through a change in the Prony series coefficients is more difficult as the coefficients are based on the integral of certain material properties.

The most useful adjustment of the Prony series for development purposes is a multiplication of the time coefficients. Reducing these by a factor of 10 will simulate the damping effects of the material when strained 10 times slower. This is useful when attempting to model quasi-static loadings in an Explicit analysis.

7.9 Modelling Material Degradation

In addition to the static and dynamic data collected during physical testing, the Mullins effect was also recorded. This allowed input of the breaking-in effect of plastics to be modelled within ABAQUS.

The Mullins material model for the UR1175 material was calibrated using uniaxial tension results as these gave the least noisy data. Hysteresis loops to 5, 10, 15, 20, 25, 50, 75 and 100% strain were inputted and the output verified using a 1 mm cube model consisting of C3D20H elements (considered to be the most accurate and efficient element available). The cube was loaded to 25, 50 and 100% strain.

Figure 7.25 shows the results. Good agreement was seen between the test data and the FE results indicating that the fitting algorithm within ABAQUS worked well for this data. The difference between the loading curves on the 100% strain was due to the test sample having previously undergone the extra 75% strain loading, while the FE model has taken its data directly from the unload curve of the 50% strain cycle.

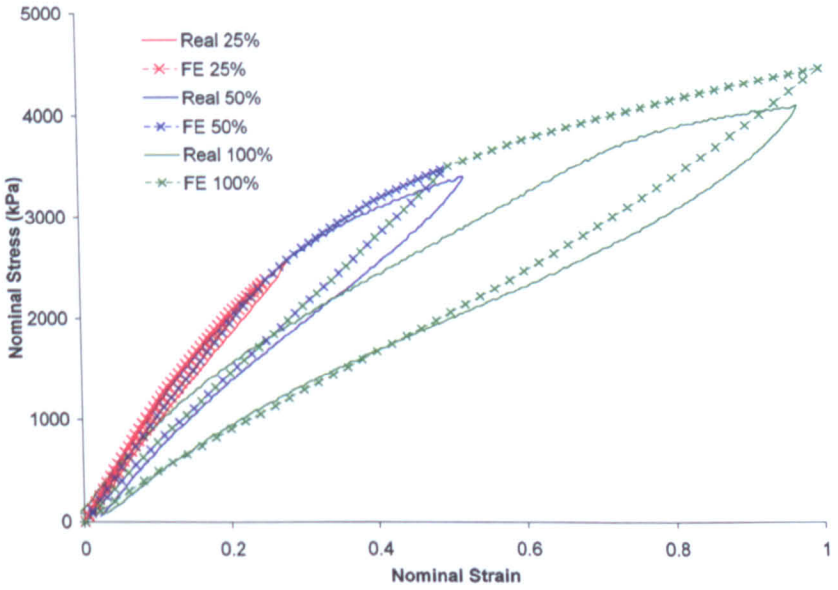

Figure 7.25: Comparison between input data and 1 mm cube model for progressive damage using the *MULLINS EFFECT command.

7.10 Chapter Summary

This chapter discussed the entire process of creating material models, and the following conclusions have been reached:

Materials Testing showed no significant change of the stiffness of any material with the orientation of the test sample to the grain of the material. There was however, a significant difference in response between dog bone samples cut from sheets, and those which were pre-moulded (the moulded ones being stiffer). Significant rate dependency was observed in some materials (viscoelastic foams), while others showed none at all over the range of testing speeds. Attempts to compare the material density in the Ultraride structure plate with the sample UR1175 material were inconclusive, due to the difficulty in creating and measuring samples from different sections of a structure.

Data Input Test data from progressive cycling to higher strains must have the plastic deformation effect removed before input into ABAQUS, either for use as the single-pull stress-strain response, or for use with *MULLINS EFFECT to predict material degradation.

The advice in the ABAQUS manuals for data input was found to be slightly unsuitable for this test data; input of more than one mode of deformation generally made the overall results worse, and certain sample rates of stress/strain were found to work better than simply inputting all the data collected.

This was most likely to be caused by small errors in physical testing, especially as the planar deformation mode tests were difficult to carry out on highly deformable/compressible materials. Hyperfoams were particularly difficult and time-consuming to fit well, due to the lack of a built-in comparison tool.

ABAQUS Performance The variation in results between different element types was checked, showing that care must be taken when using Explicit as a variety of results were obtained simply from changing the element type. In Standard, the results were much closer, and those elements that gave very inaccurate results usually suffered from shear locking and would crash the analysis, thus alerting the user to the problem.

The results from modelling the physical tests were mixed. It proved very difficult to model tests in all modes correctly, so the strain energy potentials were chosen on their ability to predict the performance in the main deformation mode seen in the specific shoe part during checks on operating strain levels.

Prediction With a predictive technology, this will be as far as is possible to go with physical testing as prototypes will not exist; material models must be chosen here, without physical verification. However, as this is a first attempt at full shoe modelling and prototypes are available, the next chapter looks at verification of the main shoe parts. This information allows adjustment of the material models to suit the materials found in the state they are in the shoes, but only for those parts tested - the rest will be speculative and will carry the possibility of error if consistent trends in adjustment are not found. This is particularly relevant as none of the material models created are capable of modelling all the deformation modes well.

Table 7.3 shows the results for the main deformation modes of all the materials under test. The sample mis-predictions quoted are the percentage error from the physical data, where a negative percentage indicates that the FE model is giving a result which is too soft. These single point readings are taken at the operating strain of each part, and it is very important to note that with some materials a large change in mis-prediction was observed over a small range of strains; the Rubber results are a particular example of this, where at 5% strain the FE model is too stiff, while at 15% strain it is too soft.

Other points to note from this data are that most of the models show a consistent prediction between quadratic and linear elements. Only the rubber testing at 5% strain and the elastic results (B64D, PX, L20G and LX materials) show significant changes between quadratic and linear for the uniaxial tension or compression tests used.

The decision to perform additional testing on certain materials could be made at this stage, but some materials may play less of a role in a shoes' performance than others. If resources are limited, then only the critically important materials need to be investigated in more depth. The next chapter addresses these issues.

Material	Deformation Mode	Operating Strain (%)	Material Model	–% Sample Mis-prediction– Quadratic	Linear
LS3016	Uni. Comp.	15	1st HFoam	-10	-10
LSA52CCM	Uni. Comp.	15	2nd HFoam	-7	-7
LS3017	Uni. Comp.	5	2nd HFoam	-77	-77
B64D	Uni. Tension	<1	Elastic	-50	-20
adi50CCM	Uni. Comp.	<10	2nd HFoam	-31	-31
UR1175	Uni. Tension	30	Marlow	-27	-22
C60A	Uni. Tension	<25	Marlow	-17	-18
ETH046	Uni. Comp.	20	2nd HFoam	-5	-5
PX	Uni. Tension	<5	Elastic	-50	-20
VGB	Uni. Comp.	15	2nd HFoam	0	0
GR685 (Heel)	Uni. Tension	25	Marlow	-15	-19
GR685 (Str.)	Uni. Tension	25	Marlow	-15	-19
L20G	Uni. Tension	<5	Elastic	-50	-20
LX	Uni. Tension	1	Elastic	-50	-20
Rubber	Uni. Tension	5	Marlow	24	-35
Rubber	Uni. Tension	15	Marlow	-35	-35

Table 7.3: Table of percentage mis-predictions in FE models when compared to physical tests, at the given strain. Note that a negative mis-prediction signifies that the FE model is creating a result which is too soft. 1st/2nd HFoam are the 1st and 2nd order hyperfoam models respectively.

Chapter 8

Modelling Stage 2: Moulded Shoe Parts

The application of the finite element method to the modelling of moulded parts found in running shoes is considered in this chapter. Once a satisfactory material model has been developed (as discussed in Chapter 7), the geometry of the actual part is added.

Running shoe midsoles are generally constructed from compression or injection moulded polymer parts/components. The CAD geometry of these parts was primarily designed for the construction of the moulds and not for FE modelling.

This chapter begins by explaining the processes required to import the geometry into ABAQUS, details any likely problems with importing and issues relating to the efficient representation of fine detail. The process of meshing irregular parts is then discussed at length, followed by analysis of physical testing and verification of the main components of the three shoes considered in this research.

8.1 Geometry

The process of creating a FE mesh of a shoe part typically begins with the geometry, which has been produced by the manufacturer's production design team. The geometry consists of surfaces that are defined by lines, which are in turn defined by points or nodes (an intersection of two or more lines).

As the use of FE techniques within the industry is in its infancy, the geometry files produced may not necessarily be suitable for direct import into FE programs. This is because the files are intended either as a visualisation/design tool, or for export to factories, where the information is converted for use on specific mould cutting machines. Since ABAQUS is a mathematical tool, which deals in absolutes, it cannot create meshes and perform calculations on geometry with microscopic holes, or surfaces that exist in the same physical space (both of which can be ignored by a milling machine).

There are a range of input issues that can be seen in the original geometry, these can be grouped into three main categories:

Uncomputable Surfaces These are surfaces that have become corrupted somewhere in the translation from design geometry to FE-compatable geometry. Figure 8.1 shows one such surface; the outer surface of the structure on an Ultraride midsole has been corrupted and the program does not have enough geometric information to find a unique solution to create a replacement surface.

Missing or Incorrect Surfaces Most shoe geometry is designed on surface modelling programs; the parts are built up of individual surfaces that do not have to form part of a solid object (as opposed to solid modellers where all surfaces are derived from solids). The majority of FEA software requires solid meshes, so any small gaps between surfaces will result in errors. Mould manufacturing machines can cope with surfaces overlapping as this only means that they machine away more material (or 'machine' empty space). This is also the case for surfaces that do not meet up - the mould can be hand-finished to remove any small burrs left over, but the FEA software will not allow for any gaps in a supposedly solid object.

Rounding Errors The design geometry is outputted in a given file format, to a given tolerance. As the surfaces involved become more numerous and complex, the occurrence of rounding errors increases. These errors can result in nodes and surface edges becoming combined (or split) in the wrong place, surfaces crossing over each other (creating negative space) and the formation of microscopic joints and surfaces and T-junctions in the model.

While the rounding error issue can be solved through correct exporting/importing settings, the others require re-specification of nodes and surfaces. This is what the automatic 'correction' algorithm attempts to do during import into ABAQUS, but at the present time, it is not possible for all inconsistencies in the very complex shoe part geometry to be automatically corrected.

Figure 8.2 shows an attempted import and repair into ABAQUS, where the red lines and dots are tiny errors in the geometry file or the import process that have not be corrected.

It must be noted that the majority of errors are too small to have any significant effect on the overall geometry (many have been observed at the micron level). Fixing these errors is a necessity to allow a model to be formed and run, and should not adversely affect the results. Only when errors cause an entire surface to become corrupt is there a danger of changing the original geometry to something not representative of the physical part.

To work around these import problems, the geometry was imported into a corrective meshing program, Hypermesh, as it provided a good range of corrective tools (and meshing capabilities, as discussed in Section 8.2). Manual adjustment of the geometry allowed the user to improve the meshing process, and also improved the efficiency of the final mesh by removing fine details. These processes are discussed in Sections 8.1.3-8.1.4.

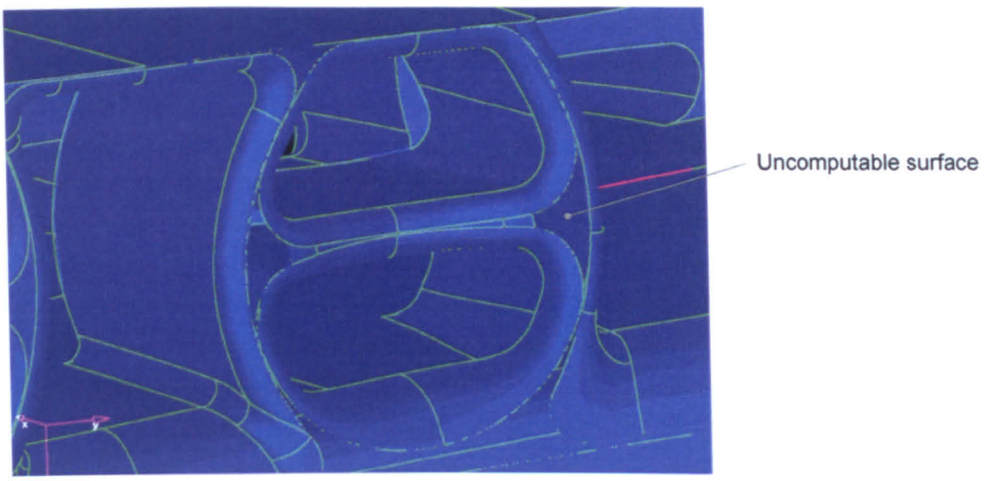

Figure 8.1: Outer surface of the structure has become corrupted and is uncomputable in the model. It must be either repaired (difficult), or replaced.

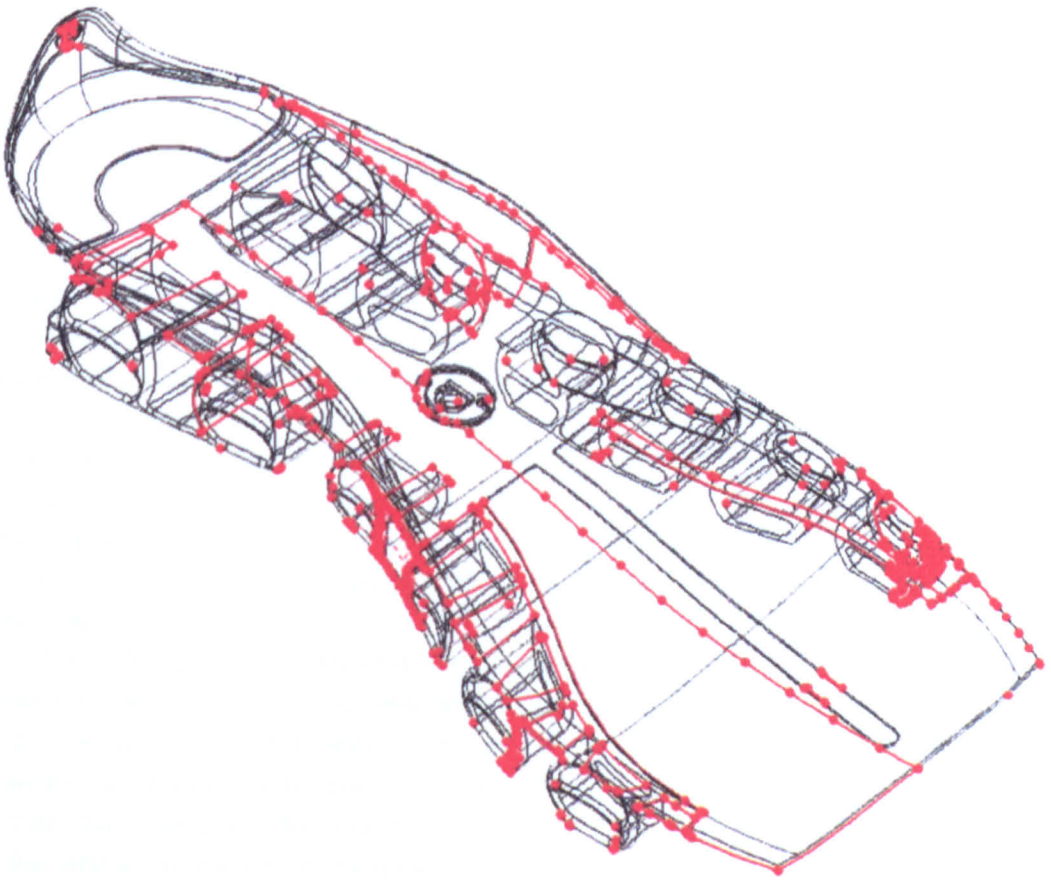

Figure 8.2: Import errors on the Ultraride structure plate when importing the geometry directly into ABAQUS.

8.1.1 Stitching

Hypermesh uses a simple tolerance control that attempts to combine nodes and surfaces that are separated by less than a given dimension (usually a fraction of a millimetre), but it is often necessary to undertake further corrections by hand. A number of techniques are available, the most fundamental of these being the stitch (or 'toggle') function. This allows the user to specify that two surfaces that are not joined together, should be. This is illustrated in Figure 8.3. Selecting one line commands the program to force the surface of the unselected line to fit to the selected one, resulting in a mathematically 'sealed' join, suitable for exporting to an FEA program.

Caution must be used, as the toggle tool will force together any two lines the user tells it to - including those that will create uncomputable surfaces.

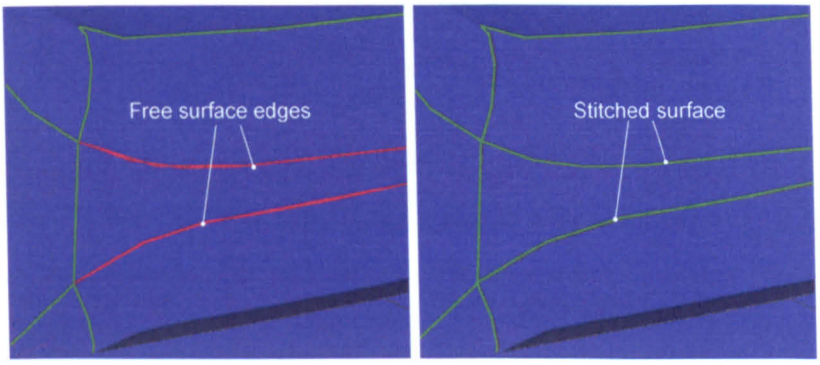

Figure 8.3: Unstitched surface edges (four red lines) and the corrected stitched surface edges (two green lines).

8.1.2 Filling

The user also has control of the re-surfacing algorithm used in the stitching process. This allows the selection of a number of free (unconnected) edges of surfaces to form the basis of a new surface. As Hypermesh is not designed to be a surface modelling program, the only control of the surface is from the edges that are selected, and the selection of forming a sharp or smooth transition from the new surfaces to the old. The rest of the computation of the surface is automatic and can be prone to failure if the selected free edges are very irregular.

The primary aim of any surface filling should be to repair the geometry with the minimum change from the original. Occasionally it is necessary to forego the ease of use of the automatic surface filling tools and manually specify lines on the new surface. This is often done when there is an unseen error in the description of the meeting point of a number of surfaces; cutting the old surfaces and rebuilding the corners can usually fix this with very little change in geometry.

Figure 8.4 shows a surface that has had this technique performed on it. As the surface was not sharply curved, it has been cut into triangles using point-to-point cuts and surface filling extending from the 'good' corner to the 'bad' one. The resulting geometry has no errors - as indicated by all green/light lines on the model. The blue/dark lines show the cut lines, that have been effectively hidden from the meshing algorithm (as explained later in this section), to reduce the instances of small elements produced.

Unfortunately it is sometimes the case that the surfaces have so many importing errors, or are so complex, that a good match between original and corrected geometry is not possible in the time available for manual correction (Figure 8.5). At this point is it up to the user to decide to either remove detail from the mesh or to approximate the part with a simple shape, both of these methods are discussed further in Section 8.1.4.

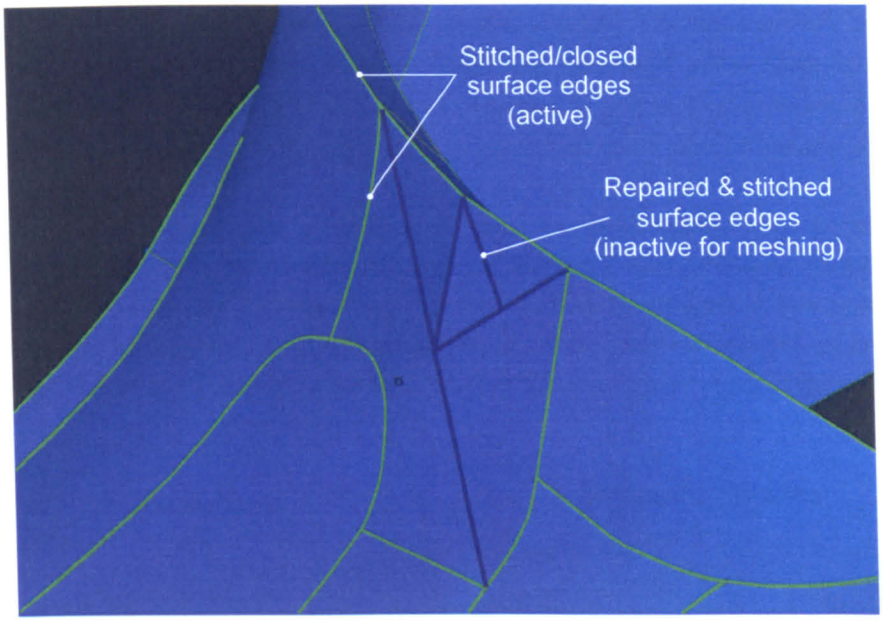

Figure 8.4: Blue lines outline triangular surfaces that have been created to replace a bad surface in the geometry. The new surface is only an approximation to the old one, but allows work to progress.

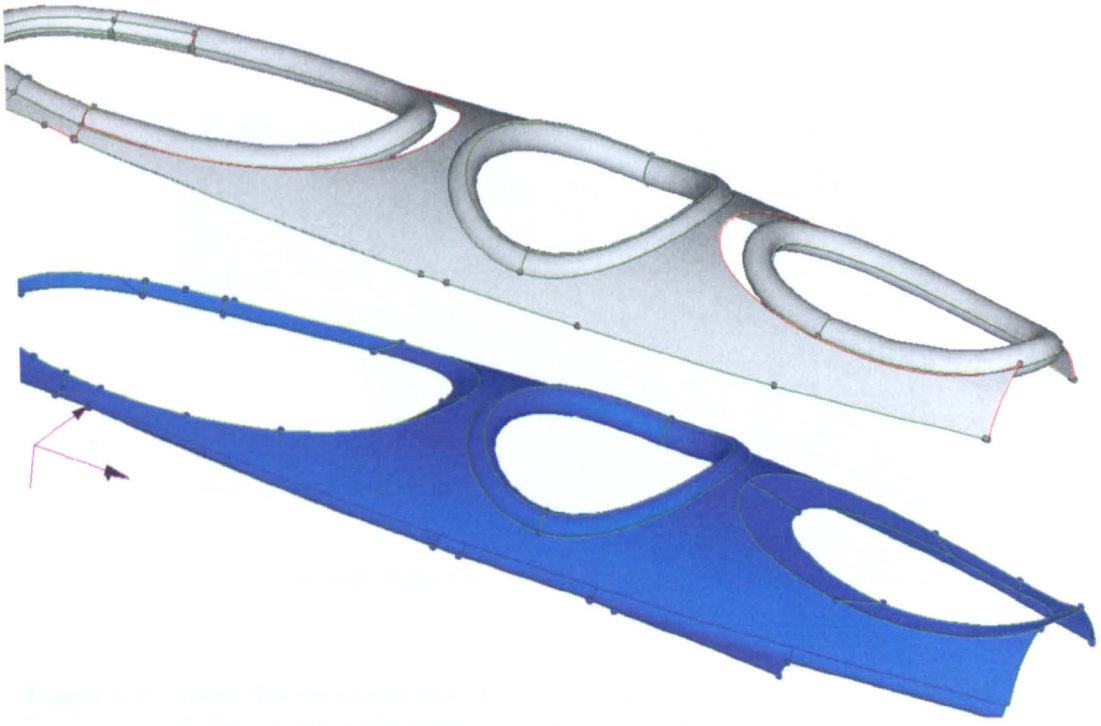

Figure 8.5: Original and modified geometry (upper and lower, respectively). Note that while the toroidal shape in the centre has been retained, the outer shapes had to be removed as attaching them to the thin body of the part caused surface corruption.

8.1.3 Mesh Control Using Surfaces

All the surfaces in the model are bounded by lines. During the meshing process, the algorithms use points along these lines to seed (begin) the mesh. The program will force these seeds onto any active lines in the geometry (displayed as green), hence there is a need to remove excessively small surfaces, such as those resulting from round-off errors and corrected surfaces (Figure 8.4), as these will result in very small (and inefficient) elements when using the Explicit solver.

The switching on and off of these lines as potential seed sites is a useful tool in the meshing process. However, switch off too many and the detail of a surface could be lost. The lines can also be used to form edges along real-life bonding boundaries, where parts may be mathematically tied together in the FE model (Figure 8.6), however, keeping these lines can be difficult if they lie on a corrupted surface, leading to un-matched bonding surfaces (Figure 8.7).

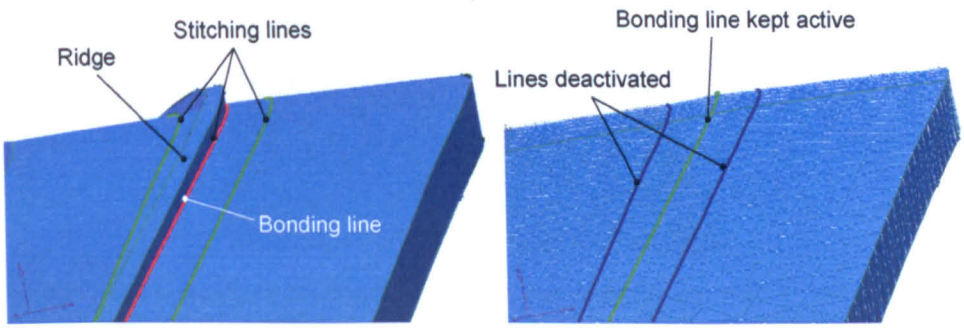

Figure 8.6: (a) Detail of rib used for bonding alignment during manufacture. (b) Geometry has been simplified, but some lines have been retained to permit accurate placement of tied nodes later in the modelling process.

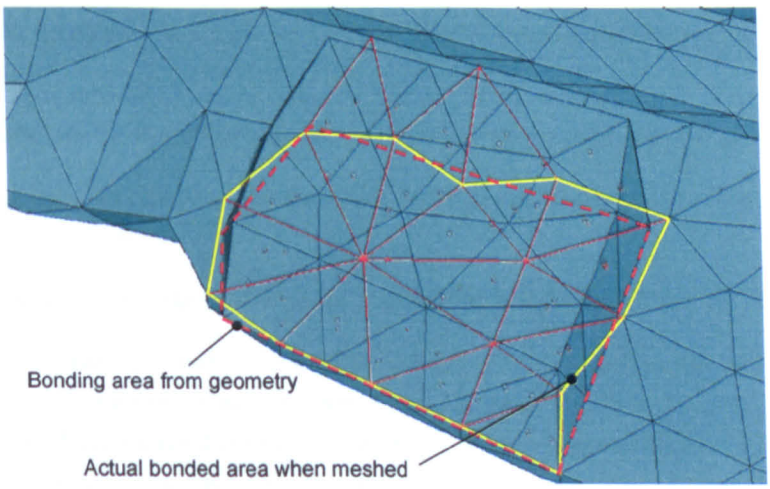

Figure 8.7: Detail of a lug on the outsole of the Ultraride. The dashed line indicates the outline of the lug, while the solid line shows the outer boundary of the tied surface on the shoe. In critical areas, this mismatching of physical and mesh bonding areas may cause problems.

8.1.4 Fine Detail Removal

Ideally the available computer systems would be able to process a very finely meshed shoe within minutes. This is unfortunately not the case, so care needs to be taken to eliminate small elements by removing fine detail from within the model, such as sections of the mesh that either provide no information to the final result, or provide an accuracy that is above what is desired. Small geometry will generally create small elements that will slow processing time (by limiting the time increment in Explicit, or increasing the number of DOF to be processed). The shoe geometry includes all of the detail to go into the final moulds, this includes some textures and even text (Figure 8.8). These details are generally smaller than the element size that is chosen to mesh the bulk of the part, so will add unnecessarily small elements if the details are not removed

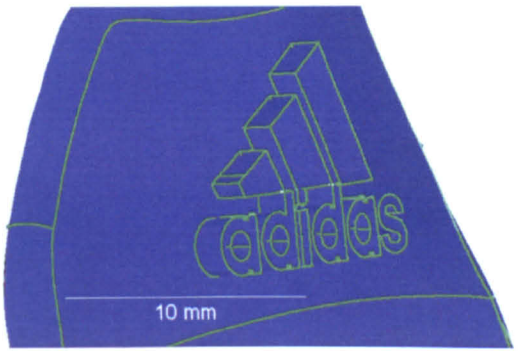

Figure 8.8: Excess detail on the outsole geometry that must be removed to give a more optimal mesh for FE modelling.

The question of how much detail should be removed to create an optimised job has been addressed many times within the modelling industry. Leon (2005) presents a paper looking at creating automatic processing for simplification of only those details that are unnecessary. It presents an overview of range of current practices for FE model preparation. The relevant points made in this paper are:

- All curved geometry is simplified to some degree when converted to a finite element mesh.
- Most parts can be simplified geometrically, allowing an even simpler mesh.
- The more complex the geometry becomes, the more difficulty there is in specifying what should be simplified.
- Simplification must take into account the loading conditions of the FE model.

The last item on the list lead to the introduction of optimisation product development processes where the output of an FE analysis is fed back into the geometry and areas of waste are removed (or meshed coarsely) and areas of interest are refined. These processes are really designed to iteratively improve geometry during the design process, and as this research is working on pre-defined geometry they are of limited use.

Other methods concentrate on adapting the mesh to the loads experienced. ABAQUS supports adaptive remeshing which refines the mesh around areas of high stress, giving a more accurate result. Unfortunately, this function currently only works in Standard, and is less accurate in models where objects are compressed and allowed to rebound (as the shoe models are required to do), as the mesh will not revert to the previous condition and some residual stress is created.

This means that removal of fine details in this case must be based purely on engineering judgement. While removing text and textures is justifiable due to very fine details, some objects require more thought, for example: the Supernova torsion bar.

The torsion bar on the Supernova affects the twisting of the midsole during a footstrike. On its lower surface it has a set of ribs, 2 mm across; these required a minimum of 2-3 elements across the smallest length for the mesh to compute correctly. So elements of 0.6-1.5 mm edge length would be needed, which was small compared to the 5 mm used to mesh the rest of the shoe. To test if removing the ribs would adversely affect the results, the torsion bar was modelled with and without its ribs. Figure 8.9 shows the models used. When loaded in the direction of stress the part will experience during a footstrike, the removal of the ribs made less than 5% difference in stiffness for a factor of three job time increase due to element size. When meshed with 5 mm elements alone, the number of elements was reduced by a factor of 19, greatly speeding up the processing.

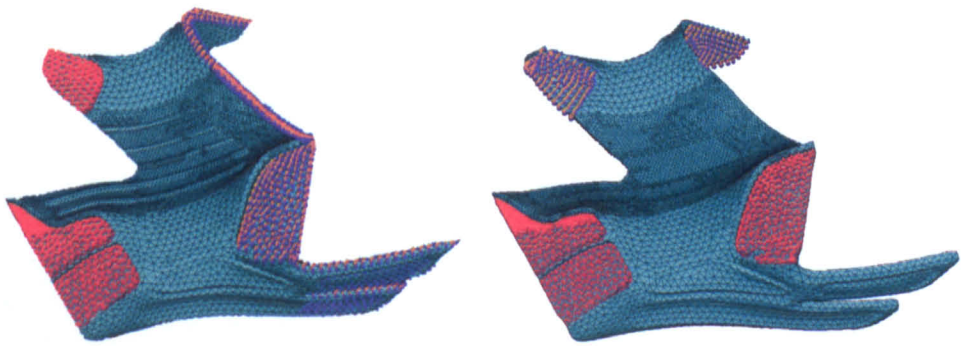

Figure 8.9: Supernova torsion bar with and without ribs.

Outsoles Outsoles generally have the most amount of fine detail. Removal of detail for those outsole sections that experience bend must be done carefully to preserve the bending stiffness of the part as much as possible, as shown in Figure 8.10. Here the irregular anterior-posterior channels are removed, while the medial-lateral ones are retained as they significantly reduce the bending stiffness of the outsole when it is bent about the medial-lateral axis (as occurs in the bend test and during a footstrike).

In some cases the complexity of an outsole prohibits repair as it could take weeks to correct using Hypermesh. In these instances the outsole was approximated by extruding the surface that contacts the midsole creating a simple part (Figure 8.11). The depth of this approximation was taken as half the distance of the largest protrusions from the midsole.

8.1.5 Parts Changed During Assembly

Outsoles are also a special case when it comes to general shape as they are normally moulded as a flat rubber part and bent around the midsole during shoe assembly. As a result the outsole geometry is flat (see Figure 8.12). The mesh morphing tool in Hypermesh can be used to distort a mesh created from the original, flat outsole geometry into the curved shape of the midsole. However, this is a fairly recent addition, so the outsoles in the models in this research were created by either extruding the lower surface of the midsole, or by using FE to 'form' the outsole onto the midsole using user defined loading. Both of these processes have serious drawbacks; extrusion means all detail on the outsole is lost, while forming using FE can be a time-consuming and unpredictable process, illustrated in Figure 8.13.

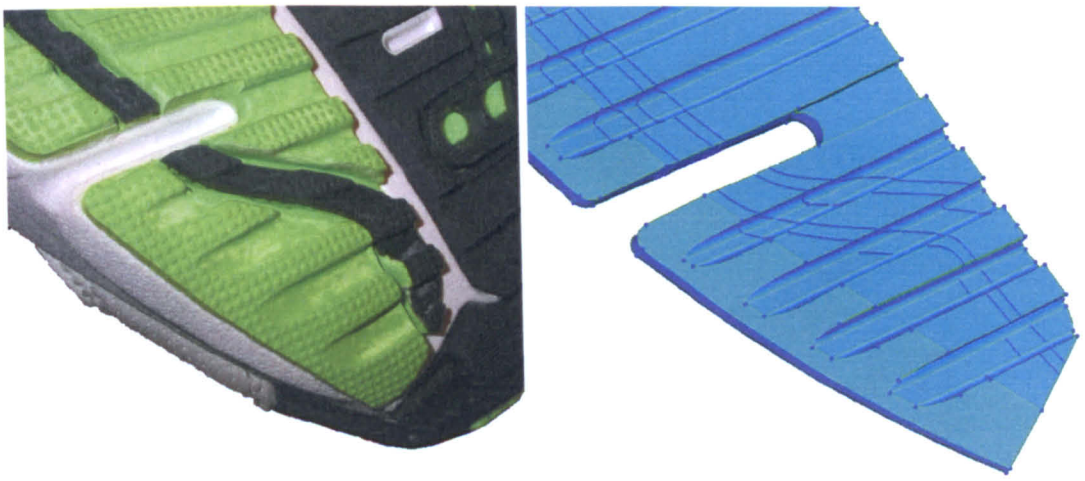

Figure 8.10: Removal of detail on the outsole of the Supernova. Note the surface lines on the geometry, showing the position of the filled-in anterior-posterior channels. Note that the medial-lateral channels are not filled, to maintain the bending stiffness of the part.

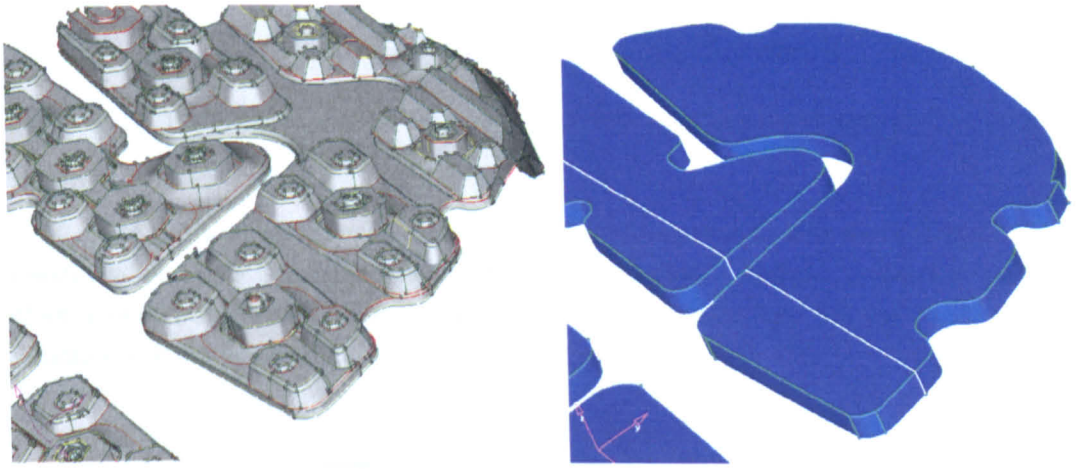

Figure 8.11: The original geometry for an outsole (left) has been simplified by extruding the upper surfaces to produce the geometry on the right.

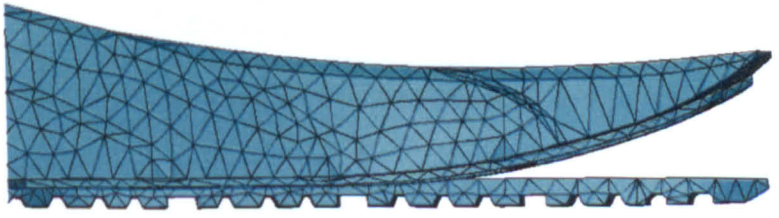

Figure 8.12: Side view of the meshed, original shape (but corrected for import) geometry of the Supernova outsole. The geometry is designed for manufacture, hence the outsole is flat.

(a) (b)

Figure 8.13: Reshaping of outsoles becomes difficult with thin, long sections of material. (a) Original shape, (b) Best result from reshaping.

Figure 8.14 shows an example of the power of the morphing tool. A mesh of high-quality hexahedral elements is created, then morphed onto a curved surface. Adjusting the mesh of an outsole would involve a similar procedure. Investigation into the use of morphing is recommended for future modelling.

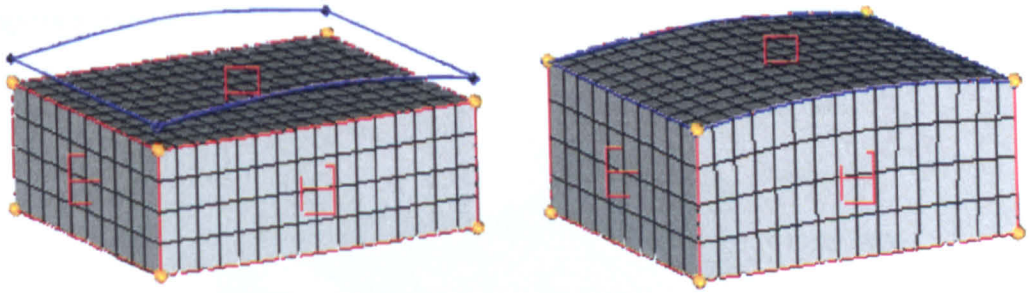

Figure 8.14: Example of the use of the morphing tool in Hypermesh. The regular mesh is morphed to fit a surface. (Adapted from the Hypermesh 7.0 User's Manual, Altair(2006)

8.2 Meshing

Engineering components are typically constructed from prismatic sections, or milled and turned from regular shapes. As such, the meshing of these parts is a fairly simple process. However, the shoe geometry used in this research was complex; it had few (if any) flat surfaces, few extruded sections and many surface intersections, meaning meshing was difficult. Due to this, meshing of the parts was done primarily in Hypermesh, as the program offered much greater control over the resulting mesh than was available in ABAQUS.

8.2.1 What is a Good Mesh?

A mesh optimised for processing speed consists of as large and as regular shaped elements as possible. Larger elements are more efficient, especially when using the Explicit solver where the size of the smallest element can have a direct link to the number of processing incrementations needed.

The underlying mathematics behind each element means the most accurate results will be produced the closer the element is to its basic shape - tetrahedral or cubic. Due to the irregular shape of shoe parts, all of the simple shoe geometry has been meshed using tetrahedral elements. While the hexahedral elements are faster and generally more accurate, there currently exists no automatic hexahedral meshing algorithm and the shoe geometry is currently too complex to create a mesh using solid meshing techniques (however, the mesh morphing function in Hypermesh shows some promise of creating a hexahedral mesh in a Gigaride structure - though this has not been achieved yet).

The following sections consider the main factors affecting the creation of a mesh.

8.2.1.1 Element Performance

It is vital to recognise that any FEA mesh and its corresponding results are only estimations of the actual physical composition and behaviour of a shoe. To verify the performance of the different elements available, a mini-study was performed using a 50 x 70 x 20 mm EVA foam sample with a 5 mm deep ridged outsole tied to it (Figure 8.15). This was a representation of the forefoot region of the Supernova. The model was then subjected to 3-point bending and cushioning tests, with a range of different meshes and sizes. The results are shown in Figures 8.16-8.19.

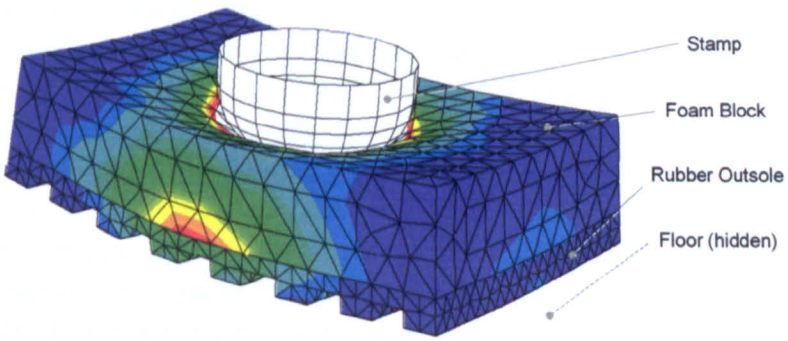

Figure 8.15: Mesh type study - Test set-up for cushioning test (analytical rigid floor is hidden).

The tests confirmed that the tetrahedral elements gave a stiffer result for an identical material model. A five-fold increase in mesh density produced a result closer to that of the hexahedral elements, but efficiency was low so a better solution was found in the use of quadratic elements in critical areas and a recognition that there was an artificial increase in stiffness in areas with linear tetrahedrals.

This study into mesh size sensitivity showed that there was only a small deviation between elements of 10 and 2.5 mm for tetrahedral and 10 to 1 mm hexahedral. This meant that development could take place with coarser meshes, to allow for multiple re-runs to set up other parameters, with the results still being similar to models with finer meshes.

One technique to calculate the accuracy of any finite element model is to perform the given test on two or more models of different mesh sizes and extrapolate the results. Theoretically, the correct result should occur when the mesh size is zero, providing the underlying mathematics is correct and all effects have been included in the model. Setting up multiple models from orphan meshes (those imported into ABAQUS rather than created from geometry inside the program), as is the case in this research, is time consuming as the altered orphan mesh needs to be re-imported into the model and all its interactions set up again. This method is more suited to models where the mesh size can be changed quickly (e.g. where the geometry is imported and meshed in ABAQUS). The mesh size for the models in this and the following chapters are verified against physical samples, so the material models are developed for those specific meshes.

8.2.1.2 Submodelling

Where accurate stress prediction is required only in a small area, the results from an initial coarse mesh simulation of a large object can be used as the boundary conditions of a finely meshed model of the area of interest. This submodelling approach is widely used in mechanical simulations, where large beams and panels can be simulated with very coarse meshes while the joints are meshed finely. It is of less use in this particular research where the aim is to model the entire shoe accurately, but is likely to be needed in future if the technology is used for predicting component failure and other localised phenomenon.

8.2.1.3 Sensitivity to Shape

In addition to the overall mesh size chosen in the previous section, the ability of the mesh to fit to and model the small and highly curved geometry was assessed. A structure was sectioned, shown in Figure 8.20(f), and a range of mesh sizes and curve fitting tolerances were tested for both hexahedral and tetrahedral elements, with the aim of deducing if adjustments to these parameters made a predictable change to the overall stiffness of the component. To check on the sensitivity of the mesh to small changes in the geometry (that may have occurred during the import correction process), the size of the four radii where the structure's curved sections meet the top and bottom flat sections were also varied.

Figures 8.20(a-b) show that adjusting the size of the mesh or radii of the geometry with a tetrahedral mesh gave a reasonably constant change in stiffness. However, (c-d) show that while the hexahedral mesh varied predictably with the radii variation, there was more tendency of the mesh to 'clump' into discrete levels of stiffness with a variation in size. This was due to the meshing algorithm attempting to fit the geometry by creating a range of mesh sizes, for example; in the case of (c), requesting an element size of 1.5 or 2 mm would give a similar result. As it was not practical to check for the existence of this 'clumping' effect on a full shoe model, the tetrahedral mesh offered a more predictably correctable mesh. Figure 8.20(e) shows that the hexahedral mesh was only slightly sensitive to the given curve fitting values.

One last point of note is that all the hexahedral mesh results showed failure of the elements near the end of the test. This was due to the edges of elements on the small radii collapsing in on themselves under high load. The tetrahedral elements resisted this deformation better due to their shape, so while they were found to be less accurate overall, in models with this

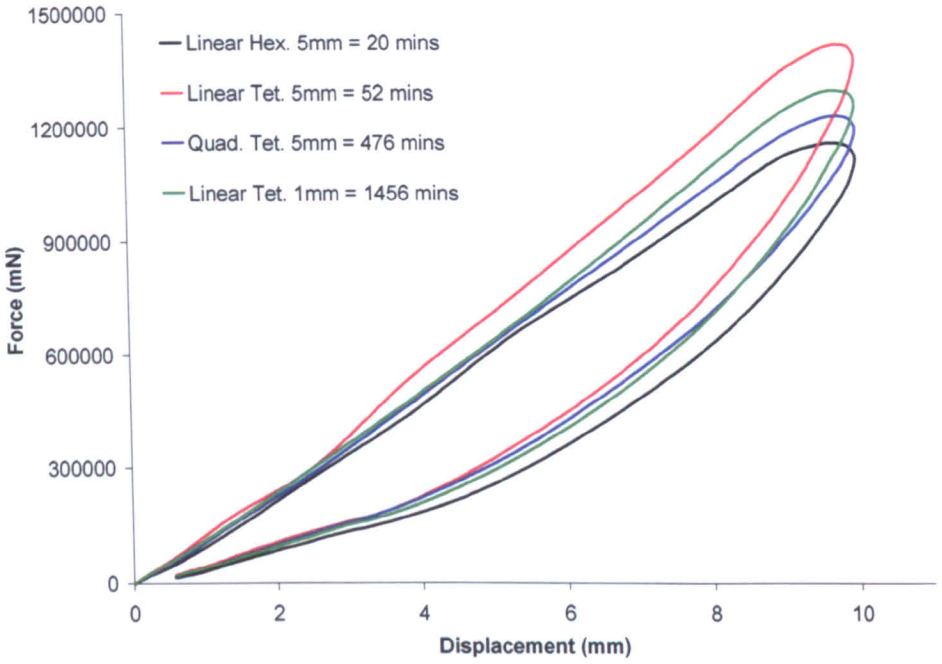

Figure 8.16: Mesh type study - cushioning test results with processing times.

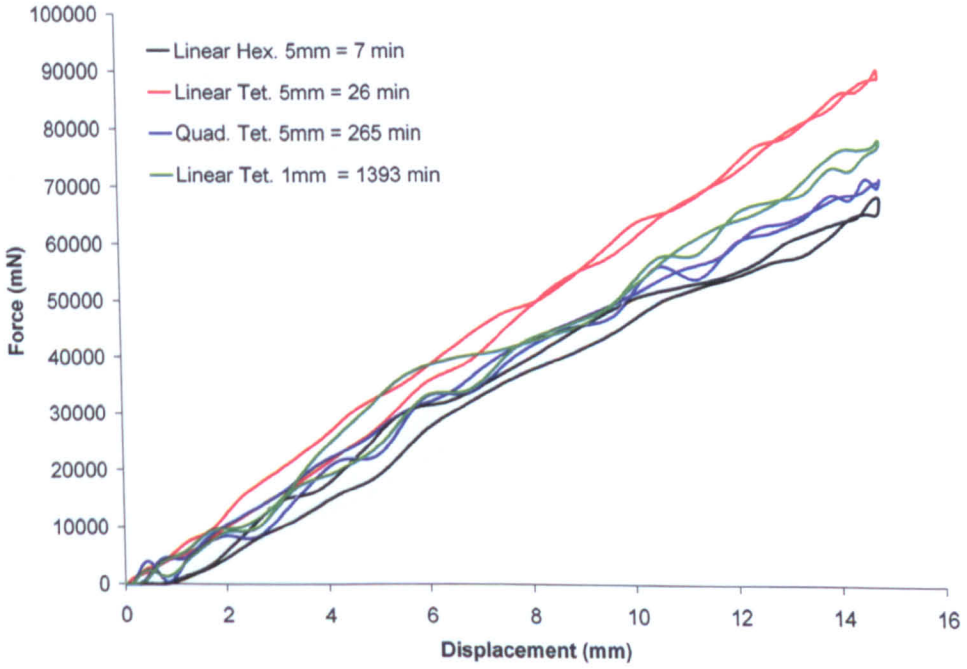

Figure 8.17: Mesh type study - 3-point bend test results with processing times.

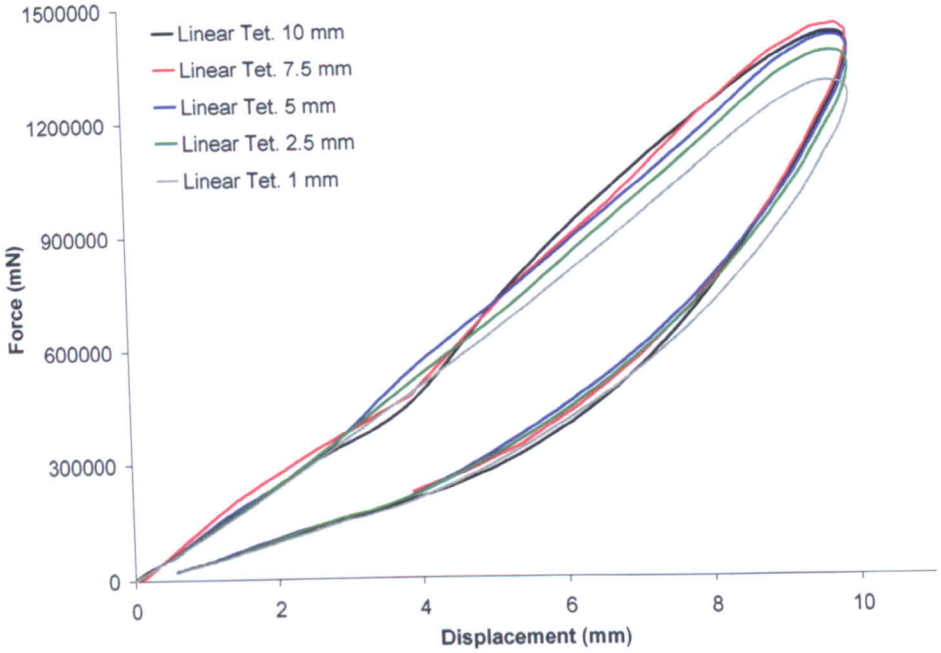

Figure 8.18: Mesh size study - Tetrahedral cushioning test results.

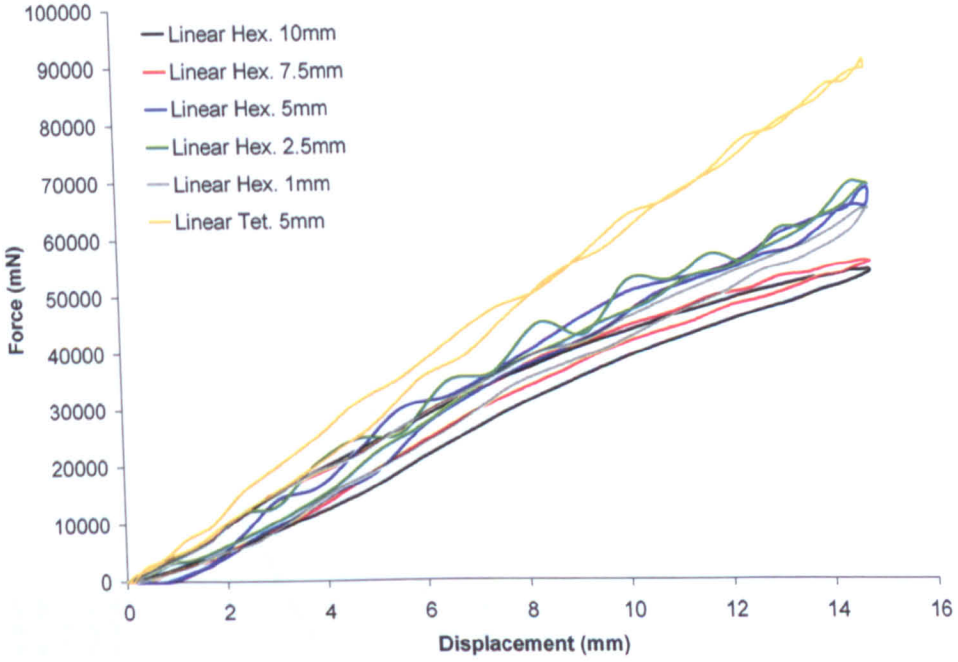

Figure 8.19: Mesh size study - Hexahedral cushioning test results.

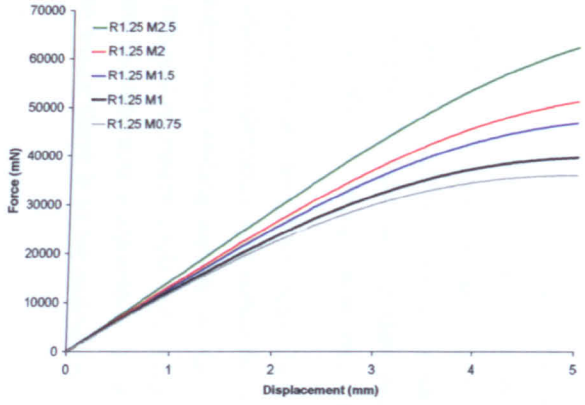

(a) Tetrahedral size variation

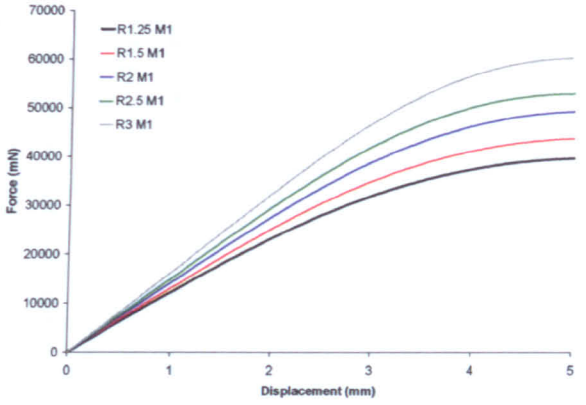

(b) Tetrahedral with radii size variation

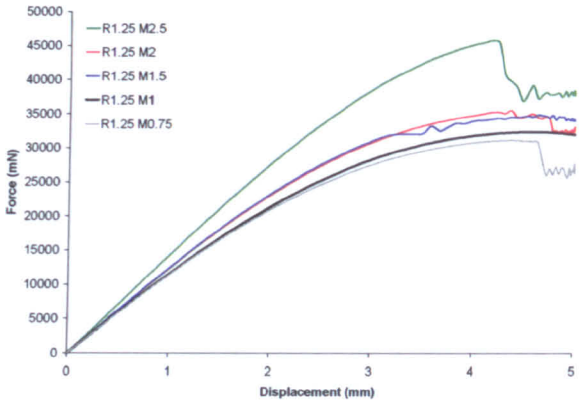

(c) Hexahedral size variation

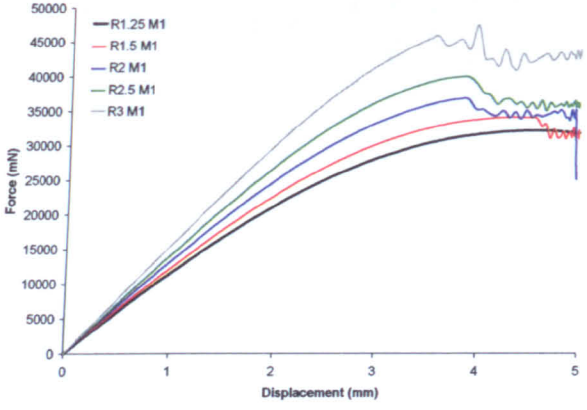

(d) Hexahedral with radii size variation

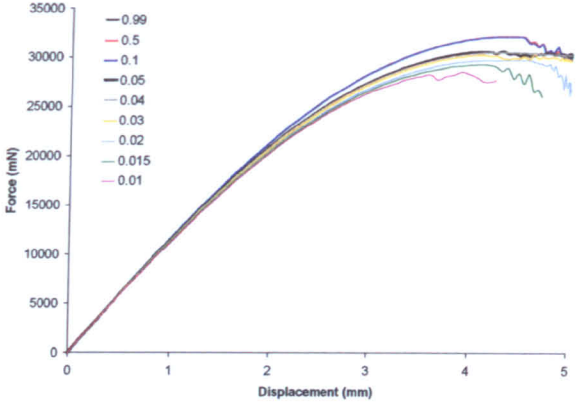

(e) Hexahedral with curve fitting variation

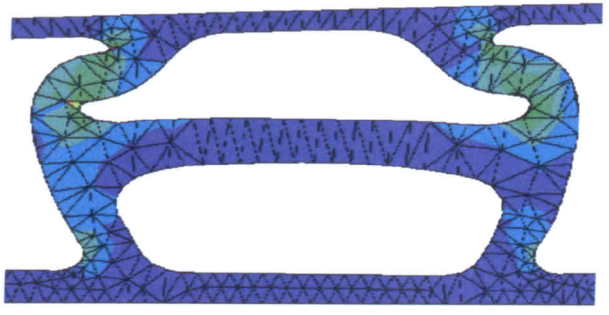

(f) Example of the test part

Figure 8.20: Results from sensitivity studies using a sectioned Ultraride structure, shown in (f) at maximum deflection.

kind of tight radii geometry, tetrahedral elements will give more stable models and more consistent results.

8.2.1.4 Shell Elements

For the majority of shapes found in the shoe geometry, the three dimensional continuum tetrahedral and hexahedral elements are able to fill the required volumes satisfactorily. Some of the elements are highly distorted, but this was necessary to achieve the desired mesh density, and care was taken that these poor elements are not used in regions of high stress. However, the upper portion of the shoe consisted of very thin volumes which could be adequately modelled without a very fine 3D mesh. For these shapes 2D shell elements might be used in future. While they were not used directly in the models here, their integration with the solid element midsole models should be considered when attempting to construct an entire shoe model.

8.2.2 Surface Meshing

When meshing irregularly shaped objects, the creation of a 2D surface mesh, upon which a 3D mesh is then based, can provide more control over the mesh quality. Additionally, better meshes may be obtained from complex shapes than when directly meshing a 3D object (which is covered in the Section 8.2.3).

All meshes can be specified node by node, but for large models (as in the case of shoe models), this is a prohibitively long process, so automated methods must be used. In Hypermesh an automatic 2D surface mesh can be created in three main ways:

Automatic The program only requires inputs for the general element size and type, in order to automatically generate a mesh based on the given element type, seed lines and seed size.

Interactive The program seeds the surface edges with the given element size. Seeds can then be added or subtracted by the user, or recalculated to fit edges with a bias (more dense mesh at one end) or a chordal deviation (more dense at points of tighter curvature). Once the seeds are specified, the mesh is generated accordingly.

QI Optimised The Quality Index (QI) optimisation mesh algorithm utilises a table of performance criteria inputted by the user. This table gives comprehensive instructions on the shape of elements, including: smallest/greatest length, interior angles, chordal deviations, skew (deviation from the basic shape), and a number of others. These parameters are given a ranking, with undesirable characteristics receiving a higher number. A quality index value is then generated and the mesh created and optimised to reduce the value of the QI value over a number of iterations.

For most parts, the QI meshing algorithm produces the best results as it is able to remove the smallest elements and redistribute the rest of the mesh to close the gaps (even ignoring user-specified seeding lines if the QI values are high enough), giving a mesh that is close to the original geometry while still being efficient during solving. For some parts it is necessary to use the interactive algorithm to tightly control the mesh, normally this is done in critical areas where there is to be contact or tie constraints (see Section 9.2.1).

Once the 2D mesh has been produced it must be checked for performance, usually to remove the smallest and/or badly skewed elements. Figure 8.21 shows a 2D meshed Ultraride structure plate that is undergoing element performance checking - the light elements around the heel indicate that these elements are failing the required criteria. Failing elements can be deleted and rebuilt manually, but it is often the case that the elements are there due to poorly defined geometry (in Figure 8.21, this is due to the thin wall thickness relative to the element size). Very tightly spaced nodes and infinitely thin surfaces can normally only be detected by meshing and checking for bad elements. A general rule of thumb for creating an accurate, but reasonably time-efficient mesh for simple parts is that no element should be below 25% of the seed length (i.e. for a 5 mm mesh the minimum length should be 1.25 mm). This is easily achievable with thick-set shapes such as a foam insole, but structures often need to be given a smaller seeding to allow the detail of the small curves to be modelled. A method of optimising meshes for job speed when using mass scaling is presented in Section 10.4.

Figure 8.21: Ultraride structure plate showing highlighted elements (white edges) that have failed a mesh-checking limit.

A satisfactory 2D mesh can then be extended to 3D using the 2D element nodes as seeding points (Figure 8.22). The resulting mesh will usually have very similar performance characteristics to the 2D mesh, but it should still be run through the same checks to confirm this.

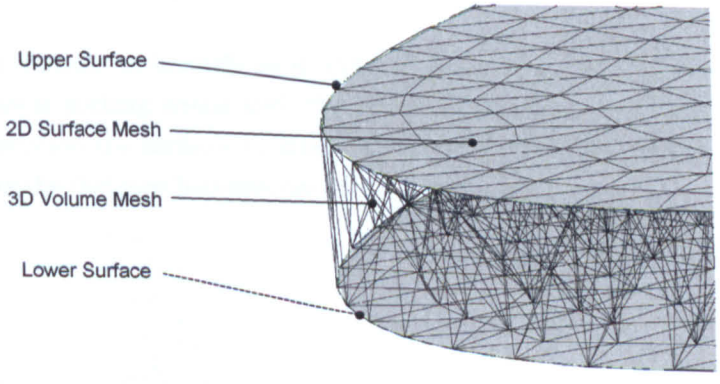

Figure 8.22: 3D mesh created in a plate from 2D element seeds. The 3D mesh incorporates the 2D, forming the outer faces of elements (The edge surface of the plate had been hidden).

On some occasions a 2D mesh will fail to run through the 3D algorithm - this is often due to the creation of a non-physical shell mesh (i.e. the mesh does not form a single completely enclosed shell around a 3D space). Hypermesh offers little assistance in diagnosing the error in the 3D meshing process, so the root cause must be identified in the 2D mesh.

One example of a non-physical mesh is shown in Figure 8.23. The size of the feature shown is close to that of the mesh seed and results in two possible meshes: one acceptable, and one with a T-joined element. The T-join is not physically realistic as it creates two elements that enclose zero volume and will therefore result in a fault in the 3D algorithm as it tries to mesh this 'non-space'. These elements need to be manually removed and the seed changed or the geometry adjusted to give better definition to the 2D algorithm. Errors will also occur when two separate objects are selected for 3D meshing at the same time (this also includes very small import error surfaces that may not be easily visible).

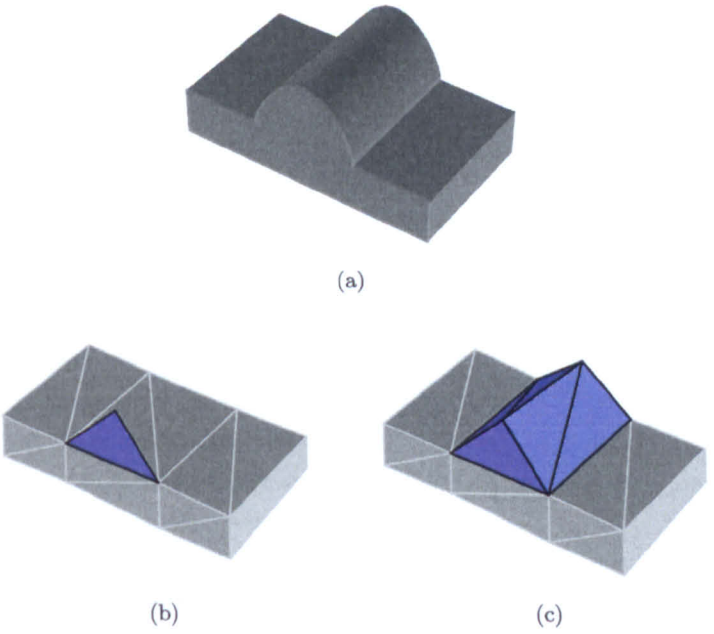

Figure 8.23: Original geometry, (a) and two surface meshes, (b)with a T-junction and (c)with a more realistic mesh.

Practical experience in meshing shoe parts shows that most of these 2D to 3D mesh problems occur where the size of features is close to that of the seed, this also includes the thickness of parts. For example; the Supernova midsole has a group of groves cut into it to assist in bending during the midfoot-push-off transition. While a good 2D mesh can be generated in these grooves, if the base of a groove is too close to the lower surface of the midsole the 3D meshing algorithm can miss-mesh the small volume of space remaining (Figure 8.24).

This error is difficult to identify as it will not show up on any of the mesh checking functions as there is nothing wrong with the 2D mesh. The only way to work around this problem is to partition the surfaces to give a better mesh definition, reduce the size of the seeds, or increase the distance between the problem surfaces.

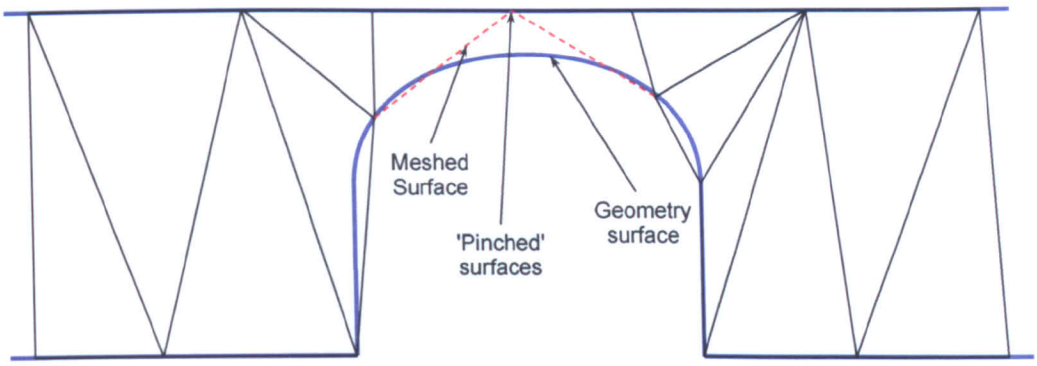

Figure 8.24: Thin 'solids' lead to 3D meshing errors at the point marked.

8.2.3 Solid Meshing

The process of solid meshing is similar to that of the 2D mesh to solid 3D meshing process, although the user has much more control over the resulting mesh. The simplification of the Ultraride midsole into a very coarse, but quick-running, mesh for development purposes demonstrates a solid meshing process (Figure 8.25). First a shape is created by joining outlying points on the original geometry. This shape may still have too much detail, in this case thin ridges around the top, so these are removed. This shape now has a reasonably regular cross-section, and can be meshed using the sweep technique. The lower surface is meshed in 2D, then this mesh is swept along the lines on the side of the shape, to the top surface. The meshing algorithm adjusts the 2D mesh to fit the small changes in shape as it passes the object and a final 3D mesh is created.

Solid meshing generally produces meshes of much better quality and allows the creation of hexahedral meshes. However, it normally requires user intervention on all but the very simplest of shapes and currently there is no automatic random-volume hexahedral meshing algorithm available, so meshing the structured midsole geometry would require the user to create many regions of reasonably constant cross-section, which is currently prohibitively time-consuming. However, future shoe designs may allow hexahedral meshing.

8.2.4 Mesh Modification

If a mesh has been created, and checks on its quality reveal inadequacies, then the offending elements must be removed or modified. Generally this can be achieved by tightening the tolerances on the QI mesher used for surface modelling, or by removal of more detail on the geometry. If only a few elements are unsatisfactory then they can be removed, or have their vertices modified. Both of these operations need to be done by hand, so it is generally better to get the meshing algorithms working well if the object is to be remeshed frequently.

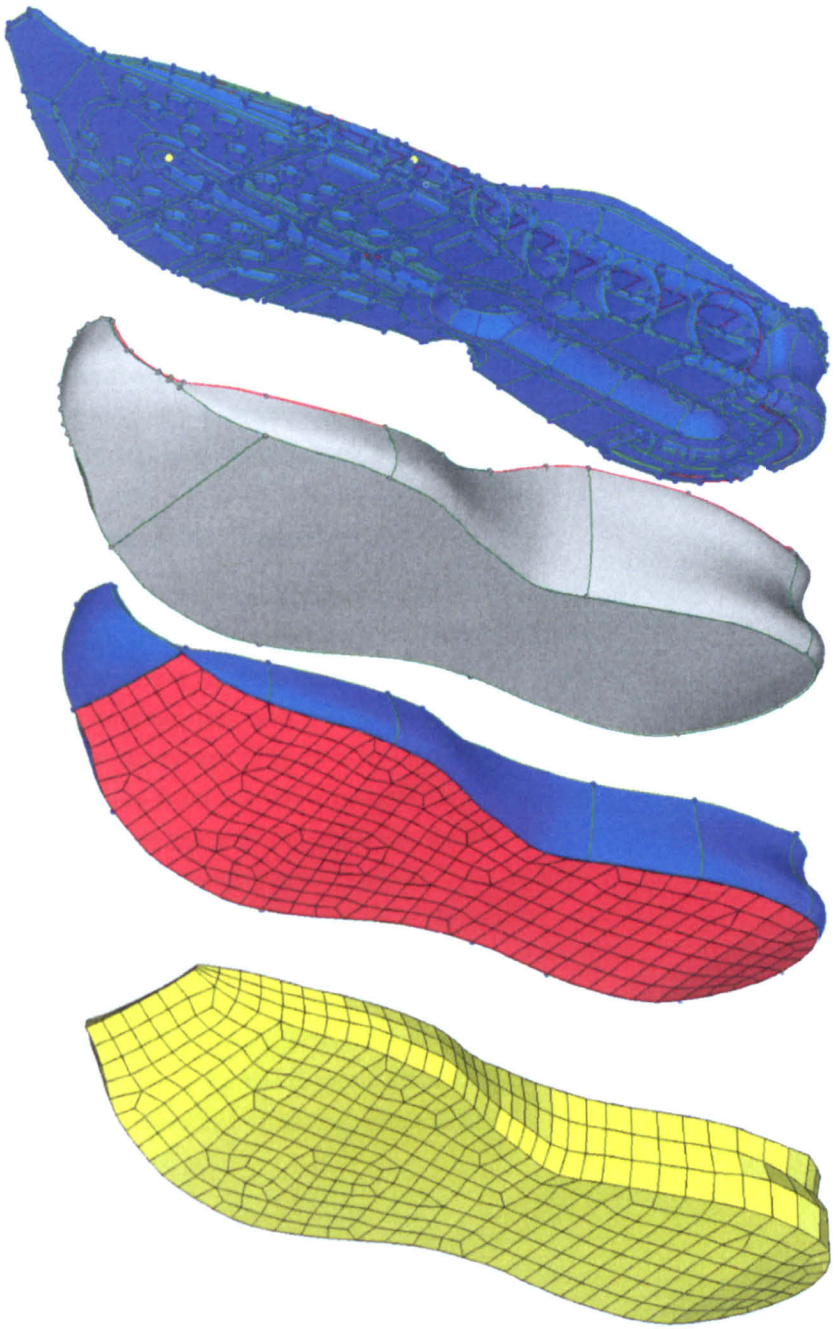

Figure 8.25: Simplification of the Ultraride to create a fast-processing mesh for development purposes.
Original Geometry (Top)
Outer Shell - Outlying surface points are joined to form a shell.
Meshable Volume - The thin edges on top of the outer shell are removed to create more of a smooth surface. The lower surface is then meshed in 2D.
Swept 3D Mesh - The 2D mesh is then swept from the lower surface to the top, creating a 3D mesh (the very anterior of the shoe not meshed as very small elements are generated).

8.3 Quasi-Static Testing

Once a satisfactory mesh has been created, it can be imported into ABAQUS, given a material model, and tests may be performed on it. To have confidence in the accuracy of these models it is vital to obtain data for verification. It is also necessary to check for any variability between physical parts which were designed to be identical, but may have different properties due to their process of manufacture.

Compression tests were carried out on the Supernova midsole, Ultraride structure plate and the Gigaride posterior structure and heel units (the test setups are described in Section 5.3).

This section will look at the results from the physical testing, while the next section covers the results from the FE models and the verification of these results against the physical data.

Required Measurements For these tests the force/deflection response was recorded, along with images of the deformed shapes of the parts under loading. The structural response of the part was also captured using the tracking technique detailed in Section 5.5.

8.3.1 Physical Test Results

Figures 8.26-8.31 show the results of controlled boundary condition tests, with the curves giving the 6th, 7th and 8th compressions of each component.

The foam Supernova (Figure 8.26 -8.27) midsole showed greater variation in the heel region than the forefoot, this may be due to the more complex moulding in this region.

The Ultraride structures (Figure 8.28) were found to be the most consistent part, with deviation of one part from another observed only at higher deformations.

Due to the smaller parts of the Gigaride, mounting of the samples was more difficult and resulted in an audible cracking sound coming from de-bonding of the sample from its mount (this can be seen in Figure 8.31). Sample GRS-1 (Heel) was only loaded to 500 N after pre-loading to see if this noise could be avoided in the test, but it persisted, so the original test level of 750 N was resumed (as the samples had been pre-loaded to this level). The most likely cause of the larger hysteresis loops seen on some of the samples is this de-bonding. Hysteresis loops were not recorded for the Supernova and Ultraride samples due to limitations of the Instron software at the time of testing those parts.

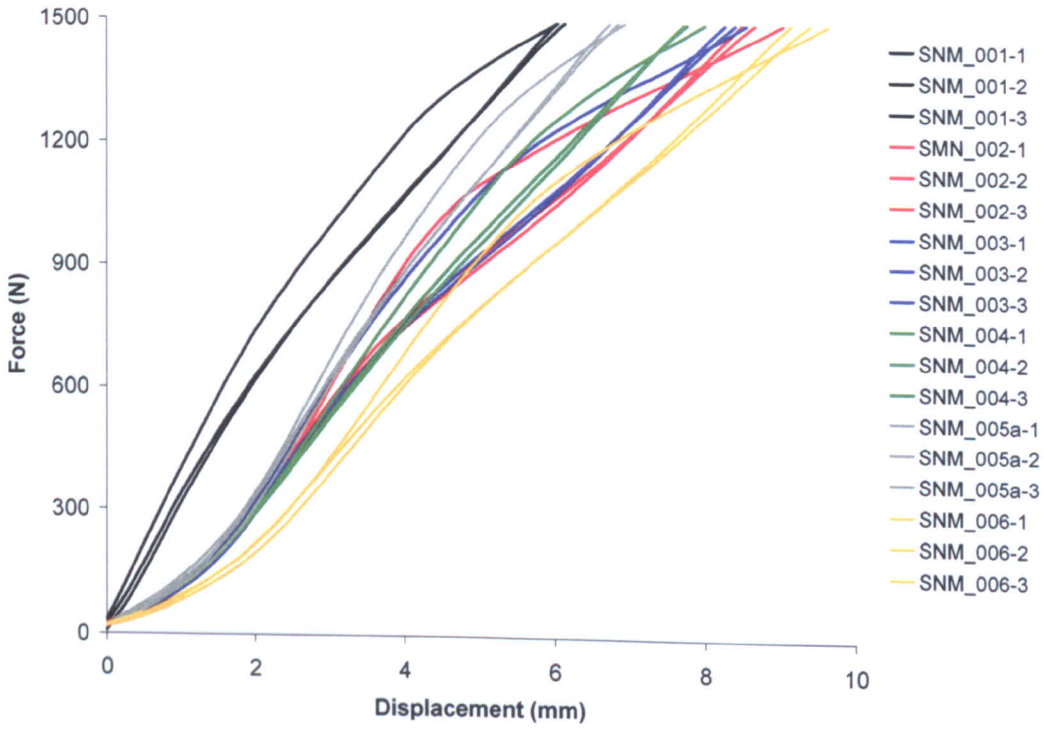

Figure 8.26: Supernova midsole part compression test results - heel region.

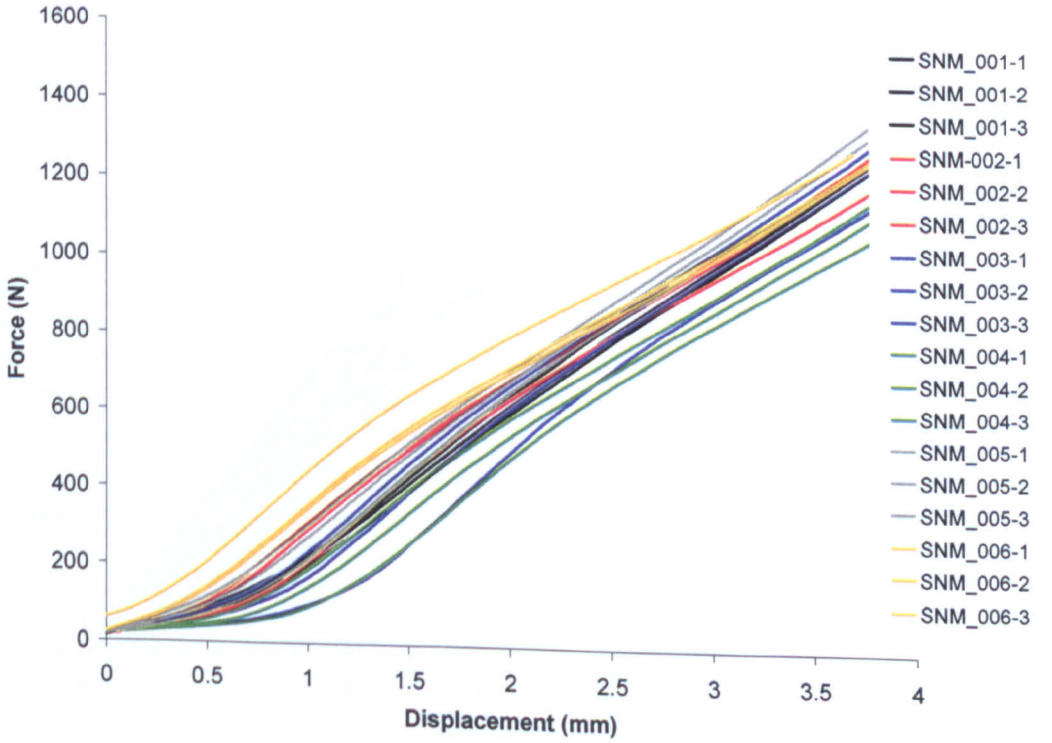

Figure 8.27: Supernova midsole part compression test results - forefoot region.

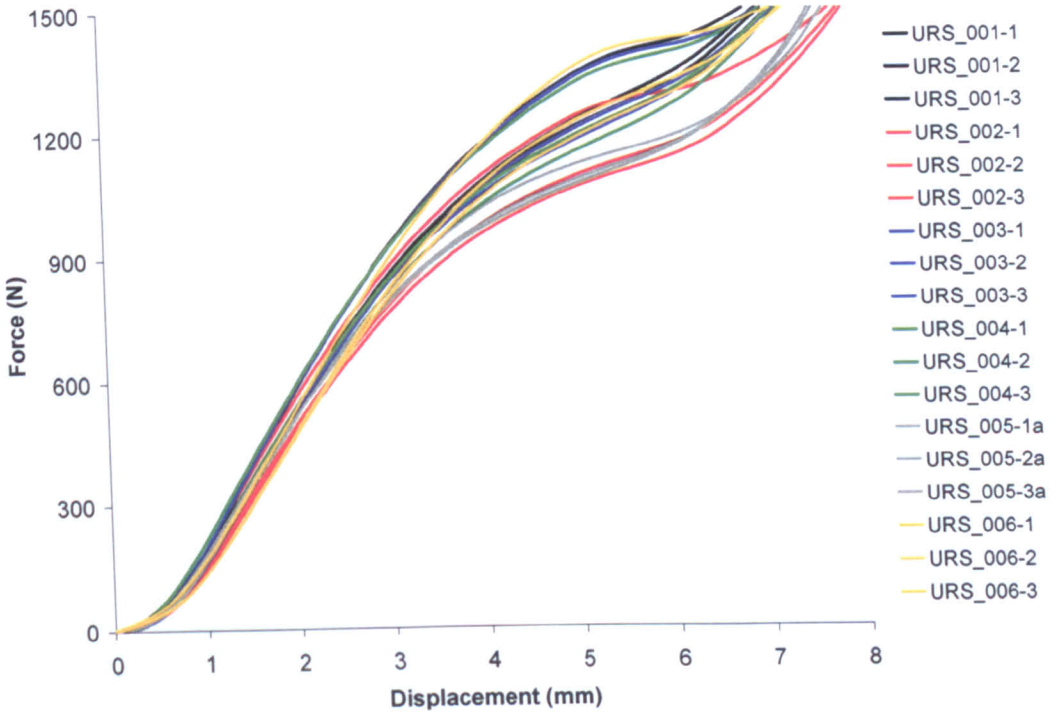

Figure 8.28: Ultraride structure plate compression test results.

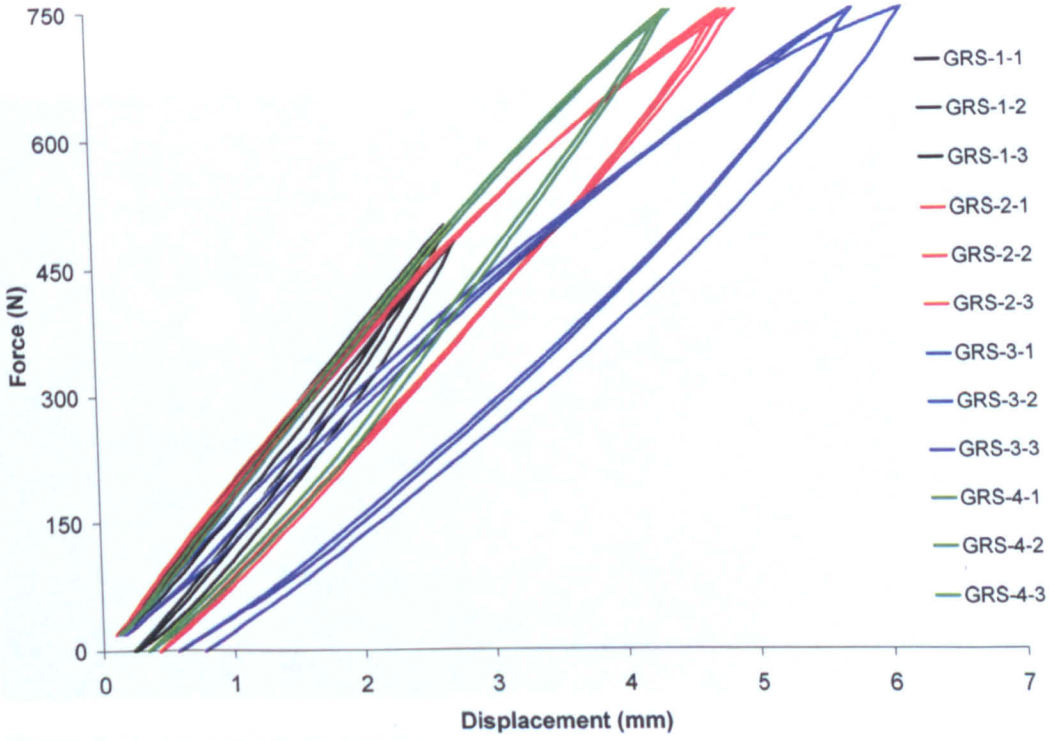

Figure 8.29: Gigaride posterior structures compression test results.

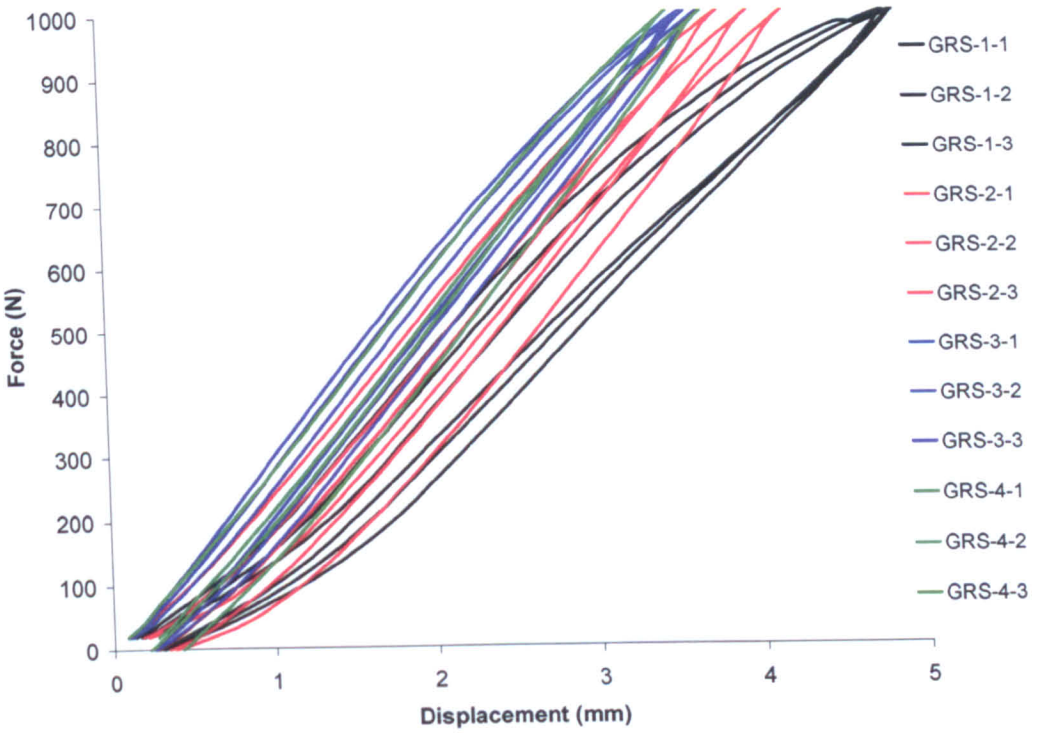

Figure 8.30: Gigaride heel structure compression test results.

Figure 8.31: De-bonding of a Gigaride heel from its mounting during compression testing (Sample: GRS-3).

8.4 Quasi-Static Modelling

8.4.1 Test Setups

As the physical tests were designed to limit any movement between surfaces, and to compress the part vertically, the FE models consist of the respective part held in space by pin constraints on their lower surface, and compressed using a displacement boundary condition on the top surface(s). The pin constraints allowed rotation of the nodes at the surface, which prevented the linear tetrahedral elements from locking and artificially stiffening the part.

All compressions were carried out in Explicit, over a period of one second, which was sufficient to give a kinetic/internal energy level of less than 5%, indicating that inertial effects could be considered negligible. Parts were initially tested with the material models developed from the sample testing performed in Chapter 7. Both linear (C3D4) and quadratic (C3D10M) tetrahedral elements were used as either element could be used in the final full shoe models, depending on its purpose (for processing speed or accuracy).

8.4.2 Job Controls

The concept of mass scaling was introduced in Section 4.6.4.2 as a method of reducing the processing time of an Explicit analysis by artificially increasing the density of the material. This is most useful when quasi-static processes must be modelled in Explicit due to complex contact preventing the analysis being run in ABAQUS Standard.

To produce accurate results, it is advised in the ABAQUS manual to check that the kinetic energy of the analysis is low when compared to its internal energy. This will occur when the deformation processes are the major contributor to the energy stored within the component, as occurs during a quasi-static process.

As this research considers how fast the modelling process can be achieved (a faster process will add value in an industrial application), tests were carried out on the Supernova midsole part to assess how much mass scaling can be applied without adversely affecting the results.

Figure 8.32 shows the results from four identical test set-ups, with only the level of mass scaling adjusted between the models. A negligible difference was seen between the 1×10^{-6} sec time increment analysis (considered to be effectively no mass scaling) and that of the 1×10^{-4} sec analysis. This corresponded to a 100 times reduction in the processing time. Only at a time increment of 1×10^{-3} sec were significant kinetic effects apparent in the reaction force results.

However, Figure 8.33 shows the energy traces for these analyses. Above a time increment of 1×10^{-5} sec, significant kinetic effects can be seen. These were also visible in animations of the FE results, which show the highly scaled models behaving as though they were highly viscous. This has also been seen in a trace of the position of the node that represents the tip (used for structural tracking), in Figure 8.34.

This study shows that the level of mass scaling that should be applied to a job is dependant on what needs to be gained from the results. In models where little motion is expected, then very high mass scaling can be applied without significantly affecting force results. However, if the model contains a large mass (such as in a drop test), if this mass is even slightly scaled then it will have a large effect on the results. It is recommended to run a highly scaled job first, as it will run quickly, and check the force, energy and visual results for signs of non-physical behaviour (such as being overly-viscous). Doing this will also quickly alert the user to other problems in the model, such as incorrect contact specification.

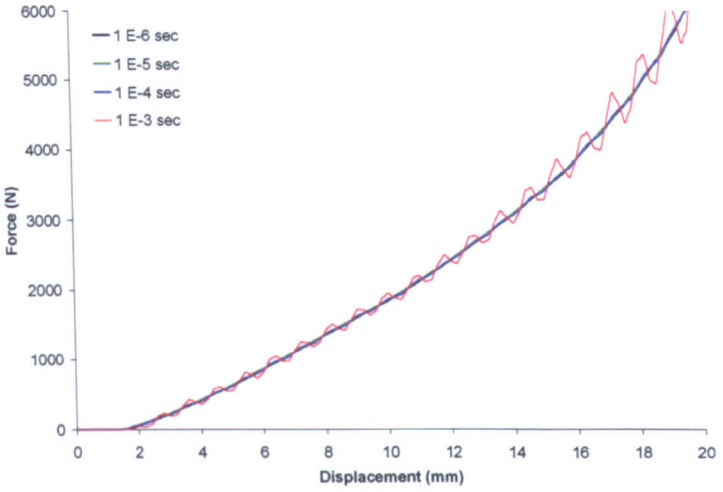

Figure 8.32: Force/displacement results from compression of the Supernova midsole part with a variation in minimum time increment applied by mass scaling.

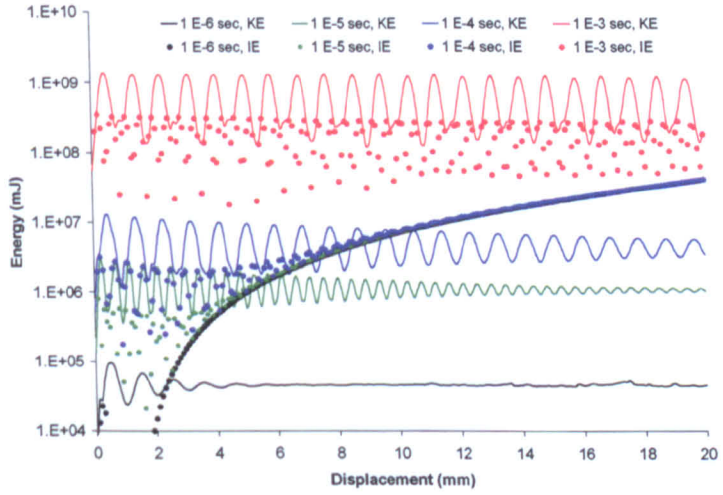

Figure 8.33: Logarithmic kinetic (KE) and internal (IE) energy results from compression of the Supernova midsole part with a variation in minimum time increment applied by mass scaling. For a quasi-static analysis, the KE should be less than 5% of the IE (ideally it would be 0%), indicating the energy in the model is stored as elastic energy.

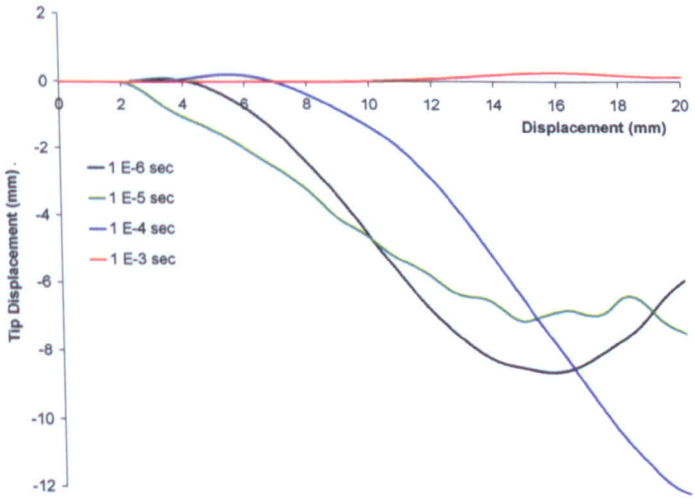

Figure 8.34: Positions of the tip of the part under loading with varying levels of mass scaling. Note the longer time needed for the end of the shoe to begin moving on the higher scaled models due to increased viscous-like effects from the mass scaling.

8.4.3 FE Results

The comparison of real and FE force/deflection results was addressed on two fronts; the overall stiffness (of the result), and the shape of the curve generated. Figures 8.35-8.39 show the FE results overlayed onto a physical result. All the data inputted into the models were the no-preload data, so it was the stiffest, first cycle data that needed to be matched.

None of the FE results fully matched the physical when using the material models from samples, and a clear difference was seen between using linear and quadratic elements. However, this was not considered a major issue as the aim of this shoe part testing was to verify the models against reality.

The foam results generally did not match the curve shape of the test data, probably due to no volumetric data being included in the model (as it caused unstable material models). The TPU models did predict the shape of the deformation curve well, indicating that the physical processes involved were reasonable, so the only adjustment needed at this point was a relatively simple change in overall stiffness (as detailed in Section 7.8). This has been included in the result figures.

The adjustment required to to match the TPU results was clear as the curve had a distinct shape which had to be fitted onto the physical results. The foam results were less clear as the adjustment was made to fit a straight line onto a curve for all but the quadratic result shown in Figure 8.36. A deliberate offset was introduced in the displacement values of the FE result in an attempt to match the overall stiffness of the physical result.

It should be noted that although the relationship between stiffness and the potential coefficients was found to be directly proportional for the TPUs (e.g. a 40% increase in the coefficients gave a 40% rise in stiffness), the foams did not behave as predictably. This may be due to a non-constant Poisson's ratio. Due to this, adjustments for foams had to be obtained by trial and error.

There was also a marked difference in the stiffness prediction between the Marlow and Ogden models for the Ultraride structures which demonstrated that any adjustment of the material model to account for moulding, must also take into account which strain energy potential is being used.

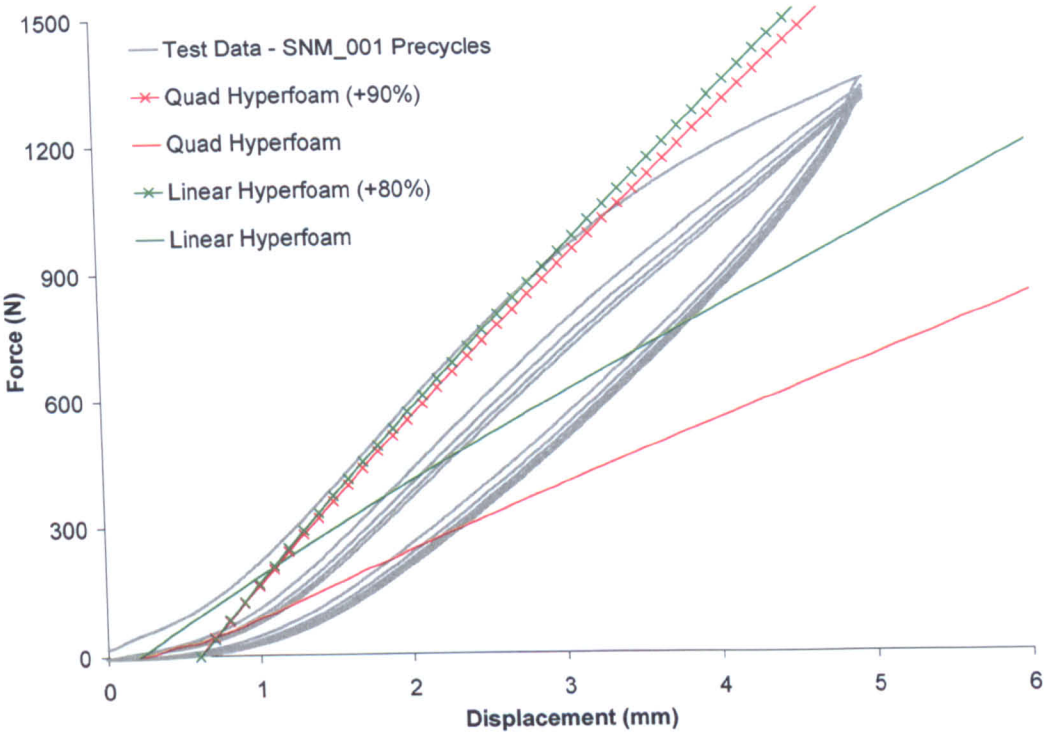

Figure 8.35: Results of FE modelling on the Supernova midsole under controlled boundary condition heel loading. Results from the original and adjusted material models are shown.

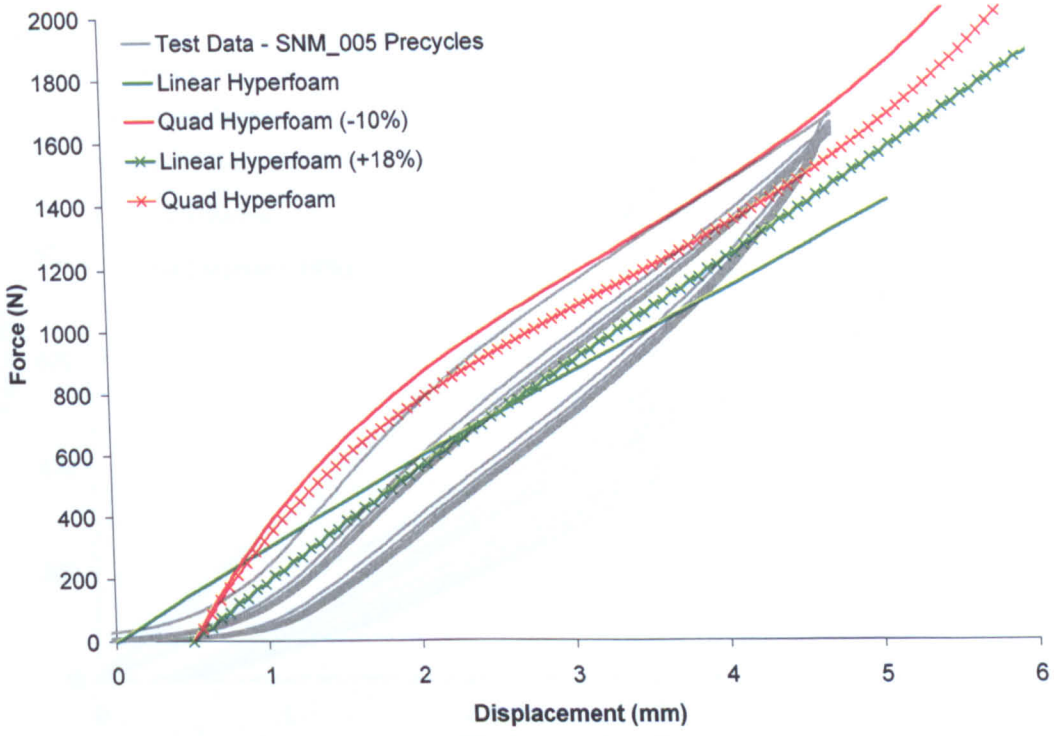

Figure 8.36: Results of FE modelling on the Supernova midsole under controlled boundary condition forefoot loading. Results from the original and adjusted material models are shown.

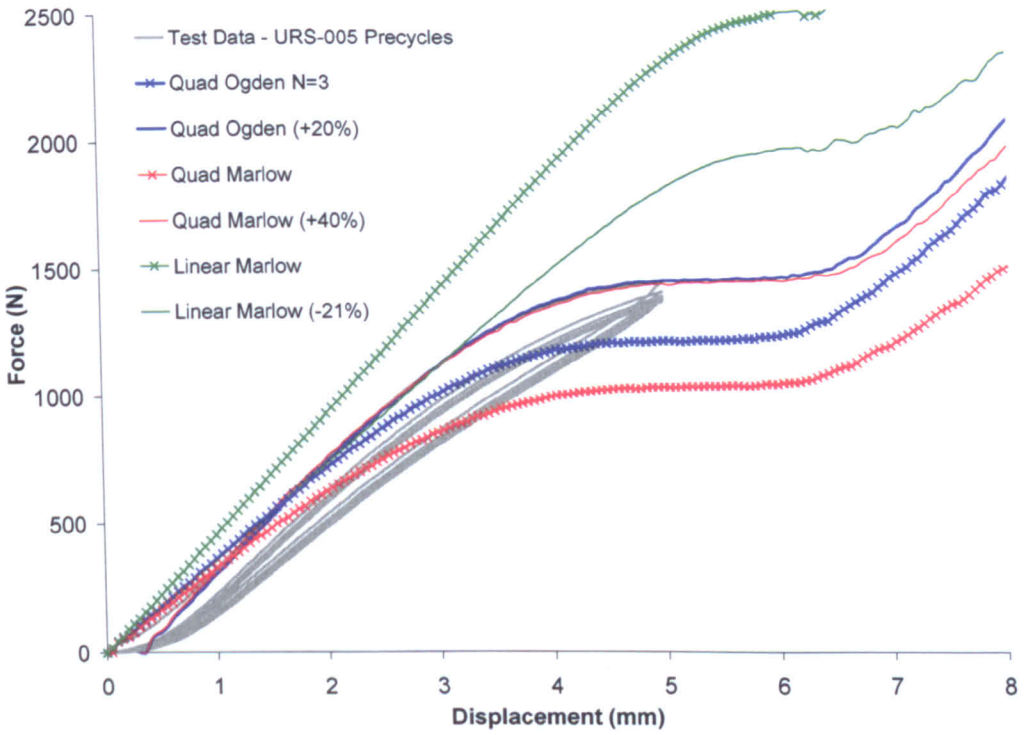

Figure 8.37: Results of FE modelling on the Ultraride structure plate under controlled boundary condition loading. Results from the original and adjusted material models are shown.

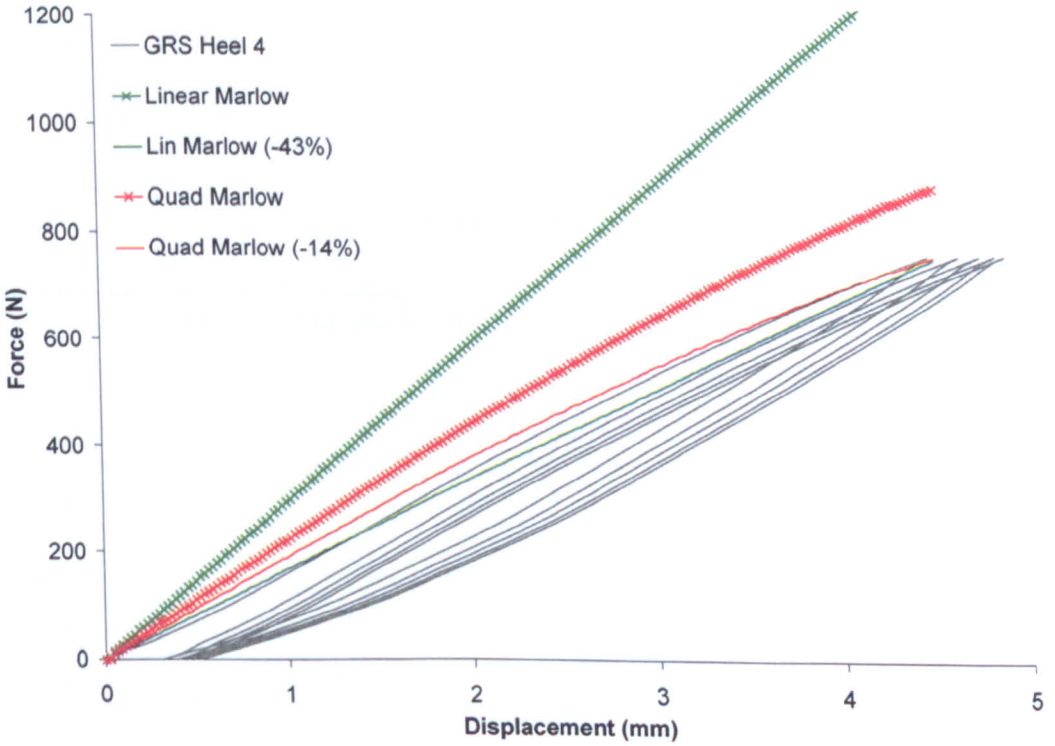

Figure 8.38: Results of FE modelling on the Gigaride heel under controlled boundary condition loading. Results from the original and adjusted material models are shown.

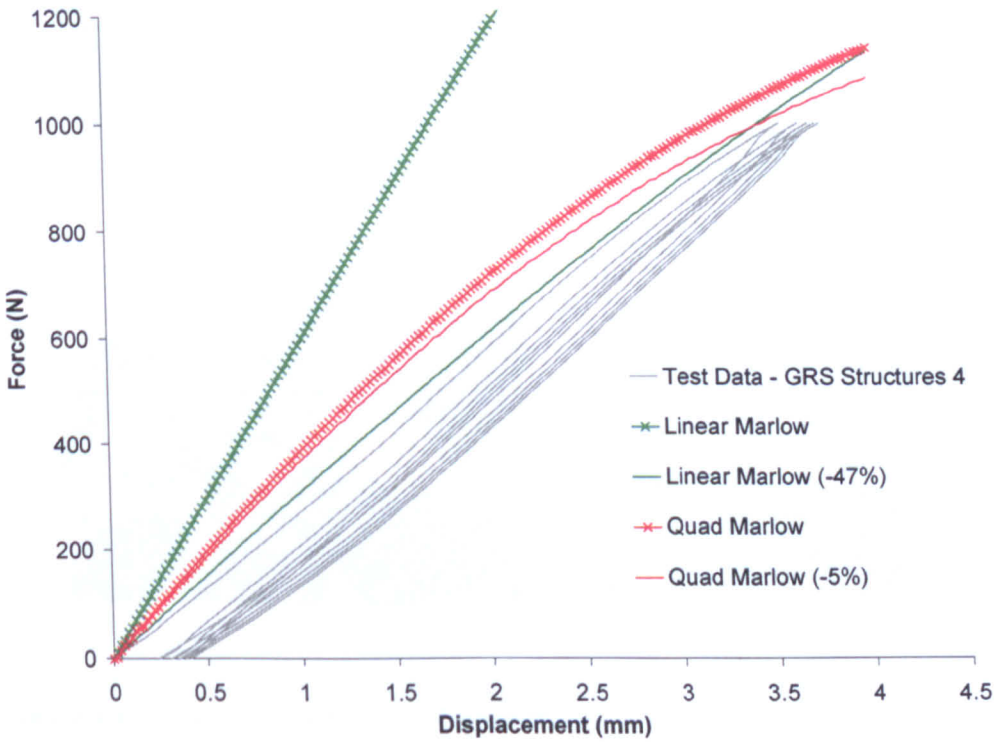

Figure 8.39: Results of FE modelling on the Gigaride main structures under controlled boundary condition loading. Results from the original and adjusted material models are shown.

8.4.3.1 Shape Comparison: By Image

While the quadratic and linear elements were adjusted to give a similar overall stiffness for the entire part under test, the structural details of the model were different (for each element type) from the physical, when using the adjusted material models. Figure 8.40 shows detail of the Gigaride heel and main structures under the same load for linear and quadratic models. The stiff linear elements were found to distribute the load more evenly than the quadratics, which showed much higher peak stresses at the intersections of the structures in the heel, and higher curvature of the main structures' shape. Figure 8.41 shows an overlay of the physical response (red), taken from video of the test, with the linear and quadratic FE responses (dark and light respectively).

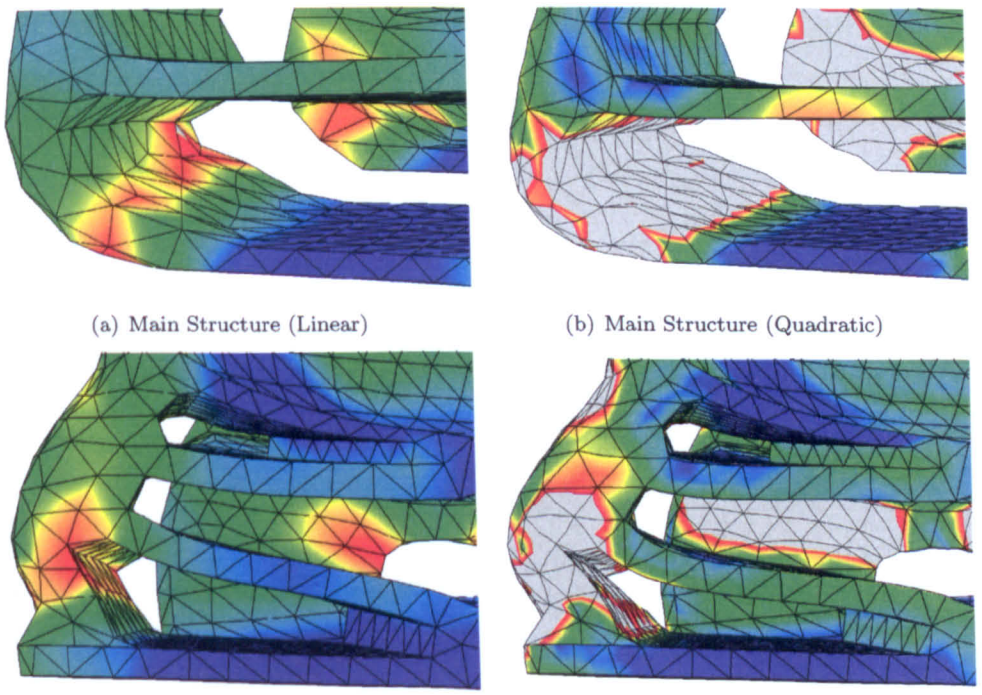

(a) Main Structure (Linear)

(b) Main Structure (Quadratic)

(c) Heel Structure (Linear)

(d) Heel Structure (Quadratic)

Figure 8.40: Shape and stress differences between the linear and quadratic element models of the Gigaride heel and main structures.

Figure 8.41: Overlay of the physical response, taken from video of GRS-4 (red) with the linear (dark) and quadratic (light) shape results.

8.4.3.2 Shape Comparison: By Structural Tracking

To give a more quantitative comparison, the effective strain in the part under test was measured externally by structural tracking (see Section 5.5 for details). For the Ultraride structure plate, the extension of the horizontal middle section of the structure was of particular interest as this was designed to be one of the main load bearing parts, and should extend under loading instead of forming an s-shape. The image comparison in Figure 8.41 showed clearly that the s-shape was not formed, but structural tracking allowed measurement of the actual extension in the vertical plane. Figure 8.42 shows the averaged results from the 18 compressions (6 structure plates with three repeats) recorded. The increase in separation of the tracking points placed at either end of the middle of the structure was taken as the extension, and the displacement was the vertical compression of the part, both in mm. Assuming the centre of a point could be tracked to within a 3 pixel diameter (as the error bars indicate), then there was very good agreement between the physical and the FE model.

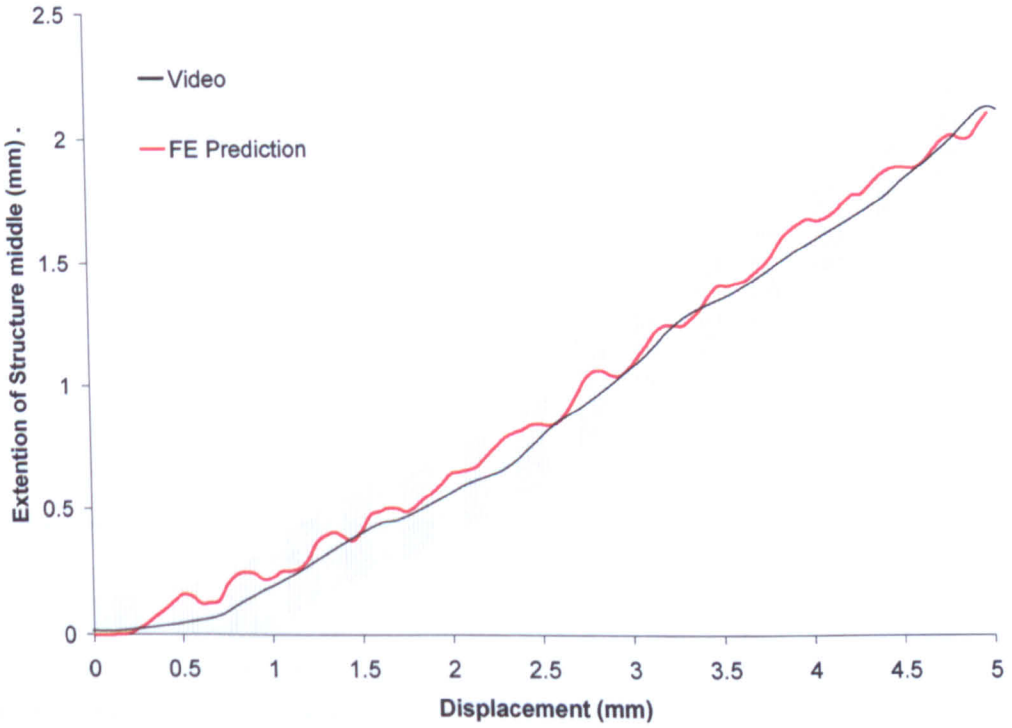

Figure 8.42: Comparison of measurements of the extension of the middle section of the medial posterior structure of the Ultraride structure plate during controlled boundary condition compression. The video results are averaged over three compressions on each of 6 structure plates. The shaded area indicates the error of the structural tracking system.

8.5 Modelling Material Degradation

The theory behind the modelling and testing of the Mullins effect was discussed in Section 7.9, and this is developed here for use on realistic geometry.

Figure 8.43 shows the stress/strain response of the controlled boundary compression test carried out on the Ultraride structure plate. The structures were cycled 5 times to 5 mm with the *MULLINS EFFECT option enabled. The adjusted Marlow potential was used with linear elements, and the result closely followed the test data curve on the full-scale model (Figure 8.37). The level of stiffness loss from the first cycle was also a good match for the higher stress part of the cycle.

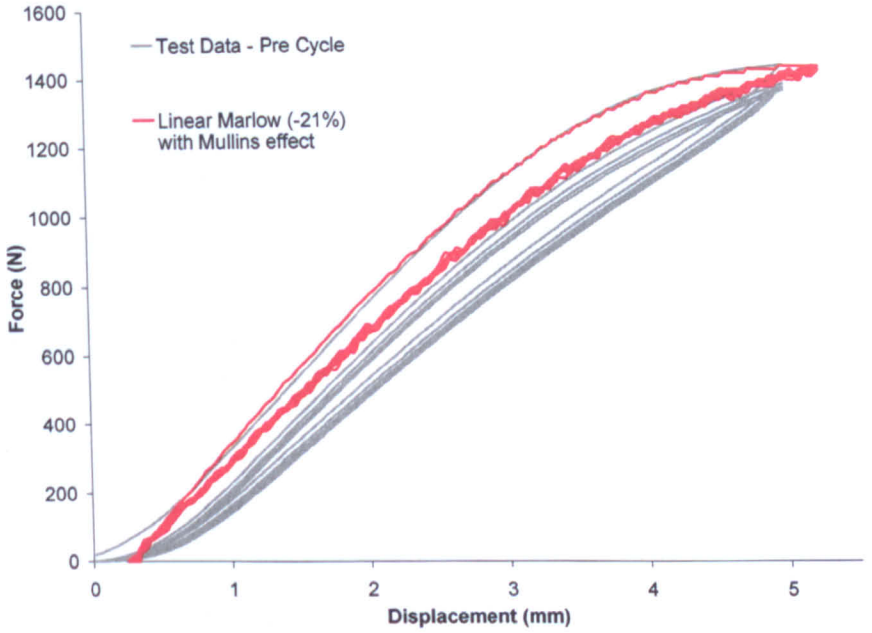

Figure 8.43: Comparison of the force/deflection results of the Ultraride structure plate compression model, with and without the Mullins effect included.

It should be noted that the FE model returns to a point of zero strain, as the loading conditions force the elements to do this, but the physical part may experience some settling in its fittings on the first loading cycle of the test, which explains the need to translate the start point of the FE prediction to illustrate the closeness of the results. This effect has been observed during most of the shoe and part testing, so a good match should be primarily determined from the stiffness and shape of the curve, rather than it sitting precisely over the physical results.

Figure 8.44 shows the stress, strain and damage energy for the Ultraride structure test. The damage energy is the energy loss through plastic damage to the material caused by the Mullins effect included in this model. The images have been chosen to show the location of peak stress/strain within the structure shape under vertical loading, and also to illustrate that the damage is not linearly related to the strain level; at higher strains the increase in damage per unit strain is greater. This concentrates the maximum damage in the regions of very high strain. For the structure geometry this has a positive effect in reducing the peak stresses seen in the model over time; the peak stress regions become softer and spread the load out over a larger area. This can be seen in Figure 8.45, even over the small number of cycles in this test. This has implications in the failure analysis of components when based on peak stress, as ignoring the Mullins effect may lead to over-engineered parts in a product where weight is important.

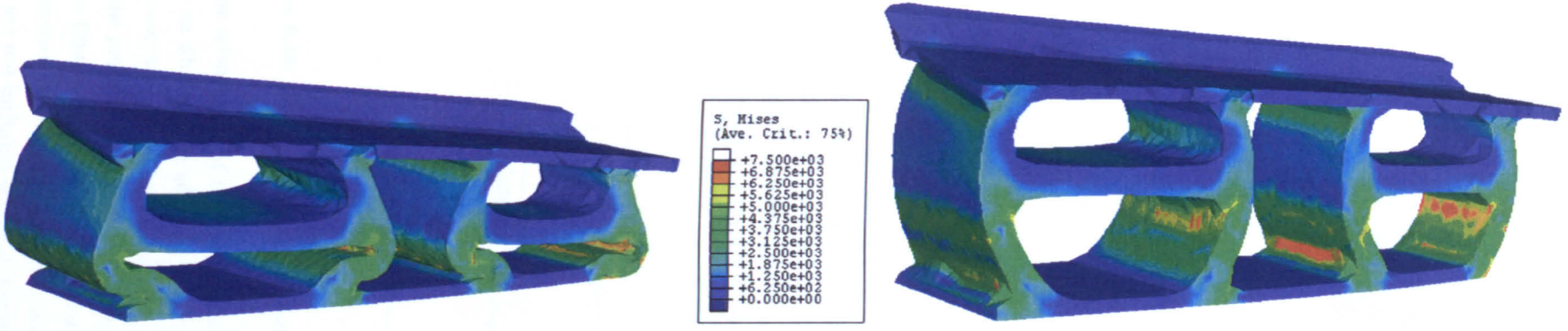

(a) Von Mises Stress (S, Deformed Shape)

(c) Von Mises Stress (S, Undeformed)

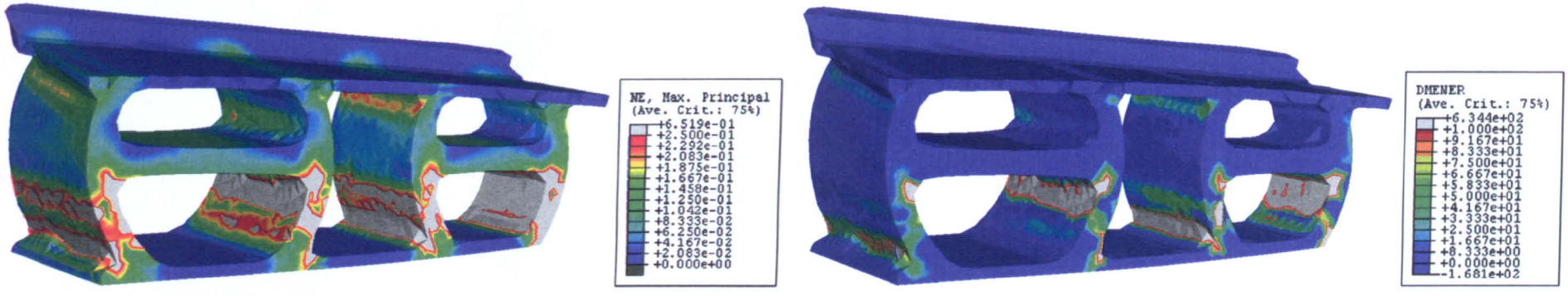

(d) Nominal Strain (NE, Undeformed)

(f) Damage Energy (DMENER, Undeformed)

Figure 8.44: Stress, strain and damage in two Ultraride structures cycled vertically to 5 mm, 5 times.

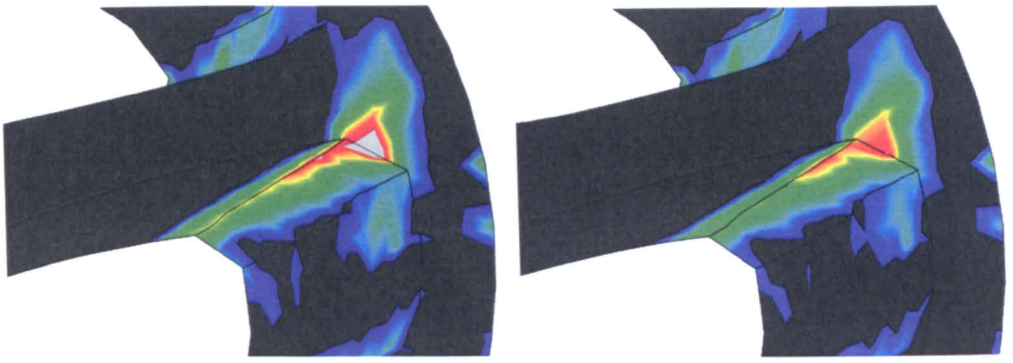

(a) 1st Cycle (b) 5th Cycle

Figure 8.45: Detail of the reduction in peak stress seen at a join in the centre of an Ultraride structure after cyclic loading.

Currently, ABAQUS cannot use the *MULLINS option with *VISCOELASTICITY, limiting the use of the Mullins effect in models that rely on viscoelastic effects, either for stress prediction or noise removal (such as from impacts on shoe assembly models, as discussed in Section 9.3.1).

A Visual Basic program was developed to allow adjustment of material data by re-specifying the material applied to any element based on the output from a model, Figure 8.46 illustrates the process. Once a job has been run, the desired critical variable (e.g. stress, strain or any other quality) is outputted and the program uses these results to specify new materials (by re-assigning sections) on an element-by-element basis, creating a new ABAQUS input file. The program bases its re-assignment on data supplied to it by the user, so the adjustment does not necessarily have to follow any progression (e.g. it could model the Mullins effect over a range of strains, or could have a single threshold where a property of the material changes). Figure 8.47 shows the result of four iterations of re-assignment for a forefoot cushioning test on the Supernova.

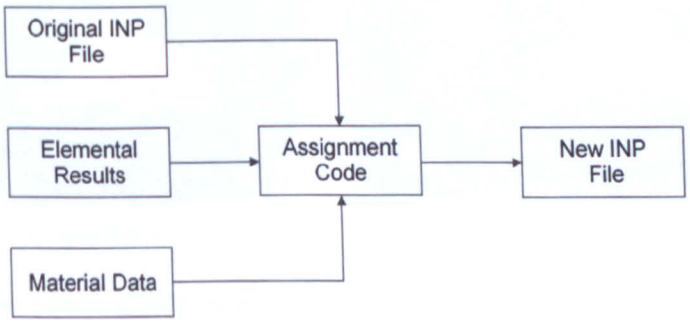

Figure 8.46: Flow chart showing information flow in the processing of ABAQUS input (INP) files.

The advantages of this method are that the material itself is changed, so there are no limits on what can be adjusted (an elastic material could become a foam if necessary), and it can overcome material conflicts, such as Mullins and viscoelasticity. The disadvantages are that the process is not in-line with the ABAQUS, it requires multiple running of jobs which can be time consuming. The application of user material models within ABAQUS (such as that written by Bergstrom 2006b) may provide a better solution, although at the moment these are not included with the ABAQUS package.

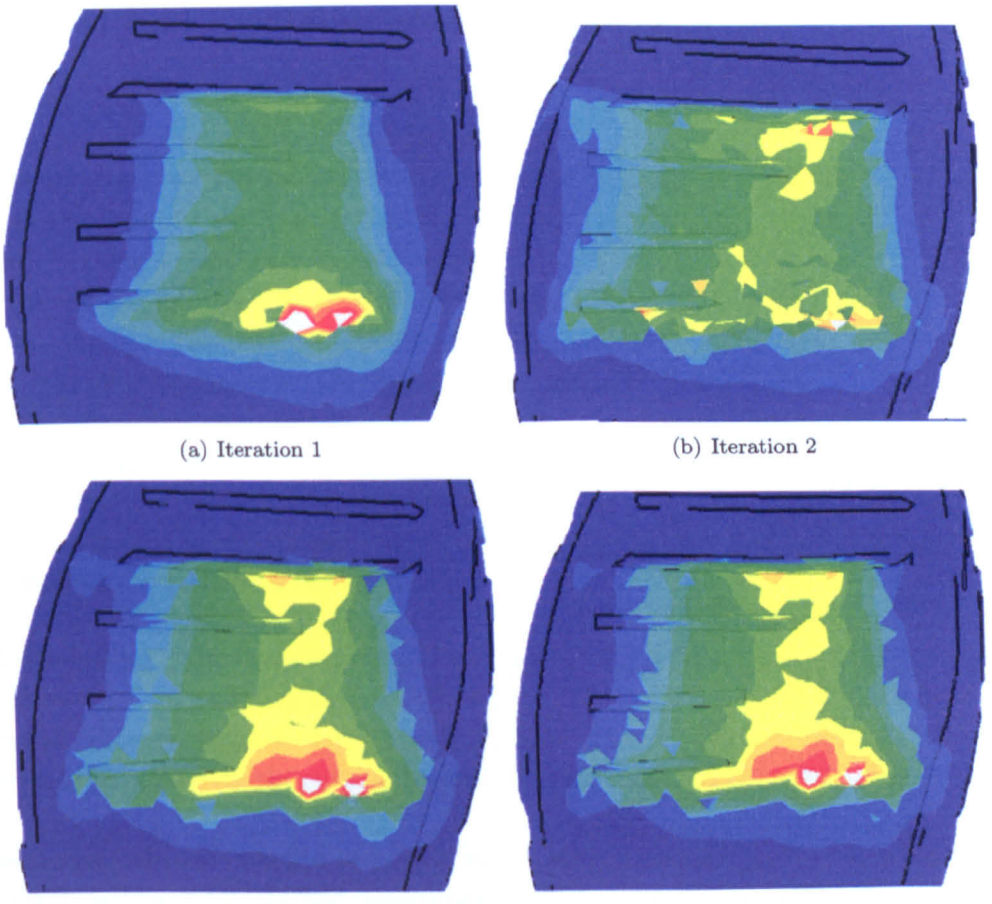

(a) Iteration 1

(b) Iteration 2

(c) Iteration 3

(d) Iteration 4

Figure 8.47: Stress results of four iterations using the section re-assignment program. Note how the stress pattern stabilises between the 3rd and 4th iterations.

8.6 Chapter Summary

The work reported in this chapter aimed to address the feasibility of creating FE models from complex shoe geometry designed for manufacture, not modelling. The accuracy of the models produced, when processed using the material models developed in the last chapter were also assessed, along with the variation of physical properties in the sample shoe parts.

Geometry FE programs such as ABAQUS cannot generally import highly complex surface geometry easily, as they are designed to deal with solid geometry. Repair of geometry that has many surface-to-solid import problems is very time consuming as it requires correction by a skilled user. If time is limited, then it is critically important that the original surface geometry is of high quality - that is it should have a high tolerance on specification of node positions and should be checked for duplicate and non-intersecting surfaces before export.

Meshing It is difficult to mesh shoe parts with the most accurate and quick-running hexahedral elements, due to the complex shapes involved. However, new techniques such as morphing may allow this on some of the newer, more regularly shaped shoes. While the tetrahedral element does cause an artificial stiffening due to its shape, and the linear tetrahedrals can lock up and become rigid if used incorrectly, the element has been able to predict the shape of the force/deflection curves of the parts well in both linear and quadratic formulations. Use of tetrahedrals also allows automatic meshing of shoe shapes, so a tetrahedral mesh may make up for slower calculation by saving the user set-up time.

Part Testing The Ultraride structure plate showed the most consistent results, with the stiffest Supernova heel showing approximately half the compression needed to achieve the test load than the softest sample. The Gigaride results were less consistent due to difficulties in mounting the samples in the test machines.

FE Modelling The models matched the shape of the test data curve well, but only after adjustment. This indicates that the FE models are predicting the large-scale underlying physical processes correctly, including the damage caused by they Mullins effect, but may not necessarily describe the stiffness accurately when using sample material data.

Predictive Ability Testing and modelling of two TPUs (UR1175 and GR685) and two foams (LS3016 and LSA52CCM, both from the Supernova), did not show any consistency in the error of prediction of the FE models between sample materials and shoe parts. As all the models used the same elements, any variation in performance due to the element shape or order was eliminated.

The inconsistency in prediction error could be attributed to the materials, three possible reasons for this could be; the materials differed in the amount of change they experienced during moulding, the sample sheets and the structures on test contained slightly different mixes of the same material, or that ABAQUS was modelling the test data differently.

The first two hypothesis cannot be proved without further physical testing. However, as the samples tests were modelled in the last chapter, it was possible to compare the difference between the ABAQUS material model, which assumed the material data was from a perfect test, and the output from models which captured some of the inaccuracies inherent in the sample tests.

Table 8.1 shows the over/underpredicition of the FE results (relative to the physical result) seen in the sample test that best fits the deformation mode seen in the part, and at the estimated operating strain (as detailed in Table 7.2). The adjustment values may appear large, but the models use highly non-linear material models and have been seen to show discrepancies between element types for the same material of up to 90%.

Material	Deformation Mode	Operating Strain (%)	Material Model	Sample Error		% Part Error	
				Quad.	Linear	Quad.	Linear
LS3016	Uni. Comp.	15	1st HFoam	-10	-10	-62	-45
LSA52CCM	Uni. Comp.	15	2nd HFoam	-7	-7	-9	-27
LS3017	Uni. Comp.	5	2nd HFoam	-77	-77	-	-
B64D	Uni. Tension	<1	Elastic	-50	-20	-	-
adi50CCM	Uni. Comp.	<10	2nd HFoam	-31	-31	-	-
UR1175	Uni. Tension	30	Marlow	-27	-22	-29	27
C60A	Uni. Tension	<25	Marlow	-17	-18	-	-
ETH046	Uni. Comp.	20	2nd HFoam	-5	-5	-	-
PX	Uni. Tension	<5	Elastic	-50	-20	-	-
VGB	Uni. Comp.	15	2nd HFoam	0	0	-	-
GR685 (Heel)	Uni. Tension	25	Marlow	-15	-19	16	75
GR685 (Str.)	Uni. Tension	25	Marlow	-15	-19	5	89
L20G	Uni. Tension	<5	Elastic	-50	-20	-	-
LX	Uni. Tension	1	Elastic	-50	-20	-	-
Rubber	Uni. Tension	5	Marlow	24	-35	-	-
Rubber	Uni. Tension	15	Marlow	-35	-35	-	-

Table 8.1: Table of percentage mis-predictions (errors) in FE models when compared to physical tests, at the given strain. Note that a negative mis-prediction signifies that the FE model is creating a result which is too soft. 1st/2nd HFoam are the 1st and 2nd order hyperfoam models respectively.

For the models where physical data was available for verification of both material samples and shoe parts, only the quadratic element models of LSA52CCM and UR1175 showed a consistent error. The other 8 models did not. This data indicates that there is not a predictive method available for all materials. However, it must be noted that this is a small sample of tests, so the possibility of a predictive method cannot be ruled out entirely without much more testing on other materials, and parts from different batches and production lines - a process which is not possible in this course of research due to time constraints.

However, what can be done is to estimate the over/underpredicition in the other shoe parts by comparing the results from shoe assembly testing with the FE models, taking account of the known adjustments calculated in this chapter. This process is carried out in the latter half of Chapter 9.

Chapter 9

Modelling Stage 3: Midsole Assemblies

9.1 Introduction

A FE assembly consists of a set of equations that connect together the various meshes in a model, and specify how those meshes interact with each other. Three main stages are required to set up an assembly: correct positioning and orientation of part meshes, simulation of the interaction between meshes, and a description of the movement or load applied. Once this has been established, the assembly is combined with the material models and job controls to form the complete model.

9.2 Interactions: Joining Materials

The adhesive bonds found in the shoes are simulated in the model by the use of tie constraints. These specify that a set of element nodes is physically joined to another set, allowing no separation and transferring all spatial (and optionally, rotational) stresses from the 'master' surface to the 'slave'.

9.2.1 Tie Constraints in Practice

The selection of nodes and elements for surfaces to be tied must be considered carefully to avoid overconstraining the mesh. This occurs when a node has one of its degrees of freedom constrained more than once. This will normally cause ABAQUS to stop the job and report an error, however it was found that ABAQUS version 6.4-1 would simply hang and not report the error. This made correction of the problem difficult as the element that was becoming over-constrained could not be identified easily. The overconstraining condition that caused this problem is illustrated in Figure 9.1, where a t-join between three parts leads to errors if the tied surfaces are defined right up to the join, as the adhesive used in manufacture would be. This problem is solved by de-selecting elements on the slave surface definition, ensuring none remain that overlap other tie definitions.

For all the shoe models investigated, the geometry is designed for manufacture and parts will occasionally fit together poorly, leaving gaps or having one part partially inside another in the initial condition (which is not a physical possibility). This is not a problem in manufacture as the parts are pressed together one by one, and cannot penetrate one another. However, the geometry is the start point of the model and unless corrections can be made, the model must accommodate these problems.

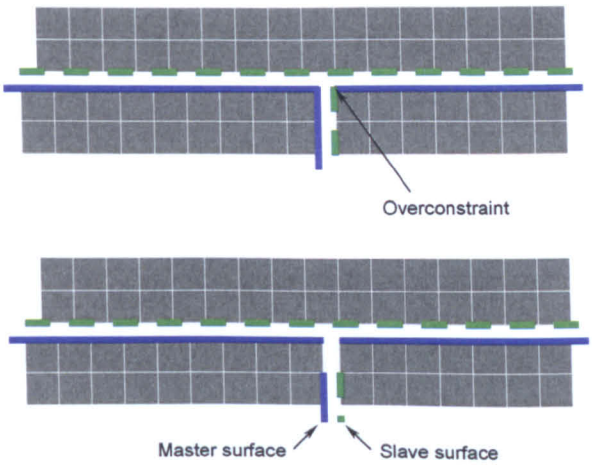

Figure 9.1: Tie constraints at the mesh interface. Master/slave surfaces are shown in dark/light. Top: Overconstrained join, bottom: Correctly constrained, but non-physical model.

The tie constraint function in ABAQUS includes a distance specifier that allows the user to dictate a sphere of influence of the tie. Any nodes defined in the surface definition within the given radius are locked together, those outside the radius are ignored. Tie surfaces that are not in initial contact can be moved together before the analysis starts, but this can cause unwanted strains and velocities in the initial state of the model. In all of the ties used in the three shoe models, the surfaces were left in their original positions as the resulting 'corrected' mesh was poor.

The use of large radii tie constraints allows models to be created where parts are missing; for example, the Ultraride is constructed with an EVA midsole bonded into the upper, which is then bonded onto the assembled structures. At the time of modelling there was no geometry available for the upper section, which left a large gap between the EVA midsole and the structures. By specifying a large tie radius, interaction between these two parts could be modelled, although the stiffness contribution of the upper part was missing (Figure 9.2).

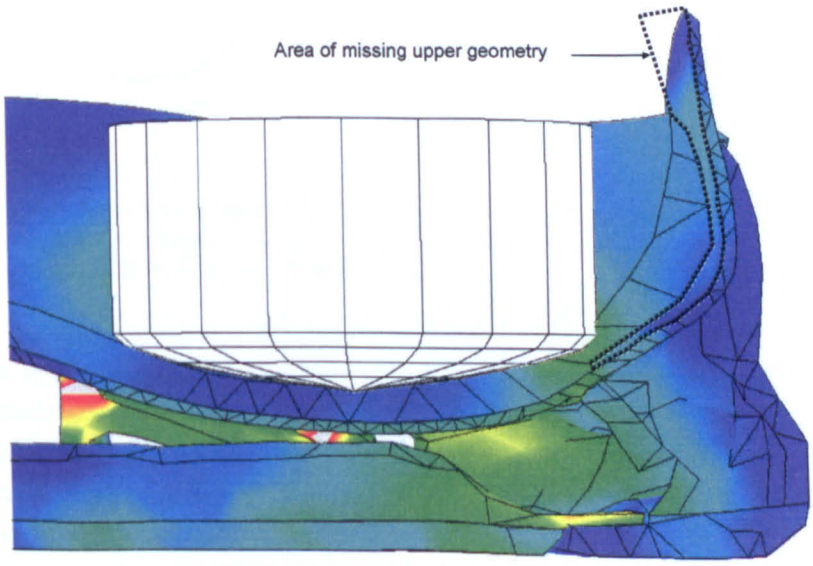

Figure 9.2: Cut-away view of Ultraride heel cushioning test. Note the continuation of stress lines across the gap left by the missing shoe upper.

Use of large radii can have some unwanted effects if not applied correctly. As an example, this section will discuss the GSCB shoe, which contains an internal mechanism, and is detailed in Chapter 10. Figure 9.3 shows a GCSB running shoe heel unit, which comprises of two sliding plates held in place by two springs and a seal. The specification of larger tie constraints causes an increase in the operational stiffness of the unit (Figure 9.4).

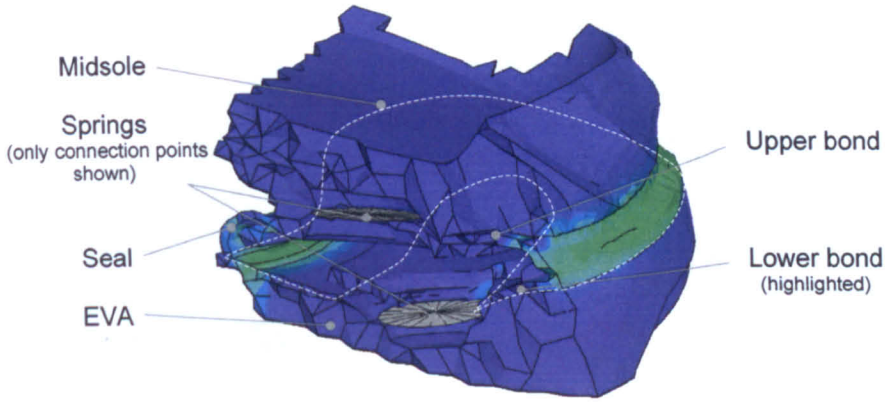

Figure 9.3: Illustration of the mechanism in the GCSB shoe (mechanisms are detailed in the Chapter 10). This is found in the posterior lateral area of the shoe and is shown sectioned across the 'O'-shaped seal.

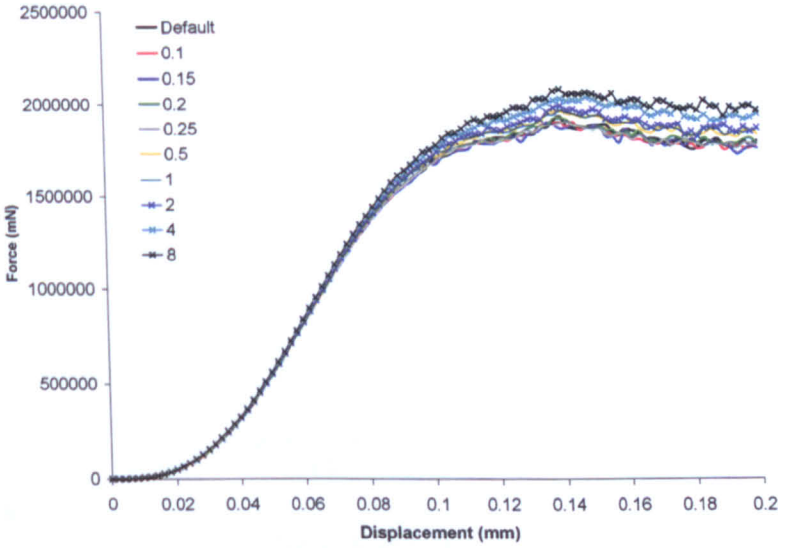

Figure 9.4: Variation in force/deflection for the GCSB mechanism under side loading with a change in the tie tolerance value (specified in mm). The default value is 5% of the element size, which in this case equates to 0.05 mm.

Studies on simple shaped components, illustrated in Figure 9.5, showed that there was no stiffness increase when the seal met the bonding surface at 90°. It did have an effect on the realistic geometry because ABAQUS included all elements that had a surface angle within a given limit into the tie constraint, if they were within the tie tolerance radius. This meant a tie defined on a sharp-edged surface was the same as the user specified, but one on a curved surface was extended as far as the tie tolerance (see ABAQUS Analysis User's Manual: 20.2.1). This tie surface extension effect was introduced into the code to avoid failure of models due to elements on the edge of the tie surface but out of the tolerance, that were not under the influence of a surface contact, penetrating the master surface (as shown in Figure 9.6). An alternative would have been to use a node-based master surface specification, which does not automatically extend its tie range.

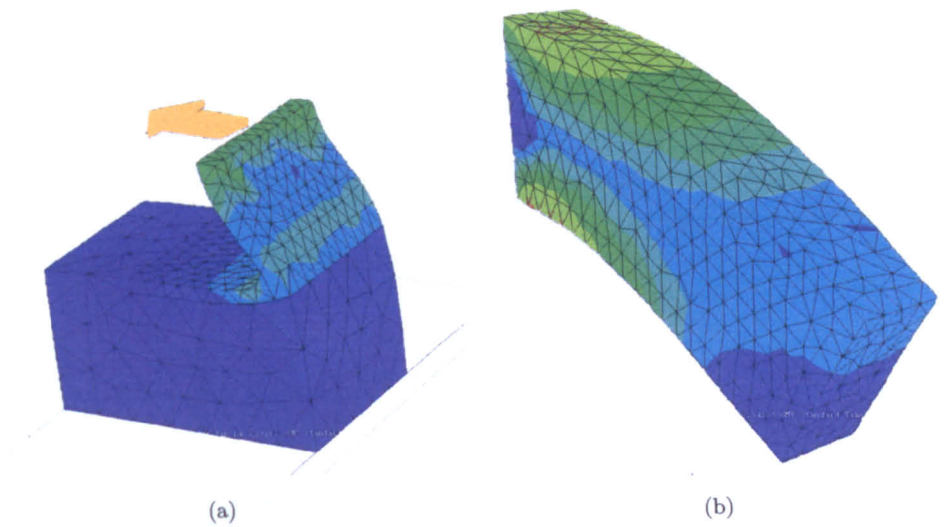

(a) (b)

Figure 9.5: (a) Simplification of the seal/EVA join in the GCSB mechanism using geometrically regular shapes, (b) Model set up for investigating the effect of tie tolerances on components in bend (laminate component is shown).

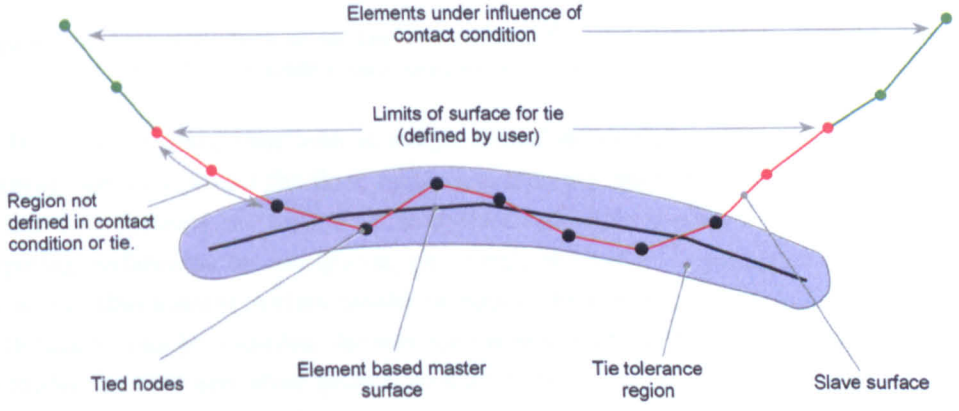

Figure 9.6: Detail of the risk of penetration when the tie tolerance does not extend over the entire surface specified in the tie.

9.3 Interactions: Surface Contact

While the interaction between two connected surfaces can be modelled using ties, surface-to-surface contact is used to model surfaces that are permitted to come into contact. The workings of the contact algorithms are described in Section 4.6.5, with the Supernova, Ultraride and Gigaride models using the general contact algorithm, where possible. This creates interactions between every deformable and discrete rigid surface and all others should they come into contact. This is very useful in the more structurally complex shoes like the Ultraride, where individual specification of surface contacts would significantly increase model set-up time. Figure 9.7 shows a section through the assembled midsoles of the Supernova and Ultraride under heel stamp testing - the Supernova has no open internal structure, while the Ultraride shows multiple internal contacts.

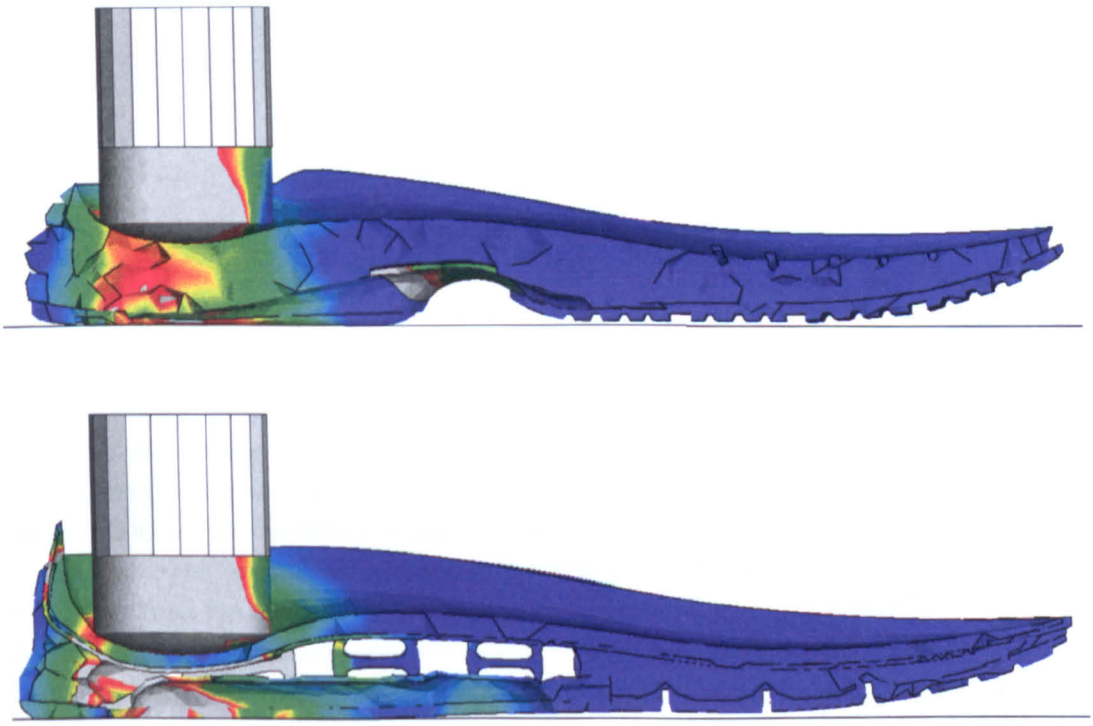

Figure 9.7: Sectional views of the heel stamp test: The Supernova shows little self-contact (top), while the Ultraride shows complex self-contact.

It should be noted that even in simple 'block' shoes such as the Supernova, the contact between the outsole and the floor requires a separate definition for each part, or section of a part that contacts the floor if an analytical rigid floor is used. This is due to ABAQUS requiring surfaces to be contiguous, i.e. single groups of elements/nodes with no internal holes, and that general contact cannot be applied to analytical rigid surfaces. In shoe models with highly complex outsoles, the less computationally efficient discrete rigid surface is used to model the floor and allow general contact to be specified.

In certain instances, exclusions to general contact must be added to stop overconstraining of elements, such as when contacts are defined in addition to the general contact. It may also be necessary to exclude surfaces where the interactions differ from the general situation; for example, the vast majority of interactions in the Ultraride model are between TPU surfaces in the structures, but the co-efficient of friction of a TPU-TPU interaction is likely to be different from that of the steel-TPU and steel-rubber interactions at the stamp and floor respectively.

9.3.1 Contact Noise

The FE model will only include physical effects if it is instructed to. If energy loss mechanisms such as viscoelasticity or the Mullins effect are not included then the energy generated from two surfaces contacting each other is not dissipated and can create oscillations in the model. Figure 9.8 shows the reaction force measured at the stamp for an Ultraride heel cushion test with an analytical rigid stamp.

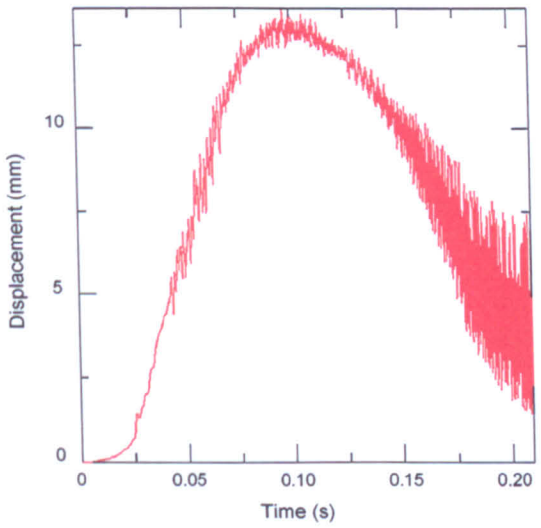

Figure 9.8: Time-displacement result measured from the heel stamp in a heel cushioning test on the Ultraride, displaying large amounts of contact noise caused by a lack of damping.

These very high speed oscillations caused the model to fail after the shoe had been impacted and the impactor had moved away from the shoe. Figure 9.9 shows a model that has failed due to similar oscillations causing collapse of the elements in the thin insole part.

This issue can be resolved by reducing the peak forces generated in the contact by removing energy from the interface. Damping can be added through the *CONTACT DAMPING function, and a small amount of this is included as a default in all Explicit analyses. However, for this research the choice was made not to increase the contact damping, as it would have introduced another means of energy loss, and one that could not be measured physically. Instead, the energy is temporarily removed from the surface contact by using a deformable stamp, with realistic material properties (in this case steel).

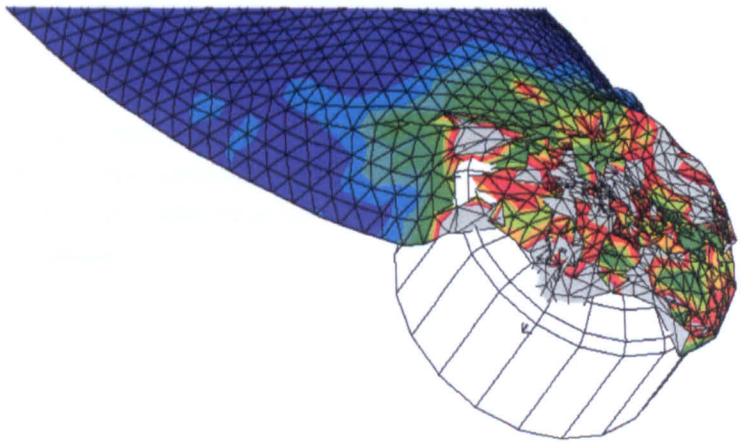

Figure 9.9: View of contact between heel stamp and insole in a Supernova heel cushioning test, viewed from below (all other parts of the shoe have been hidden). Note the excessive deformation of the insole at the point of contact with the stamp due to contact noise.

9.4 Interactions: Boundary Conditions

Boundary conditions can be specified as velocities, displacements, accelerations and rotations of nodes and elements in each step. Constraining the motion of the nodes in the outsole can be used to model the presence of a floor in the model, with nodal positions at a given time used to model stamps. There is an efficiency benefit in using boundary conditions over extra parts and contact due to the reduction in DOF in the model.

Because of their relative methods of solving the matrices, there is bigger slow-down with the addition of contact in Standard, up to the point where it fails to converge on a solution and Explicit must be used. Table 9.1 shows the times for early Supernova forefoot cushioning models for various levels of contact. Example 'Boundary Conditions' and 'Floor and Stamp Contact' models are shown in Figure 9.10.

Model Type	Standard	Explicit
Boundary Conditions	11.1	274.5
Floor Contact	61.2	315
Floor & Stamp Contact	∞	360

Table 9.1: Processing times in minutes for early model Supernova forefoot cushioning test.

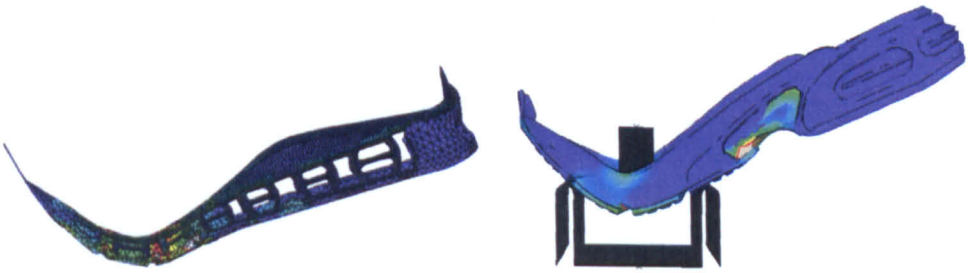

(a) (b)

Figure 9.10: Forefoot bend models with: (a) specified boundary conditions with no contact, (b) modelled test equipment with full contact.

Although the Standard model with limited contact is a degree of magnitude faster at processing than the Explicit job, the failure to process complex contact conditions prevents the modelling of shoes with internal structures such as the Ultraride and Gigaride. If simple models are required quickly, then Standard would be the best solution, but all the models in this research have used Explicit to keep consistency between the models, allowing direct comparison.

However, boundary conditions are still essential in the models to control the motion of the virtual test equipment: locking the floor in place and prescribing motion for the stamps. Control of the position and velocity of the stamp is of critical importance as it directly affects the results of the model.

9.4.1 Stamp Placement

In the physical tests performed by adidas (see Section 2.9.5.3), the shoe is aligned to the stamp with a combination of crude measurement and alignment by eye, based on practical experience. When aligning the stamps in FEA, all attempts are made to position the stamp in the same location and orientation as of that in testing - based on photographs of the shoes under test as shown in Figure 9.11.

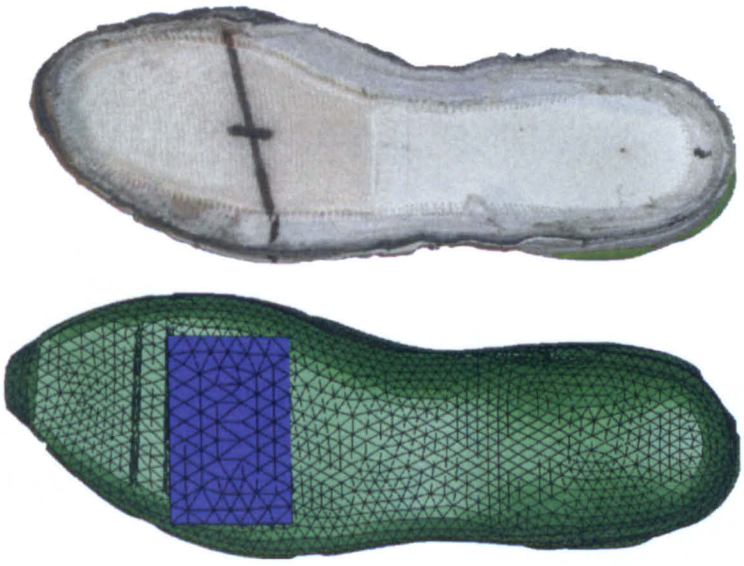

Figure 9.11: Stamp alignment in model to lines drawn on real shoe.

In order to quantify the level of error induced in the results by a misplacement of the stamps, physical and virtual tests were performed. Figures 9.13 and 9.14 show the results from these tests. A test was also performed to check the ability to align the shoe in the same place repeatedly; although some softening of the shoe was seen over ten repeated tests, the variation in displacement at 1500 N was a maximum of 0.3 mm.

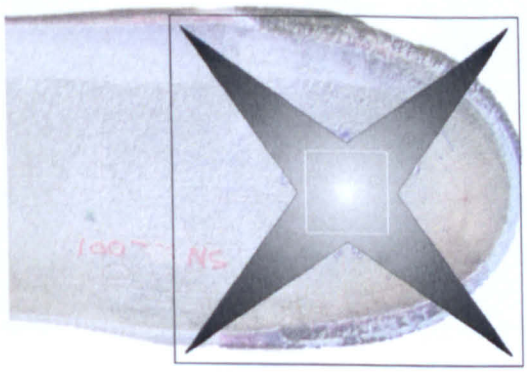

Figure 9.12: Area of the shoe over which the stamp is moved in the heel cushion positional sensitivity test (white square), which is represented by the maps in Figures 9.13 and 9.14

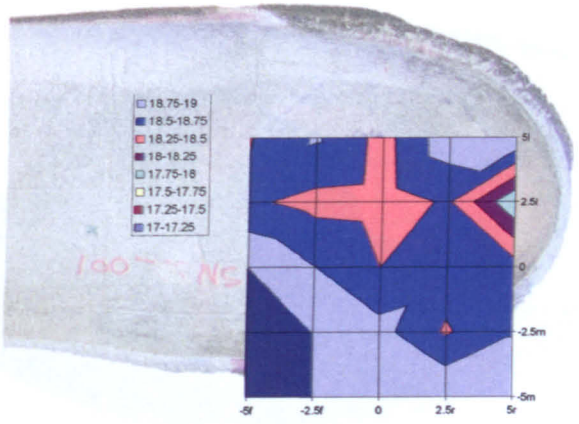

(a) Supernova Heel Cushion (Physical)

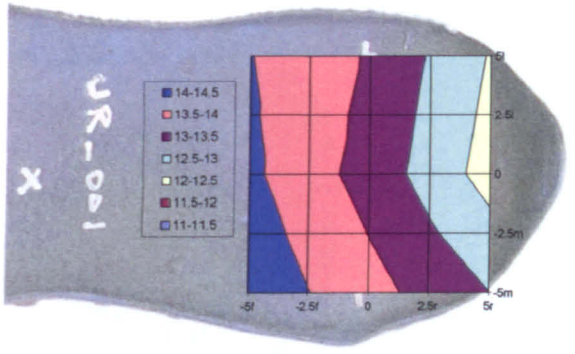

(b) Ultraride Heel Cushion (Physical)

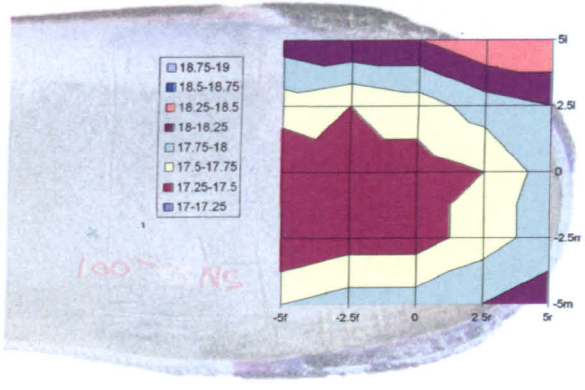

(c) Supernova Heel Cushion (Virtual)

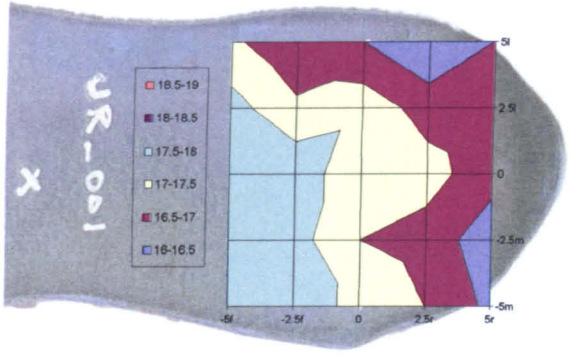

(d) Ultraride Heel Cushion (Virtual)

Figure 9.13: Stamp position sensitivity analysis. All results show the displacement required to achieve a ground reaction force of 1500 N (contours are therefore a measure of increasing softness, measured in mm). Each grid represents a 10 x 10 mm square where the centre of each stamp was aligned (not to scale).

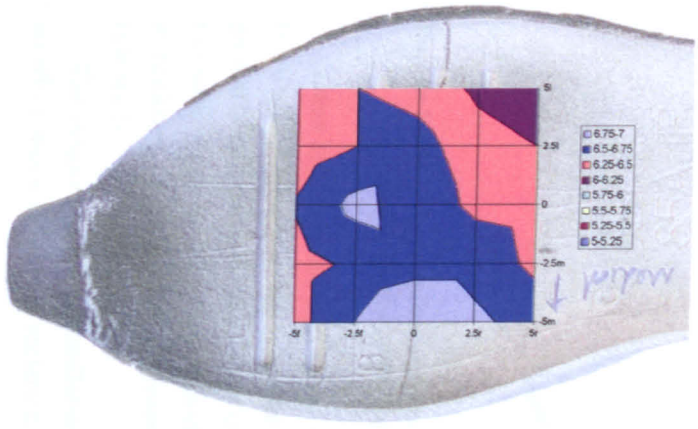

(a) Supernova Forefoot Cushion (Virtual)

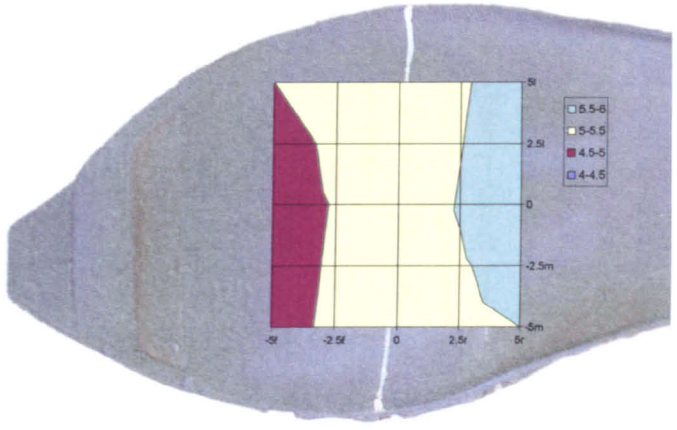

(b) Ultraride Forefoot Cushion (Virtual)

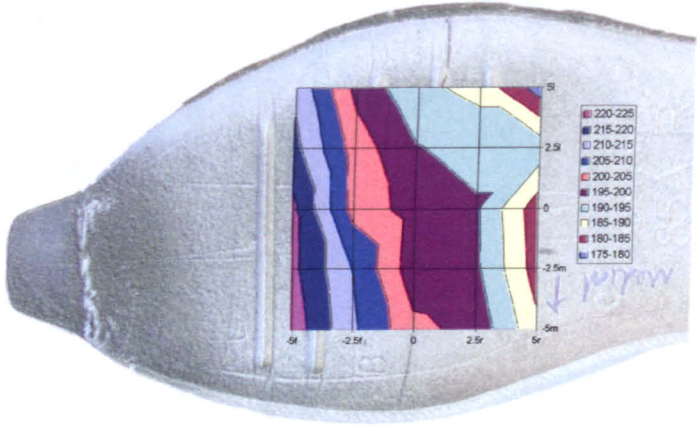

(c) Supernova Forefoot Bend (Virtual)

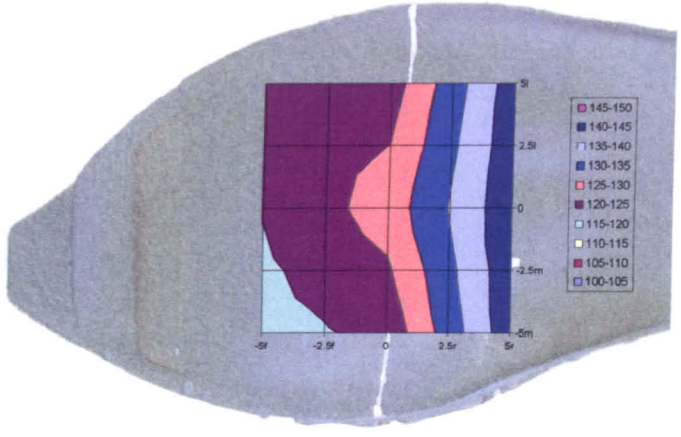

(d) Ultraride Forefoot Bend (Virtual)

Figure 9.14: Stamp position sensitivity analysis. Forefoot cushioning results show the displacement required to achieve a ground reaction force of 1500 N (contours are therefore a measure of increasing softness, displayed in mm). Forefoot bending results show the peak force at 15 mm displacement (displayed in N). Each grid represents a 10 x 10 mm square where the centre of each stamp was aligned (not to scale).

9.4.2 Loading and Displacement

The movement in the shoe models was controlled by specifying boundary conditions, regardless of whether no contact or full stamp/floor contact was used. In the physical forefoot bend test, the motion of the stamp was controlled by a programmed displacement curve, with a maximum of 15 mm. The physical cushioning tests were controlled by a specified load at a given time, with a force-feedback loop in operation in the test device.

As the prescribed displacement and force curve data were available, this left the option of the virtual tests being load or displacement driven, with the latter having a processing time advantage due to the lack of a virtual force-feedback loop generating more distortions. As some data were available on the stiffness of the shoes, the correct displacement to generate the required force was calculated.

Where practical test data is not available (as will be the case if this technology can be developed to be prototype-free), then the load driven model must be used for the cushioning tests. However for most force driven models, oscillations can be seen in the loading phase (Figure 9.15).

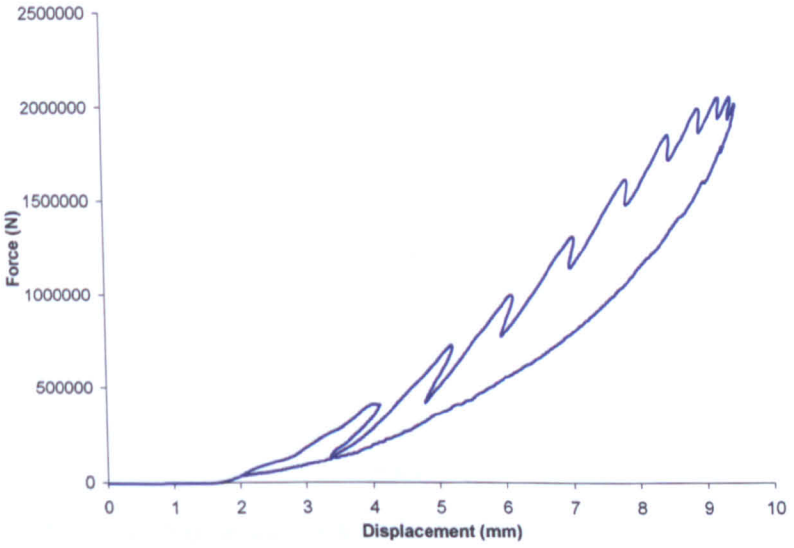

Figure 9.15: Force/displacement results for a Supernova forefoot cushion test showing oscillations in the loading portion of the cycle.

It was hypothesised that these oscillations were due to reflections of the stress wave from the floor. It this was the case the then the level of oscillation would be dependent on the geometry and material properties of the object under test. The same geometry was used as in the mesh performance study in Section 8.2.1.1, but with force driven loading and a variation in thickness of the section representing the midsole. Figures 9.16-9.18 show the results from this study.

The magnitude of the oscillation was seen to be dependant on material thickness, while no effect was seen from a variation in the mesh.

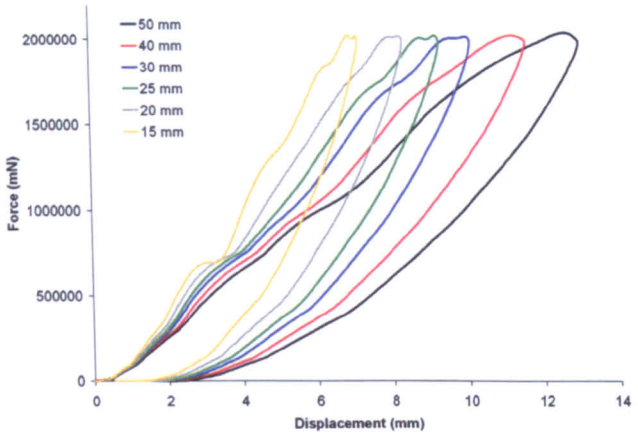

Figure 9.16: Effect on loading oscillations for 5 mm linear tetrahedral elements with a variation in model thickness. Target load ramped up to 2 kN.

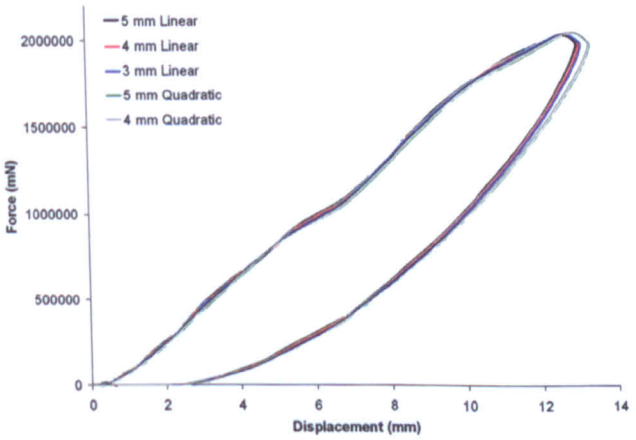

Figure 9.17: Effect on loading oscillations for 50 mm thick model with a variation in mesh size and type (all tetrahedral elements). Target load ramped up to 2 kN.

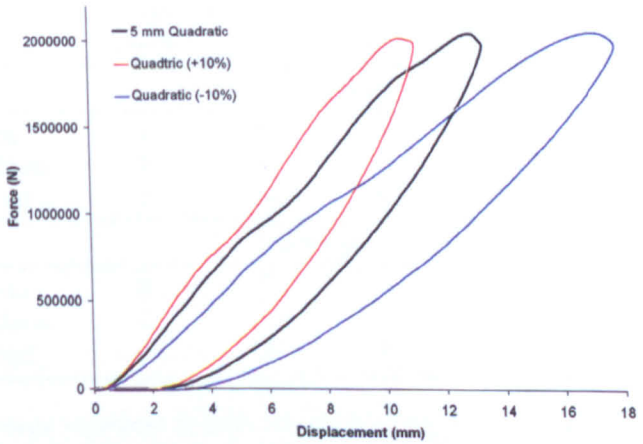

Figure 9.18: Effect on loading oscillations for 50 mm thick model with a variation in stiffness (all quadratic tetrahedral elements on a 50 mm thick model). Target load ramped up to 2 kN.

9.5 Quasi-Static and Dynamic Testing

Once the individual part geometry had been imported, meshed and assembled, mechanical testing was carried out on the shoe assemblies. To allow verification of the models, the three physical tests (Figure 9.19) were carried out on the three shoes; Supernova (SN), Ultraride (UR) and Gigaride (GR). As the modelling process used in this research determined the material stiffness responses from quasi-static testing, then added the dynamic effect through DMA, testing was performed both quasi-statically and dynamically (all test equipment and methods were detailed in Chapter 5).

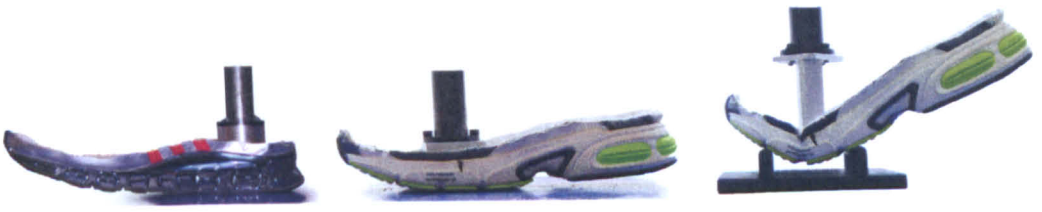

Figure 9.19: The three tests: heel cushion, forefoot cushion and forefoot bend, respectively (production shoes shown).

Figures 9.20-9.26 show the results from the physical testing. Figures 9.20-9.22 show the force/deflection responses (grouped one shoe to a page), and the latter ones show the new tip metric results derived from structural tracking of points on the shoe.

9.5.1 Static & Dynamic Force Results

When looking at the differences between shoe impacts, and between shoes, it must be taken into account that a small change in displacement can have a large effect on the peak force recorded. All tests contained a preload to attempt to put the shoes in a consistent starting position, but any differences in the geometry of the manufactured shoe could have a large overall effect on the results. With this in mind, Table 9.2 shows the variation in force at peak load between the three impacts on the same shoe and between the three or four of each shoe tested. The values were calculated as the variation in load from the peak load of the stiffest sample, at the given displacement. It was difficult to read these values from charts of the dynamic bend test, as the low forces involved meant the sample to noise ratio of the test device instrumentation was high.

Test	Supernova		Ultraride		Gigaride	
	Impacts	Shoes	Impacts	Shoes	Impacts	Shoes
			Quasi-Static			
Heel Cushion	3	25	14	17	3	5
Forefoot Cushion	3	28	5	24	2	13
Forefoot Bend	2	19	4	15	6	16
			Dynamic			
Heel Cushion	3	7	3	13	4	11
Forefoot Cushion	4	17	4	6	3	8
Forefoot Bend	17	26	2	15	0*	27

Table 9.2: Percentage variations in force (at peak loading of the stiffest sample). First values are variations between impacts, then maximum difference seen between all impacts on all assembled midsoles tested. *The dynamic bend results were too noisy to distinguish between impacts on a single shoe.

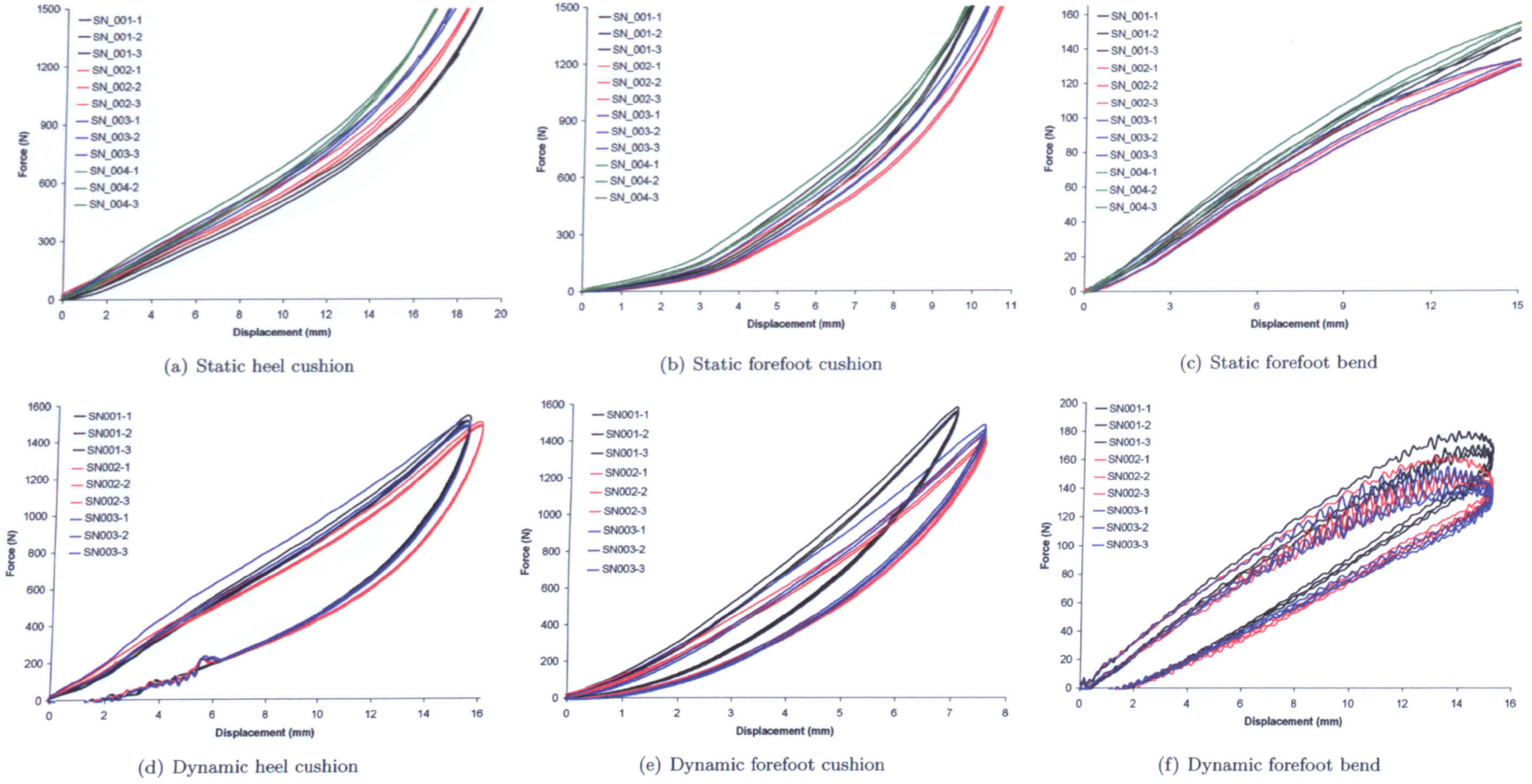

(a) Static heel cushion

(b) Static forefoot cushion

(c) Static forefoot bend

(d) Dynamic heel cushion

(e) Dynamic forefoot cushion

(f) Dynamic forefoot bend

Figure 9.20: Results of static and dynamic physical tests on Supernova midsole assemblies.

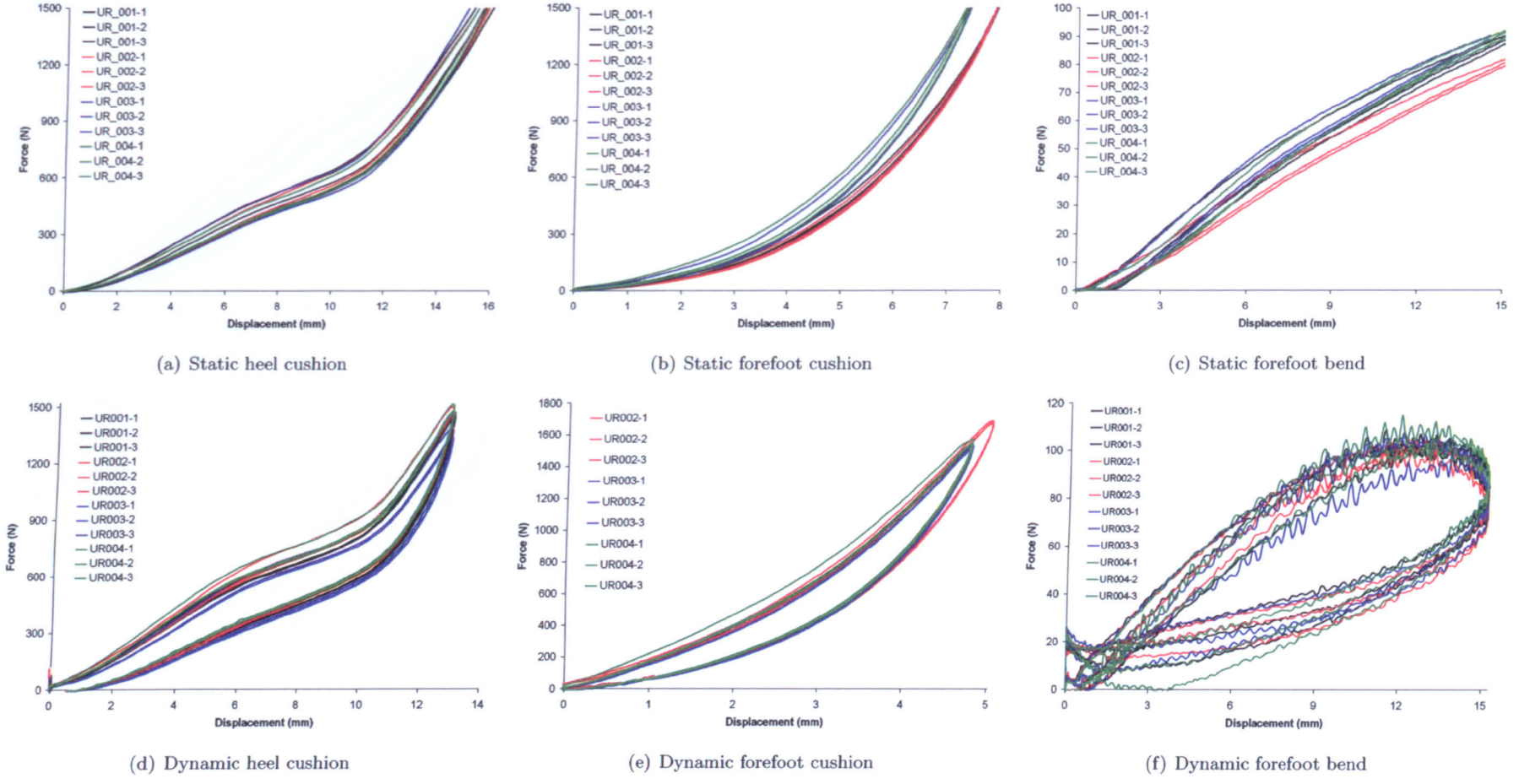

(a) Static heel cushion

(b) Static forefoot cushion

(c) Static forefoot bend

(d) Dynamic heel cushion

(e) Dynamic forefoot cushion

(f) Dynamic forefoot bend

Figure 9.21: Results of static and dynamic physical tests on Ultraride midsole assemblies.

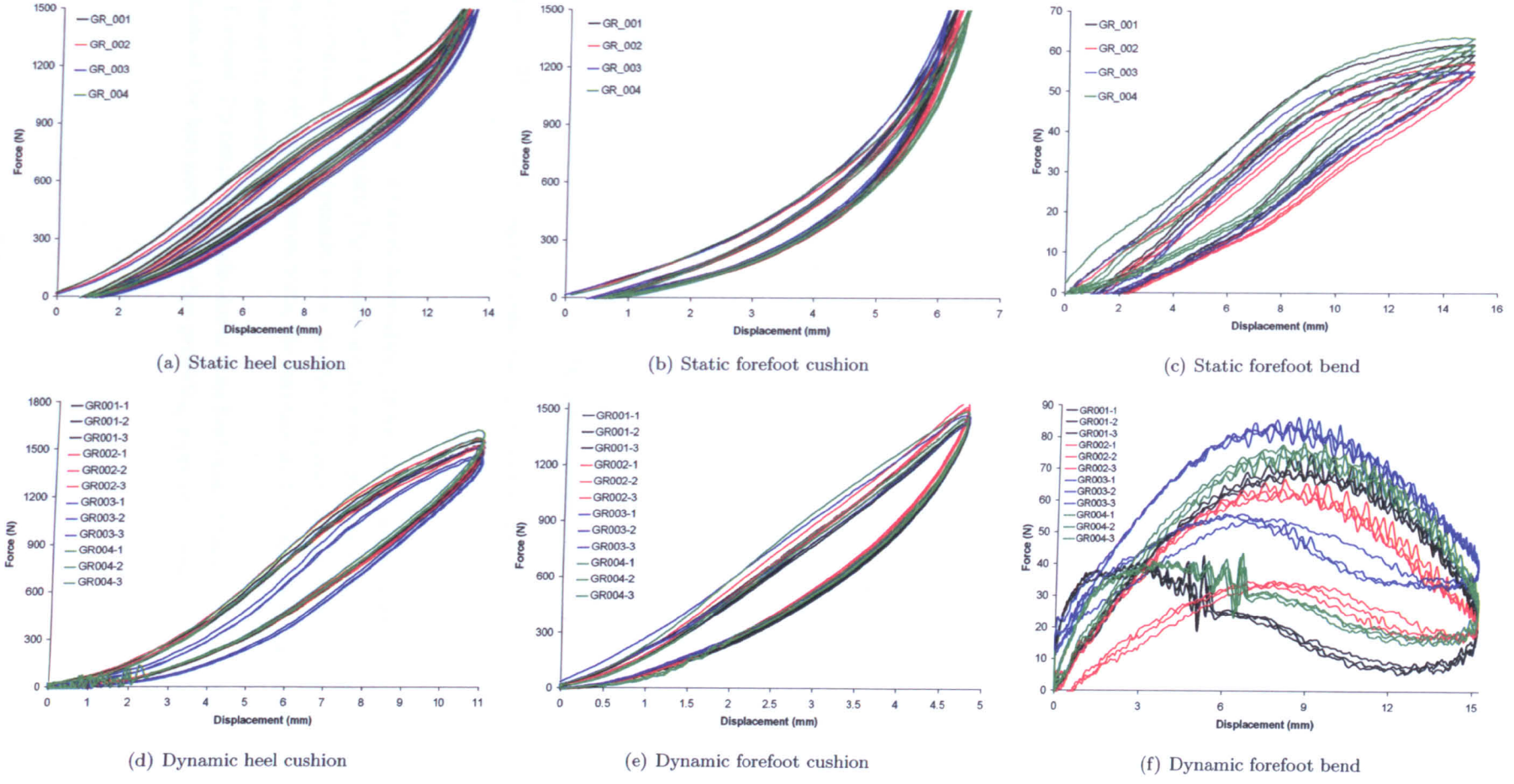

(a) Static heel cushion

(b) Static forefoot cushion

(c) Static forefoot bend

(d) Dynamic heel cushion

(e) Dynamic forefoot cushion

(f) Dynamic forefoot bend

Figure 9.22: Results of static and dynamic physical tests on Gigaride midsole assemblies.

9.5.2 Structural Metric Results

The aim of measuring the structural response of the shoes was to attempt to find new ways of comparing physical tests with FE models, so that verification could be more comprehensive, in order to improve the accuracy of the predictions.

9.5.2.1 Tip vs. RF

Figure 9.23 shows the results from static and dynamic reaction force (RF) vs. maximum tip height (Tip) for the cushioning tests. Static and dynamic tests can be compared here as the Tip height is measured as the change in height irrespective of where it starts.

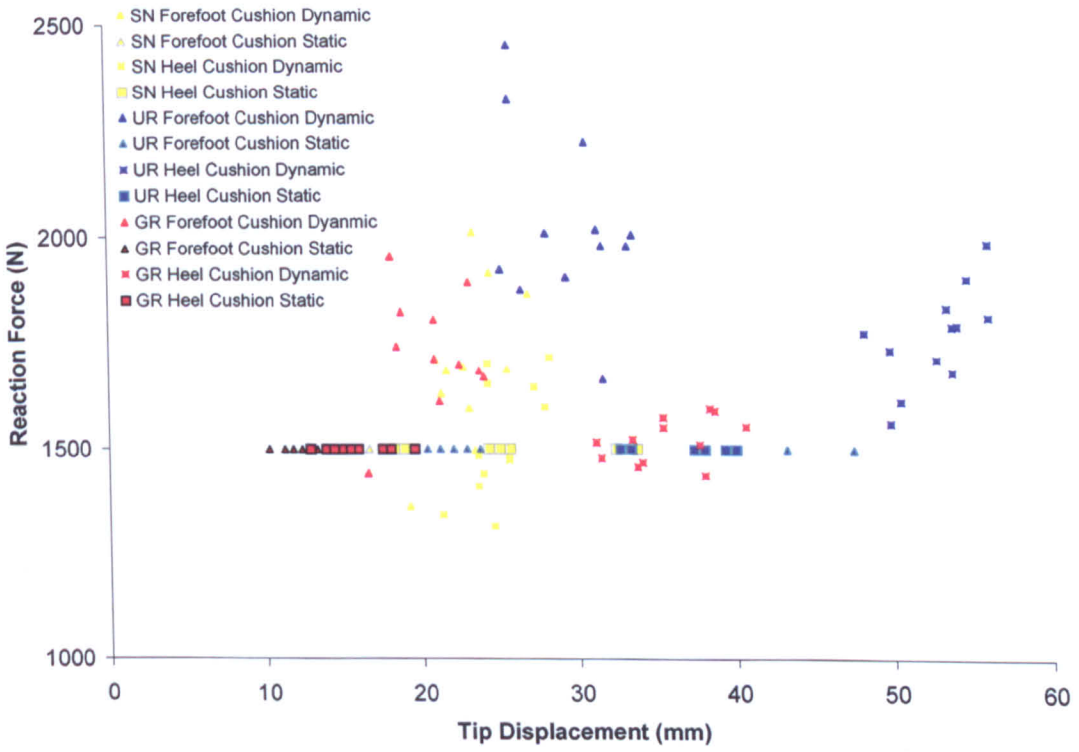

Figure 9.23: Plot of Tip against peak reaction force for static (Instron) and dynamic (drop rig) tests.

The chart shows no good correlation; there was a large variation in Tip for a constant RF. Generally the static Tip measurements were lower than the dynamic indicating a 'flick' was occurring in the dynamic tests. As the compressions for static Instron tests were higher than for the dynamic Instron tests, the increase in Tip was not caused by the added tilting of the entire assembly.

Forefoot Tip results were also lower than heel ones. This may be due to the concentration of mass at the heel part of the shoe providing more of a resistance to motion.

9.5.2.2 Maximum Compression vs. Reaction Force

Figure 9.24 shows the high sensitivity of the shoe assemblies to a small change in maximum compression (MC). This was most pronounced in the forefoot region and showed the importance of alignment of the test setup and use of preload in achieving comparable results. This metric plot could be achieved without the use of structural tracking, but it is used here to illustrate the large potential error that can be generated when the starting height of the stamp is not carefully controlled.

For the results show here, the shoes were placed in the Instron machine and loaded to 20 N, and their height calculated under this preload. This was the value used to determine the maximum compression metric. This was done in an attempt to eliminate any error caused by slight warping of the shoes, or from shoes sitting differently on a flat surface, due to variations in their geometry.

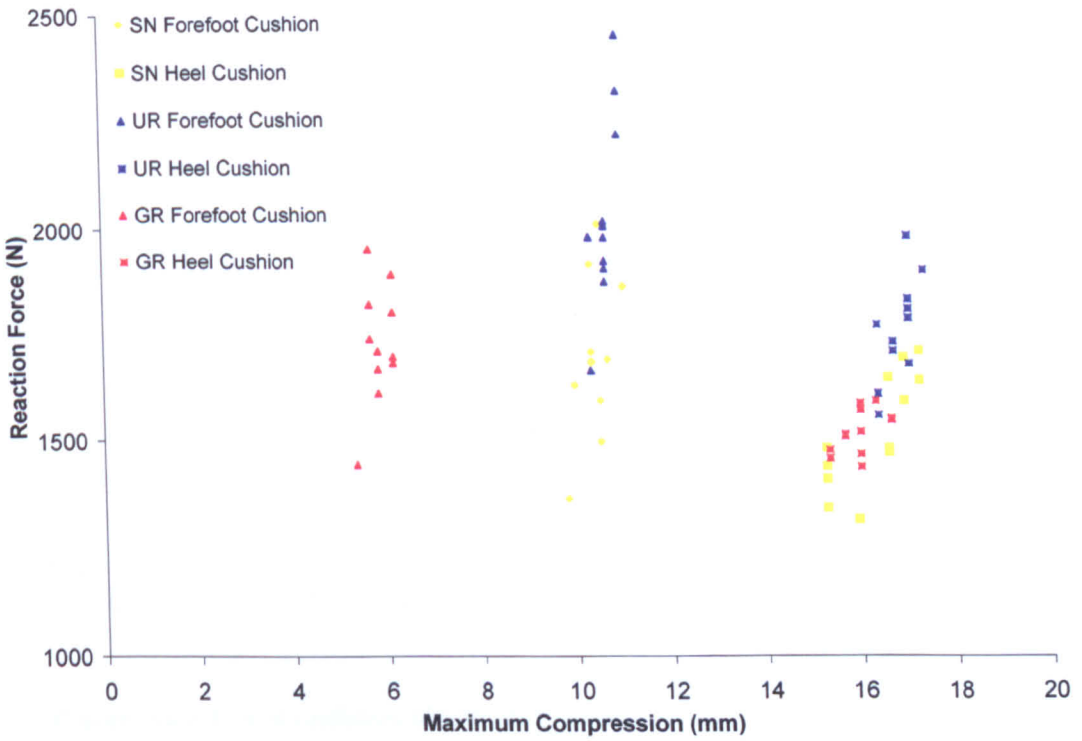

Figure 9.24: Plot of maximum compression of the midsole assembly against peak reaction force for drop testing.

9.5.2.3 COR vs. Reaction Force

Figure 9.25 shows a plot of RF against coefficient of restitution (COR) for the cushioning tests. The COR was derived from the height the mass was dropped from, and the maximum deviation of the mass from this point, so it was considered to be accurate to the resolution of the video (0.46 mm per pixel).

The chart shows that the level of energy return of the shoe materials was not significantly dependent on the reaction force used; more damage did not occur within the 2.5 kN range, which would have reduced the COR. For example, a 50% increase in load on the Ultraride forefoot gave a 0.06 increase in COR, indicating the material was becoming slightly more elastic at higher loadings.

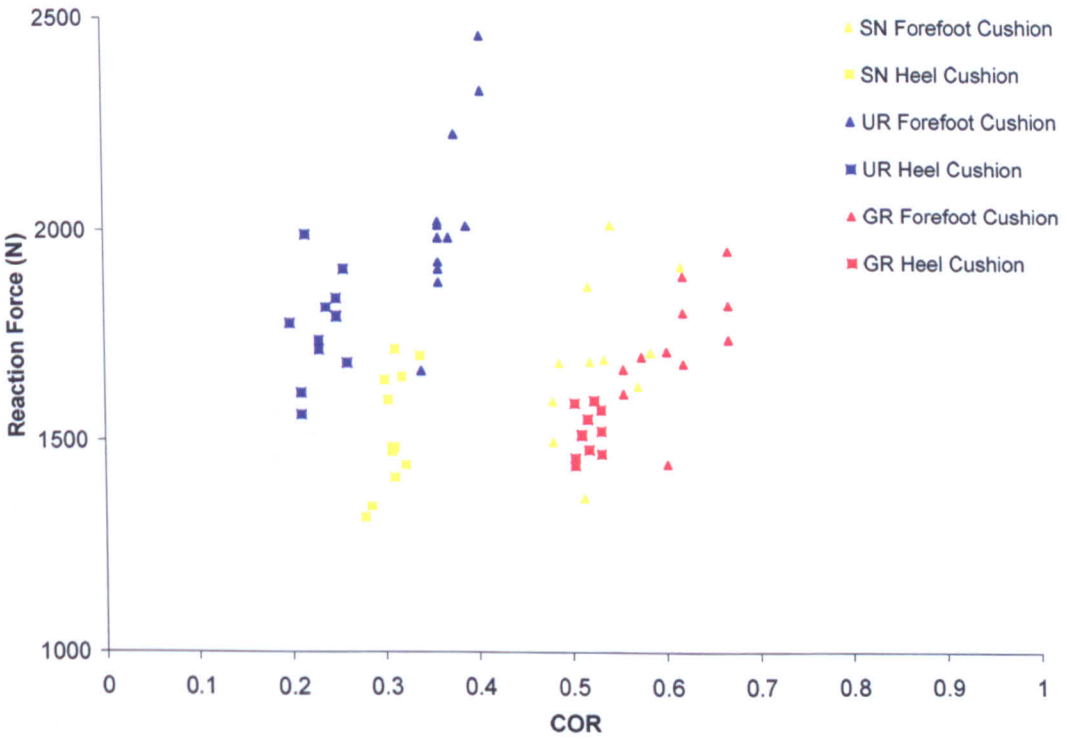

Figure 9.25: Plot of coefficient of restitution against peak reaction force for drop testing.

9.5.2.4 Delay vs. COR

The delay metric is a function speed at which the energy pulse travels through the shoe, combined with the Tip height producing mechanism. As such it was likely to be specific to each individual test, even for the same shoe. The delay measure was also based entirely on video-derived measurements so avoids the inaccuracy associated with measuring the actual compression of the midsole.

Figure 9.26 shows a plot of COR against delay. Good grouping is seen for all the shoe tests, with separation between all of the shoe groups. The smallest spread in delay was between the Supernova heel and forefoot cushion results, which may have been due to the shoe having the most homogenous construction; both forefoot and heel sections were solid blocks of foam, while the other shoes were different combinations of TPUs, foams and stiff plastics.

It is reasoned that if an FE model could reproduce the force/deflection and the delay/COR response closely, then the model would be a very good match to reality.

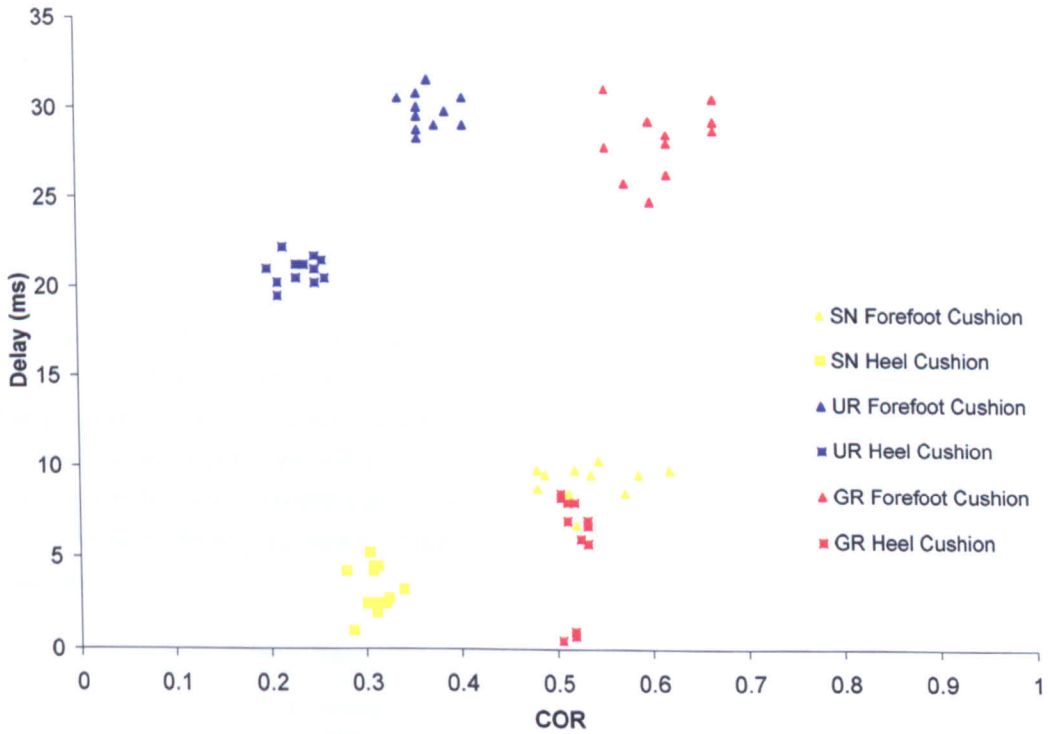

Figure 9.26: Plot of tip delay (time between maximum compression and maximum tip height) against coefficient of restitution for drop testing.

9.6 Quasi-Static and Dynamic Modelling

The physical testing carried out in the previous section permitted verification of the FE models. The physical test setups were replicated in FE, as shown in Figure 9.27. The variation between the individual physical shoe results gave the target range for stiffness response that the FE models needed to achieve to be considered accurate for force/deflection.

Figure 9.27: The three tests: heel cushion, forefoot cushion and forefoot bend, respectively (mid-sole assemblies shown).

The data from shoe testing showed fair consistency between the performance of shoes from the same batch. The largest differences occurred in the dynamic bend tests, with the Gigaride showing a similar shape, but a large variation in the size of the hysteresis loops. As the physical tests were not consistent for dynamic bend, the test setup may have been susceptible to error, and the FE results may not have matched due to this, rather than any problems with the model. As the aim was to check the models performance, the verification concentrated on the cushioning response and the static bend results.

As discussed in the conclusions of Chapter 6, the ideal process for generating FE models with new materials would occur if the material data taken directly from sample testing could be used to give a good prediction. Figures 9.29-9.31 (pages 212-214 respectively) show the FE model results using these sample test data. The orange error bars indicate the error in the results due to possible misalignment of the stamp between FE and the physical tests (see Section 9.4.1), and from using an estimation of the value of friction. Results from friction sensitivity studies are included in Appendix 12.7, along with studies into the effect of variation in density and velocity. The density study involved doubling the density of all the parts individually, to attempt to ascertain if the models were more sensitive to an error in the value of density for specific parts. As can be seen in Figure 9.28, no significant effect was found.

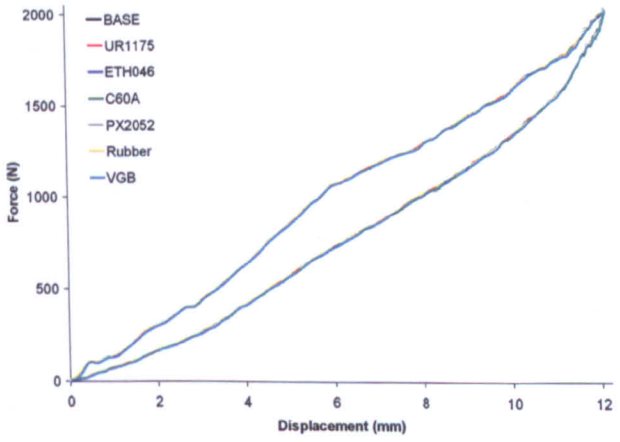

Figure 9.28: Results from density sensitivity study on the Ultraride heel cushion test. A separate model was run with one of each of the shoe materials' densities doubled (full results in Appendix A).

The friction study consisted of models with a variation in contact friction. A dependance on friction was found, with the most significant effect seen in the heel cushion tests. As the friction was not known, the total possible error over the range of values tested was combined with the positional error.

Only a small dependance on the initial velocity of the impacting mass was found, and as the velocity used in the modelling was measured from the accelerometer on the drop test rig, this was considered to be accurate, and not included in the error bars in Figures 9.29-9.31.

9.6.1 Static Force Results

The Supernova models (Figure 9.29) showed a good match of the FE results to the physical test data, whilst the Ultraride models (Figure 9.30) were all slightly too stiff, although they modelled the s-shape in the curve well. The Gigaride results (Figure 9.31) were not as good, as the s-shape in the heel cushion response was not replicated, and the model gave a very stiff response at higher compressions. The forefoot response was the opposite, as the upturn in stiffness was not modelled, resulting in a soft response at high compression. The Gigaride bend test was also very stiff and exhibited a lot of noise, which was not apparent in the other shoes, where the prediction was much better.

9.6.2 Dynamic Force Results

Generally the dynamic model results showed a magnification of the poor predictions seen in the static models, although the Supernova and Ultraride results still showed fair predictions. The dynamic bend tests showed the expected large amounts of noise in the structure shoes, but the Supernova response exhibited an unexpectedly large amount of hysteresis for a similar final force value.

In the dynamic models, the Supernova showed the best results, with good replication of the physical stiffness and hysteresis of the cushioning tests. The bend test does however show a large amount of hysteresis for only a (relatively) small over prediction of peak force.

The Ultraride results are also good, with an accurate replication of the hysteresis, and a small over-prediction of the stiffness in the cushioning tests. The bend test results exhibit a large amount of noise and appear to be roughly double the stiffness of the physical.

The Gigaride models gave the worst results, with only the forefoot cushioning test producing a reasonably accurate result. Both the heel cushion and bend test exhibit large amounts of noise; the hard impact between the stiff topplate and the stamp may be the cause of this in the cushioning tests.

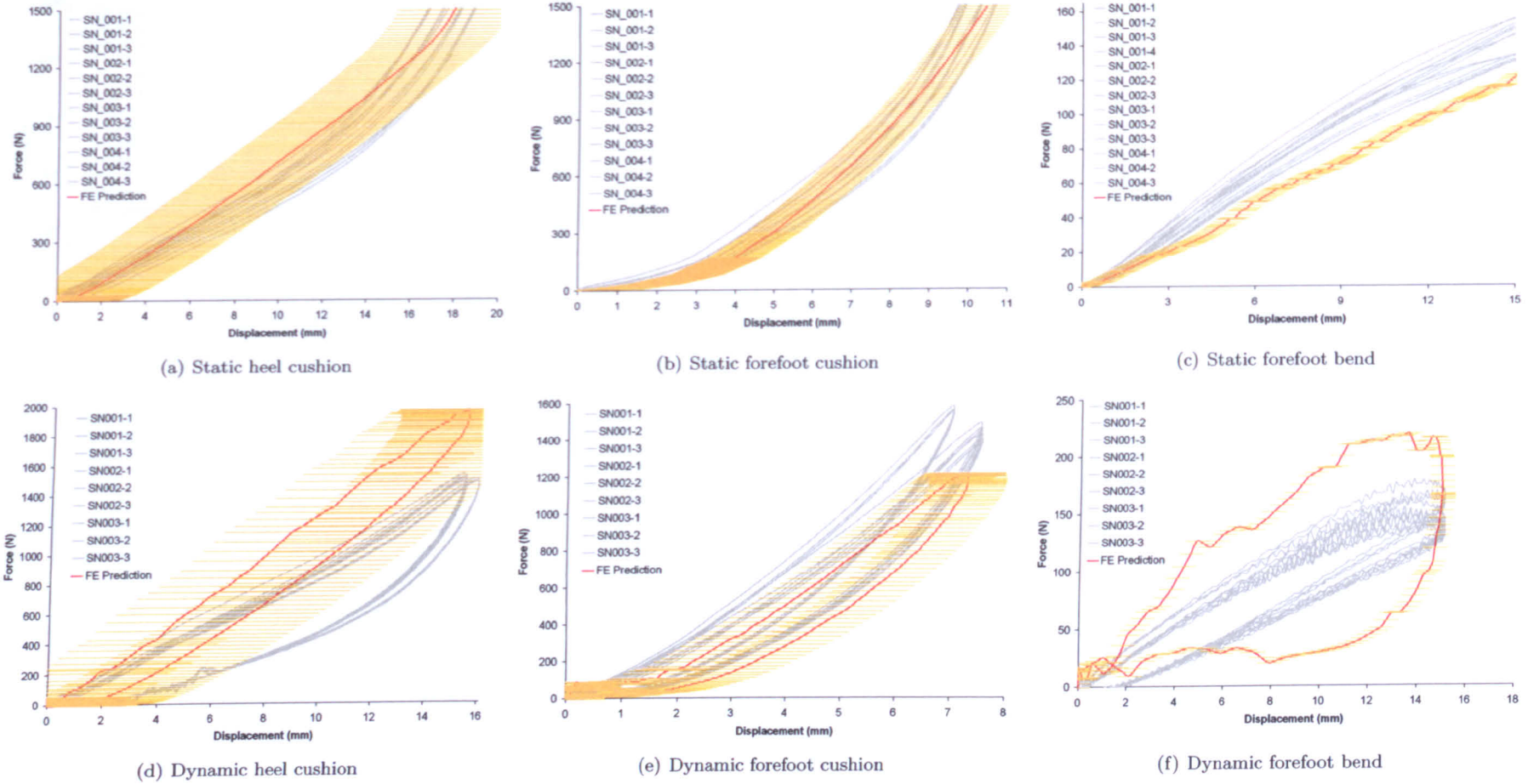

(a) Static heel cushion

(b) Static forefoot cushion

(c) Static forefoot bend

(d) Dynamic heel cushion

(e) Dynamic forefoot cushion

(f) Dynamic forefoot bend

Figure 9.29: Results of static and dynamic FE models on Supernova midsole assemblies, using material models taken directly from material samples test data. The orange bars indicate the estimated maximum error in stamp positioning and frictional effects.

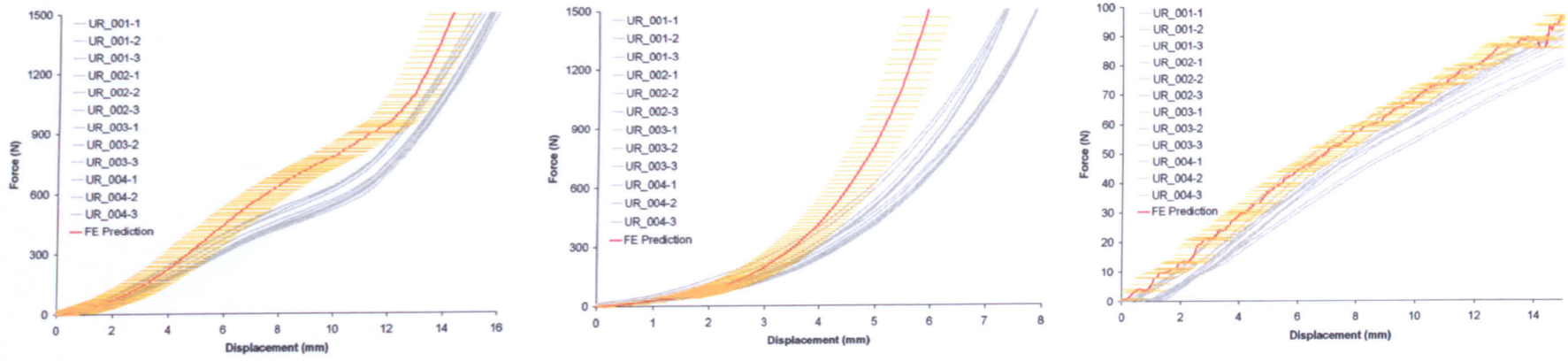

(a) Static heel cushion

(b) Static forefoot cushion

(c) Static forefoot bend

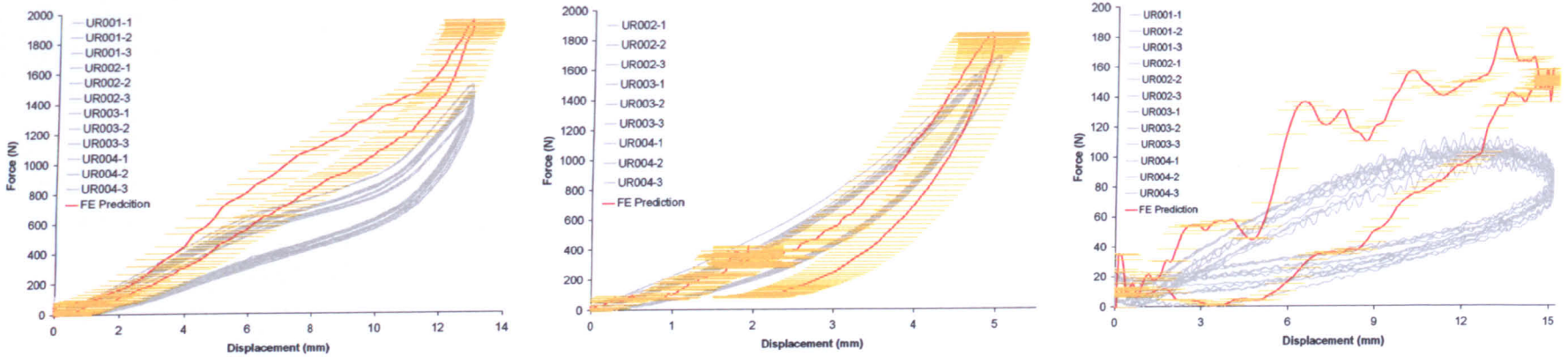

(d) Dynamic heel cushion

(e) Dynamic forefoot cushion

(f) Dynamic forefoot bend

Figure 9.30: Results of static and dynamic FE models on Ultraride midsole assemblies, using material models taken directly from material samples test data. The orange bars indicate the estimated maximum error in stamp positioning and frictional effects.

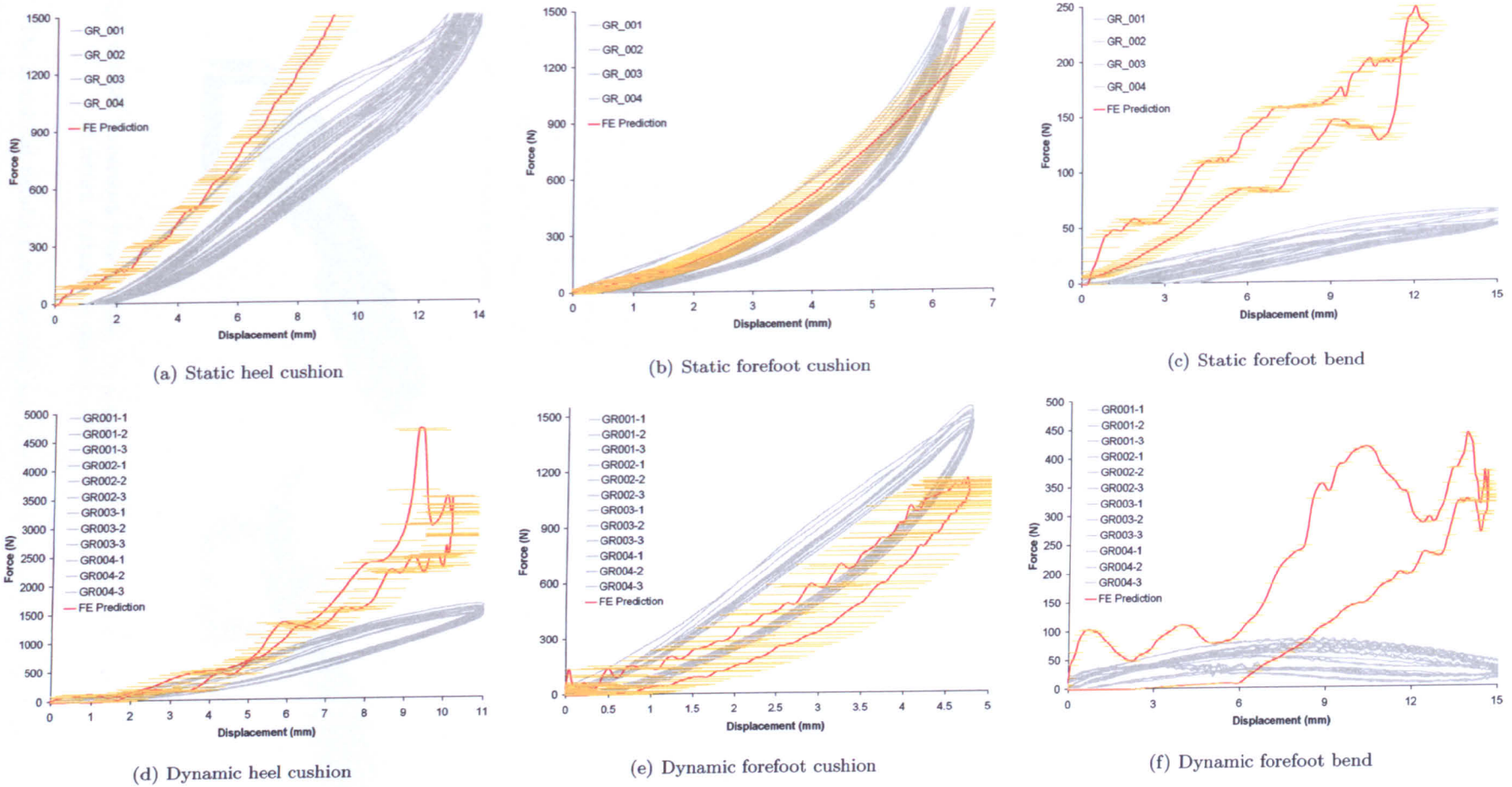

(a) Static heel cushion

(b) Static forefoot cushion

(c) Static forefoot bend

(d) Dynamic heel cushion

(e) Dynamic forefoot cushion

(f) Dynamic forefoot bend

Figure 9.31: Results of static and dynamic FE models on Gigaride midsole assemblies, using material models taken directly from material samples test data. The orange bars indicate the estimated maximum error in stamp positioning and frictional effects.

9.6.3 Structural Metric Results

While the force response of the models generally showed good agreement with experimental results, the structural metrics indicated that some physical processes were not being modelled correctly. Both the Ultraride and Gigaride showed a very low maximum tip height, lower than any of the physical results. While the cushioning response was being modelled appropriately, the flicking up of the free end of the shoe was not occurring. This was most pronounced in the Gigaride dynamic bend test, shown in Figure 9.32. The physical assembly showed a large range of movement of the posterior of the shoe, while the FE model showed a very small amount. Both images were taken at a point of maximum compression, although even if the simulation was allowed to continue the posterior of the virtual shoe does not rise more than 10 mm at any point.

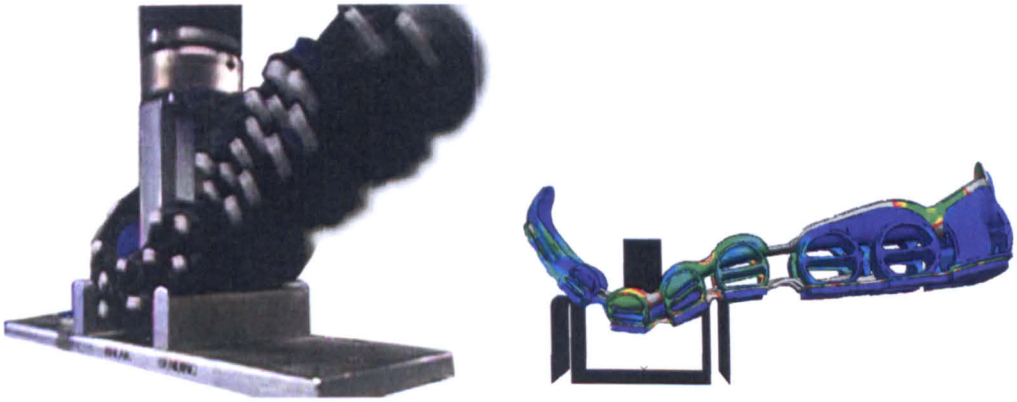

(a) (b)

Figure 9.32: Gigaride dynamic bend testing, (a) physical, (b) FE model. Both images taken at point of maximum compression.

A similar, but less pronounced effect was seen in the Ultraride, but the Supernova behaved in a more realistic manner. Figure 9.33 shows the response for static and dynamic tests on the Supernova. Both images are shown at the point of maximum posterior height, which in the dynamic case occurs after the load has been applied. The static test shows the anticipated rise of the posterior of the shoe. The large hysteresis loop seen in Figure 9.29(f) could be explained by the shoe leaving contact with the fittings and bouncing backwards at the end of a dynamic compression cycle.

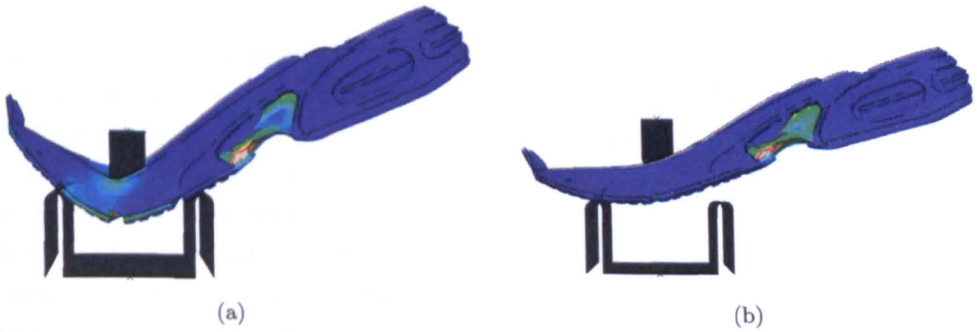

(a) (b)

Figure 9.33: Supernova bend testing, (a) static test at maximum compression, (b) dynamic test at return of stamp to starting position.

The graphical results from the first set of FE models are presented in the next section, where adjustments have been made to the FE models in an attempt to achieve better predictions. The issues are illustrated more clearly when the effect of adjustment can be seen.

9.7 Assembly Material Model Modification

The initial FE model predictions, which used material data directly from sample testing, were a reasonable match to the physical in most cases, but there was room for improvement.

Testing of shoe parts was carried out in Chapter 8 that allowed verification of the major components of the three shoes. While no overall predictive method was shown to be possible, it may be the case that shoe performance could be modelled much more accurately with the verification of a small number of critical components. This section presents a method of using these verified materials to improve the accuracy of the entire shoe.

The required final stiffness of the shoe assembly was determined from physical testing, so the values of the other components were estimated by adjusting all the materials based on their contribution to the overall stiffness of the assembly in all three tests.

Consider the simple spring system in Figure 9.34:

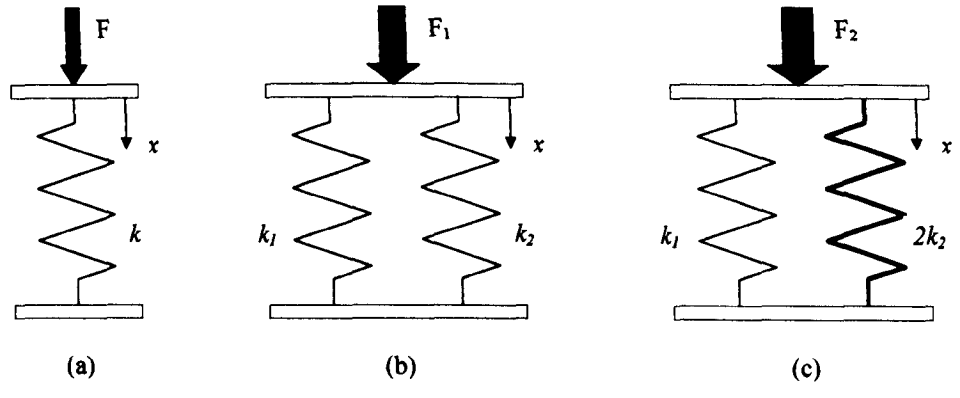

Figure 9.34: Simple spring systems

To calculate the contribution to the overall system stiffness each spring has, one of the springs has its stiffness doubled, giving the equations;

$$\text{(a) } F = kx \qquad \text{(b) } F_1 = (k_1 + k_2)x \qquad \text{(c) } F_2 = (k_1 + 2k_2)x$$

Setting equations (b) and (c) to zero, then rearranging, gives;

$$F_2 - F_1 = 2k_2x$$

Thus, if the stiffness of a material in the shoe is doubled, the resulting increase in stiffness of the entire assembly is equal to the adjusted material's stiffness. By performing this calculation on all the shoe components, a set of equations was formed that describe the contribution of each material (this method was used instead of a simple direct stiffness comparison due to the non-linear nature of the materials).

It should be noted that this was only an estimation, and some major assumptions had to be made. The first was that the percentage stiffness contributions of the materials may not add up to 100% due to the dissipation or storage of energy through friction, elemental effects (such as locking) or re-distribution of loadings inside the shoe.

The second was that an 'element shift' was added into the equations. The poor prediction of the sample models could have had two main causes; the test setup, and the elemental behaviour. As all the elements used were of the same type, this adjustment would have been shared between all materials, while the test setup error may not.

Applying these assumptions, an equation for the assembly was generated. In this example three materials were shown to have a contribution to the stiffness during the test:

$$\alpha a\phi + \beta b\phi + \gamma c\phi = \frac{F_{Target}}{F_{Current}}$$

where α, β, and γ are the stiffness contributions, a, b, and c are the material stiffness adjustments and ϕ is the element shift. The forces are the current and target loads seen at a given displacement.

This equation had too many unknowns to give a single solution, so it was rearranged and combined with the equations from the other two tests and the resulting surfaces plotted. Fortunately, none of the shoes had more than three main contributing materials, and some of these were known, so it was possible to plot the results as a 3D image without the need for higher dimensions. Figure 9.35 shows the results for the Ultraride.

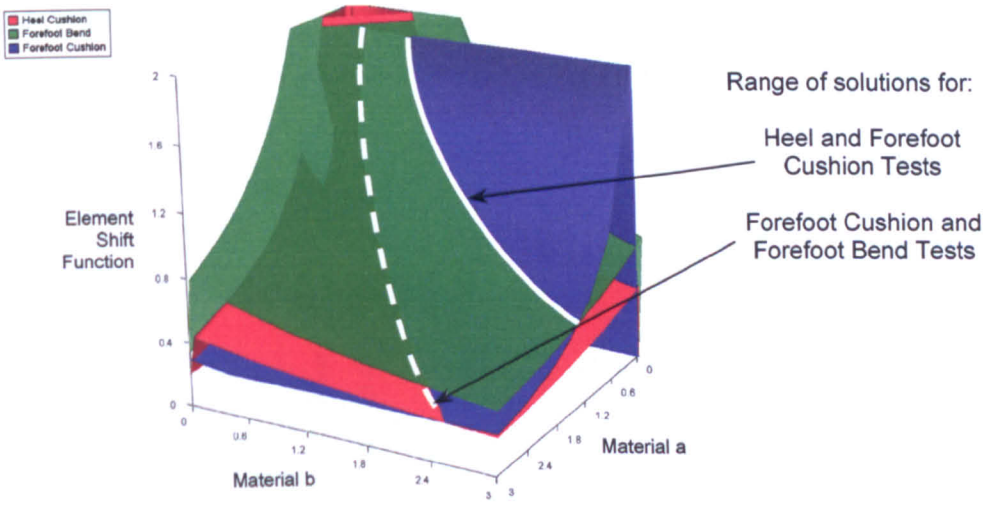

Figure 9.35: 3D plot of the solution space for material adjustment equations for the Ultraride.

Note that all three surfaces did not cross. This was due to the assumptions that have been made, so to continue the process another assumption had to be made. As the cushion test results were similar, and showed better prediction than the bend tests, a result was chosen where the forefoot and heel cushion surfaces cross. Any point could have been chosen, but for this example an attempt was made to minimise the change in material stiffness by choosing a point where a and b were closest to one.

As this shifting information was also very useful for understanding which materials were most important to model correctly for an accurate analysis, and conversely, which ones might have less time and resources spent on them, the results for all three shoes are presented in Figures 9.36-9.38. Dynamic shifts, where the energy losses due to viscoelasticity were doubled, are also presented.

Results from studies on the sensitivity of the drop tests to velocity, friction and material density are included in Appendix 12.7.

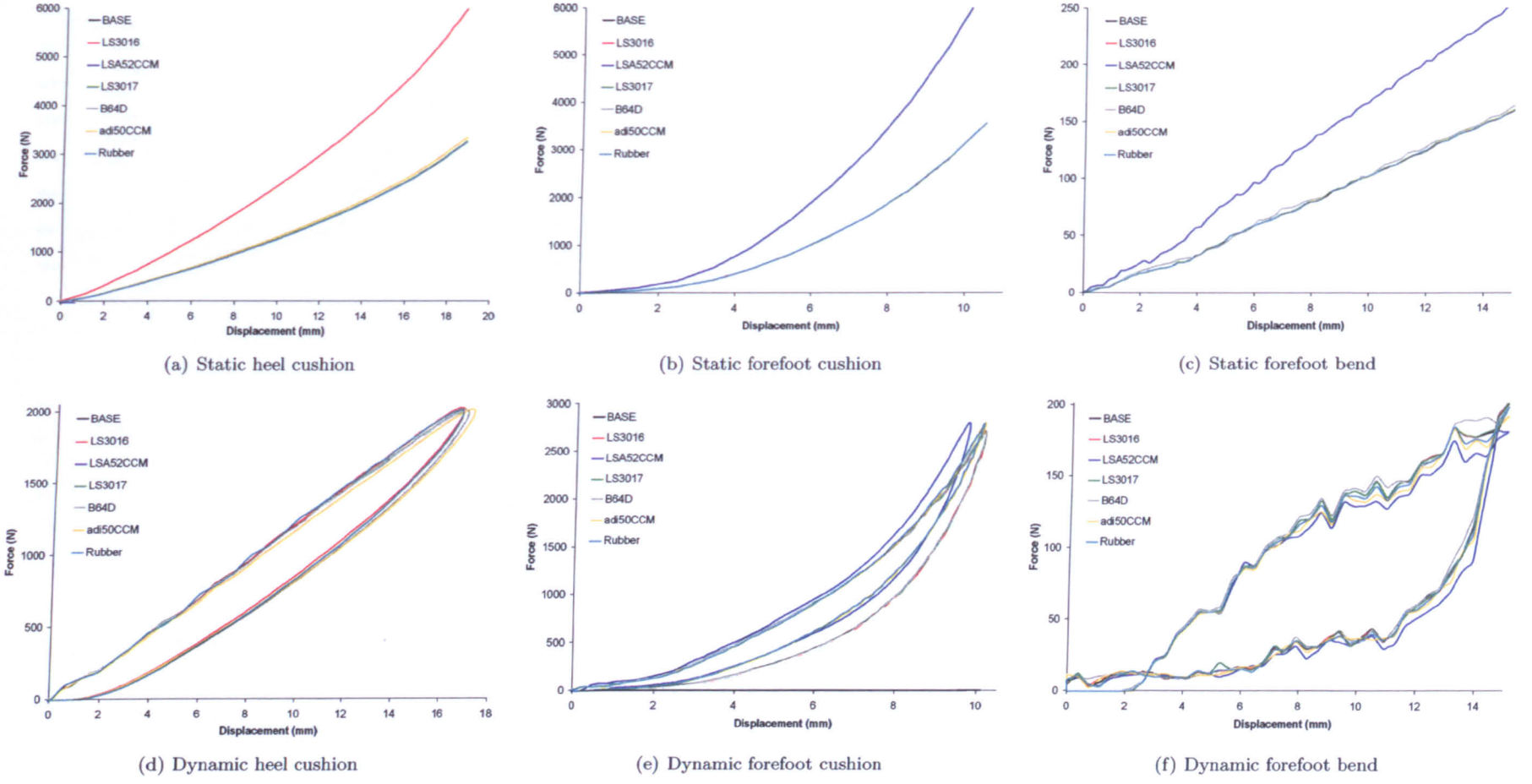

(a) Static heel cushion

(b) Static forefoot cushion

(c) Static forefoot bend

(d) Dynamic heel cushion

(e) Dynamic forefoot cushion

(f) Dynamic forefoot bend

Figure 9.36: Results of doubling the stiffness (static tests) and viscous losses (dynamic tests) on a material, for FE models of the Supernova. 'BASE' is the response of the model when using unadjusted data directly from material samples.

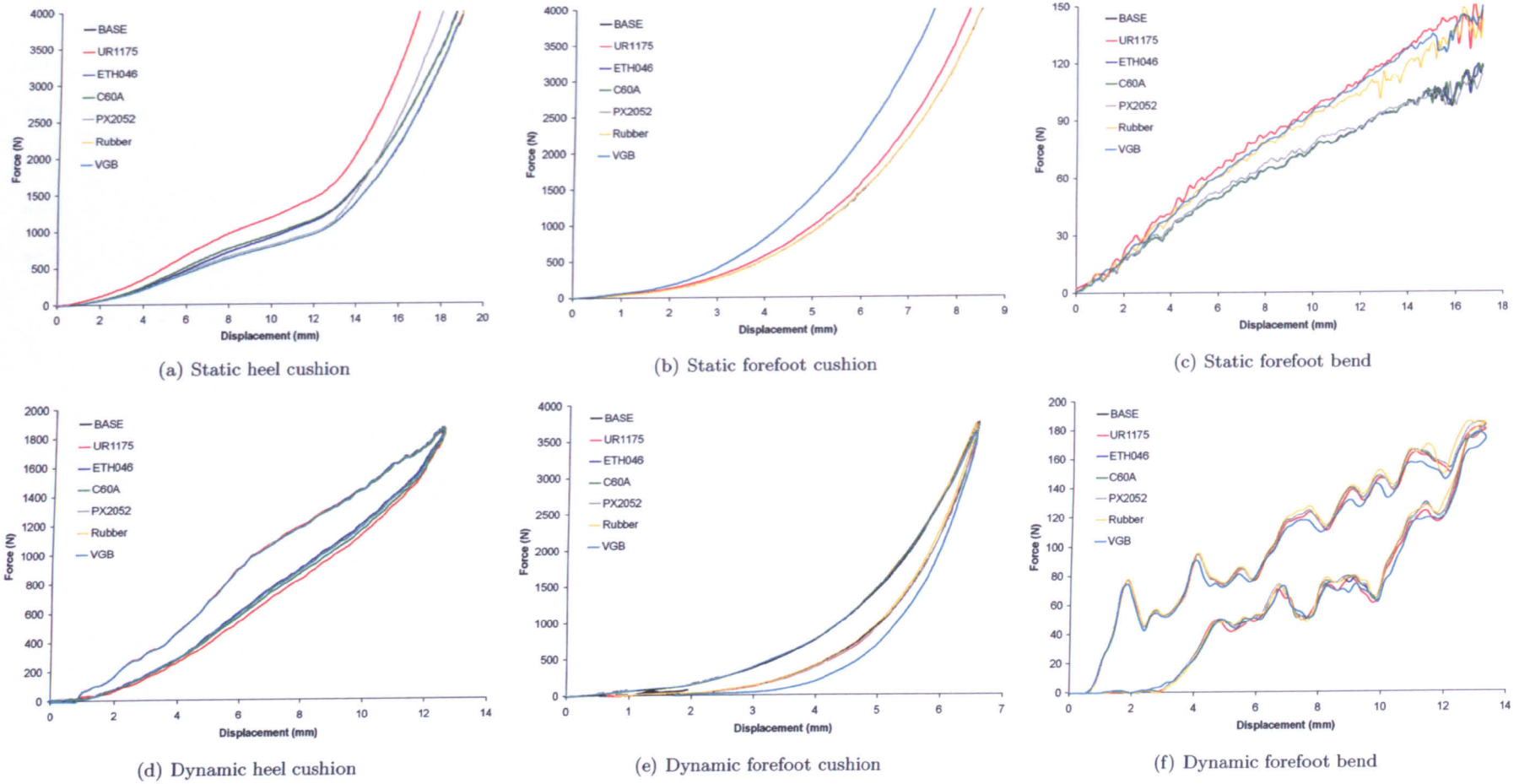

(a) Static heel cushion

(b) Static forefoot cushion

(c) Static forefoot bend

(d) Dynamic heel cushion

(e) Dynamic forefoot cushion

(f) Dynamic forefoot bend

Figure 9.37: Results of doubling the stiffness (static tests) and viscous losses (dynamic tests) on a material, for FE models of the Ultraride. 'BASE' is the response of the model when using unadjusted data directly from material samples.

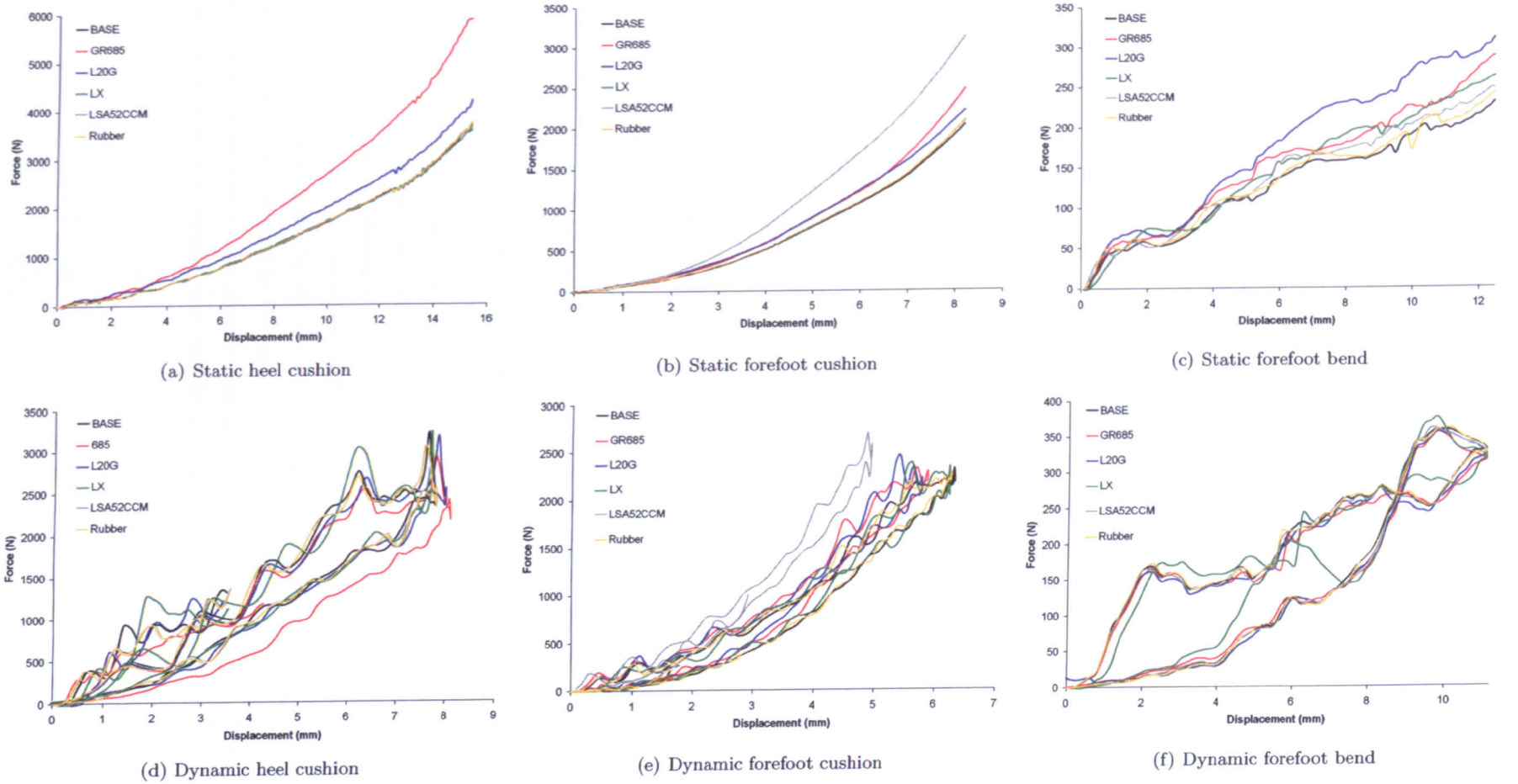

(a) Static heel cushion

(b) Static forefoot cushion

(c) Static forefoot bend

(d) Dynamic heel cushion

(e) Dynamic forefoot cushion

(f) Dynamic forefoot bend

Figure 9.38: Results of doubling the stiffness (static tests) and viscous losses (dynamic tests) on a material, for FE models of the Gigaride. 'BASE' is the response of the model when using unadjusted data directly from material samples.

Table 9.3 summarises the contributions, with the last column showing the combined adjustment. For example, the VGB material contributed 60% of the stiffness in the forefoot cushion test, but none in the heel cushion test, and its original stiffness was multiplied by 0.65 to obtain the adjusted stiffness. For UR1175 and GR685 the adjustments were obtained from physical verification of the model in Section 8.4.3.

The Gigaride bend test showed a dependency on 5 different materials, and was very noisy, so the contributions were not calculated. This did not have an adverse effect on the results however.

	Heel Cush.	Forefoot Cush.	Forefoot Bend	Multiplyer
Material	Contributions - $\alpha \setminus \beta \setminus \gamma$			$a \setminus b \setminus c \times \phi$
UR1175	0.48	0.16	0	0.79†
C60A	0.26	0	0	0.77
ETH046	0.24	0	0	0.65
VGB	0	0.6	0.29	0.65
Rubber	0	0	0.29	0.77
Others	0	0	0	0.51
GR685	0.6	0.14	‡	0.6†
L20G	0.14	0.14	‡	0.64
LSA52CCM	0	0.55	‡	1.61
Others	0	0	0	0.64

Table 9.3: Contributions of materials to assembly stiffness during tests, and estimated required material adjustments from material sample test data. Ultraride results at top. †Value derived from physical/FE verification. ‡Test data too noisy to determine contribution.

9.7.1 Results from Adjustment

Figures 9.39 and 9.40 show the adjusted responses for the Ultraride and Gigaride respectively (the Supernova was not adjusted as its original predictions were acceptable).

All results showed an improvement in prediction from the models using the original sample test data, including the bend tests, which were removed from the calculation to allow an adjustment value to be chosen. The static heel cushion responses for both shoes were now within the range seen in physical testing. Those responses that were previously dominated by noise still retained their noise, but the overall curve mimicked the physical results more closely. The steepening of the static forefoot cushion tests was still not seen in the Gigaride model, but was over-predicted in the Ultraride.

As all these notable non-linearities still occurred in the adjusted results, it was concluded likely to have been caused by the physical process rather than a combination of stiffnesses. This could have been caused by the input geometry, or the inability of the current meshes to form the same kind of loaded geometry as the physical equivalent. Both of these scenarios would require further investigation into the structural details in future.

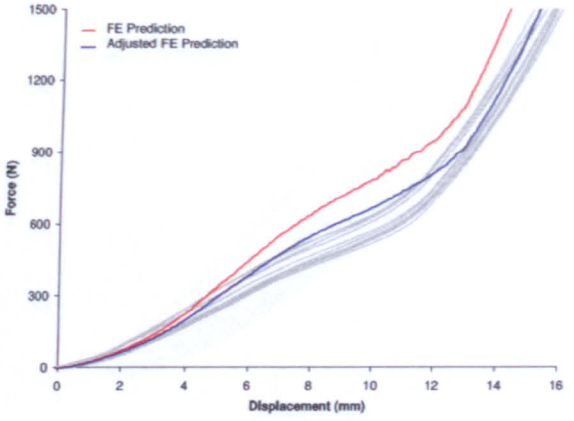

(a) Static heel cushion

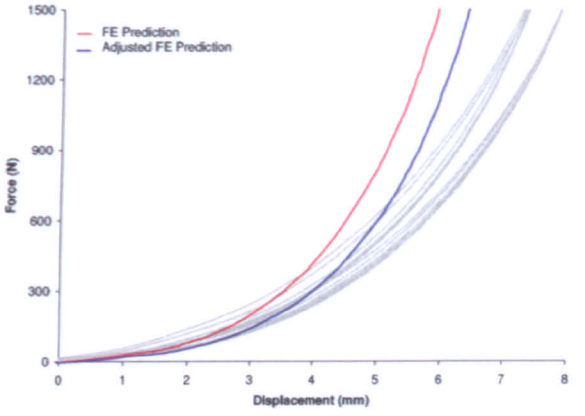

(b) Static forefoot cushion

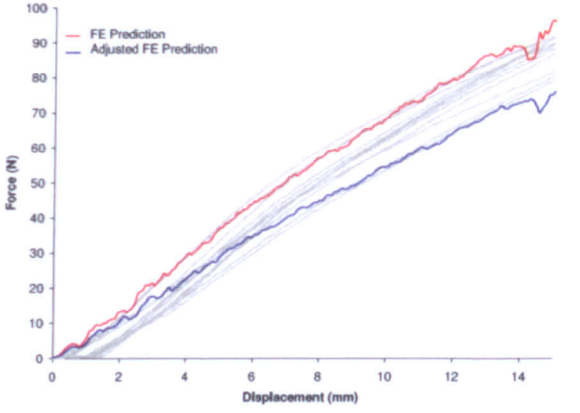

(c) Static forefoot bend

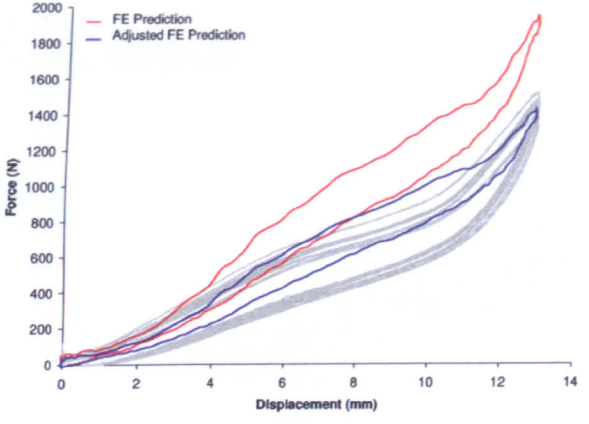

(d) Dynamic heel cushion

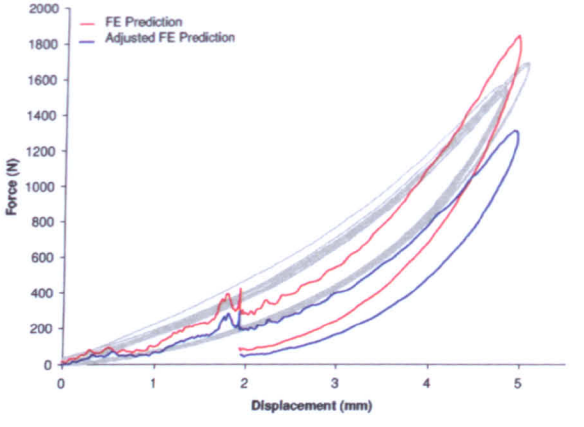

(e) Dynamic forefoot cushion

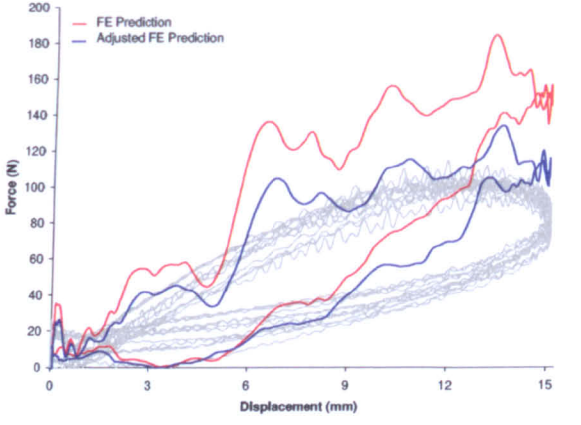

(f) Dynamic forefoot bend

Figure 9.39: Results of static and dynamic FE models on Ultraride midsole assemblies, using adjusted material models.

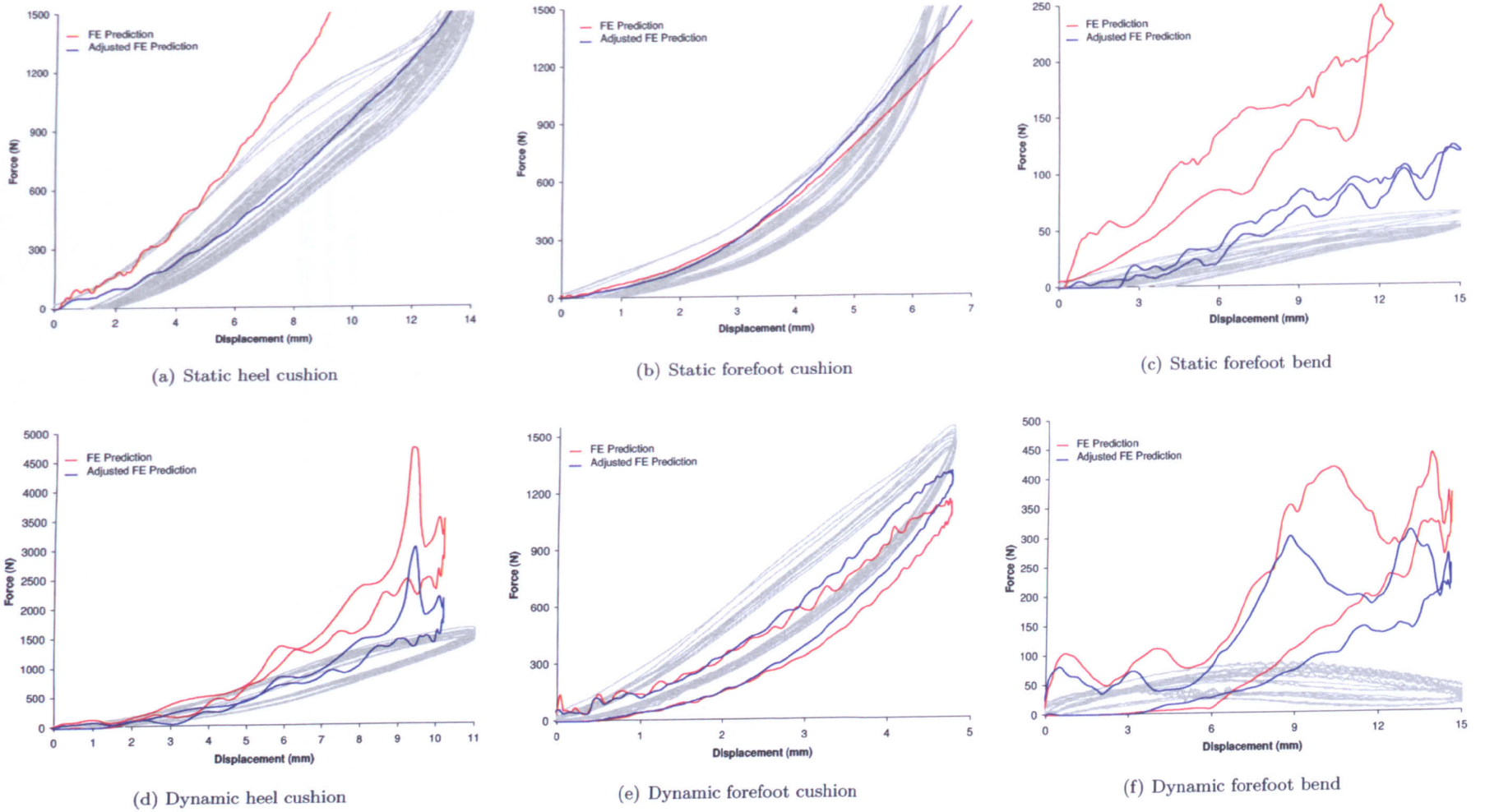

(a) Static heel cushion

(b) Static forefoot cushion

(c) Static forefoot bend

(d) Dynamic heel cushion

(e) Dynamic forefoot cushion

(f) Dynamic forefoot bend

Figure 9.40: Results of static and dynamic FE models on Gigaride midsole assemblies, using adjusted material models.

9.7.1.1 Adjusted Model Structural Results

The recording of structural metrics allowed comparison of the overall assembly shape between the FE model and the physical shoe, in addition to the force deflection results.

It can be seen in Figure 9.41 that the FE models were still underpredicting the tip height measurement in the structural shoes. The Supernova heel cushion result was good, but the forefoot result was much higher than the physical, although it still lay within that seen within the other physical shoe tests.

Figure 9.42 illustrates that the FE model impacts were more elastic than the physical impacts. This was to be expected as no effect from friction on the weight stack, air resistance nor flex in the test equipment was included within the model. However, these poor predictions were not constant between the models which indicates that the energy loss mechanisms in some of the models was not correct.

The plot in Figure 9.43 showing delay against COR, reveals that the FE models were not approaching the tight grouping of the physical results and adjustment of the material models did not have a pronounced improvement.

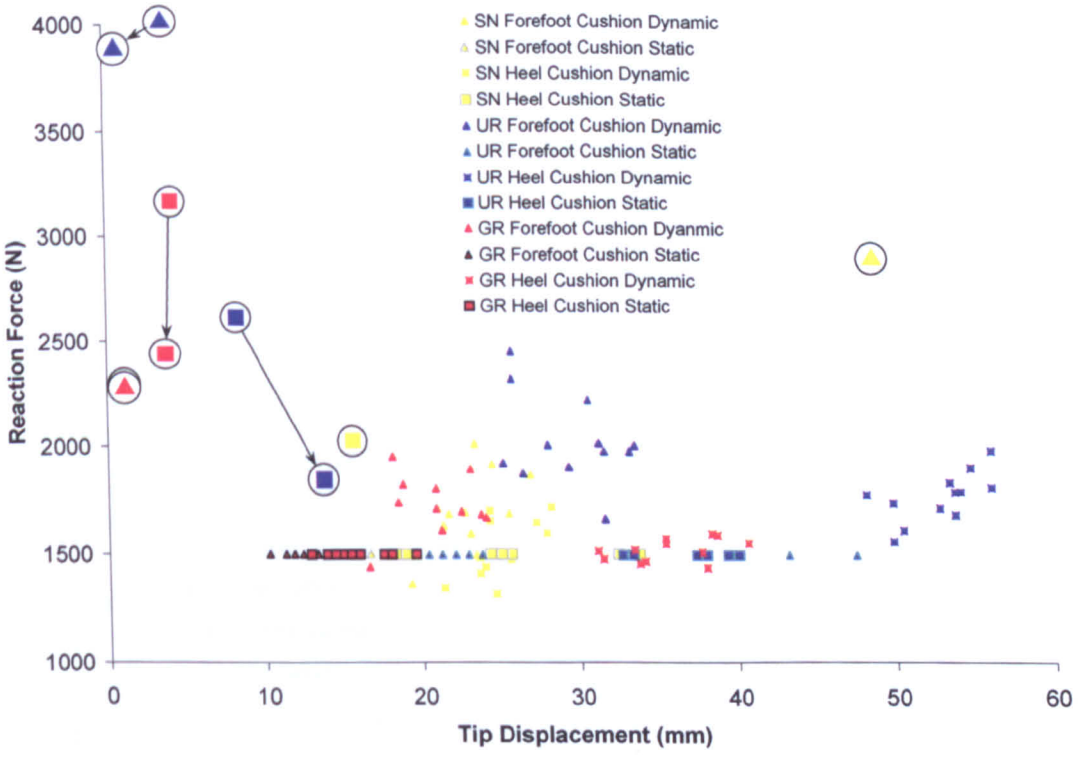

Figure 9.41: Plot of tip against peak reaction force for static (Instron) and dynamic (drop rig) tests. Points in circles indicate FE predictions. Arrows indicate change in prediction between initial predictions and those with adjusted material models.

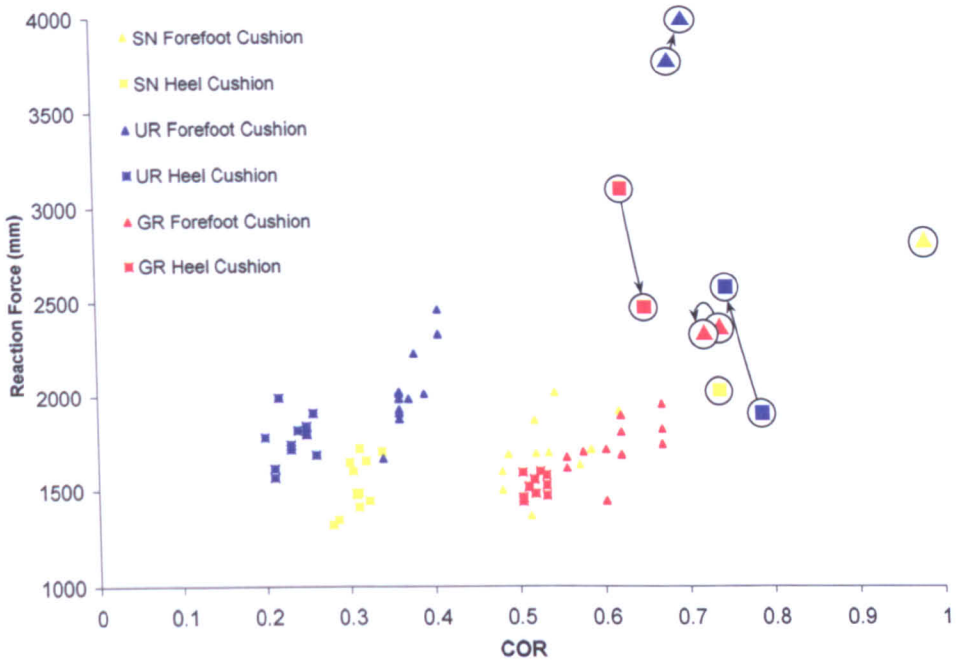

Figure 9.42: Plot of coefficient of restitution against peak reaction force for drop testing. Points in circles indicate FE predictions. Arrows indicate change in prediction between initial predictions and those with adjusted material models.

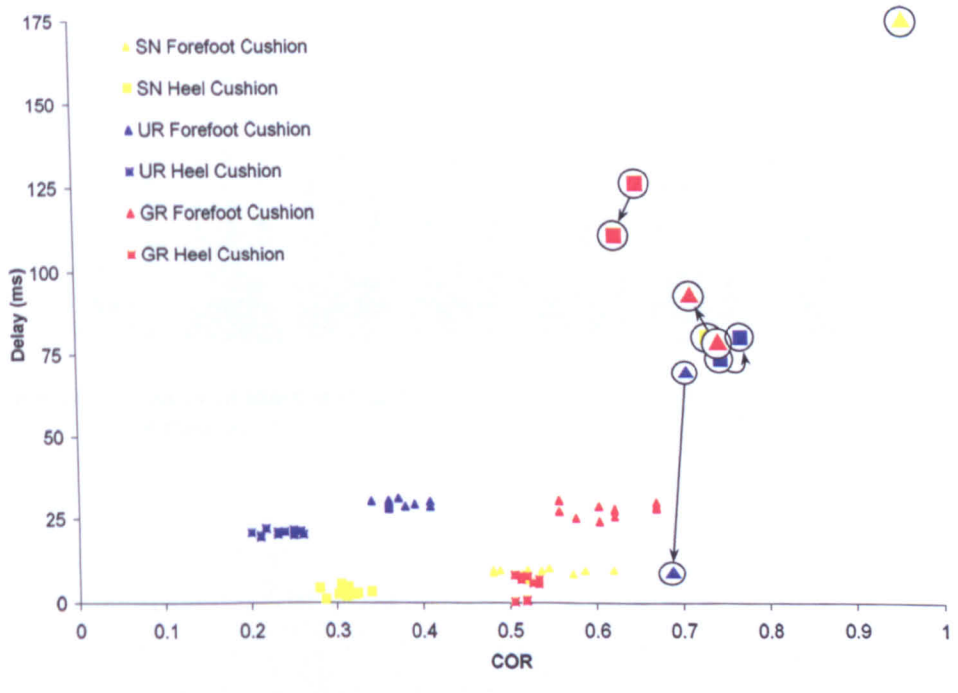

Figure 9.43: Plot of tip delay (time between maximum compression and maximum tip height) against coefficient of restitution for drop testing. Points in circles indicate FE predictions. Arrows indicate change in prediction between initial predictions and those with adjusted material models.

9.7.1.2 Adjusting for Structural Metrics

Structural metrics results were also extracted from the material property sensitivity studies. Figures 9.44-9.46 show the maximum tip deflection results from these studies. All sensitivities are for a doubling of the parameter (stiffness, damping or density), and all results excluding the VGB density change in the Ultraride bend test show less than a 30% change in tip height for a 100% change in the material properly.

It was initially thought that if the force/deflection response could be improved by adjusting the materials shown to contribute heavily to the stiffness, then the structural metrics could be adjusted by changing the materials that did not contribute to the stiffness. However, as the structural response of the TPU models was too far from reality to allow this by material adjustment alone, there was some other error in the model, not related to the material properties.

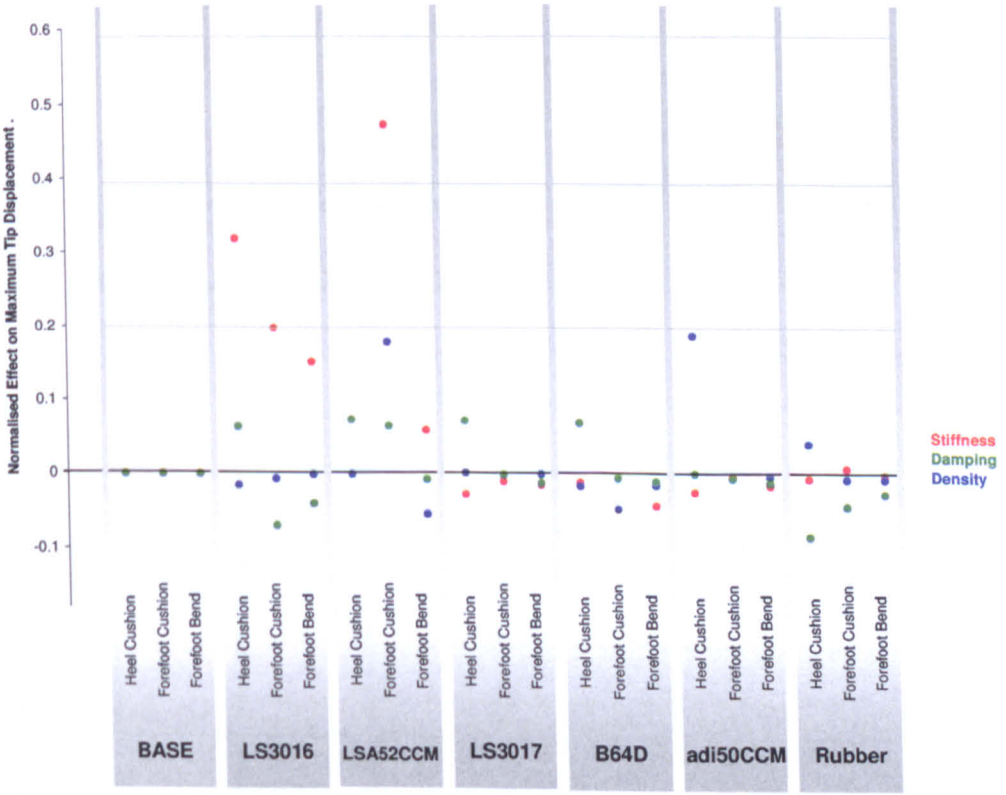

Figure 9.44: Summary of effect of doubling material parameters on metrics for all tests on Supernova models.

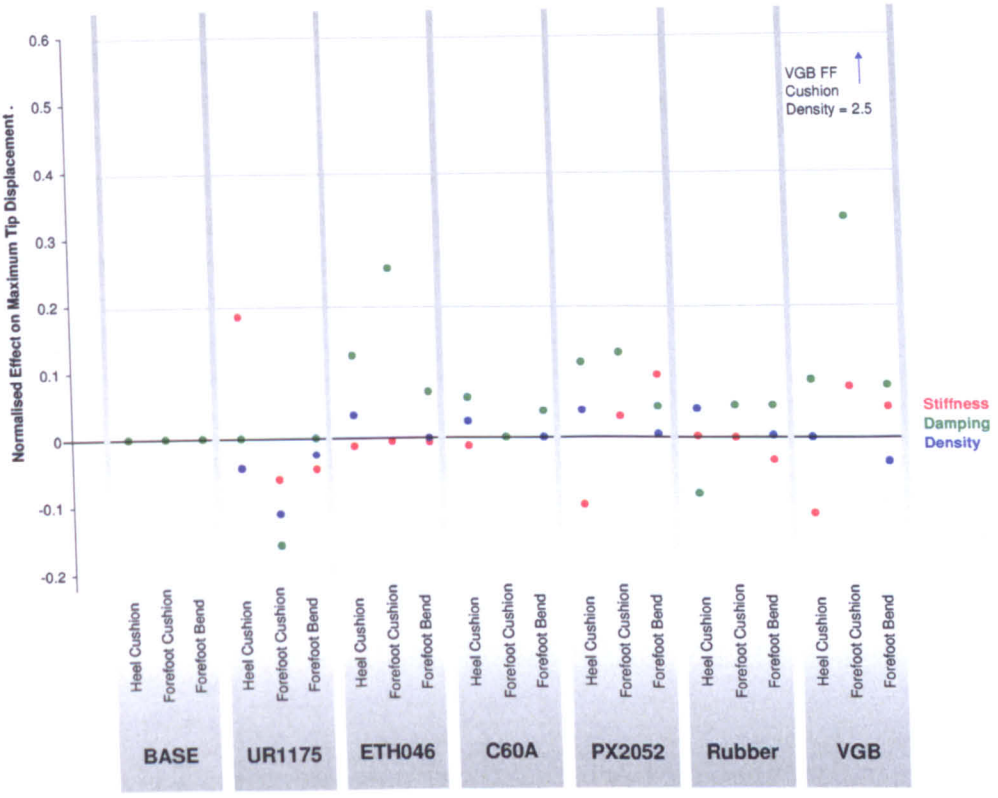

Figure 9.45: Summary of effect of doubling material parameters on metrics for all tests on Ultraride models.

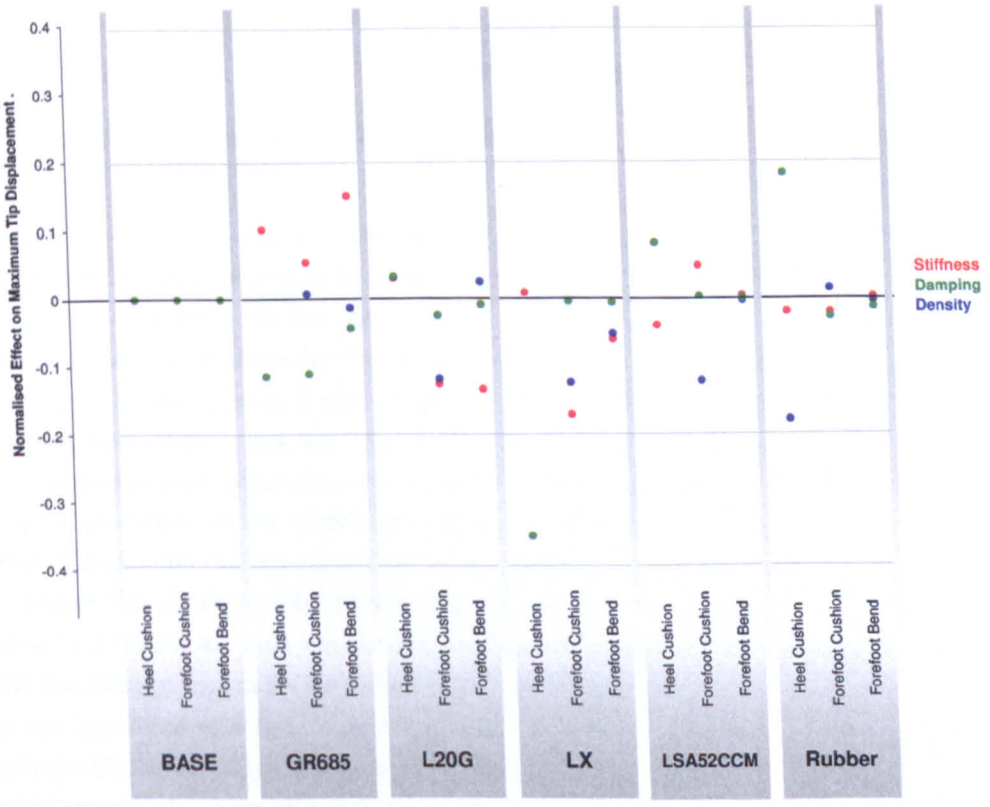

Figure 9.46: Summary of effect of doubling material parameters on metrics for all tests on Gigaride models.

9.8 Modelling Material Degradation

In Section 8.5 results were presented from a model of the Ultraride structure plate with the Mullins effect included. Here the modelling of material degradation is applied to an entire shoe assembly. The Gigaride was chosen for this as the foam models for the Ultraride would not process, due to the material pre-processor not finding a suitable combination of Mullins input data and quasi-static loading curve. As the Gigaride had no foams in the heel, the modelling could be carried out. Both the structure (GR685) and outsole (Rubber) materials were modelled for degradation, but the stiff top and bottom plates (L20G and LX materials) had no damage included as they only reached 5% strain in previous models and were still in the purely elastic region at this level during sample testing.

Figure 9.47 shows the force/displacement response of the model over 5 cycles, each lasting 5 seconds. The material models used were the unadjusted sample material models, and no viscoelastic data was included, as this was a model of a static test.

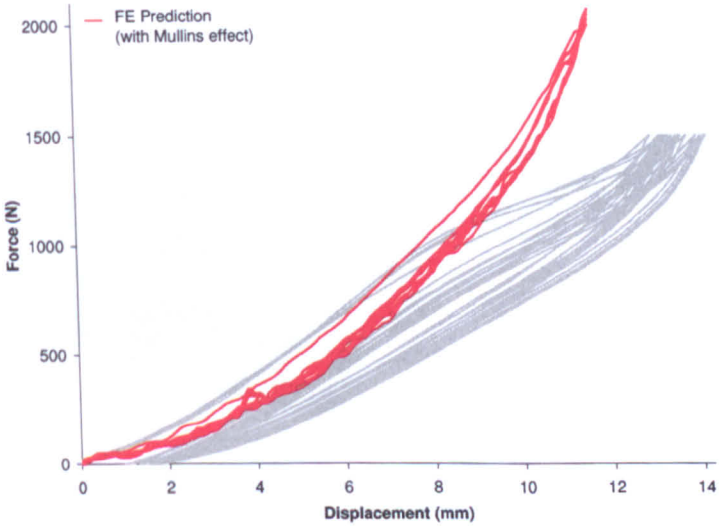

Figure 9.47: Force deflection results from physical testing (grey) and FE model which includes the Mullins effect.

The comparison in this case was the FE model to the first and subsequent loading cycles (the unloading was ignored as no damping was included within the model). A similar over-prediction was seen in the first cycle as was present in the static single cycle testing. There was a reduction in stiffness for the second and subsequent cycles, and while the results were good up to approximately 8 mm of compression, the softening at higher compressions was not modelled correctly (as was also seen in the model without the Mullins effect).

Despite the poor prediction, the overall response was similar, so it was assumed that the physical prediction of the model was reasonably realistic, and should be able to predict the areas of maximum damage, if not the exact stresses that were the cause.

Figure 9.48 shows results of stress and damage from the model. The stress plot in 9.48(a) shows that the impact load was distributed by the top plate into the structures. This indicated that the damage seen in 9.48(b) could have been achieved during running as it was not caused by the impaction of a rigid object onto the inside edges of the structures (as was the case with the Ultraride, which had no stiff top plate). Looking at 9.48(b) and (c), the damage was most severe in the posterior structures directly under the impactor. The heel unit spreads the load so that most was seen where the structure was forced into a bending deformation mode.

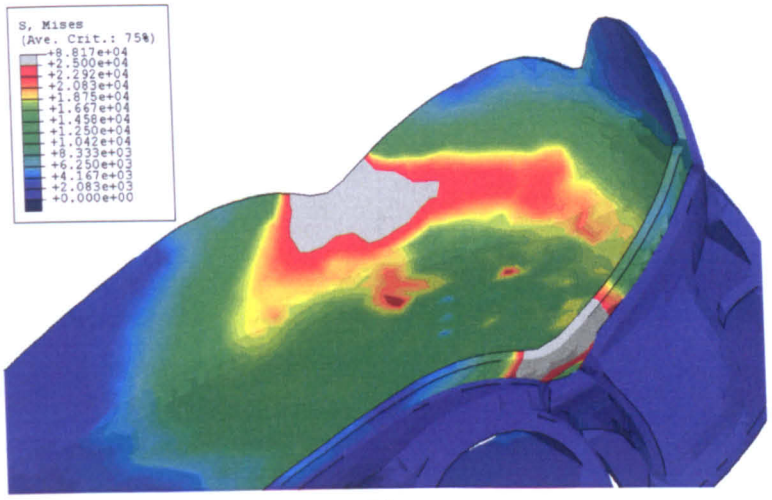

(a)

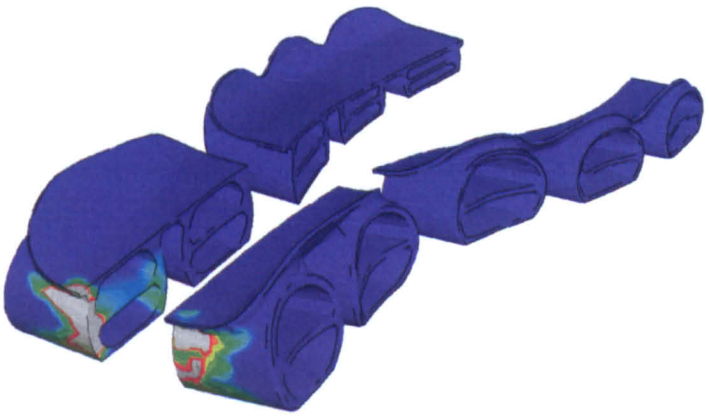

(b)

(c)

Figure 9.48: Results from modelling the Gigaride heel cushion test with the Mullins effect included. (a) is a stress plot of the posterior of the shoe, while (b) and (c) are damage plots (to the same scale) of the structures and heel structure respectively.

9.9 Chapter Summary

This chapter has considered the construction of FE models of shoe assemblies, consisting of multiple shoe components mathematically joined together, and interacting with each other and the simulated test equipment. The physical variation in shoe assemblies was assessed and the the FE models verified against these results.

Assembly Creation

It has been shown that it is possible to create shoe assemblies within ABAQUS, even if the geometry of parts does not fit together exactly. Care must be taken when specifying the location and scope of tie constraints, as they can affect the structural stiffness of the model and there are some default settings in ABAQUS that may override the users specification.

Contact between parts and themselves or other objects can cause jobs to fail if the energy transferred into the part is large and is not dissipated. High levels of vibration have been observed which lead to the collapse of elements and the failure of analyses. This was overcome by the inclusion of viscoelastic material data in dynamic testing, and through the use of deformable, but realistic, materials in the test equipment models.

It was shown that the stiffness of an assembly is dependant on the positioning of the test equipment both in physical tests and in the FE models. The most pronounced variation with position occurs for the heel cushion test, however more consistent placement of the heel stamp is possible due to it being a tighter fit in shoes with a bowl-shaped geometry under the impact site.

Load driven models exhibit vibration which is dependant on the geometry of the part, but not the mesh used. The effect was not seen in models that prescribed initial velocities and gravity (drop tests). If possible, future models should use displacement driven boundary conditions as these generate smooth loadings and will reduce error.

Physical Results

The physical testing highlighted the very high sensitivity of the reaction force with a small change in displacement, especially for the dynamic forefoot cushioning tests. However, generally the curve shapes of the shoes were very consistent, although the bend tests showed a lot of noise.

On average the variation in peak force at a consistent maximum displacement was 6% (max. 14%) between impacts on the same shoe and 15% (max. 28%) between different shoes of the same type. The Gigaride was the most consistent shoe, if its very noisy dynamic bend results are excluded, although the other two shoes were fairly consistent for the force/displacement measurement.

The structural metrics showed a large variation in reaction force for a small change in the maximum tip height which was reflected in a large variation in reaction force with a small change in maximum compression.

Some correlation between reaction force and coefficient of restitution (COR) was seen, with an increase in force giving a small increase in COR, indicating the shoes were behaving more elastically at higher loads. Tight grouping was seen in a plot of tip delay against COR, and as the delay metric is based on many different physical properties it is suggested that this is characteristic of the individual shoe undergoing a specific test. If a FE model could predict this and the force/deflection response well then it could be considered very accurate.

Initial FE Modelling

The first set of FE models used the material data taken directly from material sample testing. They showed a good match generally, with most of the models force/deflection responses being within one spread of the physical. The Supernova models produced the best results, with all of them matching the peak force/peak deflection with reasonable accuracy. The dynamic bend test showed a large amount of hysteresis which could be due to the shoe bouncing out of position on the bend test equipment.

The Ultraride and Gigaride matched the physical data well at low displacements, but under and over-predicted the stiffness at high displacements. Both the dynamic bend tests exhibited large amounts of noise for these shoes, as did the Gigaride heel model, probably due to the impact of the steel stamp with the stiff plastic top plate generating contact noise.

Looking at the structural deformation of the models, it was apparent that the structural shoes were not modelling the physical response well. Both shoes showed little lifting of the unloaded end of the shoe during a test, when the physical tests showed this response clearly. Due to this small structural response, the other structural metrics based on tip height are likely to contain significant errors. The Supernova did not produce a good match structurally, but its results were much better than the Ultraride and Gigaride results.

More accurate models that used quadratic elements were prone to failure due to the elements collapsing under high levels of deformation. It was found that this was generally due to stress waves in the model, which could be reduced by decreasing the mass scaling. However, as the use of quadratic elements gave an eight-fold increase in the number of DOF, and therefore the processing time, reducing mass scaling produced unpractically long simulations. Due to this all shoe assembly modelling was carried out with linear elements.

Adjusted FE Modelling

An approach was presented for adjustment of the stiffness of all the materials in a shoe based on the contribution of each component to the overall response of the assembly. This approach used the verified adjustments of the main components (derived in Chapter 8) and the target response given by the physical testing to estimate adjustments of all the materials.

The contribution to stiffness was found to be logical; components directly under the loading site contributed the most, while those at the unloaded end of the shoe added little or nothing to the response.

The results of modelling with these adjusted materials showed an improvement in all the results. If the stiffness of the model was not within the range seen in the physical shoes, then the difference between real and virtual was halved, indicating that the adjustment method works even with the assumptions that were made to achieve the calculations.

However, there was no real improvement seen in the structural results, indicating that the failure to model the physical shape of the shoe is independent of the material models. A sensitivity study on the variation of structural metrics with material properties indicated that it would not be possible to achieve a structural match by adjusting only the material models. This shows there is a problem with something in the model. At this point it can be determined that the problem lies within the behavior of the assembly, as the shoe part models in Chapter 8 were considered accurate in both force/deflection response and structural metrics.

Possible reasons could include:

- A change in the material properties due to the adhesive.
- An inability of the solid tetrahedral elements to model the thinner sections of the shoes that don't experience direct loading in the part testing.
- A failure of the tie constraints to realistically model the physical bonding.

Material Degradation

The static Gigaride heel cushion test was modelled with the Mullins effect included. The results showed a similar relative reduction in stiffness as the physical, but the overall stiffness curve was not modelled well at high displacements. This also indicated that there is some physical process in the model that is not being modelled correctly (the failure to model the structural response also occurs when damage is included).

Predictive Ability

Two approaches were available to create a predictive model. The first assumed that the material sample test data could be inputted directly in to the assembly model. These models did show reasonable force/deflection matches to the multi-cycled physical test results (described earlier in Section 9.9), even though the material sample data was the first-cycle data.

The second approach assumed that any error in the FE model was due to the input of non-perfect test data, and that this error could be quantified by calculating the adjustment needed to correct models of samples that included non-perfect test conditions such as friction and barreling. This was shown not to be currently possible in Section 8.6, with the range of test data available.

As a final point, although the structural response of the models was a poor representation of the physical, during a running strike all of the midsole is attached to the foot and does not necessarily need to transmit the bending loads. However, shear loads will also be formed as the forces in a running strike are not all in the vertical plane (as seen in Figure 2.11), and the ability of the models to transfer shear has not been tested. If, in a future test, only cushioning loads are applied to the models, then they will have good accuracy.

Chapter 10

Modelling Stage 3a: Mechanisms

This chapter considers the feasibility of modelling a shoe which contains a mechanism. The shoe modelled had the adidas Ground Control System (GCS) mechanism in the heel, and was in an early stage of prototyping, so physical samples of the shoe were not available for testing. The main purpose of this section of the research was to produce a working mechanism model that could be used by adidas to assist in their design process.

10.1 Mechanisms In Athletic Footwear

The GCS shoe range uses a mechanical slide-spring system to adjust the cushioning properties of the shoe. The shoe modelled was the GCS-B road shoe (referred to as GCSB, and shown in Figures 10.1 and 10.2). The design uses two stiff polymer plates and a polymer spring to form a section of a spherical bearing between the outsole and the midsole of the shoe. This has the effect of lengthening the duration of the shock experienced by the runner, which for the same impact energy, reduces the peak forces. While the GCSB shoe uses a mechanism to adjust the cushioning, it still relies on foams to provide some of the energy loss in the shoe during footstrike.

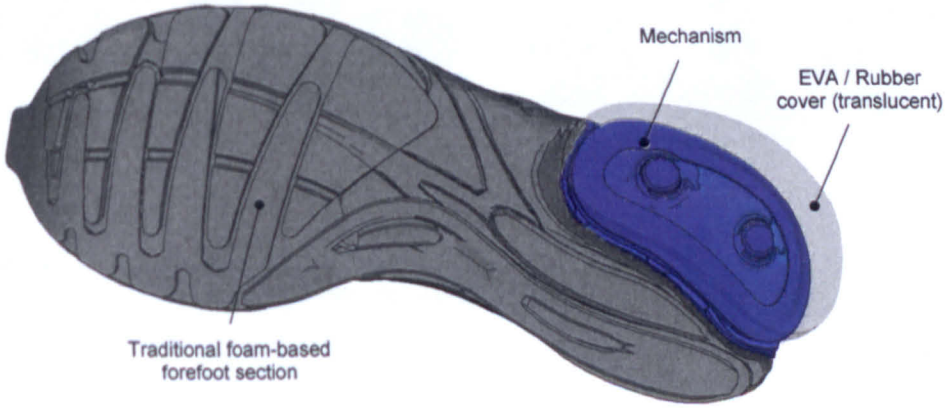

Figure 10.1: The location of the mechanism in the GCSB road shoe.

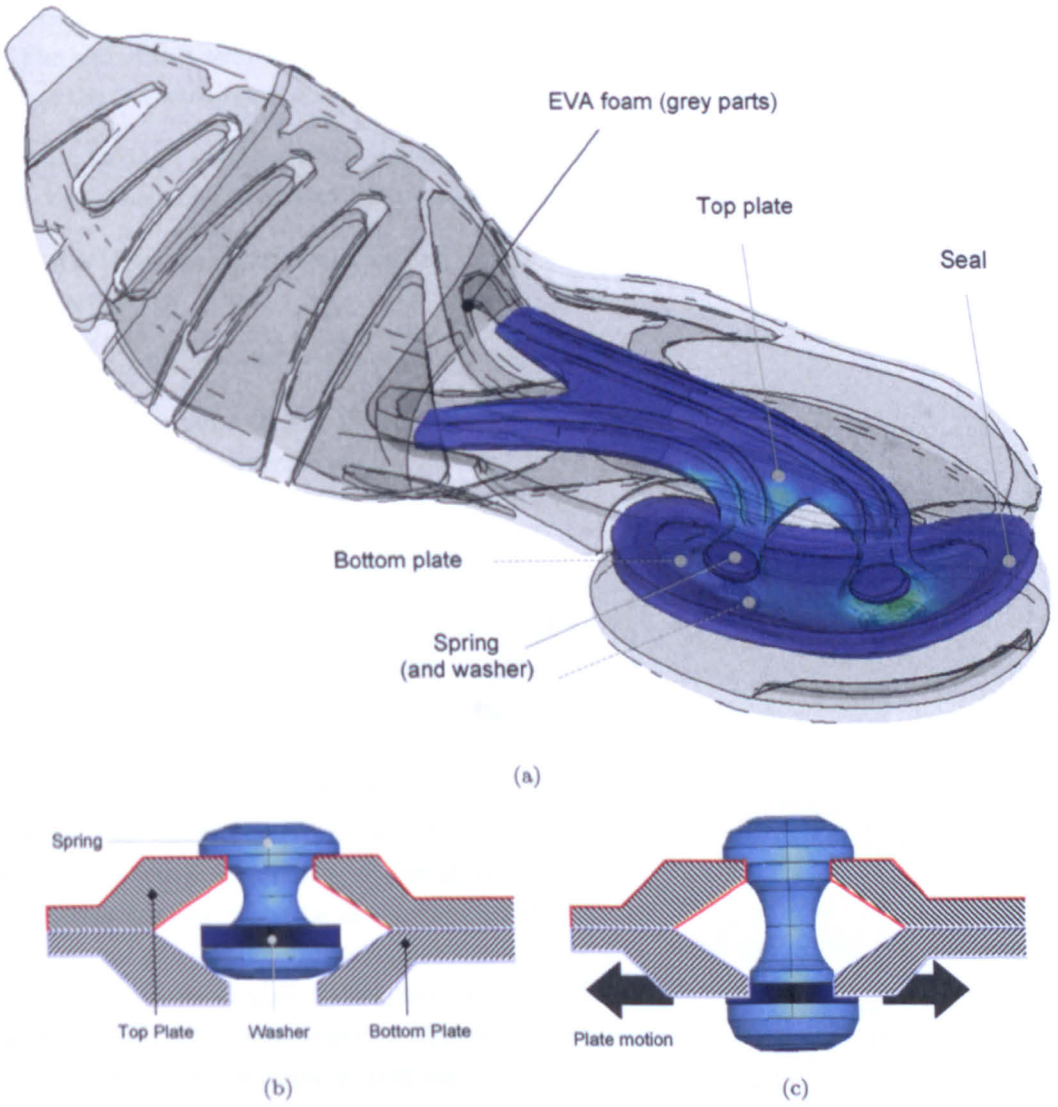

Figure 10.2: The GCSB shoe (a) location of the mechanism in the shoe, (b) schematic of the moulded part geometry, (c) schematic of the assembled part geometry.

10.2 Mechanisms In Finite Element Analysis

The FE method offers particular advantages over physical testing when it comes to observing mechanisms in practice as the model can be split up, parts hidden and the internal workings scrutinised while the mechanism is still under load. To do this physically would either be extremely difficult or impossible in most cases, resulting in widespread use of FE in industries such as automotive and aeronautical engineering to develop understanding of the inner workings of machines. The types of mechanisms normally modelled with FE consist of metallic parts and use standardised mechanical components such as bearings, shafts and bolts. Previous modelling of mechanisms made entirely from polymers was not found during the literature search.

The aim of this section of research was to create a model that could be used by adidas to answer the following questions:

- Do parts fit together when assembled, and function as intended, taking into account any preloading generated by the assembly processes?
- Are there any unwanted collisions, or does the mechanism lock up at extremes of movement?
- What are the possible avenues for failure of parts?

All of these are important if the number of design iterations and money spent on making prototypes is to be minimised.

10.3 Mechanism Geometry

The geometry import and preparation process was essentially the same as for more general shoe parts (as discussed in Chapter 8). However, the use of mechanical parts with simpler geometry allowed direct import into ABAQUS of some components. The GCSB spring was derived from a revolved curve, so a copy was constructed in ABAQUS. This allowed quick mesh adjustment as the part did not have to be re-integrated into the model for every mesh change. As the geometry was simpler for this part, it did not require stringent meshing controls, so there was no need to use Hypermesh.

However, although some of the mechanism components were simple, some contained a high degree of geometric complexity. The top plate of the GCSB (Figure 10.3) distributes the stress generated from the mechanism along the midsole. It was made of a stiff polymer and was ribbed for extra stability. These ribs could not be removed as they contributed a critical part of the structures' stiffness. The part was meshed in Hypermesh to ensure the maximum element size was generated whilst maintaining a good fit of the elements to the shape.

The mechanism parts were generally smaller than those in normal shoes, and the geometry had shown errors where parts have been so thin that poor export/import has caused negative volumes in the original geometry (where two sides of an object cross each other - which is not physically possible, illustrated in Figure 10.4). Special care needs be taken with these small/thin parts to ensure the geometry is representative of the design, as it is very likely to be critical to performance of the mechanism. In this case the surfaces were corrected so as to retain the overall shape, but with a thickness the same as the desired smallest element.

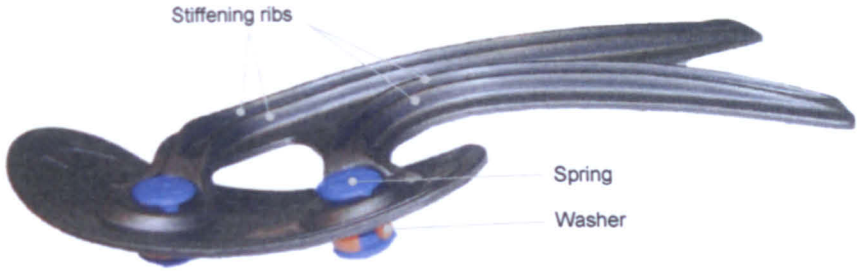

Figure 10.3: Image of the top plate of the GCSB mechanism.

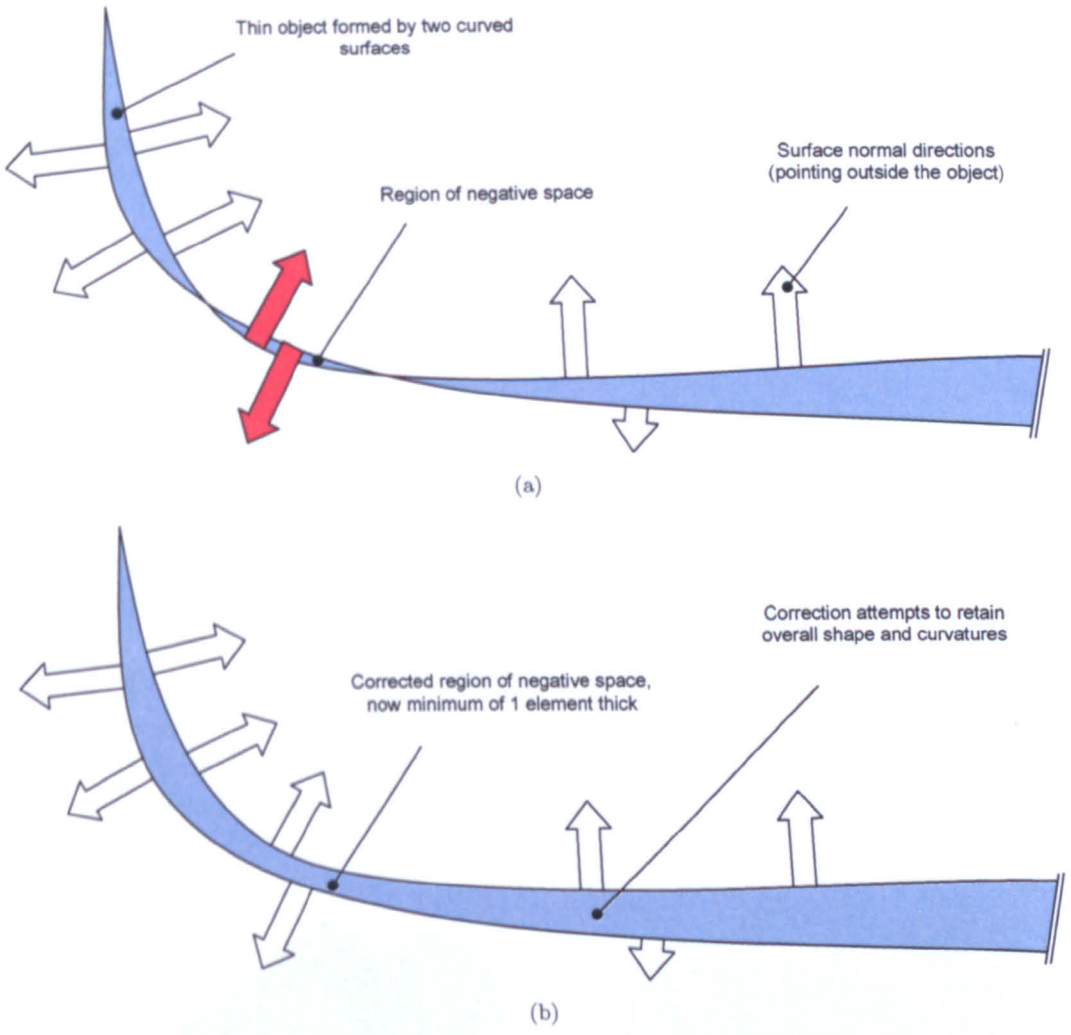

Figure 10.4: Illustration of the concept of negative space, (a) thin section of a component with an incorrect surface specification, (b) the corrected surface specification.

A critical point in the construction of an accurate mechanism model is the specification of the correct bonding of parts. This was necessary for all the shoes, but was highlighted in Section 9.2.1 using the GCSB, as the specification of tie constraints affected the overall stiffness of the mechanism. It was also important to carefully consider which seeding lines were left in the geometry, as this affected how accurate the placement of the tie constraints could be after meshing.

10.4 Mechanism Meshing

The GSCB mechanism contains soft rubber and foam parts, but also stiff plastic components with small details. As the processing time of a job is linked to the time increment, the mesh was optimised with respect to the time increment each element will require. This is based on material properties as well as size (see Section 4.6.4.2), so refinement in soft, light materials did not necessarily result in a significant reduction of processing time.

Table 10.1 lists the part properties that affect the time increment, the last column containing the element criticality: a relative measure of the difference in wave speed generated for the smallest element. The most critical element has a value of one, less critical elements have a lower value. In a fully optimised mesh all criticalities should be one, indicating that the minimum time increment for all elements is the same.

Part Name	E (N.m-2)	ν	ρ (kg.m-3)	Length (mm)	≈Time Inc(s)	Criticality
Washer	6.00E+09	0.3	1.00E+02	0.87	9.68E-08	0.75
Bottom plate	6.00E+09	0.3	1.00E+02	0.85	9.46E-08	0.76
Top plate	6.00E+09	0.3	1.00E+02	0.65	7.23E-08	1.00
Foam	5.18E+07	0.3	1.10E+03	0.41	5.15E-06	0.01
Spring	1.00E+09	0.3	1.00E+02	0.7	1.91E-07	0.38

Table 10.1: Example of optimising the stable time increment by looking at the overall effect of both the stiffness and element size in a part.

The mechanism also contained objects that had a significantly different geometry during normal operation than they had before they were assembled. For illustrative purposes, Figure 10.5 shows an example of a part which undergoes a large deformation from its initial state, to its operating state. This occurs in the GCSB springs, but to a lesser extent. In cases such as these it was essential to bias the mesh in the initial state so the elements had a good shape after assembly and before the loading occurs. This adjustment was also accounted for when optimising for time increment - optimising for the mesh size in the assembly steps may not give the optimal speed in the testing steps of the analysis. For the GCSB this was not an issue as the most time increment critical elements were in the top plate, which did not undergo a significant shape change during the analysis.

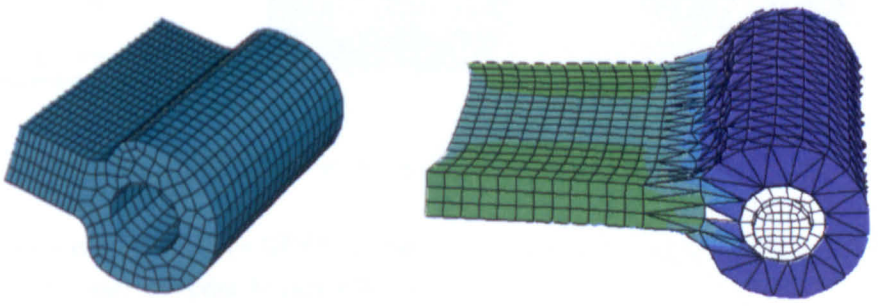

(a) Initial state

(b) State after assembly

Figure 10.5: Simple spring part, note the significant deformation of the mesh between the two situations. The initial mesh was specified so that the elements were of regular shape after assembly.

10.5 Modelling the Assembly Process

As the mechanism components required assembly in the physical shoe, so this process needed to be replicated in the FE model. If the components did not undergo any deformation between their original state and their assembled state, then the modelling process would be essentially the same as that for creating shoe assemblies, as discussed in Chapter 9.

However, in the GCSB some critical components underwent large deformations during the assembly process, and the resulting pre-loaded component had different properties to the original. This was a critical consideration for the non-linear materials used, where a small change in initial strain could have a large effect on the stiffness. Modelling the assembly process would also reveal the geometry of the spring in its assembled state, which was not accurately known due to its deformable nature.

10.5.1 The Snap Method

Performing the GCSB spring pre-load step during hand assembly was a complex procedure, but successfully modelling it in ABAQUS was perhaps more difficult as the forced movement of objects must be specified before the analysis begins.

However, the advantage of computer modelling was that objects can be made to pass through other objects without interaction. This was the most simple way of creating a pre-loaded model; position one end of the spring in place, turn off any surface contacts and pull the other end just past its final position, then turn the contacts back on and release the spring (Figure 10.6). This would cause the spring to snap back into its final resting position.

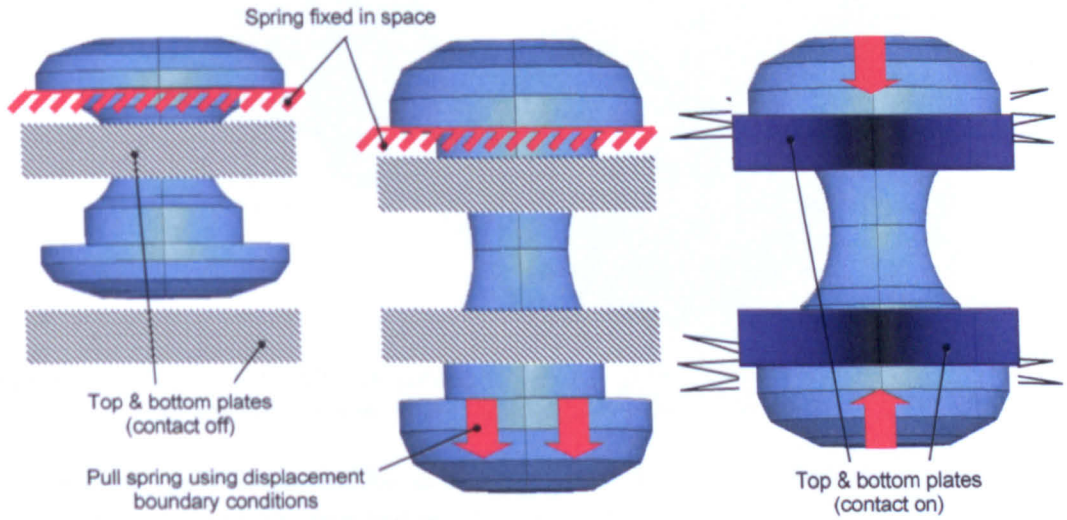

Figure 10.6: 'Snap' method of positioning and pre-loading spring in GCSB model.

This process was applied to the GCSB springs, but it was found that the method generated large amounts of noise. In order to minimise the amount of noise, the minimum amount of movement was specified, although this did involve some trial and error to optimise.

Other problems with this method arose where contacting surfaces between the spring and the plates were poorly defined by the mesh. In the GCSB this was a particular problem as the spring fits tightly in the top plate, causing some of the element nodes to initially penetrate the plate surface. This in turn caused the surface contact to fail at these nodes, and allowed parts of the spring to pass through the plate (Figure 10.7).

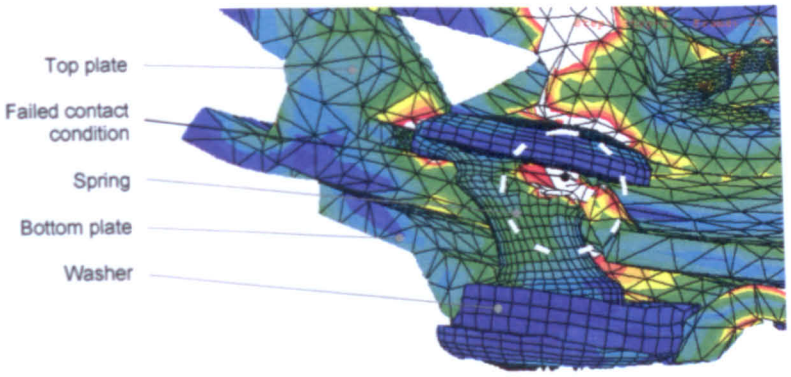

Figure 10.7: Poor alignment and a coarse mesh leads to contact failure in the circled region.

Refinement of the surfaces was found to solve the contact problem, but would generate very small elements that significantly slowed processing. To work around this problem a compromise was made between accuracy and speed; the spring was fixed in place with tie constraints to the plate, which removed the poor contact, and reduced set-up time as there was more tolerance in initial positioning of the spring.

The assumption for this method was that the foam part bonded to the top of the spring would hold it in place despite the high sideways deformation seen in Figure 10.8. However, this would be a very difficult situation to verify even with physical samples, as the spring would be sealed inside the shoe, and the foam part bonded to its upper surface would prevent any filming of the mechanism in use.

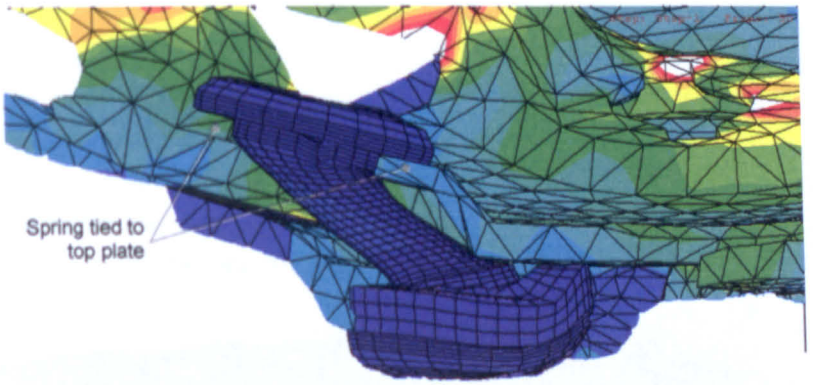

Figure 10.8: Section of GCSB unit under full load. The spring is tied to the plates at either end, but appears as though it may pull out of its slot if it were not tied in place.

The most successful method found for locating the lower part of the spring was to apply a tie constraint at the interface between the spring and the top-plate, and another between the spring and the washer part (that fits into the bottom-plate). By creating an extra washer for each spring in the FE assembly, one in the initial position and one aligned at the final position, movement of the washer tied to the spring was specified by mapping the position of the first washer onto the second. This mapping was carried out by specifying displacements of the washer over time, then releasing the washer once it was in position. Figure 10.9 illustrates the process.

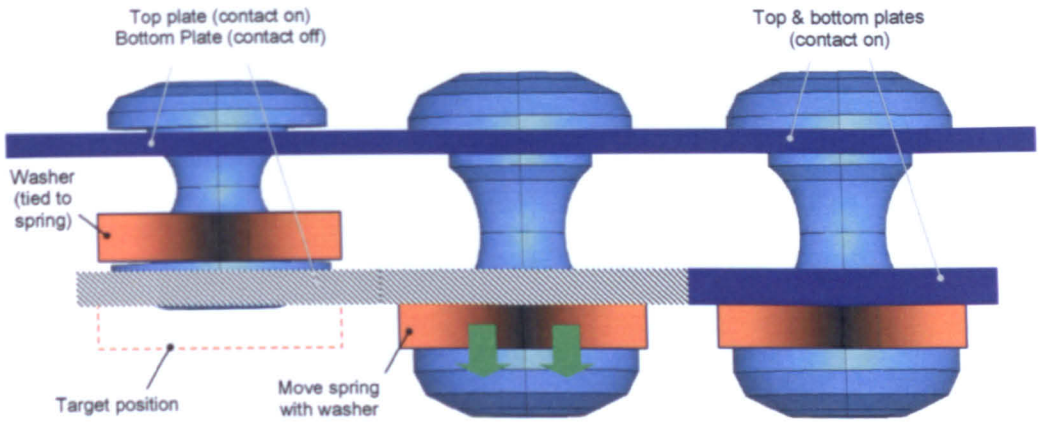

Figure 10.9: Spring-washer method of pre-loading. Left to right: Washer axially aligned to spring (which was positioned by eye), washer displaced to correct position with contacts turned off, contacts turned on and boundary conditions on spring released allowing it to settle.

10.5.2 Assembly of Mechanism into the Shoe

The GCSB springs were preloaded not only in tension, but also in compression. The design of the shoe requires that a foam part is bonded onto the underside of the bottom-plate after the springs have been fitted. This offers more cushioning and protects the springs that protrude from the underside of the bottom-plate. However, the geometry of the spring and the recess it sits in are slightly different, resulting in some stress between the foam and the spring after assembly.

This would not have been a problem in a simple shoe, as a tie constraint with a large radius could have been applied to hold the penetrating parts together, but this was not possible after the pre-loading step as ABAQUS requires that all tie constraints are specified only at the beginning of an analysis. If this issue was left uncorrected, the spring passed through the foam under load and impacted the floor causing failure of the analysis. Figure 10.10 shows this (the foam has been removed from view, but was included in the model).

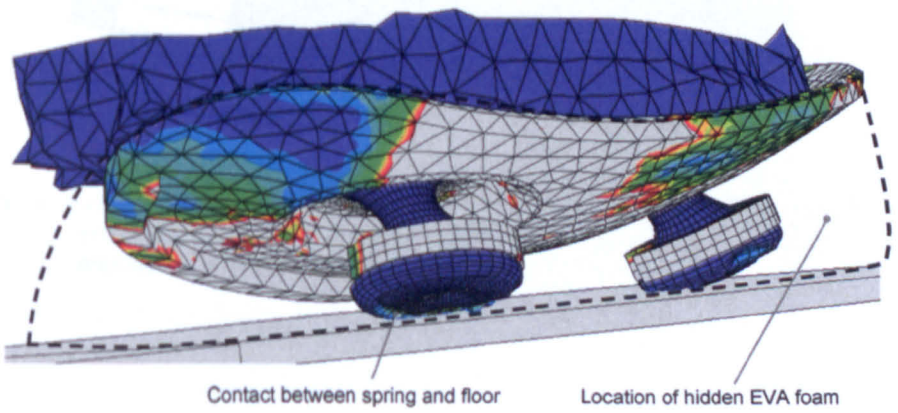

Figure 10.10: Cut-away figure showing the springs of the GCSB contacting the floor, due to the surface contact between the springs and the (hidden) EVA foam part beneath the springs failing.

The method used to overcome this problem was to specify displacement of the foam during the preloading step, then release the foam after the spring had settled. The use of a surface contact that did not allow any separation after contact could then approximate the use of ties in this area, after the the spring and foam had come into contact (see Figure 10.11).

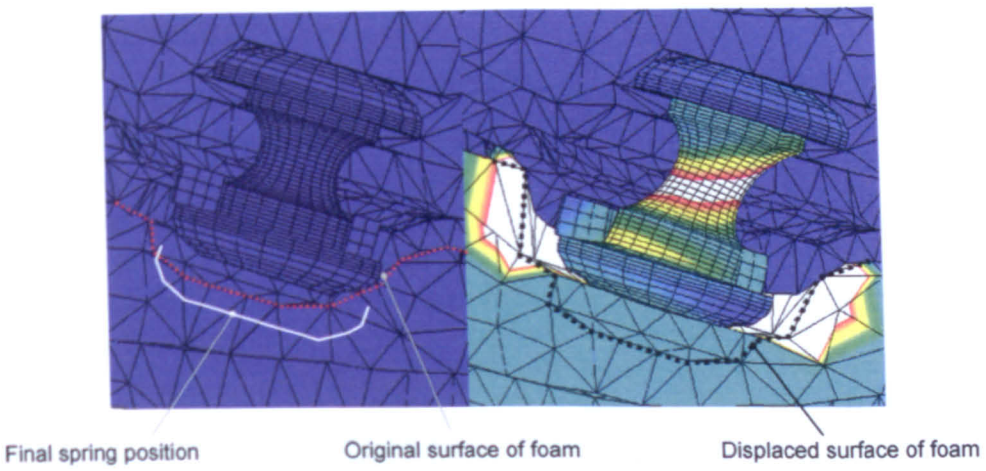

Figure 10.11: Section views of the GCSB heel unit. Left: original position of spring between plates, right: surface of EVA is moved with the spring during pre-loading to ensure surface contact is set up correctly. Dotted lines indicate the EVA foam surface.

This method allows the job to be run successfully, provided all other interactions are unaffected by the new changes. For example; Figure 10.12 shows the corrected heel unit penetrating the floor under load, due to the increased constraints in the unit causing an overconstraint in the outsole. This lead to failure of the surface contact between the floor and the outsole and was corrected by either using a two-element thick outsole, or one with quadratic elements, both of which remove the overconstraint.

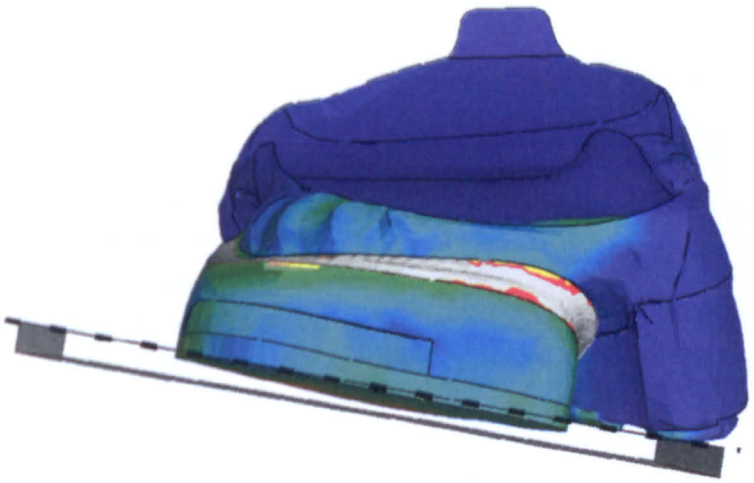

Figure 10.12: Example of overconstraints on the outsole of the GCSB heel unit (viewed from the rear of the shoe)- note the penetration of the outsole into the upper floor surface (highlighted with a dotted line).

10.6 Connectors

Connector elements were designed by ABAQUS to help create mechanisms by allowing the user to specify mathematical controls that replicate mechanical components such as hinges and pivots. Axial connectors were used to add piston-like measurement devices to the GCSB. The springs were replaced by two rigid surfaces at the springs' connection points, and an axial connector was placed between the surfaces (Figure 10.13). By specifying a stiffness for the connector, a reaction force trace could be plotted over the range of motion of the mechanism.

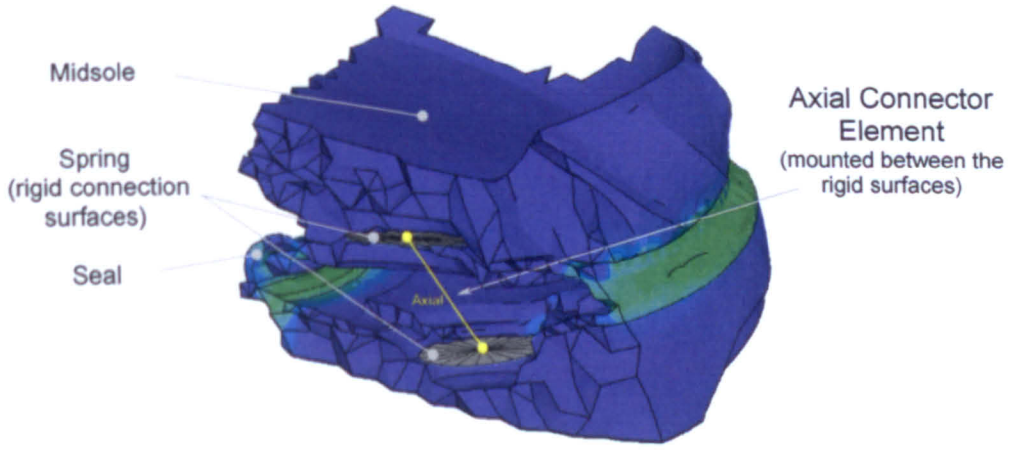

Figure 10.13: Section through the GCSB mechanism showing the use of connectors as a measuring tool.

Connectors could also be used to form more complex mechanisms within shoes, or for modelling sophisticated shoe testing equipment such as that used by Mara (2006). However, if connectors are used in future models, the users must be aware that while they are very useful, they have proven susceptible to precision problems. Nodes that should stay at the same point in space have been observed to drift in analyses with large numbers of increments. The unexpected failure of connectors part way through an analysis has also been seen, and many of these problems remain unresolved, even with assistance from ABAQUS. Therefore, the outputs from models that used connectors should be checked very carefully for these kind of errors.

10.7 Chapter Summary

This chapter has shown that it was possible to model mechanisms within shoe assemblies. A working model of the GCSB shoe was created which contained a spherical bearing and spring mechanism.

It was shown that the method of assembly of the mechanism was important in the construction of a model that could be capable of producing accurate results (assuming all the material models and other parts of the model were correct).

A method of reducing the processing and development time of mechanism shoe analysis was demonstrated, which could also be applied to other shoe models with a large range of stiffnesses in the component parts. This method directs the user to increase the size of elements only in parts that have a direct effect on the time increment based on the element size, stiffness and density.

It was also shown that the mechanism FE models are very useful for gaining an insight into the processes occurring in objects that cannot be measured internally in physical samples.

Chapter 11

Modelling Stage 4: Production Shoe Assemblies

This chapter considers the differences in physical response between shoe assemblies and test samples of cut-down production shoes. These samples are the ones generally used by adidas for shoe performance testing and include those sections of the upper beneath a physical cut line approximately 15 mm above the midsole. As the role the upper plays in the cushioning and flexibility response of the shoe is not well understood, comparison of these production shoes with the shoe assemblies tested in Chapter 9 is anticipated to yield useful information.

11.1 Production Shoe Construction

The methods of assembly for all the shoes under test are similar. The upper is sewn and bonded separately from the midsole assembly, then the two are bonded together under compression.

The construction of the upper does vary between the shoes, however. The Supernova has the least amount of extra cushioning material, its upper is there primarily to locate the midsole onto the foot and keep it there during running, whilst the Ultraride and Gigaride both have thick foam inserts in the base of the upper (which can be seen in Figures 7.4-7.6). This foam is included to provide more cushioning and to ensure the load is distributed across the individual structures. The Ultraride insert also has extra viscoelastic and elastic sections moulded into it.

For the structure shoes, the extra cushioning inserts are an integral part of the upper. Figure 11.1 shows the assembly and production shoe samples prepared for testing. In the TPU structure shoes, the uppers form a larger proportion of the shoe than in the traditional foam shoes, due to the inclusion of the extra cushioning (Figure 11.2). Because of this, it was expected that there would be a larger difference between the shoe assemblies and the production shoes of the structural type.

(a) Supernova midsole assembly

(b) Supernova production shoe (cut for testing)

(c) Ultraride midsole assembly

(d) Ultraride production shoe (cut for testing)

(e) Gigaride midsole assembly

(f) Gigaride production shoe (cut for testing)

Figure 11.1: Medial views of the shoes used in the physical tests. The uppers have been removed to a depth of approximately 10 mm on the production shoes by hacksaw.

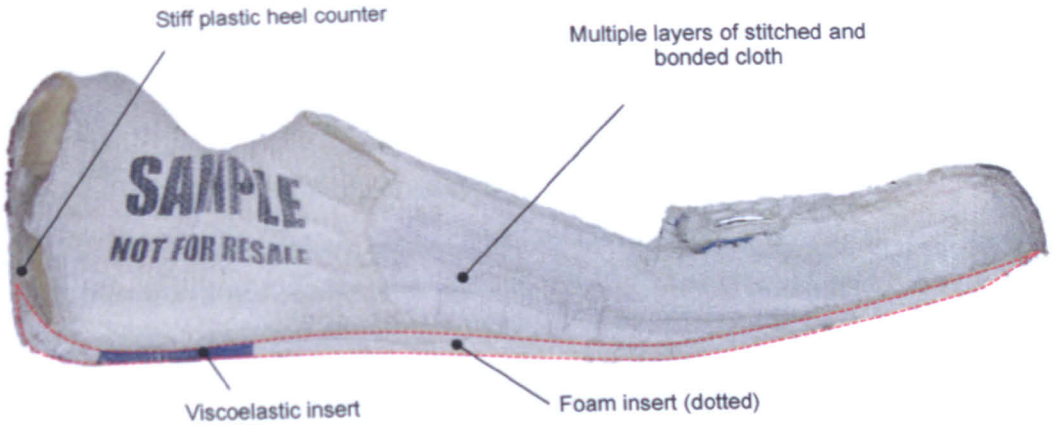

(a) Medial view of the assembled upper section of the Ultraride.

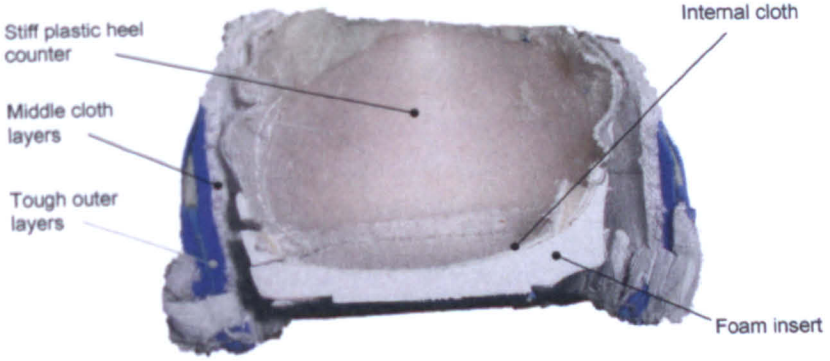

(b) Posterior view of the assembled upper section of the Ultraride.

(c) 5 mm slice through the forefoot region of theSupernova production shoe

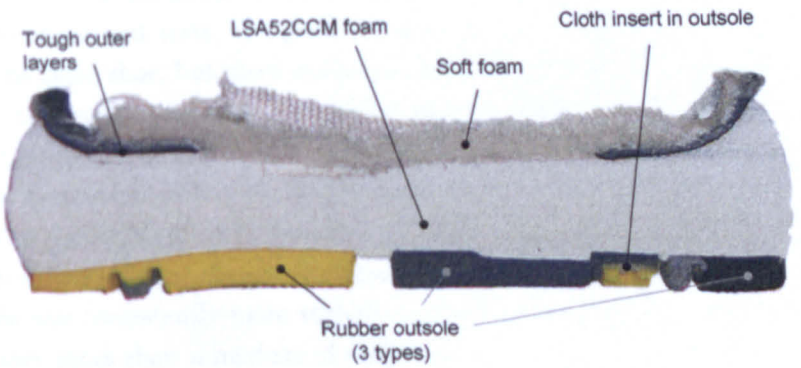

(d) 5 mm slice through the heel region of the Supernova production shoe

Figure 11.2: Sectioned views of the Ultraride and Supernova production shoes.

11.2 Physical Testing

The physical testing procedures undertaken on production shoes are identical to those carried out on the assembled midsoles, detailed in Section 5.4.

11.2.1 Force/Deflection Results

Figures 11.3-11.5, show the force deflection results for tests on production shoes. As the aim of these tests is to assess the variation in production shoes, and the effect the upper had on the shoe. Table 11.1 summarises the percentage variations seen between impacts on the same shoe and between all the impacts of that type of shoe for that test. The increase or decrease in variation over the midsole assembly is also included in brackets for comparison.

Test	Supernova		Ultraride		Gigaride	
	Impacts	Shoes	Impacts	Shoes	Impacts	Shoes
Quasi-Static, % Variation (% change from shoe assemblies)						
Heel Cushion	4 (+1)	16 (-9)	4 (-10)	15 (-2)	4 (+1)	10 (+5)
Forefoot Cushion	2 (0)	22 (-6)	1 (-4)	2 (-22)	5 (+3)	12 (+1)
Forefoot Bend	6 (+4)	9 (-10)	7 (+3)	8 (-7)	4 (-2)	11 (-12)
Dynamic, % Variation (% change from shoe assemblies)						
Heel Cushion	3 (0)	13 (+6)	5 (+2)	19 (+6)	4 (0)	6 (-5)
Forefoot Cushion	4 (0)	13 (-4)	5 (+1)	10 (+4)	4 (+1)	20 (+12)
Forefoot Bend	10 (-7)	18 (-6)	14 (+12)	21 (+6)	20 (*)	30 (+3)

Table 11.1: Percentage variations in force (at peak loading of the stiffest sample). First values are variations between impacts, then maximum difference seen between all impacts on all production shoes tested. *The midsole assembly dynamic bend results are too noisy to distinguish between impacts on a single shoe.

The average variation in force between impacts was 6% with a maximum of 20% and the average variation for all the impacts on the same type of shoe for the same tests was 16% with a maximum of 30%.

One method of comparison of production shoes with shoe assemblies was through the change in percentage variation, with a lower variation more desirable. The average change in variation from the assembled shoes was 0.25% with a maximum of +12% between impacts and was -2.5% with a maximum of -22% between similar shoes. This meant that, averaged across all the shoes and tests, the production shoes were slightly less consistent between impacts on the same shoe, but more consistent between shoes of the same type.

However, the results showed a large spread of percentage variation values, both positive and negative, so the use of an averaged variation metric has limited use for direct comparison. It was better to compare each of the tests separately. For example, the Ultraride quasi-static tests showed a reduction in variation over the shoe assemblies, except for one shoe on the bend test that had a larger change in response over its impacts. The dynamic response of the Ultraride was consistently more variable in the production shoes than shoe assemblies, while the other shoes show a mixture of results.

Significant, repeated improvements in the consistency of the force/deflection response of production shoes over shoe assemblies has not been seen.

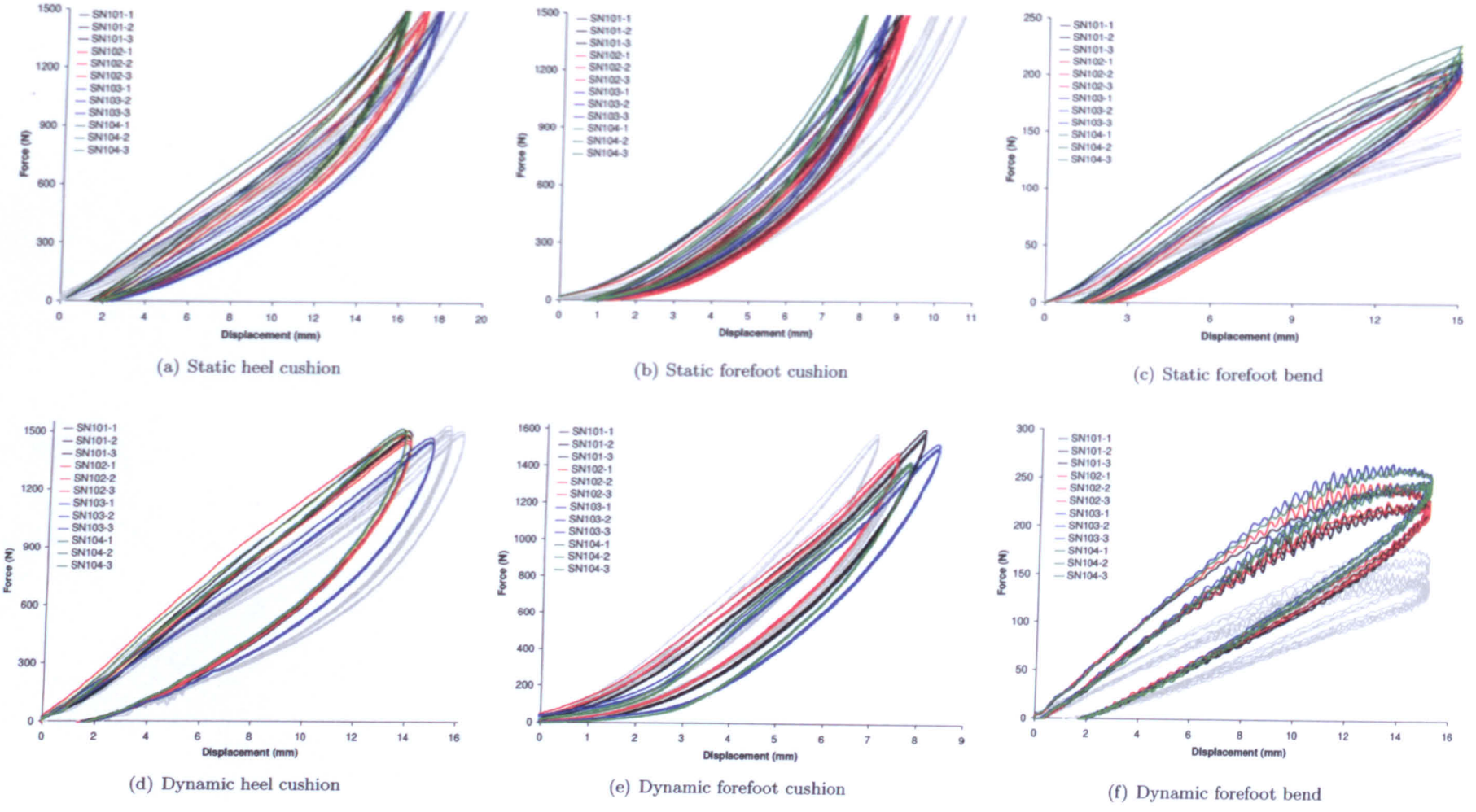

(a) Static heel cushion

(b) Static forefoot cushion

(c) Static forefoot bend

(d) Dynamic heel cushion

(e) Dynamic forefoot cushion

(f) Dynamic forefoot bend

Figure 11.3: Results of static and dynamic physical tests on Supernova midsole assemblies.

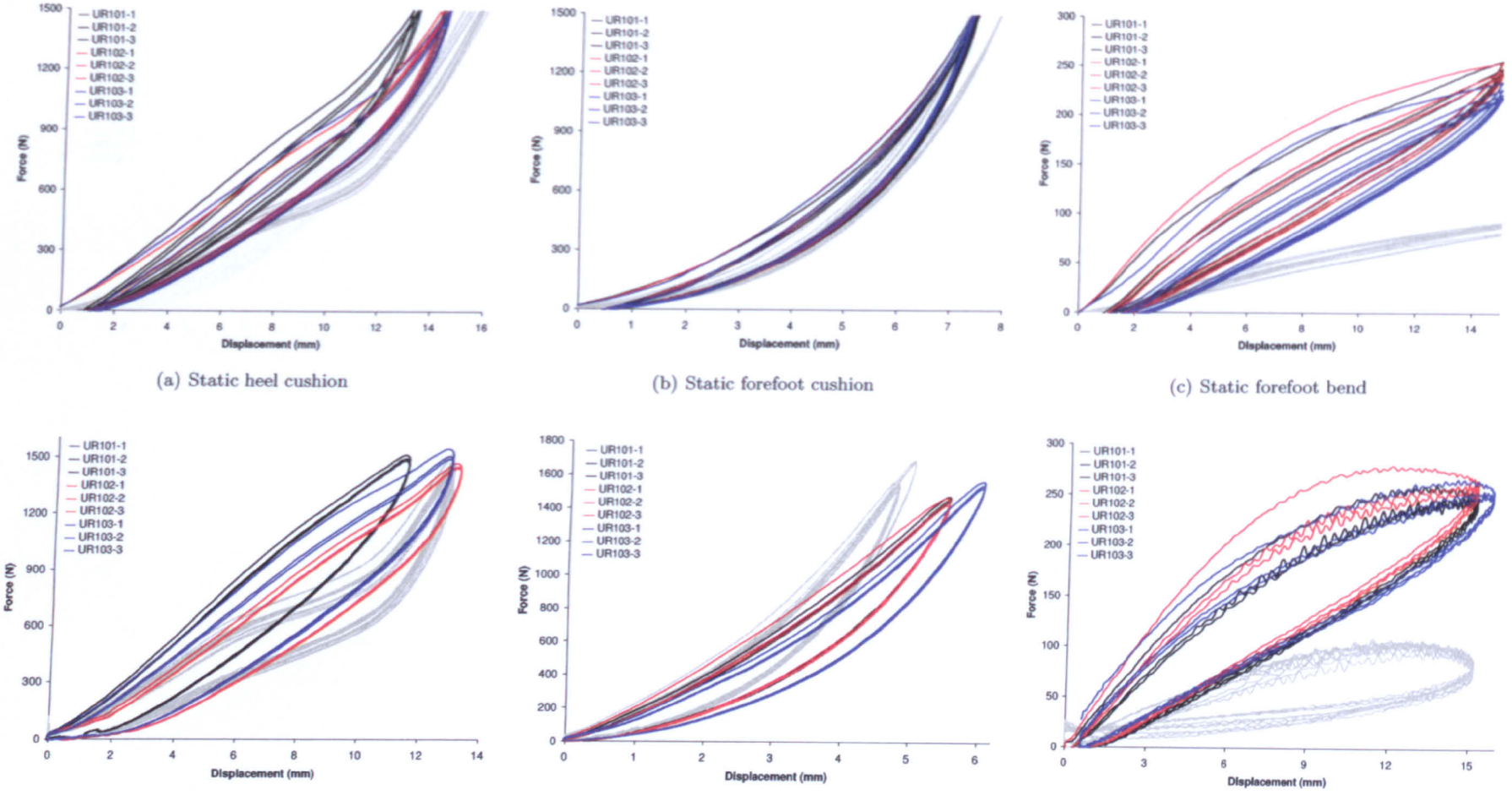

(a) Static heel cushion

(b) Static forefoot cushion

(c) Static forefoot bend

(d) Dynamic heel cushion

(e) Dynamic forefoot cushion

(f) Dynamic forefoot bend

Figure 11.4: Results of static and dynamic physical tests on Ultraride midsole assemblies.

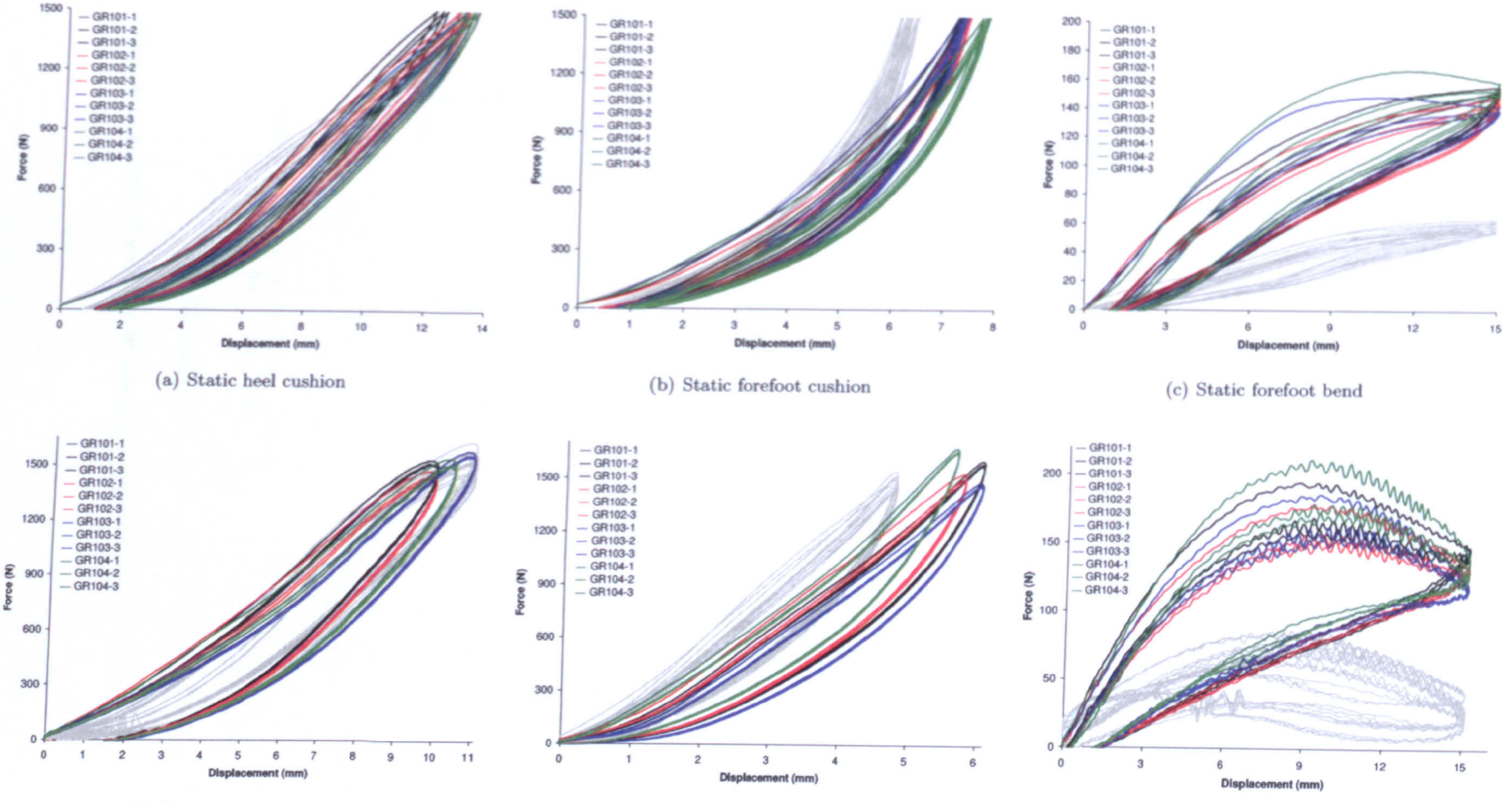

(a) Static heel cushion

(b) Static forefoot cushion

(c) Static forefoot bend

(d) Dynamic heel cushion

(e) Dynamic forefoot cushion

(f) Dynamic forefoot bend

Figure 11.5: Results of static and dynamic physical tests on Gigaride midsole assemblies.

11.2.2 Structural Metric Results

The same structural tracking measurements were recorded for the production shoes tests as were recorded for the assembled midsole tests. Figure 11.6 shows plots of coefficient of restitution (COR) against peak reaction forces. The charts show that while little change was seen in the COR of the Supernova, both the Ultraride and Gigaride production shoes behaved more similarly to the Supernova, indicating that for a given reaction force, the production shoes gave a more consistent energy return that the midsole assemblies alone.

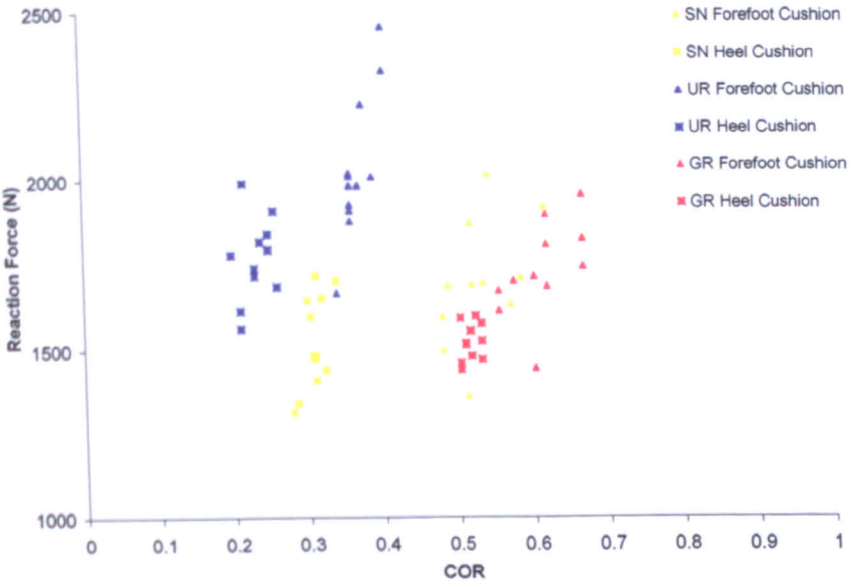

(a) Results from midsole assemblies

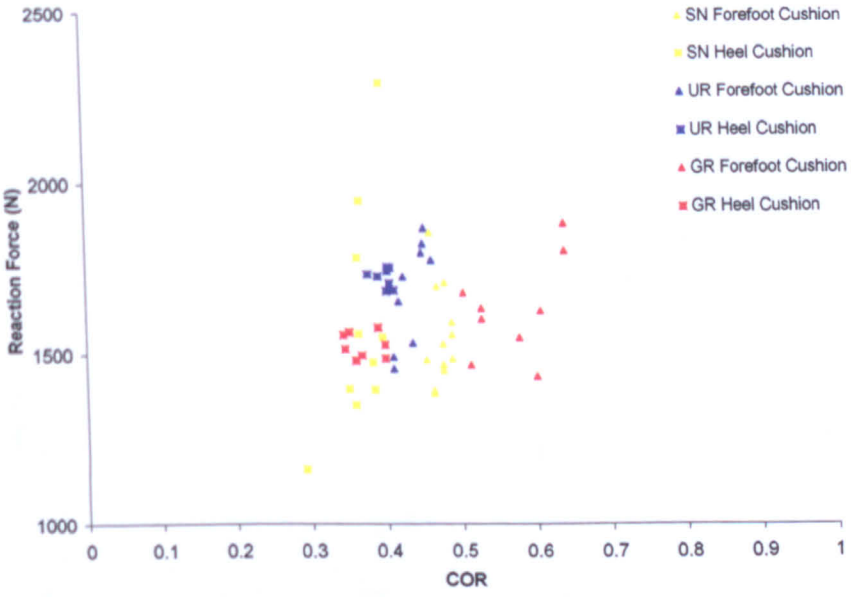

(b) Results from production shoes

Figure 11.6: Plot of coefficient of restitution against peak reaction force for drop testing.

Figure 11.7 shows plots of tip delay against COR. These metrics are dependent on a large range of properties, and it is hypothesised that the grouping seen in Figure 11.7(a) was specific to a particular shoe undergoing the particular cushioning test. The comparison with the production shoes showed that the overall structural response of the shoes coalesced around a specific area. This was particularly prevalent in the heel cushion tests where most of the points occupied a small area.

It was speculated that the point about which the production shoe metrics gathered may be a quantification of the desired properties of a shoe. This would be valid if the production shoes on test were designed based on input from runners concerning their consideration of a 'good' midsole unit. This may be confirmed by testing a much larger range of production shoes that have been designed for the same purpose.

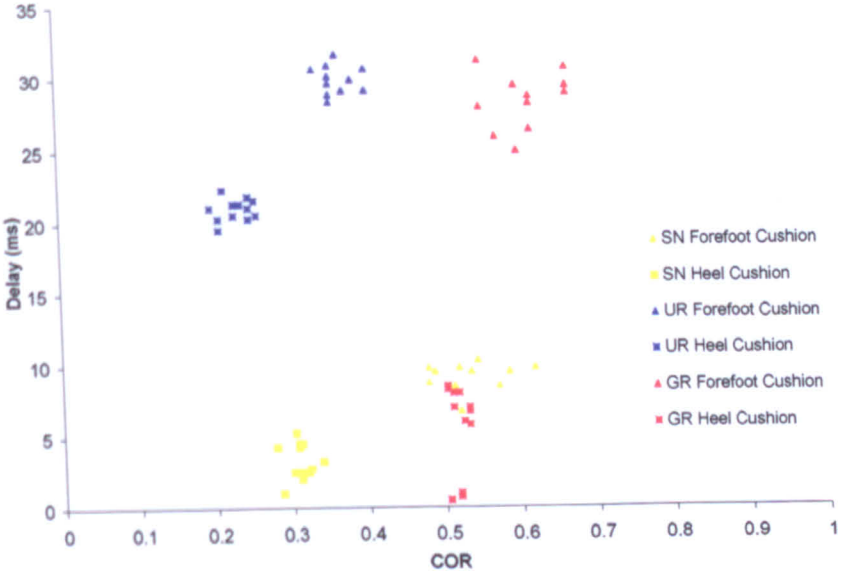

(a) Results from midsole assemblies

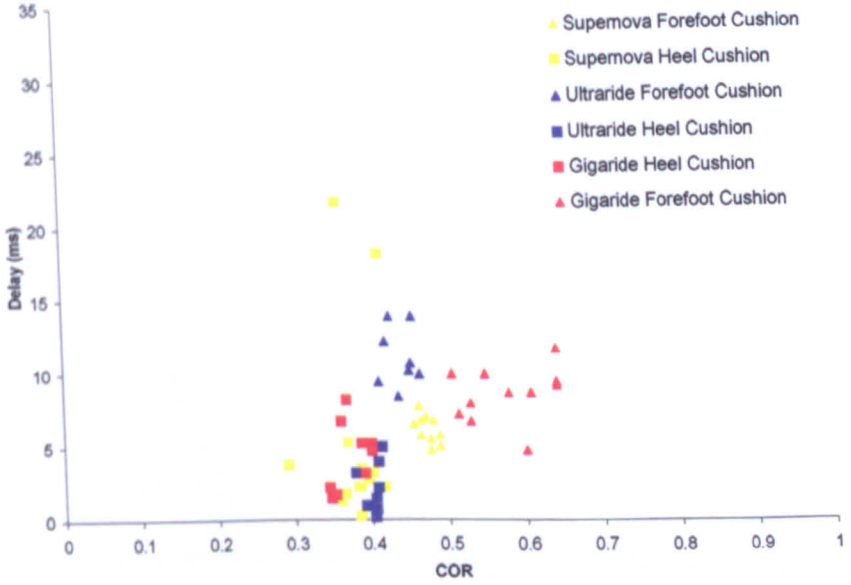

(b) Results from production shoes

Figure 11.7: Plot of tip delay (time between maximum compression and maximum tip height) against coefficient of restitution for drop testing. (a) Shoe assemblies, (b) production shoes.

11.3 Chapter Summary

Physical testing on fully assembled shoes taken from the production line was reported in this chapter. The same tests were performed on shoe assemblies and on the production shoes with most of their uppers cut off.

No significant improvement or degradation in the overall variation between impacts and shoes was seen between the production shoes and the shoe assemblies.

However, it was noted that there was large change in variation between different tests and shoes, so these average values may not be a useful way of comparing the shoes, it is better to look at the individual tests in Tables 9.2 and 11.1 (pages 202 and 247 respectively).

The structural metric results from the production shoes showed stronger grouping between the different shoes and cushioning tests than the shoe assemblies. This suggests that the shoes may be moving around some 'good shoe' metric point which may be useful as a design tool in future.

Chapter 12

Conclusions

Before this research began, work was already being carried out on reverse engineered single part models at adidas, but technology that could produce more detailed models was commercially desirable, ideally one with a performance predicting capacity. More details were given in Chapter 1, but fundamentally the purpose of this research was to answer the question:

Can shoes/shoe components be modelled using FEA techniques purely on the basis of anticipated geometry and sample material properties, with sufficient accuracy to permit reliable prediction of satisfactory/unsatisfactory shoe performance, under laboratory testing conditions and enable subsequent design improvement without physical prototypes?

This chapter responds to this question by splitting it into its constituent parts.

12.1 Athletic Footwear Modelling in FEA

Current FE programs were capable of creating meshed parts of highly irregular shapes and combining these into assemblies, as was shown in Chapter 9. For this research ABAQUS version 6.5 was used in conjunction with Hypermesh 6 for the creation of meshes from complex geometry.

The ABAQUS Explicit solver was used for the majority of the models in this research as the Standard solver was shown to be unable to cope with the complex contact conditions generated by shoe models.

Chapter 10 shows that it was also possible to model internal mechanisms within shoes, including accounting for the initial pre-loading of structures during assembly.

12.2 The Use of Anticipated Geometry

Most of the shoe components used in the models were derived from CAD geometry primarily intended for export to mould-making machines. This original geometry was found to have a large number of import anomalies: very small gaps and extra nodes generated either during the design process or during conversion between one file format and another (as described in Chapter 8). As the geometry was not intended for use in FE analyses, this was not necessarily the fault of the designers. Making them aware of the needs of FE programs may drastically reduce future model set-up times as these small errors prevent the analysis from running and many had to be corrected by hand, which was a very time consuming process.

Most of the components used in the models were derived from the original CAD geometry, except some of the outsole parts, where the level of detail was so great that it caused 1000's of anomalies and thus prevented hand repair within the available time. These parts were approximated by extruding some surfaces of the shoe and outsole.

12.3 The Use of Sample Material Data

The materials issue was much more complex than that of the geometry. The process of taking data from physical samples and inputting this into ABAQUS to generate a workable material model was undertaken in Chapter 7. The accuracy of these models is addressed in the next section. The important points to note from this section of the research are:

- It was proven difficult to create regular shaped test samples from the highly compressible foam materials. Irregular shapes introduce errors into the material calculations as the cross sectional area, and thus the stress, must be averaged.
- The standard clamping equipment used for material testing was found to be unable to hold the highly deformable materials, especially at high strains. This affects the readout of strain and introduces more error. New clamping techniques were presented and shown to be an improvement over the previous equipment.
- No grain dependence or directionality was seen in samples cut from moulded flat sheets. However, a significant difference was observed in the stiffness of material samples cut from sheets, and those pre-moulded into dog-bone shapes, with the pre-moulded samples shown to be up to 100% stiffer at high strains.
- Although multiple modes of deformation (uniaxial, planar and volumetric) were tested, the use of more than the uniaxial mode caused ABAQUS to form an unstable, unrealistic material model. It is suspected that the difficulties experienced with creating accurate samples and tests with the shoe materials, causes too many errors in the data to form a realistic material model, which assumes all tests were perfect.

12.4 The Accuracy of Prediction of Laboratory Testing Models

The laboratory conditions were defined for this research as the heel and forefoot cushion tests and the forefoot bend test (detailed in Section 2.9.5.3). These tests were performed using static and dynamic uniaxial compression/tension machines and a drop testing rig.

12.4.1 Physical Tests

To be able to say how accurate a model was, it was important to assess how accurate the physical shoes were. All testing was carried out on shoes from the same batch, so while shoe-shoe and impact-impact variation can be assessed, the variation between shoes of different batches is unknown. On average the variation in peak force at a consistent maximum displacement was 6% (max. 14%) between impacts on the same shoe and 15% (max. 28%) between different shoes of the same type. The Gigaride was the most consistent shoe, if its very noisy dynamic bend results are excluded, although the other two shoes were fairly consistent for the force/displacement measurement. The variation seen in structural response is discussed later in this section.

During testing it became apparent that the shoe tests were highly sensitive to a small change in displacement loading, resulting in some shoes becoming damaged due to overloading. Care needs to be taken in alignment of the shoe during the tests to prevent damage that may affect future results. All shoes that were damaged in this way were excluded from later testing.

12.4.1.1 Force/Deflection Response

FE models that used the material models generated in Chapter 7, produced reasonably accurate force/deflection results. Figure 12.1 shows the result from the Ultraride dynamic heel cushion test. The graph includes error bars calculated to include the effects of misalignment of the test equipment on the shoe, and between the real and virtual tests. The models were also checked for their sensitivity to changes in velocity and friction (these are included in Appendix 12.7). The s-shapes in the curve were matched, but the FE model was still too stiff. This was generally representative of the inaccuracies seen in the other shoes and tests, with the Supernova giving the best results using the sample material data (all initial results are on pages 203-209).

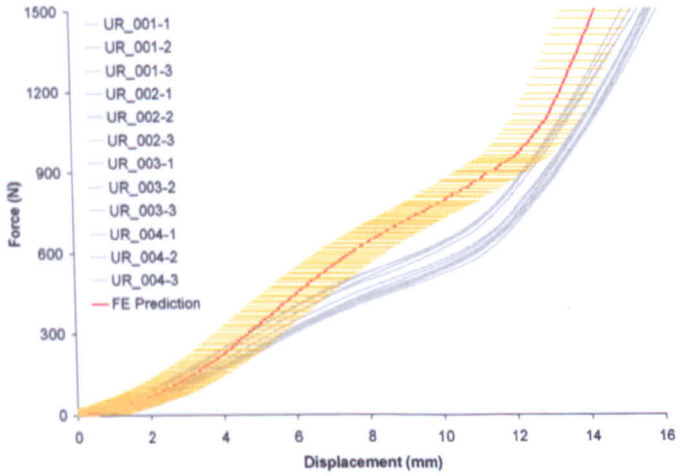

Figure 12.1: Results of the dynamic heel cushion FE model of the Ultraride midsole assembly, using material models taken directly from material sample test data. Orange bars indicate possible error in the FE result due to stamp placement and friction.

The testing of individual parts in Chapter 8 allowed the effect of bonding and boundary conditions to be removed from the test. Figure 12.2 shows the results from compression of the Ultraride structure plate. While the initial prediction is either too soft or too stiff depending on the element used, after the model stiffness is adjusted there is a very good match to the curve shape, indicating the model is capable of predicting the deformation of the part well.

However, no consistency was seen in the error in prediction of the model between the material samples and the shoe part models. Based on this small sample of tests, prediction of shoe part material response, by using material models verified through modelling of material sample tests, is not possible. Much more testing is recommend.

Applying adjustments from verified parts testing to the shoe assembly model, and using the physical data to estimate those materials for which adjustment values were not available, improved all of the test results. Figure 12.3 shows the adjusted Ultraride dynamic heel cushion test. With this adjustment, all of the model results either fell within the range of variation of the shoe testing, or had the error in prediction halved (see pages 212-214).

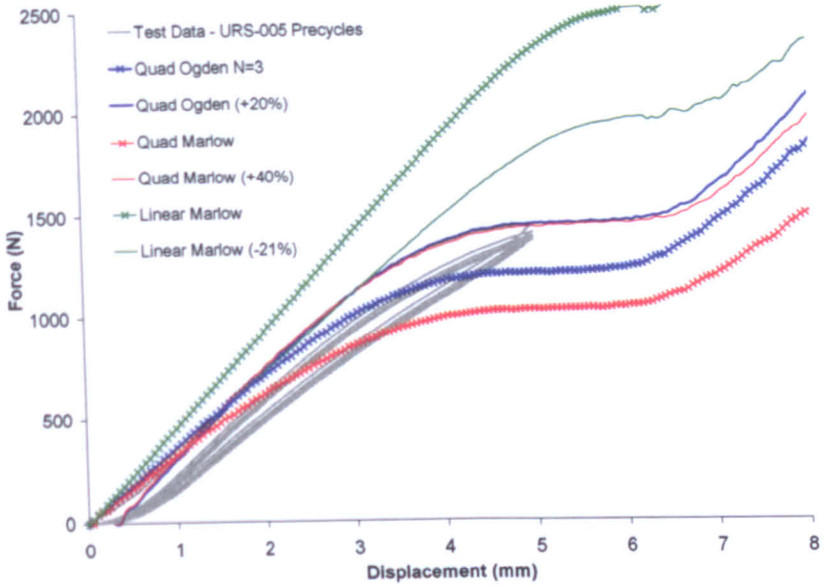

Figure 12.2: Results of FE modelling on the Ultraride structure plate under controlled boundary condition loading. Results from the original and adjusted material models are shown.

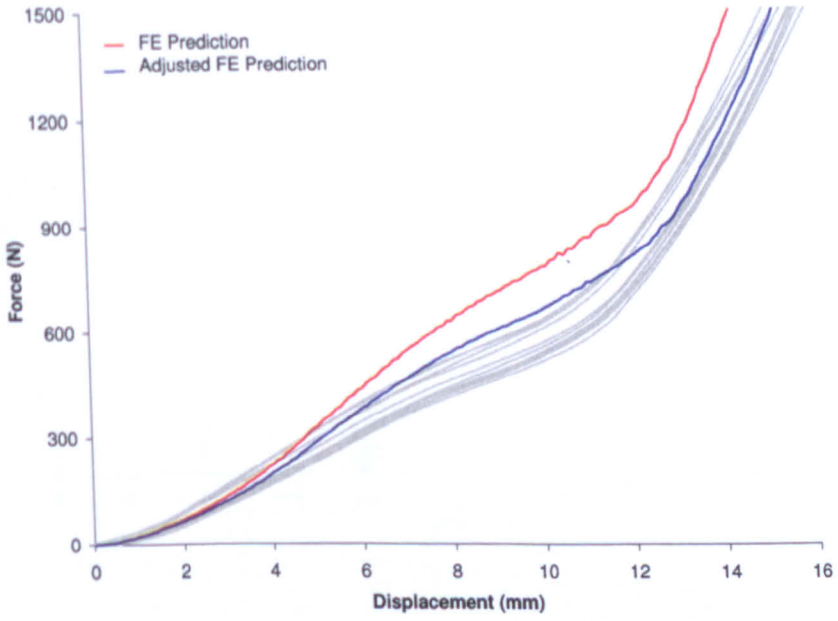

Figure 12.3: Results of dynamic heel cushion FE models of Ultraride midsole assembly, using adjusted and unadjusted material models.

12.4.1.2 Structural Response

The structural tracking method developed in Section 5.5, allowed the analysis of the shape the shoe forms during loading. Figure 12.4 shows that each shoe assembly in each test had a grouping around an individual value for a plot of coefficient of restitution against tip delay. These measures are dependant on a large range of variables which gave a good match between the same shoe assemblies, but a clear difference between different shoe assemblies or tests. Once the shoes are fully assembled on the production line, their physical responses begin to coalesce, suggesting that the response of an acceptable running shoe would fit within the range seen.

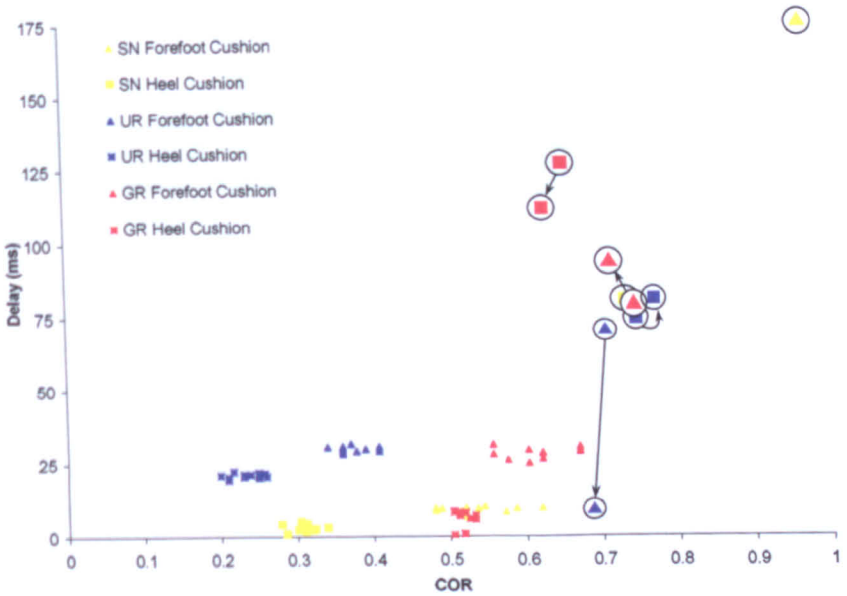

(a)

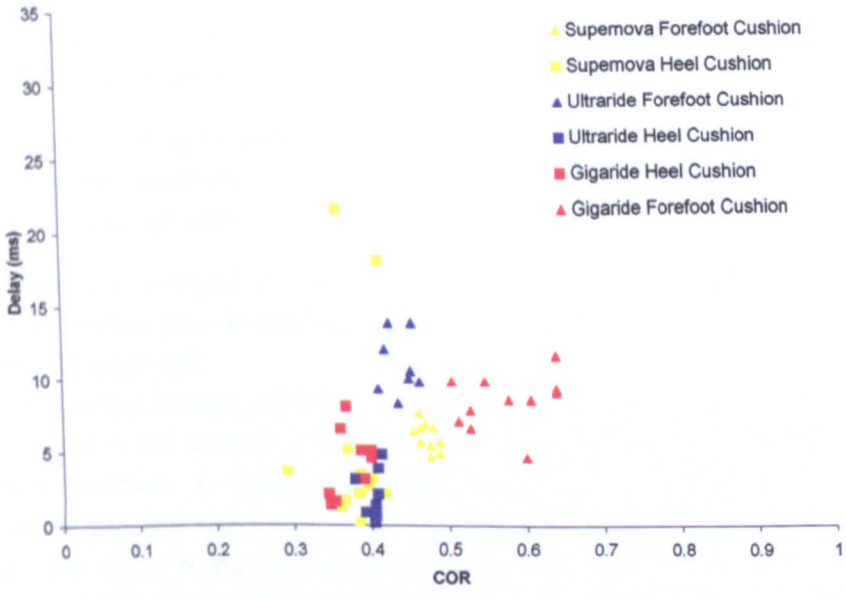

(b)

Figure 12.4: Plot of tip delay (time between maximum compression and maximum tip height) against coefficient of restitution for drop testing. (a) shoe assembly and FE results, (b) production shoe results. Points in circles indicate FE predictions. Arrows indicate change in prediction between initial predictions and those with adjusted material models.

For all the models of samples and parts in this research, it has been easier to obtain a result from a model that matches the deformation well, but poorly predicts the stresses. This occurred when the geometry, boundary conditions and elements were modelling the physical process well, but there had been an error in the material model, or a shift caused by the element type or size that had not been accounted for.

This was reversed in the case of the shoe assembles, where even after the material models had been corrected to give a very good force deflection response, only the Supernova model was capable of producing a structural response that was anywhere close to that seen in reality. Figure 12.5 shows the Gigaride model in a forefoot test, and a still from a high speed video recording of the same test.

(a) Real (b) Virtual

Figure 12.5: Real and virtual Gigaride dynamic forefoot cushion tests at point of maximum tip height (tip is at the posterior for forefoot tests).

Sensitivity studies into the effect of material properties on the structural response indicated that it would not be possible to match the virtual with the real by adjusting the materials; this indicates that the problem is related to a deficiency in the model. Three possible reasons for this have been identified and would need further modelling and/or physical testing to verify:

- The mathematical ties in the assembled model were not connecting the parts together in a realistic way.
- The physical properties of the part-bond-part composite were different from that of the summation of the individual part responses.
- The elements were not transferring bending/tension loads through thin structures (such as the top/bottom plates in the Gigaride and the structure-supporting sections of the Ultraride structure plate).

There is currently no evidence to prove or disprove any of these hypotheses, but it has been observed that bending models under-predicted the stiffness of foam parts by a factor of ten (see Figure 7.20, page 144).

However, during a running strike the shoe is not required to transmit the kind of bending loads experienced in the laboratory tests, as it is strapped to the foot, which forces the shoe into its bent condition. In their current state, the models should predict the cushioning response of the physical shoes well, if used to simulate a type of test that involves only cushioning. The ability to transmit shear forces or other loads has not been assessed, so no conclusion can be drawn on the models' ability to replicate other load conditions.

12.5 Design Improvement Without Physical Prototyping

Based on the material testing, modelling and verification in Chapters 7-9, the ability to create models that accurately predict the response of shoes only from sample material data is not currently possible. However, the majority of the models show a reasonable prediction of the physical results, and can be used within the design process to identify areas that require further investigation, such as areas of high stress and possible failure sites.

This would also extend to wear modelling. It has been shown with the Ultraride structure plate Mullins effect model, that very good agreement with the physical results is possible with sample test data and adjustment based on sample test modelling.

It is believed that the only way to achieve a fully predictive technology is with significant research directed at the nature and processing of the materials used, along with extensive physical testing.

12.5.1 Setup and Processing Times

Because of the work undertaken in this research the time it takes to set-up and run FE shoe models of a range of types is well understood.

12.5.1.1 Geometry Import and Meshing

The conversion of CAD design geometry, designed for mould construction, into a form suitable for creating FE meshes was highly dependant on the amount of small anomalies in the geometry. The Ultraride model contained many of these, and a combination of this and relative inexperience with the correcting tools at the time, resulted in the model taking 2-3 months to construct. However, the geometry found in the Gigaride was much more suitable for FE, which, combined with more experience with the correcting tools and the knowledge concerning what needed to be corrected (Chapter 8), allowed a full CAD geometry to FE model construction time of two days. This timescale is expected to be quicker than the process of constructing moulds, creating and testing prototypes, and so would be useful for checking for any major performance problems before the final moulds are created.

12.5.1.2 Processing Times

The computer used in this research was a twin Xeon (2.8 GHz) processor 32-bit workstation with IDE hard drives. The times quoted in Table 12.1 are for a single CPU, so using a twin/quad processor should halve/quarter the time, and using fast hard drives (such as SATA) will reduce the time further for analyses where large amounts of output data are required. For the sensitivity studies in Section 9.7, both dynamic cushioning and the bend test models could be run overnight, although the static tests were much slower. For the processing of the static results, four similar computers were linked up allowing approximately 20 analyses to be run over a weekend. Set up time for these jobs was minimal (less than 5 minutes) as only single parameters were changed. New tests on existing models generally took 15-30 minutes to set up (with no large changes in the model assembly). Processing models that require assembly steps, such as those for mechanisms, or models that simulate cyclic damage, required much longer. The Mullins effect model of the full Gigaride assembly in Section 9.8, took 88 CPU hours to run for 5 quasi-static compression cycles (modelling a physical time of 25 seconds). The mechanism models generally took 24 CPU hours to model the assembly process then 4 CPU hours to run the test.

Test	Supernova	Ultraride	Gigaride
	Static (CPU hours)		
Heel Cushion	14	28	9
Forefoot Cushion	14	30	15
Forefoot Bend	14	20	18
Part (C3D4 elements)	0.4	1.5	0.5
Cyclic (full shoe assembly)	-	-	88
	Dynamic (CPU hours)		
Heel Cushion	2.5	5	5
Forefoot Cushion	2	3.5	3
Forefoot Bend	4	9	7

Table 12.1: Processing times in CPU hours for the adjusted models used to calculate the majority of the results presented in this thesis.

12.5.1.3 Material Testing

Material testing was by far the longest process during modelling, as the samples had to be created, tested, then the results analysed, converted for input into ABAQUS and the accuracy checked by modelling the tests. This process, even with experience of test methods and data handling, took in excess of two months of solid work. However, the material sensitivity studies in Section 9.7 have shown that acceptable force/deflection results can be obtained if only certain critical materials are modelled specifically; the rest of the materials need only a fair estimation. The material models created for this research could be used in future models, significantly reducing the work needed to create an accurate shoe model.

In general, if the material properties are available, then the entire modeling and initial processing could be completed within three days on a single computer, for a set of the three standard dynamic mechanical tests.

12.5.1.4 Optimal Modelling Process

In an attempt to assess the quickest modelling process that would elicit the most amount of useful information, the flowchart in Figure 12.6 was drawn up. The setup time of the geometry is assumed to be consistent between shoes, and it is also assumed that the required critical materials are determined by engineering judgement (such as those materials directly under the impactor for cushioning tests), or from previous testing. At this point three models with three meshes are created; a performance model that is designed to accurately predict stresses, a development model that is used for sensitivity studies, and a fast model that consists of the minimum amount of elements and could be used for feasibility studies for such things as new test devices (where many trial and error analyses may be required).

After the models are created, the development model is run to obtain the initial operating strains and the material models are then adjusted to fit these (as was shown in Section 7.2.1). These material models are then applied to the development and fast models and these could then be used in the knowledge that they will give reasonable accuracy, but will process quickly so numerous analysis could be run.

For the performance model, the first analysis is run, then the operating strains checked for any slight changes, and adjusted. This model will now process the slowest, but will give the highest accuracy, and should be run once the error in the model due to friction/setup/density/velocity is derived using the faster models. Following this approach, the minimal processing time for the maximum enlightenment should be achieved.

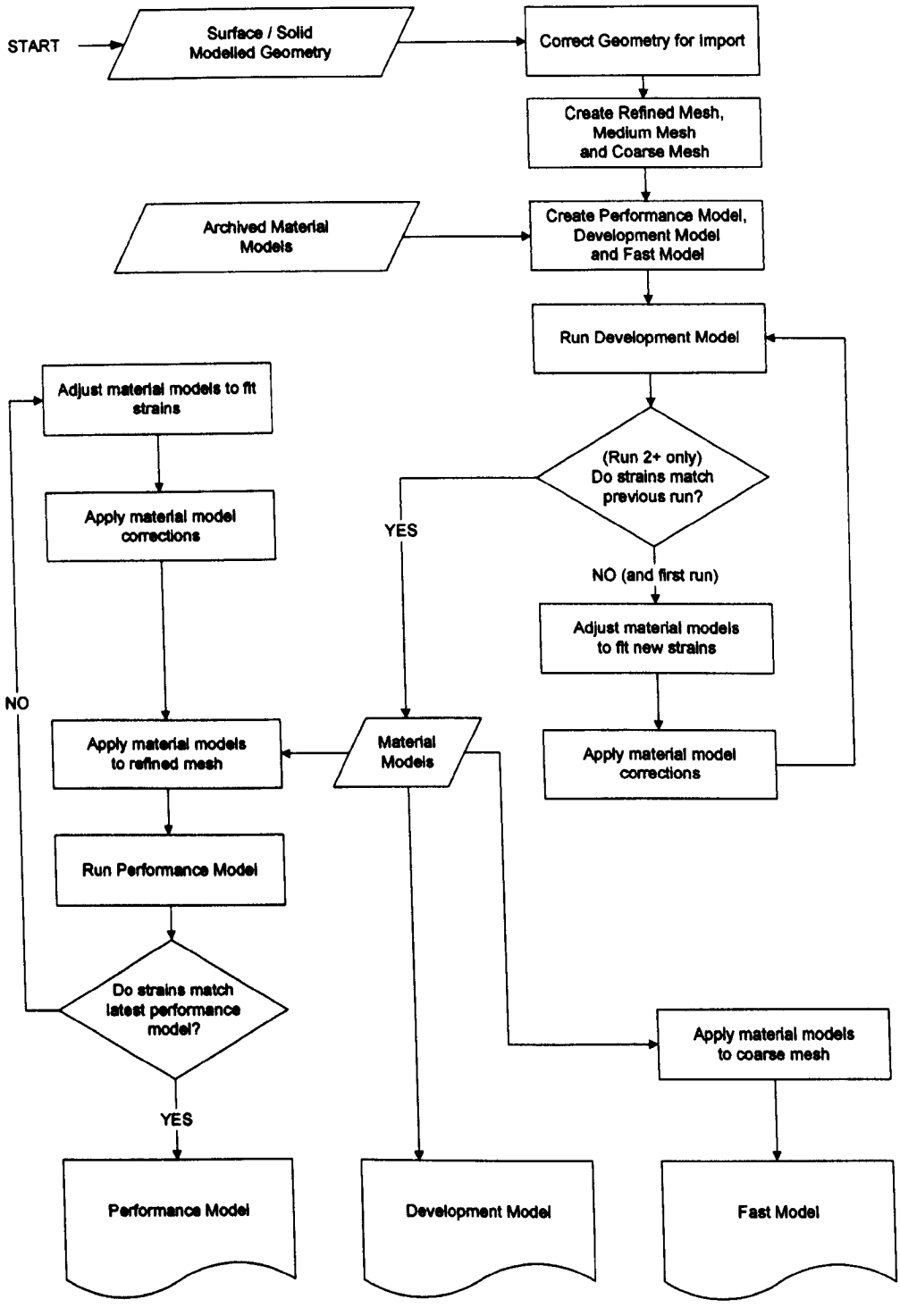

Figure 12.6: Overall process flowchart for creation of tuned predictive shoe models.

12.6 Future work

This work has shown that the FE modelling of athletic footwear is possible. This section details areas where additional research could take the technology much further.

12.6.1 Shoe Remodelling

The rapid development of computer systems and programs is part of the nature of computer-based research. New techniques and methods have presented themselves during the course of the research and many of these have been included, but there had to be a cut-off point.

One of the most useful of these advancements that have not been included is the morphing capability of Hypermesh. This allows regular hexahedral meshes to be distorted into irregular shapes. There is scope for this to be performed on the Gigaride geometry, as it contains more regularly shaped structures than the Ultraride. Use of the hexahedral elements would require more distortion controls (see Section 4.6.3), but the large performance advantage they offer over tetrahedrals could outweigh the risk of them collapsing during an analysis.

New material potentials have emerged that allow the combination of viscoelastic and Mullins effect modelling over a large range of strains. These would be extremely useful for cyclic wear modelling as they could use the Mullins and DMA data already collected.

The reconstruction of the TPU shoes using a combination of 3D solid and 2D shell elements may improve the poor structural metric results.

12.6.2 Physical Testing

While this research has generated new testing methods and taken physical measurements which show trends, all the shoes tested were from the same batches. The shoe parts and assemblies were taken off the same production line as the production shoes. Because of this, the variation between different batches of shoes has not been assessed. This may be a difficult task to achieve, as the loading history of test samples should be known, so purchasing shoes from shops may introduce significant errors into testing, and does not allow parts or midsoles to be tested. What is needed is a systematic removal and testing of shoes of many types, and from different production lines at different times. This can only be done practically by the shoe manufacturer or someone working specifically on testing on their behalf.

The same systematic approach is also needed for the assessment of material properties. A 100% difference was seen in stiffness between two sample material sheets of the same material. The ability to understand the difference between the materials being tested and the ones in the shoes (including any changes caused by adhesives) would allow much more accurate prediction. Assuming the batch variability in properties is low, and the structural modelling issue can be solved, then this materials knowledge is the last step in creating a fully predictive technology.

One other point that has come from the physical testing concerns the damage shoes receive from large impacts. It is hypothesised that a large jump could alter the properties enough for a runner to notice the change, or alternatively, a deliberate damaging of the shoe during production could pre-stress the shoe in a controllable way, reducing peak stresses that could cause part failure. A pre-stressing may also have the effect of reducing variability between shoes, but all of these hypothesis would require extensive testing to verify.

12.7 Future Use of Technology

This research has advanced the FE modelling of athletic footwear to a stage where a models can be used to predict shoe performance with an acceptable accuracy. It is predicted that one or two more research projects would be able to complete the future work required to address the issues with materials and the poor structural response, making the technology fully predictive. At this point it could have a massive impact on the industry, as shoes could be designed and thoroughly tested without any prototyping, making the process quick and inexpensive.

With new design process tools emerging that can integrate FE and CAD software, there is scope for standardised FE testing to be run as a macro function in the CAD program; a design could be created, then the shoe/part mesh automatically created and the results compiled and reported back to the designer. This would allow new, more radical (and possibly more headline-grabbing) designs to be assessed very quickly, perhaps using a bank of more realistic tailored test conditions (85 kg overpronator, 65 kg sprinter etc.).

Programs also exist that can optimise geometry based on a desired output (such as cushioning), iterating through design changes, meshing, processing an FE analysis and automatically feeding the results back into the next iteration. If this kind of technology was applied to shoes, it may be possible to quickly engineer lighter TPU structures, or create novel new designs. These kinds of integrated processes are already being carried out on high-volume consumer goods such as mobile phones, so adapting the technology to shoes should be a relatively straightforward process.

Perhaps the most novel part of this research is the suggestion that the grouping of the production shoe structural metrics around a point indicates the possibility of putting a number onto what runners consider to be a good running shoe in terms of its structural response. Stiffness measures at specific points on the force/deflection curve are already used for comparison of shoes, but if these were combined with the metrics that included shock transmission properties, there is the possibility of creating a design specification of a 'good' shoe. This quantified, measurable set of rules would allow much better comparison of shoe designs and quicker identification of designs that may or may not be able to achieve the desired values. This would help direct development costs to the most promising areas, and ensure a competitive advantage was maintained.

Publications Arising from this Work

Gibbs, P.J., Mitchell, S.R., Harland, A.R. (2006) The use of Stereoscopy and High-Speed Video for the Measurement of Quasi-Static and Dynamic Shoe Loading Scenarios, In: Haake, S., Moritz, E.F. (Eds.) *The Engineering of Sport 6: Developments for Innovation*, Blackwell Science Ltd., pp409-414.

References

adidasSalomon (2004). Katalog frhjahr/sommer 2004 - shuhe damen. *http://www.adidas.com*, Last Accessed: 25 May 2004.

Aerts, P. & De Clercq, D. (1993). Deformation characteristics of the heel region of the shod for during a simulated heel strike: The effect of varying midsole hardness. *Journal of sports sciences.*, **11**, 449–461.

Akhlaghi, F. & Pepper, M.G. (1996). In-shoe biaxial shear force measurement the kent shear system. *Medical & biological engineering & computing*, **34**, 315–317.

Alley, L. & Nichols, G. (1999). Future technical challenges for the pu industry in athletic footwear production. *Utech Asia '99.Conference proceedings*, 1–4.

Anon. (2003). Performance technology. *adidas-Salomon internal report.*.

Anon. (2004). Human evolution. *http://sci.waikato.ac.nz/evolution/HumanEvolution.shtml*, Last Accessed; 8 July 2004.

Arendse, R. (2003). Pronation and the mechanisms of running injuries. *http://www.time-to-run.com/footwear/mechanisms.htm*, Last Accessed; 7 July 2004.

ASTM D3183 (1992). Practice for rubber - preparation of test pieces for test purposes from products. *ASTM International*, West Conshohocken, PA, 19428–2959 USA.

ASTM D3574 (1995). Standard test method for flexible cellular materials - slab, bonded and molded urethane foams. *ASTM International*, West Conshohocken, PA, 19428–2959 USA.

ASTM D3575 (1993). Standard test method for flexible cellular materials made from olefin polymers. *ASTM International*, West Conshohocken, PA, 19428–2959 USA.

ASTM D3767 (1996). Practice for rubber - measurements of dimensions. *ASTM International*, West Conshohocken, PA, 19428–2959 USA.

ASTM D638 (1996). Standard test method for tensile properties of plastics. *ASTM International*, West Conshohocken, PA, 19428–2959 USA.

ASTM F1614 (1999). Standard test method for shock attenuating properties of materials systems for athletic footwear. *ASTM International*, West Conshohocken, PA, 19428–2959 USA.

ASTM F1976 (1999). Standard test method for cushioning properties of athletic shoes using an impact test. *ASTM International*, West Conshohocken, PA, 19428–2959 USA.

ASTM F869 (2001). Standard terminology relating to athletic shoes and biomechanics. *ASTM International*, West Conshohocken, PA, 19428–2959 USA.

Bates, B.T. (1985). *Testing and evaluation of running shoes*, 128–132. Biomechanics IX-B, University Park Press, Baltimore.

Bates, B.T., James, S.L., Osternig, L.R. & Sawhill, J.A. (1981). *Effects of running shoes on ground reaction forces*, 226–233. Biomechanics VII-B.

Bates, B.T., Osternig, L.P., Sawhill, J.A. & James, S.L. (1983). An assessment of subject variability, subject-shoe interaction and the evaluation of running shoes using ground reaction force data. *Journal of Biomechanics*, **16**, 181–192.

Bauman, J.T. (1998). A theory of the elastomer stress-strain curve. In *Meeting of the Rubber Division, American Chemical Society, Nashville, Tennessee*, 1–45.

Baumann, W., Krabbe, B. & Galbierz, P. (1995). Life characteristics of running shoes and shoe material. In *Second Symposium of the International Society of Biomechanics Working Group on Functional Footwear*, 38–39.

Beals, J.T. & Thompson, M.S. (1997). Density gradient effects on aluminium foam compression behaviour. *Journal of Materials Science*, **32**, 3595–3600.

Ben-Dor, G., Cederbaum, G., Mazor, G. & Igra, O. (1996a). Well tailored compressive stress-strain relations for elastomeric foams in uni-axial stress compression. *Journal of Materials Science*, **31**, 1107–1113.

Ben-Dor, G., Mazor, G., Cederbaum, G. & Igra, O. (1996b). Stress-strain relations for elastomeric foams in uni-, bi- and tri-axial compression modes. *Archive of Applied Mechanics*, **66**, 409–418.

Bergmann, G., Kniggendorf, H., Graichen, F. & Rohlmann, A. (1995). Influence of shoes and heel strike on the loading of the hip joint. *Journal Of Biomechanics*, **28**, 817–827.

Bergström, J.S. (2006a). User subroutines section. *http://www.polymerfem.com/*, Last Accessed; 16 July 2006.

Bergström, J.S. (2006b). Advanced finite element modeling of polymer foam components. *ABAQUS Users' Conference 2006, Boston, MA, USA.*, 81–94.

Blatz, P.J. & Ko, W.L. (1962). *Application of Finite Elastic Theory to the Deformation of Rubbery Materials*, vol. VI of *Transactions of the Society of Rheology*, 223–251.

Brandel, B. & Lakes, R.S. (2001). Negative poisson's ratio polyethylene foams. *Journal of Materials Science*, **36**, 5885–5893.

BS 903-A35: 1995 ISO 471:1995 (1995). Rubber - temperatures humidity's and times for conditioning and testing. *British Standards Institution*, London, UK.

BS 903-A36: 1995 ISO 4661-1:1993 (1999). Physical testing of rubber - method of preparation of samples and test pieces - part 1: Physical tests. *British Standards Institution*, London, UK.

BS 903-A38: 1991 ISO 4648:1981 (1999). Rubber, vulcanised or thermoplastic - determination of dimensions of test pieces and products for test purposes. *British Standards Institution*, London, UK.

BS EN 12743:1999 (2005). Footwear - test methods for outsoles - compression energy. *British Standards Institution*, London, UK.

BS EN 13400:2002 (2005). Footwear - sampling location, preparation and duration of conditioning of samples and test pieces. *British Standards Institution*, London, UK.

BS ISO 23529:2004 (2005). Rubber, general procedures for preparing and conditioning test pieces for physical test methods. *British Standards Institution*, London, UK.

BS ISO 37:2005 (2005). Rubber, vulcanized or thermoplastic - determination of tensile stress-strain properties. *British Standards Institution*, London, UK.

Burge, C. (2001). Comment on barefoot running. *Sports Science; http://www.sportsci.org*, Last Accessed; 1 June 2004.

Cavanagh, P.R. (1980). *The Running Shoe Book*. Anderson World, Inc, Mountain View, CA, 1st edn.

Chakravarty, U., Mahfuz, H., Saha, M. & Jeelani, S. (2003). Strain rate effects on sandwich core materials, an experimental and analytical investigation. *Acta Materialia*, **51**, 1469–1479.

Chen, W.P., Ju, C.W. & Tang, F.T. (2003). Effects of total contact insoles on the plantar stress redistribution: a finite element analysis. *Clinical Biomechanics*, **18**, S17–S24.

Cheung, J.T.M. & Zhang, M. (2006). Finite element modeling of the human foot and footwear. *ABAQUS Users' Conference 2006, Boston, MA, USA.*, 145–159.

Chino, Y., Mabuchi, M., Yamada, Y., Hagiwara, S. & Iwasaki, H. (2003). An experimental investigation of effects of specimen size parameters on compressive and tensile properties in a closed cell al foam. *Materials Transactions*, **44**, 633–636.

Clarke, T.E., Frederick, E.C. & Cooper, L.C. (1983). Effects of shoe cushioning upon ground reation forces in running. *International Journal of Sports Medicine*, **4**, 25–33.

D'Agati, M. (1993). A nonlinear finite element analysis of a running shoe midsole. *14th International Society of biomechanics congress, paris France*, 302–303.

Day, J. & Miller, K. (2000). Equibiaxial stretching of elastomeric sheets, an analytical verification of experiemental technique. *Axel Products Inc; www.axelproducts.com*, Tech. Rep. - EquibiaxialStretchingRev2, Last Accessed; 4 Mar 2006.

De Clercq, D., Aerts, P. & Kunnen, M. (1994). The mechanical characteristics of the human heel pad during foot strike in running, an in vivo cineradiographic study. *Journal of Biomechanics*, **27**, 1213–1222.

De Wit, B. & De Clercq, M., D. L. (1995). The effect of varying midsole hardness on impact forces and foot motion during foot contact in running. *Journal of Applied Biomechanics*, **11**, 395–406.

De Wit, B., De Clercq, D.A. & Aerts, P. (1996). Ground reaction forces and spatio-temporal variables during barefoot and shod running. In *14th International Symposium on Biomechanics in Sports*, 252–255.

De Wit, B., De Clercq, D. & Aerts, P. (2000). Biomechanical analysis of the stance phase during barefoot and shod running - some possible relationships. *Journal of Biomechanics*, **33**, 269–278.

Dhingra, P. & Jablonski, N.G. (2004). Comparative bipedalism - how the rest of the animal kingdom walks on two legs.

Dixon, S., Collop, A. & Batt, M. (2000). Surface effects on ground reaction forces and lower extremity kinematics in running. *Medicine Science in Sports Exercise*, **32**, 1919–1926.

El-Ratal, W.H. & Mallick, P.K. (1996). Elastic response of flexible polyurethane foams in uniaxial tension. *Journal of Engineering Materials and Technology*, **118**, 157–161.

Foto, J.G. (1995). Bench-top testing of insole orthotic materials for use in therapeutic footwear.

Frederick, E.C. & Clarke, C., T. E. H. (1984). The effect of running shoe design on shock attenuation. *Sports Shoes and Playing Surfaces*.

Frederick, E.C. & Hagy, J.L. (1986). Factors affecting peak vertical ground reaction forces in running. *International Journal of Sports Biomechanics*, **2**, 41–49.

Garcia, A.C., Ramiro, J., Ferrandis, R., Clement, V., Alwpuz, R., Vera, P. & Hoyos, J.V. (1992). Dynamic study of footwear materials simulating real loads. *Institute of biomechanics of Valencia (IBV), Spain*, **15**, 239–242.

Gent, A.N. & Thomas, A.G. (1959). The deformation of foamed elastic materials. *Journal of Applied Polymer Science*, **1**, 107–113.

Gibson, L.J., Ashby, M.F. & Kumar, K.S. (1998). *Cellular Solids, Structure and Properties, 2d ed.* Cambridge University Press, UK, 2nd edn.

Henning, E.M. & Milani, T.L. (1995b). In-shoe pressure distribution for running in various types of footwear. *Journal of Applied Biomechanics*, **11**, 299–310.

Henning, E.M., Lafortune, M.A. & Lake, M.J. (1995a). The influence of midsole material and knee flexion on energy return in simulated running impacts. In *Second Symposium of the International Society of Biomechanics Working Group on Functional Footwear*, 2–3.

James, B., S.L. Bates & Osternig, L.R. (1978). Injuries to runners. *American Journal of Sports Medicine*, **6**, 40–50.

Kinoshita, H. & Bates, B.T. (1996). The effect of environmental temperature on the properties of running shoes. *Journal of Applied Biomechanics*, **12**, 258–268.

Knoerr, K. & Rouiller, V. (2002). Integrating high performance pu-materials in sportshoe's. In *Polyurethanes Expo*, 533–537.

Krantz, G.S. (1972). Anatomy of the sasquatch foot. *http://www.rfthomas.clara.net /papers/anatomy.html*, Last Accessed; 25 May 2004.

Léon, J. & Fine, L. (2005). A new approach to the preparation of models for FE analyses. *Int. J. of Computer Applications in Technology*, **23**, 166–184.

Lewis, G. (2003). Finite element analysis of a model of a therapeutic shoe, effect of material selection for the outsole. *Biomedical Materials and Engineering*, **13**, 75–81.

Lucas, T. (2004). Condfiential foam research. *adidas-Salomon internal report*.

Luethi, S.M., Denoth, J., Kaelin, X., Stacoff, A. & Stuessi, E. (1987). *The influence of the shoe on foot movement and shock attenuation in running.*, 931–935. International Series on Biomechanics, Human Kinetics Publishers, Inc., biomechanics x-b edn.

Mara, G. (2006). Boundary conditions for the virtual testing of athletic footwear. *Unpublished Thesis*, Loughborough University, UK.

McCauley, M. (1999). VB FTT Release 2-B Computer code. *www.fullspectrum.com/deeth/programming/fft.html*, Last Accessed; 4 April 2006.

McNeel (2006). Rhinoceros - nurbs modeling for windows. *http://www.rhino3d.com/*, Last Accessed; 15 May 2006.

Miller, K. (2000a). Experimental loading conditions used to implement hyperelastic and plastic models. *Axel Products Inc; www.axelproducts.com*, Last Accessed; 7 Mar 2006.

Miller, K. (2000b). Testing elastomers for hyperelastic material models in finite element analysis. *Axel Products Inc; www.axelproducts.com*, Tech. Rep. – TestingForHyperelastics, Last Accessed; 4 Mar 2006.

Mills, N.J. (2003a). *Foam Protection In Sport*, chap. 2, 9–46. Materials In Sports Equipment.

Mills, N.J. (2003b). *Running Shoe Materials*, chap. 4, 65–99. Materials in Sports Equipment.

Mills, N.J. & Gilchrist, A. (1997). The effect of heat transfer and poisson's ratio on the compressive response of closed cell polymer foams. *Cellular Polymers*, **16**, 87–109.

Mills, N.J. & Gilchrist, A. (2000a). High strain extension of open-cell foams. *Journal of Engineering Materials and Technology*, **122**, 67–73.

Mills, N.J. & Gilchrist, A. (2000b). Modelling the indentation of low density polymer foams. *Cellular Polymers*, **19**, 389–412.

Mills, N.J. & Lyn, G. (2002). Experiments and modelling of air flow in impacted flexible polyurethane foams. *Cellular Polymers*, **21**, 343–367.

Mills, N.J. & Rodriguez-Perez, M.A. (2001). Modelling the gas-loss creep mechanism in eva foam from running shoes. *Cellular Polymers*, **20**, 79–100.

Mills, N.J. & Zhang, P.S. (1989). The effects of contact conditions on impact tests on plastics. *Journal of Material Science*, **24**, 2099–2109.

Mills, N.J. & Zhu, H.X. (1999). The high strain compression of closed-cell polymer foams. *Journal of the Mechanics and Physics of Solids*, **47**, 669–695.

Nakabe, N. & Nishiwaki, T. (2002). *Development of simplified numerical foot model for sole stability design*. The Engineering of Sport 4.

Nigg, B.M., Bahlsen, H.A., Luethi, S.M. & Stokes, S. (1987). The influence of running velocity and midsole hardness on external impact forces in heel-toe running. *Journal of Biomechanics*, **20**, 951–959.

Nike Inc. (2004). Nike running homepage. *http://www.nike.com/nikerunning/*, Last Accessed; 25 May 2004.

Nishiwaki, T. & Nakabe, N. (2002). *Numerical design of running shoes based on human response.*, 393–399. The Engineering of Sport 4.

Noe, D.A., Voto, S.J., Hoffmann, M.S., Askew, M.J. & Gradisar, I.A. (1993). Role of the calcaneal heel pad and polymeric shock absorbers in attenuation of heel strike impact. *Journal of Biomedical Engineering*, **15**, 23–26.

O'Neil, D. (2004). Neandetals. *http://anthro.palomar.edu/homo2/neandertal.htm*, Last Accessed; 15 July 2004.

Onoda, K.K. & Kawasima, Y.K. (1985). Midsole assembly for an athletic shoe. *USA Patent: 522700, application 4561195*, Class Codes;36/30R; 36/28; 36/31; 36/32 R, Issue Date; 31 December 1985.

Pajon, M. & Backacha, M. (1996). Modelling of pu foam behaviour - applications in the field of automotive seats. Tech. Rep. SAE SP-1155 960513.

Patterson, J. (1998). Vinyl foam: Effect of density on physical properties. *Journal of Vinyl & Additive Technology*, **4**, 26–29.

RAD Game Tools Inc. (1997). Radvideo. *http://www.radgametools.com/*, Last Accessed; 9 June 2006.

Radin, E.L., Parker, H.G., Pugh, J.W., Steinberg, R.S., Paul, I.L. & Rose, R.M. (1973). Response of joints to impact loading. relationship between trabecular microfractures and cartlidge degeneration. *Journal of Biomechanics*, **6**, 51–57.

Rasband, W. (1997). Imagej. *http://rsb.info.nih.gov/ij/*, U. S. National Institutes of Health, Bethesda, Maryland, USA. Last Accessed; 17 Aug 2006.

Raue, F. & Ehrenstein, G.W. (1997). Prediction of the static deformation behavior of thermoplastic polyurethane (tpu) by using dynamical tesing procedures. In *55th Spe. Proceedings ANTEC*, vol. 3, 3440–3444, The Society, [Brookfield Center, CT].

Reebok (2004). Reebox premier road lite. *http://www.reebok.com/us/vector/running/products*, Last Accessed; 25 May 2004.

Reyes, A., Hopperstad, O.S., Berstad, A.G., Hanssen, A.G. & Langseth, M. (2003). Constitutive modelling of aluminium foam including fracture and statistical variation of density. *European Journal of Mechanics A/Solids*, **22**, 815–835.

Rudy, M.F. (1980). Insole construction for articles of footwear. *USA Patent*, Class Codes; 36/44; 36/29, A43B 013/38; A43B 013/20; A61N 000/00.

Runner's World (2004). Runner's world buyer's guide spring 2004. *Magazine Pamphlet*, Rodale Ltd., UK.

Runner's World (2004a). Runner's world jargon buster. *http://www.runnersworld.ltd.uk/jargon.htm*, Last Accessed; 25 May 2004.

Russell, R. & Wilson, M. (1991). Calculating flex crack risks by fea computer analysis. *SATRA Bulletin Oct.1991*, 268–269.

Saucony Inc. (2003). Running Shoes - Mens Training - 3D Grid Triumph. *http://www.saucony.com/*, Last Accessed; 25 May 2004.

Shiang, T. (1997). The nonlinear finite element analysis and plantar pressure measurement for various shoe soles in heel region. *Proceedings of the National Science Council, Republic of China.Part B, Life sciences.*, **21**, 168.

Shiba, N., Kitaoka, H.B., Cahalan, T.D. & Chao, E.Y.S. (1995). Shock-absorbing effect of shoe insert materials commonly used in management of lower extremity disorders. *Clinical Orthopaedics and Related Research.*, **310**, 130–136.

Shulmeister, V., Nijhof, A.H.J., Marissen, R. & for Materials Science, N.S. (1997). Linear elastic closed-cell foam modelling. 2/13.

Sims, G.L.A. & Pentrakoon, D. (1997). Initial impact studies on open and closed-cell foams. *Cellular Polymers*, **16**, 431–443.

Snel, J.G., Delleman, N.J., Heerkens, Y.F. & van Ingen Schenau, G. (1983). Shock-absorbing characteristics of running shoes during actual running. In *9th Congress of Biomechanics*, 133–138.

Swigart, J.F. & Erdman, A.G. (1995). modelling the impact load buffering characteristics of footwear midsoles.

Thomson, R.D., Birkbeck, A.E., Tan, W.L., McCafferty, L.F., Grant, S. & Wilson, J. (1999). The modelling and performance of training shoe cushioning systems. *Sports engineering (Oxford, England.*

Throne, J.L. & Progelhof, R.C. (1984). Closed-cell foam behaviour under dynamic loading. i. stress-strain behaviour of low-density foams. *Journal of Cellular Plastics*, **20**, 437–442.

Throne, J.L. & Progelhof, R.C. (1985a). Closed-cell foam behaviour under dynamic loading. ii. loading dynamics of low-density foams. *Journal of Cellular Plastics*, **21**, 43–50.

Throne, J.L., Progelhof, R.C. & Kumar, S. (1985b). Closed-cell foam behaviour under dynamic loading. iii. impact loading of high-density foams. *Journal of Cellular Plastics*, **21**, 123–140.

Ujihashi, S., Woo, S.H. & Inou, N. (1998). Method of measurement and evaluation for the mechanical characteristics of running shoes.

Valiant, G.A., McMahon, T.A. & Frederick, E.C. (1987). *A new test to evaluate the cushioning properties of athletic shoes.*, 937–941. Biomechanics X-B, Human Kinetics Publishers, Inc.

Vanderbilt, T. (1998). *The Sneaker Book*. The New Press, New York, 1st edn.

Verdejo, R. & Mills, N.J. (2002). *Performance of EVA foam in running shoes*, 580–587. The Engineering of Sport 4.

Verdejo, R. & Mills, N.J. (2004). Simulating the effects of long distance running on shoe midsole foam. *Polymer Testing*, **23**, 567–574.

Warren-Forward, M.J., Goodall, R.M. & Pratt, D.J. (1992). Three-dimentional displacement and force transducer. *IEE Proceedings-A*, **139**, 21–29.

Westerman, B., Stringfellow, P.M., Eccleston, J.A. & Harbrow, D.J. (2002). Effect of ethylene vinyl acetate (eva) closed cell foam on transmitted forces in mouthguard material. *British Journal of Sports Medicine*, **36**, 205–208.

Zhang, Z. (1999). A flexible new technique for camera calibration. *International Conference on Computer Vision (ICCV'99), Corfu, Greece*, 666–673.

Zhu, H.X., Mills, N.J. & Knott, J.F. (1997). Analysis of the high strain compression of open-cell foams. *Journal of the Mechanics and Physics of Solids*, **45;**, 1875–1904.

Zysk, T.H. & Ehrenstein, G.W. (1992). Property changes of thermoplastic polyurethane elastomers (tpu) in dynamic loading. *ANTEC '92*, 846–850.

Appendix A

Sensitivity Studies

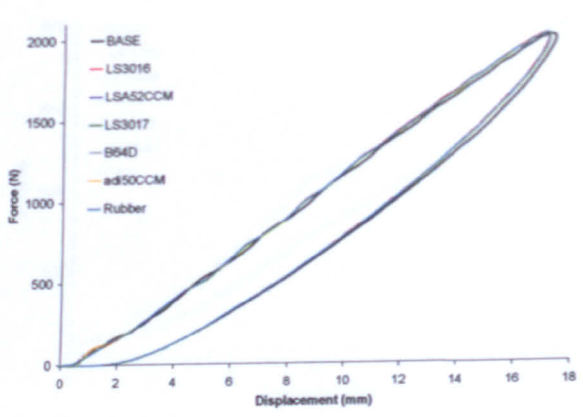

(a) Heel Cushion

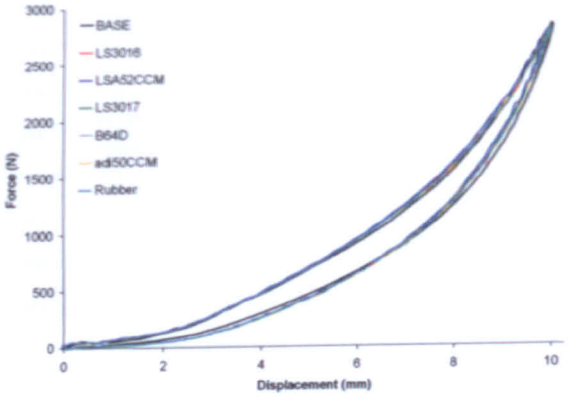

(b) Forefoot Cushion

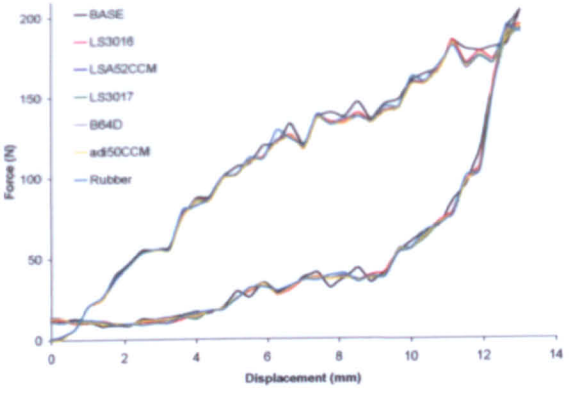

(c) Forefoot Bend

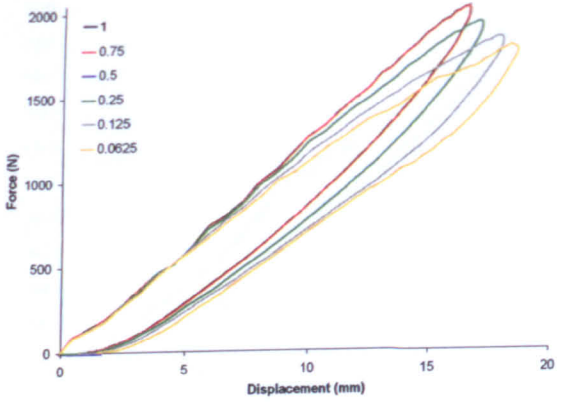

(d) Heel Cushion

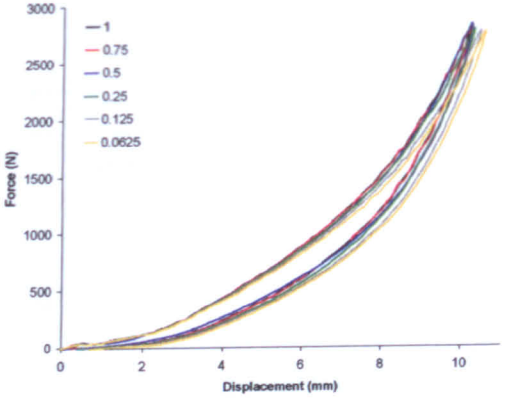

(e) Forefoot Cushion

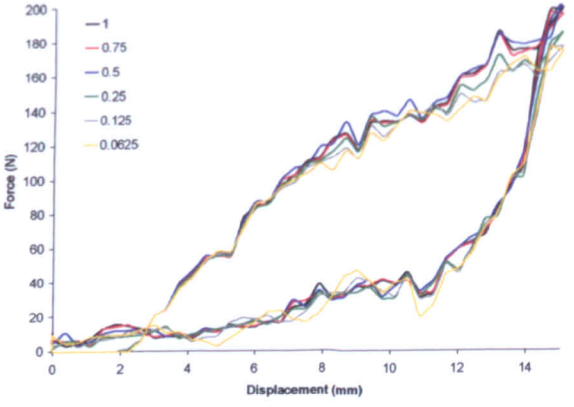

(f) Forefoot Bend

Figure A-1: Dynamic density and friction sensitivity studies for the Supernova midsole assembly.

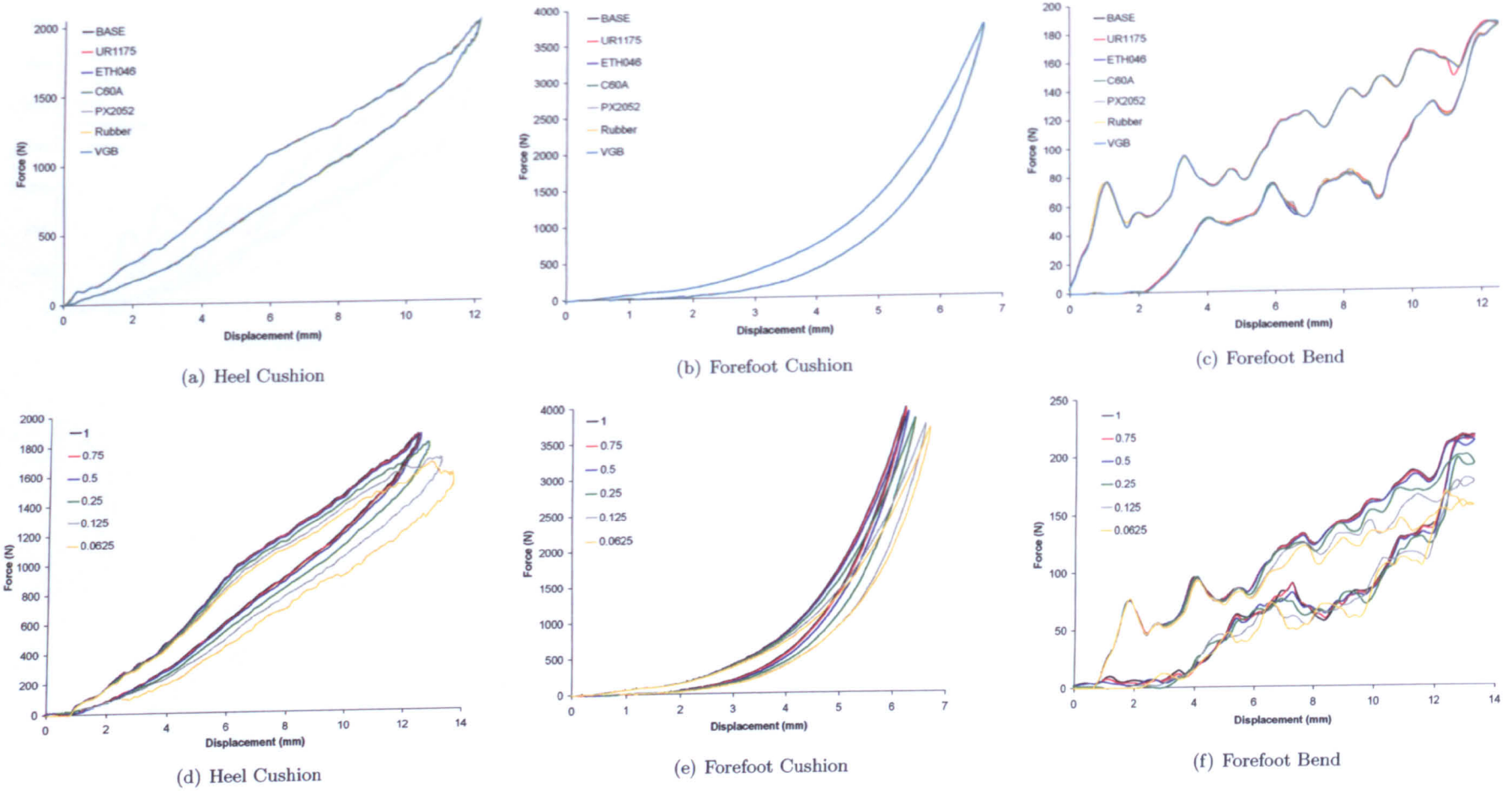

(a) Heel Cushion

(b) Forefoot Cushion

(c) Forefoot Bend

(d) Heel Cushion

(e) Forefoot Cushion

(f) Forefoot Bend

Figure A-2: Dynamic density and friction sensitivity studies for the Ultraride midsole assembly.

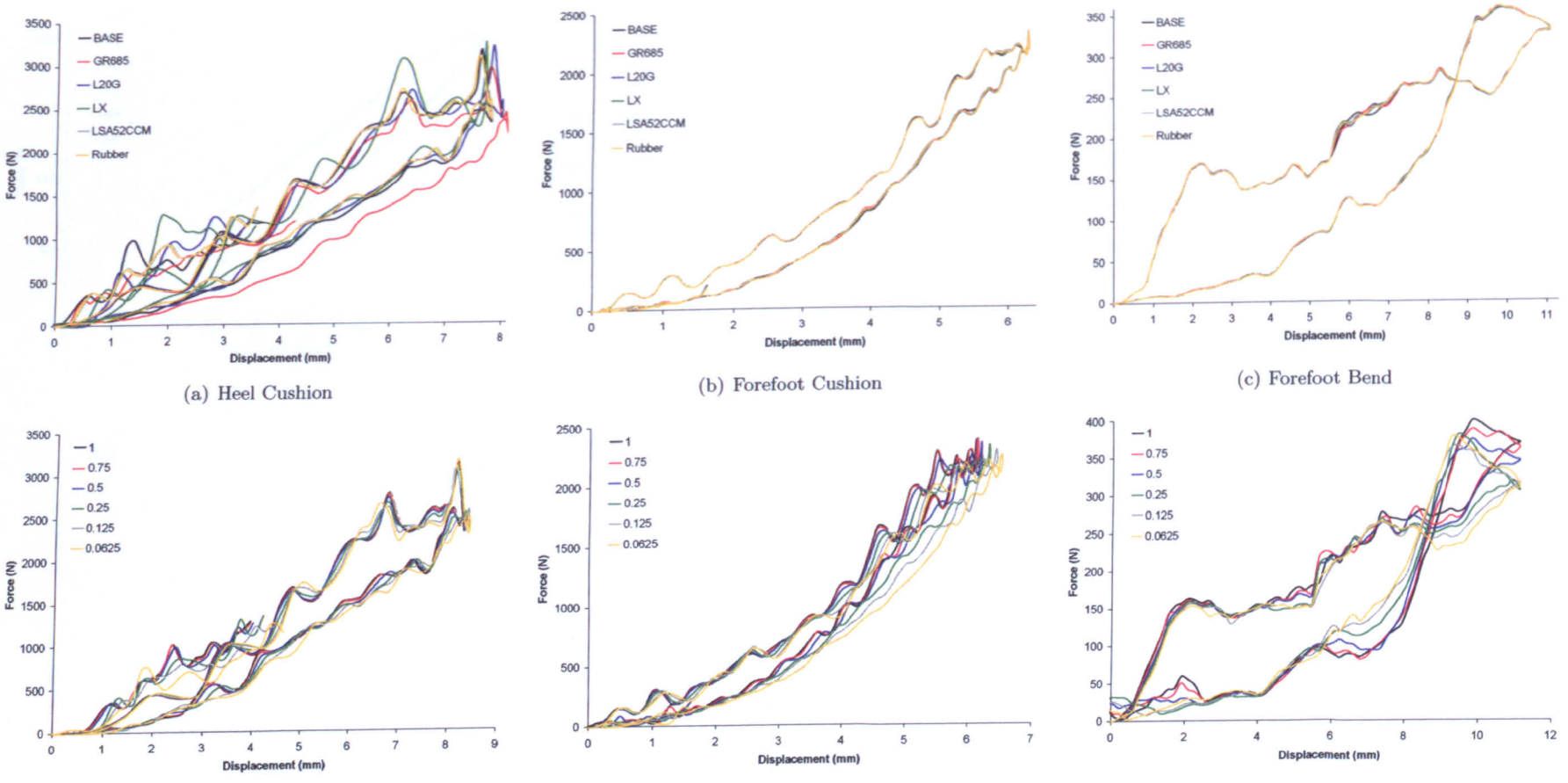

(a) Heel Cushion

(b) Forefoot Cushion

(c) Forefoot Bend

(d) Heel Cushion

(e) Forefoot Cushion

(f) Forefoot Bend

Figure A-3: Dynamic density and friction sensitivity studies for the Gigaride midsole assembly.

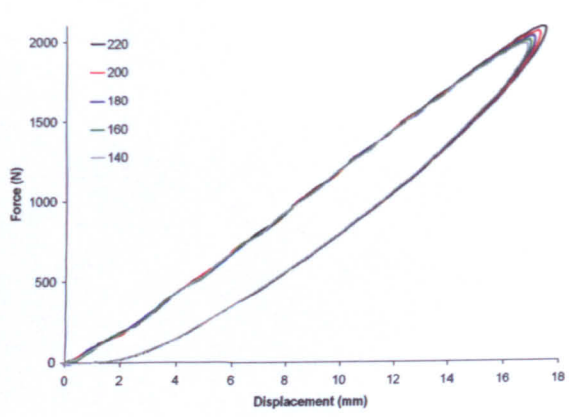

(a) Heel Cushion

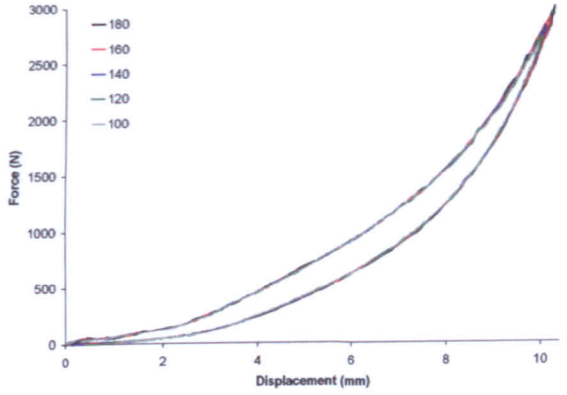

(b) Forefoot Cushion

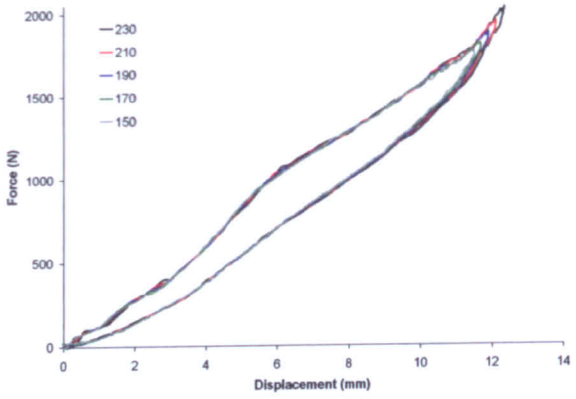

(c) Heel Cushion

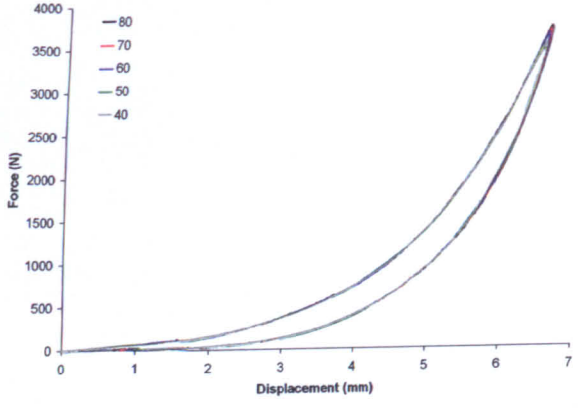

(d) Forefoot Cushion

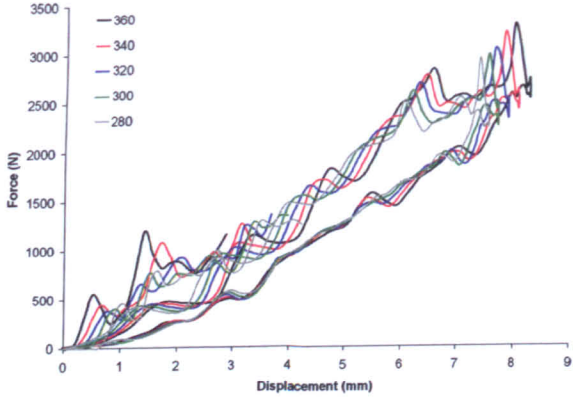

(e) Heel Cushion

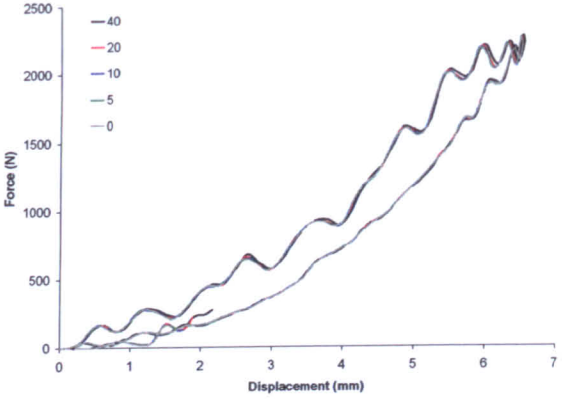

(f) Forefoot Cushion

Figure A-4: Dynamic velocity sensitivity studies for all midsole assemblies.

Appendix B

PinTracker Source Code

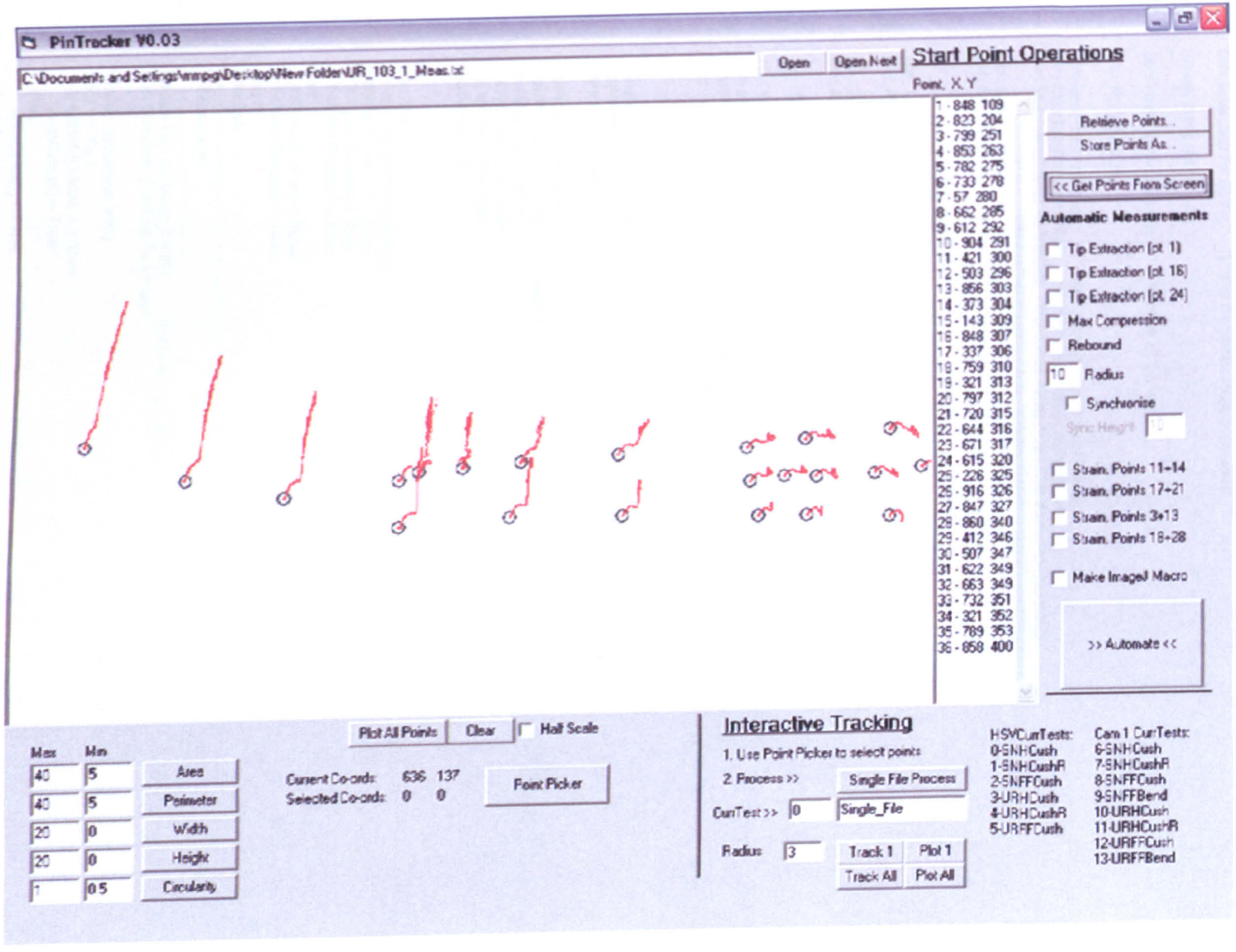
PinTracker V0.03
C:\Documents and Settings\mrpgi\Desktop\New Folder\UR_103_1_Meas.txt
Open
Open Next
Start Point Operations
Point, X, Y
1 - 848 109
2 - 823 204
3 - 799 251
4 - 853 263
5 - 782 275
6 - 733 278
7 - 57 280
8 - 662 285
9 - 612 292
10 - 904 291
11 - 421 300
12 - 503 296
13 - 856 303
14 - 373 304
15 - 143 309
16 - 848 307
17 - 337 306
18 - 759 310
19 - 321 313
20 - 797 312
21 - 720 315
22 - 644 316
23 - 671 317
24 - 615 320
25 - 226 325
26 - 916 326
27 - 847 327
28 - 860 340
29 - 412 346
30 - 507 347
31 - 622 349
32 - 663 349
33 - 732 351
34 - 321 352
35 - 789 353
36 - 858 400
Retrieve Points..
Store Points As..
<< Get Points From Screen
Automatic Measurements
Tip Extraction (pt 1)
Tip Extraction (pt 16)
Tip Extraction (pt 24)
Max Compression
Rebound
10 Radius
Synchronise
Sync Height 10
Strain, Points 11+14
Strain, Points 17+21
Strain, Points 3+13
Strain, Points 18+28
Make ImageJ Macro
>> Automate <<
Plot All Points
Clear
Half Scale
Max
Min
40 5 Area
40 5 Perimeter
20 0 Width
20 0 Height
1 0.5 Circularity
Current Co-ords: 636 137
Selected Co-ords: 0 0
Point Picker
Interactive Tracking
1. Use Point Picker to select points
2. Process >>
Single File Process
CurrTest >> 0 Single_File
Radius 3
Track 1
Plot 1
Track All
Plot All
HSVCurrTests:
0-SNHCush
1-SNHCushR
2-SNFFCush
3-URHCush
4-URHCushR
5-URFFCush
Cam 1 CurrTests:
6-SNHCush
7-SNHCushR
8-SNFFCush
9-SNFFBend
10-URHCush
11-URHCushR
12-URFFCush
13-URFFBend

```
'----- FILES / PATHS -----
'
Dim Results() As Single        'Orignal Input File
                               '  (Area/Perim/Width/Height/Circ/XStart/YStart, Point)
Dim FrameResults() As Single   'Results file converted into frames
                               '  (Area/Perim/Width/Height/Circ/XStart/YStart, Point, Frame)
Dim DirPath As String          'Directory Path
Dim FilePath As String         'Path of inputfile
Dim FilesList() As String      'List of filenames to be processed

'----- FRAME DATA ------
'
Dim TotalFrames As Long        'Number of frames

'----- POINT DATA
'
Dim MaxPoint As Long           'Max number of points per frame
Dim MaxStartPoint As Single    'Number of points in start frame
Dim StartPointStore() As Variant   'Container Array of starting points for each test
                                   '(Refinement(0)/X(1)/Y(2), Points), Name in ()(0,0), NumPoints in ()(1,0)
Dim StartPointList() As Variant    'Array of starting points held temp in txtPoint
Dim SaveAPointArr() As Variant     'Array holding tracks of selected point over all tests

'----- TRACKS AND RESULTS
'
Dim Track() As Single          'Track of given points - Track(Frames, X/Y)
Dim AllTracks() As Variant     'Array of Track Arrays - AllTracks(Track())

Dim PostProcessingResults() As Variant  'Holder for results from postproceesing (each file)
Dim AllPPR() As Variant                 'Holder for results from postproceesing (each test)

'----- OTHER VARIABLES
'
Dim TestToStore As String      'The name of the test selected by the user from cmbTestNames
Dim PickerOn As Boolean        'Declares if PointPicking mode is on/off
Dim PickerTemp() As Integer    'Temporary array of points from picking - PickerTemp(X/Y, points)
Dim AutoCalcs(4) As Boolean    'Array holding which calculations to perform during Auto.

'-------------------------------------------------------------------------------------------

Private Sub Form_Load()
'PointPick mode off
PickerOn = False

Dim NumPoints As Integer
'ReDim StartPointStore(21) '(TestNum, Refinement(0)/X(1)/Y(2), Points), Name in (x,0,0), NumPoints in (x,1,0)
Dim StartPointTEMP()
ReDim StartPointTEMP(2, 10)
ReDim SaveAPointArr(2, 1)
chkSync_Click


End Sub
Private Sub chkSync_Click()
If chkSync.Value = 1 Then
   lblSync.Enabled = True
   txtSync.Enabled = True
Else
   lblSync.Enabled = False
   txtSync.Enabled = False
End If
End Sub
'-------------------------------------------------------------------------------
'  Automation
'--------------------------------
Private Sub cmdAuto_Click()      'Click on Auto button
Dim CurrStart, CurrEnd As Integer

'Set up calculation array
For i = 0 To 4
   If AutoM(i).Value = 1 Then
      AutoCalcs(i) = True
   Else
      AutoCalcs(i) = False
   End If
Next 'i
```

```
Call Automate

End Sub
Private Sub cmdSingleProcess_Click() 'Click on Single File Process button

'1. Get filename and directory path
SingleFileName = txtSingle.Text & ".txt"
'FilePath = CommonDialog1.FileName    '<< already collected as user loads first file
'DirPath = CurDir

'2. Take start points from PickerTemp (user has done 'PointPicker' operation),
'      temp. write over StartPointStore in correct Curr(ent)Test
'arrMyTEMP = StartPointStore
'CurrTest = txtCurrTest.Text
'TestToStore = StartPointStore(CInt(CurrTest))(0, 0)    'string, testname
'Call Store(True)

'3. Process
ReDim FilesList(0)
ReDim AllPPR(1) 'set up postprocess results array
Call SingleFileAuto(1, CInt(txtRadius.Text))

'4. Export PostProcess data
SavePostProcessing (SingleFileName)

'5. Return StartPointS
'StartPointStore = arrMyTEMP

End Sub
Private Sub Automate()
'Automatically process the files for a given test
'
'   All subs operate on module-level arrays Results() and FrameResults()
'

'1. Load in start points + refinement values!! <<<< store refinements in sep file?
'** Already done on form_load
TestNames = Array("SNHCush", "SNHCushR", "SNFFCush", "URHCush", "URHCushR", "URFFCush")

'2. Get directory + create file list
Me.CommonDialog1.ShowOpen
FilePath = CommonDialog1.FileName
DirPath = CurDir

MyFile = Dir(DirPath & "\*MEAS.txt")
ReDim FilesList(0)
Do While MyFile <> ""
   If Right(MyFile, 4) = ".txt" Then
      If FilesList(UBound(FilesList)) <> "" Then
         ReDim Preserve FilesList(UBound(FilesList) + 1)
      End If
      FilesList(UBound(FilesList)) = MyFile
   End If
   MyFile = Dir
Loop

'3. Declare range of filenumbers for each test (in test order)
'REMOVED

'4. Loop through each test
'>>> MAIN CURR TEST LOOP REMOVED - process by folder only
'For CurrTest = CurrStart To CurrEnd

   'Re-dimension post-process results array to size of files in folder
   ReDim AllPPR(UBound(FilesList) + 1)

"FILE LOOP REPLACED BY A LIST OF FILES IN A GIVEN FOLDER
For MyFileNumber = 1 To UBound(FilesList) + 1

   '5. Set up filename
   FilePath = (FilesList(MyFileNumber - 1))

      Rad = CInt(txtRad.Text)
```

```
'----------SINGLE FILE PROCESS----------
'
Call SingleFileAuto(MyFileNumber, Rad)
'
'----------END OF SINGLE FILE PROCESS----------

Next 'MyFileNumber

    SavePostProcessing (FilePath) 'exports PostProcessingResults to .txt file with "_PPR.txt" extension

'Next 'CurrTest

'ReDim Preserve SaveAPointArr(2, UBound(SaveAPointArr, 2) - 1) 'Remove spare row <<SPARE ROW HAS
DATA IN

Call SaveAPoint   'exports a given point (e.g. rows-frame, col-point(Y) data for 12 repeats)
                  '  for easy excel input
MsgBox "Automatic Process Complete: " & MyFileNumber - 1 & " Files Processed"
End Sub
Private Sub SingleFileAuto(MyFileNumber, Rad)
'6. Open File + Read in data
    OpenFiles     'needs FilePath and DirPath

    '7. Refine Data
    'Read, Upper, Lower, Measure from StartPointStore(0, 1-8)
    For i = 1 To 9 Step 2
       Upper = StartPointStore(0, i)
       Lower = StartPointStore(0, i + 1)
       Call FilterPoints(Upper, Lower, ((i + 1) / 2)) 'all as single
    Next 'measure

    '8. Track Data
    'Find X,Y coord of point from StartPointStore(CurrTest, x/y, points) array

    CurrPoint = 0
    ReDim AllTracks(1)
    For MyPoint = 1 To UBound(StartPointStore, 2)
       XCoord = StartPointStore(1, MyPoint)
       YCoord = StartPointStore(2, MyPoint)


       If XCoord > 0 And YCoord > 0 Then
          'Track Points
          ' Adjust Rad for Stamp and tip

          "If MyPoint = UBound(StartPointStore, 2) Then     'LAST (stamp)
          "    If CurrTest < 6 Then Rad = Rad * 10 'big radius for HSV tests (stamp)
          "End If

          If MyPoint = 1 Then
             Rad = Rad * 2  'larger radius for tip point
          End If

          Call PointTrackerNearest(Rad, XCoord, YCoord)

          '8a. Store Track - AllTracks(Points, [Track(Frames,X/Y)]
          CurrPoint = CurrPoint + 1
          If UBound(AllTracks) < CurrPoint Then
             ReDim Preserve AllTracks(UBound(AllTracks) + 1)
          End If

          AllTracks(CurrPoint) = Track()

       End If
    Next 'MyPoint

    '9. Post Processing
    '  Set up post processing results array
    ReDim PostProcessingResults(6) '(Tip/MC/R/DATUM_Min/DATUM_Max/Vel(2D))

    'Synchronise mode
    If chkSync.Value = 1 Then
       SyncHeight = CInt(txtSync.Text)
       Call Synchronise(SyncHeight)          'syncs data so it starts at given stamp height
    End If
```

```
    SmoothData (3)          'applies Gaussian filter of radius (x)


    '---- Automatic Calculations ----
    'Finds max/min deflection of a point and time (in frames, from given start)
    '
    ' NOTE!! 0,0 if top left, so 'up' in reality is DOWN in pixel co-ords,
    '       e.g. max tip deflection is MINIMUM point.
    '
'DATUM (penultimute pin)
'       Datum Min
      Call MinMaxExtraction(UBound(AllTracks, 1) - 1, 1, False, "Datum_MIN")
        'Max Compression: Point = 2nd Last, Start = 1, Min(False)
'       Datum Max
      Call MinMaxExtraction(UBound(AllTracks, 1) - 1, 1, True, "Datum_MAX")
        'Max Compression: Point = 2nd Last, Start = 1, Max(True)
'TIP MAX (Pin 1)
      If AutoCalcs(0) = True Then
        Call MinMaxExtraction(1, 1, False, "Tip")
        'Tip: Point = 1, Start = 1, Min(False)
      End If
'TIP MAX FOR FFCUSH (Pin 16)
      If AutoCalcs(1) = True Then
        On Error Resume Next
        Call MinMaxExtraction(16, 1, False, "Tip")
        'Tip (FFCush): Point = 16, Start = 1, Min(False)
      End If
'TIP MAX FOR FFCUSH (Pin 24)
      If AutoCalcs(2) = True Then
        Call MinMaxExtraction(24, 1, False, "Tip")
        'Tip (FFCush): Point = 24, Start = 1, Min(False)
      End If
'MAXUMUM COMPRESSION (Last Pin)
      If AutoCalcs(3) = True Then
        Call MinMaxExtraction(UBound(AllTracks, 1), 1, True, "MC")
        'Max Compression: Point = Last, Start = 1, Max(True)
        On Error Resume Next
      End If
'REBOUND (Last Pin)
      If AutoCalcs(4) = True Then
        Call MinMaxExtraction(UBound(AllTracks, 1), PostProcessingResults(2)(3), False, "R")
        'Rebound: Point = Last, Start = Max Compression point, Min(False)
      End If
'MAX VELOCITY
      Call MaxVelocity(UBound(AllTracks, 1))
      'Max Velocity: Point = Last, Start = 1
      On Error GoTo 0

      'Add PostProcessing Data to AllPPR() container
      AllPPR(MyFileNumber) = PostProcessingResults
      AllPPR(MyFileNumber)(0) = FilesList(MyFileNumber - 1)

'STRAIN
      'UR
      'If chkStrain1114.Value = 1 Then Call StrainMeasure(11, 14)
      'If chkStrain1721.Value = 1 Then Call StrainMeasure(17, 21)
      'GR
      If chkStrain1114.Value = 1 Then Call StrainMeasure(12, 16)
      If chkStrain1721.Value = 1 Then Call StrainMeasure(19, 23)
      'URS
      'If chkStrain0313.Value = 1 Then Call StrainMeasure(3, 13)
      'If chkStrain1828.Value = 1 Then Call StrainMeasure(18, 28)
      'GRS
      'If chkStrain0313.Value = 1 Then Call StrainMeasure(5, 6)
      'If chkStrain1828.Value = 1 Then Call StrainMeasure(5, 8)

      '10. Export Data
      'SavePostProcessing  'exports PostProcessingResults to .txt file with "_PPR.txt" extension

      SaveTrack     'exports AllTracks() to .txt file with "_OUT.txt" extension

      If chkImageJ.Value = 1 Then
        Stop    '
            ' User needs to add start times, fps and no. frames
        SaveJavaTrack  'exports AllTracks() to an ImageJ macro file for overlay onto an animation
      End If
```

```
    'Resize array if smaller than current number of files processed
    If UBound(SaveAPointArr, 2) < MyFileNumber Then
       ReDim Preserve SaveAPointArr(2, MyFileNumber)
    End If
    'Record Track (last point = stamp)
    SaveAPointArr(1, MyFileNumber) = AllTracks(UBound(AllTracks)) 'stores given point track to array for output
at end with SaveAPoint
    'Record Name of Point
    SaveAPointArr(1, 0) = UBound(AllTracks)

    SaveAPointArr(2, MyFileNumber) = AllTracks(9)
    SaveAPointArr(2, 0) = 9

End Sub

'-------------------------------------------------------------------------------
'  File I/O
'---------------------------------
Private Sub cmdOpen_Click() 'Open Results File

'1. Get Filename
Me.CommonDialog1.ShowOpen
FilePath = CommonDialog1.FileName
txtOpen.Text = FilePath


'2. Get Directory Path
DirPath = CurDir

'3. Open File

OpenFiles

'MsgBox "Done"

'Plot Points from frame 1
Call PlotPoints(0, 0, 0)
End Sub
Private Sub OpenFiles()
'Open ImageJ output file

On Error GoTo err
Open FilePath For Input As #1   ' Open file for input.
i = 0

Do While Not EOF(1)   ' Loop until end of file.
   If i = 0 Then   'Skip title row
      Input #1, dummy
   End If
   i = i + 1
   ReDim Preserve Results(7, i)
   'Skip Point Number
   Input #1, dummy
   'Area
   Input #1, Results(1, i)
   'Skip Mean/Min/Max
   Input #1, dummy
   Input #1, dummy
   Input #1, dummy
   'Perimeter
   Input #1, Results(2, i)
   'BX/BY - bounding box, top left co-ords
   '  Bounding box used so all objects come out in
   '  correct order, allowing sorting into frames.
   Input #1, Results(6, i)
   Input #1, Results(7, i)
   'Width
   Input #1, Results(3, i)
   'Height
   Input #1, Results(4, i)
   'Circularity
   Input #1, Results(5, i)
   'Skip XStart (first encoded point)
   Input #1, dummy
   'Skip YStart
```

```
    Input #1, dummy

Loop
err:
Close #1

'Calculate Number of frames
CalculateFrames

'Sort Data Into Frames
SortIntoFrames

'Calculate centre by bounding box (assumes all points are circular,
'                        which they should be if they are pins)

For CurrPoint = 1 To UBound(FrameResults, 2)
   For Frame = 1 To UBound(FrameResults, 3)
      FrameResults(6, CurrPoint, Frame) = FrameResults(6, CurrPoint, Frame) + CInt(FrameResults(3, CurrPoint,
Frame) / 2)
      FrameResults(7, CurrPoint, Frame) = FrameResults(7, CurrPoint, Frame) + CInt(FrameResults(4, CurrPoint,
Frame) / 2)
   Next 'Frame
Next 'CurrPoint

End Sub

Private Sub CalculateFrames()
'Calculates how many frames there are based on change of YStart value

TotalFrames = 1
MaxPoint = 1
Points = 0

On Error GoTo err2
For i = 1 To UBound(Results, 2)
   Points = Points + 1
   If Results(7, i) > Results(7, i + 1) Then   'new frame
      TotalFrames = TotalFrames + 1
      If Points > MaxPoint Then MaxPoint = Points
      Points = 0
   End If
Next 'i
err2:
End Sub
Private Sub SortIntoFrames()
'Converts Results() into frame-by-frame results based on change of YStart value
ReDim FrameResults(7, MaxPoint, TotalFrames)

Frame = 1      'Number of frame
CurrPoint = 0  'Number of current point

On Error GoTo err3
For i = 1 To UBound(Results, 2)
   If Results(7, i) <= Results(7, i + 1) Then  'same frame
      CurrPoint = CurrPoint + 1   'increment point number
      For j = 1 To 7
         FrameResults(j, CurrPoint, Frame) = Results(j, i)   'Fill data line
      Next 'j
   Else
      CurrPoint = CurrPoint + 1   'increment point number

      For j = 1 To 7
         FrameResults(j, CurrPoint, Frame) = Results(j, i)   'Fill data line
      Next 'j
      Frame = Frame + 1   'Increment Frame number
      CurrPoint = 0   'reset number of current point
   End If


Next 'i
err3:

End Sub
```

```
Private Sub cmdSave_Click()
SaveTrack
End Sub
Private Sub SaveTrack()
'Tracks outputted to a txt file for export into excel. Points across columns, frames in rows
'Outputs data from AllTracks()

MyOutputPath = Left(FilePath, Len(FilePath) - 4) & "_OUT.txt"

Open MyOutputPath For Output As #3
On Error GoTo err5

'1. Write header
MyOutPut = "Frame "
For Points = 1 To UBound(AllTracks, 1)  '1 point per track....
      MyOutPut = MyOutPut & Points & "X " & Points & "Y "
Next 'Points
MyOutPut = Left(MyOutPut, Len(MyOutPut) - 1)  'remove spare space
Print #3, MyOutPut

'2. Write main
For Frames = 1 To UBound(AllTracks(1), 1)   'length of Track array

   MyOutPut = Frames & " "     'frame number

   For Points = 1 To UBound(AllTracks, 1)  '1 point per track....
      MyOutPut = MyOutPut & AllTracks(Points)(Frames, 1) & " " & AllTracks(Points)(Frames, 2) & " "
   Next 'Points

   MyOutPut = Left(MyOutPut, Len(MyOutPut) - 1)   'remove spare space
   Print #3, MyOutPut

Next 'Frames

err5:
Close #3

End Sub
Private Sub SaveJavaTrack()
'Tracks outputted to a txt file that can be read as a macro by ImageJ,
' allowing the pin tracks to be overlayed on a stack of images and saved
' as an animation.

"" REQUIRED FRAME INFO
MyStartFrame = 0        'start frame of HSV that corresponds to frame 0 of FE
MyNoFrames = 101        'max number of frames
FEfps = 101             'frames per second of output file
HSVfps = CInt(776 - (30 * 7))  'subtract timeshift
""
' Conversion needed to make track fit output anim.
'
' Skip frames according to HSVfps/FEfps
'               (for example: 4000/40 = 100 gives, For i = 1 to X Step 100)
'
fpsStep = Int((HSVfps / FEfps)) + 1
'
'
MyWidth = 8

MyOutputPath = Left(FilePath, Len(FilePath) - 4) & "_Macro.txt"

Open MyOutputPath For Output As #6
'On Error GoTo err6    'Remove handler for debugging

'1. Open AVI command
'Print #6, "open(""AVI FILENAME.avi"");"

'2. Looped list of drawing commands
'
'   This loop draws a cross hair over the given point co-ords
'
'setTool(4);   'select up the line drawing tool
'
'makeLine(x1,y1,x2,y2);     'draw the line
'run("Draw");               'emboss onto frame
'run("Next Slice [>]");     'skip to next frame
```

```
'
Zoom = 1.5      'size multiplier
XOffset = 50    'offset (+ = right)
YOffset = 35    'offset (+ = down)
FrameShift = -30  'difference in time between FE + points

'2a. Loop frames
Print #6, "setForegroundColor(255,255,255);"    'set colour
For i = (200) To UBound(AllTracks(1), 1) Step fpsStep       'i = 1 to no. frames

'
' **** Needs conversion from HSV video coords
' ****  to ABAQUS output coords
'
' X(abq) = { X(hsv) * [(HSV/ABQ)pix/mm ]} + Datum(abq)
'
' where Datum(abq)  = AlignX(abq) - AlignX(hsv)
'

    '2b. Need all points on one frame, so loop AllTracks(Point No.)(x,y)
    For j = 1 To UBound(AllTracks, 1) - 1 'Loop points,  j = 1 to no. points.
       'Set drawing co-ords
       If (AllTracks(j)(i, 1) * AllTracks(j)(i, 2)) <> 0 Then
          'Lines
          XCoord = CInt((AllTracks(j)(i, 1) * Zoom) + XOffset)
          YCoord = CInt((AllTracks(j)(i, 2) * Zoom) + YOffset)
          'X1 = XCoord - 16
          'Y1 = YCoord - 16
          'X2 = XCoord + 16
          'Y2 = YCoord + 16

          'MyOutPut = "makeLine(" & X1 & "," & Y1 & "," & X2 & "," & Y2 & ");"
          'Print #6, MyOutPut
          'Print #6, "run(""Draw"");"

          'Circles
          X1 = CInt(XCoord - (MyWidth / 2))
          Y1 = CInt(YCoord - (MyWidth / 2))
          X2 = MyWidth
          Y2 = MyWidth

          MyOutPut = "makeOval(" & X1 & "," & Y1 & "," & X2 & "," & Y2 & ");"
          Print #6, MyOutPut
          Print #6, "run(""Fill"", ""slice"");"
       End If
    Next 'j

    If i < UBound(AllTracks(1), 1) Then Print #6, "run(""Next Slice [>]"");"

Next 'i


'3. Save AVI command
'Print #6, "saveAs(""AVI..."","""AVI OUTPUTNAME.avi"");"
'Print #6, "close();"

'Stop
err5:
Close #6

End Sub

Private Sub SaveAPoint()
Dim OutputArr As Variant
'Tracks outputted to a txt file for export into excel. Points across columns, frames in rows
'Outputs Y DATA ONLY from SaveAPointArr(UBound(SaveAPointArr, 2)) = AllTracks(2)
'
'
'INPUT: SaveAPointArr(Points,Repeat_number[dynamic resize in Automate])(frame, X/Y)Names in (0))
'OUTPUT: OutputArr(Frames[in order of tests], Repeats)
'
'1. Outer Loop: Tests
'   1a. Open output file
MyOutputPath = DirPath & "\SaveAPoint.txt"
Open MyOutputPath For Output As #5
```

```
For Test = CurrStart To CurrEnd  'Due to ReDim commands, tracks are in one above their test index

  For PointNumber = 1 To UBound(SaveAPointArr, 1)

    '2. Find repeat with largest amount of frames
    Max = -9999
    For Repeat = 1 To UBound(SaveAPointArr, 2)
      If UBound(SaveAPointArr(PointNumber, Repeat), 1) > Max Then
        Max = UBound(SaveAPointArr(PointNumber, Repeat), 1)
      End If
    Next 'Repeat

    '3. Create/Clear output array: OutputArr(Frames, Repeats)
    ReDim OutputArr(Max, UBound(SaveAPointArr, 2))

    '4. Fill Array

    For i = 1 To UBound(OutputArr, 1) 'Frames
      For j = 1 To UBound(OutputArr, 2)  'Repeats
        If i > UBound(SaveAPointArr(PointNumber, j), 1) Then 'number of frames in set
          'Fill in zero
          OutputArr(i, j) = 0
        Else '<< changed this bit
        OutputArr(i, j) = SaveAPointArr(PointNumber, j)(i, 2)  'Y data only for height measurement
        End If
      Next 'j
    Next 'i

    '5. Write Data to File
    MyOutPut = "Points,"
    For i = 0 To UBound(SaveAPointArr, 2)
      MyOutPut = MyOutPut & SaveAPointArr(PointNumber, 0) & ","
    Next 'i
    Print #5, MyOutPut

    For i = 1 To UBound(OutputArr, 1)
      MyOutPut = i & " "
      For j = 1 To UBound(OutputArr, 2)  'Repeats
        MyOutPut = MyOutPut & OutputArr(i, j) & " "
      Next 'j
      Print #5, MyOutPut
    Next 'i

  Next 'PointNumber
Next 'Test

Close #5

End Sub
Private Sub SavePostProcessing(ResultsFileName)
'Writes out AllPPR() array to txt file.

MyOutputPath = DirPath & "\PPR_" & ResultsFileName

Open MyOutputPath For Output As #4
On Error Resume Next

For i = 0 To UBound(AllPPR)              'loop files
  'MyOutPut = Right(FilePath, Len(FilePath) - Len(DirPath)) & ", "  'now done out of file loop, so name is the same
  MyOutPut = "File-" & i + 1 & ", "
  MyOutPut = MyOutPut & AllPPR(i)(0) & ", " 'Title
  For j = 1 To UBound(AllPPR(i), 1)        'loop PP tests
    'MyOutPut = ""
    If AllPPR(i)(j) <> "" Then
      For k = 0 To UBound(AllPPR(i)(j), 1) 'loop results
        MyOutPut = MyOutPut & AllPPR(i)(j)(k) & ", "
      Next 'k
      'Print #4, MyOutPut
      'Print #4, "----------"
    Else
      MyOutPut = MyOutPut & "NoValue,"
      'Print #4, "----------"
    End If
  Next 'j
  Print #4, MyOutPut
Next 'i
```

```
err6:
Close #4

End Sub

'-------------------------------------------------------------------------------
'  Tracking
'-------------------------------
Private Sub cmdTrack1_Click() 'Track from current selected co-ords
XCoord = CInt(lblSelX)
YCoord = CInt(lblSelY)
Call PointTrackerNearest(2, XCoord, YCoord)

End Sub
Private Sub cmdTrackAll_Click() 'Track from points list
ReDim AllTracks(1)

'1. Get point from first frame
CurrPoint = 1
For Points = 1 To UBound(FrameResults, 2)
   XCoord = FrameResults(6, Points, 1)
   YCoord = FrameResults(7, Points, 1)
   '2. Check has not been zeroed
   If XCoord > 0 And YCoord > 0 Then
      '3. Find Track
      Call PointTrackerNearest(5, XCoord, YCoord)

      '4. Store Track - AllTracks(Points, [Track(Frames,X/Y)]
      If CurrPoint > 1 Then
         ReDim Preserve AllTracks(UBound(AllTracks) + 1)
      End If
      AllTracks(CurrPoint) = Track()
      CurrPoint = CurrPoint + 1

   End If
Next 'Points
End Sub

Private Sub PointTracker(Rad, XCoord, YCoord)
'Finds closest point to given coords in next frame
'1. Set up array - Track(Frame, X/Y)
ReDim Track(UBound(FrameResults, 3), 2)

CurrXCoord = XCoord
CurrYCoord = YCoord

For Frames = 1 To TotalFrames                'loop frames
   For Points = 1 To UBound(FrameResults, 2)  'loop points
      '2. Compare
      Distance = Sqr((FrameResults(6, Points, Frames) - CurrXCoord) ^ 2 + (FrameResults(7, Points, Frames) -
CurrYCoord) ^ 2)
      ' Increase intial distance on start frame
      If Frames = 1 Then
         MyRad = 1.5 * Rad
      Else
         MyRad = Rad
      End If
      If Distance <= MyRad Then
         '3. Track found!
         CurrXCoord = FrameResults(6, Points, Frames)
         CurrYCoord = FrameResults(7, Points, Frames)
         Track(Frames, 1) = CurrXCoord
         Track(Frames, 2) = CurrYCoord
         Exit For
      End If
   Next 'j
'If Points = Ubound(FrameResults, 2) then '
Next 'i

End Sub
Private Sub PointTrackerNearest(Rad, XCoord, YCoord)
'Finds closest point to given coords in next frame
'1. Set up array - Track(Frame, X/Y)
ReDim Track(UBound(FrameResults, 3), 2)
Dim Dist()
ReDim Dist(UBound(FrameResults, 1), 1)
```

```
CurrXCoord = XCoord
CurrYCoord = YCoord

For Frames = 1 To TotalFrames                'loop frames
   'Check distance to each point
   CurrMin = 9999
   For Points = 1 To UBound(FrameResults, 2)  'loop points
      MyDist = Sqr((FrameResults(6, Points, Frames) - CurrXCoord) ^ 2 + (FrameResults(7, Points, Frames) -
CurrYCoord) ^ 2)
      If MyDist < CurrMin Then
         CurrMin = MyDist
         CurrMinPoint = Points
      End If
   Next 'j

   'Check point is within safty radius
   If CurrMin < Rad Then
      CurrXCoord = FrameResults(6, CurrMinPoint, Frames)
      CurrYCoord = FrameResults(7, CurrMinPoint, Frames)
      Track(Frames, 1) = CurrXCoord
      Track(Frames, 2) = CurrYCoord
   End If

Next 'i
End Sub

'--------------------------------------------------------------------------------
'  Ploting
'--------------------------------
Private Sub cmdClear_Click()
pic1.Cls
End Sub
Private Sub cmdPlotAllPoints_Click()
Call PlotPoints(0, 0, 0)

For Frame = 1 To UBound(FrameResults, 3)
   For Points = 1 To MaxPoint
      If FrameResults(6, Points, Frame) > 0 And FrameResults(7, Points, Frame) > 0 Then
         If chkHalf.Value = False Then 'Normal
            pic1.PSet (FrameResults(6, Points, Frame), FrameResults(7, Points, Frame)), RGB(255, 0, 0)
         Else   'half scale
            pic1.PSet (CInt(FrameResults(6, Points, Frame) / 2), CInt(FrameResults(7, Points, Frame) / 2)),
RGB(255, 0, 0)
         End If
      End If
   Next 'i
Next 'j
End Sub
Private Sub PlotPoints(R As Integer, G As Integer, B As Integer)
'Draw Positions on frame 1
'pic1.Cls
'pic1.Line (X1, Y1)-(X2, Y2), RGB(0, 0, 0) 'screen bounding box
For i = 1 To MaxPoint
   If FrameResults(6, i, 1) > 0 And FrameResults(7, i, 1) > 0 Then
      If chkHalf.Value = False Then 'Normal
         pic1.PSet (FrameResults(6, i, 1), FrameResults(7, i, 1)), RGB(R, G, B)
         pic1.Circle (FrameResults(6, i, 1), FrameResults(7, i, 1)), 5, RGB(R, G, B)
      Else
         pic1.PSet (CInt(FrameResults(6, i, 1) / 2), CInt(FrameResults(7, i, 1) / 2)), RGB(R, G, B)
         pic1.Circle (CInt(FrameResults(6, i, 1) / 2), CInt(FrameResults(7, i, 1) / 2)), 3, RGB(R, G, B)
      End If
   End If
Next 'i

End Sub
Private Sub cmdPlot1_Click()
For Frames = 1 To UBound(Track, 1)
   If Track(Frames, 1) > 0 And Track(Frames, 2) > 0 Then
      If chkHalf.Value = False Then 'Normal
         pic1.PSet (Track(Frames, 1), Track(Frames, 2)), RGB(255, 0, 0)
      Else
         pic1.PSet (CInt(Track(Frames, 1) / 2), CInt(Track(Frames, 2) / 2)), RGB(255, 0, 0)
      End If
   End If
Next 'Frames
End Sub
```

```
Private Sub cmdPlotAll_Click()
For Points = 1 To UBound(AllTracks, 1)
  For Frames = 1 To UBound(AllTracks(1), 1)
    If AllTracks(Points)(Frames, 1) > 0 And AllTracks(Points)(Frames, 2) > 0 Then
      If chkHalf.Value = False Then 'Normal
        pic1.PSet (AllTracks(Points)(Frames, 1), AllTracks(Points)(Frames, 2)), RGB(255, 0, 0)
      Else
        pic1.PSet (CInt(AllTracks(Points)(Frames, 1) / 2), CInt(AllTracks(Points)(Frames, 2) / 2)), RGB(255, 0, 0)
      End If
    End If
  Next 'Frames
Next 'Points
End Sub
Private Sub PlotStartPoints()
For Points = 1 To UBound(StartPointStore, 2)
  If chkHalf.Value = False Then 'Normal
    pic1.Circle (StartPointStore(1, Points), StartPointStore(2, Points)), CInt(txtRad.Text), RGB(255, 0, 0)
  Else
    pic1.Circle (CInt(StartPointStore(1, Points) / 2), CInt(StartPointStore(2, Points) / 2)), CInt(txtRad.Text / 2),
RGB(255, 0, 0)
  End If
Next 'i
End Sub
'-------------------------------------------------------------------------------
'  Start Point Processes
'-------------------------------
Private Sub cmdRetrieve_Click()
'Load points into list and StartPointsStore from a file
Me.CommonDialog1.ShowOpen
StartFilePath = CommonDialog1.FileName

GetStartPoints (StartFilePath)

End Sub
Private Sub GetStartPoints(StartFilePath)

'1. Read in txt file of start points
Open StartFilePath For Input As #2   ' Open file for input.
'On Error GoTo err4

ReDim StartPointStore(2, 1)

'Name and number of points
TestNum = TestNum + 1
Input #2, StartPointStore(0, 0)  'Name
Input #2, NumPoints 'Number of points

If NumPoints > UBound(StartPointStore, 2) Then
  ReDim Preserve StartPointStore(2, NumPoints)
End If
'Point co-ordinates
StartPointStore(1, 0) = NumPoints     'record number of points in row 0
For i = 1 To NumPoints
  Input #2, StartPointStore(1, i)   'load in rest of points
  Input #2, StartPointStore(2, i)
Next 'i
'Refinement data
For i = 1 To 11
  Input #2, StartPointStore(0, i)
Next 'i


DisplayStartPoints

err4:
Close #2
End Sub

Private Sub DisplayStartPoints()
'Put StartPoints into listbox and highlight them on screen

'1. Fill StartPointList() with point info
ReDim StartPointList(2, 1)
For i = 1 To UBound(StartPointStore, 2)
  If StartPointStore(1, i) > 0 And StartPointStore(2, i) > 0 Then
    If i > 1 Then ReDim Preserve StartPointList(2, i)
```

```
        StartPointList(1, i) = StartPointStore(1, i)
        StartPointList(2, i) = StartPointStore(2, i)
    End If
Next 'i


'1a. Fill txtPoint with info
FillTxtPoint

'2. Fill Refinement boxes (with test 1 as default)
txtAreaMax.Text = StartPointStore(0, 1)
txtAreaMin.Text = StartPointStore(0, 2)
txtPerimMax.Text = StartPointStore(0, 3)
txtPerimMin.Text = StartPointStore(0, 4)
txtWidthMax.Text = StartPointStore(0, 5)
txtWidthMin.Text = StartPointStore(0, 6)
txtHeightMax.Text = StartPointStore(0, 7)
txtHeightMin.Text = StartPointStore(0, 8)
txtCircMax.Text = StartPointStore(0, 9)
txtCircMin.Text = StartPointStore(0, 10)
txtRad.Text = StartPointStore(0, 11)

Call PlotStartPoints


End Sub
Private Sub FillTxtPoint()
'Writes data from StartPointList(point, X/Y) into txtPoint
MaxStartPoints = 0
MyString = ""
For Points = 1 To UBound(StartPointList, 2)
    If StartPointList(1, Points) > 0 And StartPointList(2, Points) > 0 Then
        MaxStartPoints = MaxStartPoints + 1
        MyString = MyString & MaxStartPoints & " - " & StartPointList(1, Points) & "  " & StartPointList(2, Points) &
vbCrLf
    End If
Next 'Points
txtPoint.Text = MyString

End Sub
Private Sub cmdGetPoints_Click()
'Load points from screen into txtPoints
MyString = ""
txtPoint.Text = MyString
MaxStartPoints = 0

For Points = 1 To UBound(FrameResults, 2)
    If FrameResults(6, Points, 1) > 0 And FrameResults(7, Points, 1) > 0 Then
        MaxStartPoints = MaxStartPoints + 1
        MyString = MyString & MaxStartPoints & " - " & FrameResults(6, Points, 1) & "  " & FrameResults(7, Points,
1) & vbCrLf
    End If
Next 'Points

txtPoint.Text = MyString

End Sub
Private Sub cmdStore_Click()
Store (False)
End Sub
Private Sub Store(SingleFile)
Dim MyTEMP()

'Save points in list as selected test
'1 If in point picking mode, update StartPoint List

    ReDim Preserve PickerTemp(2, UBound(PickerTemp, 2) - 1) 'Remove spare row
    ReDim StartPointList(UBound(PickerTemp, 1), UBound(PickerTemp, 2))
    If UBound(PickerTemp, 2) > 10 Then
        ReDim StartPointStore(UBound(PickerTemp, 1), UBound(PickerTemp, 2))
    End If
    For i = 0 To UBound(PickerTemp, 2)
        StartPointList(1, i) = PickerTemp(1, i)
        StartPointList(2, i) = PickerTemp(2, i)
    Next 'i
```

```
'2. Get filename
Me.CommonDialog1.ShowSave
StoreFilePath = CommonDialog1.FileName


'3. Load new data from list
For j = 1 To UBound(StartPointList, 2)
   StartPointStore(1, j) = StartPointList(1, j)  'X
   StartPointStore(2, j) = StartPointList(2, j)  'Y
Next 'j

StartPointStore(1, 0) = UBound(StartPointList, 2)  'Number of Points
On Error Resume Next

For j = (UBound(StartPointList, 2) + 1) To UBound(StartPointStore, 2)
   StartPointStore(1, j) = 0  'Fill blanks
   StartPointStore(2, j) = 0  'Fill blanks
Next 'j

'Refinement Data
StartPointStore(0, 1) = txtAreaMax.Text
StartPointStore(0, 2) = txtAreaMin.Text
StartPointStore(0, 3) = txtPerimMax.Text
StartPointStore(0, 4) = txtPerimMin.Text
StartPointStore(0, 5) = txtWidthMax.Text
StartPointStore(0, 6) = txtWidthMin.Text
StartPointStore(0, 7) = txtHeightMax.Text
StartPointStore(0, 8) = txtHeightMin.Text
StartPointStore(0, 9) = txtCircMax.Text
StartPointStore(0, 10) = txtCircMin.Text
StartPointStore(0, 11) = txtRad.Text

WriteStoreData (StoreFilePath)

If SingleFile = True Then Exit Sub

err5:
Close #4

End Sub
Private Sub WriteStoreData(StoreFilePath)

'1. Write new file
'   1a Read in txt file of start points
Open StoreFilePath For Output As #4   ' Open file for input.
On Error GoTo err5

'Name and number of points
Write #4, StartPointStore(0, 0)  'Name
Write #4, StartPointStore(1, 0)  'Number of points

'Point co-ordinates
For i = 1 To UBound(StartPointStore, 2)
   If StartPointStore(1, i) > 0 Then Write #4, StartPointStore(1, i)   'load in rest of points
   If StartPointStore(2, i) > 0 Then Write #4, StartPointStore(2, i)
Next 'i

'Refinement data
For i = 1 To 11
   Write #4, StartPointStore(0, i)
Next 'i

err5:
Close #4

End Sub
Private Sub cmbTestNames_Click()
'User selected the test to save points as
TestToStore = cmbTestNames.Text
End Sub
Private Sub cmdPicker_Click()
'Allows user to pick points that are then placed in txtPoint and the StartPointList
PickerOn = True

ReDim PickerTemp(2, 1)
End Sub
```

```
Private Sub FillTxtPoint2()
'Writes data from PickerTemp(X/Y, Point) into txtPoint
MaxStartPoints = 0
MyString = ""
For Points = 1 To UBound(PickerTemp, 2)
   If PickerTemp(1, Points) > 0 And PickerTemp(2, Points) > 0 Then
      MaxStartPoints = MaxStartPoints + 1
      MyString = MyString & MaxStartPoints & " - " & PickerTemp(1, Points) & "  " & PickerTemp(2, Points) &
vbCrLf
   End If
Next 'Points
txtPoint.Text = MyString

End Sub
'--------------------------------------------------------------------------
'  Refinement
'-----------------------------
'
'  Order = 1. Area, 2. Perimeter, 3. Width, 4. Height, 5. Circularity
'
Private Sub cmdArea_Click()
Upper = CSng(txtAreaMax.Text)
Lower = CSng(txtAreaMin.Text)
Call FilterPoints(Upper, Lower, 1)

Call PlotPoints(255, 0, 255)

'MsgBox MaxPoint & " points" & vbCrLf & UBound(FrameResults, 3) & " frames"
End Sub
Private Sub cmdCircularity_Click()
Upper = CSng(txtCircMax.Text)
Lower = CSng(txtCircMin.Text)
Call FilterPoints(Upper, Lower, 5)

Call PlotPoints(255, 0, 0)

'MsgBox MaxPoint & " points" & vbCrLf & UBound(FrameResults, 3) & " frames"
End Sub

Private Sub cmdHeight_Click()
Upper = CSng(txtHeightMax.Text)
Lower = CSng(txtHeightMin.Text)
Call FilterPoints(Upper, Lower, 4)

Call PlotPoints(0, 255, 0)

'MsgBox MaxPoint & " points" & vbCrLf & UBound(FrameResults, 3) & " frames"
End Sub

Private Sub cmdPerimeter_Click()
Upper = CSng(txtPerimMax.Text)
Lower = CSng(txtPerimMin.Text)
Call FilterPoints(Upper, Lower, 2)

Call PlotPoints(0, 0, 255)

'MsgBox MaxPoint & " points" & vbCrLf & UBound(FrameResults, 3) & " frames"
End Sub

Private Sub cmdWidth_Click()
Upper = CSng(txtWidthMax.Text)
Lower = CSng(txtWidthMin.Text)
Call FilterPoints(Upper, Lower, 3)

Call PlotPoints(255, 255, 0)

'MsgBox MaxPoint & " points" & vbCrLf & UBound(FrameResults, 3) & " frames"
End Sub

Private Sub FilterPoints(ByVal Upper As Single, ByVal Lower As Single, ByVal Measure As Integer)
'Recreate FrameResults array ignoring iffy objects
Dim TempFrameResults
TempFrameResults = FrameResults
ReDim FrameResults(UBound(TempFrameResults, 1), UBound(TempFrameResults, 2),
UBound(TempFrameResults, 3))
MaxPoint = 0
```

```
'Loop through
For i = 1 To UBound(FrameResults, 3)    'frames
   CurrPoint = 0
   For j = 1 To UBound(FrameResults, 2)    'points

      'If within limits - record point
      If Abs(TempFrameResults(Measure, j, i)) >= Lower And Abs(TempFrameResults(Measure, j, i)) <= Upper
Then
         CurrPoint = CurrPoint + 1
         For k = 1 To 7
            FrameResults(k, CurrPoint, i) = TempFrameResults(k, j, i)
         Next 'k
      End If

   Next 'j

   If CurrPoint > MaxPoint Then
      MaxPoint = CurrPoint
      'maxi = i
   End If

Next 'i

'MsgBox "max frames " & MaxPoint & " on " & maxi

'Cut slack out of FrameResults array
TempFrameResults = FrameResults
ReDim FrameResults(7, MaxPoint, UBound(TempFrameResults, 3)) 'DEBUG<< possible issue point

For i = 1 To UBound(FrameResults, 1)
   For j = 1 To UBound(FrameResults, 2)
      For k = 1 To UBound(FrameResults, 3)
         FrameResults(i, j, k) = TempFrameResults(i, j, k)
      Next 'k
   Next 'j
Next 'i


End Sub

Private Sub pic1_MouseMove(Button As Integer, Shift As Integer, X As Single, Y As Single)
If chkHalf.Value = False Then
   lblCurrX = X
   lblCurrY = Y
Else
   lblCurrX = 2 * X
   lblCurrY = 2 * Y
End If
End Sub

Private Sub pic1_MouseUp(Button As Integer, Shift As Integer, X As Single, Y As Single)

If chkHalf.Value = 1 Then
   X = 2 * X
   Y = 2 * Y
End If

lblSelX = X
lblSelY = Y


'PointPick mode
If PickerOn = True Then

   'Store info in PickerTemp(X/Y, Point) array
   If UBound(PickerTemp, 2) >= 1 Then ReDim Preserve PickerTemp(2, UBound(PickerTemp, 2) + 1)
   PickerTemp(1, UBound(PickerTemp, 2) - 1) = X
   PickerTemp(2, UBound(PickerTemp, 2) - 1) = Y

   'Update txtPoint
   FillTxtPoint2

End If
End Sub
```

```
'-------------------------------------------------------------------------------
'  Post Processing
'-------------------------------
Private Sub SmoothData(Range)
'Sub to apply gaussian smooth to the tracks before output
'
'  reads: AllTracks   writes to: AllTracks
'
' rounds to nearest half....
For Passes = 1 To 3 'number of smoothing passes


'Loop tracks
For CurrTrack = 1 To UBound(AllTracks, 1)
   'Create Temporary holder
   TrackTEMP = AllTracks(CurrTrack)


   'Loop points in track
   For CurrPoint = 1 To UBound(AllTracks(CurrTrack), 1)
      'If CurrPoint = 29 Then Stop
      'Level off data that has partial data region
      If CurrPoint <= Range Then   'start
         TrackTEMP(CurrPoint, 1) = AllTracks(CurrTrack)(Range, 1)
         TrackTEMP(CurrPoint, 2) = AllTracks(CurrTrack)(Range, 2)
      ElseIf CurrPoint >= (UBound(TrackTEMP, 1) - Range) Then   'end
         TrackTEMP(CurrPoint, 1) = AllTracks(CurrTrack)((UBound(AllTracks(CurrTrack), 1) - Range), 1)
         TrackTEMP(CurrPoint, 2) = AllTracks(CurrTrack)((UBound(AllTracks(CurrTrack), 1) - Range), 2)
      Else

         'Smooth
         MySumX = AllTracks(CurrTrack)(CurrPoint, 1)
         MySumY = AllTracks(CurrTrack)(CurrPoint, 2)
         Counter = 1
         For i = 1 To Range
            On Error Resume Next
            'AllTracks(CurrTrack)(CurrPoint, 1)'X
            MySumX = MySumX + AllTracks(CurrTrack)(CurrPoint + Range, 1)
            MySumX = MySumX + AllTracks(CurrTrack)(CurrPoint - Range, 1)
            'AllTracks(CurrTrack)(CurrPoint, 2)'Y
            MySumY = MySumY + AllTracks(CurrTrack)(CurrPoint + Range, 2)
            MySumY = MySumY + AllTracks(CurrTrack)(CurrPoint - Range, 2)
            Counter = Counter + 2
         Next 'i
         TrackTEMP(CurrPoint, 1) = Int(Round((MySumX / Counter), 1))
         TrackTEMP(CurrPoint, 2) = Int(Round((MySumY / Counter), 2))
      End If
   Next 'CurrPoint

   'Overwrite with temp array
   AllTracks(CurrTrack) = TrackTEMP

Next 'CurrTrack

Next 'Pass
End Sub
Private Sub Synchronise(SyncHeight)
'Synchronises the track - time 0 is when stamp is at given height
'
'(for each track, find point where stamp height is just above shoe and use
'that as zero position)
'
'1. Set array holding info on heights for each test
' Indexes:
' 0. SN HCush   (High Speed Video) - note, HSV are cropped and processed in a single macro
' 1. SN HCushR
' 2. SN FFCush
' 3. UR HCush
' 4. UR HCushR
' 5. UR FFCush
' 6. SN HCush   (3D Cams)
' 7. SN HCushR
' 8. SN FFCush
' 9. SN FFBend
' 10. UR HCush
' 11. UR HCushR
```

```
' 12. UR FFCush
' 13. UR FFBend
SyncPoint = 0
Dim SyncNEW()

MySyncPoint = UBound(AllTracks, 1)  'set point to use as sync (last = stamp)

'2. Loop through track of stamp point until height found
For i = 1 To UBound(AllTracks(MySyncPoint), 1)
   If AllTracks(MySyncPoint)(i, 2) = SyncHeight Then
      SyncPoint = i
      Exit For
   End If
Next 'i

If i >= UBound(AllTracks(MySyncPoint), 1) Then Exit Sub   'failed to sync

'3. Remove any points before this point (set point as frame 1)
For k = 1 To UBound(AllTracks, 1)
   MySyncPoint = k
   SyncTEMP = AllTracks(MySyncPoint)                    'set up temporary copy
   ReDim SyncNEW(UBound(AllTracks(MySyncPoint), 1) - i, 2)    'create new smaller array

   For j = 1 To UBound(SyncNEW)                         'copy required data
      SyncNEW(j, 1) = SyncTEMP(i + j, 1)
      SyncNEW(j, 2) = SyncTEMP(i + j, 2)
   Next 'j

   AllTracks(MySyncPoint) = SyncNEW                     'add new array to holder
Next 'k

'4. RECORD number of removes frames (for sync with accelerometer data).
'goes into 0,0 point
PostProcessingResults(0) = i '<<<< cant go in here, needs a separate PPR test holder


End Sub
Private Sub MinMaxExtraction(MyPoint, MyStart, MinMax, TestType)
'Finds maximum deflection of tip point, and time it occurs.
'
'MyPoint = Point to be tested, MyStart = Start frame,
'MinMax = to look for: True(Max) False(Min), TestType = Type of test
'      ---                    ----
'         ---      -      ----
'            @------ ------@
'
'aviods above scenario by checking for first and last max/min deflection (@)
'and finding the centre of these two frames.
'
'Check for non-pickup of point
If AllTracks(MyPoint)(1, 2) = 0 Then Exit Sub

MyRange = 10   'value used to check slope is rising/falling

On Error GoTo err
'1. Scroll through to find first max/min deflection
If MinMax = False Then
   'pixel MINIMA
   MyMin = 99999
   For CurrFrame = MyStart To UBound(AllTracks(MyPoint), 1)
      If AllTracks(MyPoint)(CurrFrame, 2) < MyMin Then
         MyMin = AllTracks(MyPoint)(CurrFrame, 2)
         FirstMin = CurrFrame
      End If
   Next 'CurrFrame
Else
   'pixel MAXIMA
   MyMin = -99999
   For CurrFrame = MyStart To UBound(AllTracks(MyPoint), 1)
      If AllTracks(MyPoint)(CurrFrame, 2) > MyMin Then
         MyMin = AllTracks(MyPoint)(CurrFrame, 2)
         FirstMin = CurrFrame
      End If
   Next 'CurrFrame
End If
```

```
'2. Scroll through to find last max/min deflection
'pixel MINIMA/MAXIMA
LastMin = FirstMin
For CurrFrame = FirstMin To UBound(AllTracks(MyPoint), 1)
   If MinMax = True Then
      If (AllTracks(MyPoint)(CurrFrame + 10, 2)) < AllTracks(MyPoint)(CurrFrame, 2) Then
         Exit For
      End If
   Else
      If (AllTracks(MyPoint)(CurrFrame + 10, 2)) > AllTracks(MyPoint)(CurrFrame, 2) Then
         Exit For
      End If
   End If

   If AllTracks(MyPoint)(CurrFrame, 2) = MyMin Then
      LastMin = CurrFrame
   End If
Next 'CurrFrame

'3. Calculate max/min point
MyLocation = Int((FirstMin + LastMin) / 2)
MyFrameDiff = MyLocation - MyStart
MyPixDiff = AllTracks(MyPoint)(MyLocation, 2) - AllTracks(MyPoint)(MyStart, 2)
'MyData = Array(TestType,Point NO., Start Frame, MinMax Frame, Frame Diff, Start Pix,          End Pix,
Pix Diff)
MyData = Array(TestType, MyPoint, MyStart, MyLocation, MyFrameDiff, AllTracks(MyPoint)(MyStart, 2),
AllTracks(MyPoint)(MyLocation, 2), MyPixDiff)


'4. Record data
If TestType = "Tip" Then
   PostProcessingResults(1) = MyData
ElseIf TestType = "MC" Then
   PostProcessingResults(2) = MyData
ElseIf TestType = "R" Then
   PostProcessingResults(3) = MyData
ElseIf TestType = "Datum_MIN" Then
   PostProcessingResults(4) = MyData
ElseIf TestType = "Datum_MAX" Then
   PostProcessingResults(5) = MyData
End If
Exit Sub

'ERROR handler
err:
'4. Record error data
If TestType = "Tip" Then
   PostProcessingResults(1) = Array("No_Tip_Result", "na", "na", "na", "na", "na", "na", "na")
ElseIf TestType = "MC" Then
   PostProcessingResults(2) = Array("No_MC_Result", "na", "na", "na", "na", "na", "na", "na")
ElseIf TestType = "R" Then
   PostProcessingResults(3) = Array("No_R_Result", "na", "na", "na", "na", "na", "na", "na")
ElseIf TestType = "Datum_MIN" Then
   PostProcessingResults(4) = Array("No_DatumMIN_Result", "na", "na", "na", "na", "na", "na", "na")
ElseIf TestType = "Datum_MAX" Then
   PostProcessingResults(5) = Array("No_DatumMAX_Result", "na", "na", "na", "na", "na", "na", "na")
End If
On Error GoTo 0
End Sub
Private Sub MaxVelocity(MyPoint)
'Calculates the maximum velocity of a pin (velocity take over 3-frame window)
On Error GoTo err:
VelRange = 16

MyMax = -99999
'1. Loop through frames
For CurrFrame = (VelRange + 1) To (UBound(AllTracks(MyPoint), 1) - VelRange)

   '2. Calculate Velocity
   MyVel = (AllTracks(MyPoint)(CurrFrame + VelRange, 2) - AllTracks(MyPoint)(CurrFrame - VelRange, 2))
   '3. Compare to current max
   If MyVel > MyMax Then
      MyMax = MyVel
      MaxVelFrame = CurrFrame
   End If
Next 'CurrFrame
```

```
'MyData = Array(TestType,Point No.)
MyData = Array("MaxV", MyPoint, MaxVelFrame, (MyMax / (VelRange * 2)))

'Output
PostProcessingResults(6) = MyData

Exit Sub
err:
PostProcessingResults(6) = Array("No_Vel_Data", "na", "na", "na")

End Sub
Private Sub StrainMeasure(PinA, PinB)
'
'  A-----| Calculates hypotenuse between PinA and PinB, then exports
'        |  results to a file.
'        B
'
'1. Create new array
Dim Strain() As Single
ReDim Strain(UBound(AllTracks(PinA), 1))

'2. Loop through and calculate hypotenuse
For i = 1 To UBound(AllTracks(PinA), 1)
   Xa = AllTracks(PinA)(i, 1)
   Ya = AllTracks(PinA)(i, 2)
   Xb = AllTracks(PinB)(i, 1)
   Yb = AllTracks(PinB)(i, 2)

   Strain(i) = CSng(Sqr((Xa - Xb) ^ 2 + (Ya - Yb) ^ 2))
Next 'i

'3. Write
MyOutputPath = Left(FilePath, Len(FilePath) - 4) & "_Strain_" & PinA & "-" & PinB & ".txt"
Open MyOutputPath For Output As #7
On Error GoTo err7

For i = 1 To UBound(Strain)
   Print #7, Strain(i)
Next 'i

err7:
Close #7
End Sub
```